Geochemistry and Mineralogy of the Silver Pond Prospect in the Toodoggone District: Implications for Regional Exploration

by

Pascal Andreas Voegeli

A thesis submitted in partial fulfillment of the requirements for the degree of

Master of Science

Department of Earth and Atmospheric Sciences
University of Alberta

© Pascal Andreas Voegeli, 2022

ABSTRACT

The Lawyers Property located in the Toodoggone district hosts a well-known extensively explored low sulfidation style epithermal deposit as well as an adjacent less understood target area known as Silver Pond that shares characteristics of a high sulfidation style system. The Silver Pond prospect is a large argillic alteration lithocap, with a high degree of leaching and texturally destructive clay alteration of the intermediate volcanic host rocks.

This study characterizes the geochemical trends, key alteration assemblages, and paragenesis of the Silver Pond prospect. The argillic-advanced argillic clay alteration is extensive both at surface as well as in the subsurface. The results of combined spectral (Raman and SWIR) and petrographic analysis identified a characteristic high sulfidation epithermal zonation pattern, as represented by an advanced argillic alteration zone with high temperature, low pH mineralogy (alunite, dickite, kaolinite, pyrophyllite) in structural contact with a large argillic alteration envelope (smectite, illite, ± kaolinite). Geochemical analyses indicated complimentary trends that are associated with alteration type and intensity. Intense alteration focused along major fault surfaces indicate that known regional scale structures controlled fluid flow. Abrupt changes in alteration assemblages and geochemistry at structural contacts indicate that Silver Pond likely underwent displacement that postdates alteration. While advanced argillic alteration is relatively extensive, highly porous silicified rock is scarce at Silver Pond and typically associated with faulting. Therefore, either the silica cap has been removed by erosion or Silver Pond represents the proximal shoulders to a silica cap that has been structurally displaced. Structural displacement and subsequent burial has led to preservation of different levels of erosion within Silver Pond. As shown by the mining history in the region, this structural dismemberment of mineralized systems makes the Toodoggone district prospective for diverse hydrothermal deposit types including epithermal and porphyry systems.

PREFACE

This thesis is an original work by Pascal Andreas Voegeli. No part of this thesis has been previously published.

Acknowledgments

First and foremost, I would like to thank the APEX Geoscience Ltd staff that provided technical guidance and have helped shape my professional development through the years, including Edward Parker, Rachelle Houge, Emily Laycock, Warren Black and Rob L'Heureux, as well as the countless other members of the team for their assistance in geoteching, core logging, SWIR data acquisition and general good company. I would also like to acknowledge Christopher Gallagher and Grayson Clague of Rogue Geoscience, who were responsible for a significant portion of the structural mapping used in this study as well as for developing the logging software and data structure used for the field portion of this study. I would also like to thank the hard-working staff of Radius Drilling for their tireless efforts, specifically Lenny Blunt for her role as operations manager. I would also like to graciously thank Benchmark Metals Inc for making this study possible with funding contribution and access to data, as well as the Natural Sciences and Engineering Research Council of Canada (NSERC) and Geoscience BC for financial contributions to this project. Thank you to Pilar Lecumberri-Sanchez for sharing her wealth of knowledge and for her tireless support as my supervisor, as well as Sasha Wilson and Farhad Bouzari for agreeing to serve on my committee. I would also like to express my gratitude to Spencer Poulette and Marko Szmihelsky for their assistance in the Raman lab, as well as Jilu Feng and Benoit Rivard for the acquisition and processing of the hyperspectral core scans. Finally, I would like to thank my parents for teaching me the value of hard work, fostering a spirit of adventure, and their truly unconditional support.

TABLE OF CONTENTS

ABSTRACT……i

PREFACE……ii

AKNOWLEDGMENTS……....iii

TABLE OF CONTENTS……..…..iv

LIST OF TABLES……..…vi

LIST OF FIGURES……....vi

1. Introduction 1

2. Geologic Setting 5

2.1 Geology 5

2.2 Structure 7

2.3 Alteration and Mineralization 7

3. Methods 8

3.1 Alteration mineralogy at deposit scale 8

3.2 Geochemical zonation at deposit scale 10

3.3 Paragenetic relationships 12

4. Results 13

4.1 Alteration Assemblages and Mineralogy 13

4.2 Mineral Paragenesis 17

4.3 Geochemical Classification 17

5. Discussion 39

5.1 Mineralogy and conditions of formation 39

5.2 Spatial distribution of mineral associations 40

5.3 Controls on fluid flow and implications for exploration 41
6. Conclusions 45
7. References 51
8. Appendices 57
Appendix A: Geochemistry Data Cross Sections
Appendix B: Shortwave Infrared (SWIR) Data Cross Sections
Appendix C: Geology Cross Sections
Appendix D: Representative Raman Spectra
Appendix E: Raman Multidimensional Arrays
Appendix F: Petrography
Appendix G: ASTER Shortwave Infrared (SWIR)
Appendix H: Hyperspectral Core Scans
Appendix I:White Mica Crystallinity Versus 2200 nm
Appendix J: Proposed Mineral Paragenesis
Appendix K: EDS and SEM
Appendix L: SWIR Tabular Data

LIST OF TABLES

Table 1: Energy Dispersive (EDS) Analysis

LIST OF FIGURES

Figure 1: Regional geology of Lawyers property area in north-central British Columbia. Geological unit boundaries and faults are from the BC Geological Survey's MapPlace dataset (MapPlace, 2021). All co-ordinates are in UTM Zone 9, NAD 83.

Figure 2. Geology of main prospect areas of the north-central part of the Lawyers property: Amethyst Gold Breccia (AGB), Cliff Creek, Phoenix and Dukes Ridge (MINFILE 094E 066, MapPlace, 2021). The study area is focused on the Silver Pond group of prospects (Silver Pond North, Silver Pond Clay, Silver Pond West; MINFILE 094E 163). Geological unit boundaries and faults are from the BC Geological Survey's MapPlace dataset (MapPlace, 2021). All co-ordinates are in UTM Zone 9, NAD 83.

Figure 3: Representative endmember alteration zones present at Silver Pond with A) medium-dark green host rock with pervasive chlorite alteration and sporadic carbonate veining representing propylitic alteration B) highly oxidized argillic assemblages representing supergene overprint, C) highly altered, completely replaced host rock occurring in conjunction with a fault zone, representing advanced argillic alteration and D) light to medium grey, intensely sericitized host rock representing argillic alteration.

Figure 4: Detailed core photos of characteristic textures including major fault structures (A-B), mm scale porosity within intensely altered and residual silica (C), and semi-massive sulfide breccia (pyrite) within intensely altered and silicified host rock (D).

Figure 5: 1) Plan view of the Silver Pond prospect. Background gradient represents topography. Circles indicate surface samples with argillic (yellow) and advanced argillic-alteration assemblages (red). Locations of drillholes (i.e 20SPCDD00X) and cross-sections (A–A', B–B'; see Figure 1**)** are labeled in black. **2)** E-W cross section A-A' showing the alteration assemblages at depth **3)** SE-NW cross section B–B' showing the alteration assemblages at depth. All co-ordinates are in UTM NAD83 Zone 9 elevation is in metres (m) above sea level

Figure 6: Strip Log of illustrating mineralogical composition and abundances of cross sections A-A' and B-B' shown in figure 5.

Figure 7: Orthogonal view of the surficial extent of the Silver Pond clay anomaly including the distribution of alteration assemblages with red circles representing samples with advanced argillic, and yellow circles representing argillic alteration. Discontinuous back lines indicate mapped and inferred fault surfaces.

Figure 8: Cross section C-C' (refer to panel 1, figure 5) illustrating extensive faulting within the central advanced argillic alteration zone.

Figure 9: Plots of white mica and kaolinite crystallinity as a function of depth (A-B). Plots of SWIR 2200 nm wavelength position in white mica as a function of depth and mineral species (C-D) (see figure 5 for drill hole locations**).**

Figure 10. Hyperspectral core scans showing the extent of alunite (A-D,orange), dickite (E-H, green), kaolinite (E-G, red) and pyrophyllite (I-J, blue) alteration in selected samples.

Figure 11. Hyperspectral core scans indicating compositional variations in white mica as determined by the position of 2200 nm wavelength features. White micas in samples SPC010 and 27 have compositions dominantly muscovitic while samples SPCX075 and SPC085 have dominantly phengitic compositions. Note transitions to lower 2200 nm features occurring as halos around veins.

Figure 12: Raman Spectra of alunite/natroalunite samples within advanced argillic assemblage. Panels A-D show the high and low bands of two alunite samples. Panels E-F display the features of a natroalunite sample. All labels indicate characteristic peak positions of alunite.

Figure 13: Raman spectra of select samples associated with intense hydrothermal alteration. Panel A shows a pyrophyllite spectra, Panel B shows a muscovite spectra, panels C-F display the high (3500-3800 cm^{-1}) and low band (200-1400 cm^{-1}) features of a dickite samples. All labels indicate characteristic peak positions.

Figure 14: Petrographic thin sections with A-B) a muscovite altered phenocryst crosscut by a late sulfate (Gyp) vein, C) complete replacement of the host rock to a dickite(Dck)-alunite(Alu)-pyrite(Py) assemblage D) illustrating a K-felspar phenocryst partially altered to muscovite suspended in a highly silicified groundmass, E) kaolinite(Kao)-sericite(Ser) alteration occurring on the rims of a pyrite grain F) a feldspar grain altered to pyrophyllite(Pyr), with late stage dickite (Dck)

Figure 15: Multidimensional spectral array displaying a feldspar pseudomorph suspended in a groundmass composed of muscovite (Msc) altered feldspars, finely disseminated pyrite (py) and minor quartz (Qtz), with the pseudomorph being infilled by late-stage anhydrite and quartz fluid pulses. The pyrite phase was included in the CLS fitting, but is identifiable as the anisotropic phase in the cross polarized image on the bottom right, and as the black pixels in the spectral grid. Note that this processing method assigns all pixels to one of the loadings selected for statistical analyses.

Figure 16: Multidimensional spectral array exhibiting complete host rock replacement with no relict host rock textures. Replacement mineralogy includes dickite (Dck) and

Alunite (Al). Note that this processing method assigns all pixels to one of the loadings selected for statistical analyses

Figure 17: Veining paragenesis as seen in drill core and thin section A) late gypsum vein crosscutting earlier pyrite phase within argillic altered host rock, B) quartz (Qtz) vein within a sericite (Ser), smectite (Smt), quartz (Qtz) bearing groundmass, crosscut by late stage pyrite and gypsum veining taken in cross polarized(XPL) and reflected light (RL), C) a sphalerite (Sph) grain with a second stage quartz vein, and a third stage calcite (Cal) vein in XPL and D) Earlier generations of pyrite (Py) and quartz(Qtz) crosscut by gypsum (Gyp) in XPL.

Figure 18: Thin section photomicrographs with Raman point analyses identified. A-C) Host rock completely replaced alunite and porosity filled by late stage dickite and sulfides, D-I) igneous feldspar phenocrysts altered to pyrophyllite and crosscut by a late stage dickite phases. All thin sections images in XPL

Figure 19: Orthogonal view of the Silver Pond argillic surface expression (outlined in beige) and faults. A. Relative concentrations of Tl are indicated using a colour scheme and a corresponding symbol size. B. Relative concentrations of Ca are indicated using a colour scheme and a corresponding symbol size.

Figure 20: 1) Cross-section A–A' (from Figure 3) showing relative concentration of Se and dominant alteration assemblage. 2**)** Cross-section B–B' (from Figure 3) showing relative concentration of Se and dominant alteration assemblage.

Figure 21. Isocon plots showing elemental relationships of alteration assemblages and mineralized zones plotted against reference unaltered hostrock, where C altered (vertical axis) represents the concentration of each assayed element in the altered/mineralized hostrock, and C unaltered (horizontal axis) represents the concentration of each assayed element in the unaltered hostrock. Elements that experienced no net loss or gain lay on the line with a slope of 1, with enriched elements having a value greater than one and depleted elements having a value of less than one, and immobile elements generally staying on the line regardless of the influence of alteration events. **a)** Isocon plot of the propylitic alteration zones shows minimal enrichment/depletion due to the occurrence of dominantly lower temperature hydration reactions (i.e., chlorite, epidote). **b)** Isocon plot of representative advanced argillic-alteration shows a high degree of enrichment in epithermal suite elements (i.e., W, S, Ag, Se, Mo) and major depletion in rock-forming elements (i.e., Mg, Ca, Na). **c)** Isocon plot of elemental distribution in a 1 m drillcore interval (drillholes 20SPCDD005, 20SPCDD008 and 20SPCDD009) with 23.6 ppmAu equivalent and **d)** Isocon plot of elemental distribution in 1 m drillcore interval (drillholes 20SPCDD005, 20SPCDD008 and 20SPCDD009) with 3.05 ppm Au equivalent. The isocon plots of mineralized sections indicate a similar geochemical signature as the advanced argillic-

alteration zones, indicating the identified enrichment trends can be used for targeting mineralization. Drillhole locations shown on Figure 3. Abbreviation: gt, grams per tonne.

Figure 22: A graphic illustration of proposed T^1 paragenetic sequence, with early-stage extensional faulting and the emplacement and cooling of plutonic suites generating the hydrothermal-magmatic system responsible for the high temperature white mica-pyrophyllite transition environment at depth and moderate temperature, low pH assemblages at surface. The fluid migration pathway and rock buffering relationship is indicated by a transition of high temperature mineralogy at the core zone situated around the fault system to the broader scale argillic zone. The mineralogical transitions and compositional shifts occurring as a function of temperature and pH are supported by 2200 nm (black contour lines) wavelength and crystallinity trends. Temperature isotherms (red, orange, yellow contours) are deduced from mineralogical data.

Figure 23: A graphic illustration of proposed T^2 paragenetic sequence, with a post erosion, late stage hypogene style acid-sulfate overprint of the earlier advanced argillic-argillic assemblages associated with the onset of the Silver Pond hydrothermal-magmatic system. This generation of alteration occurs in the shallower portion of the stratigraphy and is dominated by a broad scale laterally oriented alteration assemblage(s) composed of moderate temperature, low pH assemblages (dickite-kaolinite, anhydrite/gypsum, alunite).

Figure 24: Graphic illustration of proposed development of structural wedge as part of larger horst-grabben geometry that developed within the extensional fault regime of the Toodoggone volcano-tectonic depression. This major faulting episode is the proposed mechanism of displacement of the described alteration assemblages.

Figure 25: Graphic illustration of proposed T^3 paragenetic sequence which includes the deposition of the sedimentary units of the Cretaceous Sustut Group, which preserved the underlying Jurassic age volcanic-plutonic suites and their associated mineralization.

Figure 26: Graphic illustration of proposed T^4 paragenetic sequence in which subsequent tectonic uplift represented a shift to an erosional regime which resulted in the re-exposure of the Toodoggone volcanics as well as the earlier generations of T^1 and T^2 generations at surface and shallow depths within the Silver Pond prospect.

Introduction:

The Toodoggone district of north-central British Columbia (BC) is a 35×17 km NW trending mineral district (Bouzari et al., 2019). The district includes historical precious and base-metal producers such as the Baker, Cheni, Shasta and Kemess mines, and has emerged as a high priority exploration area with major discovery potential for porphyry and epithermal deposits. These types of system form some of the world's most important ore deposits, and are some of the largest producers of Cu, Mo, Au, and Ag globally (Halley, et al., 2015).

Extensive magmatism, structural dismemberment, and early burial in the district (Bouzari, 2019) have resulted in the formation of structural blocks that are eroded to varying levels of the magmatic-hydrothermal system. Structural dismemberment in a homogeneous and vertically extensive volcanic host package (Hazelton group) makes structural reconstruction challenging. Therefore, the level of exposure of the magmatic-hydrothermal system for each structural block is best interpreted through characterization of alteration assemblages, mineralization, and lithogeochemistry.

The Lawyers property, located in the historical Cheni mine within the central region of the Toodoggone district (Figure 1), preserves some of the shallow alteration and mineralization end-members of magmatic-hydrothermal systems, and hosts an indicated resource of 2.05 million oz. Au-Ag (Benchmark Metals Inc., 2021). The Lawyers property hosts several key pre-requisites for the development of high value exploration targets, including a deep-rooted fault system with a high degree of connectivity that can provide fluid pathways and conditions for fluid mixing, multiple periods of episodic magmatism that can enhance endowment and further mobilize precious and base metals, as well as late sedimentary units that provide high preservation potential for earlier magmatic products. The district was subject to multiple episodes of magmatism, which provide increased opportunities for the generation of hydrothermal-magmatic systems that yield significant mineralization events.

The majority of known Au-Ag mineralization at the Lawyers property is hosted in narrow multiphase quartz-carbonate, quartz-adularia, quartz-sulphide vein, stockwork and hydrothermal breccia zones, typical of low sulphidation epithermal systems (Duuring at al., 2009).

Mineralization is often closely associated with narrow (~5–30 m) potassic (potassium feldspar+sericite±kaolinite) alteration zones and broad regional-scale propylitic alteration (chlorite+hematite±epidote). Rare occurrences of phyllic style alteration (quartz, sercite, pyrite) occur in association with mineralized zones. Proximal to the extensively developed, low sulphidation–style prospects of Cliff Creek, Amethyst Gold Breccia (AGB), Phoenix and Dukes Ridge, but separated from them by a regional-scale fault, there is a less explored group of prospects known as Silver Pond (Figure 2). In contrast to the Lawyers property's dominant mineralization style, Silver Pond shows argillic-advanced argillic alteration *s.l.*, which occur in hydrolytic alteration conditions. Advanced argillic alteration is described by Meyer and Hemley (1967) as an assemblage of minerals occurring due to hydrothermal alteration systems and typically include "dickite, kaolinite, pyrophyllite usually with sericite, quartz, and frequently alunite, pyrite, tourmaline, topaz, zunyite and amorphous clays", wherein advanced argillic assemblages represent the advanced hydrolytic reaction. Argillic assemblages typically consist of clay minerals that are stable in less acidic conditions such as illite/muscovite, montmorillonite, kaolinite and halloysite (Vickre et al., 2010; Hemley and Jones., 1964). Lithocap environments containing argillic-advanced argillic assemblages commonly occur as the near-surface expression of porphyry systems (Sillitoe., 1994; Bouzari et al., 2019), but can have very different exploration implications depending on the presence and distribution of specific minerals and the mechanism of formation that they represent (Hedenquist and Arribas, 2022). Beyond the well-developed and established low sulfidation style mineralization on the property, the Silver Pond prospect indicates that the Lawyers system could be host to valuable intermediate-high sulfidation epithermal, and porphyry style mineralization.

The mineralogy of argillic-advanced argillic assemblages provides an indication of the formation environment and can be used to vector towards the likely relative position of mineralization (Hedenquist and Arribas, 2022) in a magmatic hydrothermal system. The zonation of alteration mineralogy in porphyry systems and their associated surface expressions has been successfully characterized through SWIR in several porphyry deposits (Lypcawzeski et al., 2020). The whole rock geochemical composition in epithermal-porphyry deposits also displays vertical and/or lateral zonation patterns (Vikre & John., 2018). Trace metals generate anomalies upward and outward from the hydrothermal magmatic core in a general sequence of Mo, W, Sn, Te, Bi, Sb, As, Li and Tl (Haley et al., 2015), with element enrichments including As, Sb, Hg, Se, Te, Tl, Mo being

reported specifically in epithermal systems (White and Hedenquist, 1995; Saunders et al., 2014, Coolbaugh, 1994; Kesler, 2003). Negative geochemical anomalies of key rock forming elements (i.e, Ca, Na) also occur in epithermal systems as a result of leaching by acidic fluids.

This study determines the spatial and paragenetic distribution of minerals and lithogeochemistry in the Silver Pond prospect towards interpreting 1) the mechanisms of formation of argillic alteration, 2) the implications for exploration in the prospect, and 3) the broad implications for the distribution of magmatic-hydrothermal mineralization in the region.

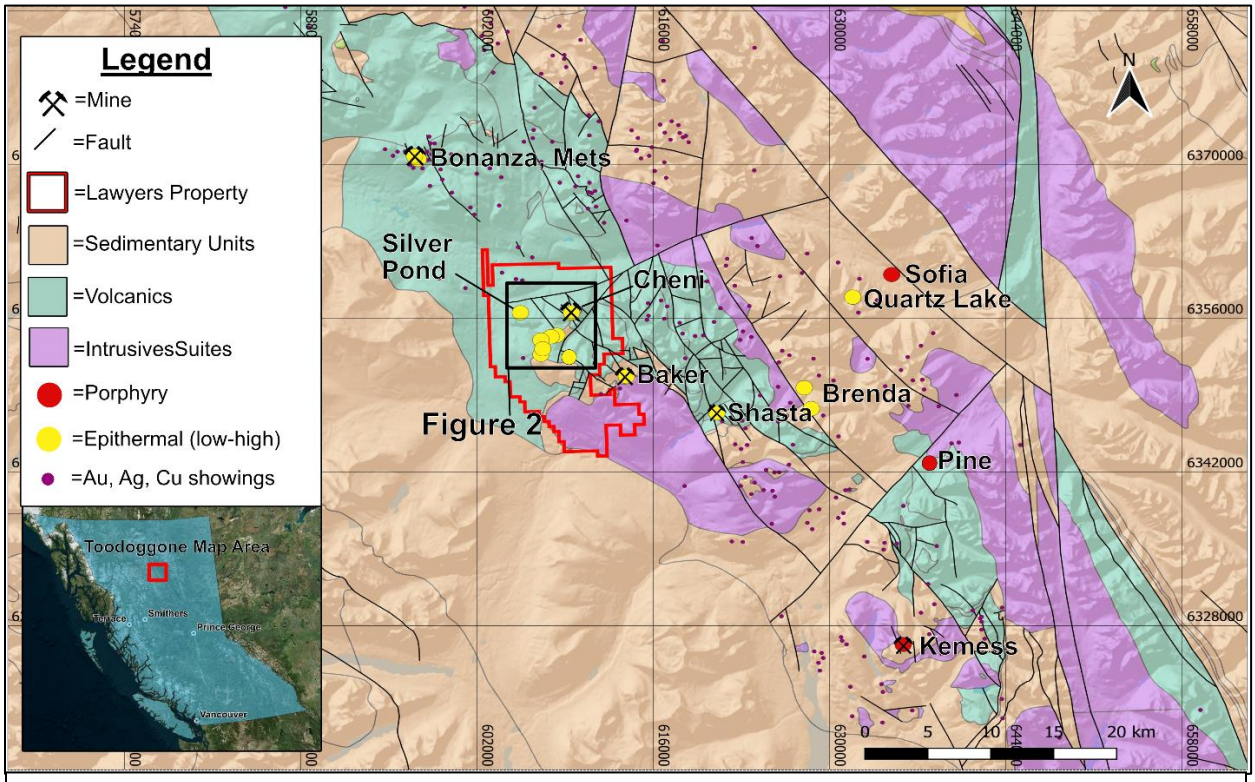

Figure 1. Regional geology of Lawyers property area in north-central British Columbia. Geological unit boundaries and faults are from the BC Geological Survey's MapPlace dataset (MapPlace, 2021). All co-ordinates are in UTM Zone 9, NAD 83.

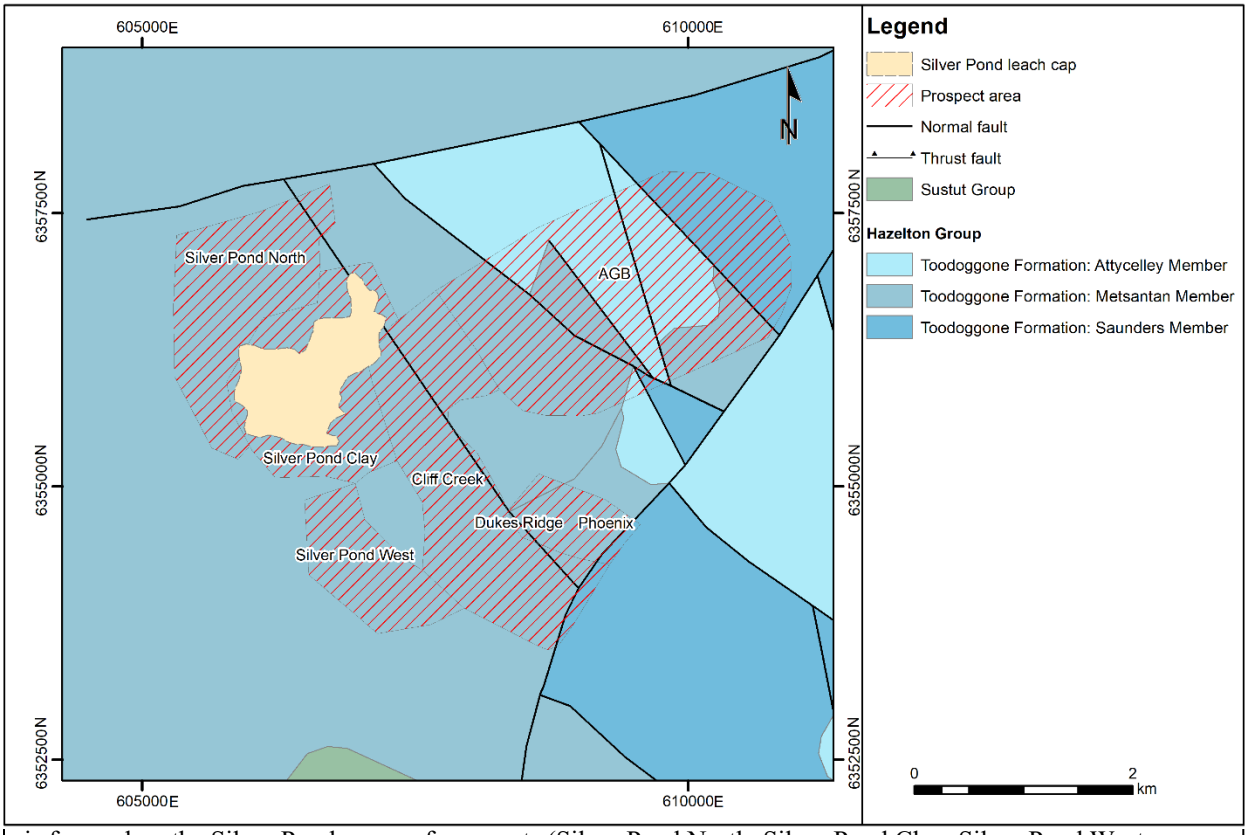

is focused on the Silver Pond group of prospects (Silver Pond North, Silver Pond Clay, Silver Pond West; MINFILE 094E 163). Geological unit boundaries and faults are from the BC Geological Survey's MapPlace dataset (MapPlace, 2021). All co-ordinates are in UTM Zone 9, NAD 83.

Geologic Setting

2.1 Geology

The Toodoggone district is located in the northern Intermontane Belt of the Canadian Cordillera and constitutes part of the eastern Stikine terrane which formed from aggregation of allochthonous Paleozoic and Mesozoic calc-alkaline arc complexes and their overlying sedimentary sequences (Monger, 1984). Late Triassic to early Jurassic magmatism is related with a series of economic porphyry and epithermal deposits that surround the Middle Jurassic to mid-Cretaceous Bowser Basin forming the prolific Golden Horseshoe trend. The Golden Horseshoe trend includes Eskay, Bruce Jack, and Red Mountain in its eastern extent, GT Gold and Red Chris to the North, and Ranch, Lawyers and Kemess to the East. The Lawyers property and the Toodoggone District are hosted in an ~2 km thick package of Lower Jurassic intermediate volcanic rocks belonging to the Toodoggone Formation, which is part of the regionally extensive Hazelton Group. The Hazelton group represents the final stage of magmatic arc activity in the Stikine Terrane prior to accretion onto the Cordillerran terrane collage (Gagnon et al, 2012). The volcanic sequences of the Toodoggone Formation include latite to dacite volcanic strata deposited in a north-northwest-elongated volcano-tectonic depression of the Toodoggone basement, which locally consists of Lower Triassic Takla Group volcanic rocks and Permian carbonate rocks (Diakow et al., 1991). The Toodoggone Formation is composed of relatively homogeneous intermediate porphyrytic andesites with feldspar, hornblende and rare biotite phenocrysts. The andesitic units exhibit textural variations that locally help define the stratigraphic units including fine grained units, volcaniclastic units, autobreccias and rare sections with interbedded ash layers. The Toodoggone formation is intruded by Jurassic porphyritic plutons known as the Black Lake intrusive suite, which consists of granodiorite to quartz monzonite crosscut by a series of felsic–intermediate cogenetic dikes (Diakow., 1991). Regionally the granitoids of the Black Lake intrusive suite are part of a belt of late Triassic to early Middle Jurassic plutons that are exposed intermittently in sections of the eastern margin of the Bowser Basin (Bouzari et al., 2019; Woodsworth et al., 1988). The emplacement of the Black Lake intrusive suite as well as a series of late unaltered felsic and mafic dikes appear to have been influenced by dominant regional deep-rooted extensional faults as evidenced by the preferred NW-NNW orientation of the various intrusive suites. Diakow et al (1991) suggest that the Toodoggone Formation formed concurrently with the establishment of the

deep-rooted extensional fault regime which likely focused magmatism and controlled the geometric distribution and subsidence of the lithologic units of the volcano-tectonic depression of the Toodoggone district. Continued tectonic extension of the Hazelton Group resulted in the generation of substantial accommodation space which, prior to the onset of contractional deformation, lead to the deposition of the marine sedimentation of the Bowser Basin (Thorkelson et al., 1995, Gagnon et al., 2009). Following the depositional hiatus of the Middle to Upper Jurassic, a thick package of Cretaceous continental sedimentary rocks known as the Sustut Group was deposited and represents the youngest unit in the Lawyers property and surrounding region (Diakow et al., 1991). The late sedimentary units are credited with preserving the epithermal deposits hosted in the Toodoggone volcanic rocks during subsequent uplift (Bouzari et al., 2019).

The prolific deposits of the Toodoggone district occur in spatial and temporal association with one another, commonly occurring along similar fault systems and displaying interrelated broad scale mineralogical transitions. These deposits exhibit the characteristics of each respective end member of the epithermal-porphyry continuum as represented by the porphyry systems of Kemess, Sofia and Pine, and the low-high sulfidation epithermal systems of Baker, Brenda, Alunite Ridge, Bonanza, Mets and Lawyers. District scale analysis by Bouzari et al (2019) underlines the porphyry affinities of various prospects within the Toodoggone Disitrct as evidenced by mineralogical and geochemical data. The key alteration characteristics described include pyrophyllite-quartz, alunite-quartz and kaolinite quartz bearing assemblages at Brenda and Alunite Ridge, indicating a surficial porphyry expression. Similar alteration relationships are also present in the Bonanza and Mets high sulfidation style deposits with mineralized silicic zones occurring in association with kaolinite-quartz, alunite-quartz bearing assemblages. Baker and Sofia display porphyry style K-silicate alteration as well as a higher relative concentration of Cu, Mo, W and Sn, indicating a more proximal porphyry environment. The low sulfidation deposits of the Cliff Creek prospect at Lawyers, as well as Shasta appear as having distal porphyry affinities, including quartz-illite-smectite dominant alteration assemblages and low-moderate relative enrichment in element suites associated with porphyry centers (i.e Cu, Mo). The significance of the alteration and geochemical characteristics present at Silver Pond with respect to the property and regional scale deposit model(s) remains largely undetermined and are further developed in this study.

2.2 Structure

The dominant property-scale structures at the Lawyers property consist of steeply dipping, north-northwest-trending (~310–340°) synvolcanic faults, which formed during extension in the Early Jurassic. This synvolcanic faulting formed a series of horst-graben blocks (Diakow et al., 1991), which define the structural geometry and displacement of the local and regional stratigraphy. Most fault blocks exhibit normal displacement with rare kinematic indicators (conjugate riedel structures and lineations) of minimal displacement and/or strike-slip movement. Major fault gouge zones are associated with potassic and propylitic alteration assemblages and are commonly pervasively silicified. The main Lawyers trend, which hosts the known hydrothermal breccia zones and their associated Au-Ag mineralization and alteration assemblages, is strongly structurally controlled, with the north-northwest-trending fault structures functioning as key fluid conduits. Isolated dilation jogs and intersections of north-northwest- and west-trending faults appear to concentrate ore shoots within the Lawyers trend. The argillic alteration assemblages of the Silver Pond prospects appear to have a strong association with deep-rooted north-northwest-trending fault structures. These faults have similar orientations to the main regional fault structures that serve as major controls for mineralization in the adjacent low sulphidation–style prospects.

2.3 Alteration and Mineralization

The volcanic sequences that host a majority of the known deposits on the Lawyers property are characterized by a regional epidote-chlorite-albite ± hematite assemblage that rarely hosts significant mineralization. Recent exploration efforts have recognized higher intensity epidote alteration and a minor sericite-smectite component that is more localized to deeper portions (~>300m) of the stratigraphy. This second alteration assemblage is associated with low sulfidation mineralization consisting of significant Au-Ag grades in the form of electrum, native gold, and finely disseminated sulfosalts, and having a distinct base metal association with Cu, Zn and Pb hosted in semi massive chalcopyrite, galena and sphalerite veins. A majority of the mineralization within the primary low sulfidation epithermal targets of Cliff Creek, AGB, Dukes Ridge, and Phoenix is hosted in mm scale metallic grey sulfosalt veinlets as well as milky quartz ± calcite, typically occurring in stockwork veining, multiphasic hydrothermal breccias and quartz stinger zones. The wall rock adjacent to the major faults associated with mineralized zones typically shows 5-30m wide alteration haloes consisting of fine-grained adularia ± sericite, and less commonly

quartz, sericite, pyrite alteration. Most mineralized zones adjacent to fault zones are moderately to intensely silicified.

The Silver Pond prospect is adjacent to the Cliff Creek low sulfidation prospect but is separated by major regional NW-NNW extensional fault structures that bound its eastern and western extent, forming a structural wedge. This block is characterized by a 5-7 km^2 as of yet uncharacterized clay alteration zone.

Low sulfidation mineralization at AGB and Cliff Creek as determined by Ar^{40}-Ar^{39} ages of K-feldspar is 188.2 ± 2.3 Ma and 189.7 ± 2.6 Ma (Clark and Williams-Jones., 1990). Molybdenite Re-Os dating of the proximal Baker Mine yielded ages of 193.8 ± 0.8 Ma (Bouzari et al., 2019). The Re-Os molybdenite dates from Baker match a series of Pb^{206}-U^{238} crystallization dates for the Duncan Pluton (oldest age of 202.3 ±2.3 Ma and a youngest date of 193.4 ± 2.6 Ma) belonging to the larger Black Lake Intrusive suite (Bouzari et al., 2019). The range of ages of intrusions and mineralization likely indicate multiple episodes of magmatism in the Toodoggone District. An age constraint for the Silver Pond alteration packages is inferred by the presence of a series of slightly altered dikes that crosscut Albert's Hump located to the north of the Lawyers Property, and Silver Pond, which are similar in composition and texture to the dikes that crosscut the intrusions of the Black Lake Suite, and therefore are synchronous or post-date the youngest date (~193-190 Ma) of cooling of the intrusive.

Methods:

3.1 Alteration mineralogy at deposit scale

Two shortwave infrared (SWIR) datasets were collected in the field: 496 surface analyses of clay/soils and 1956 subsurface analyses of drillcore. Surface spot analyses were collected with a Malvern Panalytical Ltd's portable ASD TerraSpec® Halo spectrometer. Surface datasets were collected in a 50 by 50 m grid using a GPS for navigation, with sample locations varying by up to 20 m from the grid spacing when necessary to access adequate clay exposure. Surface clay samples contained at least 1 cm of soil/clay and were dried prior to scanning. In addition to surface clay, flat unweathered/unoxidized representative host rock samples were analyzed where available.

Drillcore analyses were collected with a Malvern Panalytical Ltd's stationary ASD TerraSpec 4 Hi-Res Mineral spectrometer. All drillcore SWIR analysis were performed at regular 3 m intervals on a broken flat surface of representative core dried for ~3 hours with a Herman Nelson heating unit before scanning. The lens was regularly cleaned and the instrument calibrated with a white standard puck. Spot analyses focused on pervasive alteration mineralogy of host rock and avoided (1) planar features such as veins, faults and fractures, and (2) late stage oxidized surfaces (i.e limonite, goethite) and halos along faults and fractures.

The field dataset were processed through two commercial packages: The Spectral Geologist (TSG™) for ~15 % of the data; and IMDEX™ Ltd. aiSIRIS™ software for ~85% of data. Consistency between processing methods was verified through processing a subset of analyses both through aiSIRIS™ and through TSG. Spectra where abnormal absorption features or excessive noise were identified were discarded.

The relative crystallinity of white mica was determined by dividing the AlOH peak depth at ~2200 nm by the H_2O peak depth at ~1900 nm (Pontual el al., 1997, Guggenheim et al., 2002). For kaolinite, the mean 2181 nm absorption feature was divided by the 2161 nm absorption feature to provide the kaolinite crystallinity index (Hauff et al., 1990).

In addition to field SWIR analyses, a subset of samples was analyzed through hyperspectral core scan. Samples for hyperspectrcal core scan analyses were selected based on the presence of key diagnostic minerals (as identified through TSG or aiSIRIS), overprinting relationships and/or alteration textures. Each sample consisted of 2–10 cm length of split 2-inch core. The hyperspectral corescan dataset was collected at the University of Alberta's Spectral Imaging Facility through a SPECIM, Spectral Imaging Ltd.'s SisuROCK hyperspectral scanning system. The spatial resolution of the analyses is 250 by 250 µm/pixel. Mineral abundance maps of the samples were used to confirm representativity of field sample analysis, evaluate the abundance of each respective mineral and define paragenetic relationships of mineral assemblages where possible, including key high temperature minerals (pyrophyllite, dickite) within representative alteration zones.

The distribution of alteration assemblages identified through SWIR analyses was plotted in Micromine Pty Ltd's Micromine™ 2019 modelling software. Kaolinite associations with dickite,

alunite or pyrophyllite are categorized as advanced argillic alteration. Kaolinite associations with illite or undefined white micas are classified as argillic, noting that many of the white micas have illitic compositions and often have secondary and tertiary spectral contributions from smectite and kaolinite minerals. Chlorite associations with epidote, hematite or carbonate are categorized as propylitic alteration. While white mica-montmorillonite mixtures are identical to interlayered illite-smectite in SWIR (IMDEX aiSIRIS., 2022), mineral associations provide the context to interpret deposit zonation. Between the two processing techniques (TSG and aiSIRIS), the author recognizes and hereby wishes to state that some spectra reported as white mica with secondary montmorillonite may be illite-smectite interlayers and vice versa. All discussions and proposed models take careful consideration of individual spectra in the context of overall alteration assemblage, petrographic evidence, logging observations and broad scale zonation patterns that can nevertheless be accurately described.

The distribution of mineralogy obtained was then compared to ASTER data from the Geoscience BC's ASTER Exploration Assistant draped over a LiDAR digital elevation model (for the surface dataset) and the spatial relationship with mineralogy, geophysics, geochemistry and core logging observations was evaluated.

3.2 Geochemical zonation at deposit scale

Geochemical samples collected at the Silver Pond prospect include soil, rock and drillcore samples. Soil in-situ samples were collected in a 50 by 50 m grid avoiding sections with Quaternary (glacial) overburden. Due to poor outcrop exposure at Silver Pond, surface rock samples were collected at mapping stations and not at regular sampling intervals. Drillcore was sampled at a 2 m interval in relatively fresh host-rock with little to no mineralization, while samples with significant veining, increased alteration intensity and/or mineralization were sampled at a 1 m intervals. In sections of core with major structural breaks, isolated mineralization and/or veining, sampling intervals were adjusted to isolate the zone of interest with a minimum sample interval of 30 cm.

Silver and an additional 46 elements were commercially analyzed by four-acid digestion followed by inductively coupled plasma–mass spectrometry (ICP-MS), with samples that returned silver assays in excess of 1500 ppm being reanalyzed by fire assay of a 30 g sample with a gravimetric finish. Gold was analyzed by fire assay of a 30 g sample followed by inductively coupled plasma–

atomic emission spectroscopy (ICP-AES), with a lower detection limit of 0.001 ppm. All samples that exceeded 10 ppm gold were reassayed by fire assay of a 30 g sample with a gravimetric finish; the upper detection limit was 10 000 ppm. Quality assurance and quality control samples were inserted at a minimum of every 10 samples, with duplicates being taken in mineralized zones.

Isocon plots were used to observe quantitative changes in elemental concentrations of the rock-forming and epithermal suite elements as compared to immobile elements in order to determine the relationship between alteration types and addition/subtraction of elements (Grant, 2005). An unaltered reference was calculated from 10–150 m sections of unaltered core from 14 separate holes across the property with the same lithology as the Silver Pond prospects. In total, 179.9 m of core was used to calculate the unaltered reference. The mean, median and standard deviations of each of the elements analyzed were determined to help ensure that samples selected were representative of unaltered sections, and to remove any potential outliers within the selected sections. The mean value was then used as the unaltered reference against all sections of interest. Mineralized sections, alteration assemblages and individual alteration minerals identified by SWIR were plotted against the unaltered reference mean to help understand the composition of hydrothermal fluids responsible for mineralization and alteration.

In order to assess the possible porphyry affinity of the Silver Pond prospect, the MDRU porphyry index was applied to all geochemical drillhole data. This index is based on the work of Halley and was developed by the Mineral Deposit Research Unit at the University of British Columbia, and is a normalized element index ratio that utilizes the known occurrence of porphyry centers being enriched in Cu, Mo, W and Sn with respect to Sb, As, Ag, Li and Tl which generally are more enriched in the shallow portions of porphyry, and porphyry transitional environments (Bouzari et al., 2019). The formula is as follows:

$$\frac{\frac{Cu}{10} + Mo + (10 \times W) + (20 \times Sn)}{(5 \times Sb) + (20 \times Tl) + Ag + As + Li}$$

The MDRU porphyry index typically returns an index value ranging from ~1< to 6, with higher values indicating a geochemical signature that is more proximal to a porphyry center.

3.3 Paragenetic relationships

Determining the petrographic relationships of clay minerals through hand sample observation, petrography, or SWIR analyses is challenging due to the fine-grained nature of the minerals compared to the spatial resolution of these techniques. Therefore petrography, Raman spectroscopy and SEM were combined as potential tools to observe paragenetic relationships of clays. Thin sections were made for 105 samples from 8 drillholes. Target areas were determined from 1) SWIR data which identified key hydrothermal alteration mineralogy and 2) logging observations which displayed important paragenetic features of host rock alteration and veining. A subset of representative petrographic thin sections were selected for Raman and SEM analyses with a particular focus on samples containing high temperature phases (likely indicators of proximity to the hydrothermal fluid source).

Raman spectra were collected at the University of Alberta's Fluid Inclusion Laboratory using a Horiba Scientific's LabRAM HR Evolution mounted with an Olympus optical fiber microscope. LabSpec6 ™ was used for data reduction including smoothing, noise reduction, baseline subtraction, and multivariant (CLS) analysis techniques (Horiba Scientific., 2019). A monochromatic laser with a 532 nm frequency was used with a single holographic concave grating spectrograph with a resolution of 3 cm^{-1}/pixel and a spectral coverage of ~150-3200 cm^{-1}, operating at ≤300mW. Raman analysis included point analysis of individual phases, and 120 ×120 point grid mapping of ~800µm× 600µm areas. After spectral processing, each acquisition was plotted in CrytsalSleuth™ software for CRE (cosmic ray effect) removal and for use of the spectral matching function with representative spectra from the RRUFF database for positive mineral identification typically achieving a match confidence of ~85-95%. In addition to the use of CrystalSleuth software, all presented spectra were referenced to the current literature (primarily Gates et al.,2017) on interpretation and identification of mineral species, and where possible end member composition. Raman mapping was collected using 1 accumulation, acquisition time of 1 second, and 100% laser intensity and generated 12,000-16,000 spectra that were processed in Labspec6 software. Pixels exhibiting photoluminescence rather than Raman scattering were removed using the threshold function, typically at an assigned limit value of above 1200 counts depending on spectral profiles. Anomalous peaks associated with CRE were removed using the despike function at a maximum wavenumber width of 3 cm^{-1}. In order to remove high background results from the raw data, all multidimensional spectral arrays were baselined on a ~20^{th} degree

polynomial completed with an additional denoising operation. Images displaying the distribution of each respective phase identified in the multidimensional spectral array were generated by selecting a representative spectrum (or "loading") from within the spectral array (with a maximum of 3 reference spectra) and applying a Classical Least Squares (CLS) fitting procedure.

Scanning electron microscopy analyses were performed in a Zeiss Sigma 300VP-FESEM instrument in the University of Alberta's Scanning Electron Microscope Laboratory. All analyses were performed at high vacuum with an accelerating voltage of 15 keV, and EDS was performed on spots ranging 5-10mm in diameter.

Results:

4.1 Alteration Assemblages and Mineralogy

Three main alteration types have been identified through SWIR at the Silver Pond prospect: advanced argillic, argillic, and propylitic. The mineralogy, spatial distribution and textural characteristics at this prospect are different from the alteration types present at the low sulphidation targets on the Lawyers property.

Propylitic alteration is a broad scale alteration package composed of chlorite, hematite, carbonate and epidote, and is typically spruce green to light grey in color (Figure 3). Propyltic alteration dominantly occurs as weak to moderate intensity, weakly sulphized (0.5-2% pyrite) and is rarely weakly-moderately silicified, typically as a function of proximity with the argillic assemblages.

Argillic alteration is the dominant alteration style present at Silver Pond and overprints earlier generations of propylitic and relict phyllic style alteration in the form of K-rich white micas. The dominant argillic alteration occurs as two subcategories, including:

1) Highly oxidized assemblage consisting of low crystallinity kaolinite, illite, and smectite stained by iron oxides (limonite, goethite, hematite) likely related with the oxidation of pyrite (Figure 3). The host rock in this environment has undergone partial to complete replacement and is friable.

2) A much broader scale argillic alteration with light to dark grey appearance and feldspar phenocrysts having commonly undergone complete replacement (Figure 3). Lithologic textures such as volcanic clasts, feldspars, and layered ash beds are typically still visible with only partial replacement. Mineralogically, argillic alteration is dominantly composed of pyrite, interlayered illite and smectite, and white mica (paragonite, muscovite and phengite) with lesser kaolinite. K-rich white micas (muscovite) are most proximal to advanced argillic alteration and gradually transitioning to K-deficient, interlayered smectites and illites. Argillic alteration occurs as moderately to strongly silicified pervasively sulphidized (5-20% pyrite) zones, resembling a continuum between argillic and phyllic alteration.

Advanced argillic alteration occurs as highly sulphized (~10-30% pyrite), intensely altered rock where the original rock texture is lost (Figure 3). Proximal to fault zones this alteration results in either incompetent rocks completely replaced to clay, or in highly silicified competent rock that has also undergone partial to complete replacement, manifesting as fine-grained silica with most other mineral constituents being removed. All advanced argillic sections are moderate to dark grey in color and rarely exhibit relict host rock textures. The transition from rubbly clay rich core to competent silicified core almost always occurs at fault contacts (Figure 3 & 4). Rare sections of altered host rock exhibit possible gusano textures which are known to occur at the base of lithocaps and are dissolution features characterized by sub-rounded to rounded clusters of clay minerals, sulfides, sulfates in a fine-grained quartz groundmass (Torres., 2018). Additional textural features include rare 5-20cm sections that contain mm to cm scale dissolution pores typically proximal to fault zones. Mircoscale porosity ranging from 20-100 μm was also observed with petrographic analysis. The advanced argillic hydrothermal alteration zone is defined by the presence of high-temperature, low-pH alteration mineral assemblages including alunite, kaolinite, dickite, anhydrite/gypsum, high crystallinity white mica, and isolated occurrences of pyrophyllite and intense sulfidation (dominantly pyrite) (Figure 4D). Intense advanced argillic alteration, moderate to strongly silicified host rock, and dissolution textures causing isolated porous residual silica (Figure 4C**)** strongly correlate with fault surfaces at depth (Figure 4 A&B). The observed spatial distribution and associated assemblages of advanced argillic mineralogy occur as two general subcategories including:

1) A laterally extensive (>1.5 km) assemblage dominated by dickite-kaolinite, quartz, pyrite, gypsum/anhydrite and lesser alunite. This zone appears as partial to complete replacement of the host rock, and appears to transition outwards from the major fault zones described. This assemblage appears to resemble hypogene style alteration characteristics as described by Cooke et al 2000.
2) A narrow (~50-200 m) assemblage dominated by pyrophyllite, muscovitic white micas, alunite, dickite, quartz and pyrite. This zone appears in sections of intensely altered host rock that has typically undergone complete replacement, and is fault bound, occurring on or with proximity to major fault surfaces. This assemblage resembles the white mica-pyrophyllite transition environment described by Arribas & Hedenquist 2022.

The alteration domains at Silver Pond present gradual boundaries over 10s to 100s of meters, with sharp boundaries occurring only in association with structural features. At surface, the highest intensity hydrothermal alteration in Silver Pond is an elongated east-west advanced argillic-alteration core, with south and north shoulder zones predominantly composed of transitional argillic and propylitic alteration assemblages (Figure 5&6). The surface extent of the argillic alteration domain is largely bound within mapped, logged and inferred fault structures (Figure 7**)**. The south and north shoulder zones exhibit a transition from advanced argillic alteration to argillic alteration composed of white mica/illite, smectite and kaolinite. The argillic alteration zone is observed both at surface and at depth, typically grading outwards from the advanced argillic zones (ex 20SPCDD005, 20SPCDD006 and 20SPCDD007) or being truncated by fault structures **(**Figure 8). The deeper sections of the drillholes to the north and south of Silver Pond display a transition from argillic to propylitic alteration zones (ex. 20SPCDD001-3, 20SPCDD005, 21SPNDD003-4).

The majority of chlorite identified within the Silver Pond prospect has a fairly homogeneous low wavelength absorption feature (~2246–2252 nm) indicating a magnesium-rich end member (appendix B). In contrast, white micas show systematic zonation in terms of mineral abundance, composition, and crystallinity. The spectral contribution (i.e. relative abundance) of white micas is high across the extent of the Silver Pond prospect. Muscovitic compositions occur at depth in the advanced argillic core and closer to surface in the shoulders of the system, while phengitic compositions occur at depth in the shoulders of the system (Figure 9). Muscovitic white micas (lower 2200 nm wavelength) occur as alteration halos around veins and more phengitic

compositions are associated with groundmass (Figure 11). The crystallinity of white mica and kaolinite also increases with depth (Figure 8 a, b) and/or proximity to advanced argillic-alteration zones. Overall, white micas across Silver Pond display intermediate crystallinity values (~0.75-1.5) with a subset of highly crystalline values (~1.5-2.5) (Appendix I)**.** Regional SWIR studies of other deposits in the Toodoggone District by Bouzari et al., reported high crystallinity values (>2) in white micas are associated with quartz sericite alteration associated with intrusive porphyry stocks at the Baker and Black Gossan deposits.

The presence and abundance of pyrophyllite and dickite (Figure 10), as examples of high temperature phases, was identified with SWIR analysis and verified through hyperspectral core scans. Several samples contain over 90% volume of dickite or pyrophyllite. Isolated sections of the advanced argillic alteration core zone exhibit texturally-destructive pervasive alunite alteration of the host rock (Figure 10). The hyperspectral corescans also identified narrow zones of advanced argillic mineralogy (i.e alunite, pyrophllite, dickite) in zones that are broadly argillic-propylitic suggesting that transitions between alteration domains are, in detail, broader than shown by field analyses.

Raman spot analyses confirmed the presence, compositional variations, assemblage associations, and paragenetic relationships of key hydrothermal alteration minerals. Alunite-bearing samples displayed Raman peak position indicative of K-Na alunites to Na-alunite (Figure 12), which were confirmed through EDS analyses. Dickite, pyrophyllite and white mica SWIR identification was also verified through Raman analyses (Figure 13). White micas showed variable positions in the 1000-1150 cm^{-1} Raman peak representing the solid solution between phengite and muscovite, with phengite occurring at the upper 1150 cm^{-1} range and muscovite in the lower 1000 range cm^{-1} (Li et al., 2011; Arbiol., 2021). White micas generally exhibited intermediate composition peak positions (~1075-1125 cm^{-1}) but, similarly to the hyperspectral maps few consistent spatial trends in composition were observed at the hand sample scale. All major phases identified were verified with EDS analysis (Table 1) and assemblage associations were observed in backscatter images. There were some discrepancies between the hyperspectral and Raman identification of dickite/kaolinite such that some minerals identified through hyperspectral analyses as kaolinite locally showed Raman peaks characteristic of dickite (Gates et al., 2013).

4.2 Mineral Paragenesis

Feldspars phenocrysts are replaced by pyrophyllite; alunite-dickite; coarse grained muscovite-quartz; or kaolinite-muscovite associations. A multiphase quartz-pyrite component appears to be prior to coeval to these replacements in different samples (Figure 14)

Microporosity cements (10-500 μm) within advanced argillic domains were analyzed and mapped through Raman showing late-stage infill with quartz, anhydrite/gypsum, pyrite (Figures 15) as well as complete replacement by an alunite-dickite assemblage (Figure 16). These textural features are important precursors to deposit formation as they provide the host rock for mineralization in high sulfidation style settings.

The main vein types present at Silver Pond include quartz, semi-massive sulfide (pyrite), gypsum/anhydrite and calcite (Figure 17). The earliest generations of veining are typically either mm-cm scale quartz veinlets or broad-scale fine grained-silicification of groundmass and pseudomorphs replacements of feldspars. Pyrite veining crosscuts quartz in veins and breccias and also occurs as finely disseminated throughout the prospect, typically with increasing modal percentage as a function of increasing alteration intensity. Gypsum and anhydrite veins crosscut both quartz and pyrite veins. The final stage of veining is a late calcite generation that commonly infills open space in earlier quartz, pyrite and sulfate veins as well as microporosity in the host rock. Kaolinite veins identified through hyperspectral mapping (Figure 10) are found in samples pervasively altered to dickite are crosscut by gypsum veins. Dickite veins were identified through Raman in samples pervasively altered to pyrophyllite and alunite (Figure 18).

4.3 Geochemical Classification

The surface area of Silver Pond is characterized by a systematic depletion in common rock-forming elements, such as Mg, Ca and Na, as well as enrichment in epithermal suite elements, such as Tl, Te, Se, As and Sb (Figure 19, Appendix A). Similar chemical relationships were also displayed in the subsurface with the highest degree of relative enrichment closely correlating with the intensity and type of clay alteration present. The geochemical fingerprint of each respective alteration domain, as illustrated in the isocon plots (Figure 21), shows high levels of enrichment in key elements such as Mo, Se, Te, Pb, Bi, Th and Sn, coinciding with the signature of other known

intermediate to high sulphidation epithermal systems (i.e., La Coipa, Chile; Summitville, United States; Pueblo Viejo, Dominican Republic), which are commonly enriched in Cu, Pb, Zn, Mo, Bi, Sn, Te, Th and Se (John et al., 2018). Samples with intense advanced argillic-alteration generally exhibit the highest degree of enrichment in epithermal suite elements and a corresponding depletion in rock-forming elements (Figure 21), with argillic and propylitic alteration assemblages sequentially having a lower degree of enrichment/depletion of indicative element suites. Select samples within isolated mineralized intervals (0.3–1 m) from three different drillholes (20SPCDD005, 20SPCDD008, 20SPCDD009) show a correlation between the occurrence of Au-Ag and W, Pb, Bi, Cu, Te, Mo and Se (Figure 21). In addition, positive anomalies of Mo, Se, Te, Pb, Bi and Sn systematically increase from argillic to advanced argillic-alteration zones.

A series of modelled and logged north-northwest-trending faults appear to have an influence on the spatial distribution of geochemical trends, with areas proximal to the fault system experiencing a higher degree of enrichment in select epithermal suite elements. Similar degrees of enrichment and elemental associations can be found within isolated Au-Ag intersections. Historical drilling on the Silver Pond prospects also indicates select zones of mineralization occur along a northern extension of the fault system, possibly indicating extensive mineralization along the strike of these major fault structures. The close spatial correlation of the enrichment of pathfinder elements with advanced argillic alteration (high-temperature low-pH) clay assemblages provides evidence that the system at Silver Pond site has a strong structural control, as suggested by observed fault structures exhibiting a strong association with highly anomalous geochemical signatures and a corresponding mineralogical shift that suggests intense fluid alteration. Sharp boundaries between alteration assemblages at faults indicate that those structures were likely reactivated after mineralization.

The MDRU porphyry index applied to the Silver Pond generally reports isolated (~10-50 meter) zones with higher porphyry affinity (~3-5) within the faulted central block with the highest degree of alteration intensity, which generally grades out to lower scores (<1-2) in the more distal portions. The results from the MDRU porphyry index mirror the high temperature alteration zones with anomalous geochemical signatures, but however do not show any clear broad scale relationship with increasing depth as would be expected in an ideal vertical zonation patten of the described elemental ratios.

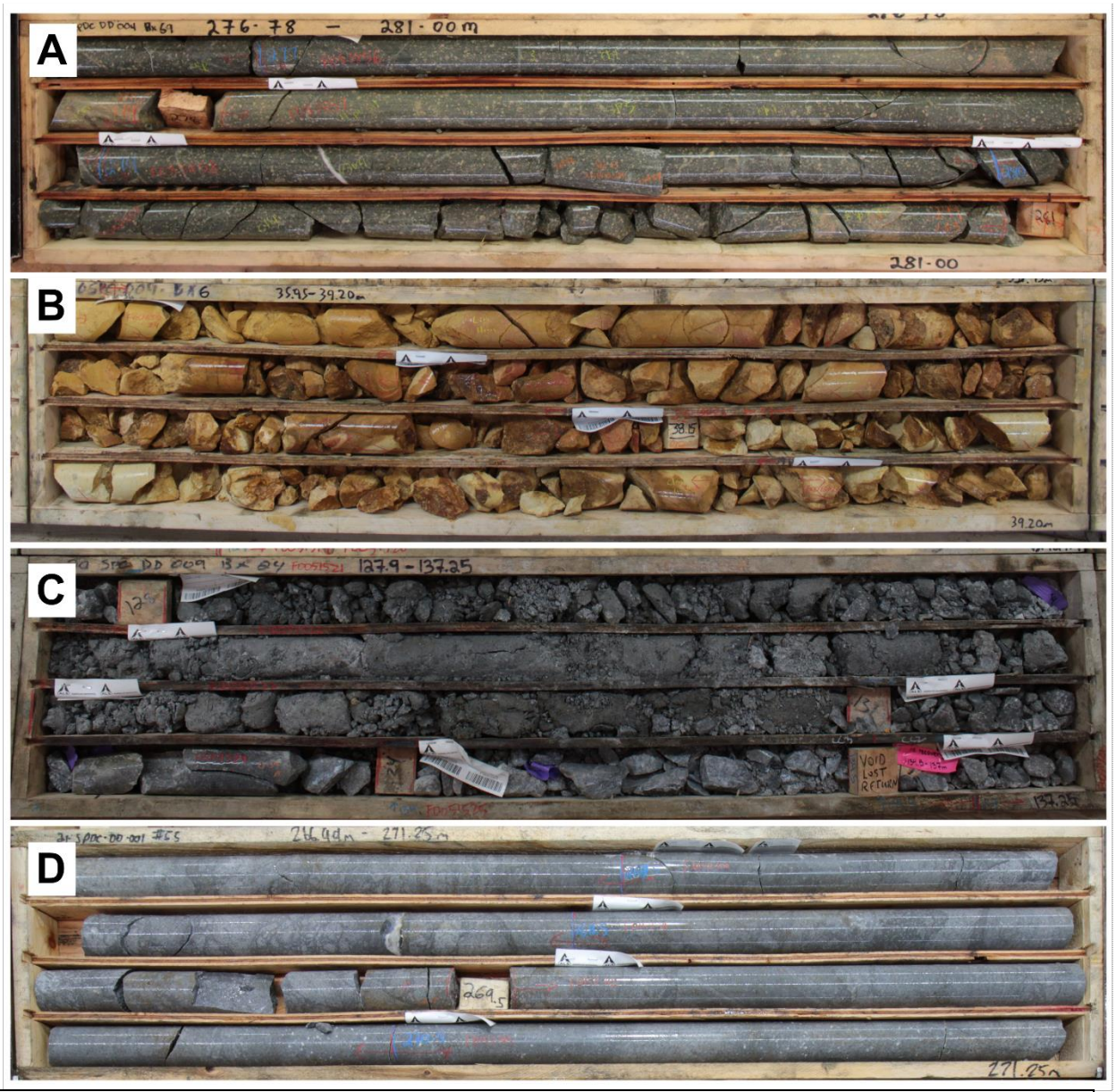

Figure 3: Representative endmember alteration zones present at Silver Pond with A) medium-dark green host rock with pervasive chlorite alteration and sporadic carbonate veining representing propylitic alteration B) highly oxidized argillic assemblages representing supergene overprint, C) highly altered, completely replaced host rock occurring in conjunction with a fault zone, representing advanced argillic alteration and D) light to medium grey, intensely sericitized host rock representing argillic alteration.

Figure 4: Detailed core photos of characteristic textures including major fault structures (A-B), mm scale porosity within intensely altered and residual silica (C), and semi-massive sulfide breccia (pyrite) within intensely altered and silicified host rock (D).

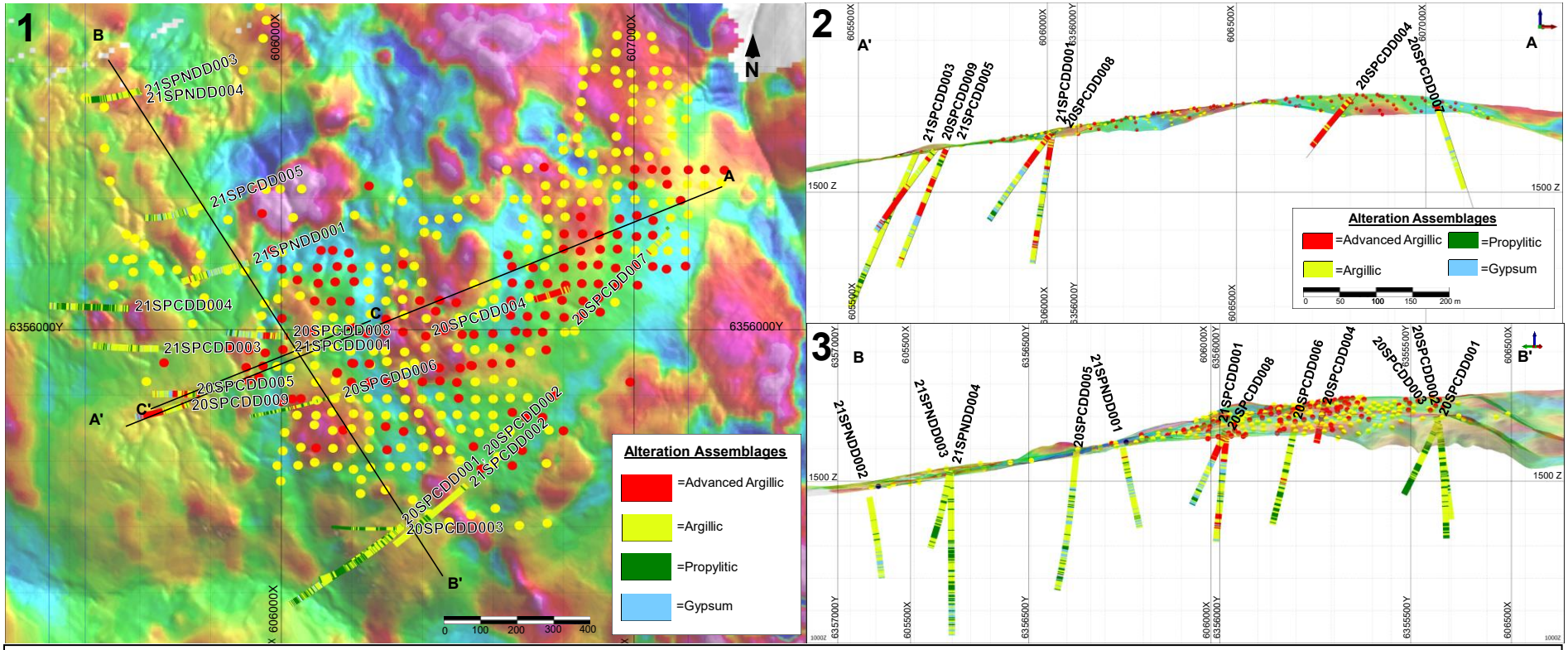

Figure 5: 1) Plan view of the Silver Pond prospect. Background gradient represents topography. Circles indicate surface samples with argillic (yellow) and advanced argillic-alteration assemblages (red). Locations of drillholes (i.e 20SPCDD00X) and cross-sections (A–A', B–B'; see Figure 1**)** are labeled in black. **2)** E-W cross section A-A' showing the alteration assemblages at depth **3)** SE-NW cross section B–B' showing the alteration assemblages at depth. All co-ordinates are in UTM NAD83 Zone 9 elevation is in metres (m) above sea level

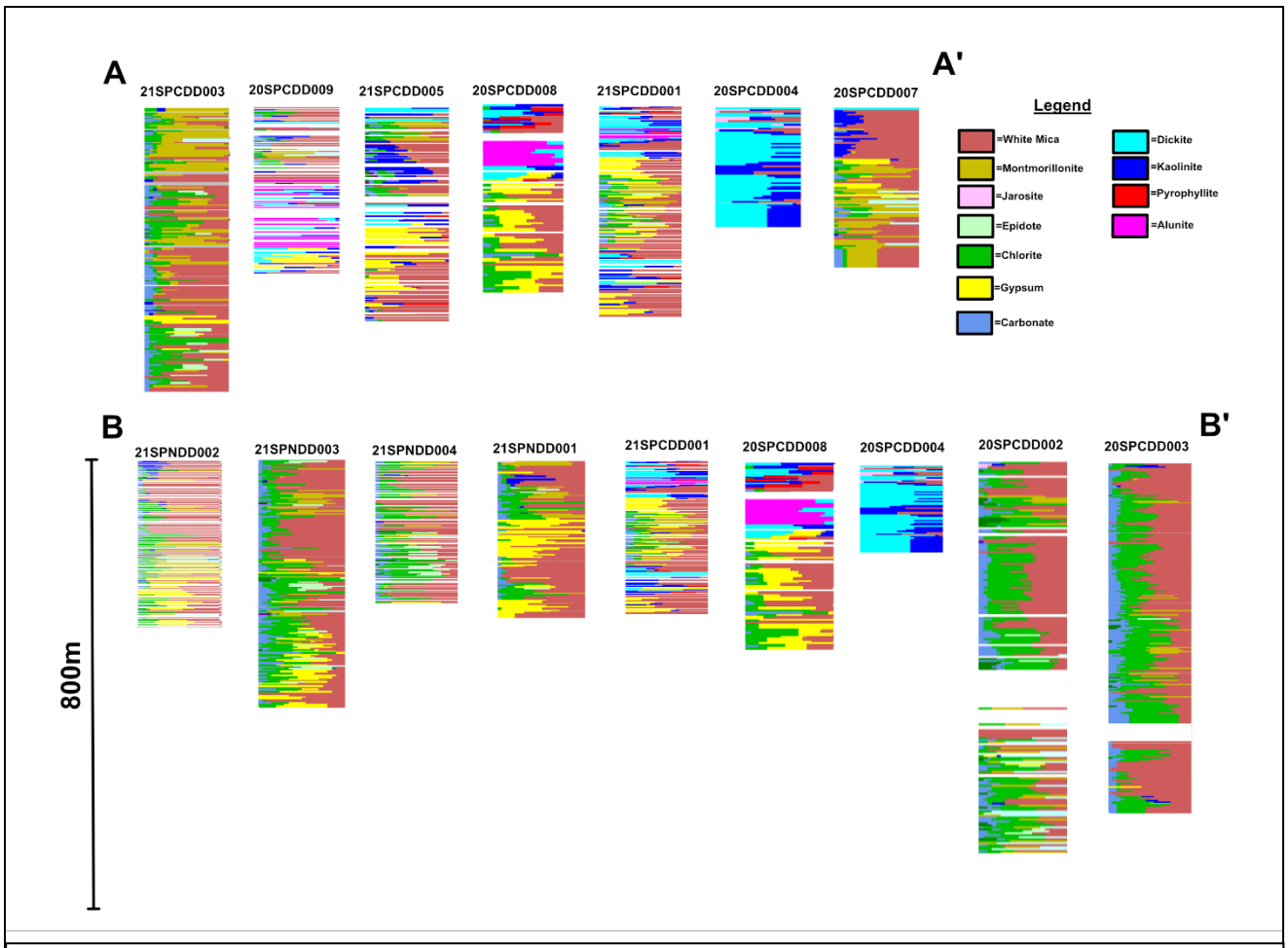

Figure 6: Strip Log of illustrating mineralogical composition and abundances of cross sections A-A' and B-B' shown in figure 5.

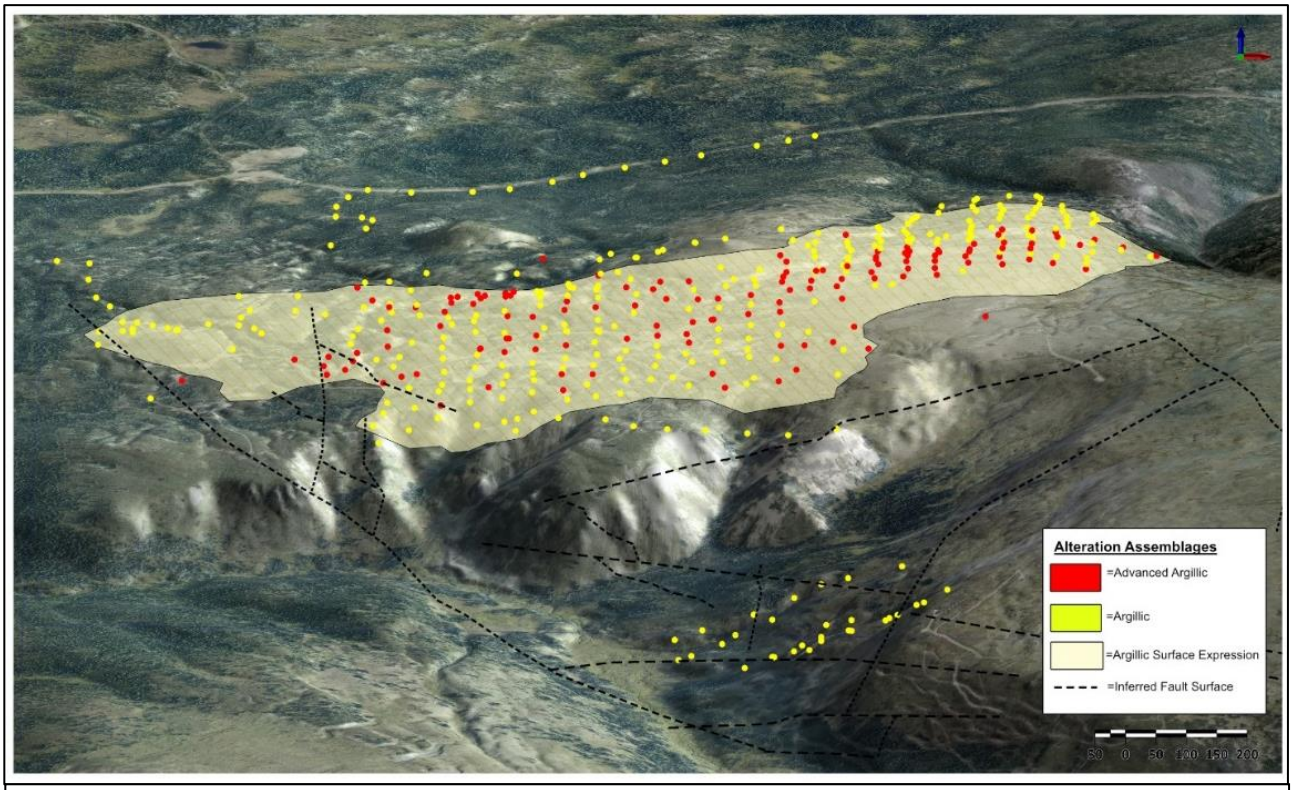

FIGURE 7: Orthogonal view of the surficial extent of the Silver Pond clay anomaly including the distribution of alteration assemblages with red circles representing samples with advanced argillic, and yellow circles representing argillic alteration. Discontinuous back lines indicate mapped and inferred fault surfaces.

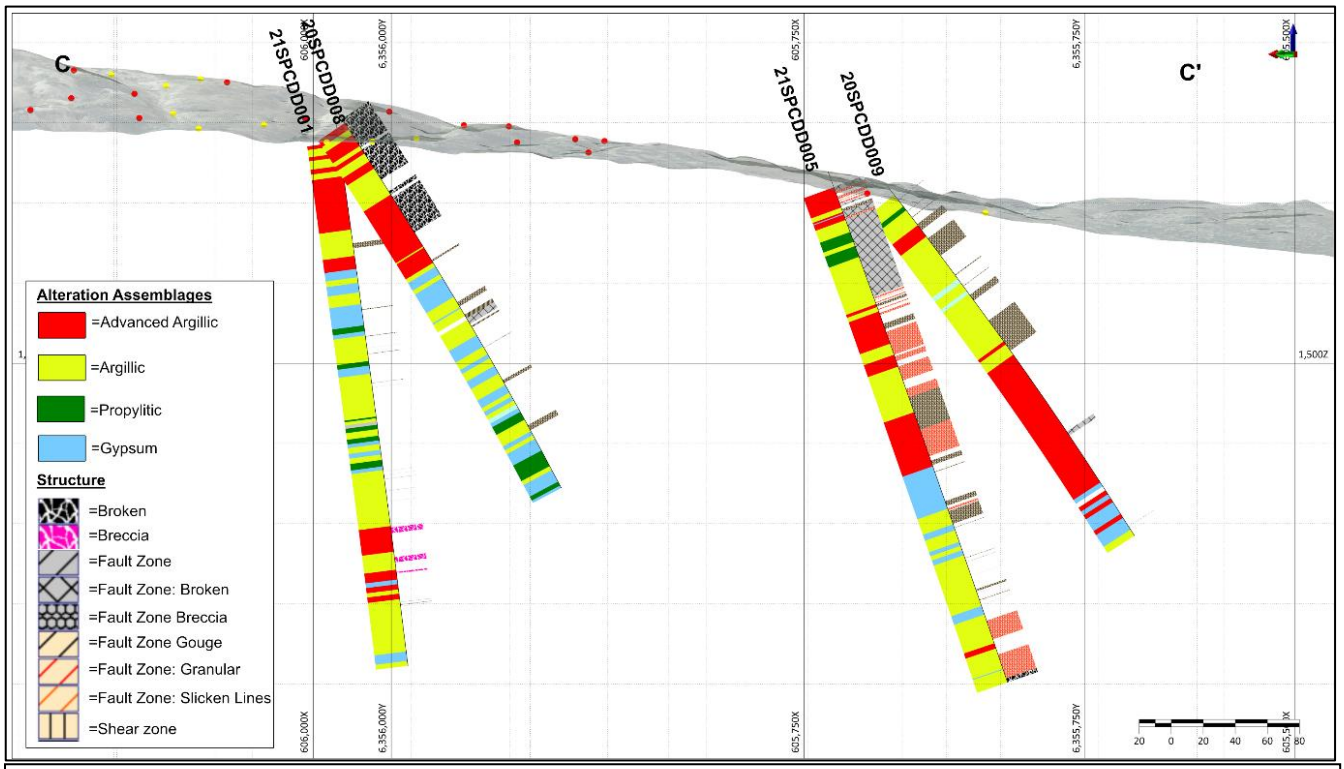

Figure 8: Cross section C-C' (refer to panel 1, figure 5) illustrating extensive faulting within the central advanced argillic alteration zone.

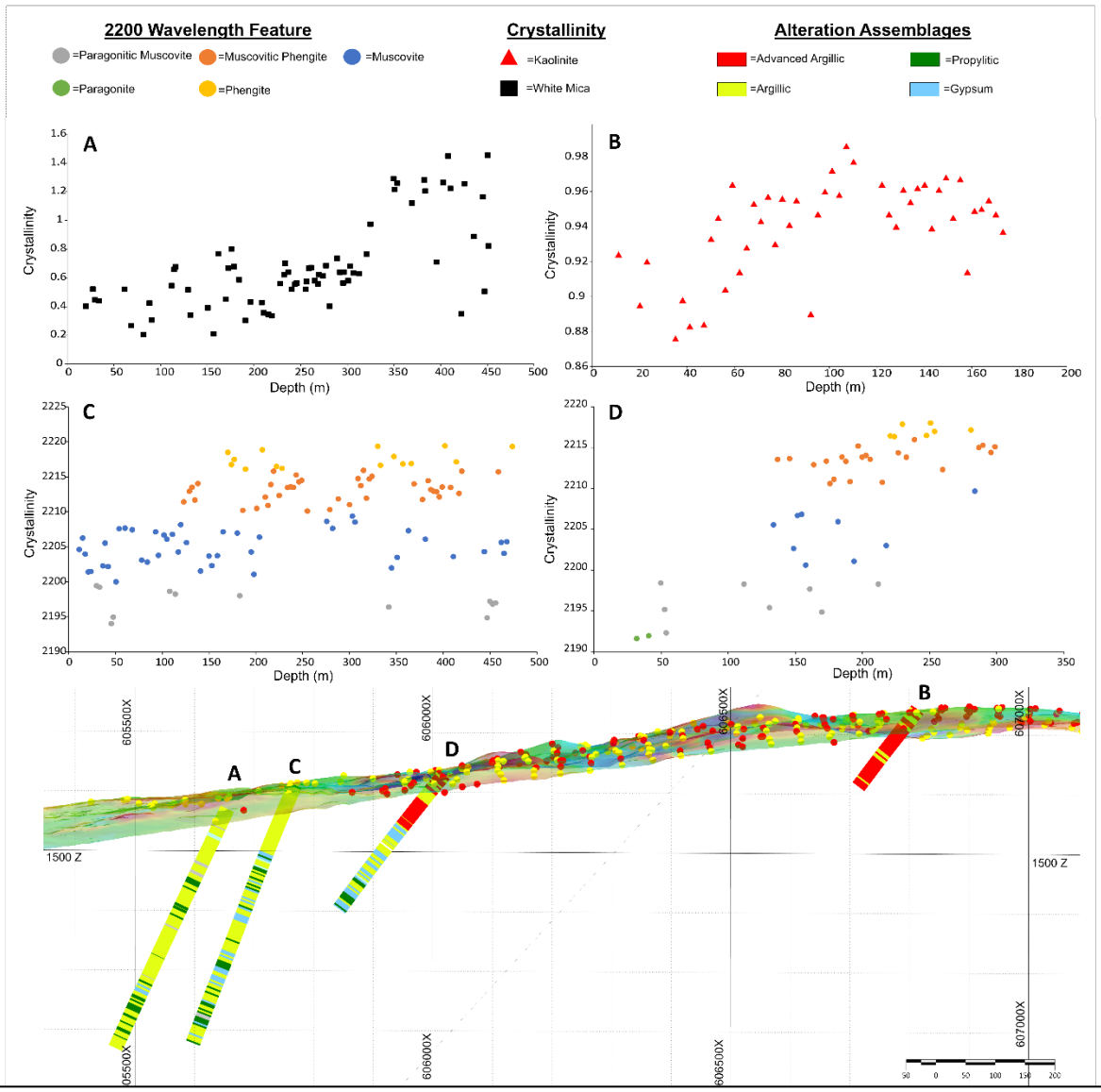

Figure 9: Plots of white mica and kaolinite crystallinity as a function of depth (A-B). Plots of SWIR 2200 nm wavelength position in white mica as a function of depth and mineral species (C-D) (see figure 5 for drill hole locations**).**

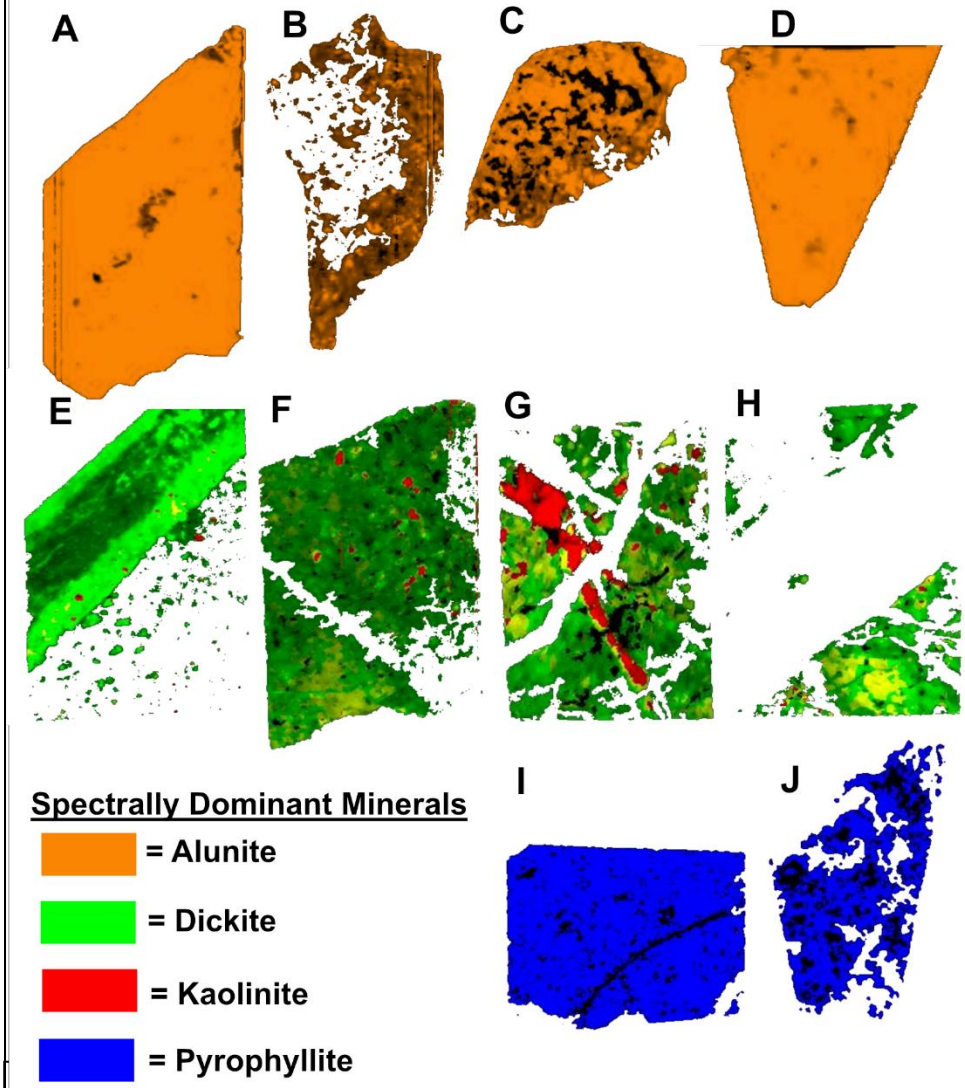

Figure 10. Hyperspectral core scans showing the extent of alunite (A-D,orange), dickite (E-H, green), kaolinite (E-G, red) and pyrophyllite (I-J, blue) alteration in selected samples.

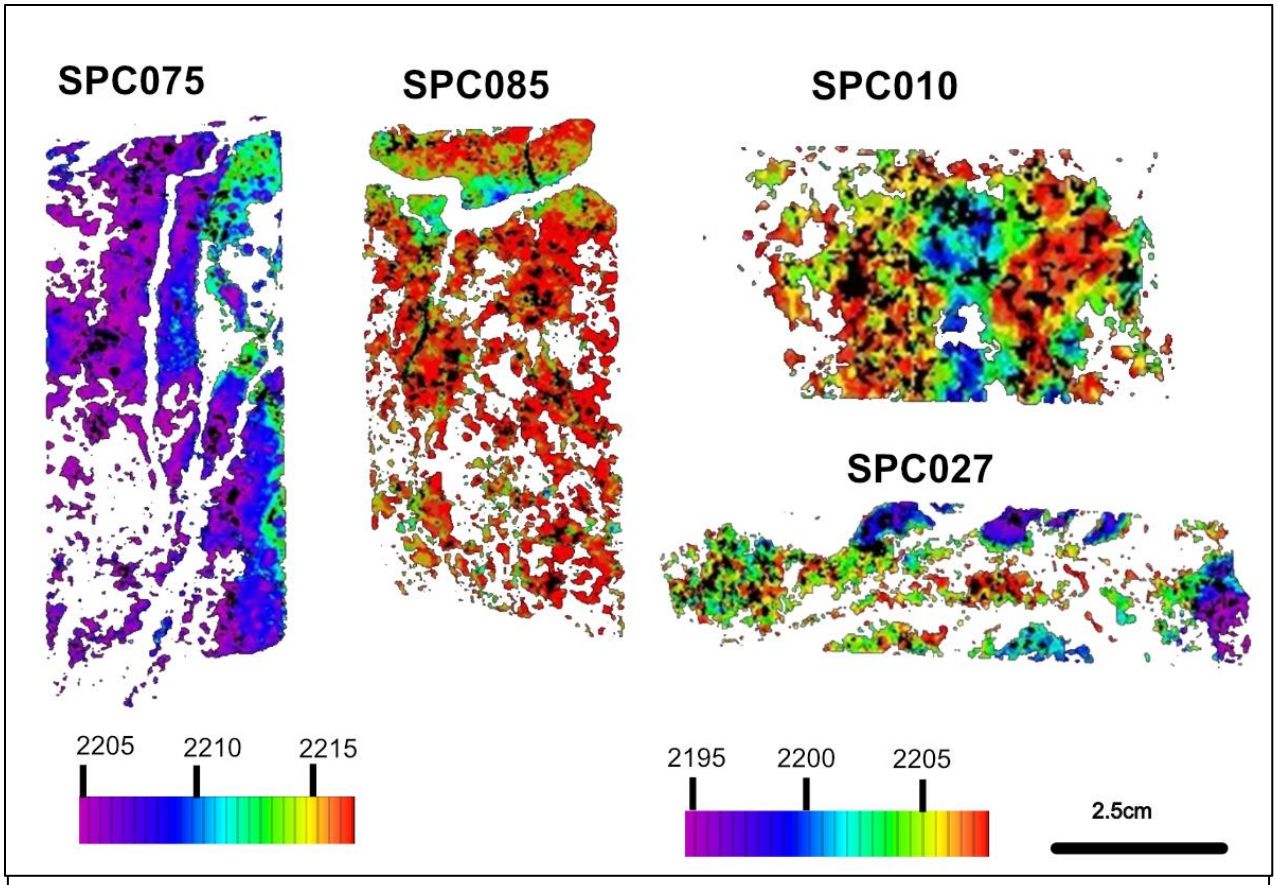

Figure 11. Hyperspectral core scans indicating compositional variations in white mica as determined by the position of 2200 nm wavelength features. White micas in samples SPC010 and 27 have compositions dominantly muscovitic while samples SPCX075 and SPC085 have dominantly phengitic compositions. Note transitions to lower 2200 nm features occurring as halos around veins.

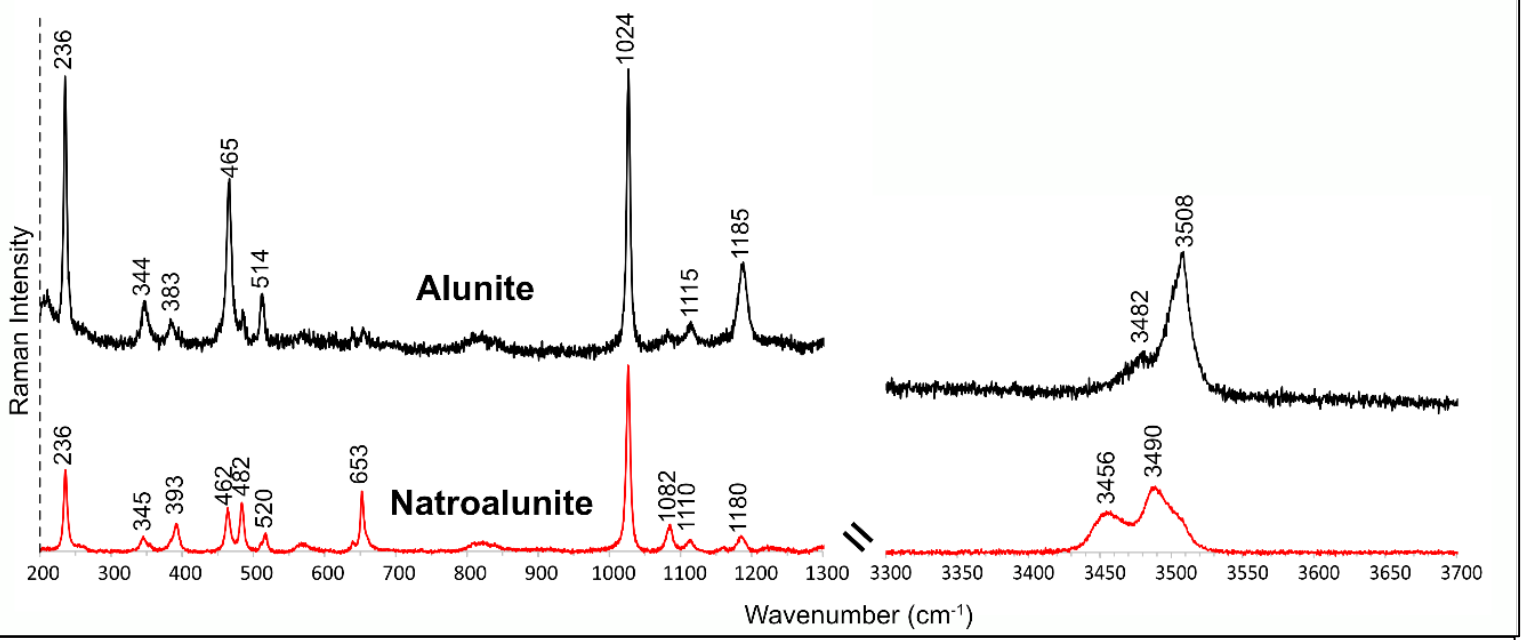

Figure 12: Raman Spectra of alunite/natroalunite samples within advanced argillic assemblage. Panels A-D show the high and low bands of two alunite samples. Panels E-F display the features of a natroalunite sample. All labels indicate characteristic peak positions of alunite.

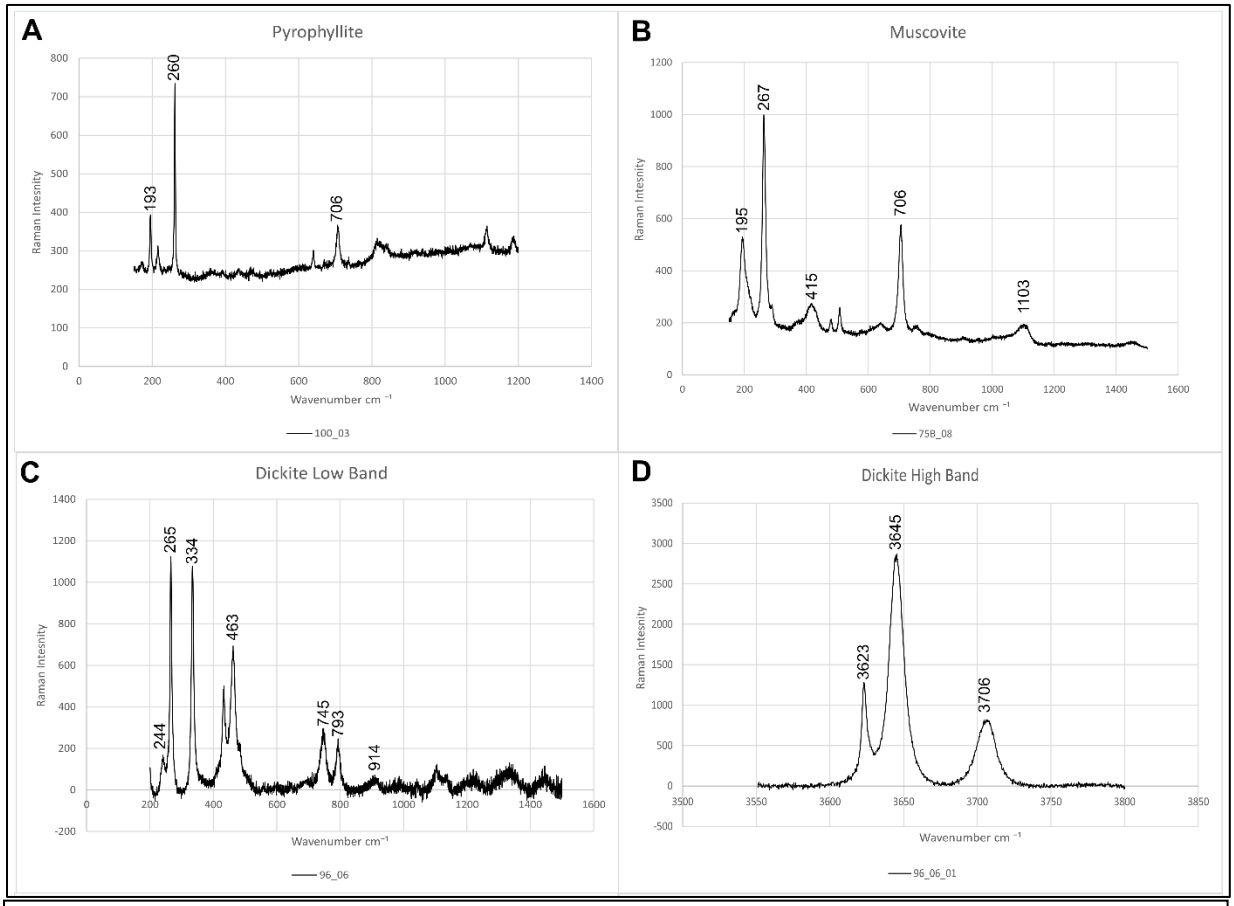

Figure 13: Raman spectra of select samples associated with intense hydrothermal alteration. Panel A shows a pyrophyllite spectra, Panel B shows a muscovite spectra, panels C-F display the high (3500-3800 cm^{-1}) and low band (200-1400 cm^{-1}) features of a dickite samples. All labels indicate characteristic peak positions.

Table 1: EDS Analysis

Spectrum	O	Na	Mg	Al	Si	S	K	Mineral ID
SPC097_ 10	54.6	1.6		21.0		16.5	6.3	Alunite
SPC097_ 12	55.1	1.9		21.2		16.0	5.4	Alunite
SPC097_ 14	54.5	0.9		19.2		16.9	8.5	Alunite
SPC097_ 5	56.8	3.1		20.6		15.7	3.7	Alunite
SPC097_ 6	54.8	0.7		19.8		15.5	9.2	Alunite
SPC097_ 8	54.2	1.4		21.2		16.9	6.3	Alunite
SPC097_ 9	55.6	3.2		20.9	1.4	15.6	3.3	Alunite
SPC096_ 1	56.4			21.0	22.6			Dickite/Kaolinite
SPC096_ 2	55.8			22.1	22.1			Dickite/Kaolinite
SPC097_ 1	56.4			21.4	22.2			Dickite/Kaolinite
SPC097_ 11	55.1			21.8	23.1			Dickite/Kaolinite
SPC097_ 2	56.7			21.4	22.0			Dickite/Kaolinite
SPC097_ 3	57.0			21.1	21.9			Dickite/Kaolinite
SPC097_ 4	56.7			21.2	22.1			Dickite/Kaolinite
SPC097_ 7	55.3			21.5	23.2			Dickite/Kaolinite
SPC100_ 2	54.3			19.9	25.8			Dickite/Kaolinite
SPC100_ 4	55.4			21.2	23.4			Dickite/Kaolinite
SPC100_ 6	55.9			21.0	23.1			Dickite/Kaolinite
SPC100_ 8	55.9			21.3	22.8			Dickite/Kaolinite
SPC101B_ 3	56.4			21.2	22.4			Dickite/Kaolinite
SPC101B_ 5	56.1			21.3	22.5			Dickite/Kaolinite
SPC101B_ 8	56.1			19.6	24.3			Dickite/Kaolinite
SPC101B_ 1	49.2	0.3	0.2	18.9	25.1		6.3	Muscovite
SPC101B_ 4	49.1	0.5		19.7	24.5		6.2	Muscovite
SPC101B_ 6	49.6		0.7	18.7	24.6		6.4	Muscovite
SPC100_ 1	51.4			16.4	32.2			Pyrophyllite
SPC100_ 3	51.3			16.0	32.7			Pyrophyllite
SPC100_ 5	51.6			15.9	32.5			Pyrophyllite
SPC100_ 9	51.5			16.2	32.3			Pyrophyllite
SPC096_ 3	52.6				47.4			Quartz
SPC097_ 13	52.3			1.0	46.7			Quartz
SPC100_ 7	51.6			1.4	47.0			Quartz
SPC101B_ 7	52.4			1.4	45.7		0.4	Quartz

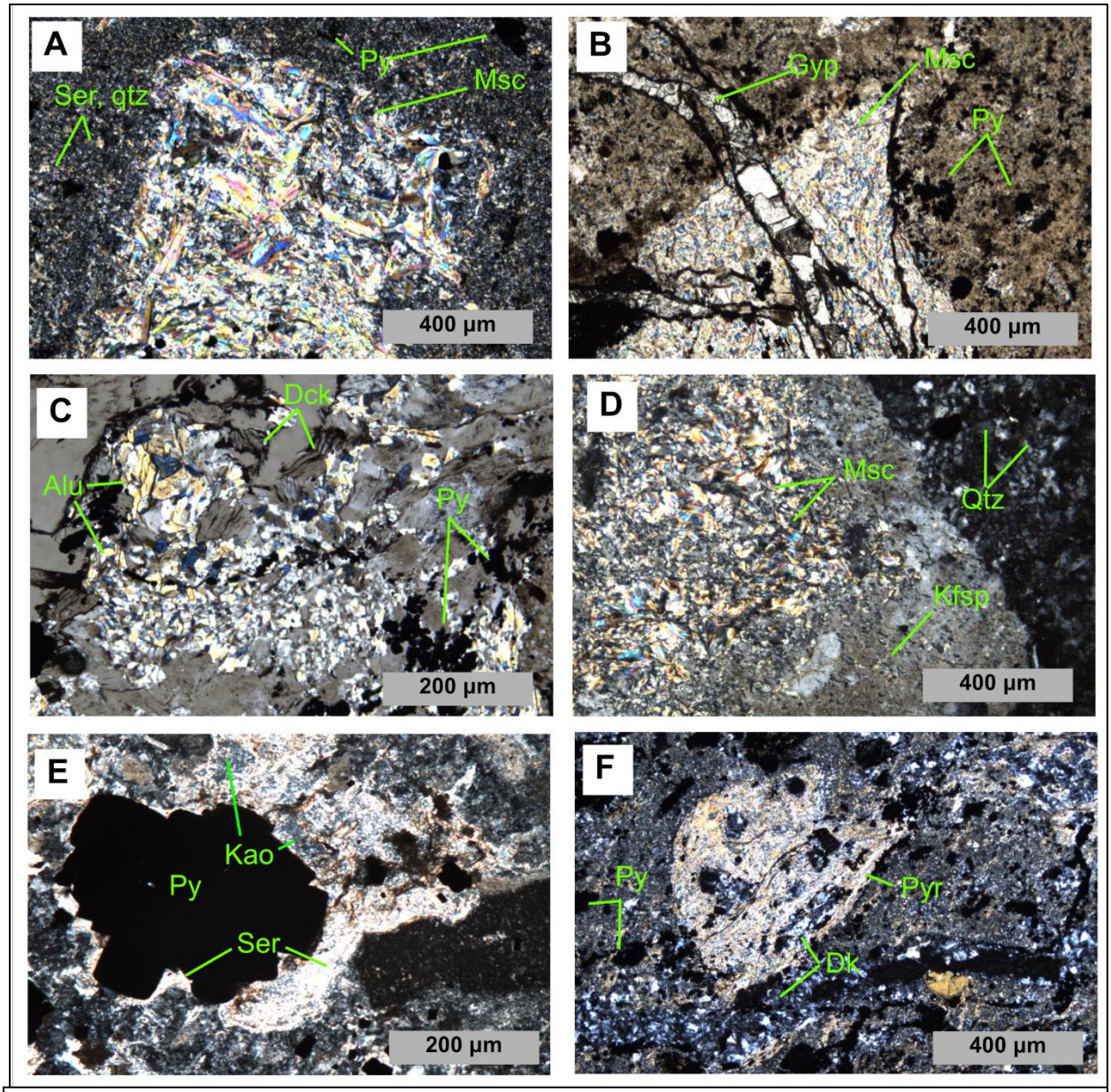

Figure 14: Petrographic thin sections with A-B) a muscovite altered phenocryst crosscut by a late sulfate (Gyp) vein, C) complete replacement of the host rock to a dickite(Dck)-alunite(Alu)-pyrite(Py) assemblage D) illustrating a K-felspar phenocryst partially altered to muscovite suspended in a highly silicified groundmass, E) kaolinite(Kao)-sericite(Ser) alteration occurring on the rims of a pyrite grain F) a feldspar grain altered to pyrophyllite(Pyr), with late stage dickite (Dck)

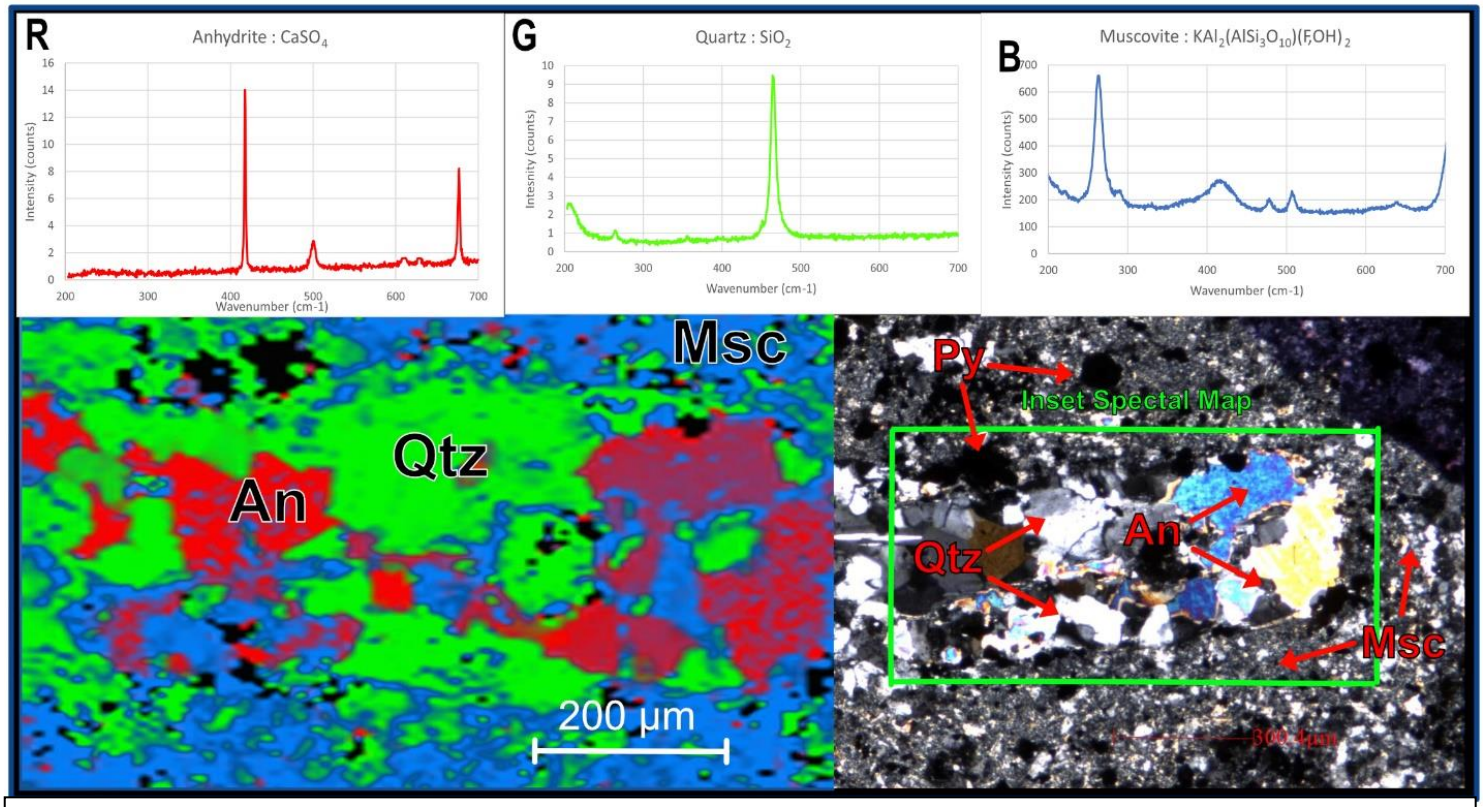

Figure 15: Multidimensional spectral array displaying a feldspar pseudomorph suspended in a groundmass composed of muscovite (Msc) altered feldspars, finely disseminated pyrite (py) and minor quartz (Qtz), with the pseudomorph being infilled by late-stage anhydrite and quartz fluid pulses. The pyrite phase was included in the CLS fitting, but is identifiable as the anisotropic phase in the cross polarized image on the bottom right, and as the black pixels in the spectral grid. Note that this processing method assigns all pixels to one of the loadings selected for statistical analyses.

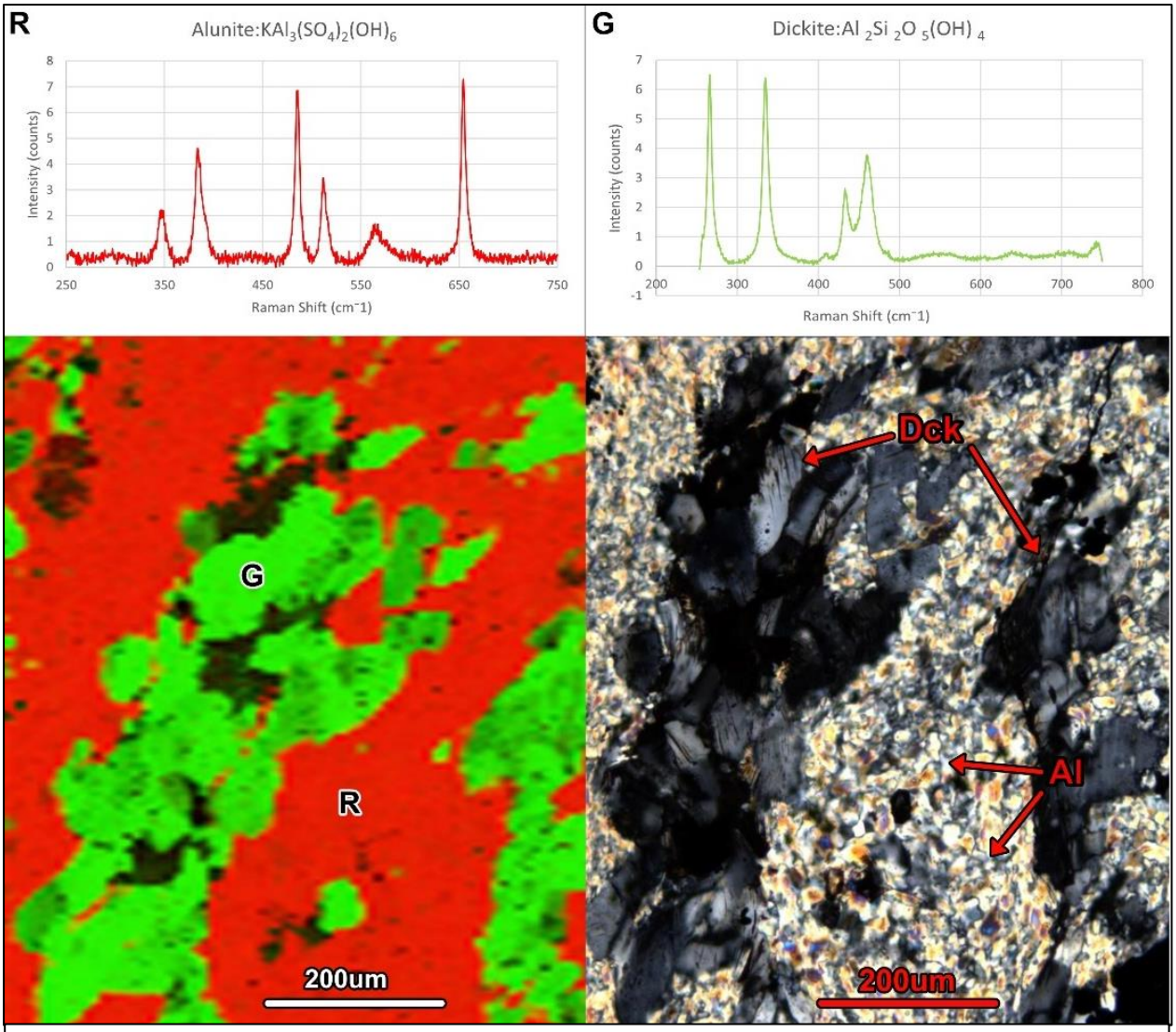

Figure 16: Multidimensional spectral array exhibiting complete host rock replacement with no relict host rock textures. Replacement mineralogy includes dickite (Dck) and Alunite (Al). Note that this processing method assigns all pixels to one of the loadings selected for statistical analyses.

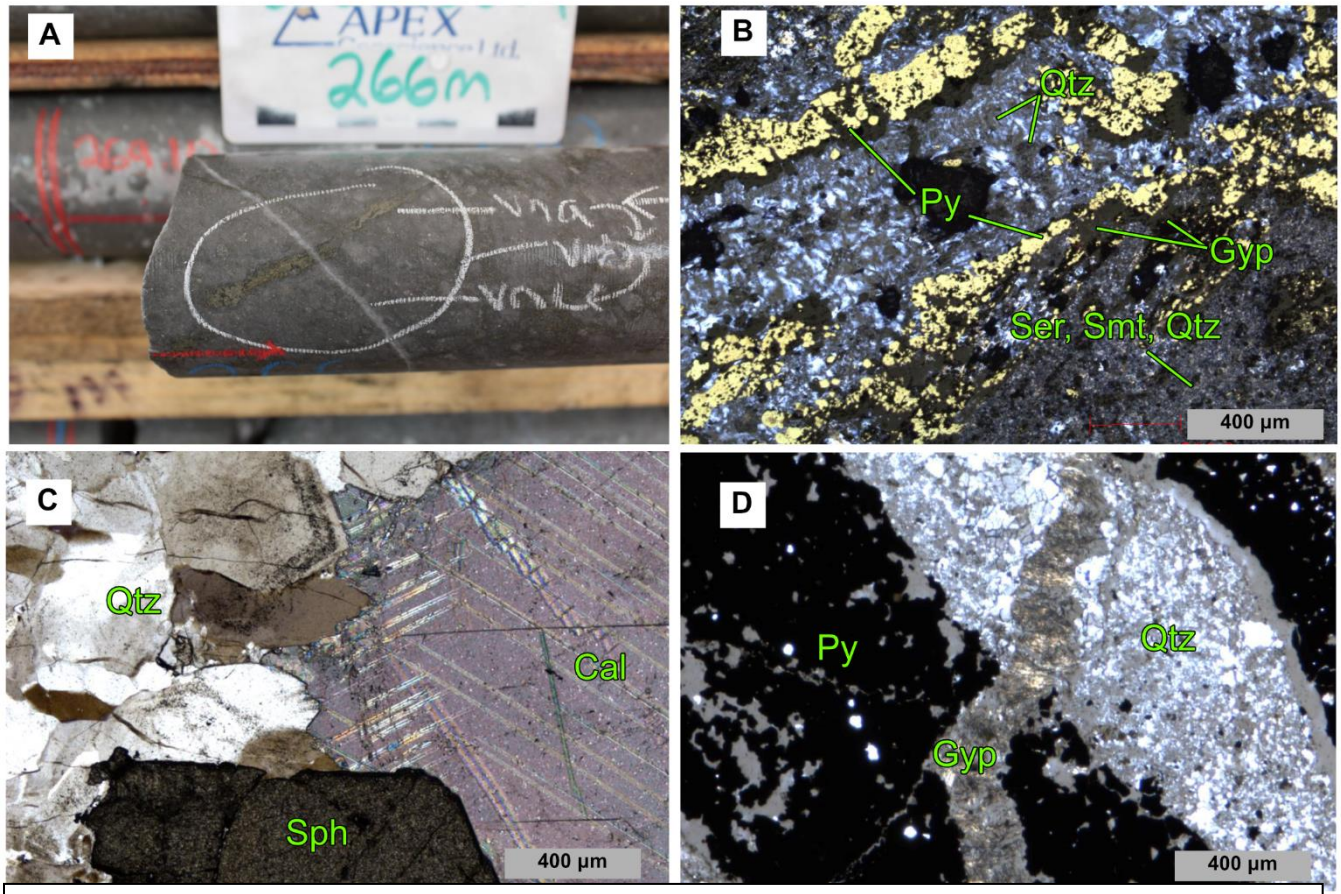

Figure 17: Veining paragenesis as seen in drill core and thin section A) late gypsum vein crosscutting earlier pyrite phase within argillic altered host rock, B) quartz (Qtz) vein within a sericite (Ser), smectite (Smt), quartz (Qtz) bearing groundmass, crosscut by late stage pyrite and gypsum veining taken in cross polarized(XPL) and reflected light (RL), C) a sphalerite (Sph) grain with a second stage quartz vein, and a third stage calcite (Cal) vein in XPL and D) Earlier generations of pyrite (Py) and quartz(Qtz) crosscut by gypsum (Gyp) in XPL.

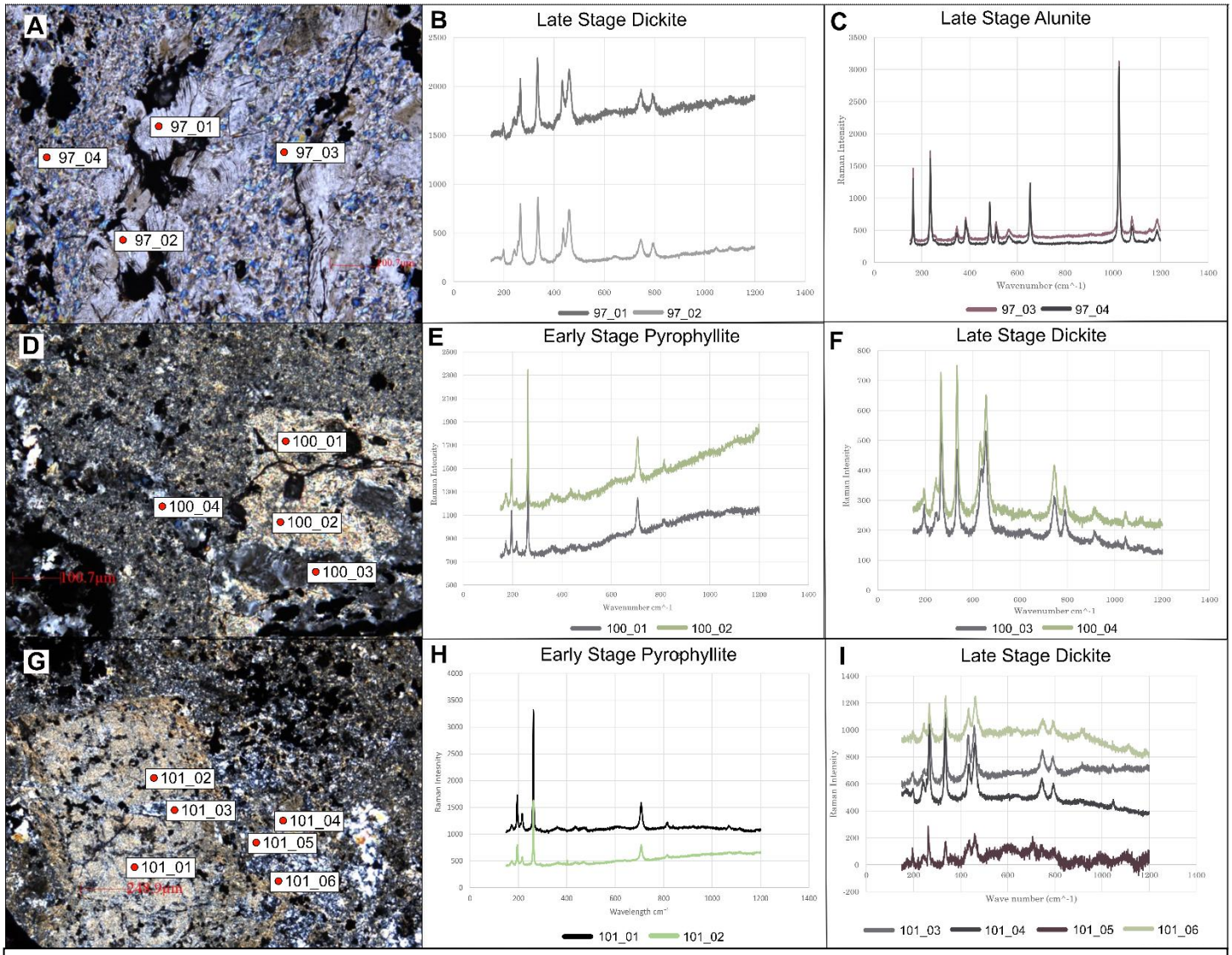

Figure 18: Thin section photomicrographs with Raman point analyses identified. A-C) Host rock completely replaced alunite and porosity filled by late stage dickite and sulfides, D-I) igneous feldspar phenocrysts altered to pyrophyllite and crosscut by a late stage dickite phases. All thin sections images in XPL

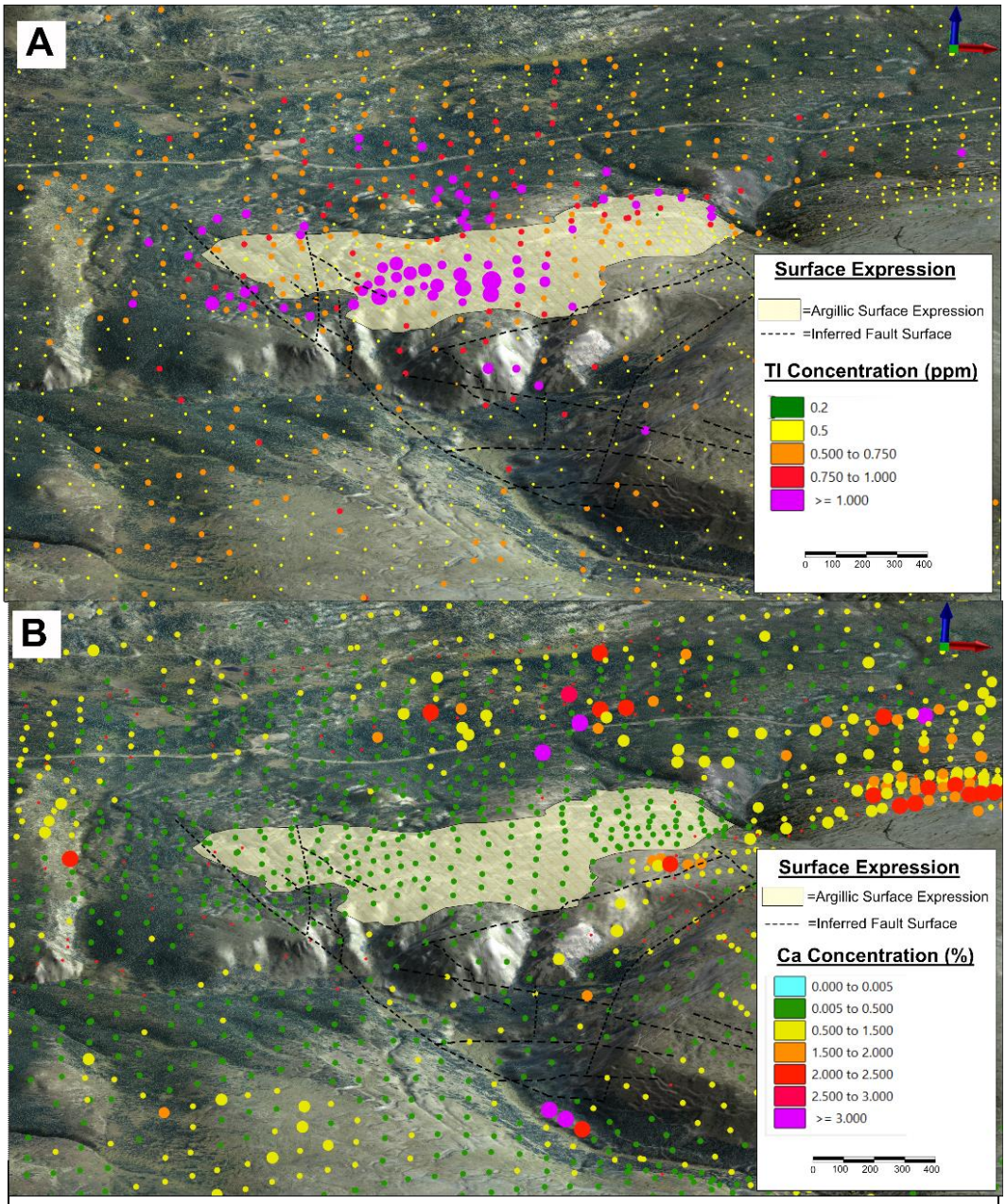

Figure 19: Orthogonal view of the Silver Pond argillic surface expression (outlined in beige) and faults. A. Relative concentrations of Tl are indicated using a colour scheme and a corresponding symbol size. B. Relative concentrations of Ca are indicated using a colour scheme and a corresponding symbol size.

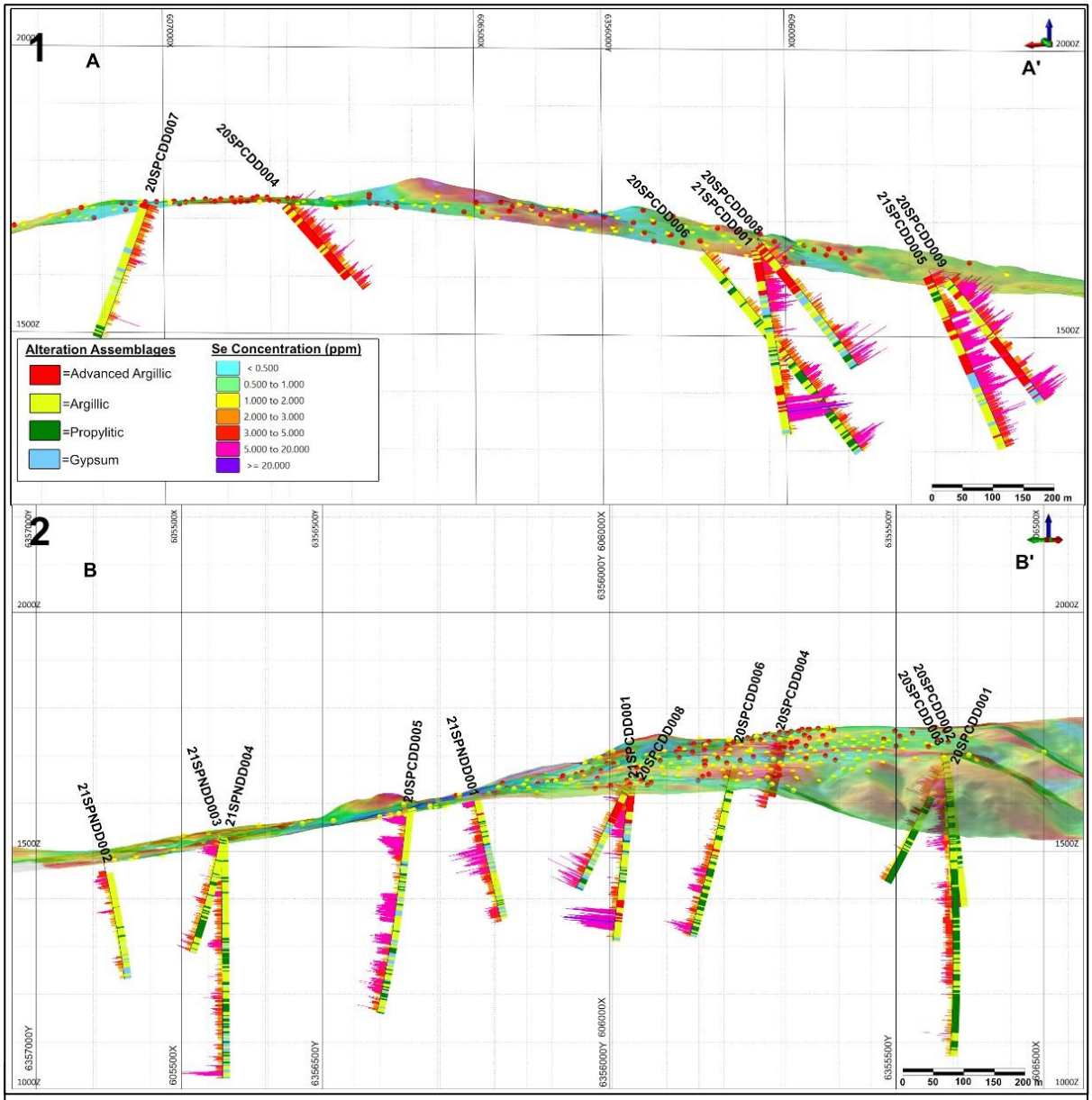

Figure 20: 1) Cross-section A–A' (from Figure 3) showing relative concentration of Se and dominant alteration assemblage. 2**)** Cross-section B–B' (from Figure 3) showing relative concentration of Se and dominant alteration assemblage.

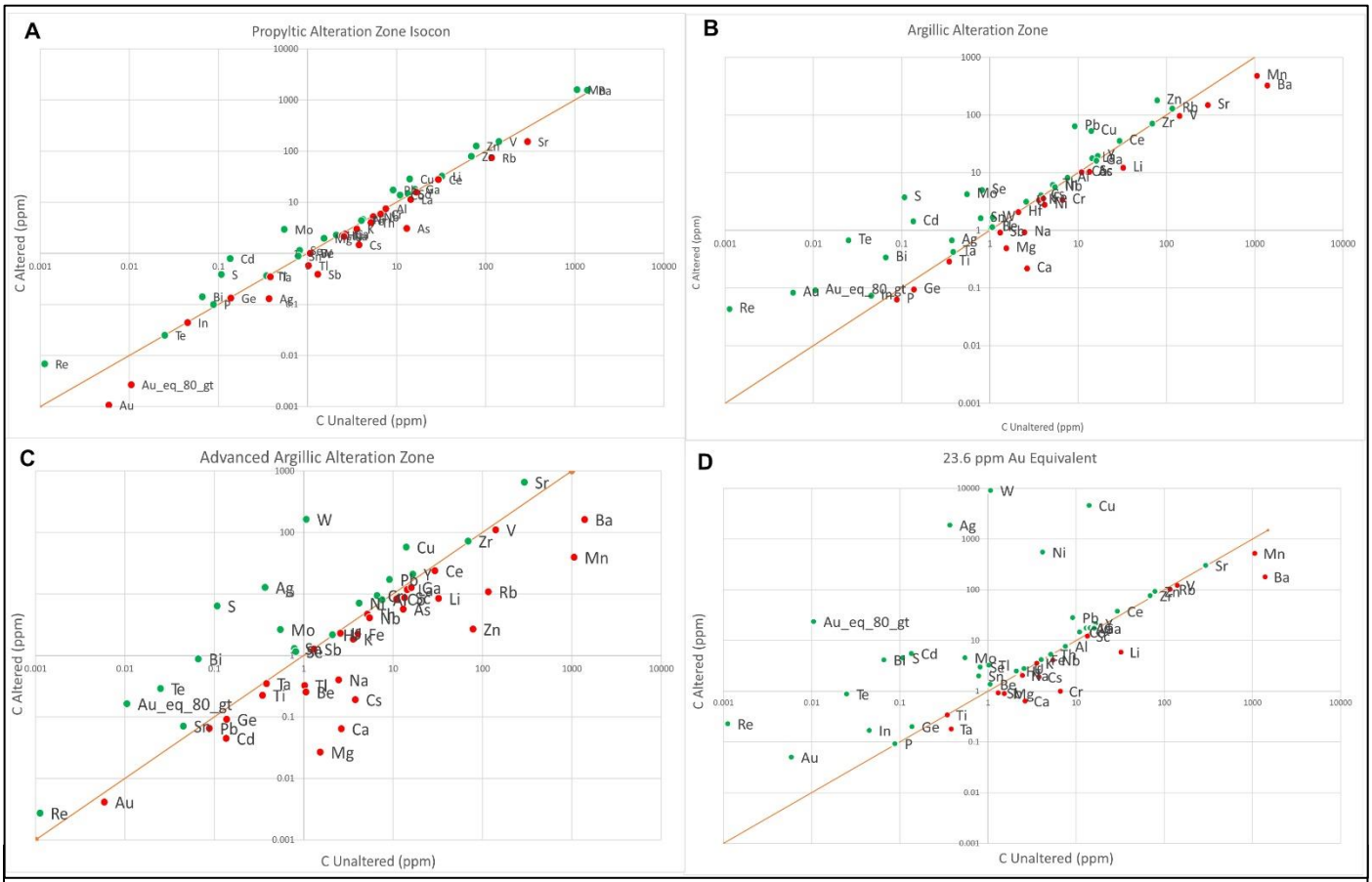

Figure 21. Isocon plots showing elemental relationships of alteration assemblages and mineralized zones plotted against reference unaltered hostrock, where C altered (vertical axis) represents the concentration of each assayed element in the altered/mineralized hostrock, and C unaltered (horizontal axis) represents the concentration of each assayed element in the unaltered hostrock. Elements that experienced no net loss or gain lay on the line with a slope of 1, with enriched elements having a value greater than one and depleted elements having a value of less than one, and immobile elements generally staying on the line regardless of the influence of alteration events. **a)** Isocon plot of the propylitic alteration zones shows minimal enrichment/depletion due to the occurrence of dominantly lower temperature hydration reactions (i.e., chlorite, epidote). **b)** Isocon plot of representative advanced argillic-alteration shows a high degree of enrichment in epithermal suite elements (i.e., W, S, Ag, Se, Mo) and major depletion in rock-forming elements (i.e., Mg, Ca, Na). **c)** Isocon plot of elemental distribution in a 1 m drillcore interval (drillholes 20SPCDD005, 20SPCDD008 and 20SPCDD009) with 23.6 ppmAu equivalent and **d)** Isocon plot of elemental distribution in 1 m drillcore interval (drillholes 20SPCDD005, 20SPCDD008 and 20SPCDD009) with 3.05 ppm Au equivalent. The isocon plots of mineralized sections indicate a similar geochemical signature as the advanced argillic-alteration zones, indicating the identified enrichment trends can be used for targeting mineralization. Drillhole locations shown on Figure 3. Abbreviation: gt, grams per tonne.

Discussion:

5.1 Mineralogy and conditions of formation

Mineral associations and mineral chemistry can be indicators of genetic environments. Kaolinite polymorphs provide information on the temperature and pH conditions of formation. The isochemical transition from kaolinite (low temperature phase) to dickite (high temperature phase) occurs at ~200 ºC (Reyes., 1990). As a result, kaolinite occurs in a broad range of environmental conditions, ranging from weathering at low temperature surface conditions to higher temperature conditions present in hydrothermal-magmatic systems. Dickite, in contrast, is more commonly associated with higher temperature, lower pH conditions present exclusively in hydrothermal-magmatic systems. SWIR and Raman analysis in this study indicate that dickite is largely associated with the highest intensity alteration zones, while kaolinite species occur dominantly in the surficial zones as well as in the lower temperature illite/smectite assemblages.

The presence and composition of alunite is also dependent on conditions of formation. Modeling studies indicate that aluminum rich minerals (pyrophyllite, diaspore, and locally andalusite) are stable at high temperatures at depth and, in a gradually lower-temperature shallow-regime, Na and K alunite become stable (Hedenquist & Taran., 2013). As a result, alunite occurs associated with 1) fumarolic steam heated settings where it is associated with kaolinite and interlayed illite-smectite occurring in a 100-160 C temperature range, as well as in 2) hypogene hydrothermal-magmatic conditions occurring with diaspore, pyrophyllite, kaolinite, dickite and zunyite within acidic conditions and a temperature range of 200-350 ºC (Arribas, 1995). Experimental data suggest that more sodic alunite is favored in higher temperature conditions (Deyell and Dipple, 2004), thus the identification of alunite versus natroalunite further helps constrain temperature conditions present in the alteration system in question. The alunite at Silver Pond as indicated by the shift in the 1480 SWIR absorption feature (Chang et al., 2011) has intermediate composition suggesting moderate temperature ranges. Alunite at Silver Pond, however, commonly occurs in conjunction with higher temperature minerals including dickite and rarely pyrophyllite. The occurrence of minerals that form in significantly different conditions in the same samples suggest either extreme geothermal gradients or overprinting events whose paragenetic relationships remains unclear.

5.2 Spatial distribution of mineral associations

Mineral assemblages provide more comprehensive information on genetic environments. Five end member environments can result in advanced argillic alteration (Arribas and Hendequist, 2022) including low temperature oxidation of pyrite, steam heated (CO_2 and H_2S type), hypogene condensate, and high temperature white mica-pyrophyllite transition zone typical to porphyry transitional environments (which commonly occurs at the base of lithocaps). The mineral assemblages at Silver Pond underline the presence of multiple advanced argillic environments that evolved in space and time. All advanced argillic alteration assemblages are located in a relatively shallow, EW fault-bounded block that displays the highest abundance of predominantly muscovitic white micas (low 2200 nm feature) and pyrophyllite, and a systematic increase in kaolinite and white mica crystallinity with depth and/or proximity to fault structures indicative of decreasing pH and increasing temperature (280–400°C) regimes (Monier and Robert, 1986; Cohen, 2011). The first advanced argillic assemblage identified consists of either (1) large alunite-kaolinite-dickite haloes with isolated sections of pyrophyllite in intervals that display the highest degree of texturally destructive alteration, intense leaching of the host rock, and likely represent feeder zones or (2) narrow fault-related occurrences of residual silica, pyrite, fine grained alunite-pyrophyllite rich zones with a white mica association (typically K-rich, muscovite). This style of advanced argillic alteration resembles the white mica-pyrophyllite zone characteristic of the base of lithocap zones. The muscovite to pyrophyllite transition (~350 ºC, Hemley et al., 1980; Watanbe and Hedenquist, 2001) as described at Silver Pond represents the deepest, highest temperature advanced argillic alteration type and likely has a direct association with magmatic fluids exsolved from underlying intrusions commonly at the top of porphyry systems and/or at the base of lithocaps (Sillitoe, 1994).

In contrast to the pyrophyllite-bearing advanced argillic alteration, the second style of advanced argillic alteration occurs in a broader scale E-W elongated alteration zone consisting of dickite ±kaolinite and sulfates that occur both as replacements and cements spatially associated with pyrite, residual silica, and lesser alunite. The mineralogy of this zone resembles hypogene, acid-sulfate conditions which form as a result of the disproportionation of high temperature magmatic vapors such as HCl and SO_2 to H_2SO_4 and H2S, and typically occurs in a 200-300ºC range, with a pH range as low as <pH 1 (Arribas & Hedenquist., 2022; Arribas., 1995; Giggenbach., 1997). Hypogene assemblages are known to occur in the shallow portions (~150-400 m) of intrusions

within the epithermal environment (Arribas & Hedenquist., 2022; Sillitoe., 1999; Steven and Ratté., 1960).

A final stage of advanced argillic alteration broadly represents shallow (~0-50m), late stage, low temperature (<40 ºC) supergene style alteration that occurs as a result of the oxidation of pyrite from exposure to atmospheric oxygen within highly sulphidized zones. This zone occurs in isolated sections and is characterized by the presence of iron-oxides, kaolinite, and pyrite. Surface waters measured at Silver Pond reported pH readings as low as ~2, indicating the ongoing process of supergene style weathering and alteration in the modern-day environment.

The fault bound advanced argillic zone is in sharp structural contract with broad dominantly illite-smectite± chlorite alteration assemblages to the north and south, which are zonation patterns characteristic of intermediate to high sulphidation deposits as classified by John et al. (2018). These illite-smectite assemblages are associated with white micas of more phengitic composition with depth and distance to likely feeder zones. While the identification of illite-smectite through SWIR is not conclusive, the absence of high-temperature minerals (i.e.. dickite, pyrophyllite) and the presence of phengite is indicative of a likely change to an argillic alteration environment. This broad argillic halo likely occurred as the host rock buffered hydrothermal magmatic fluids, resulting in gradually lower temperature and neutral pH assemblages.

In the north and south structural blocks argillic alteration transitions to propylitic assemblages with depth. The chlorites at Silver Pond have Mg-dominant compositions. The magnesium content of chlorites in other mineral deposits increases with proximity to high temperature centers (Neal et al.,2018; Feng et al., 2019), where they have been used as a vectoring tool. The lack of systematic trends in magnesium chlorite contents at Silver Pond and the abundance of chlorite in the Hazelton volcanics regionally suggests that not all the chlorites in the host rock are of hydrothermal origin and chlorite chemistry systematics at Silver Pond may be difficult to interpret as a proxy for hydrothermal fluid pathways.

5.3 Controls on fluid flow and implications for exploration

The Silver Pond prospect area has been previously described as a lithocap defined by a high degree of clay alteration caused by a downfaulted acid sulfate outflow (Diakow et al., 1991). The highest degree of texturally destructive alteration identified in this study are associated with structural

feeder zones and correspond to samples altered to alunite-kaolinite-dickite haloes and isolated sections of pyrophyllite. These narrow advanced argillic alteration zones are bounded by a broad muscovite (±illite±smectite) alteration assemblage characteristic of intermediate to high sulphidation deposits (John et al., 2018; Arribas, 1995). To date, exploration efforts at Silver Pond have intersected the main alteration envelopes associated with high sulfidation systems (i.e., sericite-pyrophyllite, quartz-dickite/kaolinite, quartz-alunite, illite-smectite) but not a zone of residual quartz, which typically hosts Au-Ag mineralization in analogous deposits. Advanced argillic-alteration assemblages commonly cap porphyry copper systems (Sillitoe, 1973). The Silver Pond zone likely represents the surface expression of a hydrothermal-magmatic system derived from the intrusion of the Black Lake Intrusive Suite. The elevated base-metal associations elsewhere in the Toodoggone district including at Baker, Sofia, Black Gossan (Bouzari et al 2019), and at depth in isolated sections of Cliff Creek and AGB are indicative of deep hydrothermal system(s) associated with shallower mineralization and alteration domains. The relatively small footprint of the argillic leach cap at Silver Pond possibly signifies that it represents a shoulder zone of the main circulation conduit, and/or post alteration tectonism resulted in the displacement of the structural bloc that contained the main surface extent of the lithocap.

The largest degree of depletion in rock forming elements and enrichment in epithermal-suite elements corresponds to texturally destructive advanced argillic alteration. Texturally destructive advanced argillic alteration and its association with epithermal suite elements is focused in zones proximal to faulting suggesting a structural control on fluid flow. The compositional ratios of epithermal elements in these fault zones as represented by the MDRU porphyry index are comparable to geochemical signatures in other systems proximal porphyry signatures within the Toodoggone District. The link between the enrichment of individual elements associated with porphyry centers such as W and Sn and high temperature mineralogy assemblages occurring along major fault surfaces, suggests that the Silver Pond experienced conditions that occur in close spatial association with a porphyry style environment.

The distinct mineralogical and geochemical features of Silver Pond, as well as mapped and logged fault structures indicate that the larger domain represents a fault bound wedge, which is consistent with the horst-grabben geometry observed elsewhere in the broader Toodoggone volcano-tectonic depression. The fault surfaces that confine the Silver Pond structural wedge and serve as a primary

conduit for hydrothermal magmatic fluids have a similar orientation as the main north-northwest-trending regional high angle fault system that served as a key control for mineralization in the adjacent low sulphidation–style deposits in the property, as well as elsewhere in the Toodoggone District including the high sulfidation deposits of the Ranch Property located directly north of the Lawyers property. These regional fault structures are broadly responsible for the development of graben and half graben geometries that define the main structural domains on the Lawyers Property. Fault blocks within known extensional regimes typically exhibit normal faulting which conceptually lends itself to the possible downfaulting of the earlier magmatic products and potential mineralized zones of Silver Pond within a graben structure. At the low sulfidation prospects, faults associated with mineralization commonly have multiple generations of reactivation. Given the similar fault regime and structures present at Silver Pond, fault displacement and truncation of mineralized zones coincident with earlier generations of faulting could be possible. Although the direction and extent of fault displacement was not determined due to a lack of kinematic indicators, it likely played a role in the preservation of the Silver Pond alteration zones.

The identification of key indicator minerals (i.e quartz-pyrophyllite-alunite-muscovite) coupled with diagnostic geochemical associations with direct hydrothermal-magmatic implications at the Silver Pond prospect expands the area within the Toodoggone District with demonstrable porphyry linkages. The similarities between Silver Pond and other prospects within the Toodoggone District with shallow porphyry expressions such as Brenda and Alunite Ridge to the east, and the Mets and Bonanza to the north, underlines a regional scale trend of clustered porphyry systems within a relatively narrow geographic area. To date, the porphyry deposits discovered (i.e Sofia, Pine, Kemess) lie on the eastern extent of the Toodoggone District. The lithocap environments at Ranch (Mets, Bonanza, Thesis) and Lawyers (Silver Pond), as well as the high temperature porphyry style K-silicate alteration present at Baker, suggests porphyry style conditions throughout a broader extent of the western portion of the district, underlining the likelihood of undiscovered porphyry deposits occurring elsewhere in the district.

The distribution of alteration mineralogy is interpreted as occurring in four major stages (Figures 22-26). The first stage is likely linked to the onset of hydrothermal-magmatism driven by the emplacement of the Black Lake Intrusive suite, with magmatic fluids being derived from

crystallization and devolatilization processes of the underlying plutons. Broad scale, synvolcanic faulting provided the fluid conduits that were exploited by the magmatic fluids into the overlying volcanic stratigraphy of the Toodoggone Formation. Upon ascent, fluids went from equilibrium with K-rich white mica to equilibrium with pyrophyllite-dickite during cooling and sulfur disproportionation. The central advanced argillic assemblage transitioned to a broad scale argillic zone as the magmatic fluids were buffered by the surrounding volcanic host rock. Porosity infill with quartz and sulfates indicates a later stage of fluids responsible for cement precipitation. Interaction of a later magmatic fluid with meteoric water at the paleowater level may have caused the precipitation of these cements. If that is the case, this overprinting relationship maybe indicative of telescoping process common to volcanic plutonic arcs, in which shallow epithermal style alteration assemblages overprint earlier assemblages associated with porphyry, and porphyry transition type environments (Sillitoe., 1994). Displacement along the fault conduits at least in part postdates hydrothermal alteration and caused the central block of Silver Pond to be structurally displaced with respect to the surrounding blocks and possibly to be partially eroded. Following the cessation of magmatism in the Toodoggone District and a depositional hiatus in the Middle to Upper Jurassic, a thick package of Cretaceous sediments was deposited forming a large regional unconformity of the Sustut Group underlain by the earlier Jurassic magmatic products and preserving the mineralized systems of the Toodoggone District. Late-stage uplift resulted in a return to an erosional regime, with high rates of denudation exposing the alteration domains close to the modern surface. Continued supergene oxidation of highly sulphidized assemblages of host rock expanded the argillic surface expression on the modern surface, resulting in overprinting relationships in the shallow portions of the main alteration domain and lateral expansion of its edges.

Conclusions

Silver Pond represents an environment resembling the surface expression of deep porphyry systems with late-stage overprinting of shallow hypogene and supergene assemblages. Despite the evidence for a high sulfidation epithermal system including favorable stratigraphy, geochemical signatures, textural evidence, and major alteration zones and their associated transitions, a significant mineralized silicic alteration zone that commonly hosts economic mineralization in analogous deposits has yet to be intersected. Further research that would help refine the Silver Pond exploration model would ideally include deeper drilling to evaluate elemental associations, and identification of constraints on structural displacement.

The adjacent high grade, low sulfidation deposits on the Lawyers property and extensive mineralization throughout the Toodoggone District are associated with fault structures and stratigraphy similar to the Silver Pond prospect suggesting a fertile environment for the generation of mineralized systems. In a regional context, the Silver Pond system represents a detailed example of the broad scale potential of the Toodoggone District as a major target for the exploration of porphyry style systems. The presence of porphyry style surface expressions as defined by advanced argillic alteration lithocaps and/or high sulfidation style mineralization at exploration targets throughout the district including Baker, Black Gossan, Brenda, Ranch and Silver Pond underlines multiple centers with hydrothermal-magmatic products, often associated with proven mineralization within the interrelated shallow epithermal regimes. Renewed interest, validated by the results of various active exploration programs throughout the Toodoggone District delivers the necessary momentum that will help develop its full discovery potential and further build upon the growing understanding of the geology of the region.

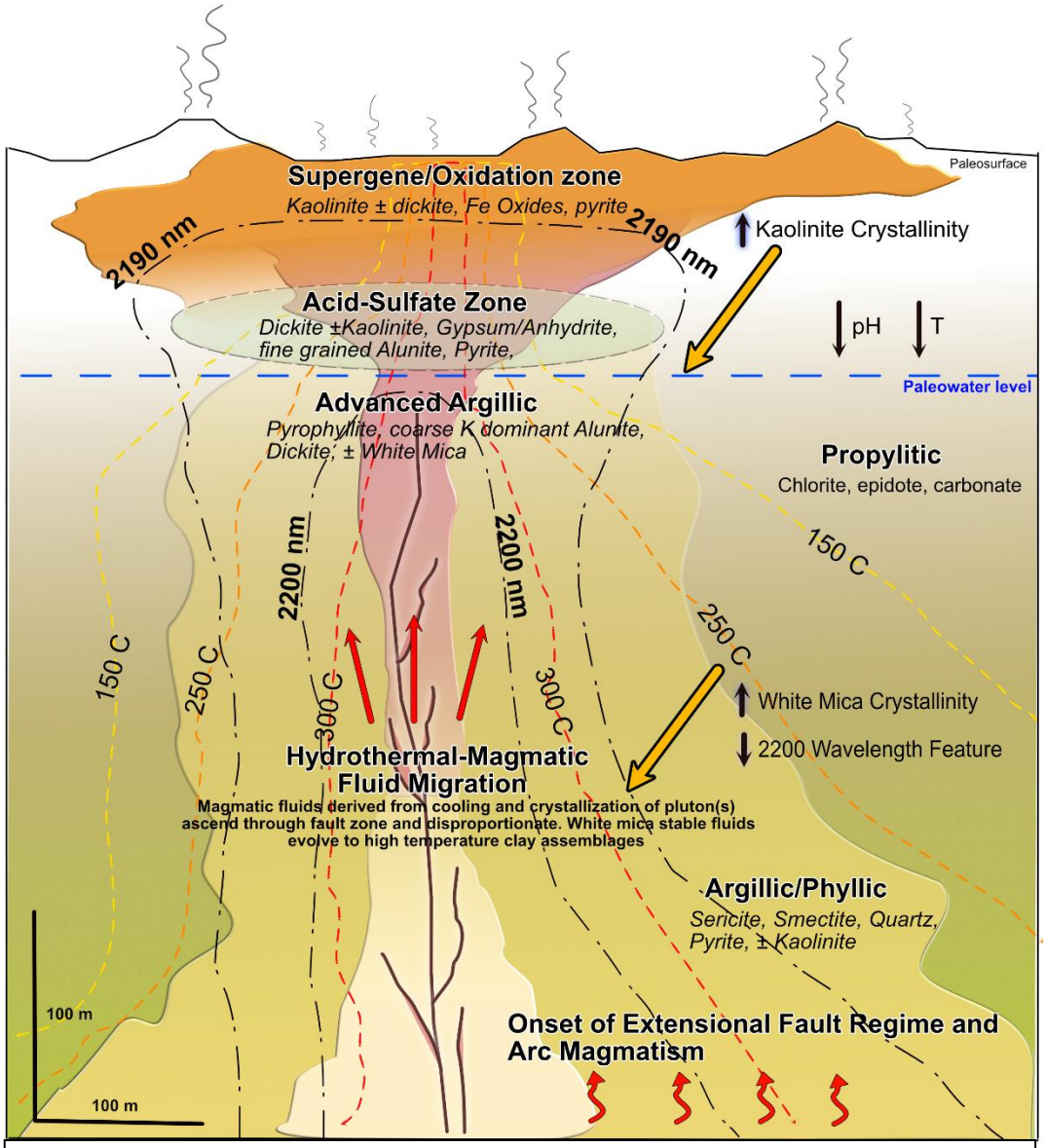

Figure 22: Schematic cross section of proposed T[1] paragenetic sequence, with early-stage extensional faulting and the emplacement and cooling of plutonic suites generating the hydrothermal-magmatic system responsible for the high temperature white mica-pyrophyllite transition environment at depth and moderate temperature, low pH assemblages at surface. The fluid migration pathway and rock buffering relationship is indicated by a transition of high temperature mineralogy at the core zone situated around the fault system to the broader scale argillic zone. The mineralogical transitions and compositional shifts occurring as a function of temperature and pH are supported by 2200 nm (black contour lines) wavelength and crystallinity trends. Temperature isotherms (red, orange, yellow contours) are deduced from mineralogical data.

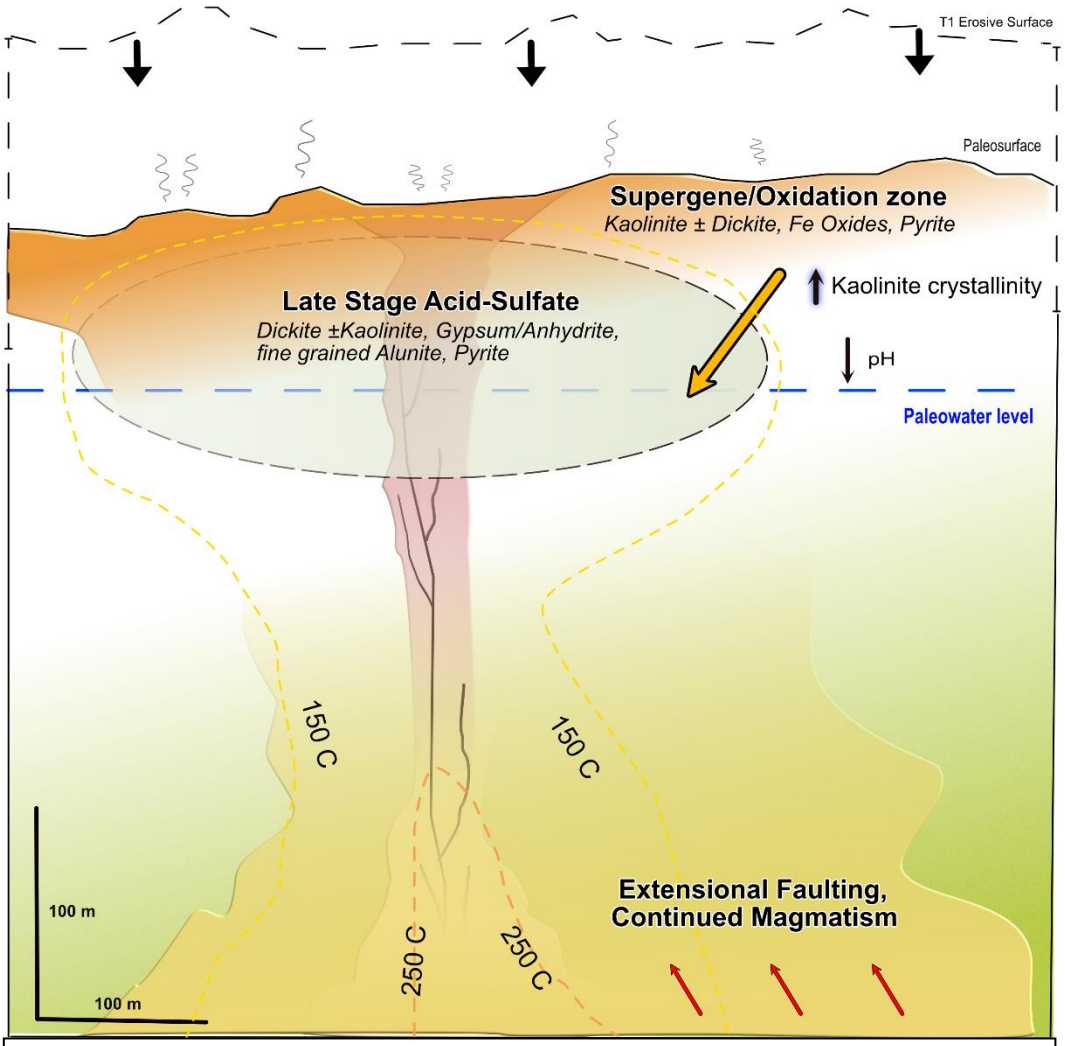

Figure 23: Schematic cross section of proposed T^2 paragenetic sequence, with a post erosion, late stage hypogene style acid-sulfate overprint of the earlier advanced argillic-argillic assemblages associated with the onset of the Silver Pond hydrothermal-magmatic system. This generation of alteration occurs in the shallower portion of the stratigraphy and is dominated by a broad scale laterally oriented alteration assemblage(s) composed of moderate temperature, low pH assemblages (dickite-kaolinite, anhydrite/gypsum, alunite).

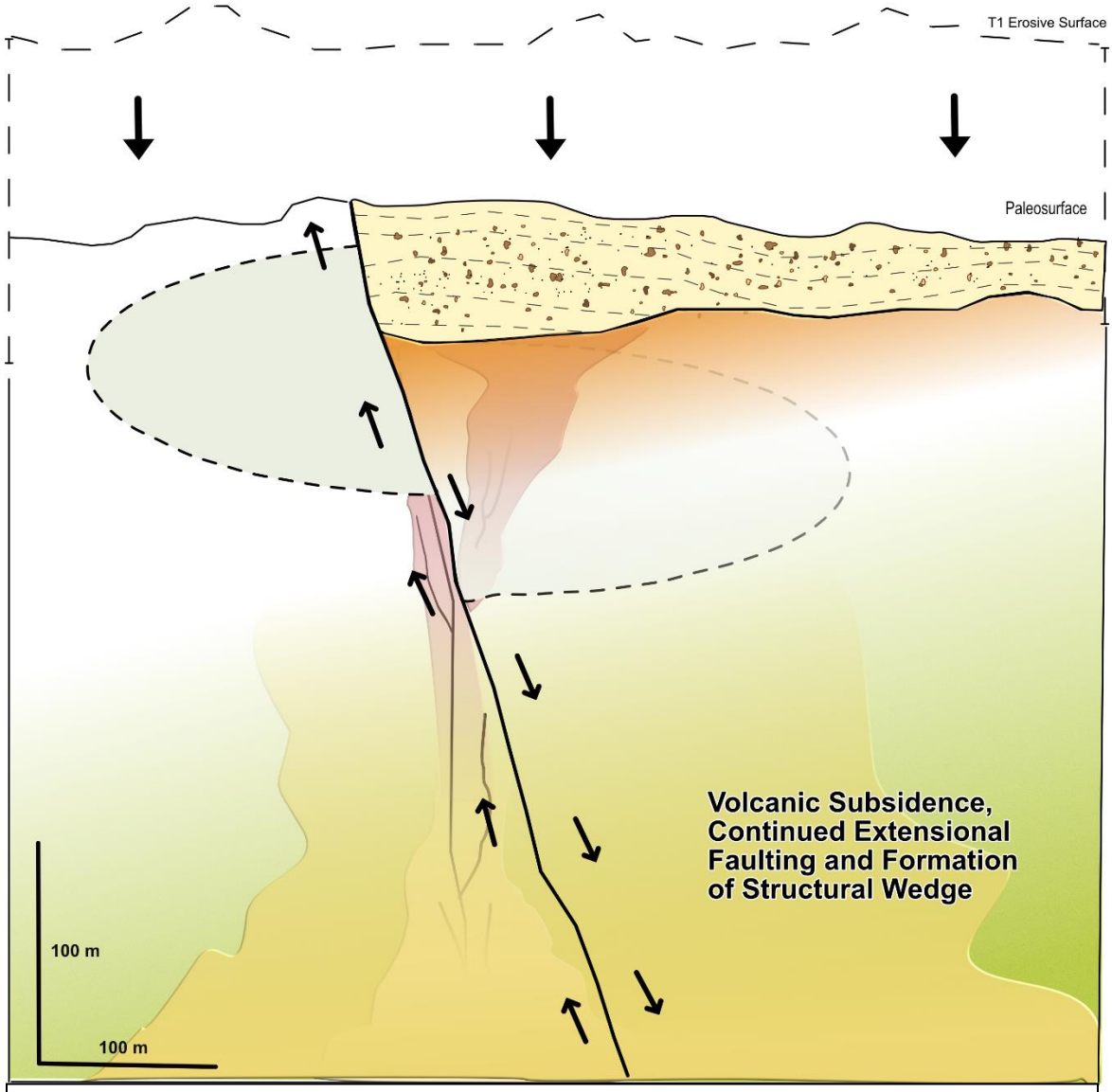

Figure 24: Schematic cross section of proposed structural displacement as part of larger horst-grabben geometry that developed within the extensional fault regime of the Toodoggone volcano-tectonic depression. This major faulting episode is the proposed mechanism of displacement of the described alteration assemblages.

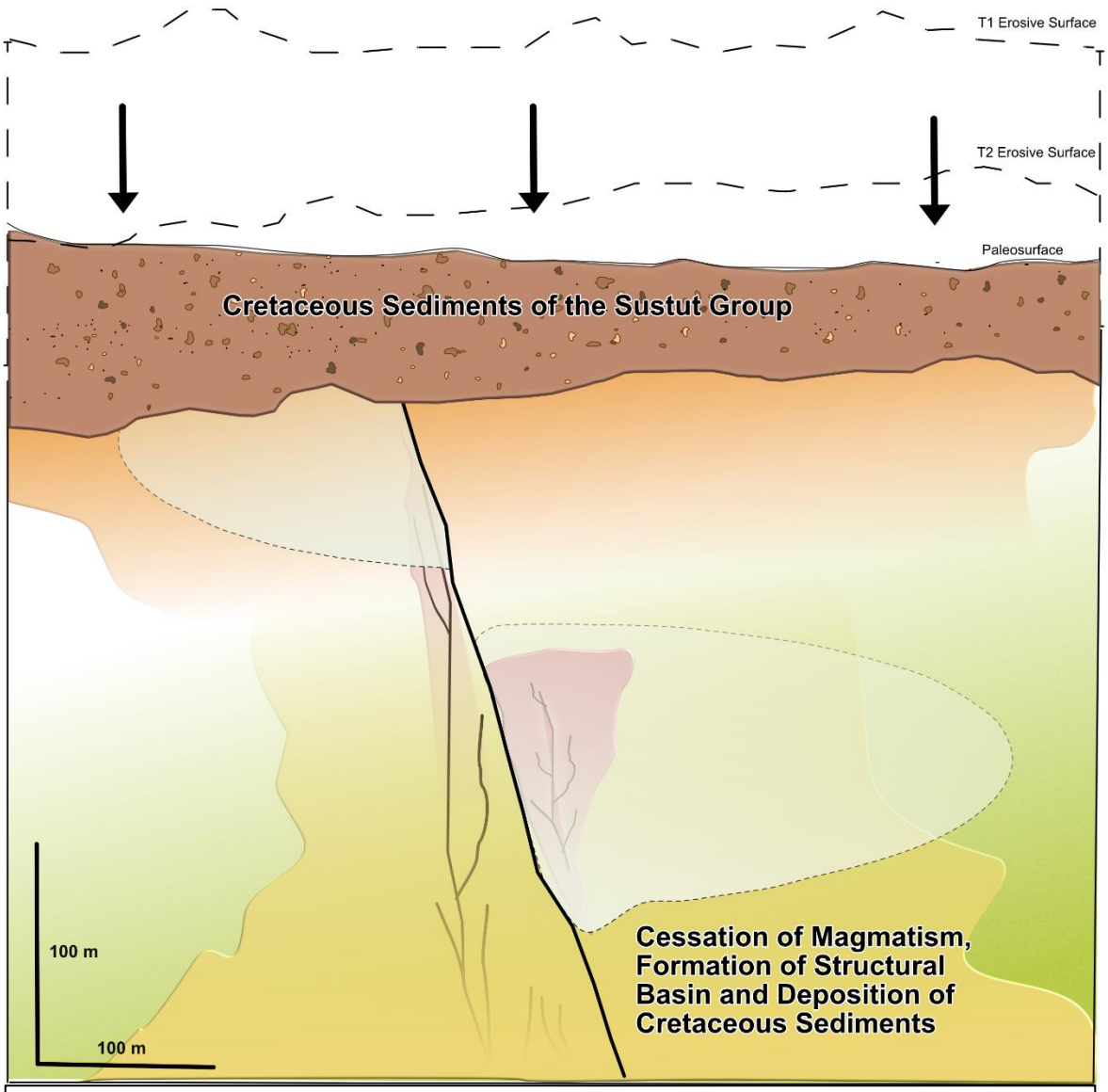

Figure 25: Schematic cross section of proposed T^3 paragenetic sequence which includes the deposition of the sedimentary units of the Cretaceous Sustut Group, which preserved the underlying Jurassic age volcanic-plutonic suites and their associated mineralization.

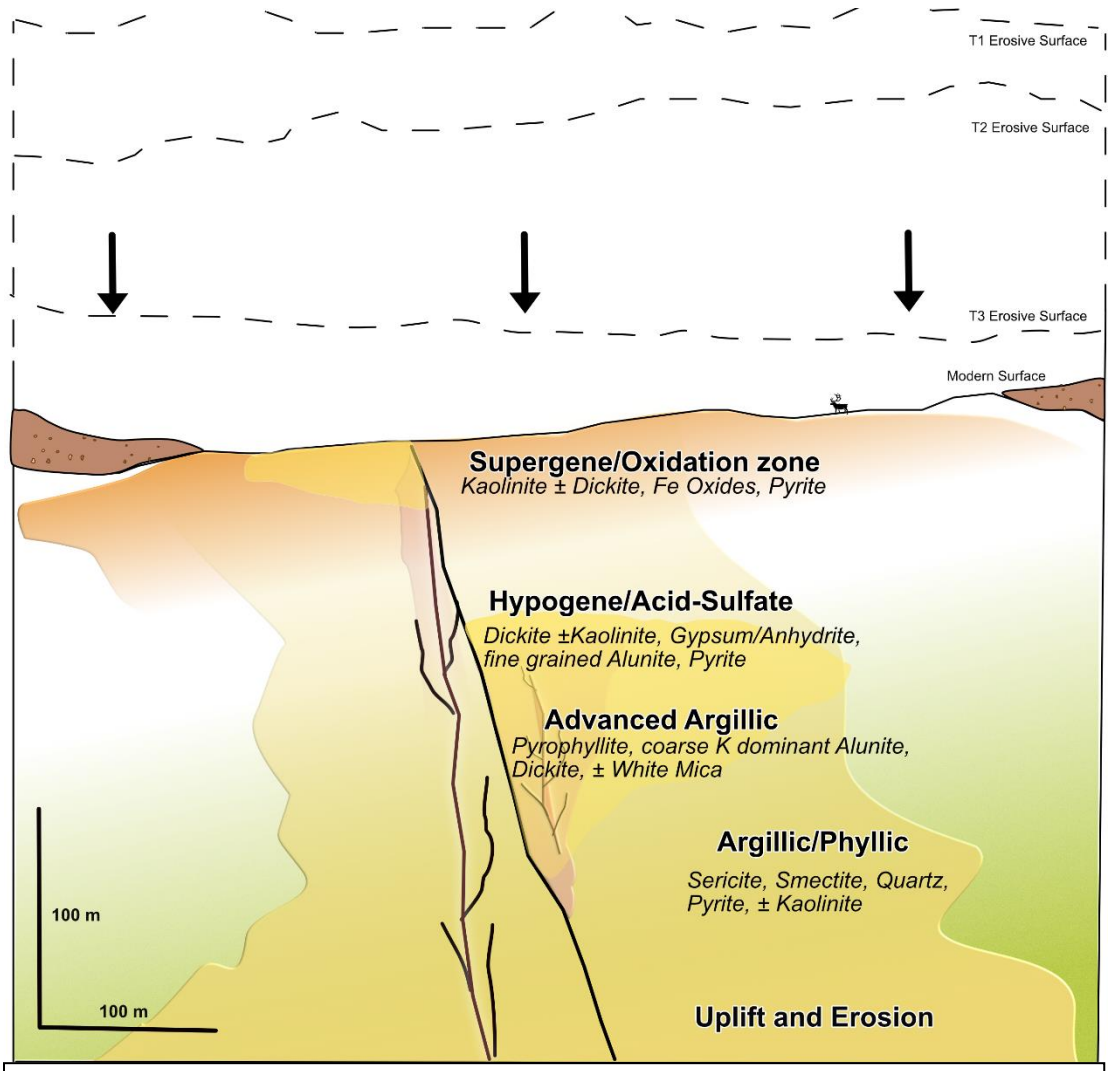

Figure 26: Schematic cross section of proposed T^4 paragenetic sequence in which subsequent tectonic uplift represented a shift to an erosional regime which resulted in the re-exposure of the Toodoggone volcanics as well as the earlier generations of T^1 and T^2 generations at surface and shallow depths within the Silver Pond prospect.

References

Abrams, M., Hook, S., & Ramachandran, B. (2002). ASTER user handbook, version 2. *Jet propulsion laboratory*, *4800*, 135.

Arribas Jr., A. (1995): Characteristics of high-sulfidation epithermal deposits, and their relation to magmatic fluid; Mineralogical Association of Canada, Short Course 23, p. 419–454.

Arbiol, C., & Layne, G. D. (2021). Raman Spectroscopy Coupled with Reflectance Spectroscopy as a Tool for the Characterization of Key Hydrothermal Alteration Minerals in Epithermal Au–Ag Systems: Utility and Implications for Mineral Exploration. *Applied spectroscopy*, *75*(12), 1475-1496.

Benchmark Metals Inc. (2021): Benchmark delivers 2.1 million ounces of 1.62 g/T Au eq indicated and 821,000 ounces of 1.57 g/T Au eq inferred for its initial mineral resource estimate; Benchmark Metals Inc., press release, May 14, 2021, URL <https://www.benchmarkmetals.com/news/news-releases/benchmark-delivers-2-1-million-ounces-of-1-62-g-t-aueq-indicated-and-821000-ounces-of-1-57-g-t-aueq-inferred-for-its-initial-mineral-resource-estimate/> [November 2021].

Bouzari, F., Bissig, T., Hart, C.J.R. and Leal-Meja, H. (2019): An exploration framework for porphyry to epithermal transitions in the Toodoggone mineral district (94E); Geoscience BC, Report 2019-08 and MDRU Publication 424, 101 p., URL <http://www.geosciencebc.com/wp-content/uploads/2019/11/Geoscience-BC-Report-2019-08.pdf> [November 2021].

Buzgar, N., Buzatu, A., & Sanislav, I. V. (2009). The Raman study on certain sulfates. *Analele Stiintifice ale Universitatii Al. I. Cuza*, *55*, 5-23.

Chang, Z., Hedenquist, J. W., White, N. C., Cooke, D. R., Roach, M., Deyell, C. L., ... & Cuison, A. L. (2011). Exploration tools for linked porphyry and epithermal deposits: Example from the Mankayan intrusion-centered Cu-Au district, Luzon, Philippines. *Economic Geology*, *106*(8), 1365-1398.

Clark, J. R., & Williams-Jones, A. E. (1990). 40Ar/39Ar ages of epithermal alteration and volcanic rocks in the Toodoggone Au–Ag district, north-central British Columbia (94E). *British Columbia Ministry Energy, Mines and Petroleum Research, Geological Fieldwork*, 1991-1.

Cohen, J.F. (2011): Compositional variations in hydrothermal white mica and chlorite from wall-rock alteration at the Ann-Mason porphyry copper deposit, Nevada; M.Sc. thesis, Oregon State University, 121 p.

Cooke, D.R., White, N.C., Zhang, L., Chang, Z. and Chen, H. (2017): Lithocaps – characteristics, origins and significance for porphyry and epithermal exploration; *in* Mineral Resources to Discover,

Proceedings of the 14th SGA Biennial Meeting, v. 1, Society for Geology Applied to Mineral Deposits, August 20–23, 2017, Quebec City, Quebec, p. 291–294.

David R. Cooke, Stuart F. Simmons, 2000. "Characteristics and Genesis of Epithermal Gold Deposits", Gold in 2000, Steffen G. Hagemann, Philip E. Brown

Deyell, C. L., & Dipple, G. M. (2005). Equilibrium mineral–fluid calculations and their application to the solid solution between alunite and natroalunite in the El Indio–Pascua belt of Chile and Argentina. *Chemical Geology*, *215*(1-4), 219-234.

Diakow, L.J., Panteleyev, A. and Schroeter, T.G. (1991): Jurassic epithermal deposits in the Toodoggone River area, northern British Columbia; examples of well-preserved, volcanic-hosted, precious metal mineralization; Economic Geology, v. 86, no. 3, p. 529–554, URL <https://www.doi.org/10.2113/gsecongeo.86.3.529>.

Duke, E. F. (1994). Near infrared spectra of muscovite, Tschermak substitution, and metamorphic reaction progress: Implications for remote sensing. *Geology*, *22*(7), 621-624.

Duuring, P., Rowins, S.M., McKinley, B.S.M., Dickinson, J.M., Diakow, L.J., Kim, Y.-S. and Creaser, R.A. (2009): Examining potential genetic links between Jurassic porphyry Cu-Au±Mo and epithermal Au±Ag mineralization in the Toodoggone district of north central British Columbia, Canada; Mineralium Deposita, v. 44, p. 463–496.

Frost, R. L. (1995). Fourier transform Raman spectroscopy of kaolinite, dickite and halloysite. *Clays and Clay Minerals*, *43*(2), 191-195.

Feng, H., Shen, P., Zhu, R., Li, C., Ma, G., & Pan, H. (2019). Geology and He-Ar-S-Pb isotope constraints on the genesis of the Sidaogou gold deposit in Liaodong Peninsula, northeastern North China Craton. *Ore Geology Reviews*, *113*, 103080.

Gagnon, J. F., Barresi, T., Waldron, J. W., Nelson, J. L., Poulton, T. P., & Cordey, F. (2012). Stratigraphy of the upper Hazelton Group and the Jurassic evolution of the Stikine terrane, British Columbia. *Canadian Journal of Earth Sciences*, *49*(9), 1027-1052.

Gagnon, J. F., Evenchick, C. A., Waldron, J. W. F., Cordey, F., & Poulton, T. P. (2009). Jurassic subsidence history of the Hazelton Trough–Bowser Basin in the area of Todagin Mountain, north-central British Columbia, Canada. *Bulletin of Canadian Petroleum Geology*, *57*(4), 430-448.

Gates, W., Kloprogge, J. T., Madejova, J., & Bergaya, F. (2017). *Infrared and Raman spectroscopies of clay minerals*. Elsevier.

García-Vicente, A., Lorenzo, A., Morales, J., García-Romero, E., & Suárez, M. (2021). Field spectroscopy applied to the kaolinite polytypes identification. In *Environmental Sciences Proceedings* (Vol. 6, No. 1, p. 16). Multidisciplinary Digital Publishing Institute.

Grant, J.A. (2005): Isocon analysis: a brief review of the method and applications; Physics and Chemistry of the Earth, Parts A/B/C, v. 30, no. 17–18, p. 997–1004, URL <https://www.doi.org/10.1016/j.pce.2004.11.003>.

Gray, J. E., & Coolbaugh, M. F. (1994). Geology and geochemistry of Summitville, Colorado; an epithermal acid sulfate deposit in a volcanic dome. *Economic Geology*, *89*(8), 1906-1923.

Guatame Garcia, L. A. (2013). *Crystallinity variations of smectite-illite and kaolin hydrothermal alteration minerals by using SWIR spectroscopy: a study of the Rodalquilar AU deposit, SE Spain* (Master's thesis, University of Twente).

Guggenheim, S., Bain, D.C., Bergaya, F., Brigatti, M.F., Drits, V.A., Eberl, D.D., Formoso, M.L.L., Galán, E., Merriman, R.J., Peacor, D.R., Stanjek, H. and Watanabe, T. (2002): Report of the Association Internationale pour l'Etude des Argiles (AIPEA) Nomenclature Committee for 2001: order, disorder and crystallinity in phyllosilicates and the use of the 'Crystallinity Index'; Clay Minerals, v. 37, no. 2, p. 389–393.

Hauff, P.L., Kruse, F.A. and Thiry, M. (1990): Characterization of interstratified kaolinite/smectite clays using infrared reflectance spectroscopy (1.2–2.5 μm); Chemical Geology, v. 84, no. 1–4, p. 267–270, URL <https://www.doi.org/10.1016/0009-2541(90)90234-x>.

Hauff, P. (2008). An overview of VIS-NIR-SWIR field spectroscopy as applied to precious metals exploration. *Arvada, Colorado: Spectral International Inc*, *80001*, 303-403.

Hedenquist, J. W., & Arribas, A. (2022). Exploration Implications of Multiple Formation Environments of Advanced Argillic Minerals. *Economic Geology*, *117*(3), 609-643.

Hedenquist, J. W., & Taran, Y. A. (2013). Modeling the formation of advanced argillic lithocaps: Volcanic vapor condensation above porphyry intrusions. *Economic Geology*, *108*(7), 1523-1540.

Hemley, J. J., Montoya, J. W., Marinenko, J. W., & Luce, R. W. (1980). Equilibria in the system Al 2 O 3-SiO 2-H 2 O and some general implications for alteration/mineralization processes. *Economic Geology*, *75*(2), 210-228.

Herrmann, W. "Short Wavelength Infrared (SWIR) Spectral Analysis of Hydrothermal Alteration Zones Associated with Base Metal Sulfide Deposits at Rosebery and Western Tharsis, Tasmania, and

Highway-Reward, Queensland." *Economic Geology*, vol. 96, no. 5, 2001, pp. 939–955., https://doi.org/10.2113/96.5.939.

Horiba Scientific. 2019. Labspec6 Spectroscopy Suite Reference Manual. DOI: https://s3-us-west-2.amazonaws.com/oww-files-public/b/b4/LabSpec6_-_Reference_Manual.pdf

Huang, J., Chen, H., Han, J., Deng, X., Lu, W., & Zhu, R. (2018). Alteration zonation and short wavelength infrared (SWIR) characteristics of the Honghai VMS Cu-Zn deposit, Eastern Tianshan, NW China. *Ore Geology Reviews*, *100*, 263-279.

Iea. (n.d.). *The role of critical minerals in Clean Energy Transitions – analysis*. IEA. Retrieved March 13, 2022, from https://www.iea.org/reports/the-role-of-critical-minerals-in-clean-energy-transitions

J. J. Hemley, W. R. Jones; Chemical aspects of hydrothermal alteration with emphasis on hydrogen metasomatism. *Economic Geology* 1964;; 59 (4): 538–569. doi:

John, D.A., Vikre, P.G., du Bray, E.A., Blakely, R.J., Fey, D.L., Rockwell, B.W., Mauk, J.L., Anderson, E.D. and Graybeal, F.T. (2018): Descriptive models for epithermal gold-silver deposits; U.S. Geological Survey, Scientific Investigations Report 2010–5070–Q, 247 p., URL <https://www.doi.org/10.3133/sir20105070Q>.

Kesler, S. E., Russell, N., & McCurdy, K. (2003). Trace-metal content of the Pueblo Viejo precious-metal deposits and their relation to other high-sulfidation epithermal systems. *Mineralium Deposita*, *38*(6), 668-682.

Kilby, W. E., & Kilby, C. E. Examining ASTER Imagery with the MapPlace Image Analysis Toolbox.

Kruse, F., & Hauff, P. L. (1991). Identification of illite polytype zoning in disseminated gold deposits using reflectance spectroscopy and X-ray diffraction-potential for mapping with imaging spectrometers. *IEEE Transactions on Geoscience and Remote Sensing*, *29*(1), 101-104.

Lerouge, C., Beny, C., Fléhoc, C., & Guerrot, C. (2007). Constraints of Stable Isotopes, Raman Spectrometry on the Formation of the Advanced Argillic Alteration of the Breznik Epithermal Au Occurrence in Bulgaria: Impact of Weathering. In *9th Biennial SGA Meeting* (pp. 19-23).

Li, H., Zhang, L., & Christy, A. G. (2011). The correlation between Raman spectra and the mineral composition of muscovite and phengite. In *Ultrahigh-Pressure Metamorphism* (pp. 187-212). Elsevier.

Lypaczewski, P., Rivard, B., Lesage, G., Byrne, K., D'Angelo, M., & Lee, R. G. (2020). Characterization of Mineralogy in the Highland Valley Porphyry Cu District Using Hyperspectral Imaging, and Potential Applications. *Minerals*, *10*(5), 473.

MapPlace (2021): Claims data, regional geology, aeromagnetic data and MINFILE digital data for portions of NTS 094E; BC Ministry of Energy, Mines and Low Carbon Innovation, BC Geological Survey, MapPlace website, URL <http://apps.empr.gov.bc.ca/pub/mapplace/mp2/fusion/templates/mapguide/slate/index.html?ApplicationDefinition=Library://mp2.ApplicationDefinition&locale=en> [September 2021].

Monger, J. W. H., 1984, Cordilleran tectonics: A Canadian perspective: Geol. Soc. France Bull., ser. 7, v. 26, no. 2, p. 255- 278.

Monier, G. and Robert, J.-L. (1986): Muscovite solid solutions in the system K_2O-MgO-FeO-Al_2O_3-SiO_2-H_2O: an experimental study at 2 kbar P_{H_2O} and comparison with natural Li-Free white micas; Mineralogical Magazine, v. 50, no. 356, p. 257–266, URL <https://www.doi.org/10.1180/minmag.1986.050.356.08>.

Neal, L. C., Wilkinson, J. J., Mason, P. J., & Chang, Z. (2018). Spectral characteristics of propylitic alteration minerals as a vectoring tool for porphyry copper deposits. *Journal of Geochemical Exploration*, *184*, 179-198.

Omori, K. (1968). Infrared diffraction and the far infrared spectra of anhydrous sulfates. *Mineralogical Journal*, *5*(5), 334-354.

Pontual, S., Merry, N., and Gamson, P., 1997a, G-Mex Volume 1: Spectral interpretation field manual: Kew, Victoria 3101, Australia, Ausspec International Pty. Ltd

Reyes, A. G. (1990). Petrology of Philippine geothermal systems and the application of alteration mineralogy to their assessment. *Journal of Volcanology and geothermal research*, *43*(1-4), 279-309.

Reyes, A. G., Giggenbach, W. F., Saleras, J. R., Salonga, N. D., & Vergara, M. C. (1993). Petrology and geochemistry of Alto Peak, a vapor-cored hydrothermal system, Leyte Province, Philippines. *Geothermics*, *22*(5-6), 479-519.

Saunders, J.A., Hofstra, A.H., Goldfarb, R.J. and Reed, M.H. (2014): Geochemistry of hydrothermal gold deposits; *in* Treatise on Geochemistry (2nd edition), v. 13, H.D. Holland and K.K. Turekian (ed.), Elsevier, Oxford, p. 383–424.

Sillitoe, R.H. (1973): The tops and bottoms of porphyry copper deposits; Economic Geology, v. 68, p. 799–815.

Sillitoe, R. H. (1994). Erosion and collapse of volcanoes: Causes of telescoping in intrusion-centered ore deposits. *Geology*, *22*(10), 945-948.

Steven, T.A. and Ratte, J.C. (1960): Geology and ore deposits of the Summitville district, San Juan Mountains, Colorado; U.S. Geological Survey, Professional Paper 343, 70 p.

Thorkelson et al., 1995

D.J. Thorkelson, J.K. Mortensen, H. Marsden, D.C. Taylor: Age and tectonic setting of Early Jurassic episodic volcanism along the northeastern margin of the Hazelton Trough, northern British Columbia D.M. Miller, C.J. Busby (Eds.), Jurassic Magmatism and Tectonics of the North American Cordillera, vol. 299, Geological Society of America Special Paper (1995), pp. 83-94

Thompson, A.J.B., Hauff, P.L., and Robitaille, A.J., (1999). Alteration mapping in exploration: Application of short-wave infrared (SWIR) spectroscopy. *SEG Discovery*, (39), 1–27. https://doi.org/10.5382/segnews.1999-39.fea

Jimenez Torres, C. A. (2018). *Geology, hydrothermal alteration, geochemistry, mineral geochemistry, and alteration textures of the lithocap at Bantug, Negros-Philippines* (Doctoral dissertation, University of Tasmania).

John, D. A., Vikre, P. G., du Bray, E. A., Blakely, R. J., Fey, D. L., Rockwell, B. W., ... & Graybeal, F. T. (2018). *Descriptive models for epithermal gold-silver deposits* (No. 2010-5070-Q). US Geological Survey.

Wang, A., Freeman, J. J., & Jolliff, B. L. (2015). Understanding the Raman spectral features of phyllosilicates. *Journal of Raman Spectroscopy*, *46*(10), 829-845.

Watanabe, Y., & Hedenquist, J. W. (2001). Mineralogic and stable isotope zonation at the surface over the El Salvador porphyry copper deposit, Chile. *Economic Geology*, *96*(8), 1775-1797.

White, N.C. and Hedenquist, J.W. (1995): Epithermal gold deposits—styles, characteristics and exploration; Society of Economic Geologists, Newsletter 23, p. 1, 9–13.

Woodsworth, G.J., Anderson, R.G., Brookfield, A. and Tercier, P. (1988). Distribution of Plutonic Suites in the Canadian Cordillera, Geological Survey of Canada, Open File 1982

Appendix A: Geochemistry Data Cross Sections

Plan View Cross Section Reference

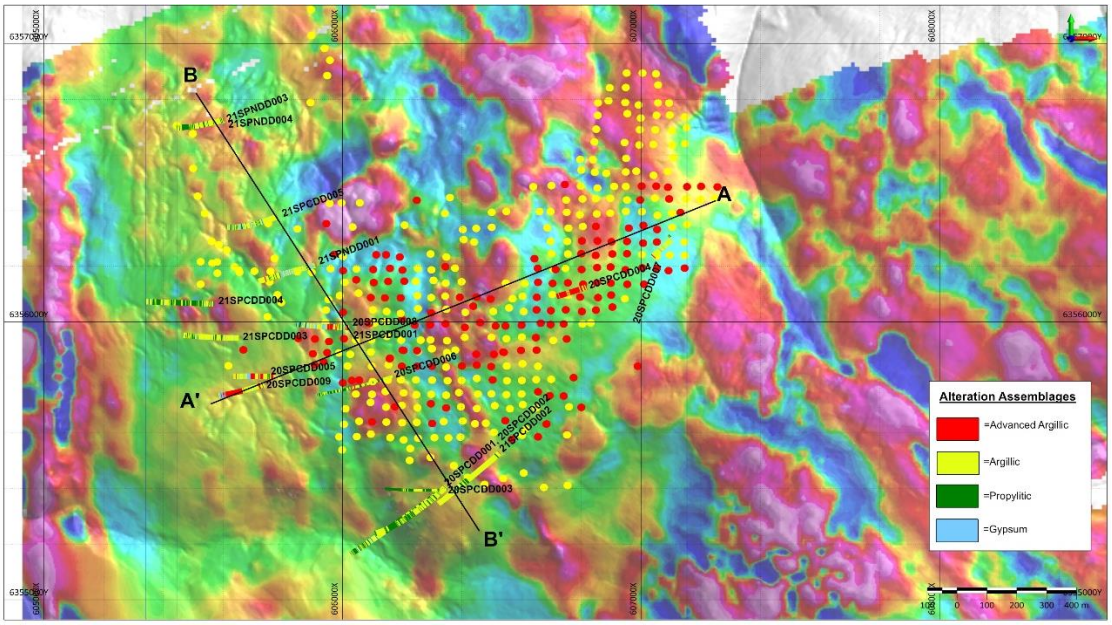

E-W Mo Concentration

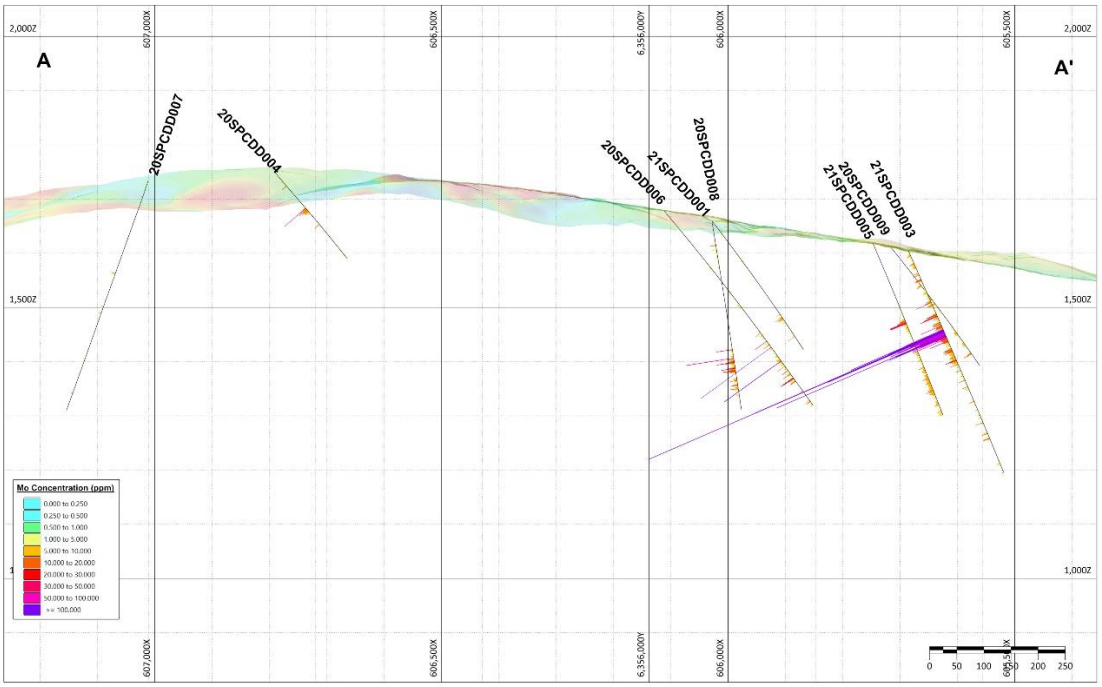

E-W As Concentration

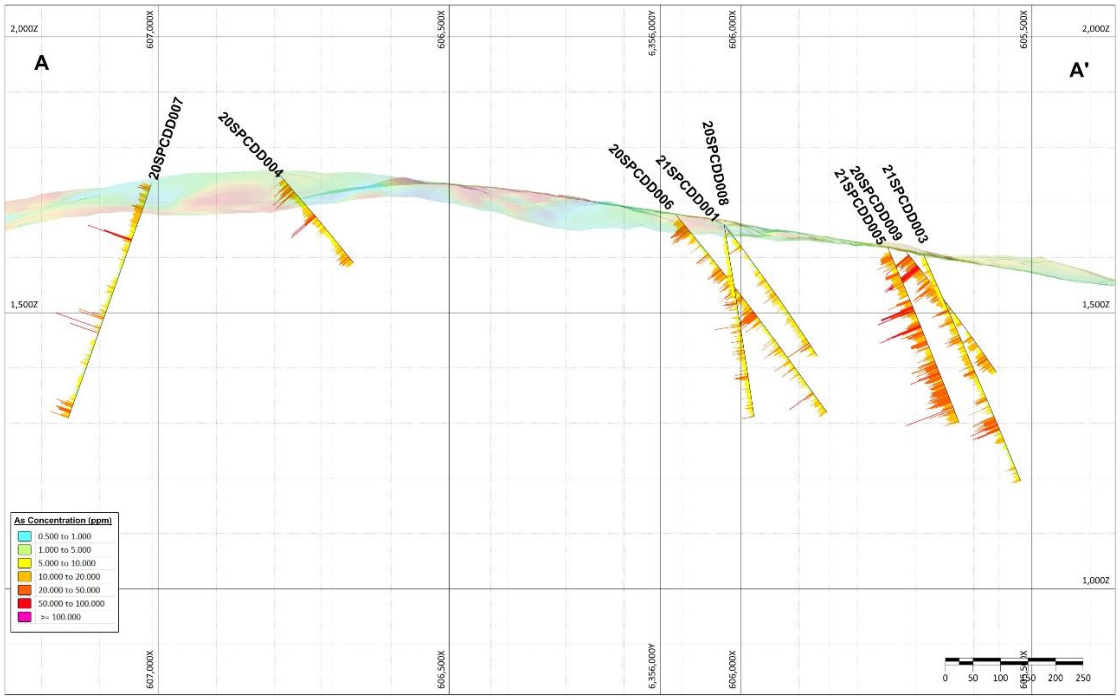

E-W Pb Concentration

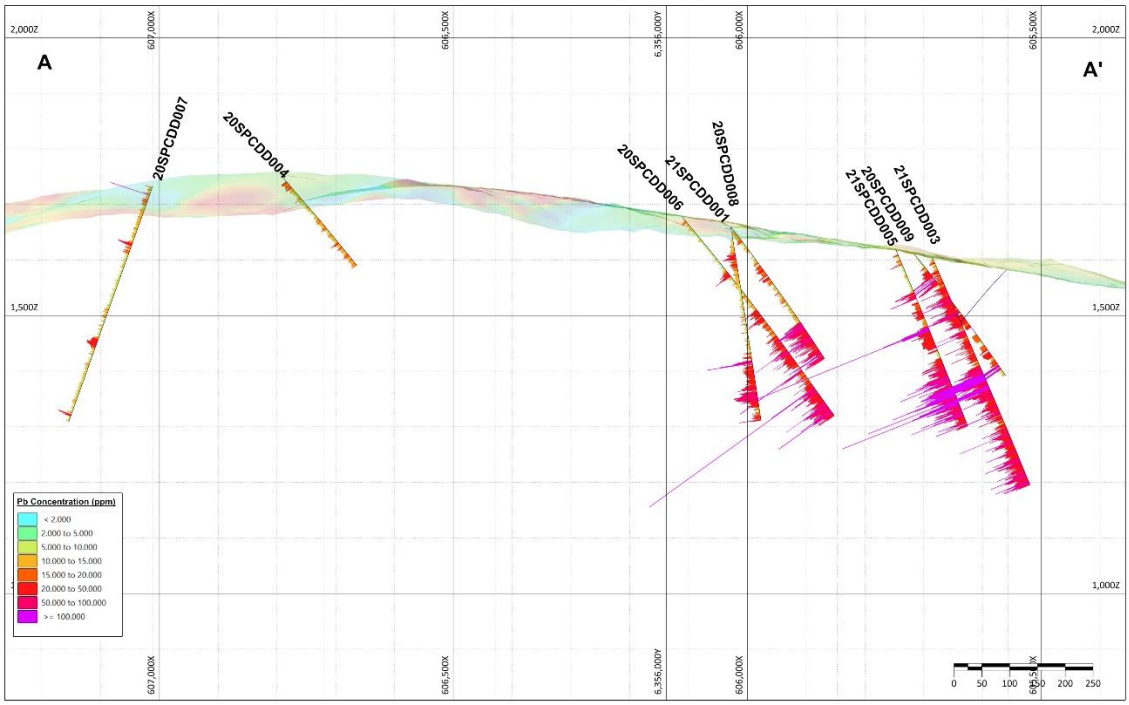

E-W S Concentration

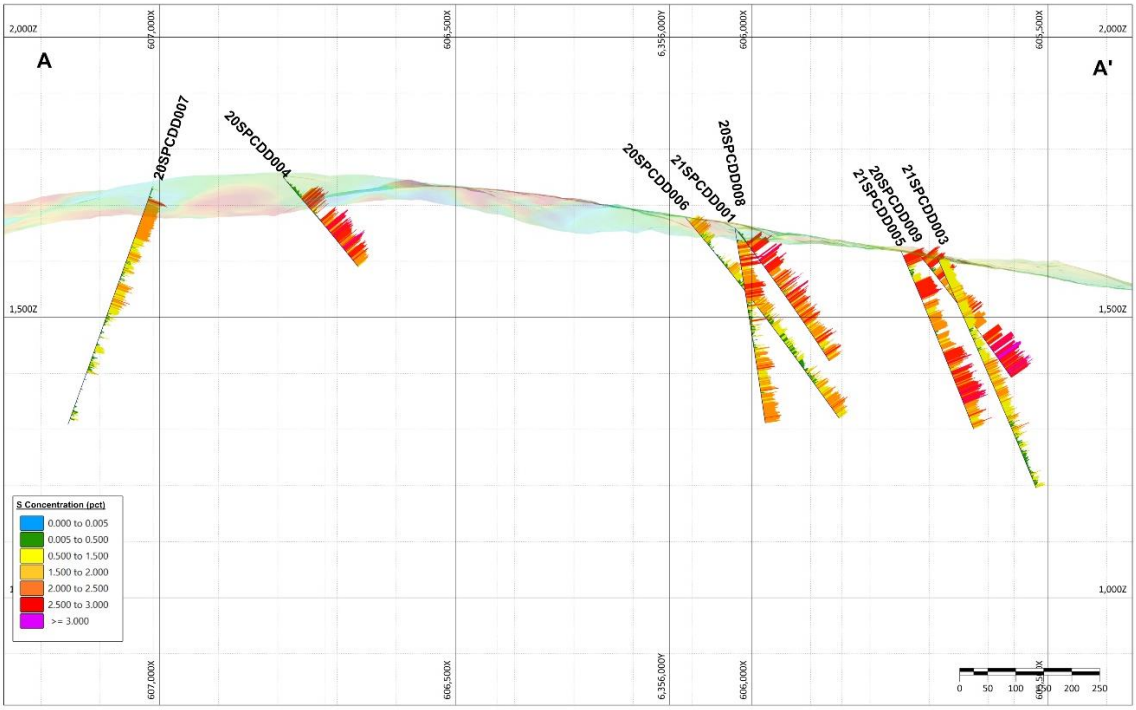

E-W Sb Concentration

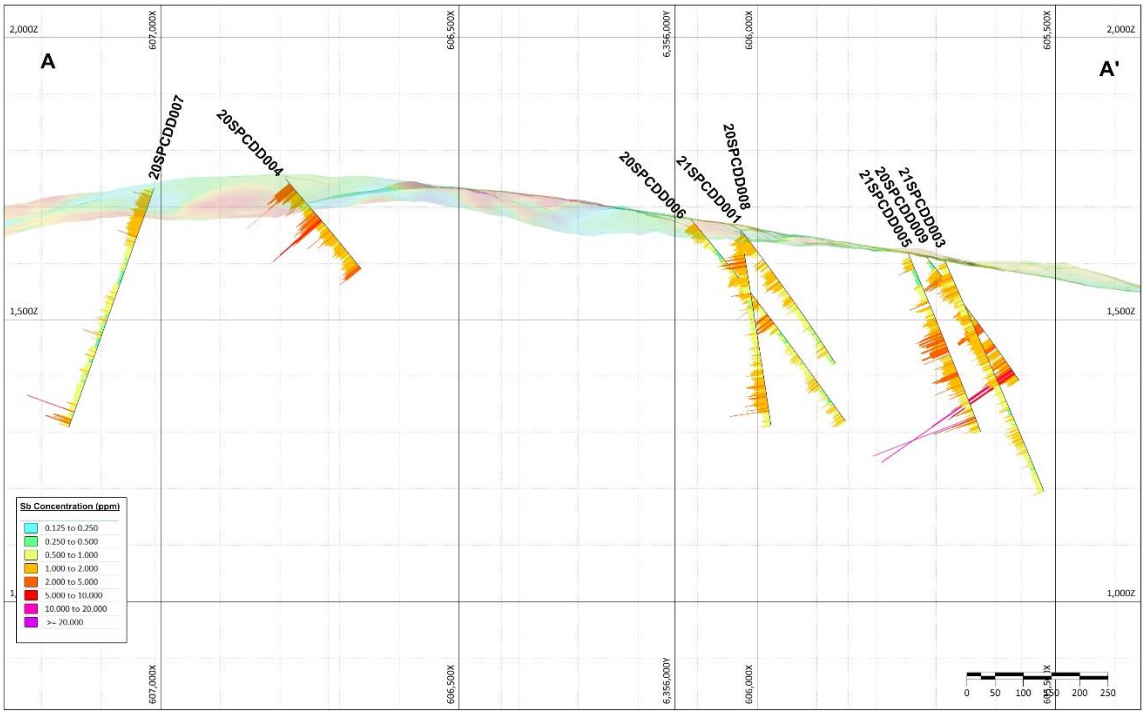

E-W Se Concentration

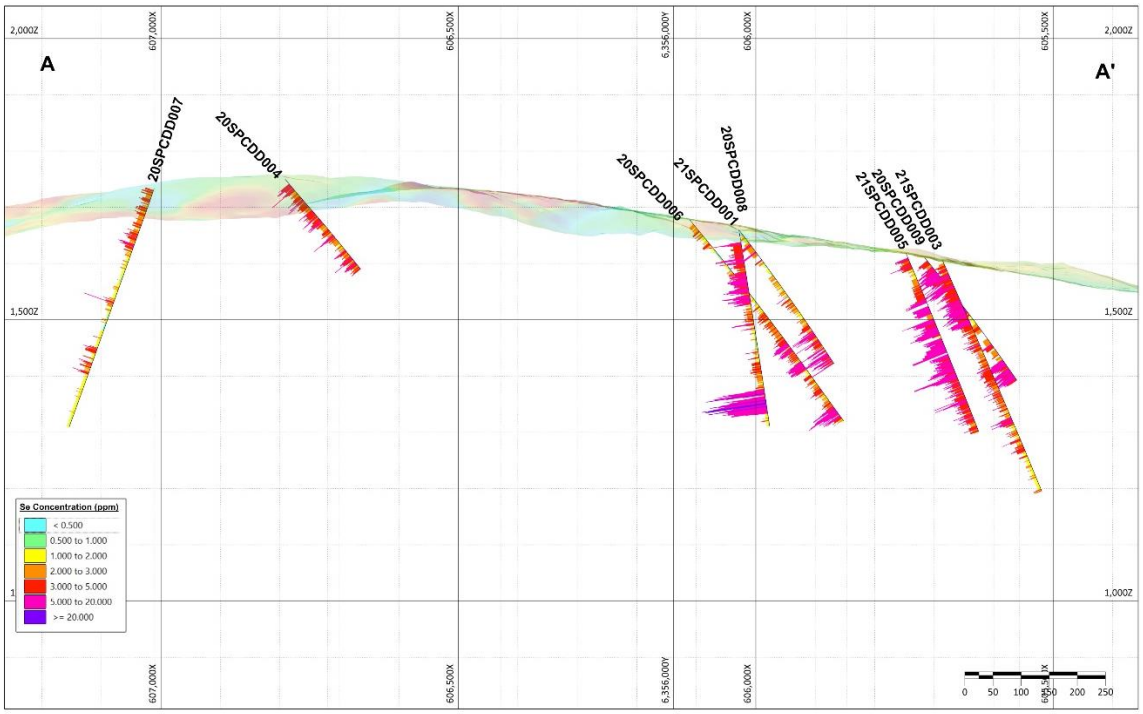

E-W W Concentration

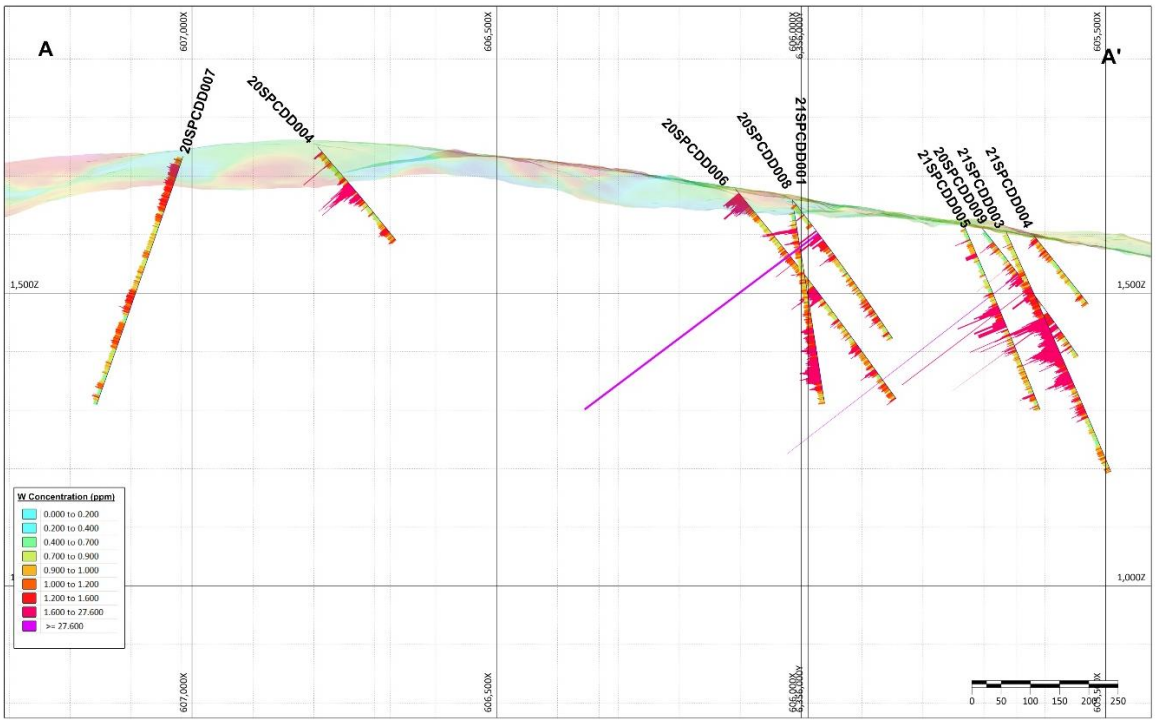

E-W MDRU Porphry Index

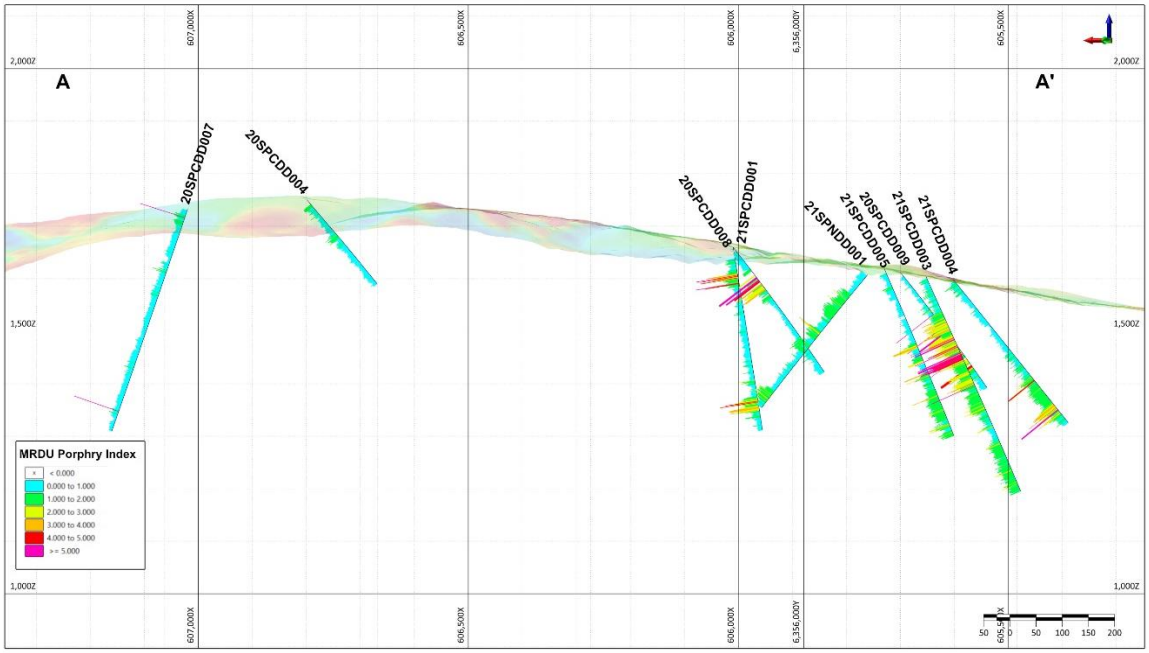

N-S As Concentration

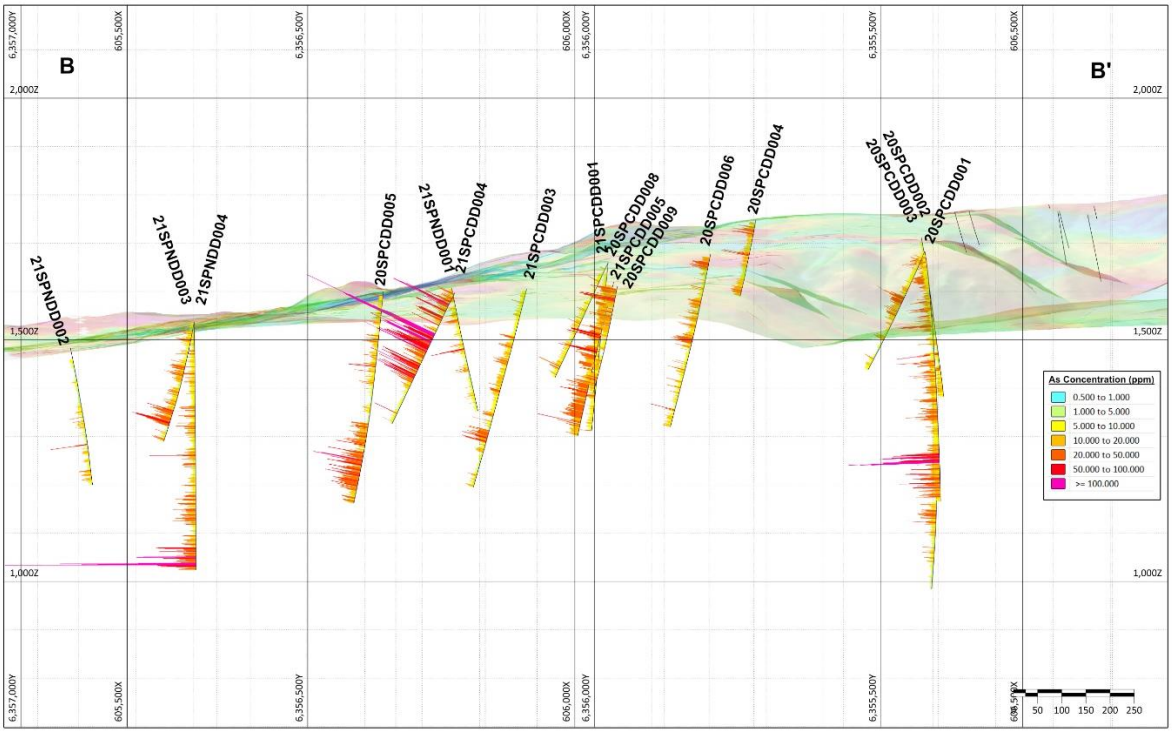

N-S Mo Concentration

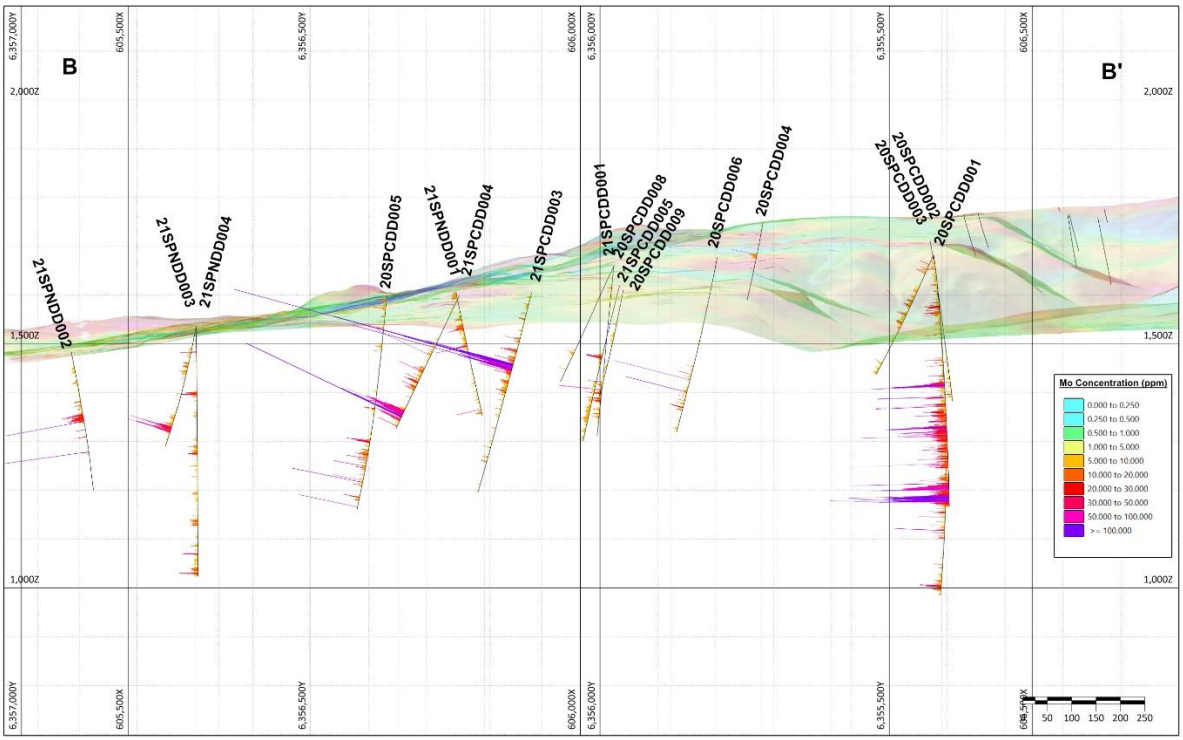

N-S Pb Concentration

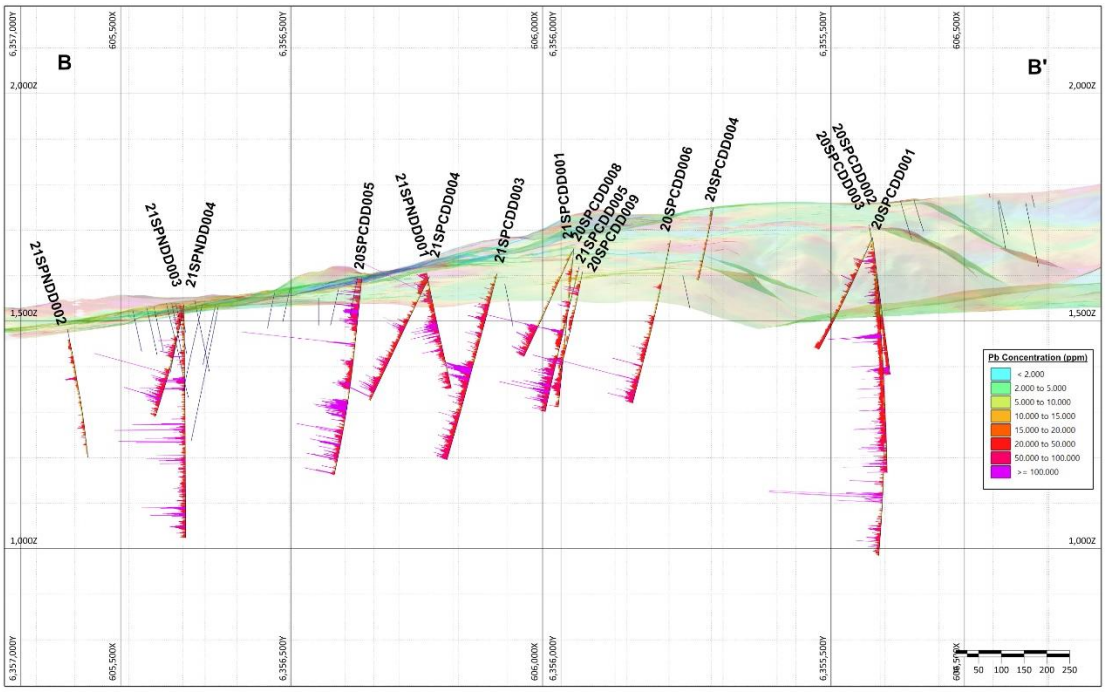

N-S S Concentration

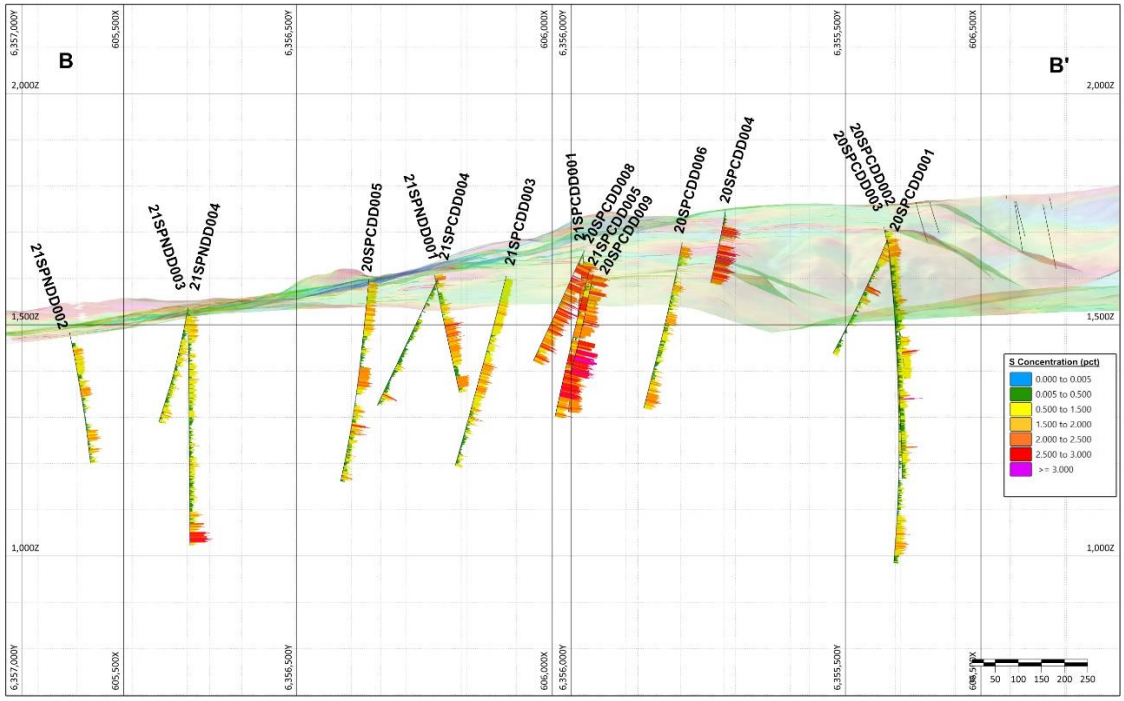

N-S Sb Concentration

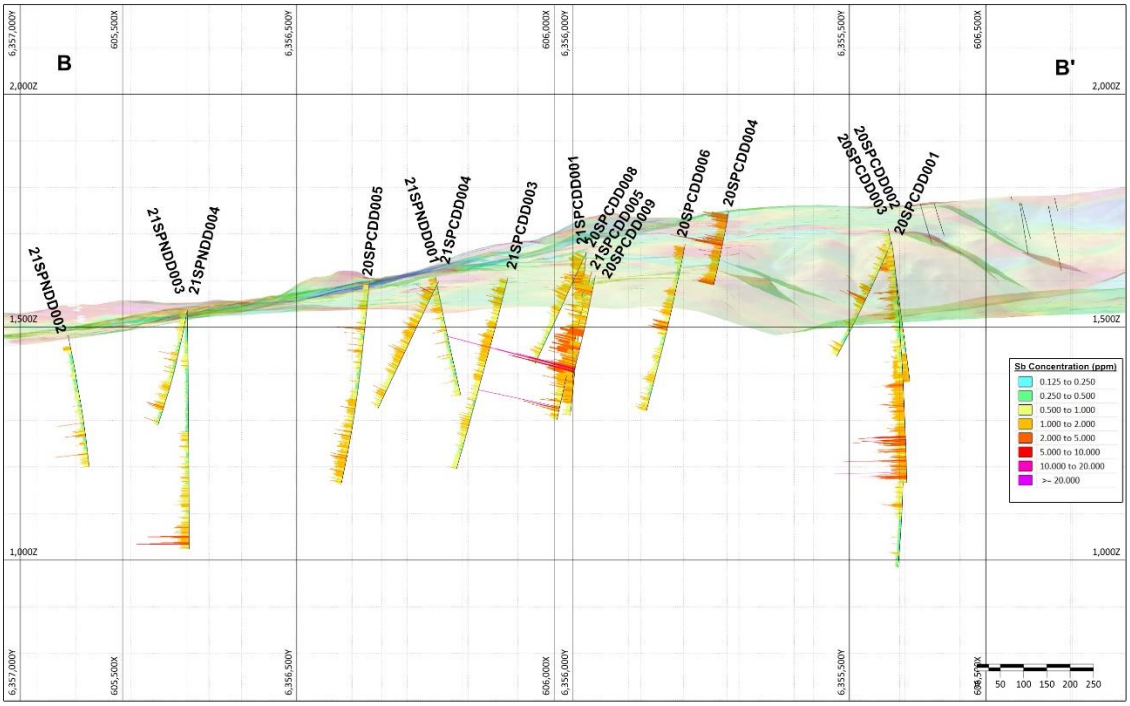

N-S Te Concentration

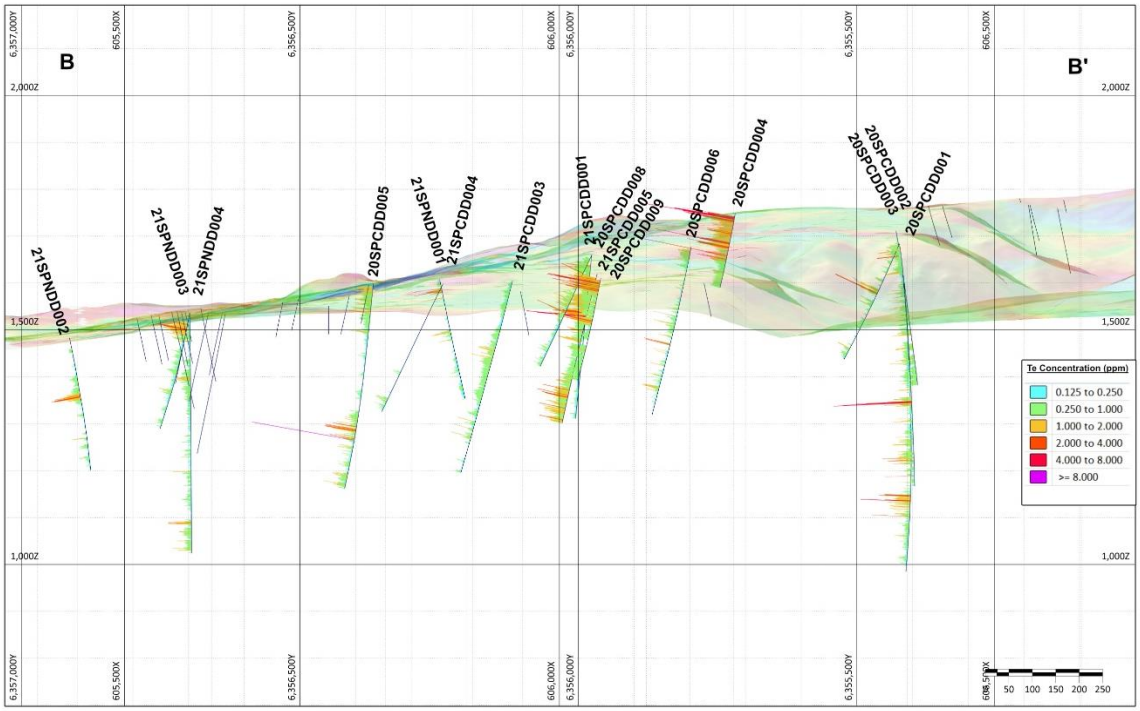

N-S W Concentration

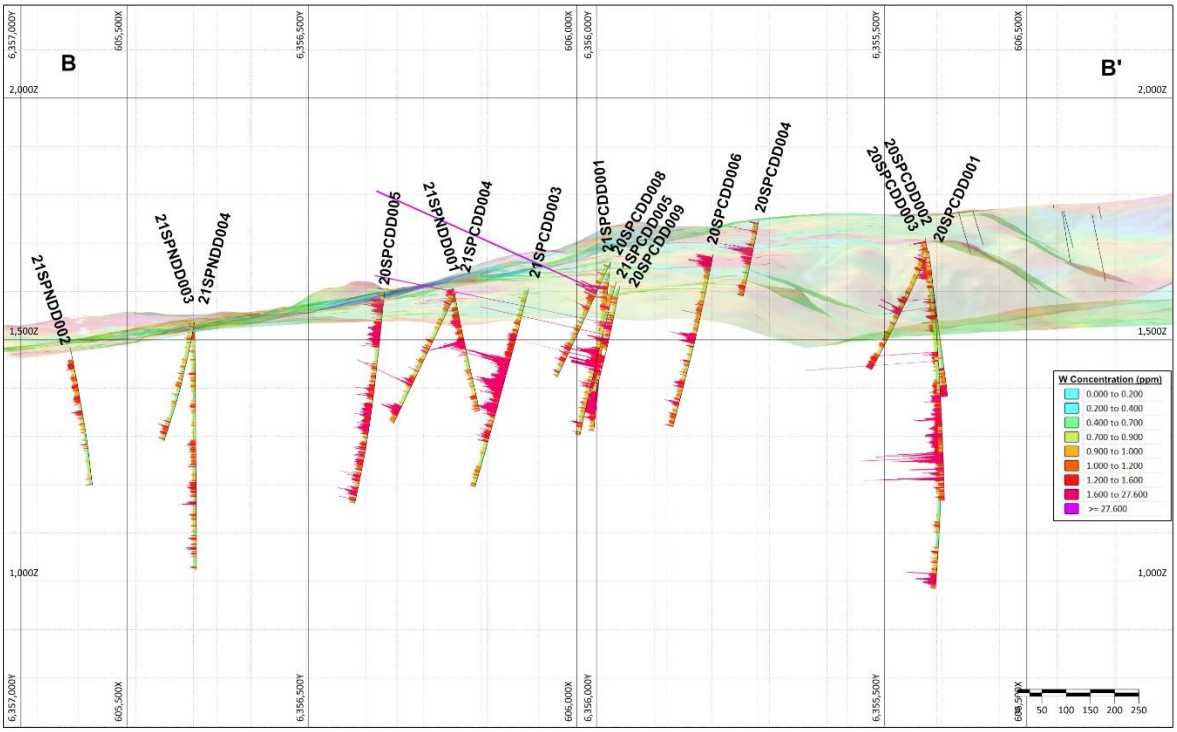

N-S MRDU Porphry Index

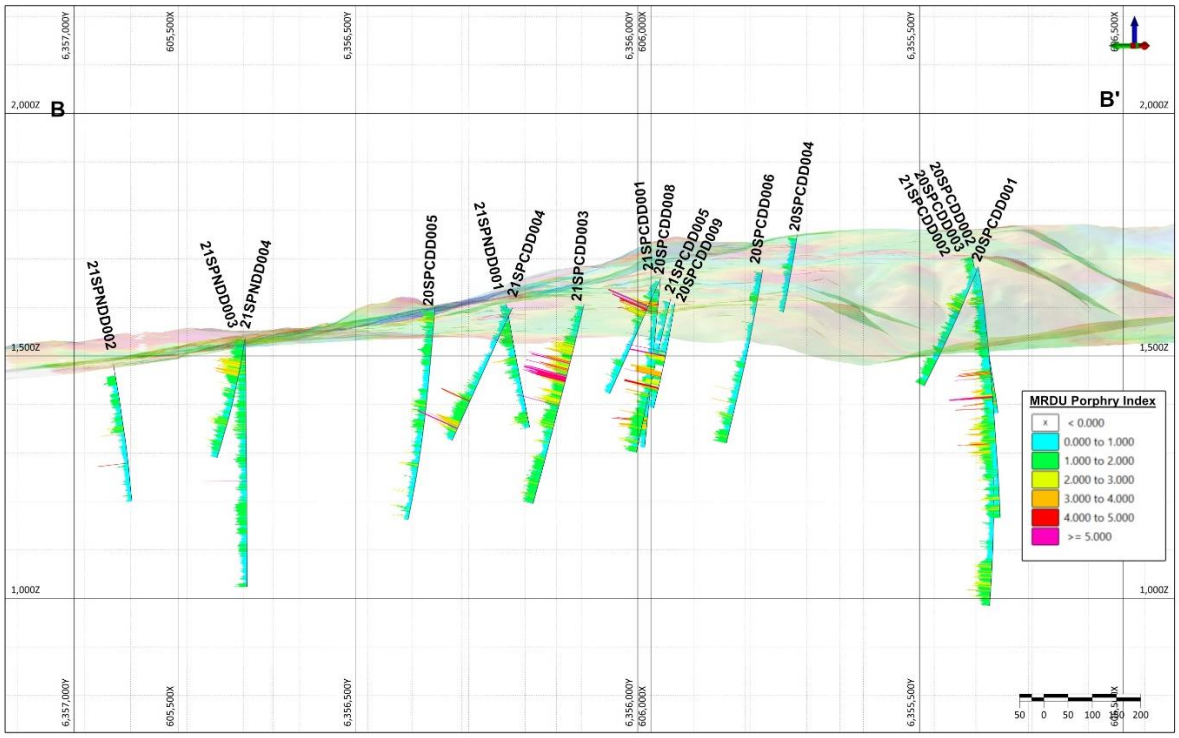

Appendix B: SWIR Data Cross Sections

N-S Alunite Abundance

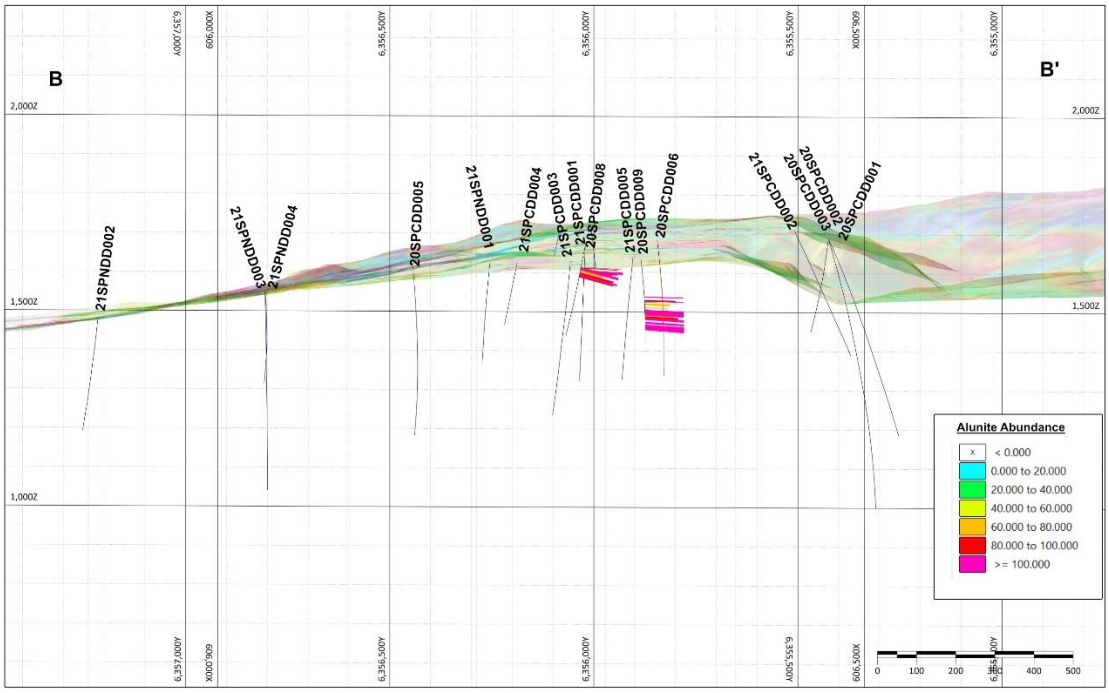

N-S Alunite Composition

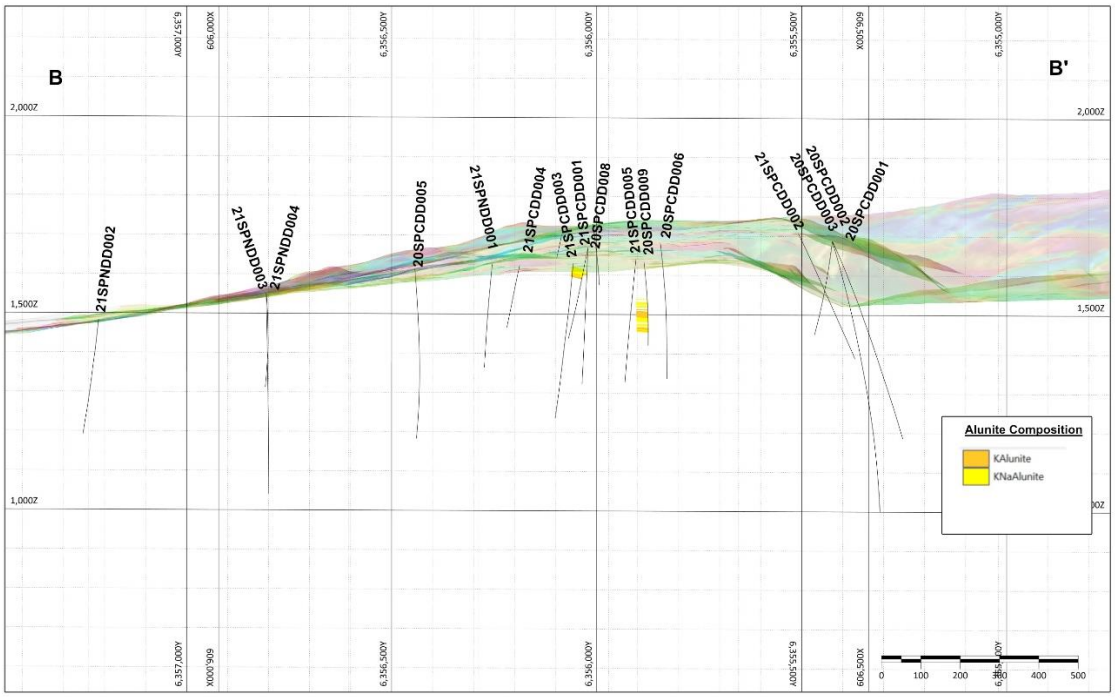

N-S Chlorite Abundance

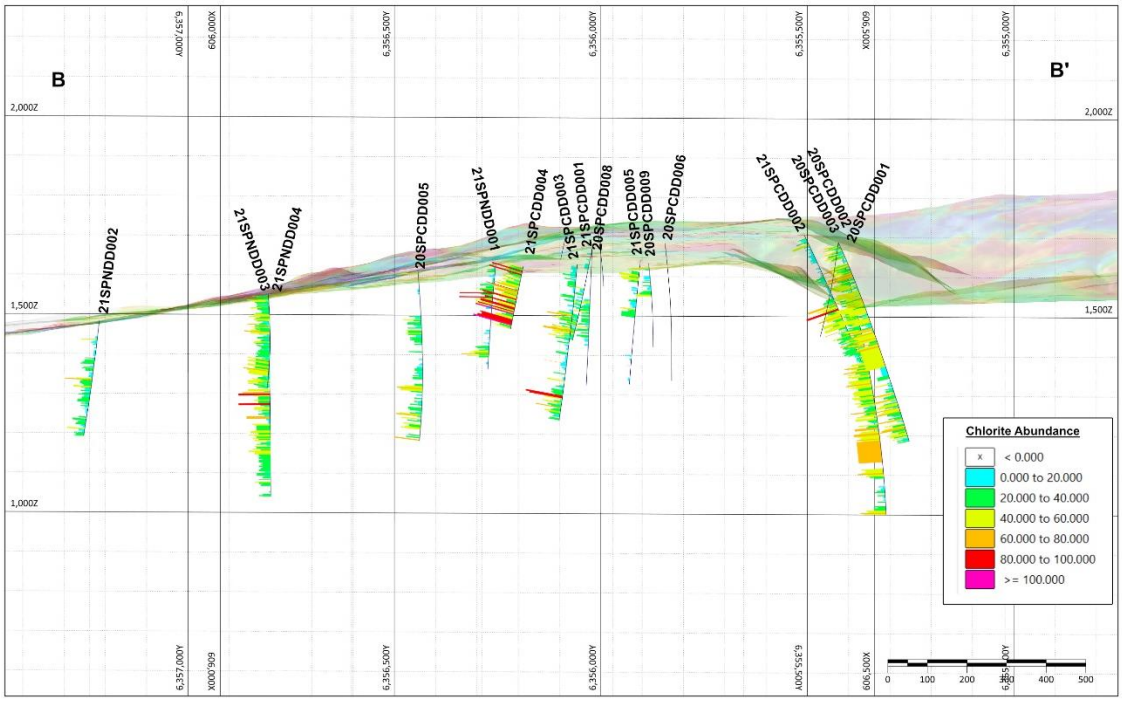

N-S Chlorite Composition

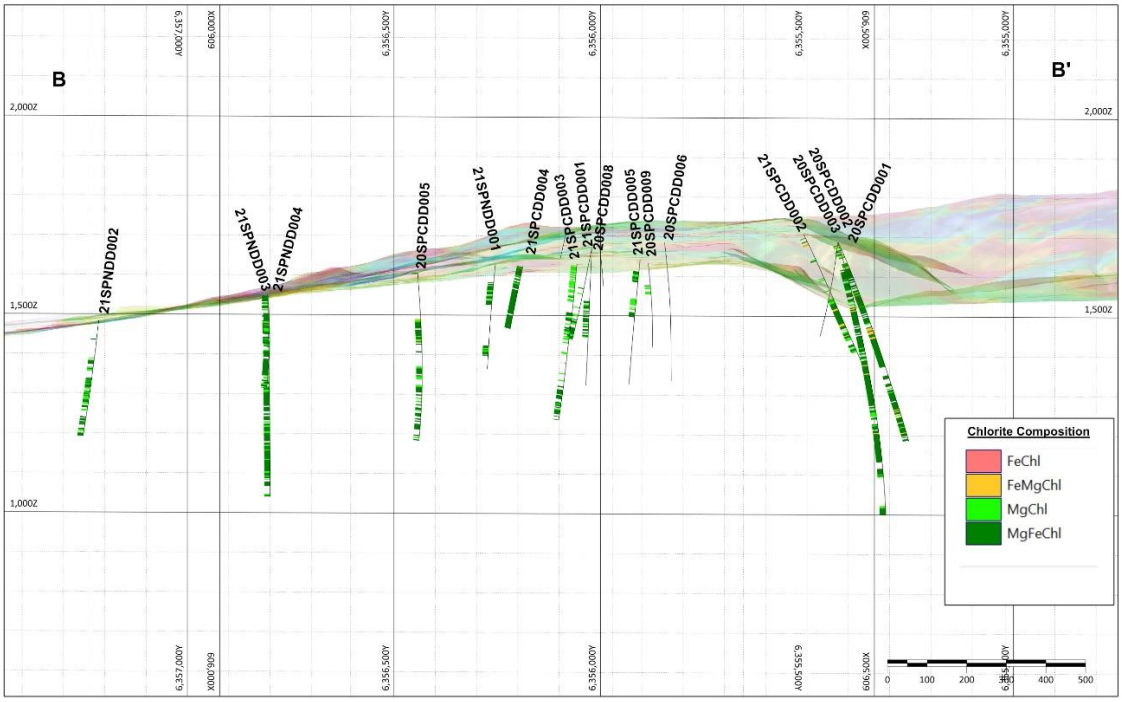

N-S Dickite Abundance

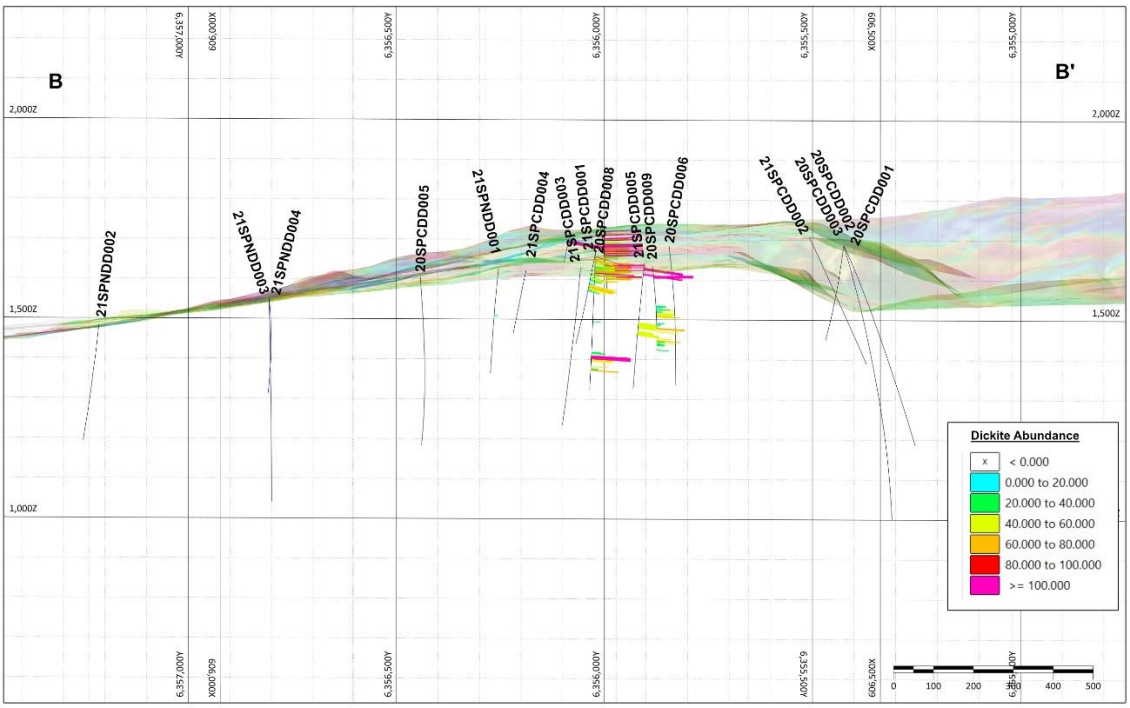

N-S Epidote Abundance

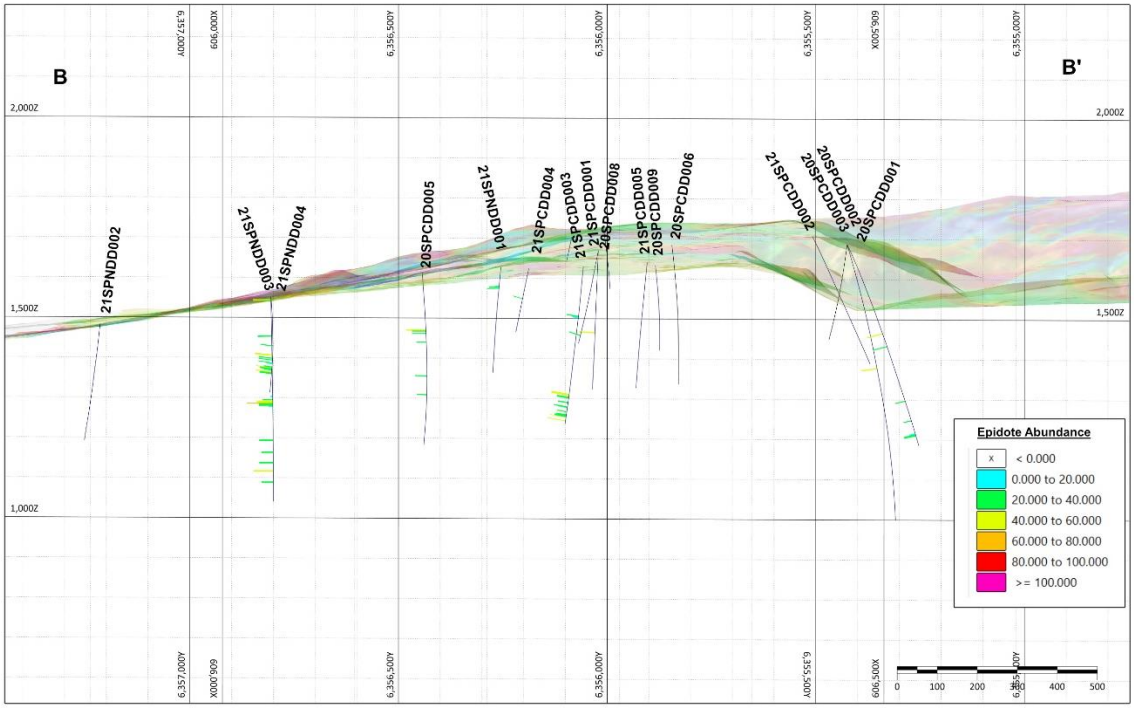

N-S Kaolinite Abundance

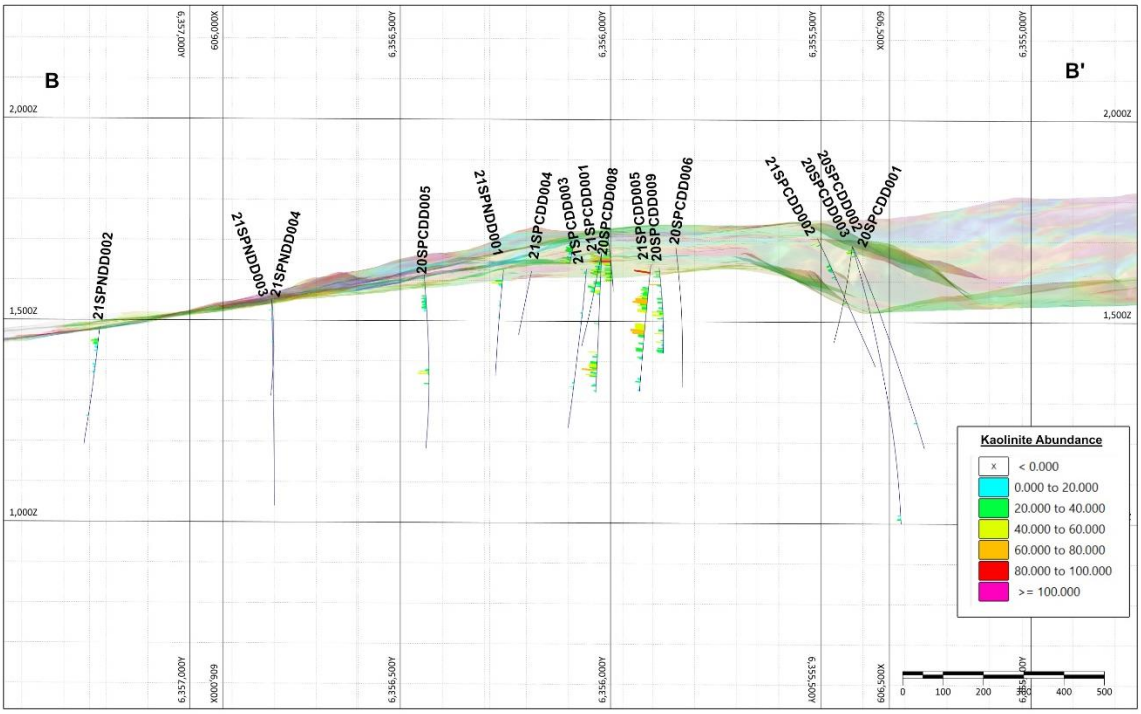

N-S Montmorillonite

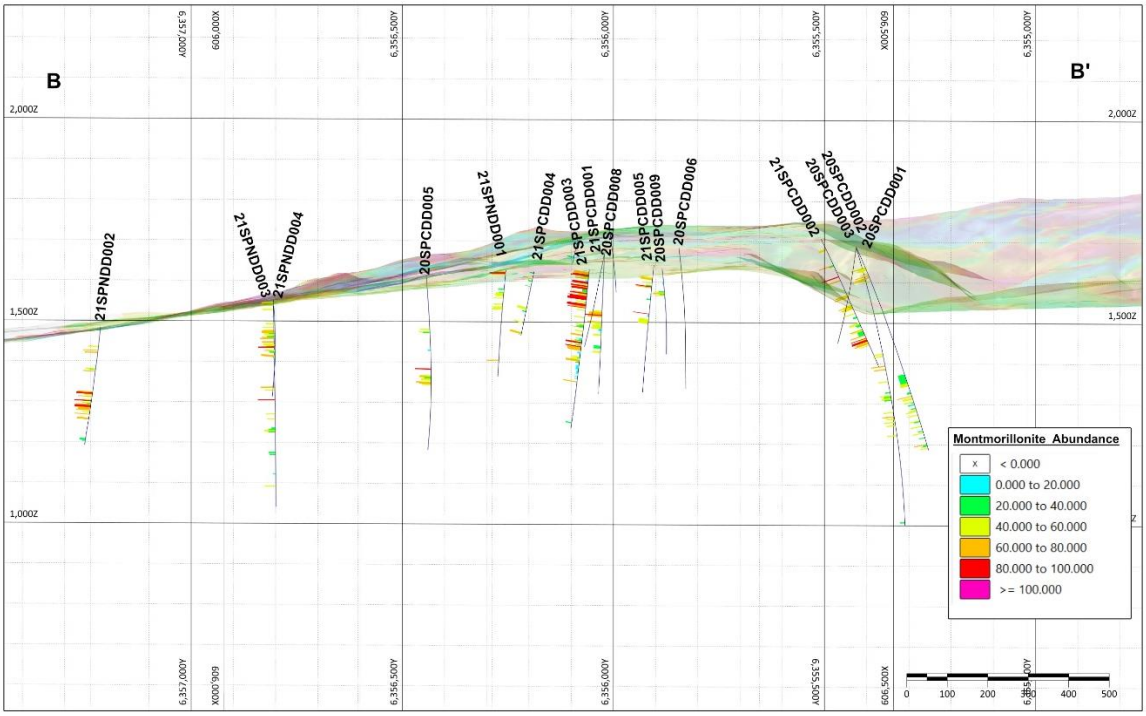

N-S Pyrophyllite Abundance

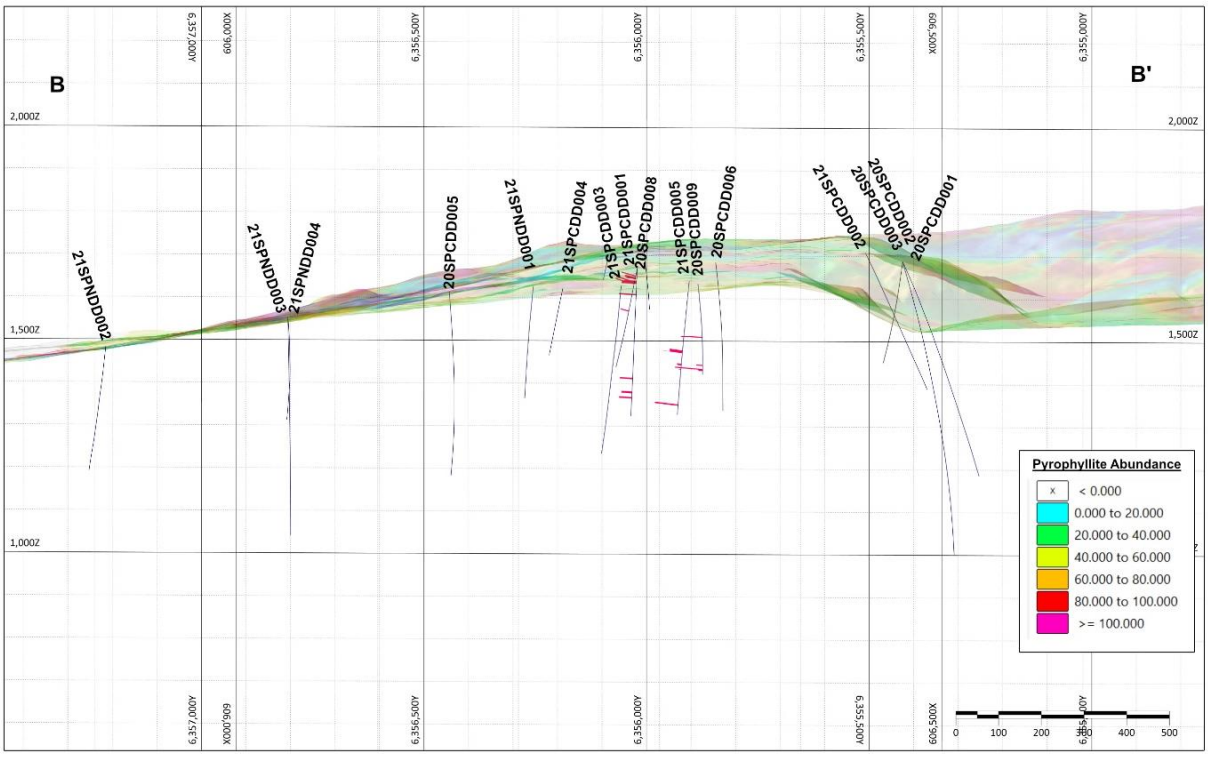

White Mica Composition

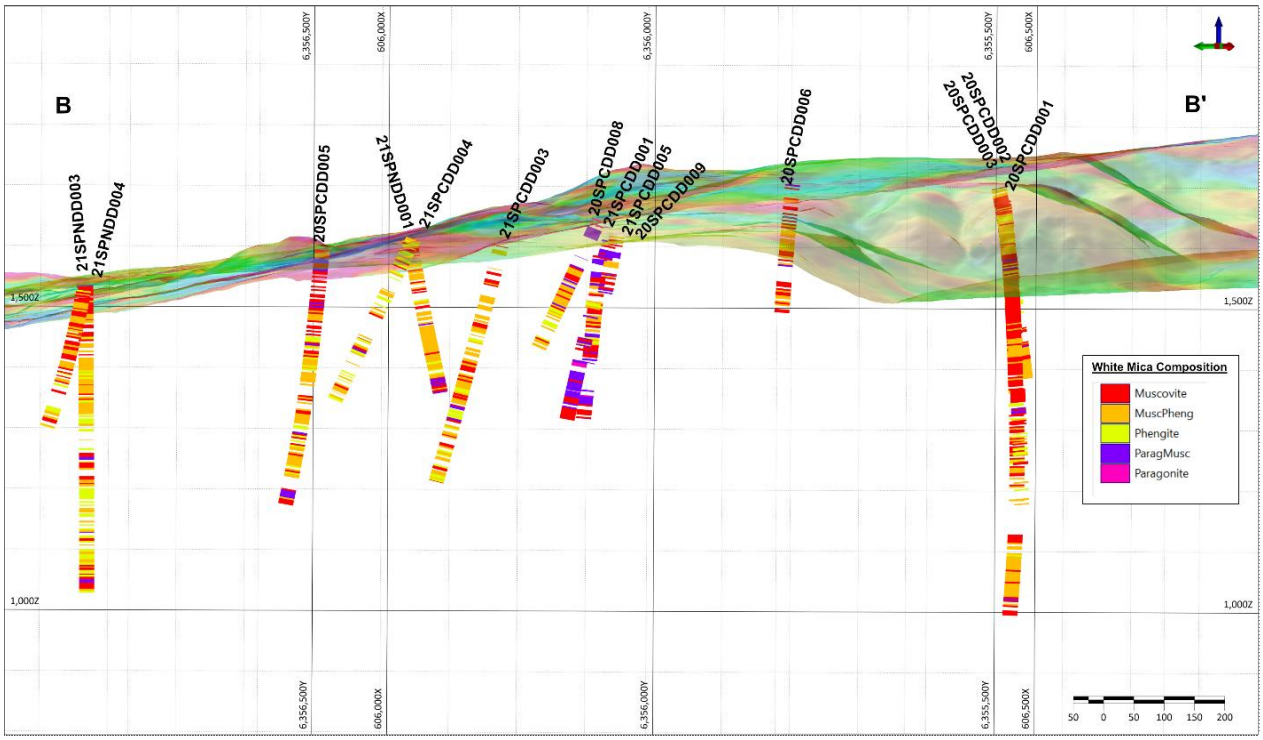

White Mica Spectral Contribution

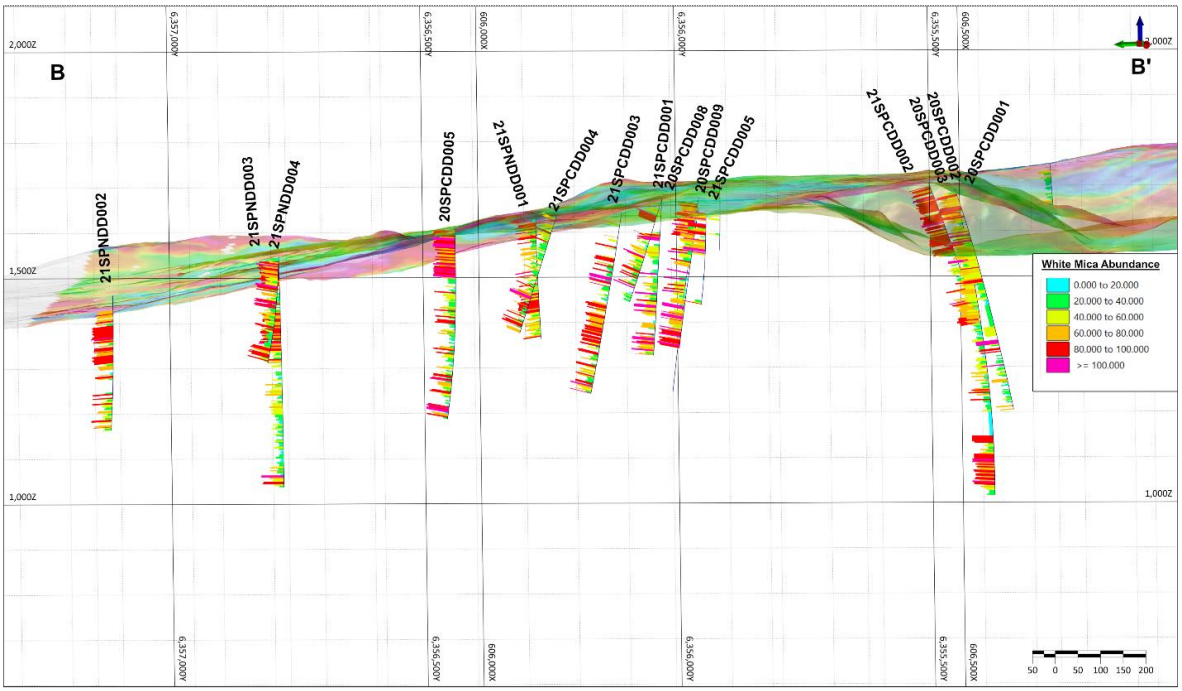

Appendix C: Geology Cross Sections

E-W Fault Structure

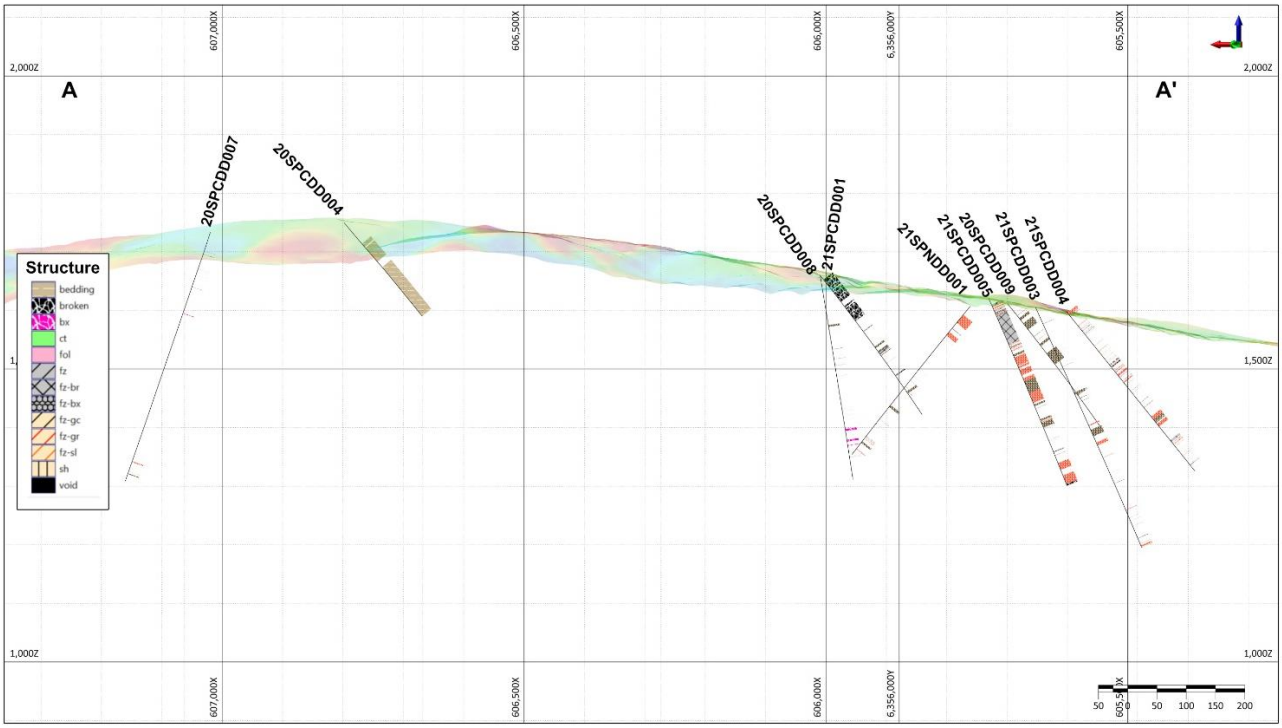

E-W Litholodgy

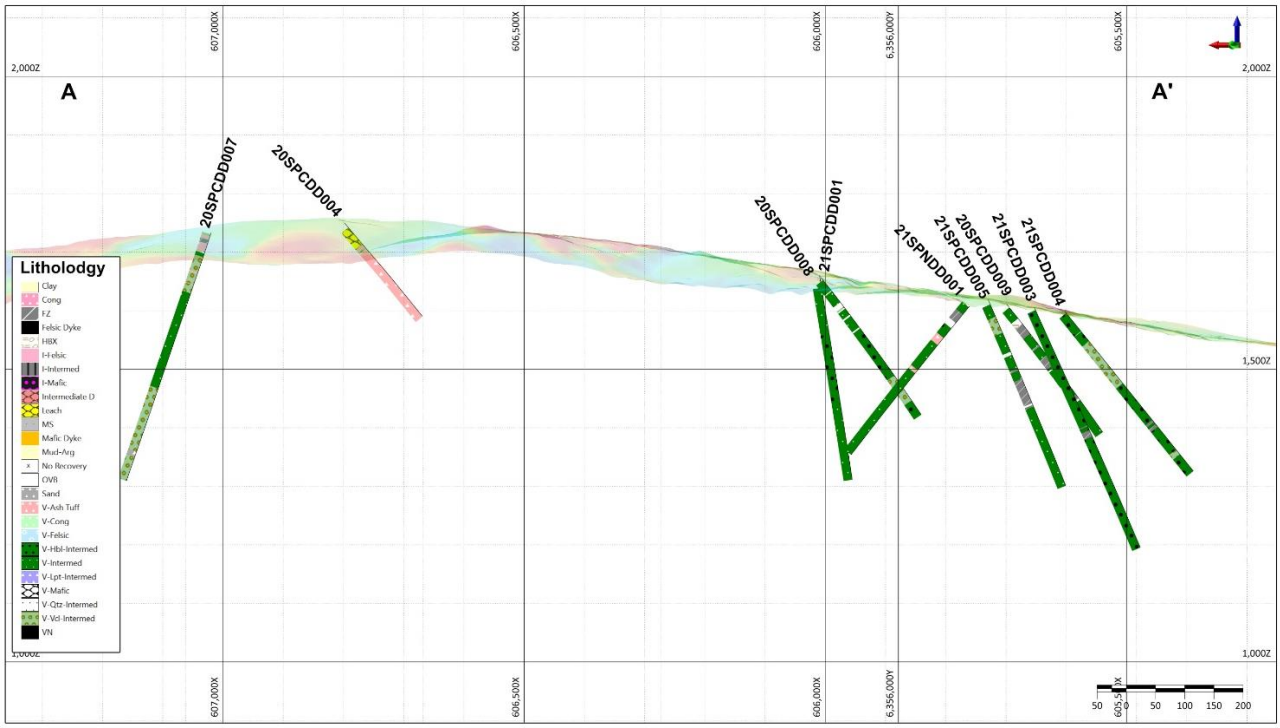

E-W MDRU Porphry Index

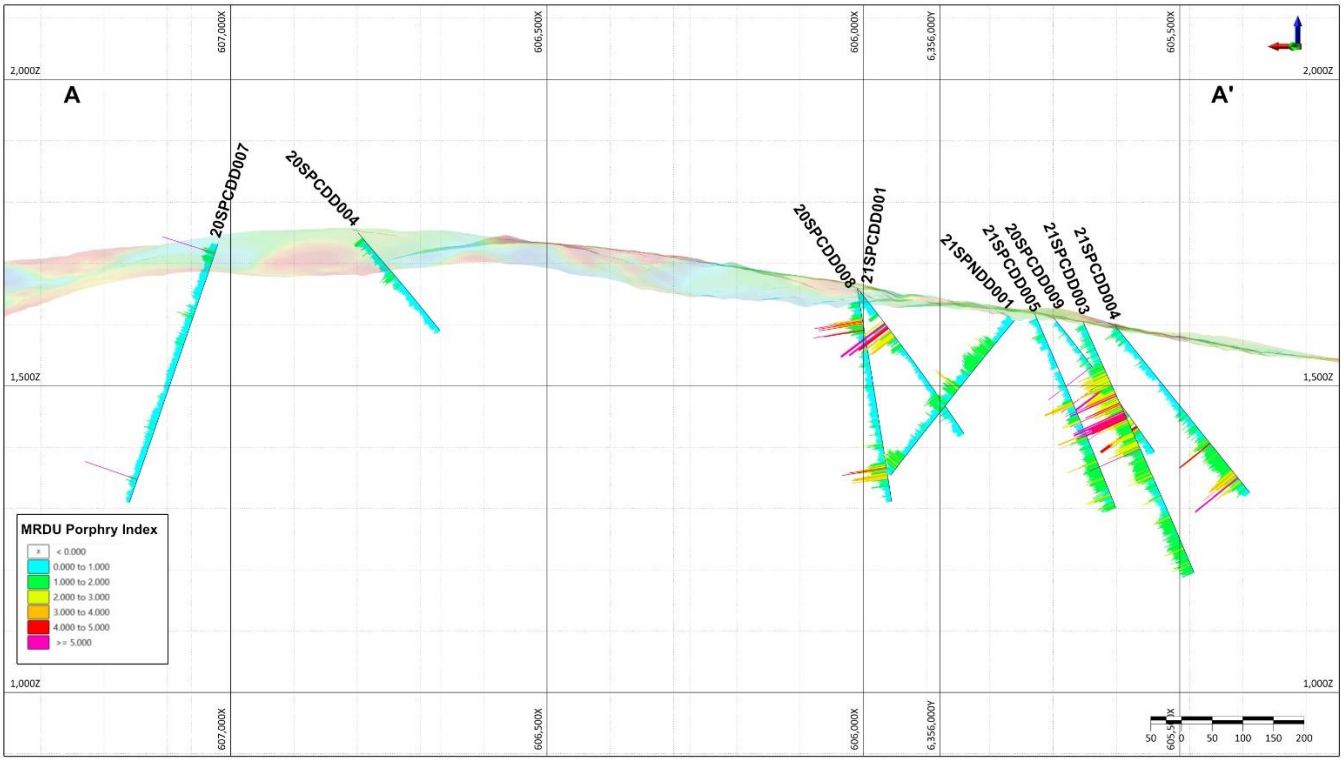

E-W Logged Pyrite Percent

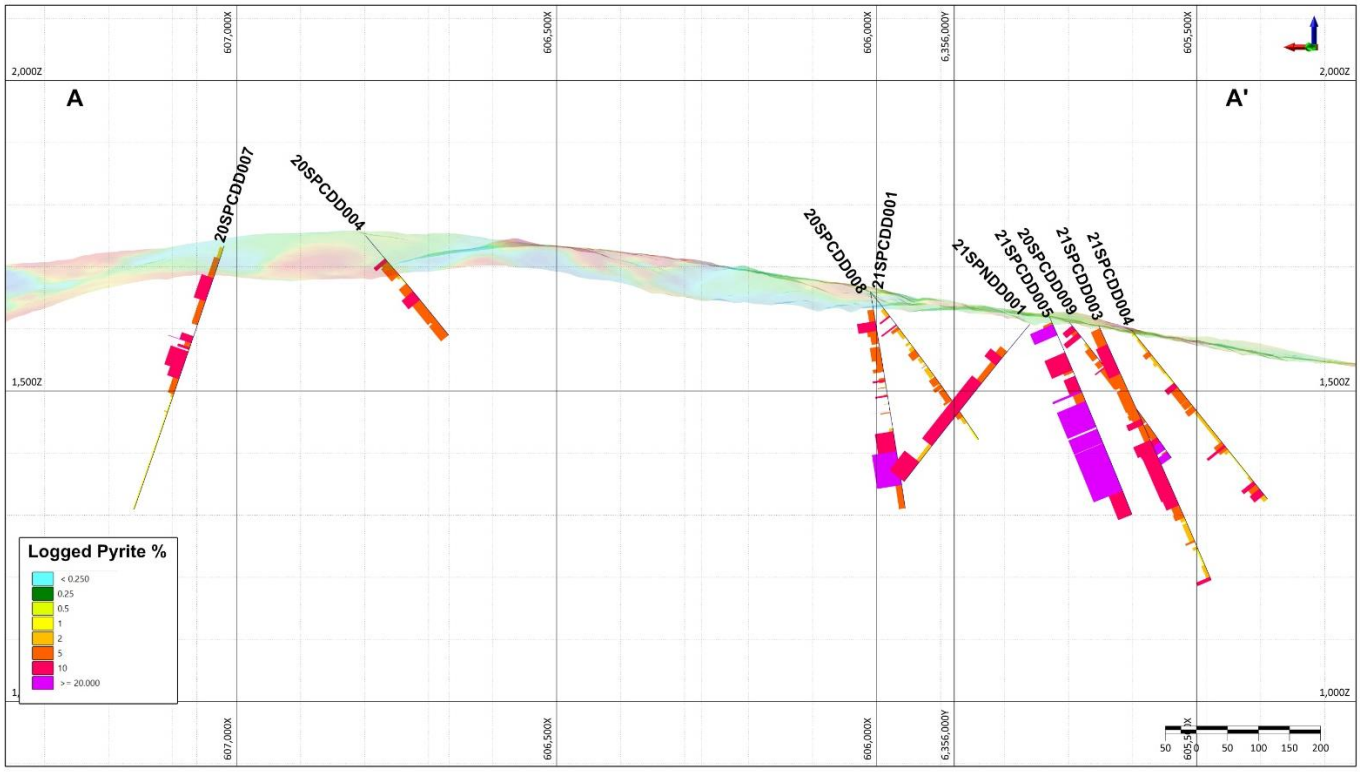

E-W Sericite Alteration Intensity

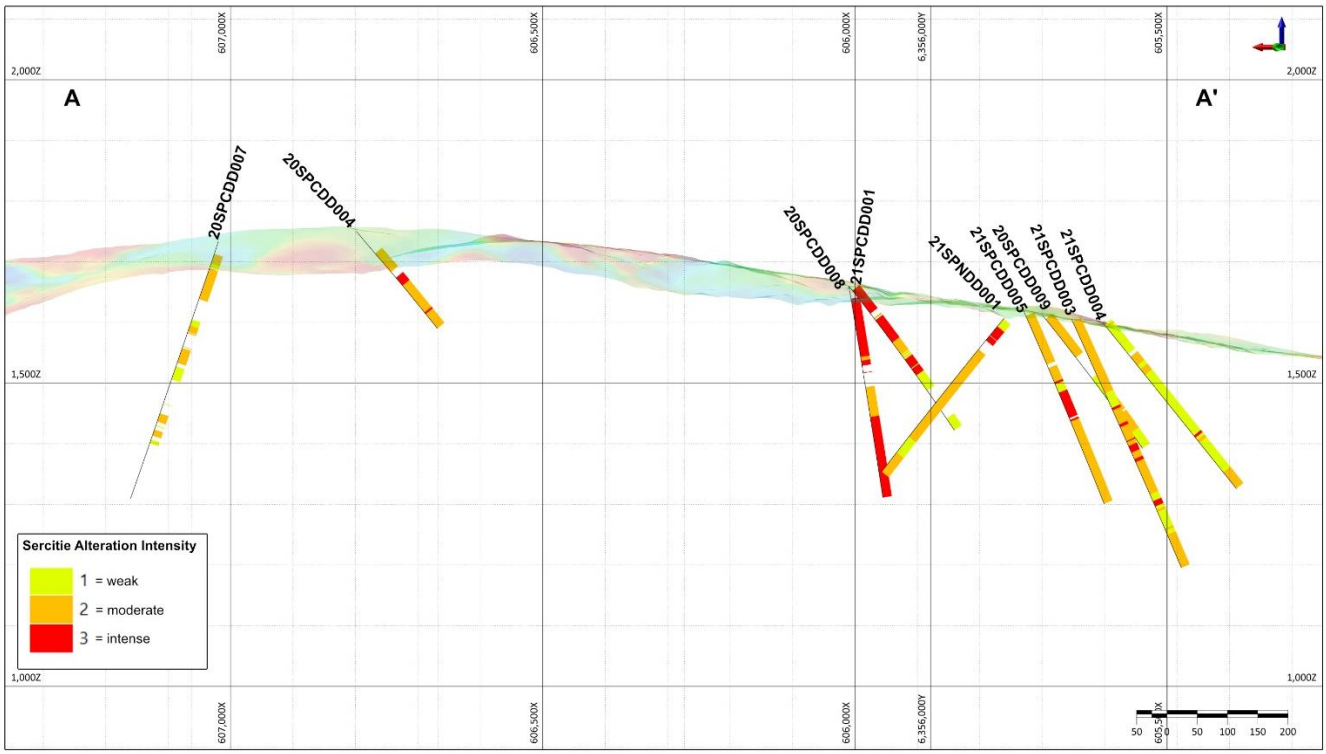

E-W Silicification Intensity

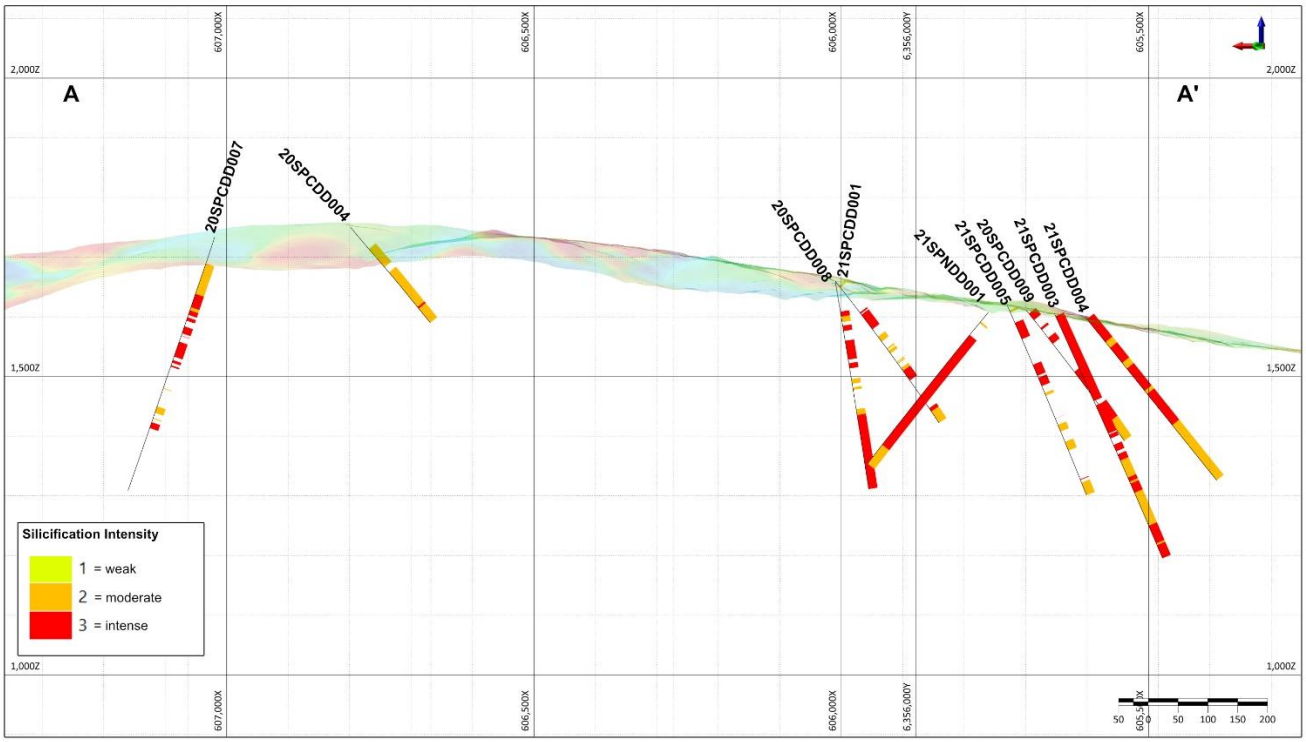

N-S Litholodgy

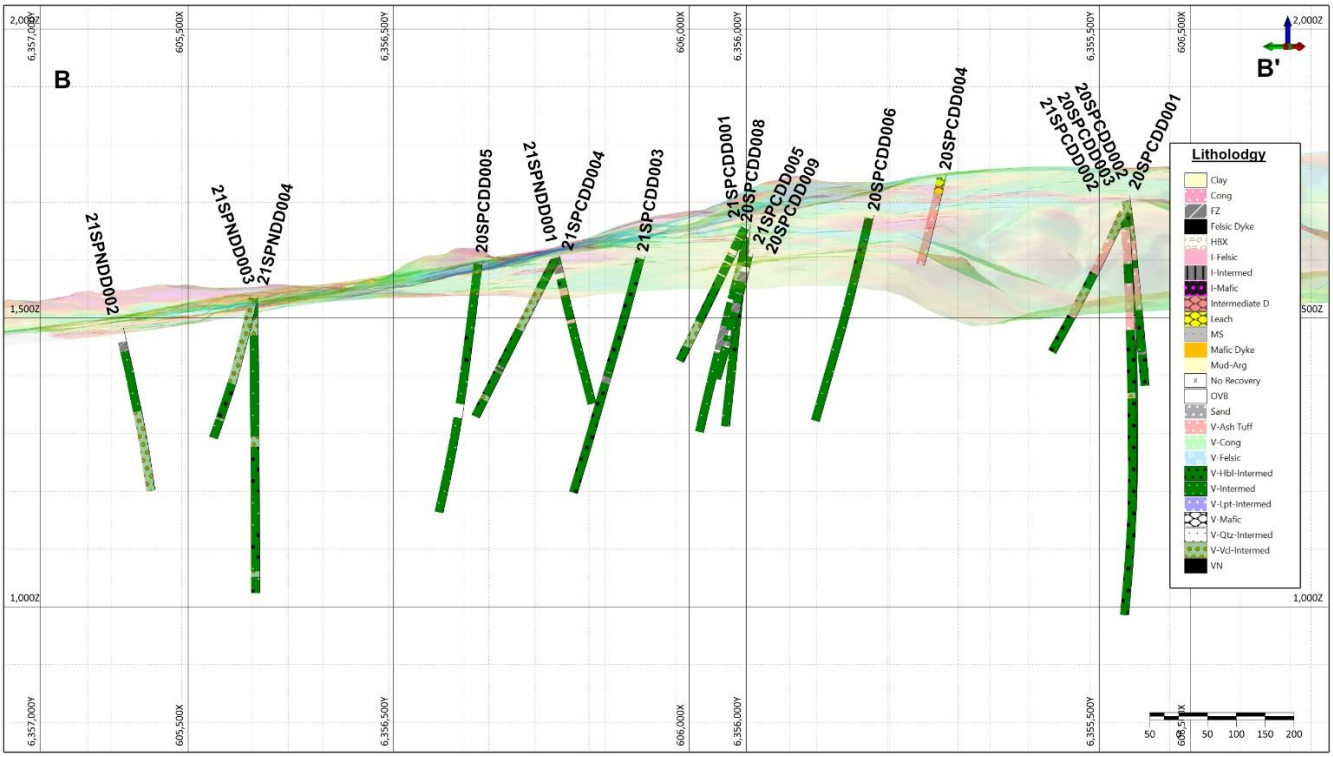

N-S Logged Pyrite

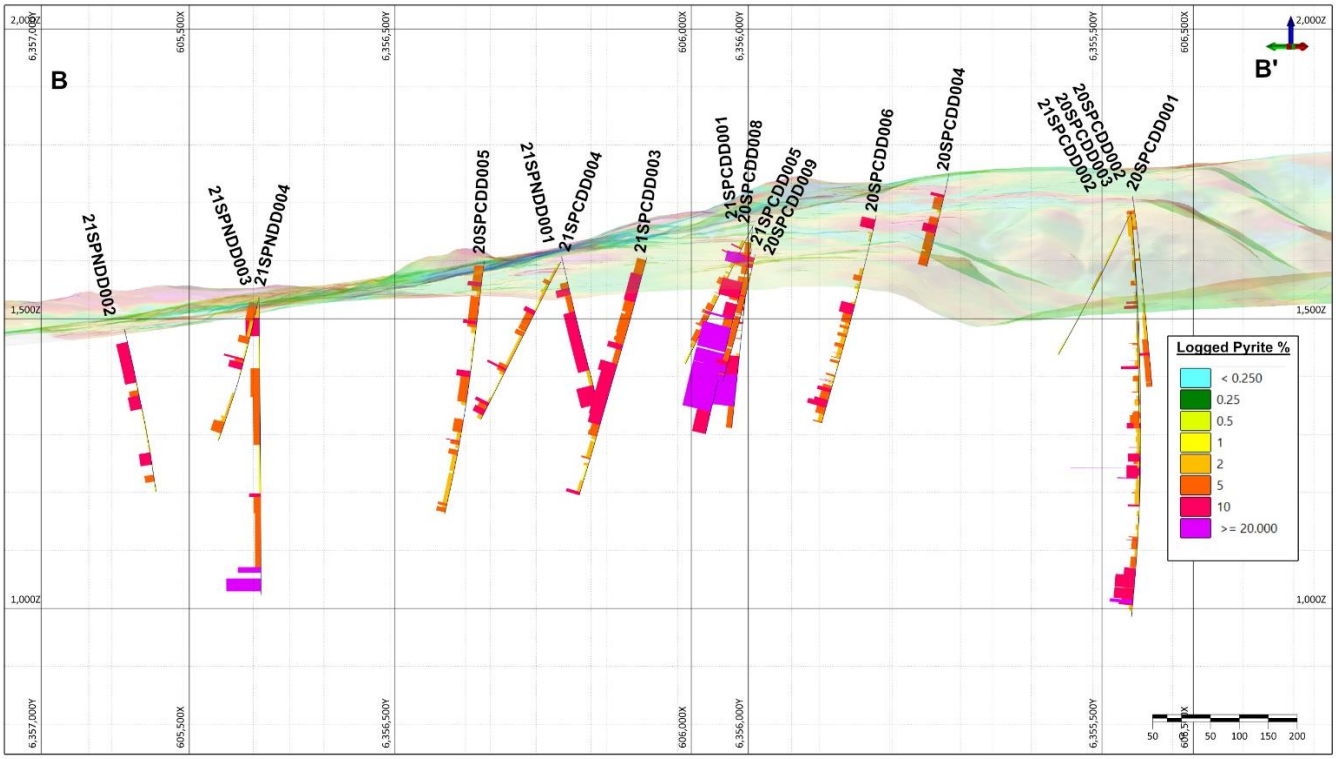

N-S Logged Sericite Intensity

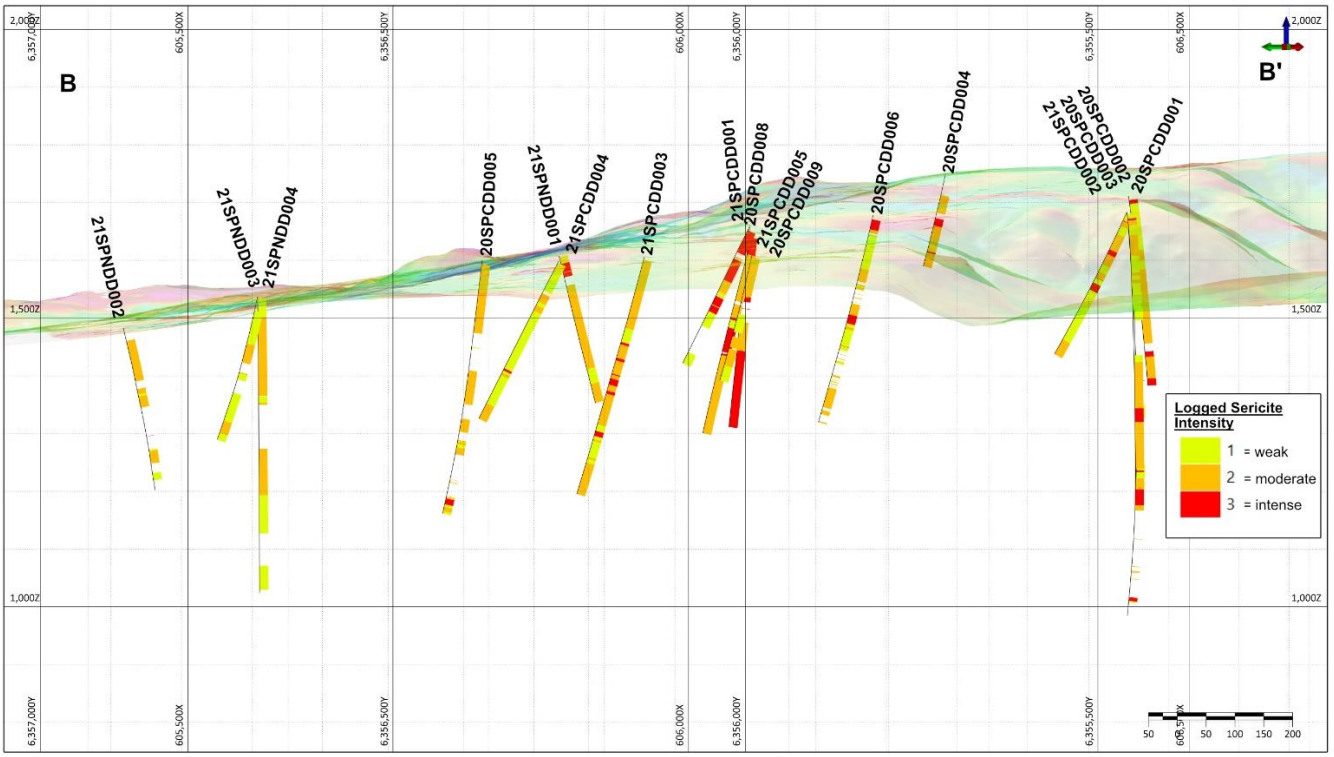

N-S Logged Silicification Intensity

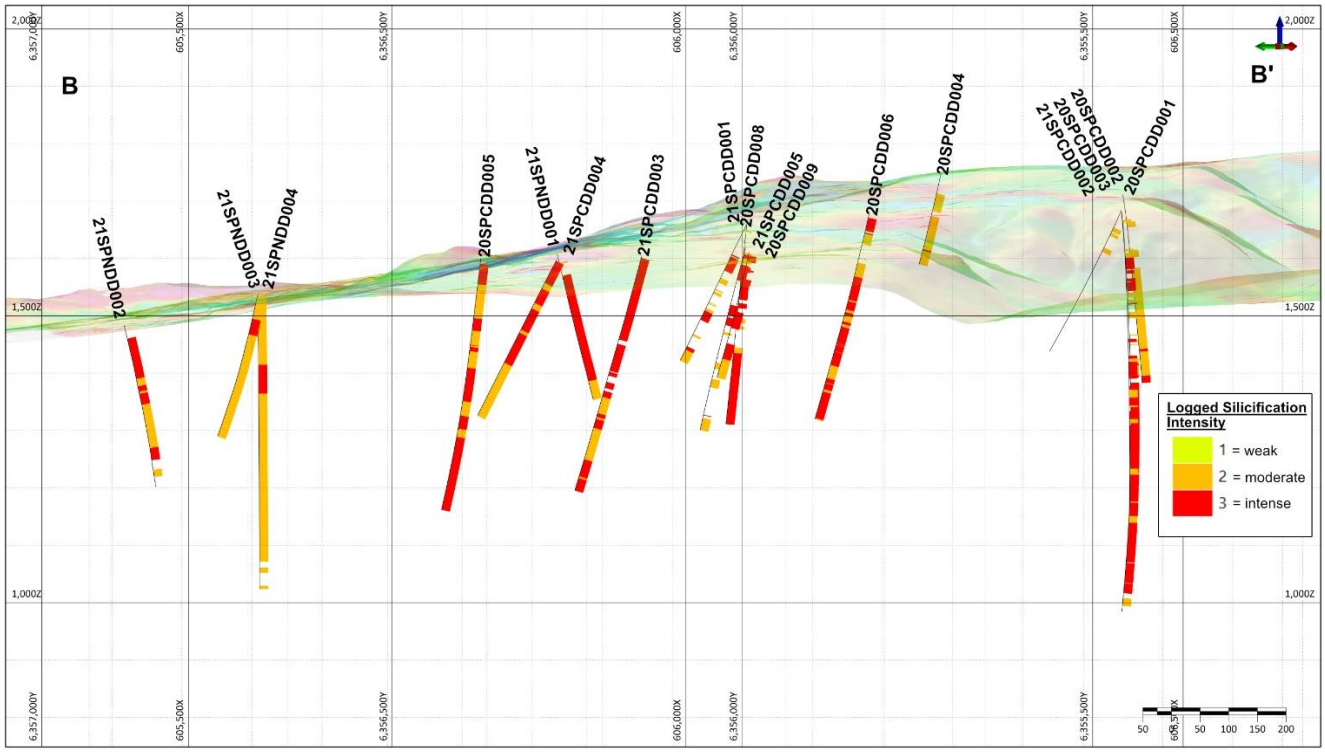

N-S Logged Broad Structure

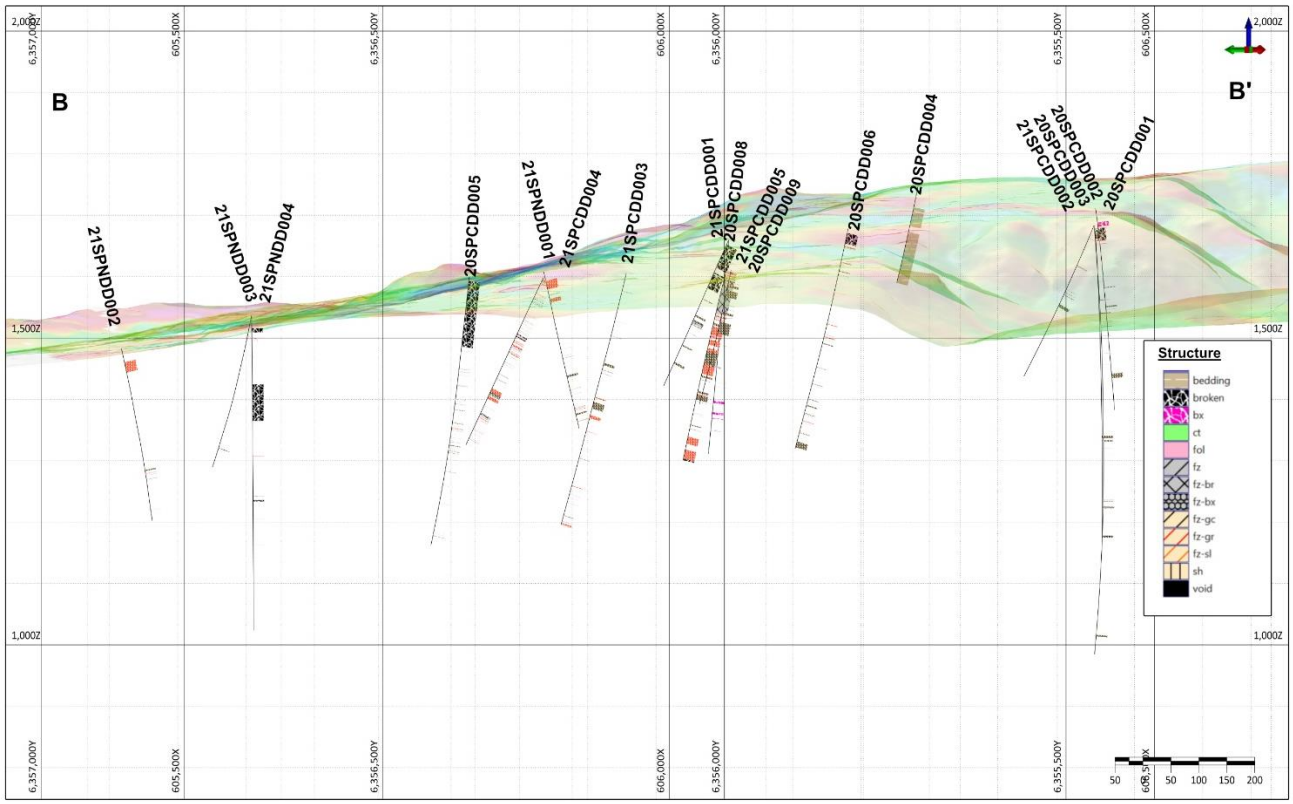

N-S MDRU Porphyry Index

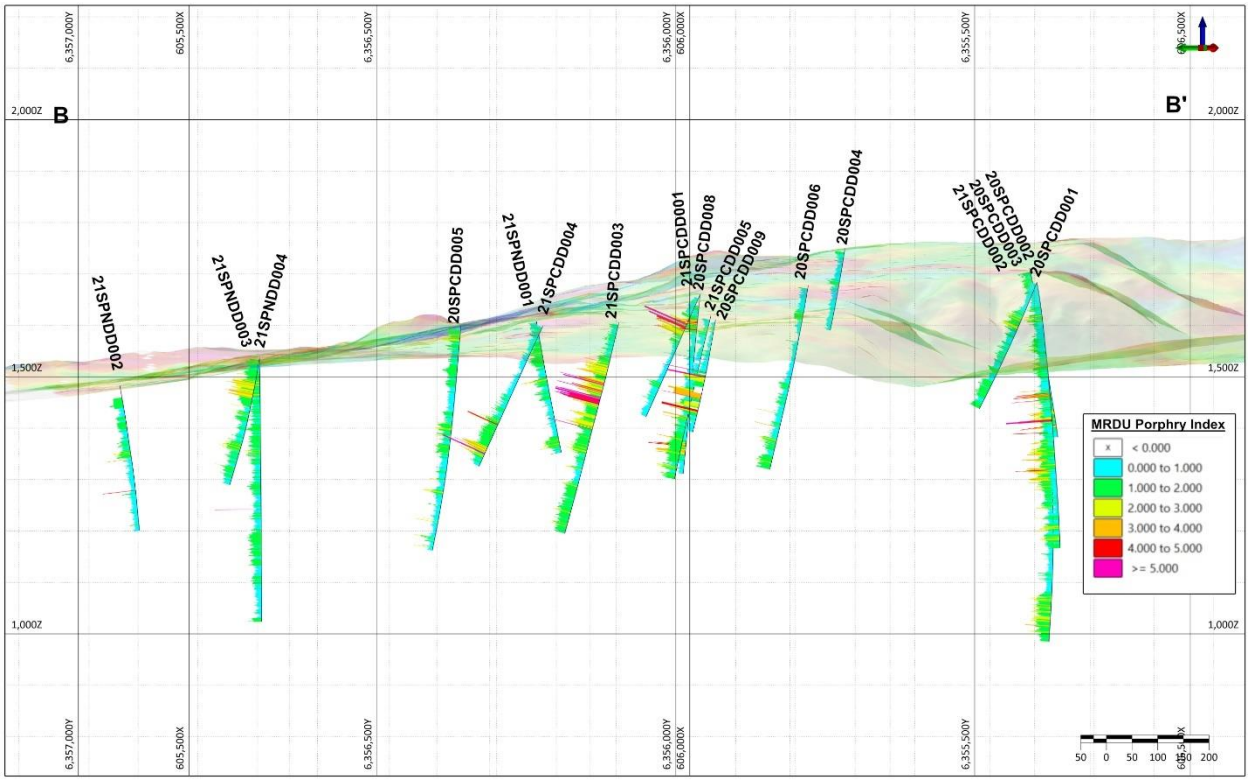

Appendix D: Representative Raman Spectra

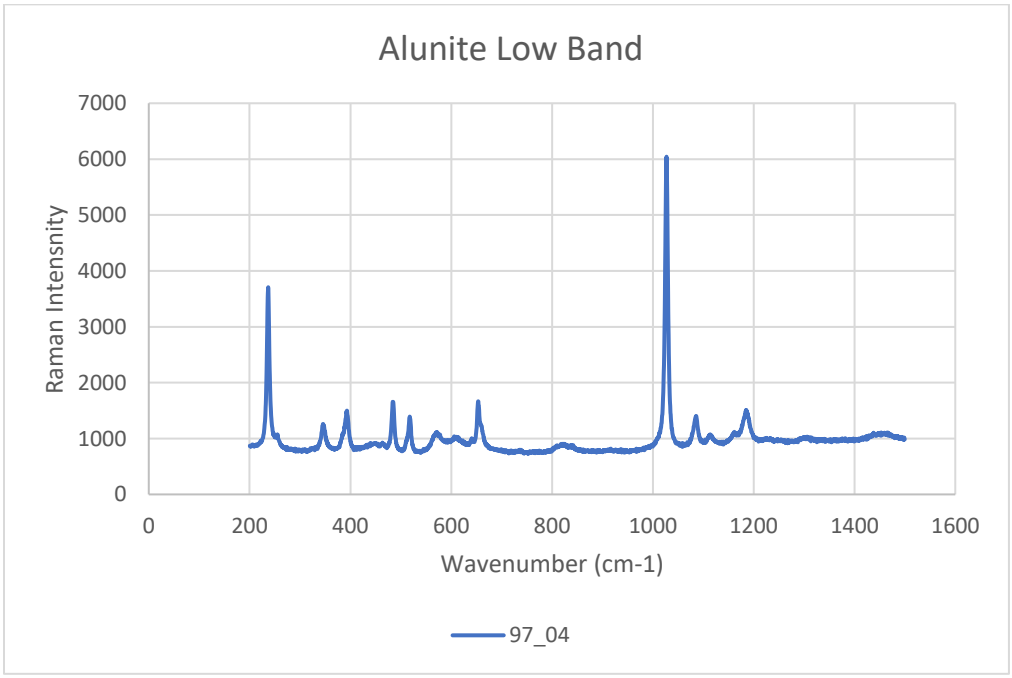

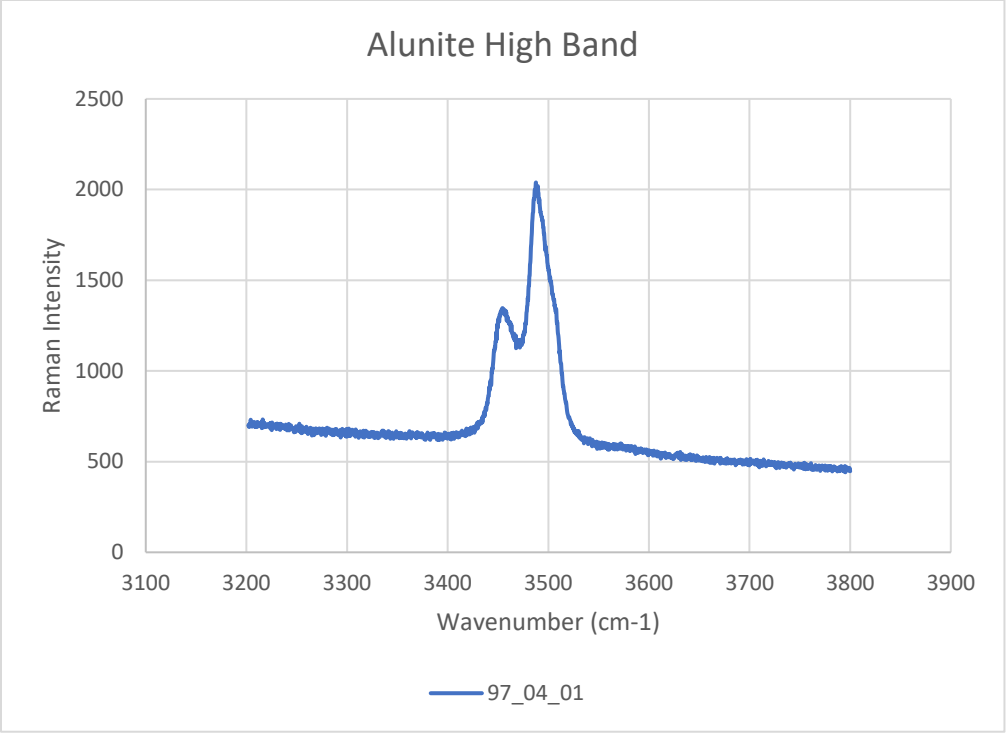
Alunite High Band
Raman Intensity
2500
2000
1500
1000
500
0
3100
3200
3300
3400
3500
3600
3700
3800
3900
Wavenumber (cm-1)
97_04_01

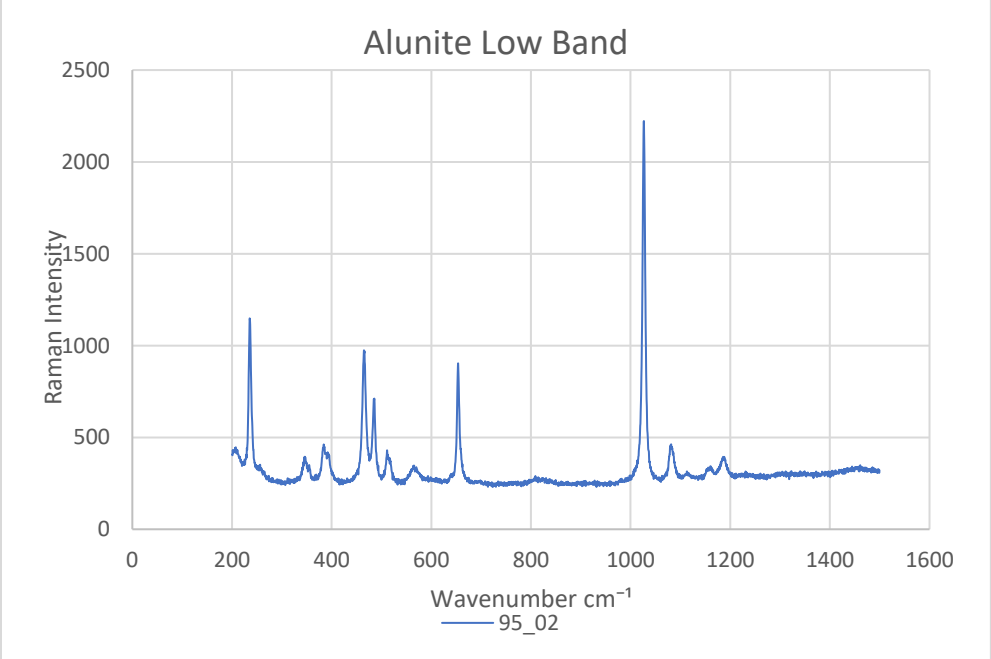
Alunite Low Band
Raman Intensity
2500
2000
1500
1000
500
0
0
200
400
600
800
1000
1200
1400
1600
Wavenumber cm⁻¹
95_02

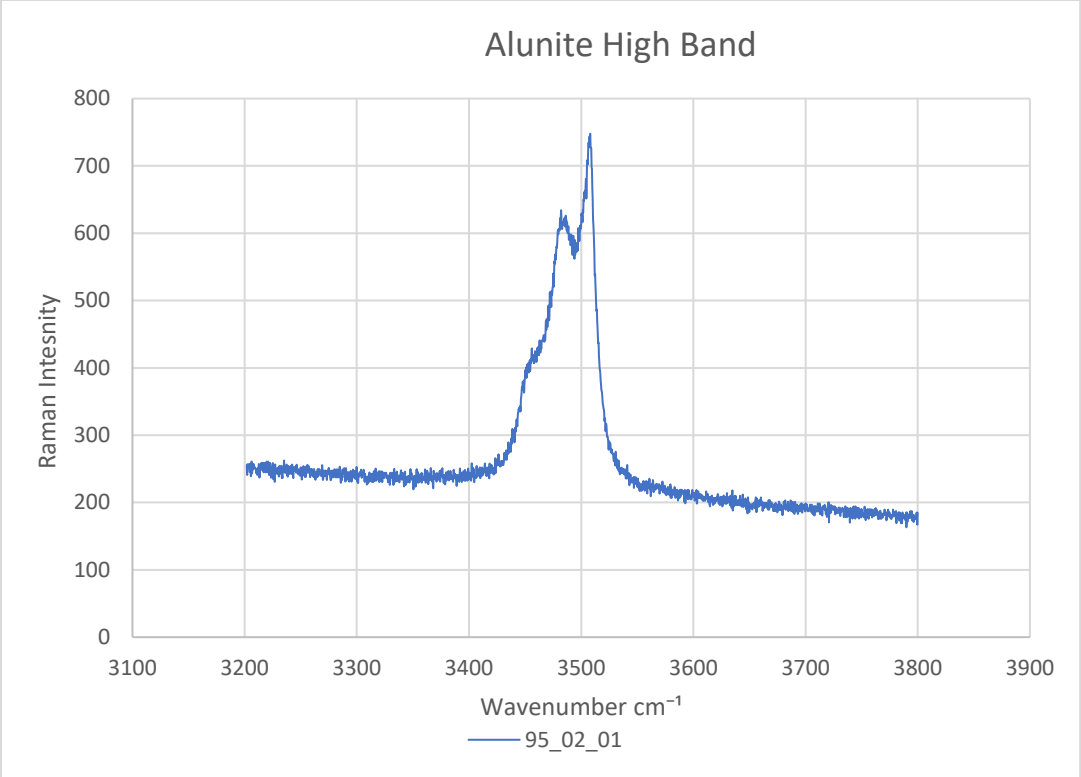
Alunite High Band
Raman Intesnity
800
700
600
500
400
300
200
100
0
3100
3200
3300
3400
3500
3600
3700
3800
3900
Wavenumber cm⁻¹
95_02_01

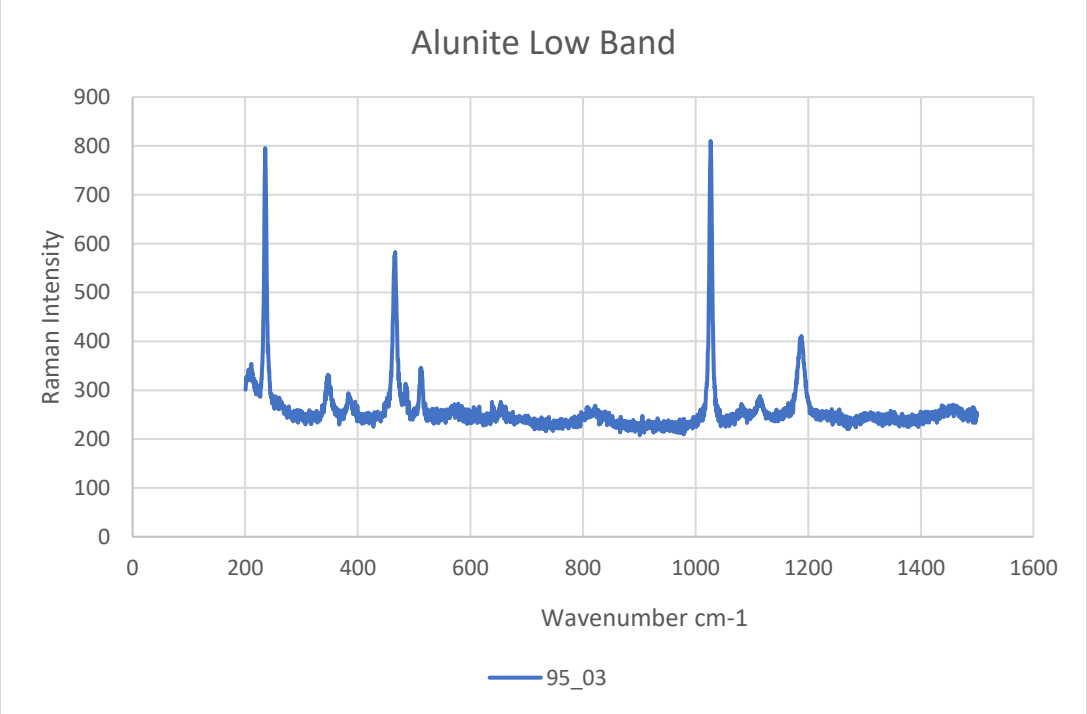
Alunite Low Band
Raman Intensity
900
800
700
600
500
400
300
200
100
0
0
200
400
600
800
1000
1200
1400
1600
Wavenumber cm-1
95_03

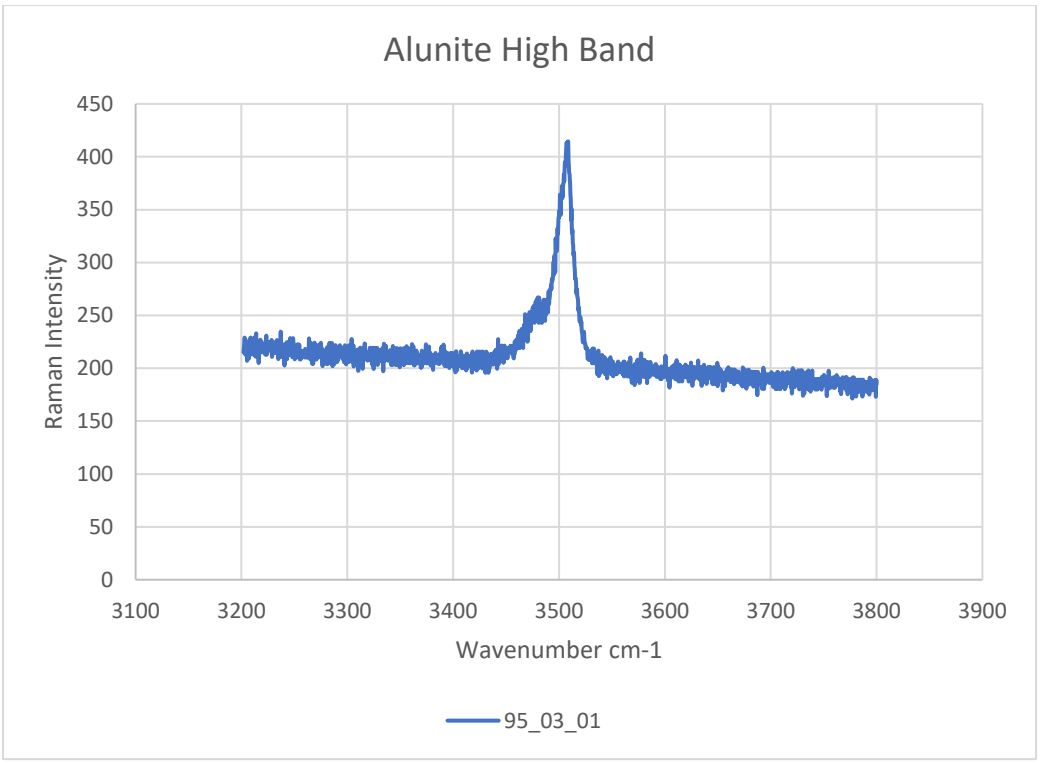
Alunite High Band
Raman Intensity
450
400
350
300
250
200
150
100
50
0
3100
3200
3300
3400
3500
3600
3700
3800
3900
Wavenumber cm-1
95_03_01

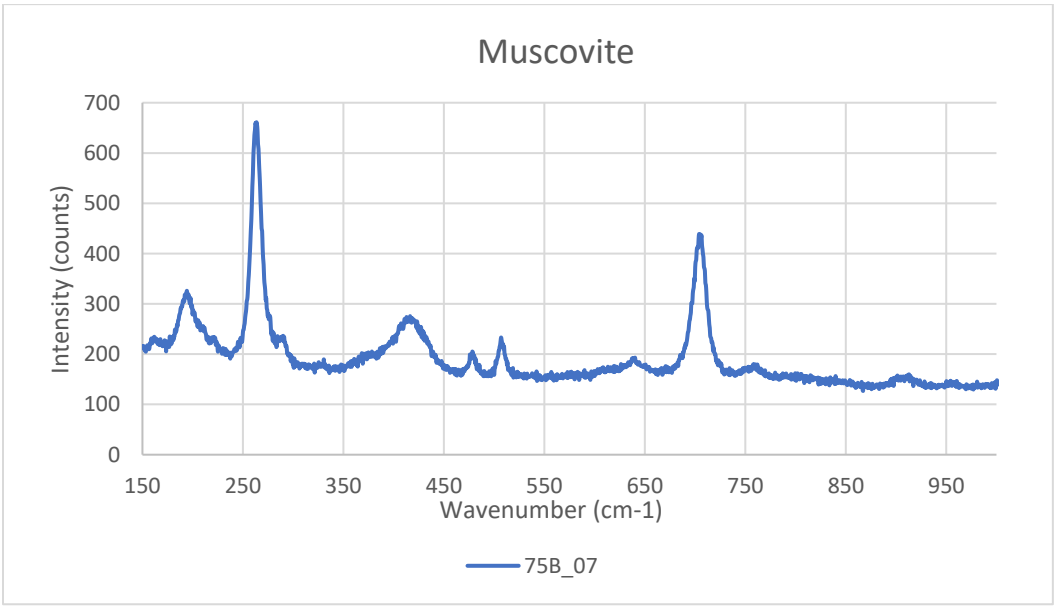
Muscovite
Intensity (counts)
700
600
500
400
300
200
100
0
150
250
350
450
550
650
750
850
950
Wavenumber (cm-1)
75B_07

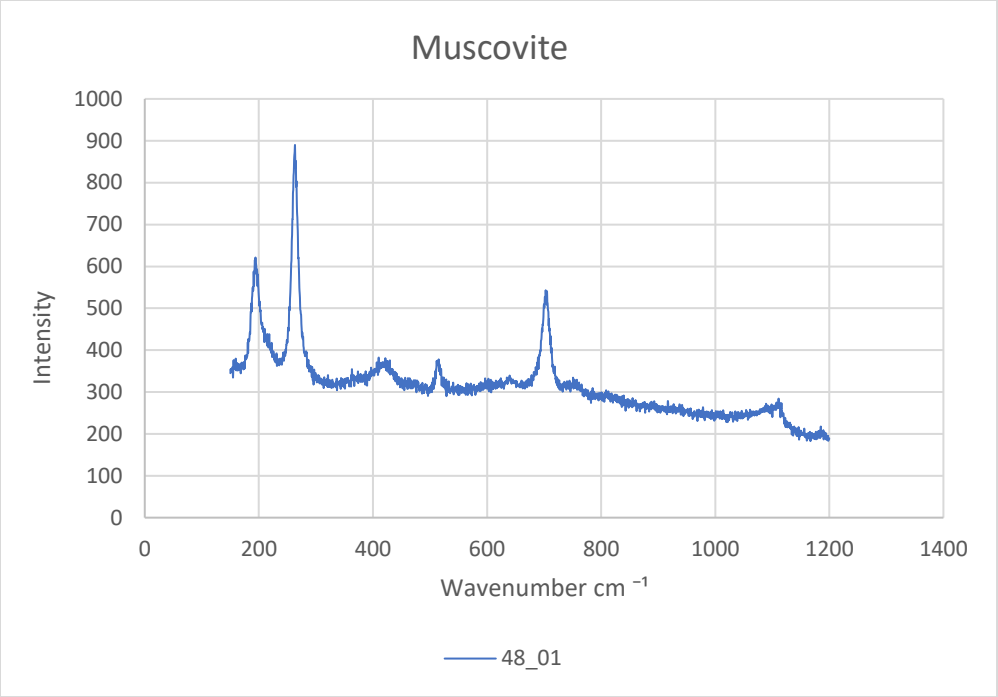
Muscovite
1000
900
800
700
600
500
400
300
200
100
0
Intensity
0
200
400
600
800
1000
1200
1400
Wavenumber cm ⁻¹
48_01

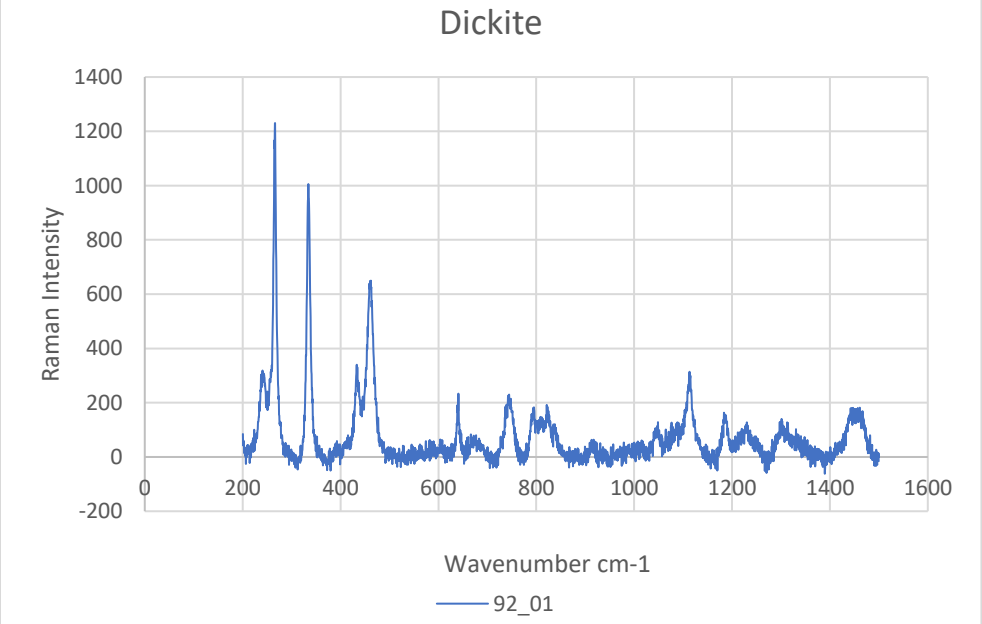
Dickite
1400
1200
1000
800
600
400
200
0
-200
Raman Intensity
0
200
400
600
800
1000
1200
1400
1600
Wavenumber cm-1
92_01

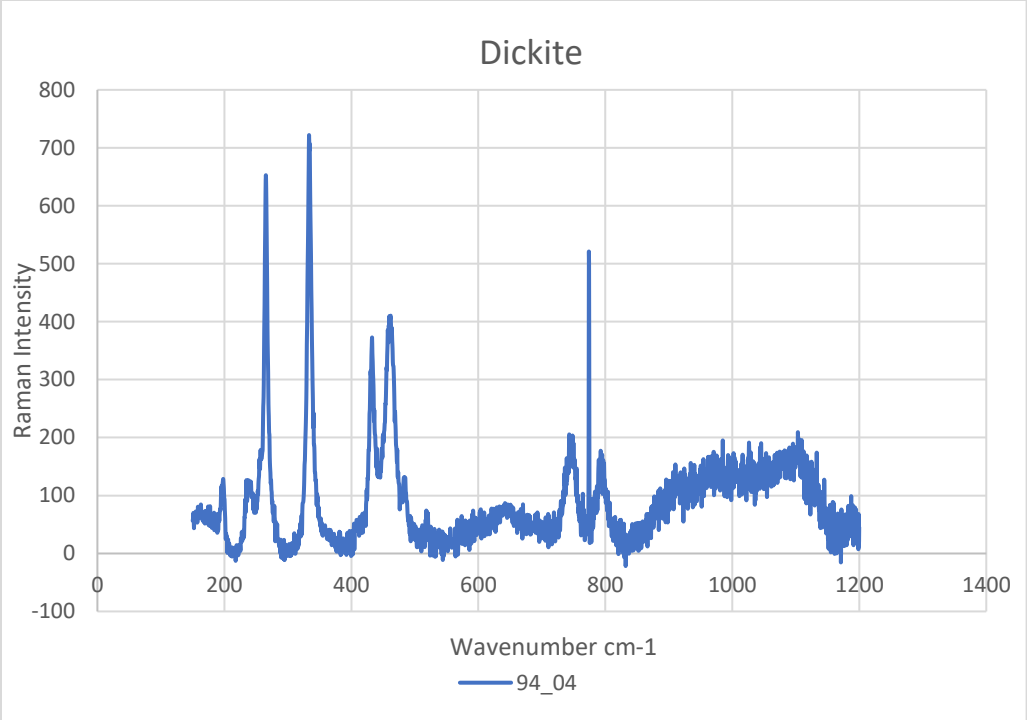
Dickite
800
700
600
500
400
300
200
100
0
-100
Raman Intensity
0
200
400
600
800
1000
1200
1400
Wavenumber cm-1
94_04

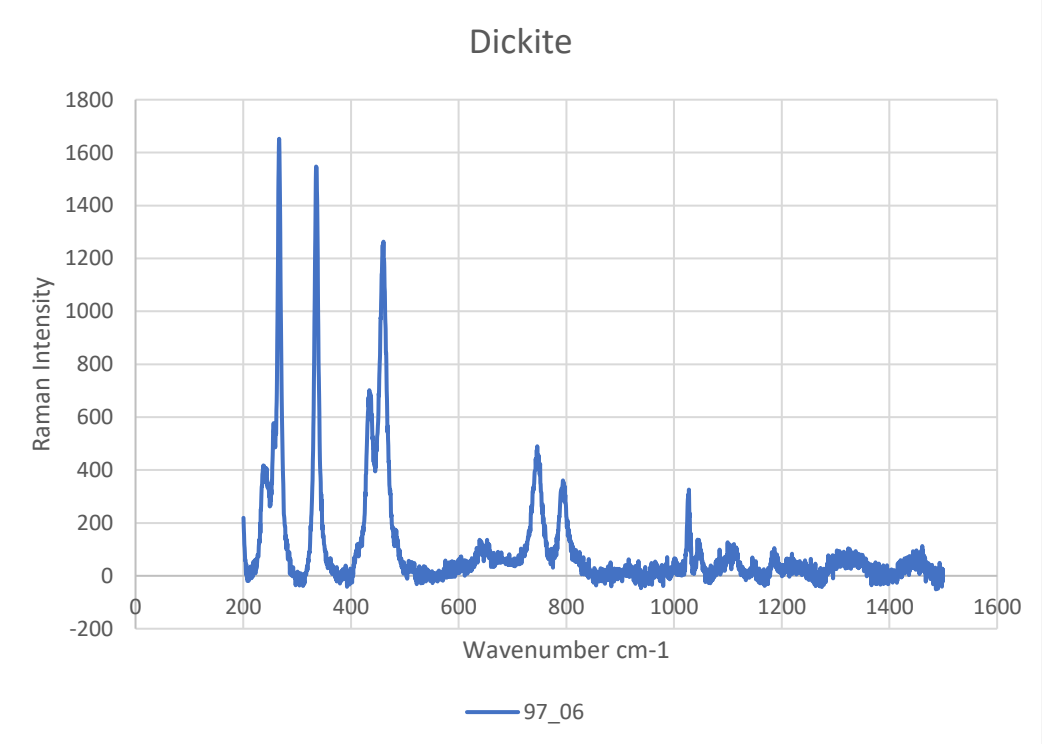
Dickite
1800
1600
1400
1200
1000
800
600
400
200
0
-200
Raman Intensity
0
200
400
600
800
1000
1200
1400
1600
Wavenumber cm-1
97_06

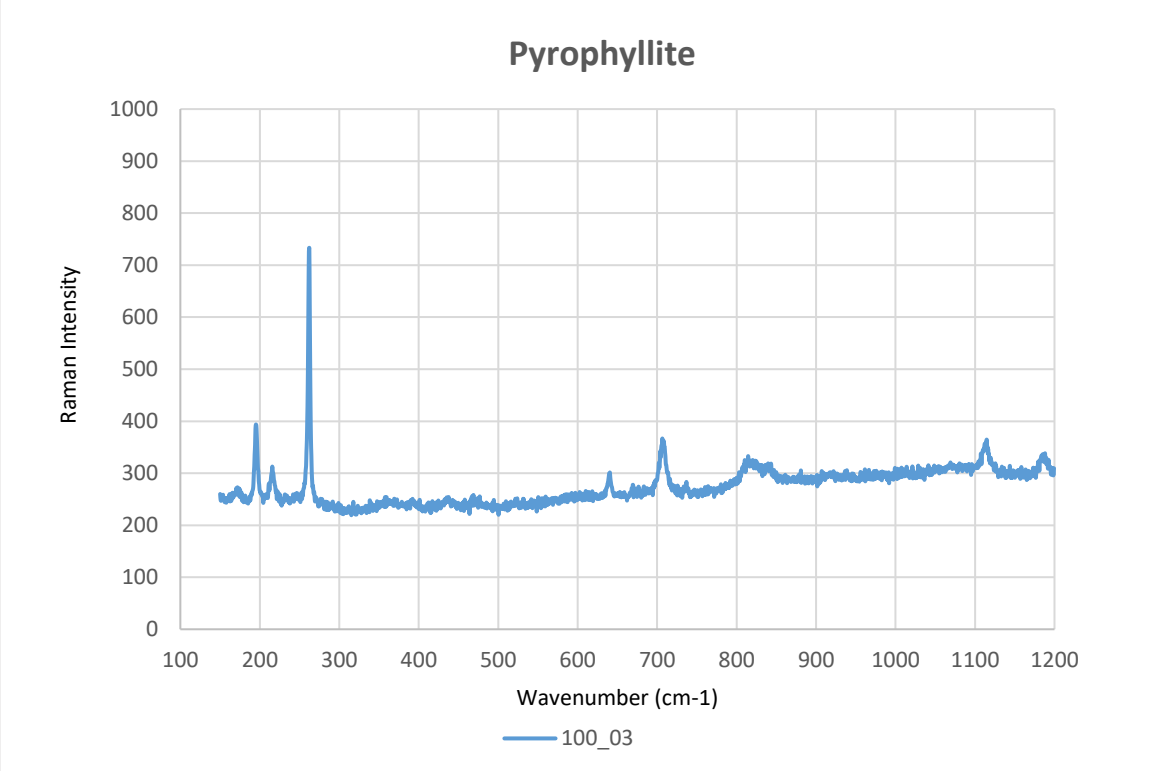
Pyrophyllite
Raman Intensity
1000
900
800
700
600
500
400
300
200
100
0
100
200
300
400
500
600
700
800
900
1000
1100
1200
Wavenumber (cm-1)
100_03

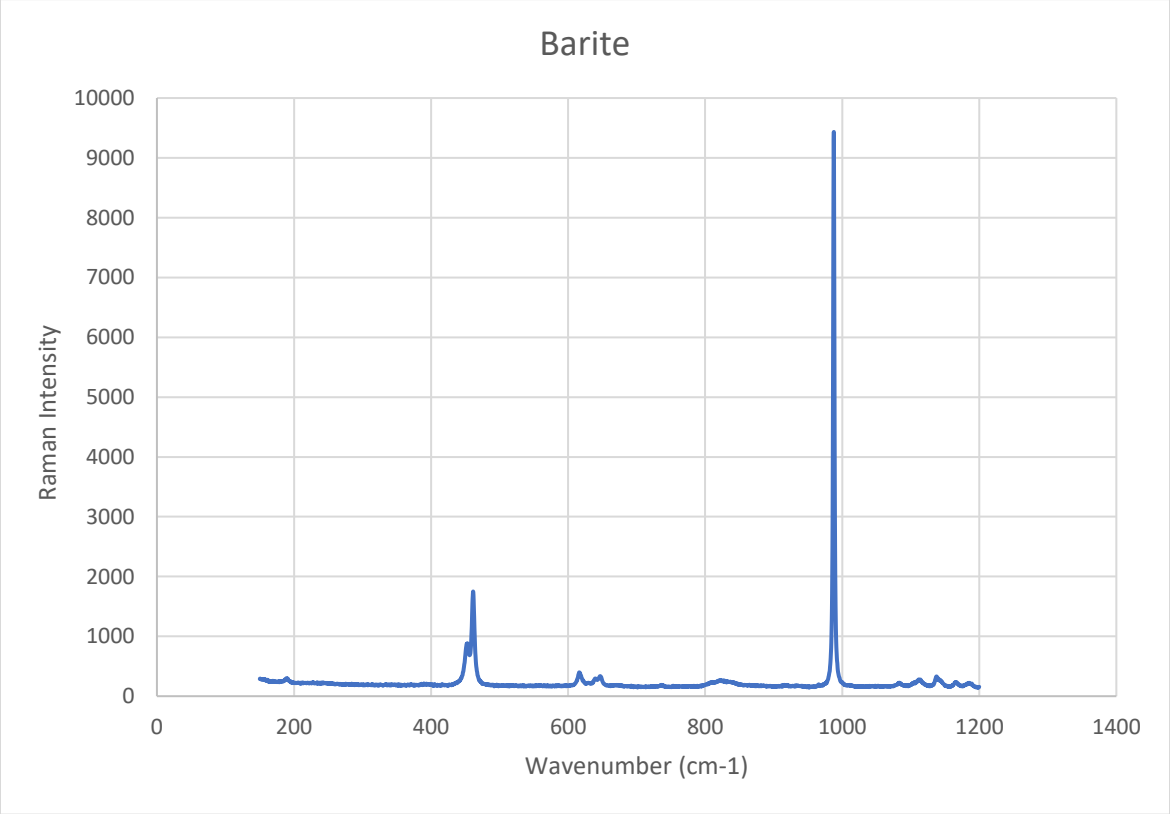
Barite
Raman Intensity
10000
9000
8000
7000
6000
5000
4000
3000
2000
1000
0
0
200
400
600
800
1000
1200
1400
Wavenumber (cm-1)

Appendix E: Raman Multidimensional Arrays

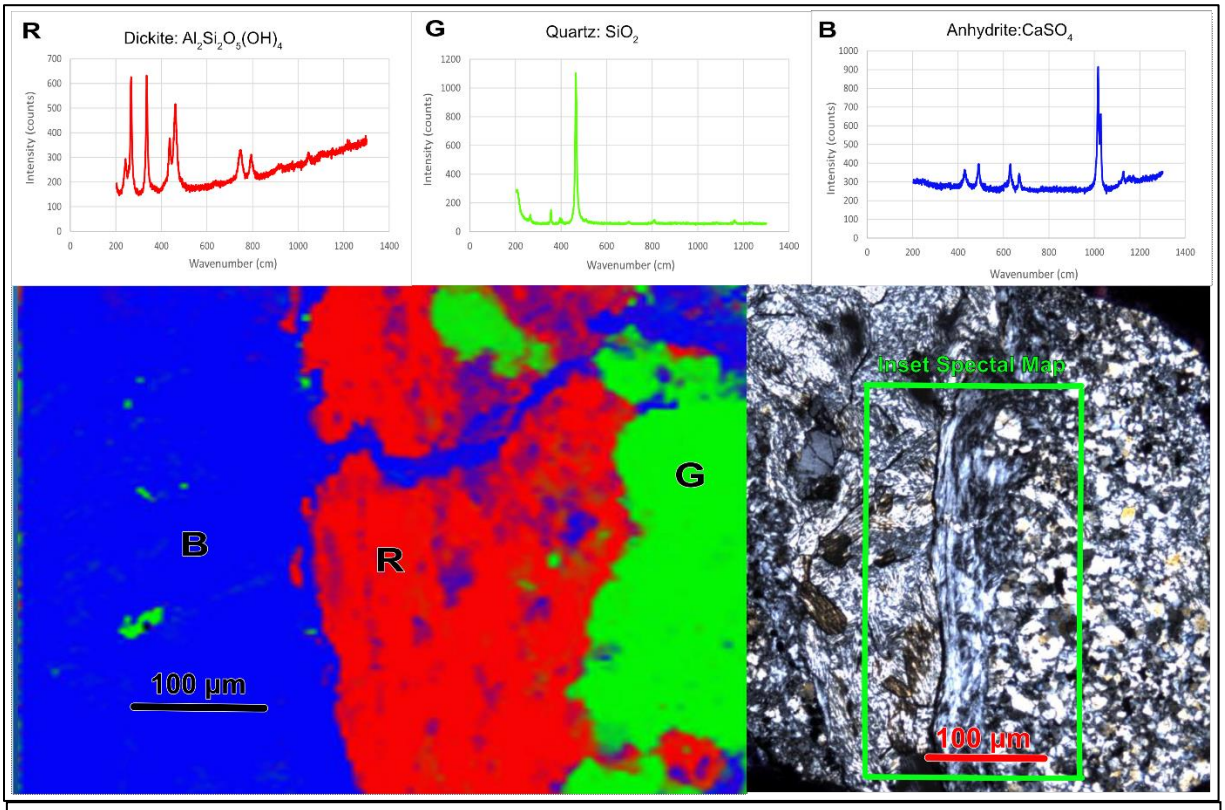

Multidimensional spectral array exhibiting a dickite, quartz, anhydrite assemblage, with late stage anhydrite crosscutting earlier generations of dickite and quartz.

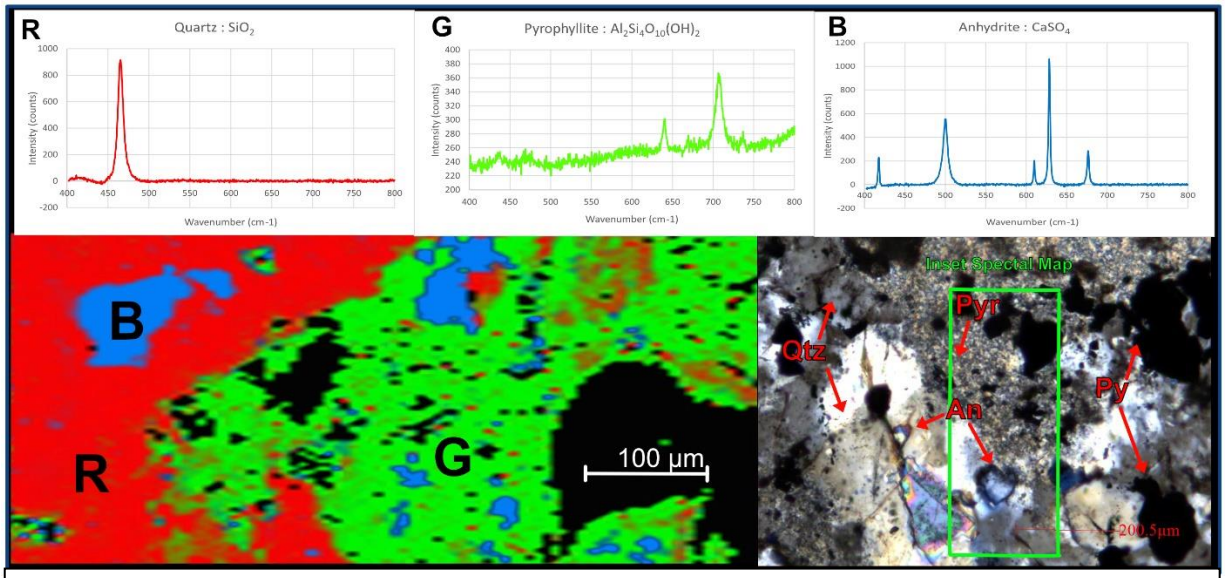

Multidimensional spectral array exhibiting a feldspar phenocryst completely replaced to pyrophyllite, suspended in a quartz rich (silicified) matrix. Anhydrite appears as a late-stage infill(?).

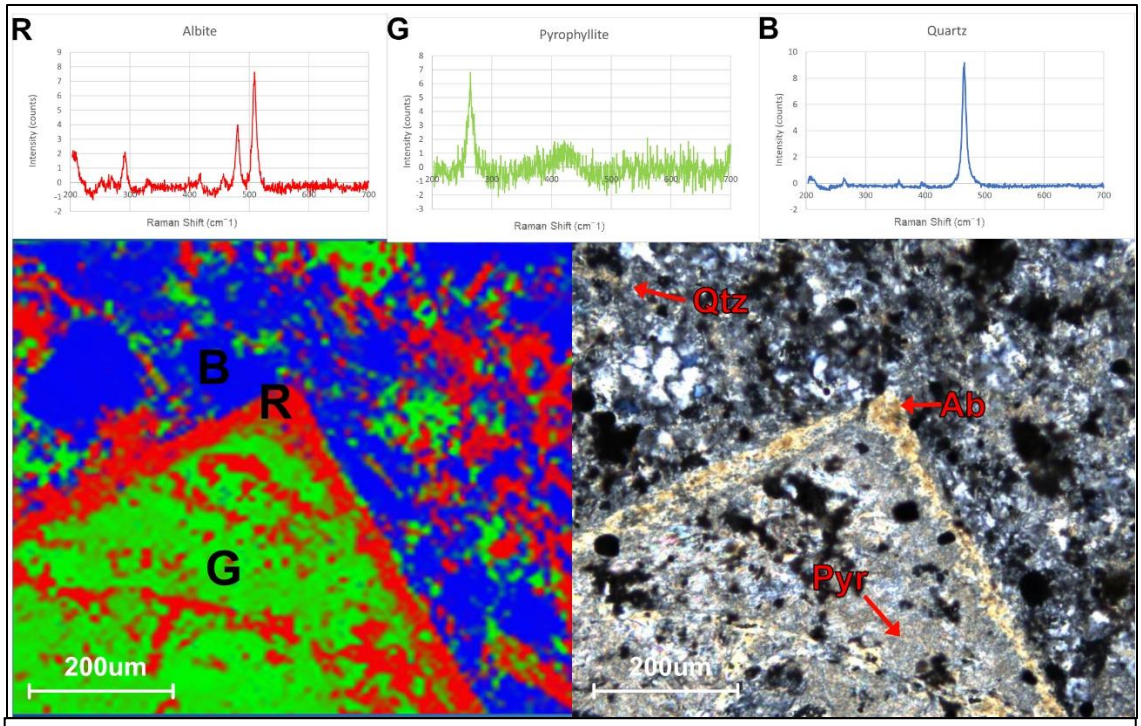

Multidimensional spectral array exhibiting a feldspar phenocryst completely replaced to pyrophyllite, suspended in a quartz rich (silicified) matrix. Albite occurs as an alteration rim surrounding the phenocryst.

Appendix F: Petrography

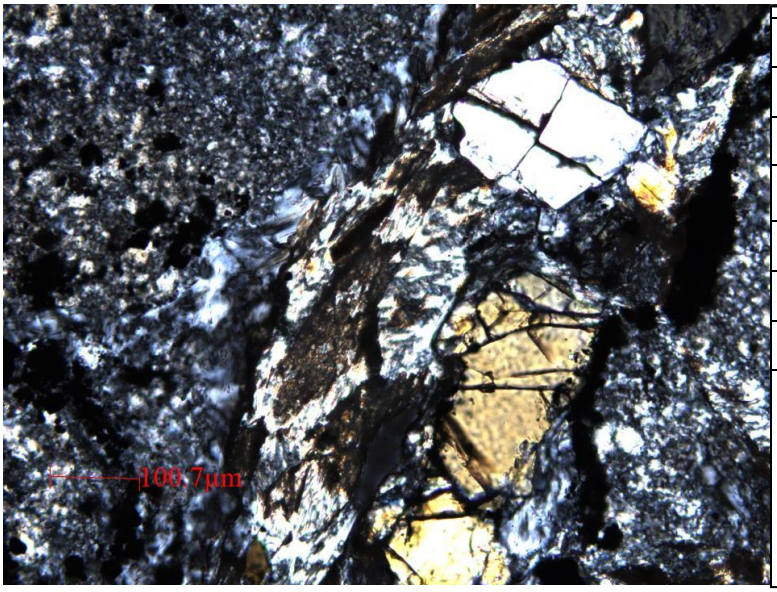

Sample ID	SPC096
Drillhole	20SPCDD009
Depth	242.53 m
Minerals Present	Barite, dickite, gypsum
SWIR Assemblage	Advanced Argillic
Light	XPL
Magnification	10X

Description: Coarse grained barite associated with gypsum vein with fine grained dickite on contact with vein

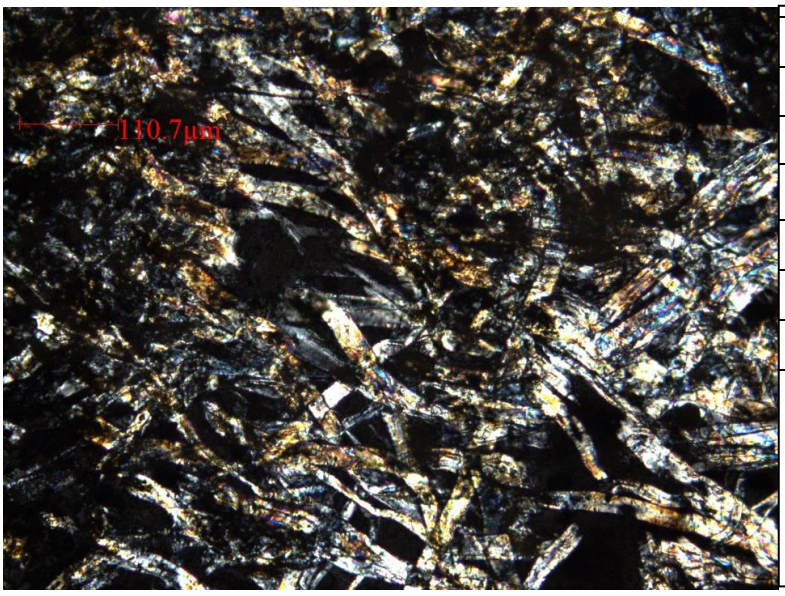

Sample ID	SPC041
Drillhole	20SPCDD004
Depth	133.3 m
Minerals Present	Alunite
SWIR Assemblage	Advanced Argillic
Light	XPL
Magnification	10X

Description: Coarse grained alunite grains.

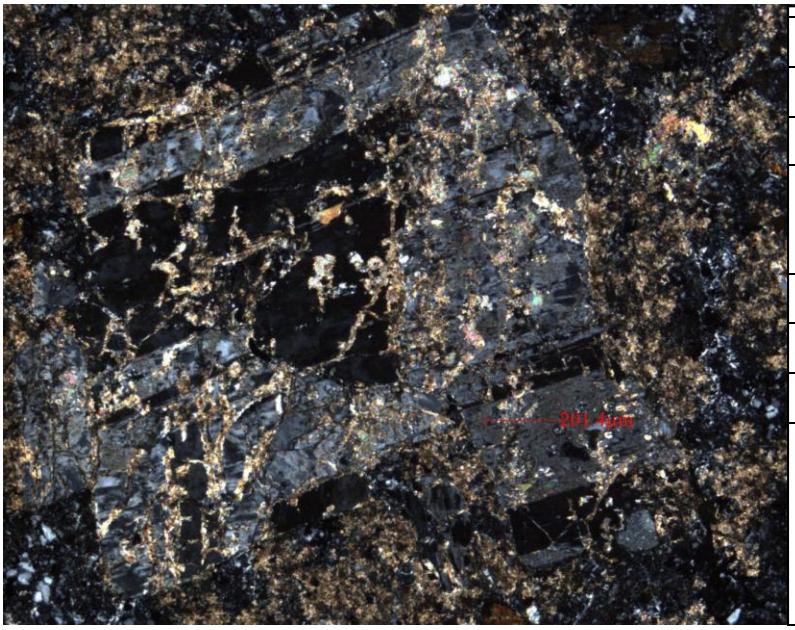

Sample ID	SPC065
Drillhole	20SPCDD007
Depth	161.54 m
Minerals Present	K Feldspar, sericite, dickite, qtz, minor pyrite
SWIR Assemblage	Advanced Argillic
Light	XPL
Magnification	4X

Description: Sericite alteration of felspar phenocryst and of groundmass. Minor dickite (late?) and fine grained quartz in groundmass.

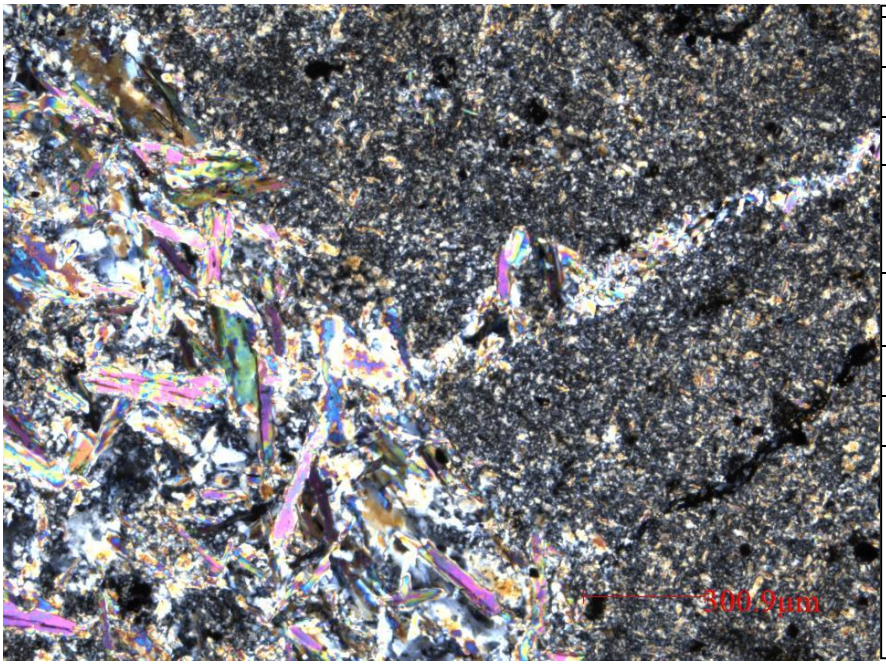

Sample ID	SPC095
Drillhole	20SPCDD009
Depth	234.5 m
Minerals Present	Muscovite, dickite, qtz, sericite, minor pyrite
SWIR Assemblage	Advanced Argillic
Light	XPL
Magnification	10X

Description: Feldspar phenocryst replaced by coarse grained muscovite. Fine grained dickite, sericite, qtz and minor pyrite in groundmass

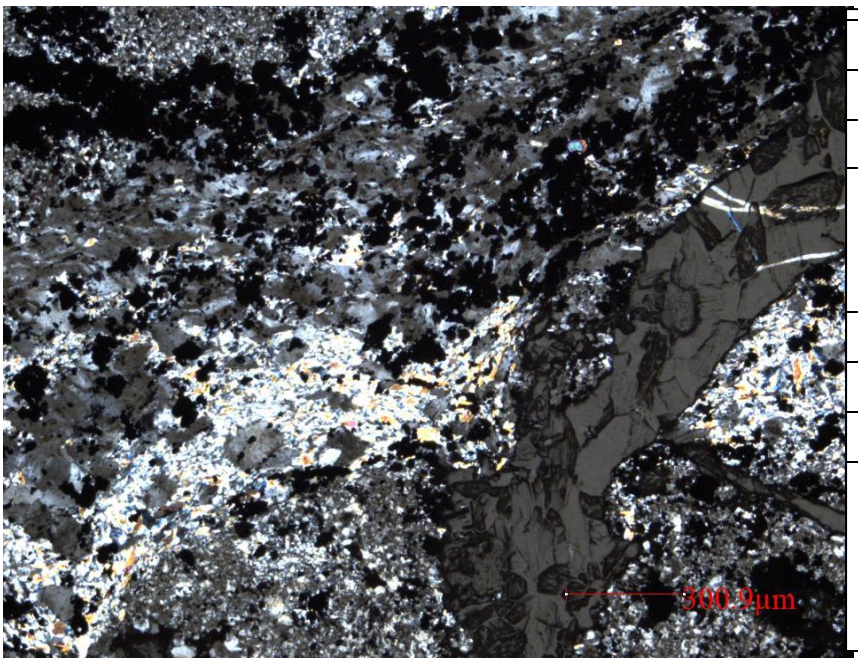

Sample ID	SPC097
Drillhole	20SPCDD009
Depth	244.05
Minerals Present	alunite, dickite, pyrite, gypusm, minor pyrophyllite, , minor quartz
Assemblage	Advanced Argillic
Light	XPL
Magnificiation	4X

Description: Bands of alunite, dickite and pyrite crosscut by a gypsum vein. Minor pyrophyllite and quartz in the groundmass.

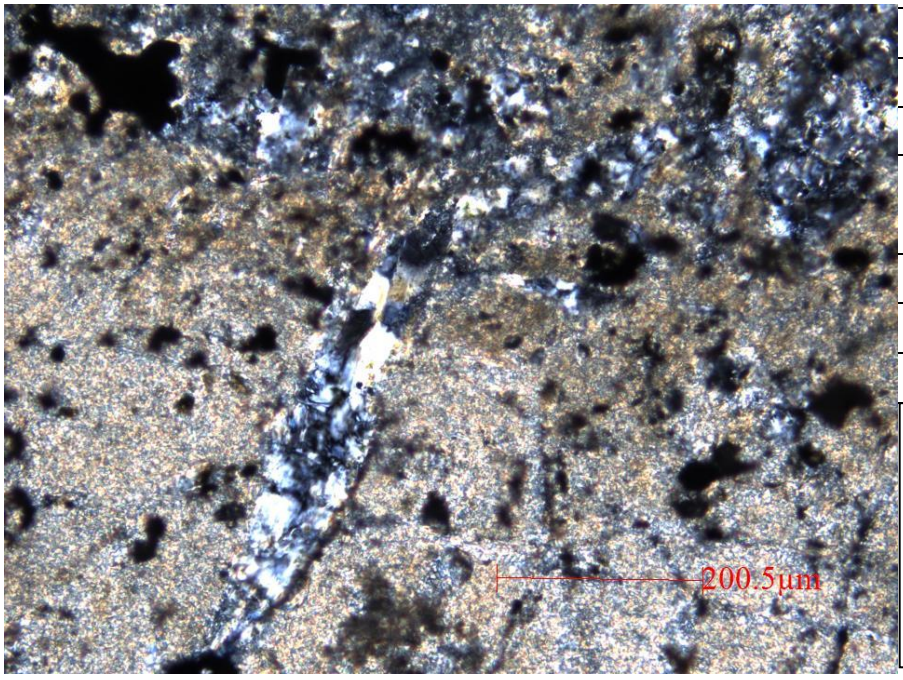

Sample ID	SPC101
Drillhole	20SPCDD009
Depth	262.60
Minerals Present	pyrophyllite, dickite, pyrite, minor quartz
Assemblage	Advanced Argillic
Light	XPL
Magnificiation	10X

Description: Feldspar phenocryst altered to pyrophyllite with dickite vein crosscutting phenocryst and groundmass. Pyrite in groundmass and phenocryst and minor fine grained qtz in groundmass

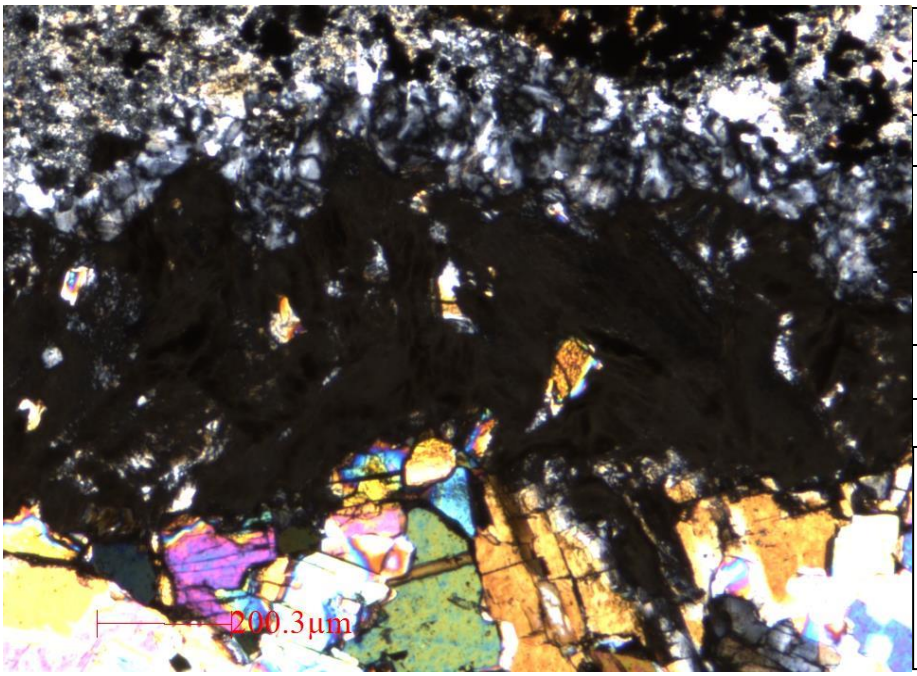

Sample ID	SPC103A
Drillhole	20SPCDD009
Depth	267.54 m
Minerals Present	dickite, gypsum, calcite, pyrite
SWIR Assemblage	Advanced Argillic
Light	XPL
Magnificiation	4X

Description: Gypsum vein associated with dickite. Late stage (?) calcite infill. Pyrite occurs in highly altered groundmass.

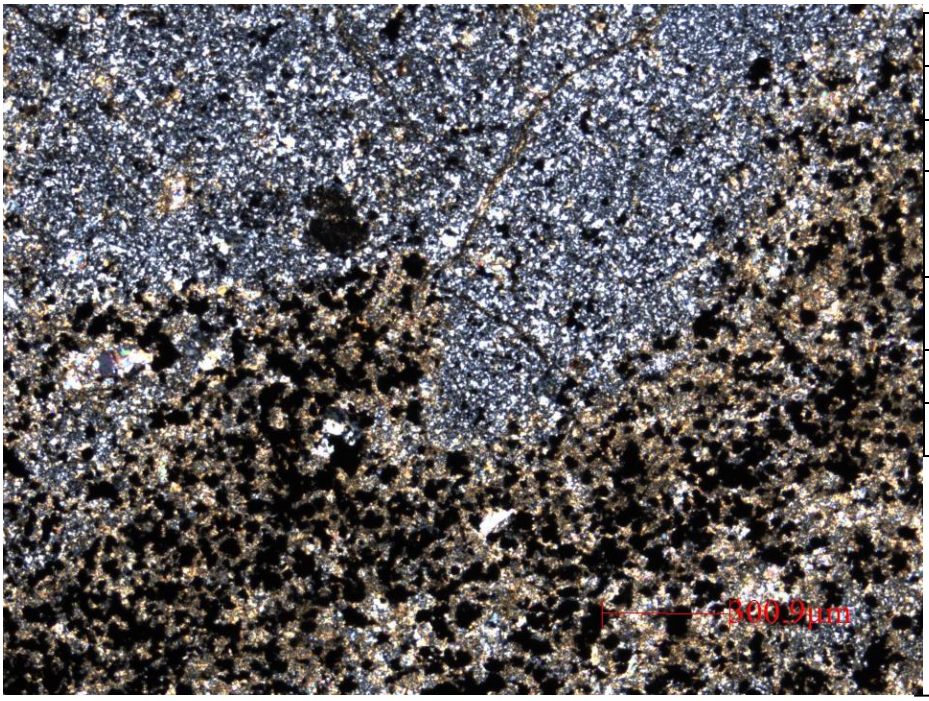

Sample ID	SPC104A
Drillhole	20SPCDD009
Depth	272.3 m
Minerals Present	dickite, pyrite, sericite/muscovite
SWIR Assemblage	Advanced Argillic
Light	XPL
Magnificiation	4X

Description: Dominantly fine grained dickite (alteration front?) in contact with highly sulphidized (pyrite) and sericitized (muscovite?) groundmass.

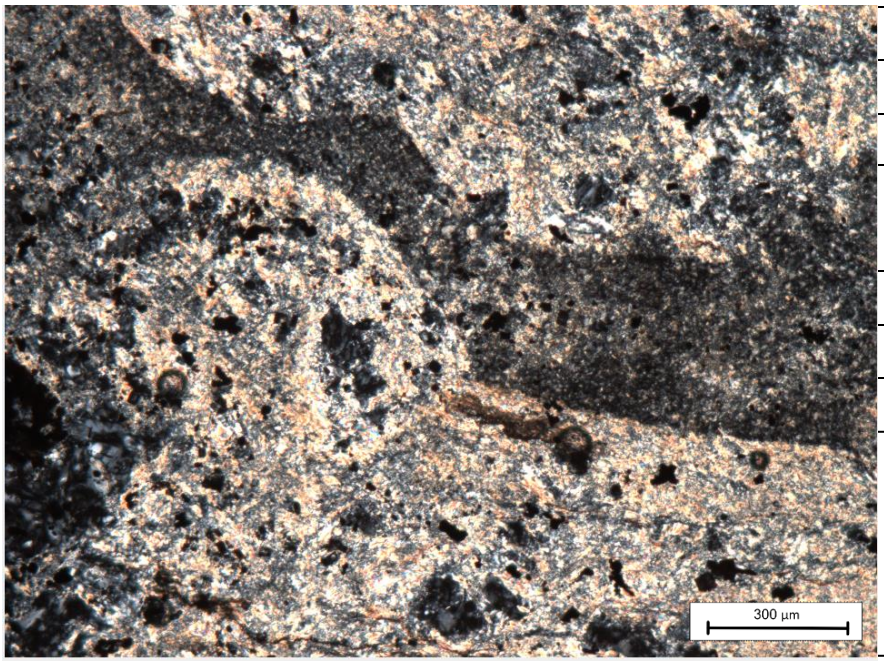

Sample ID	SPC104A
Drillhole	20SPCDD009
Depth	260.62 m
Minerals Present	Pyrophyllite, dickite, pyrite,
SWIR Assemblage	Advanced Argillic
Light	XPL
Magnificiation	4X

Description: Feldspar phenocrysts completely altered to pyrophyllite within intensely sericitized groundmass with minor dickite and pyrite.

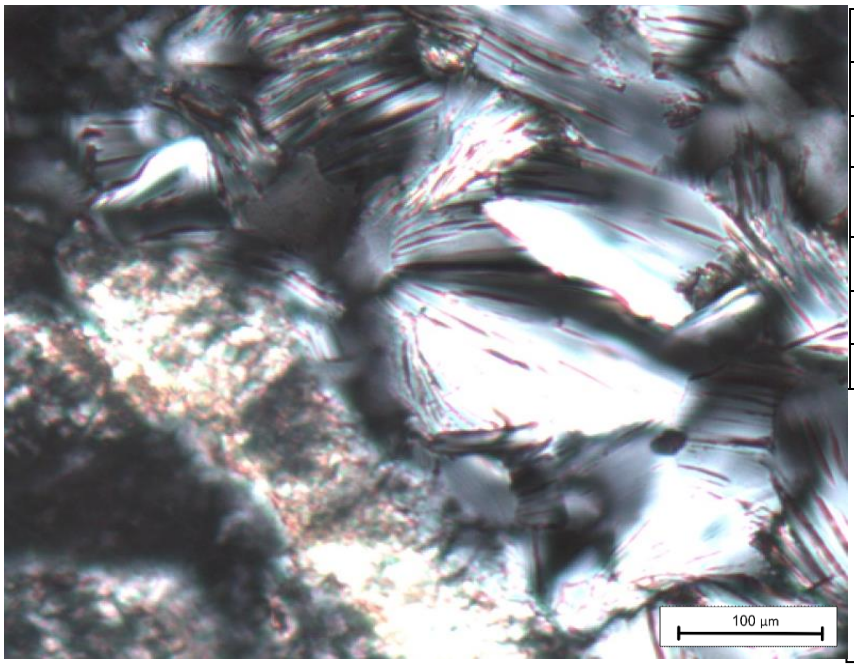

Sample ID	SPC036
Drillhole	20SPCDD004
Depth	54.9 m
Minerals Present	Dickite
SWIR Assemblage	Advanced Argillic
Light	XPL
Magnificiation	20X

Description: Platy dickite occuring as vein/vein selvage within a broader section of dickite-sericite cement.

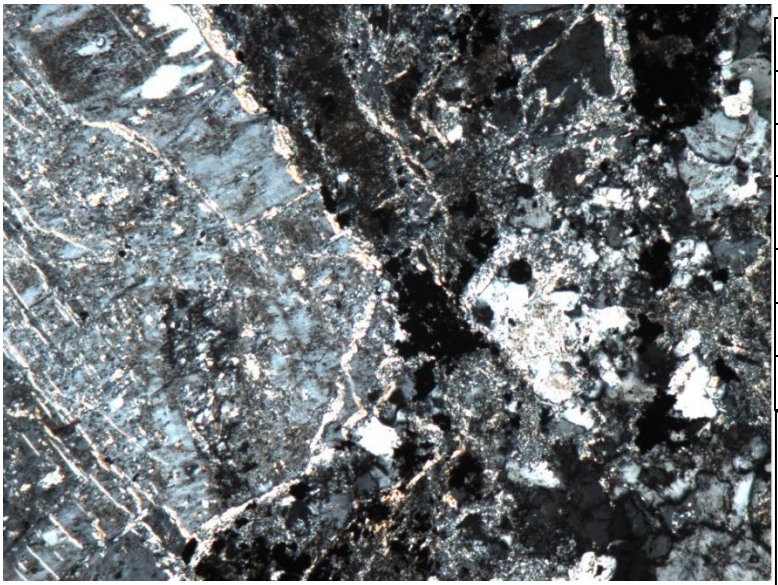

Sample ID	SPC073
Drillhole	20SPCDD007
Depth	44.75 m
Minerals Present	Kspar, illite, pyrite, quartz
SWIR Assemblage	Argillic
Light	XPL
Magnificiation	10X

Description: Altered feldspar within illite, pyrite, quartz dominant groundmass.

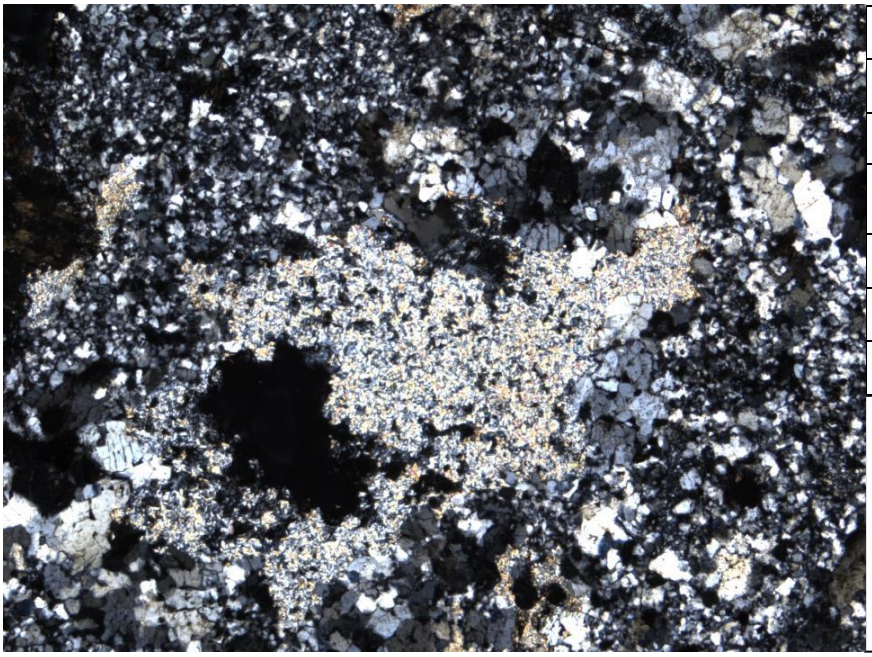

Sample ID	SPC046
Drillhole	20SPCDD005
Depth	352.88 m
Minerals Present	quartz, illite, pyrite
SWIR Assemblage	Argillic
Light	XPL
Magnificiation	10X

Description: highly silicified groundmass composed of quartz, illite, pyrite and highly altered feldspar.

Appendix G: ASTER SWIR

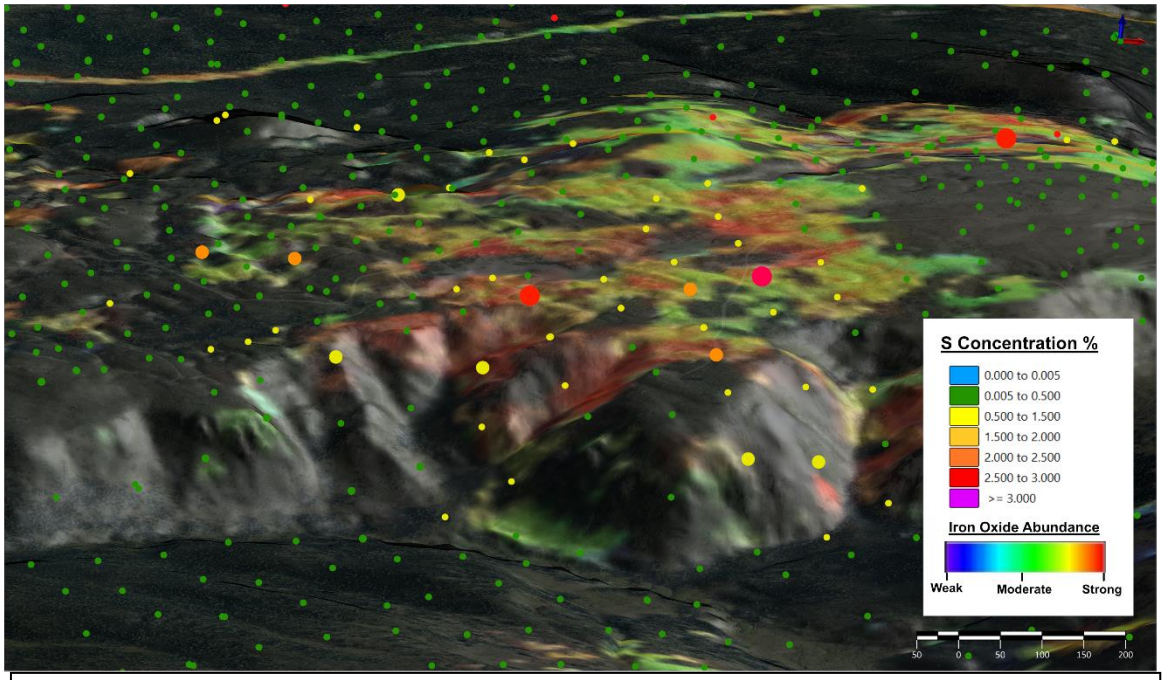

Orthogonal view of the Silver Pond prospect displayed with ASTER SWIR data, indicating a high abundance of iron oxides at surface that coincides with elevated concentrations of sulfur.

Appendix H: Hyperspectral Core Scans

Alunite-Jarosite-Pyrophyllite

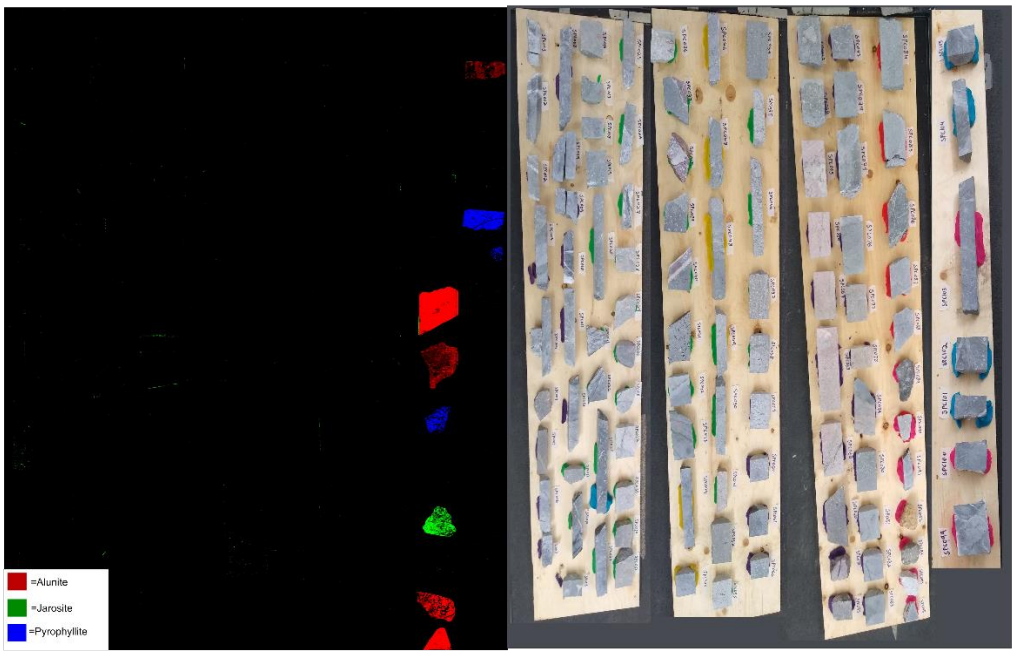

Chlorite # Mg Content

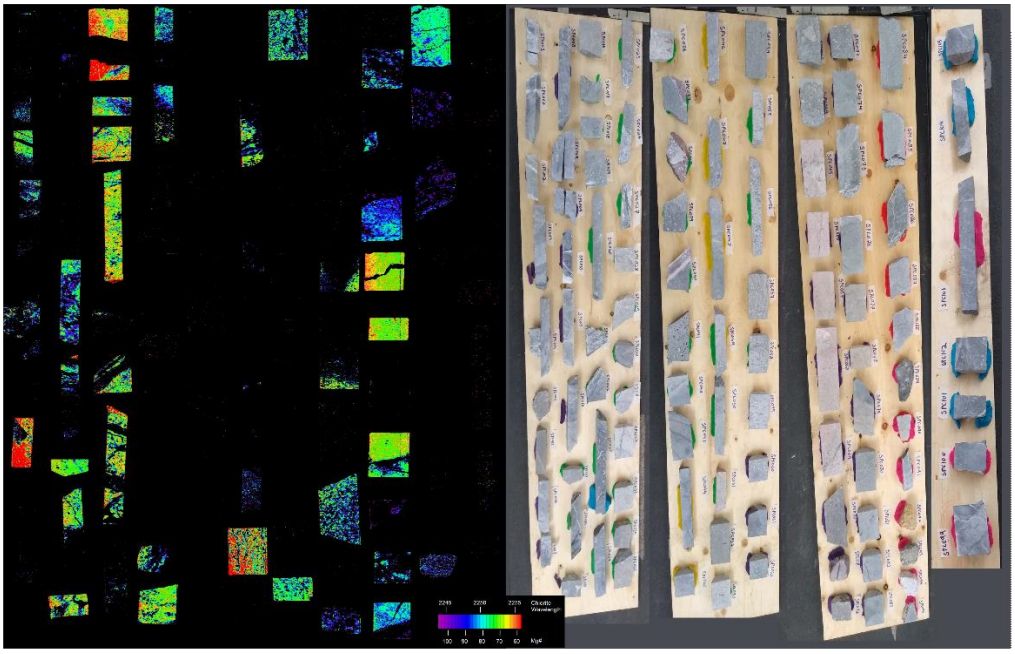

Gypsum-Paragonite-Calcite

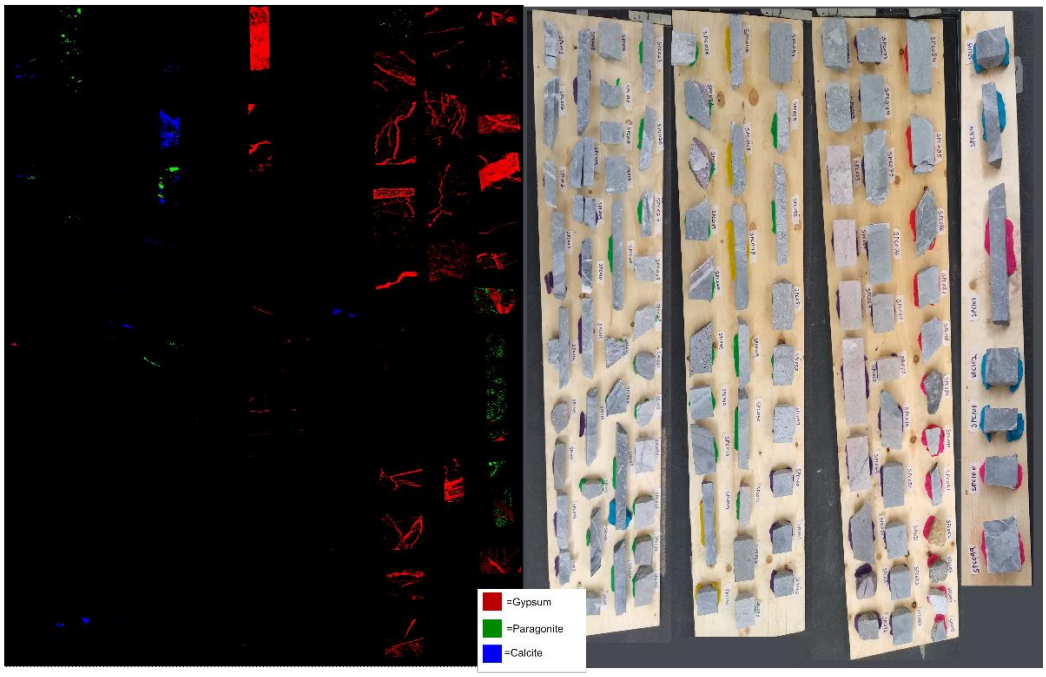

Water Absorption

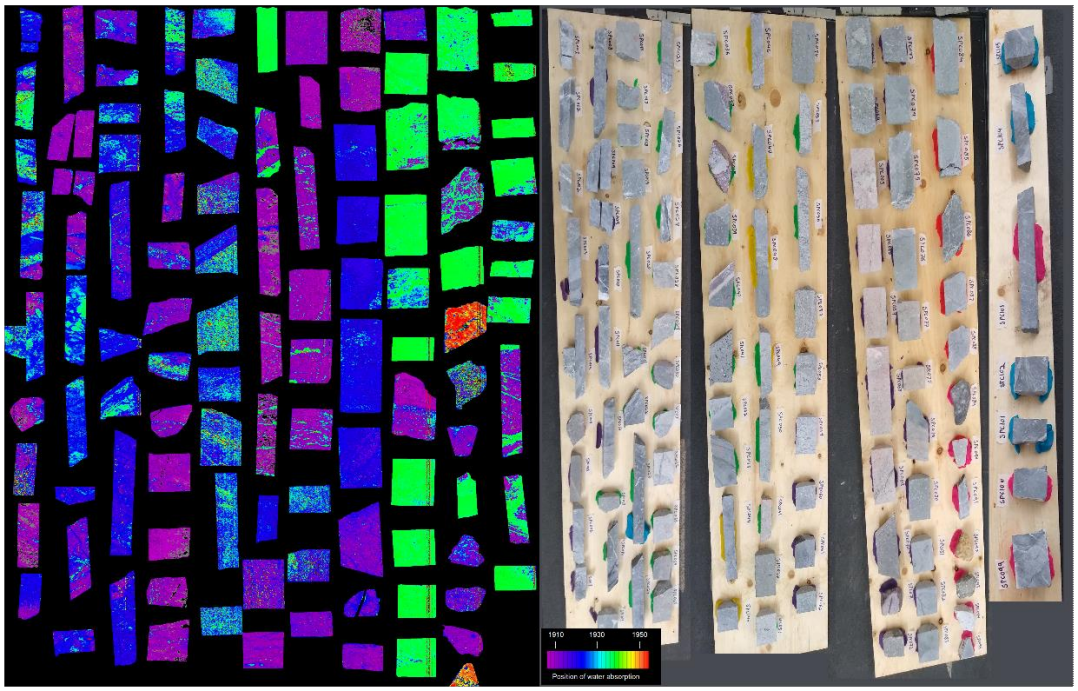

Muscovite (2195-2205 nm)

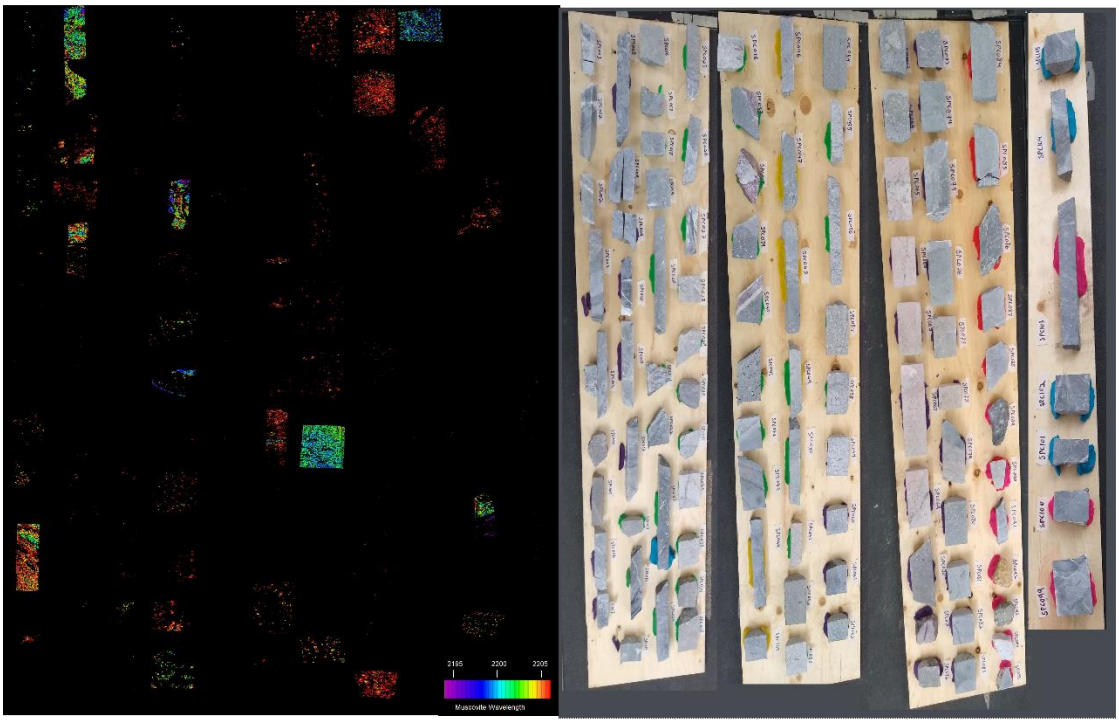

Phengitic Clays

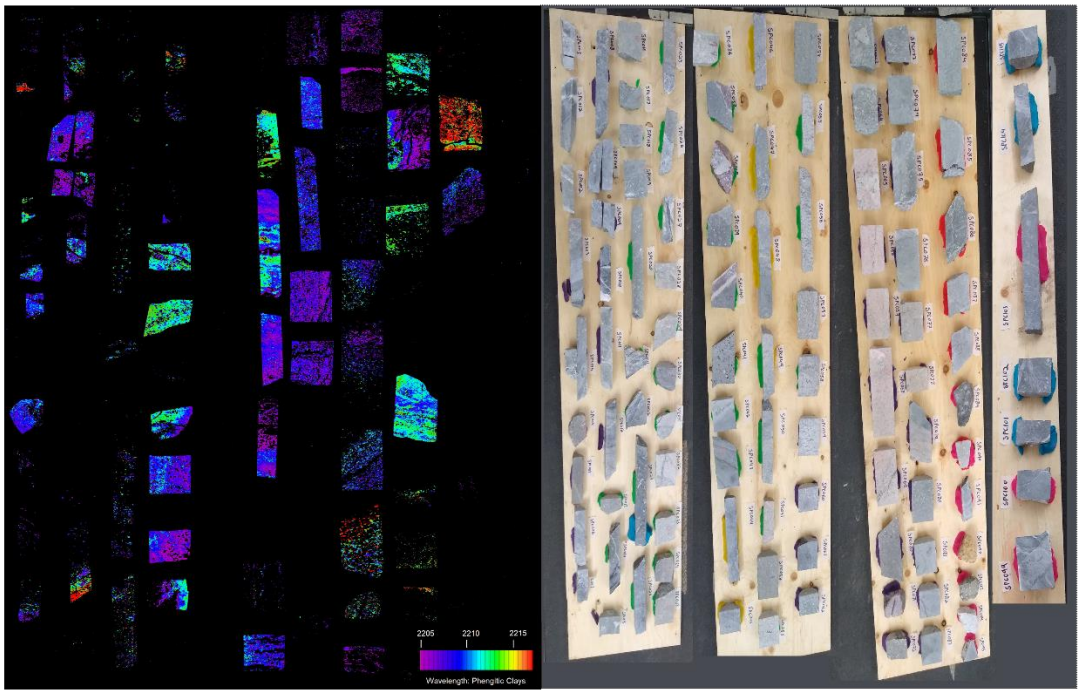

Kaolinite-Dickite-Illite/Muscovite

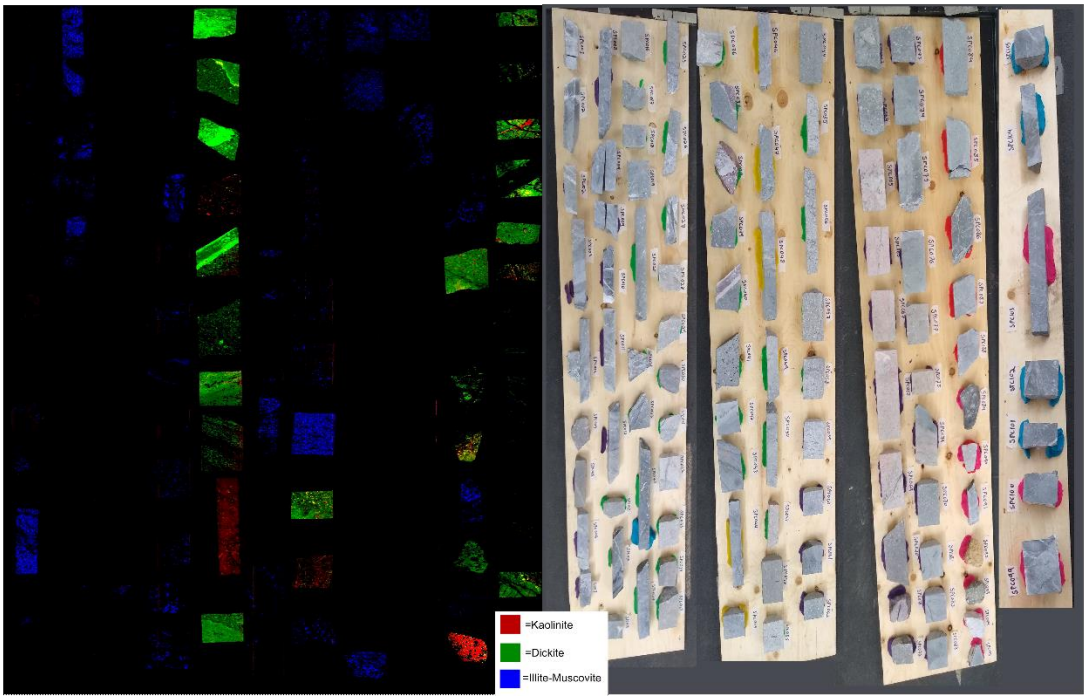

OH Feature Position (2195-2215nm)

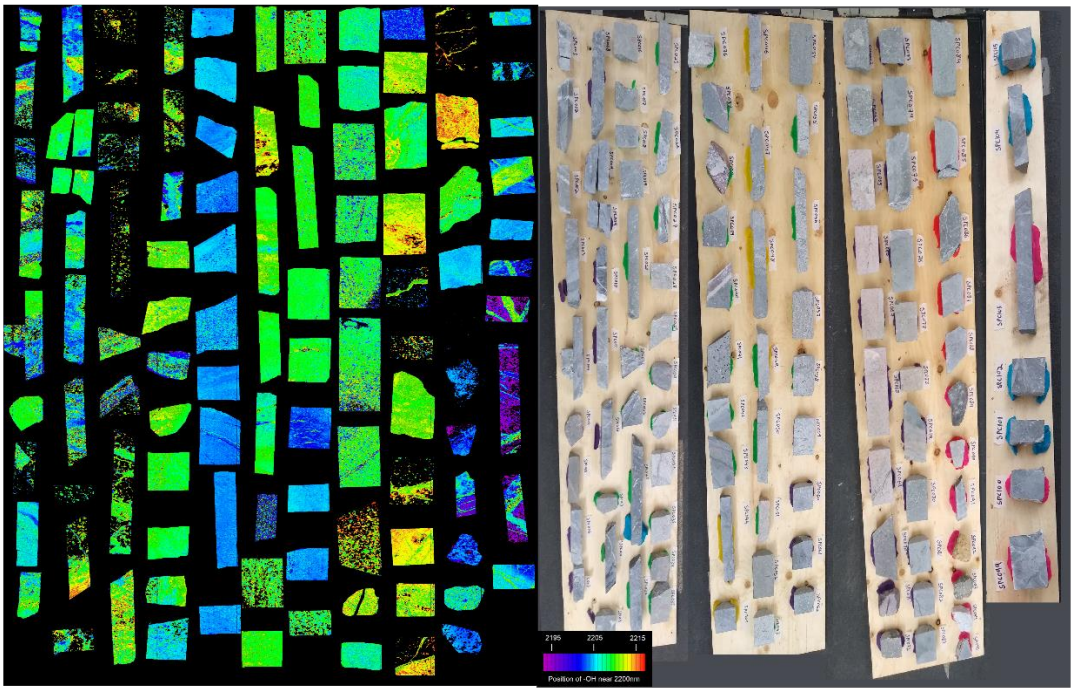

Reflectance

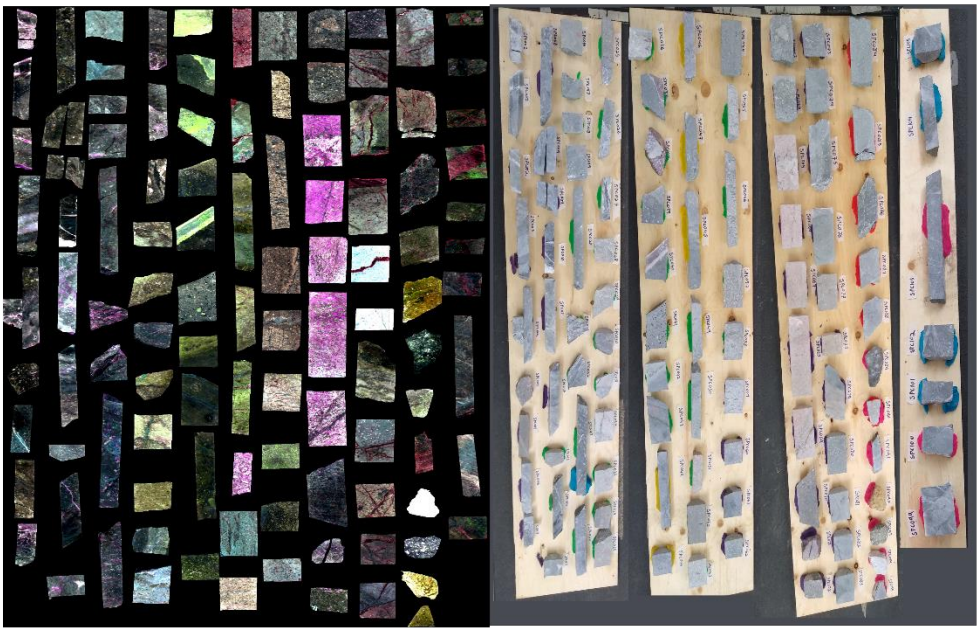

White Mica-Chlorite-Montmorrilonite

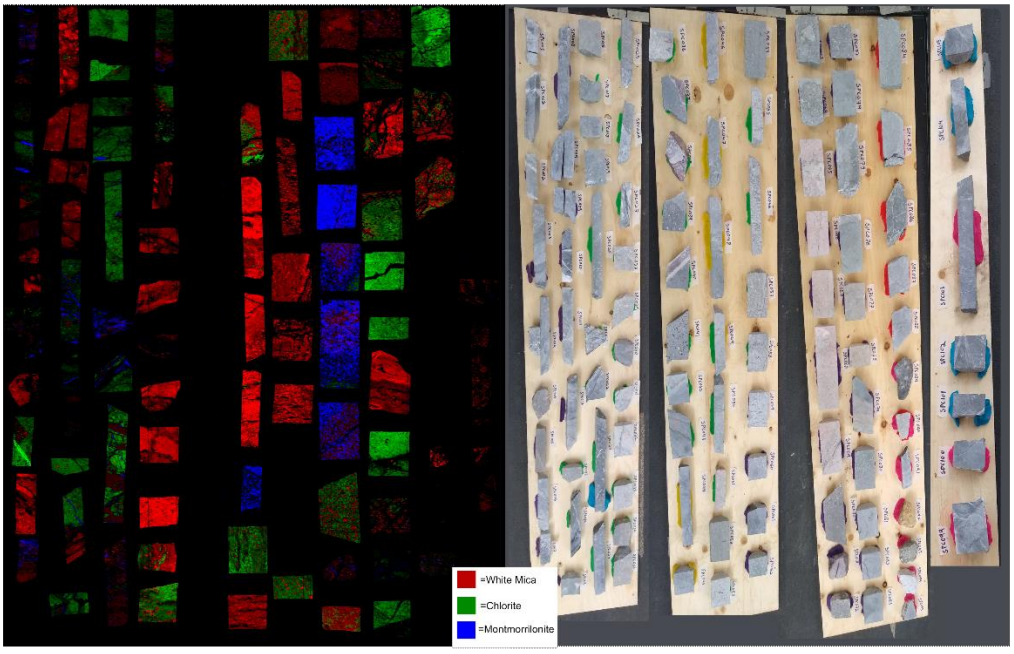

Appendix I: Crystallinity vs 2200 nm

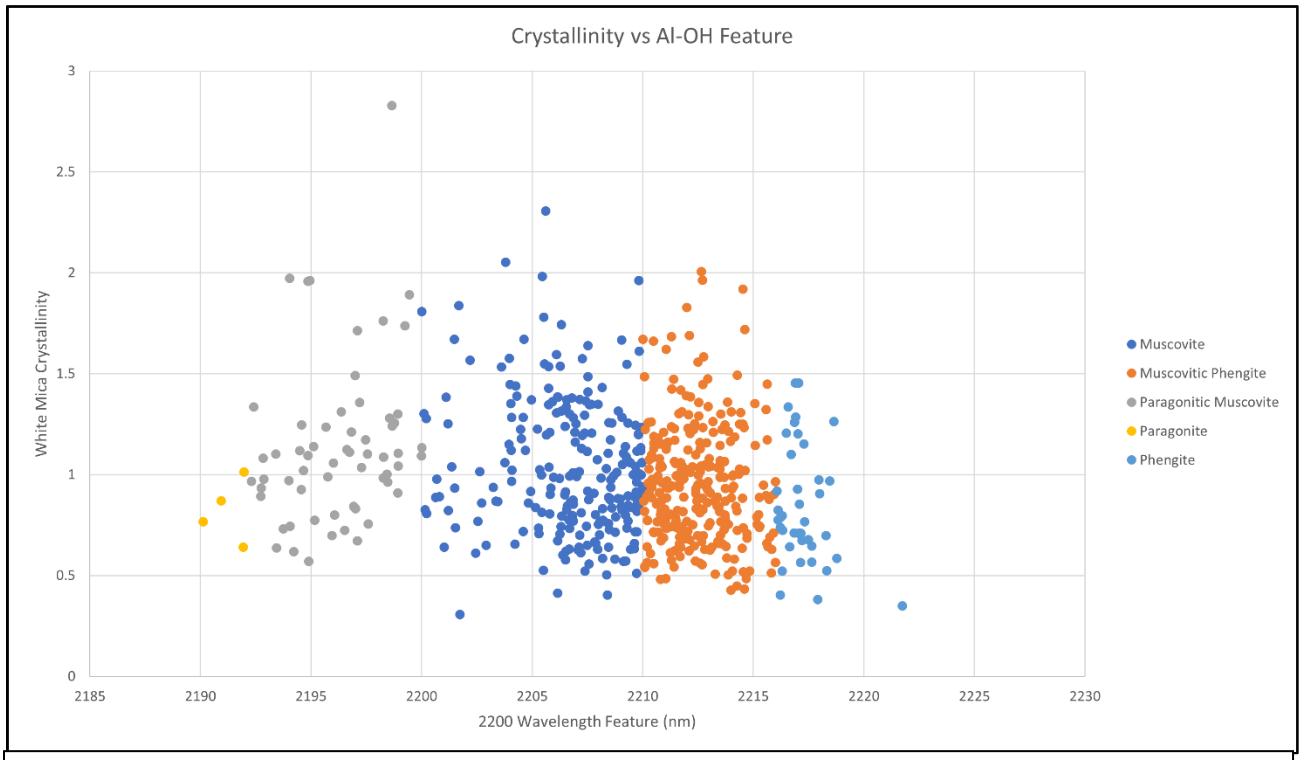

Plot of the 2200 nm Al-OH feature (x axis) versus crystallinity of white micas at prospect scale, with phengitic white micas generally displaying lower crystallinity values, and a shift to higher crystallinity values in more muscovitic compositions.

Appendix J: Proposed Paragenesis

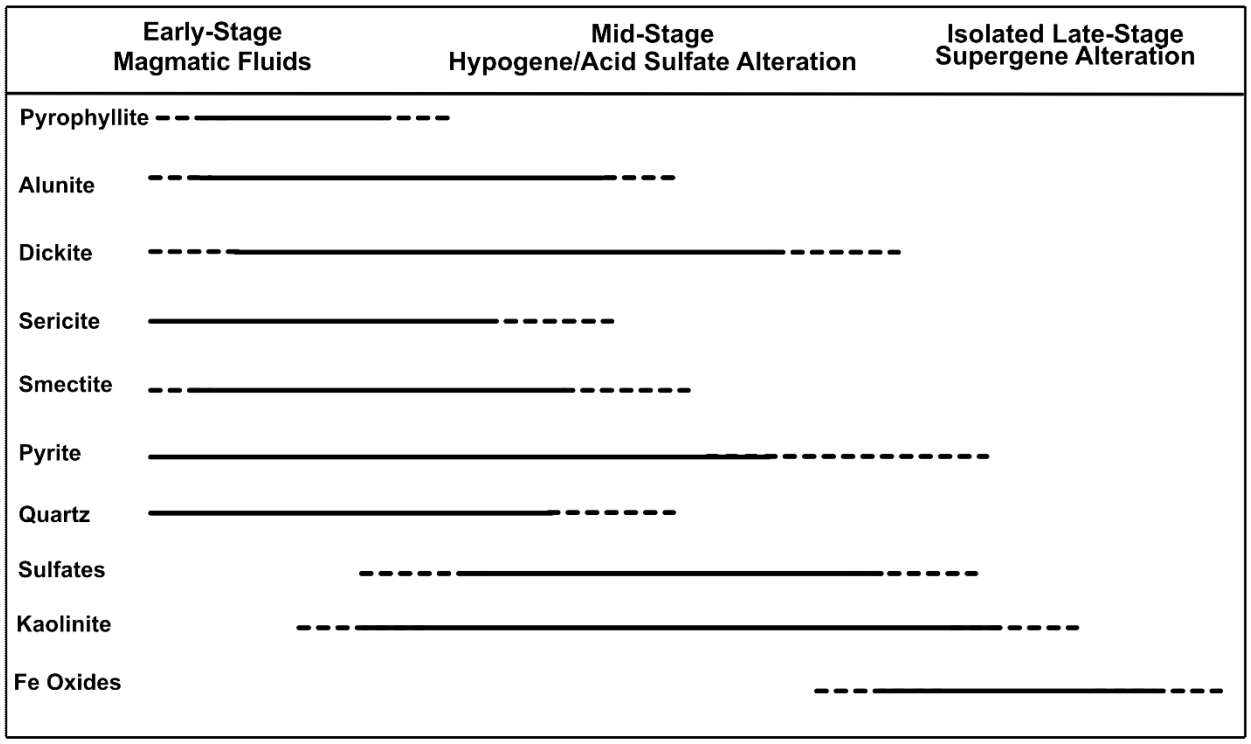

Appendix K: EDS and SEM Analysis

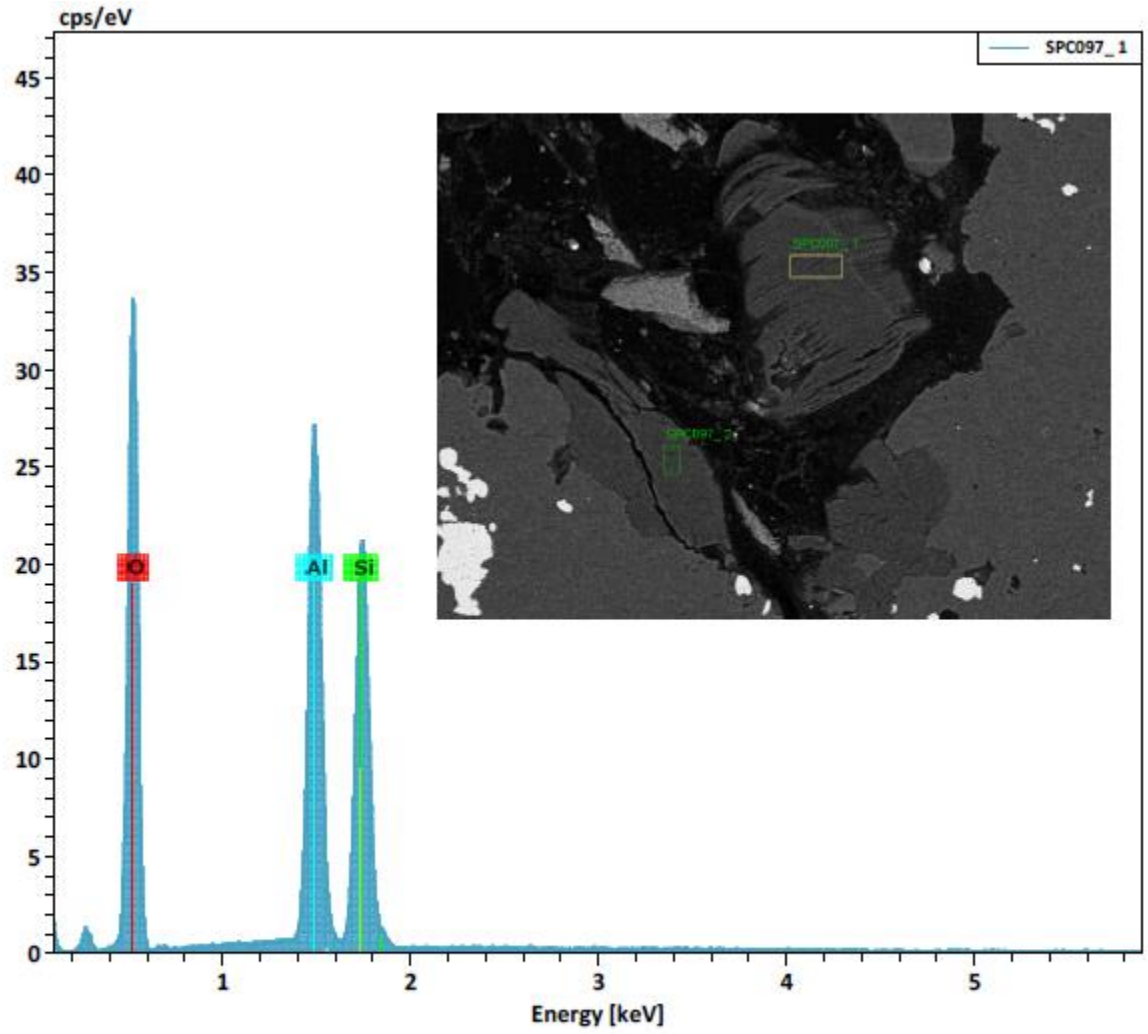

Spectrum	O	Al	Si
SPC097_1	56.4	21.4	22.2

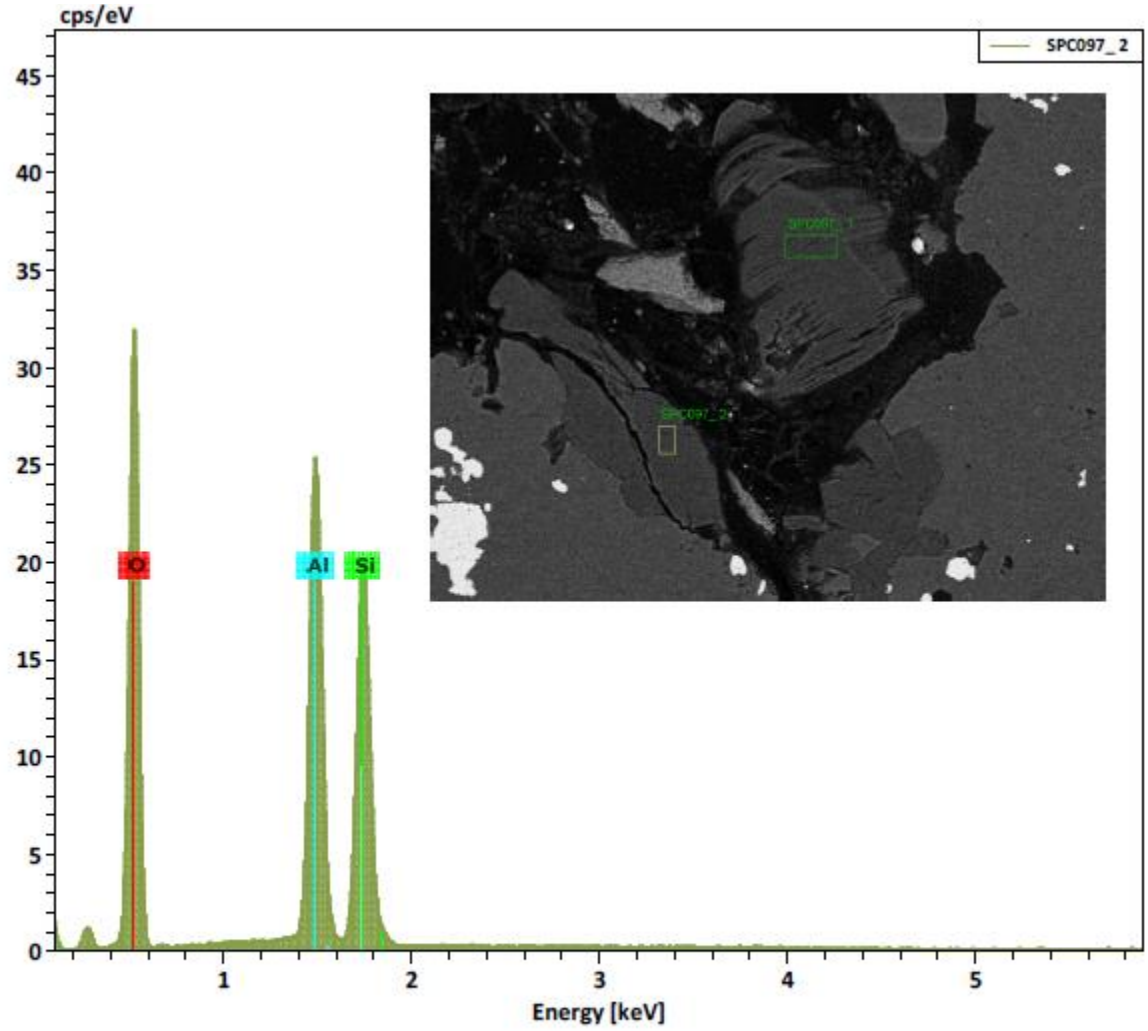

Spectrum	O	Al	Si
SPC097_2	56.7	21.4	22.0

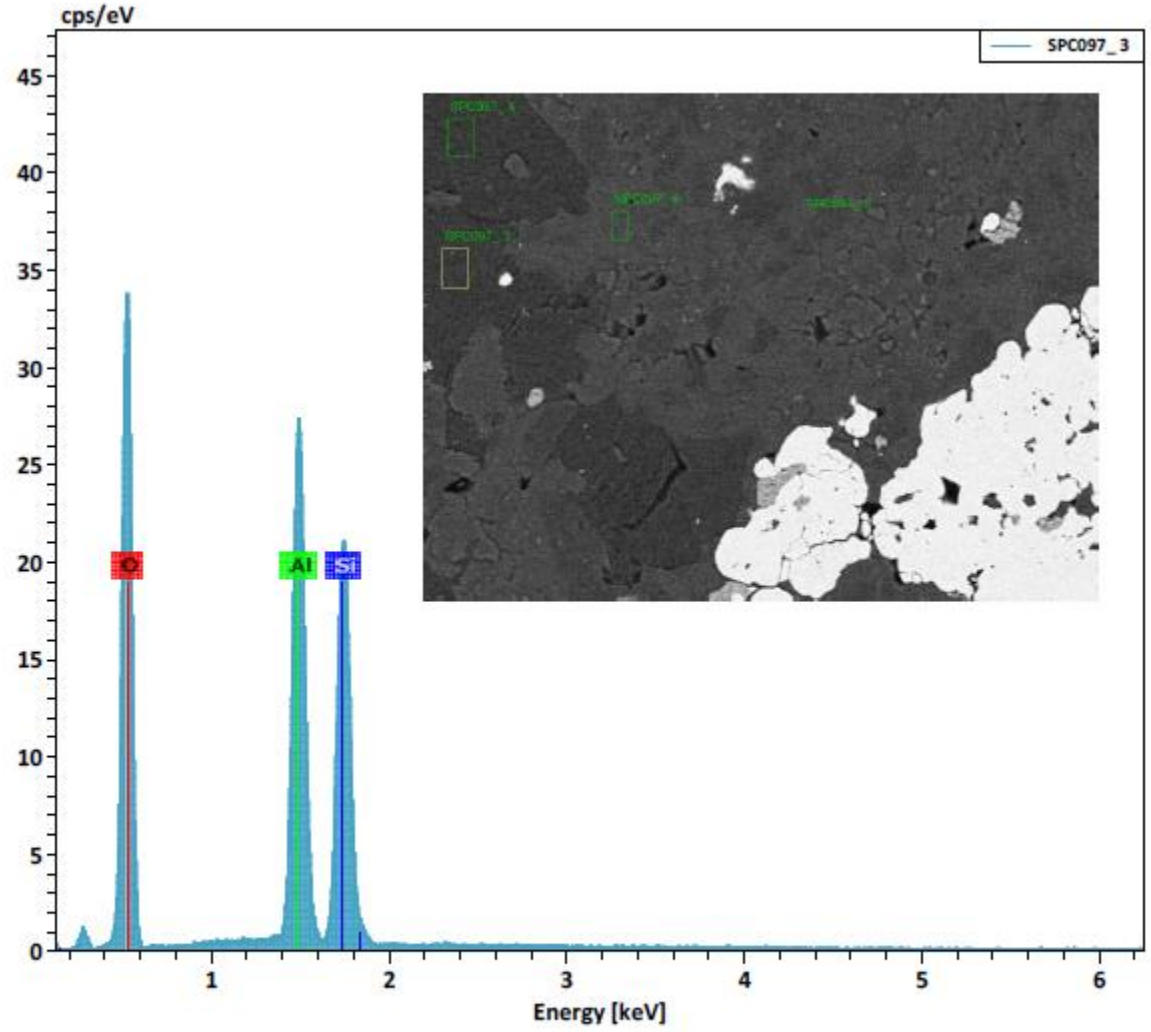

Spectrum	O	Al	Si
SPC097_3	57.0	21.1	21.9

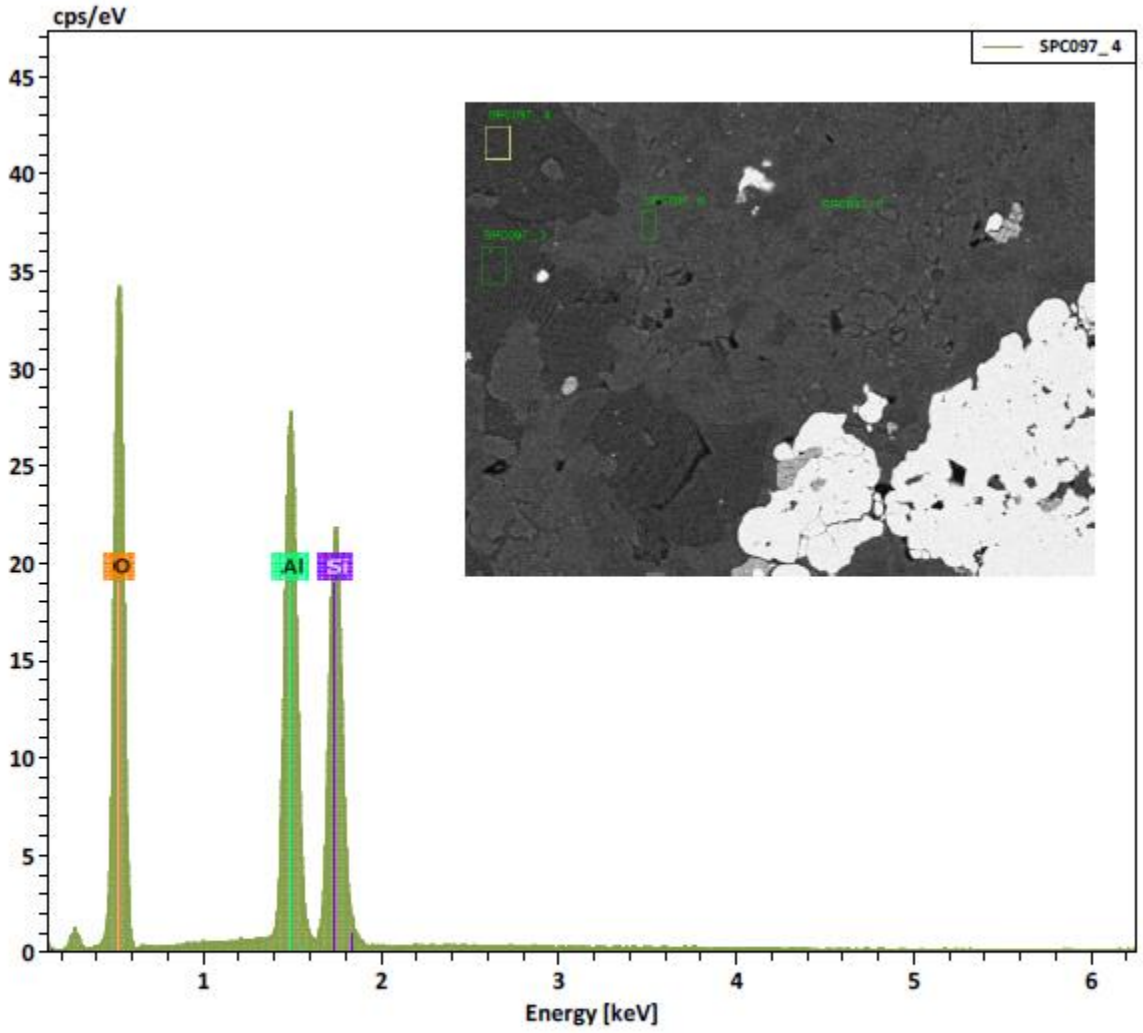

Spectrum	O	Al	Si
SPC097_4	56.7	21.2	22.1

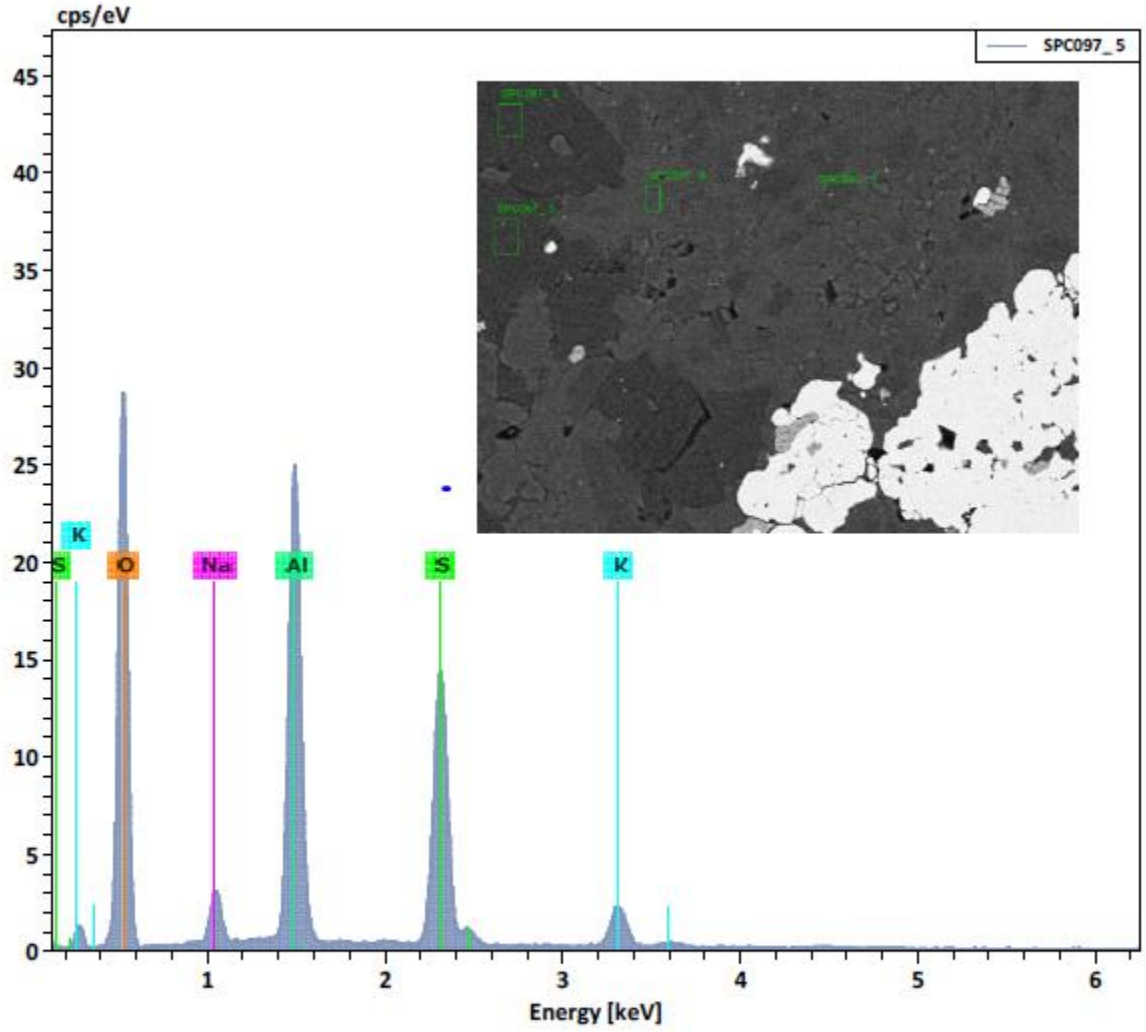

Spectrum	O	Na	Al	S	K
SPC097_5	56.8	3.1	20.6	15.7	3.7

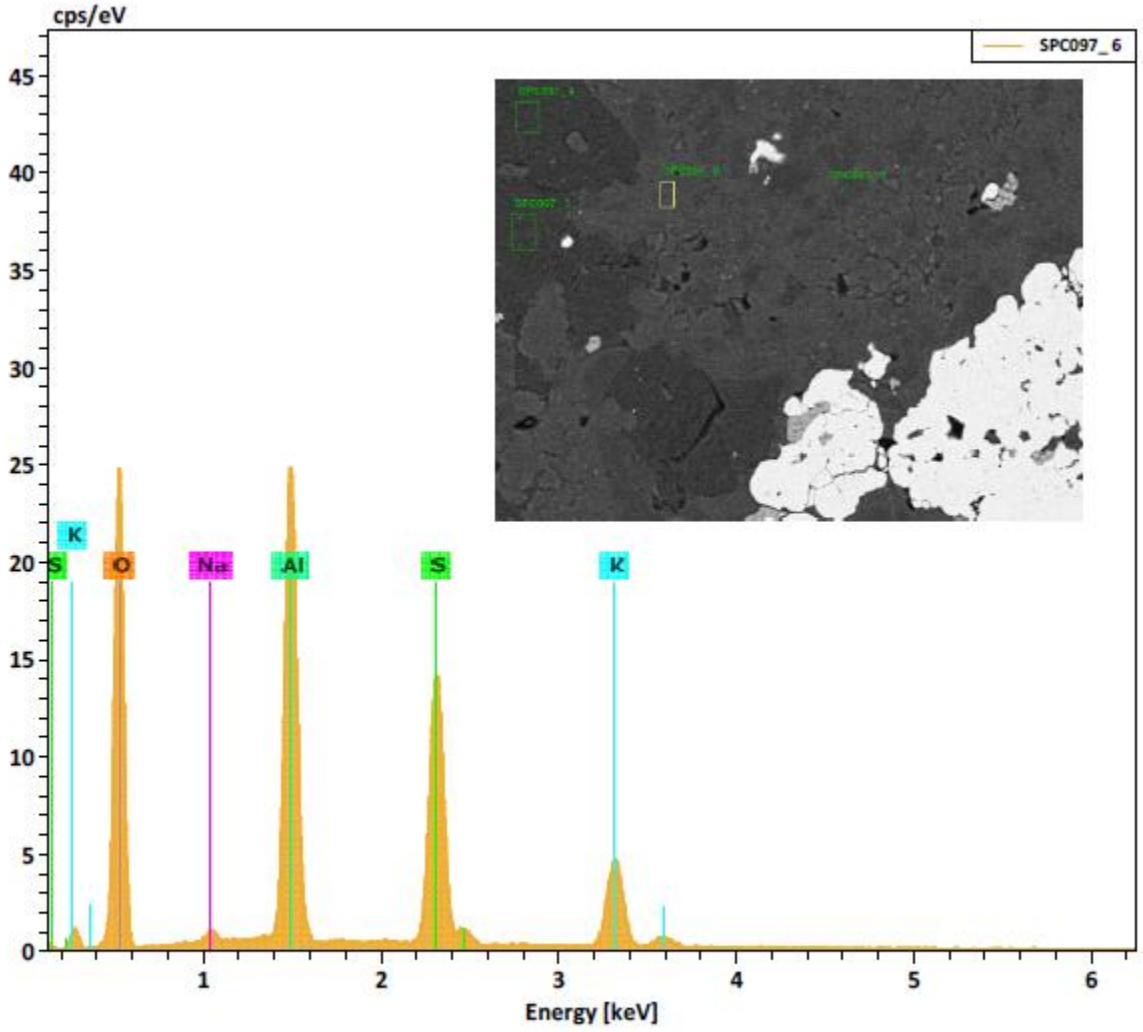

Spectrum	O	Na	Al	S	K
SPC097_6	54.8	0.7	19.8	15.5	9.2

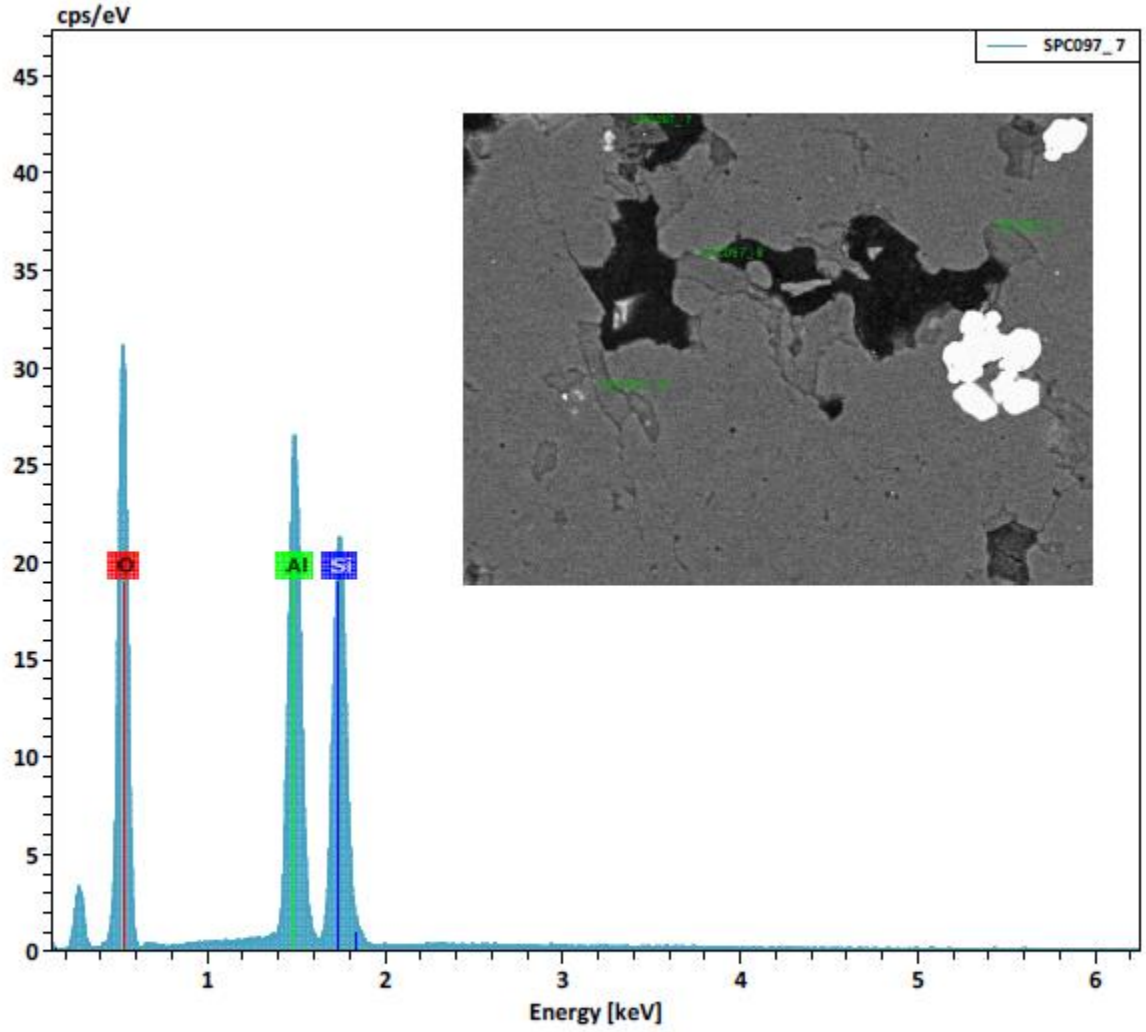

Spectrum	O	Al	Si
SPC097_7	55.3	21.5	23.2

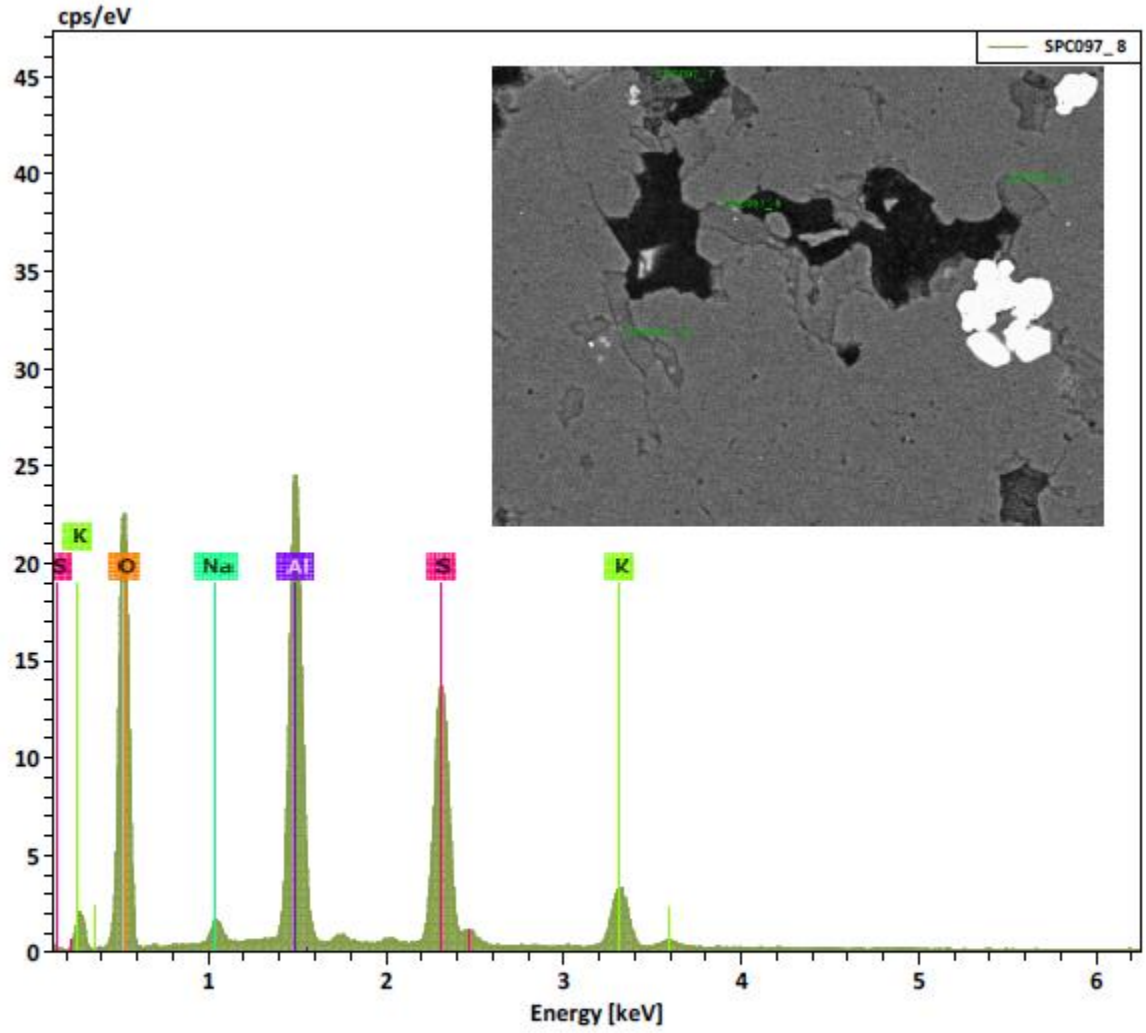

Spectrum	O	Na	Al	S	K
SPC097_8	54.2	1.4	21.2	16.9	6.3

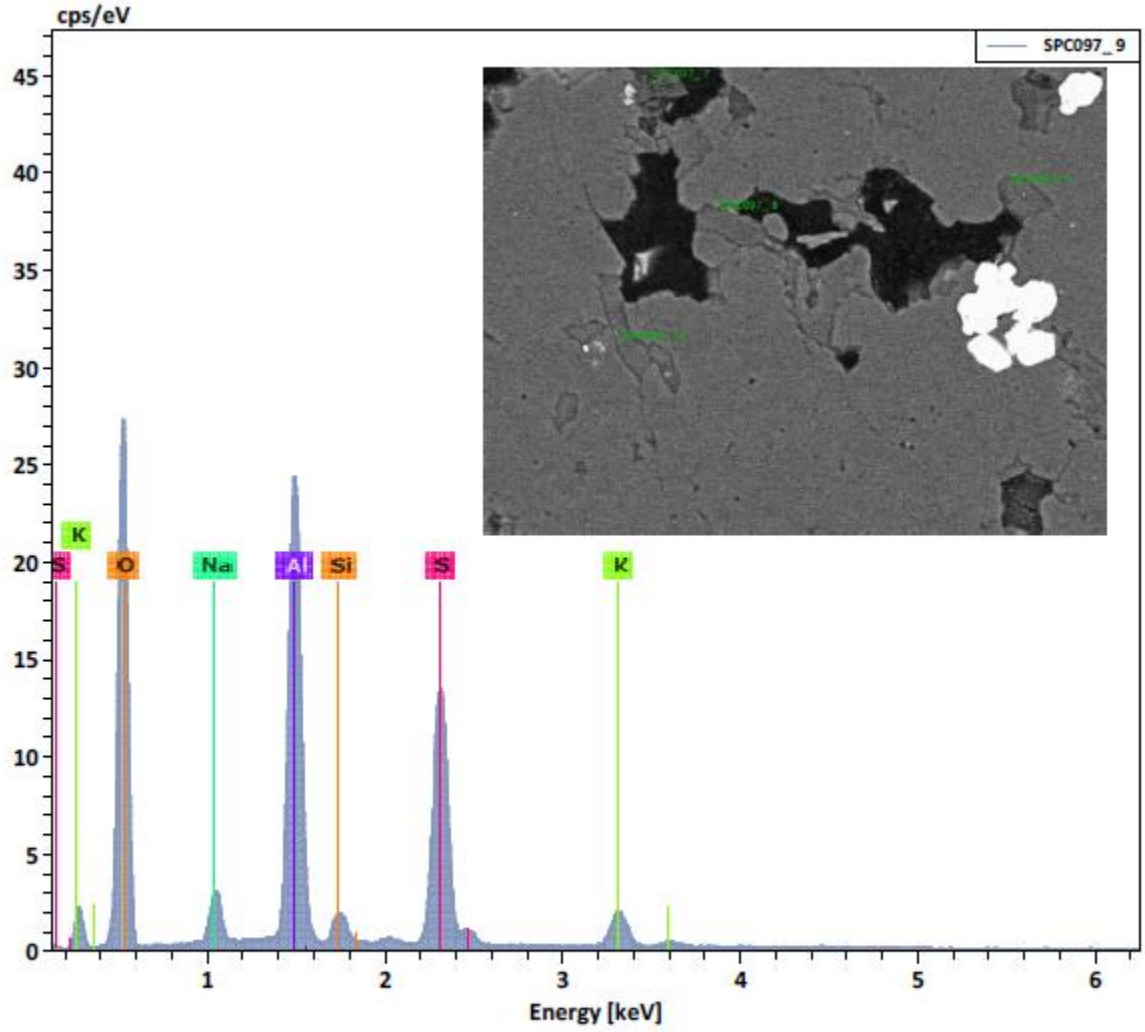

Spectrum	O	Na	Al	Si	S	K
SPC097_9	55.6	3.2	20.9	1.4	15.6	3.3

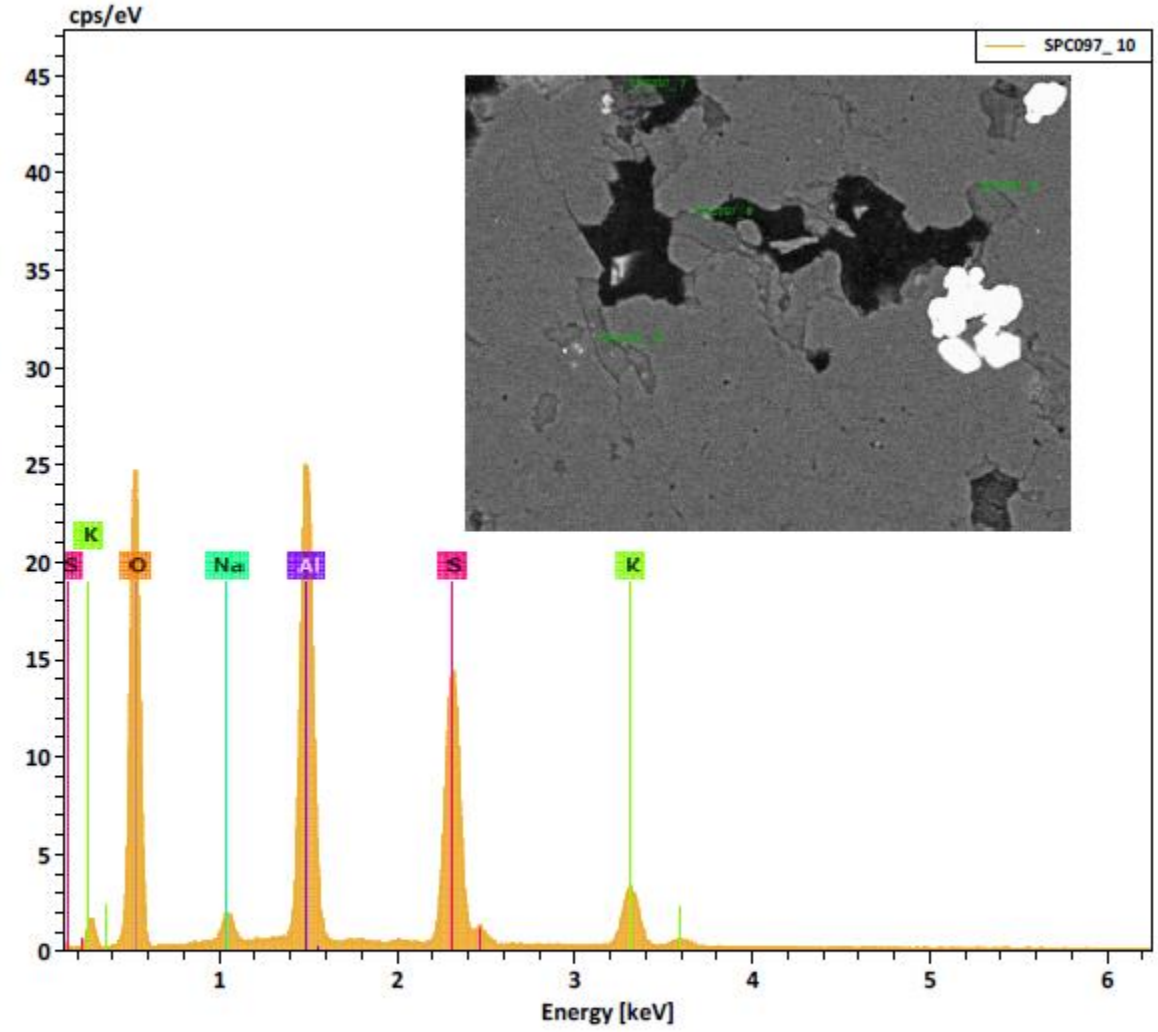

Spectrum	O	Na	Al	S	K
SPC097_10	54.6	1.6	21.0	16.5	6.3

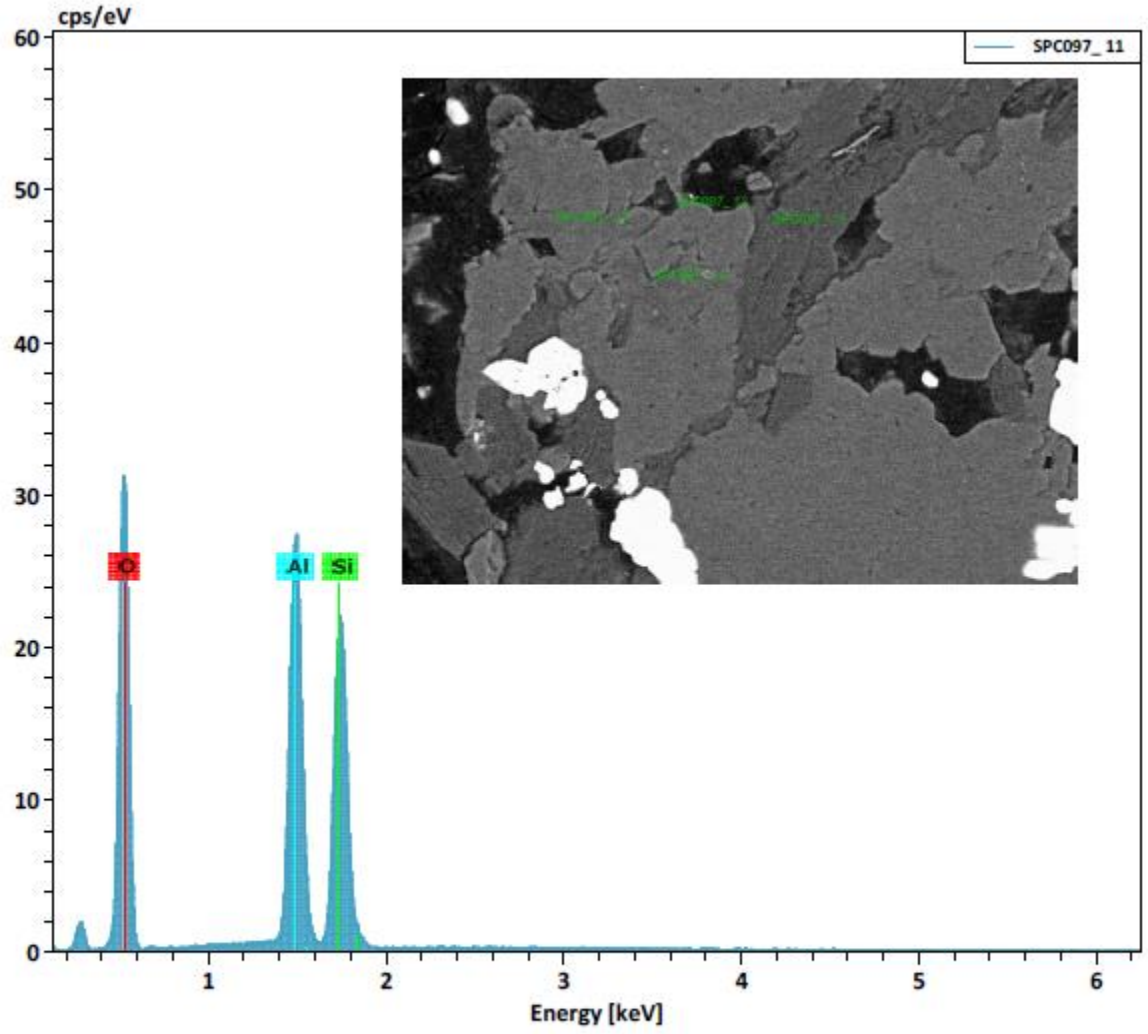

Spectrum	O	Al	Si
SPC097_ 11	55.1	21.8	23.1

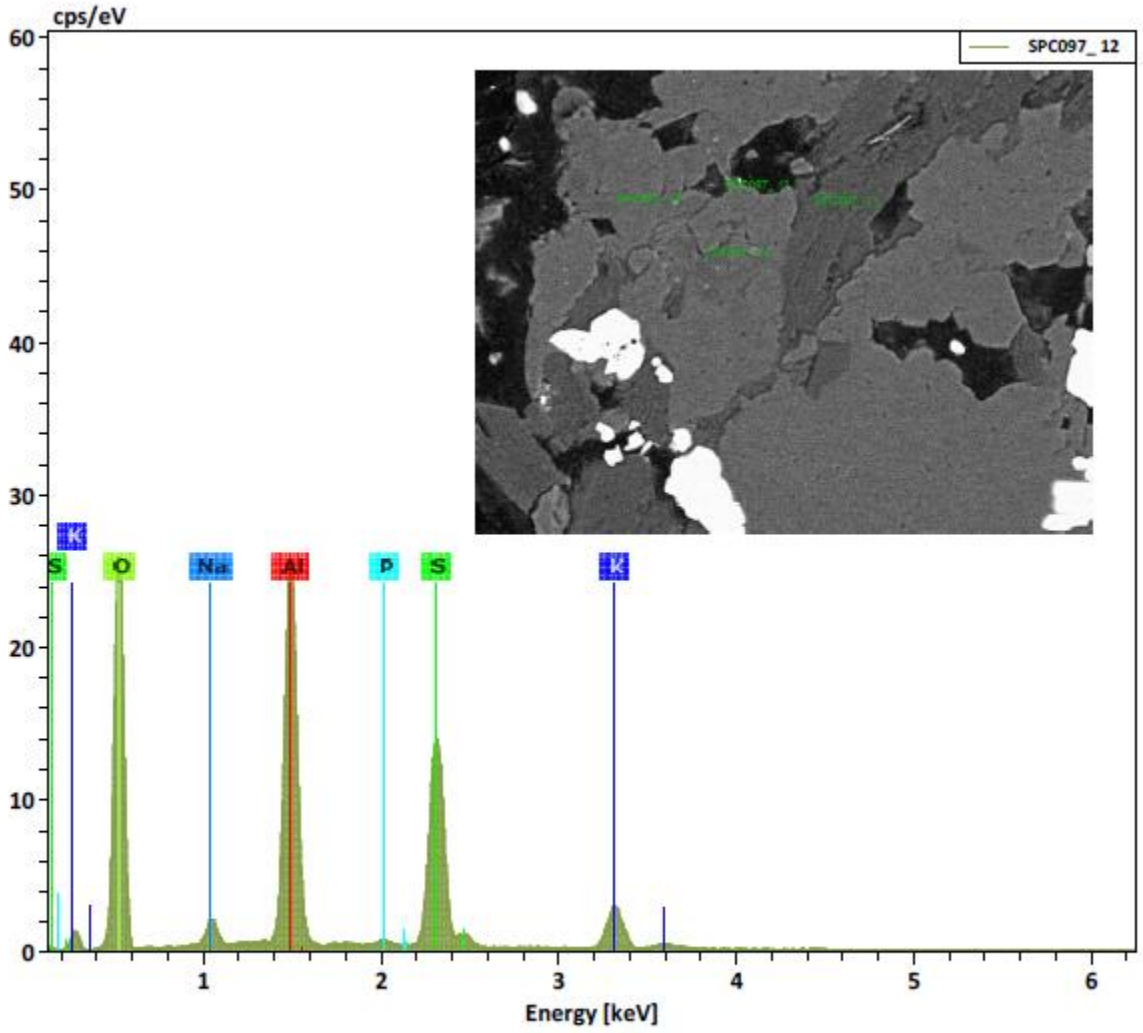

Spectrum	O	Na	Al	P	S	K
SPC097_12	55.1	1.9	21.2	0.3	16.0	5.4

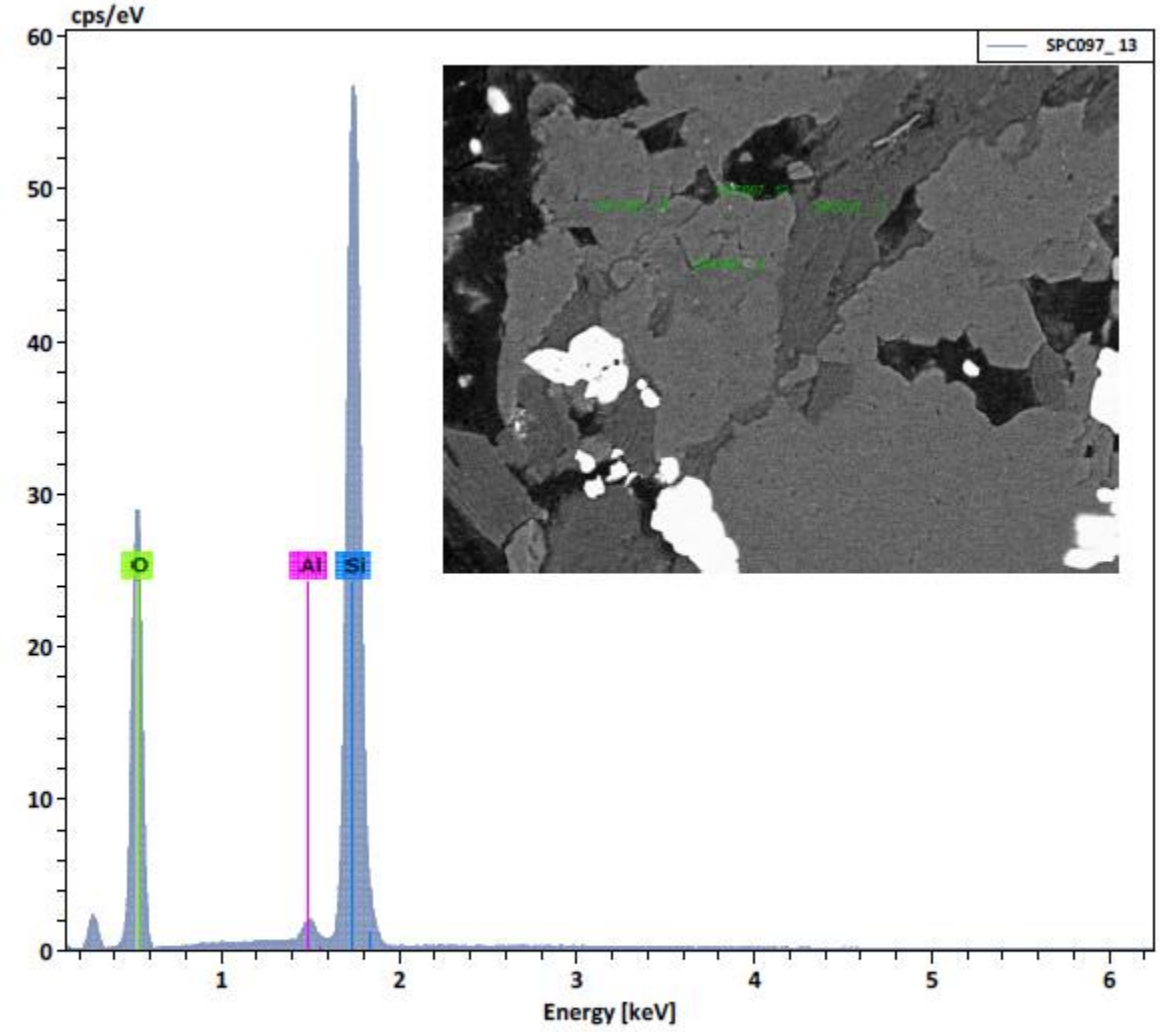

Spectrum	O	Al	Si
SPC097_13	52.3	1.0	46.7

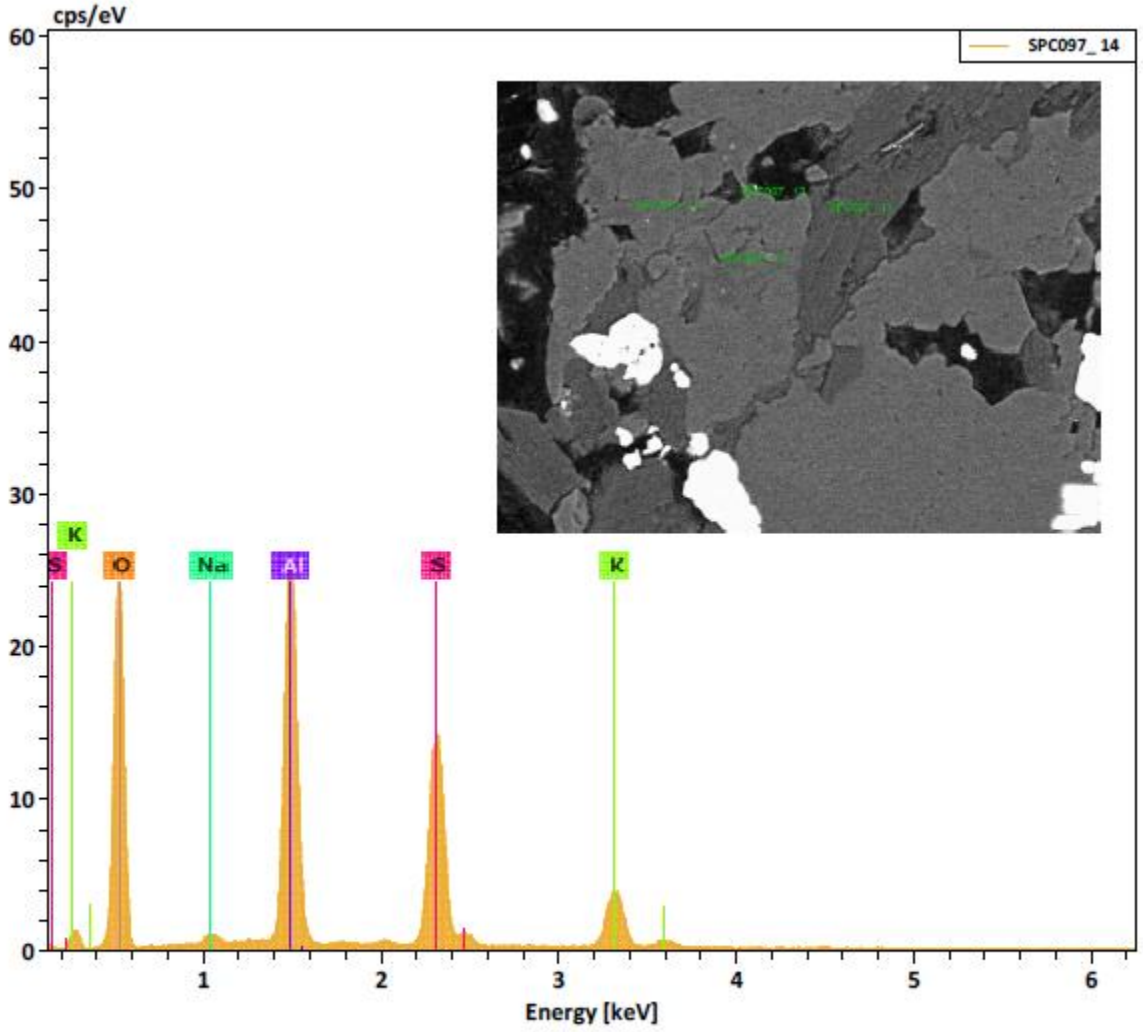

Spectrum	O	Na	Al	S	K
SPC097_14	54.5	0.9	19.2	16.9	8.5

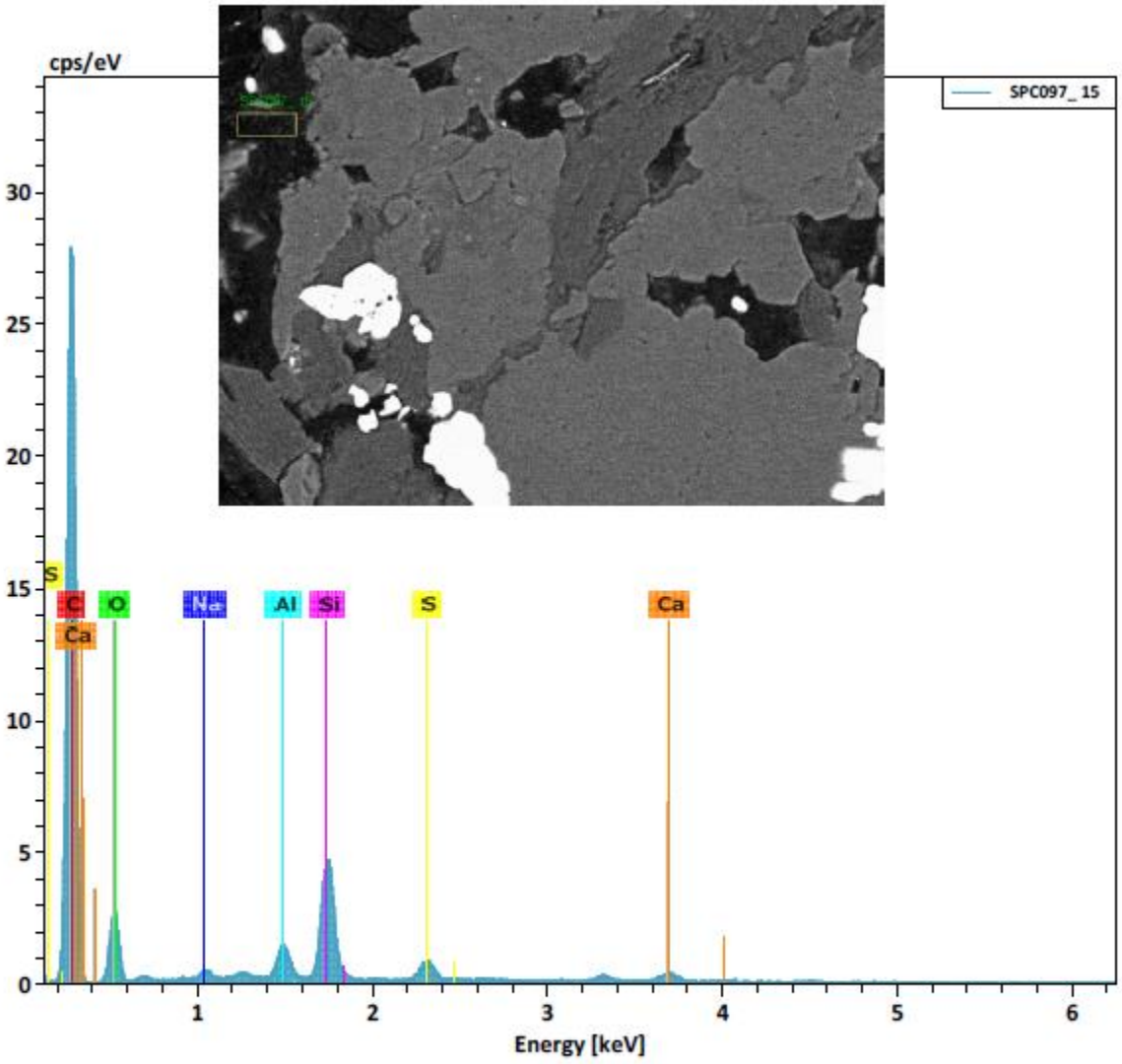

Spectrum	C	O	Na	Al	Si	S	Ca
SPC097_ 15	75.8	16.0	0.3	1.2	4.8	1.1	0.7

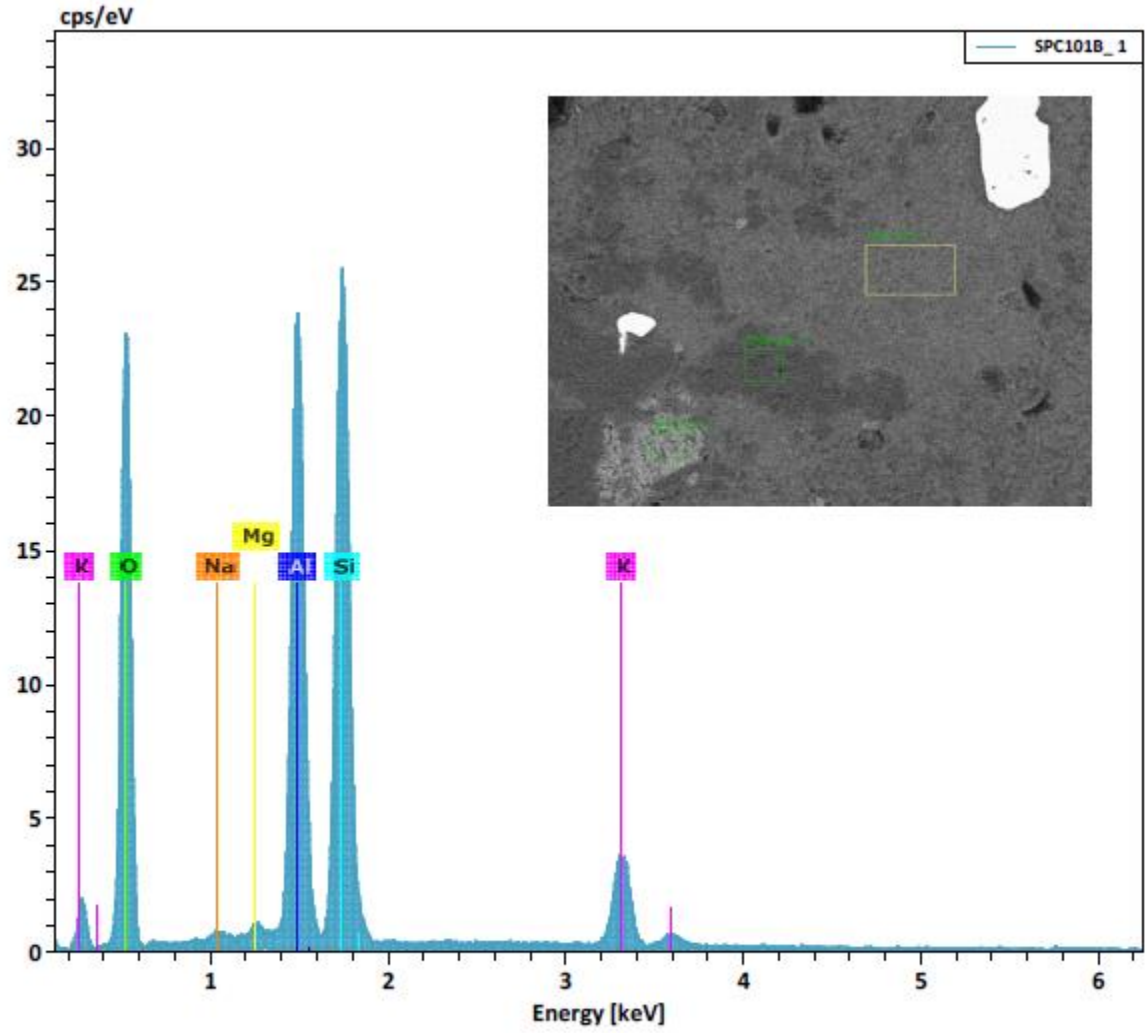

Spectrum	O	Na	Mg	Al	Si	K
SPC101B_1	49.2	0.3	0.2	18.9	25.1	6.3

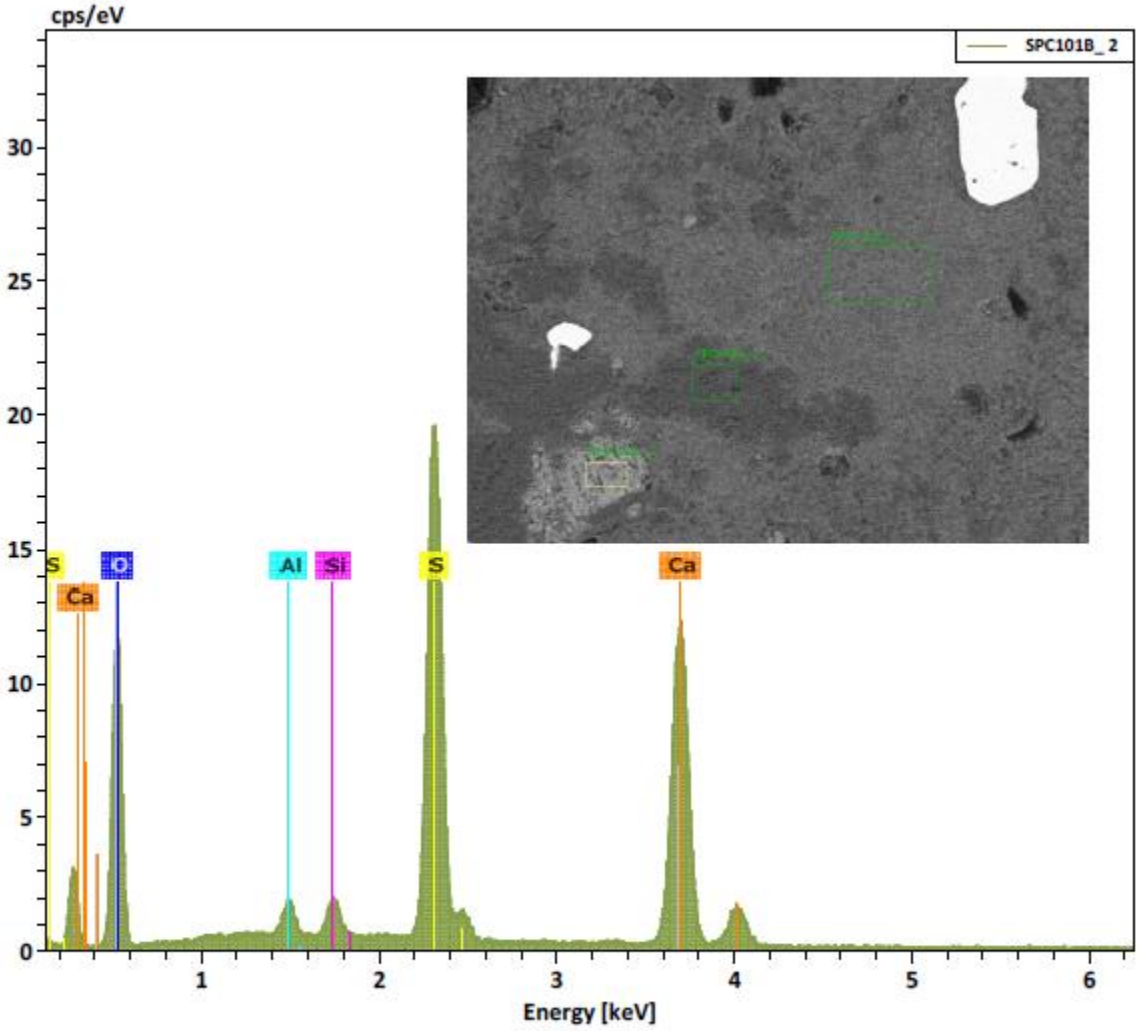

Spectrum	O	Al	Si	S	Ca
SPC101B_2	47.7	1.0	1.1	19.9	30.3

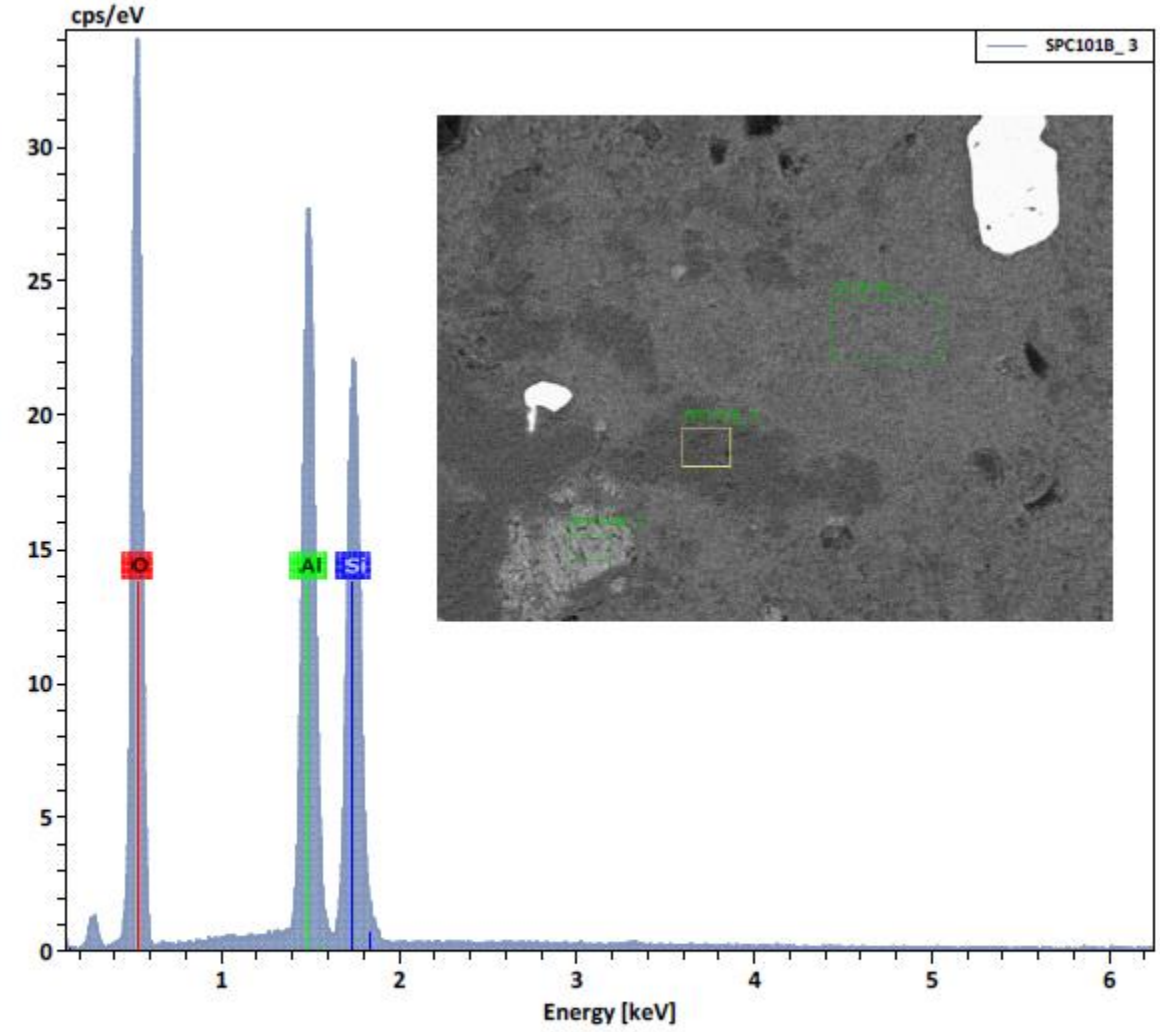

Spectrum	O	Al	Si
SPC101B_3	56.4	21.2	22.4

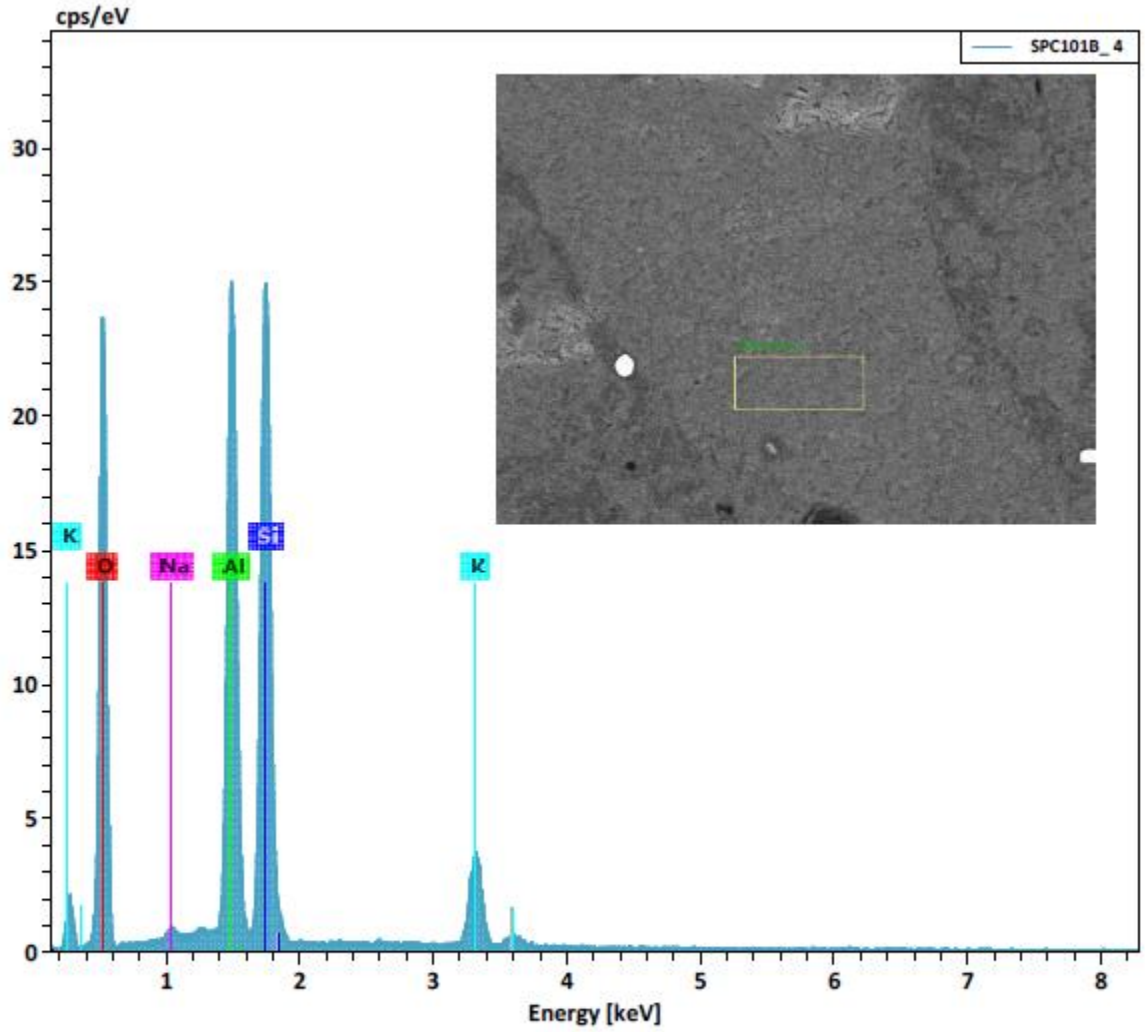

Spectrum	O	Na	Al	Si	K
SPC101B_ 4	49.1	0.5	19.7	24.5	6.2

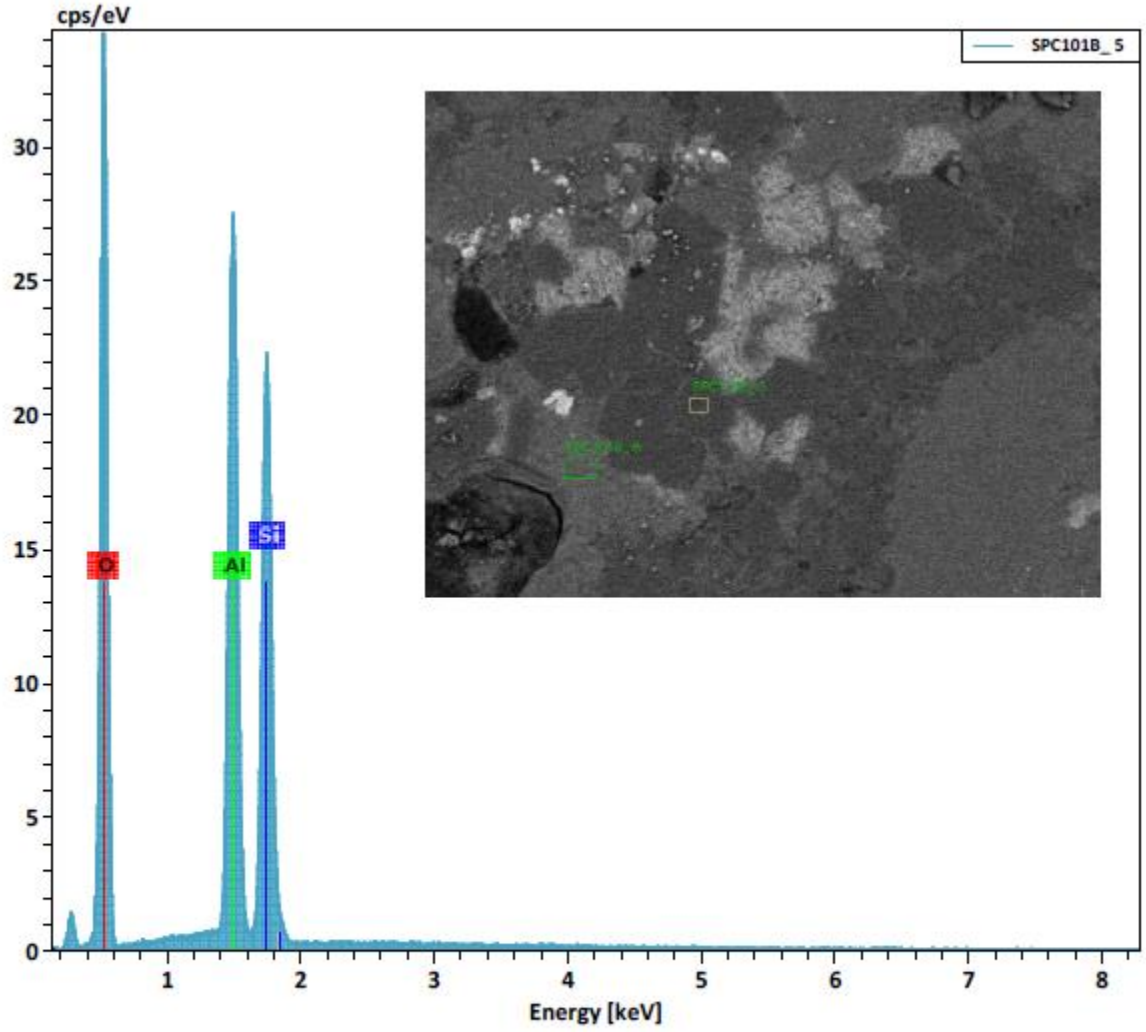

Spectrum	O	Al	Si
SPC101B_5	56.1	21.3	22.5

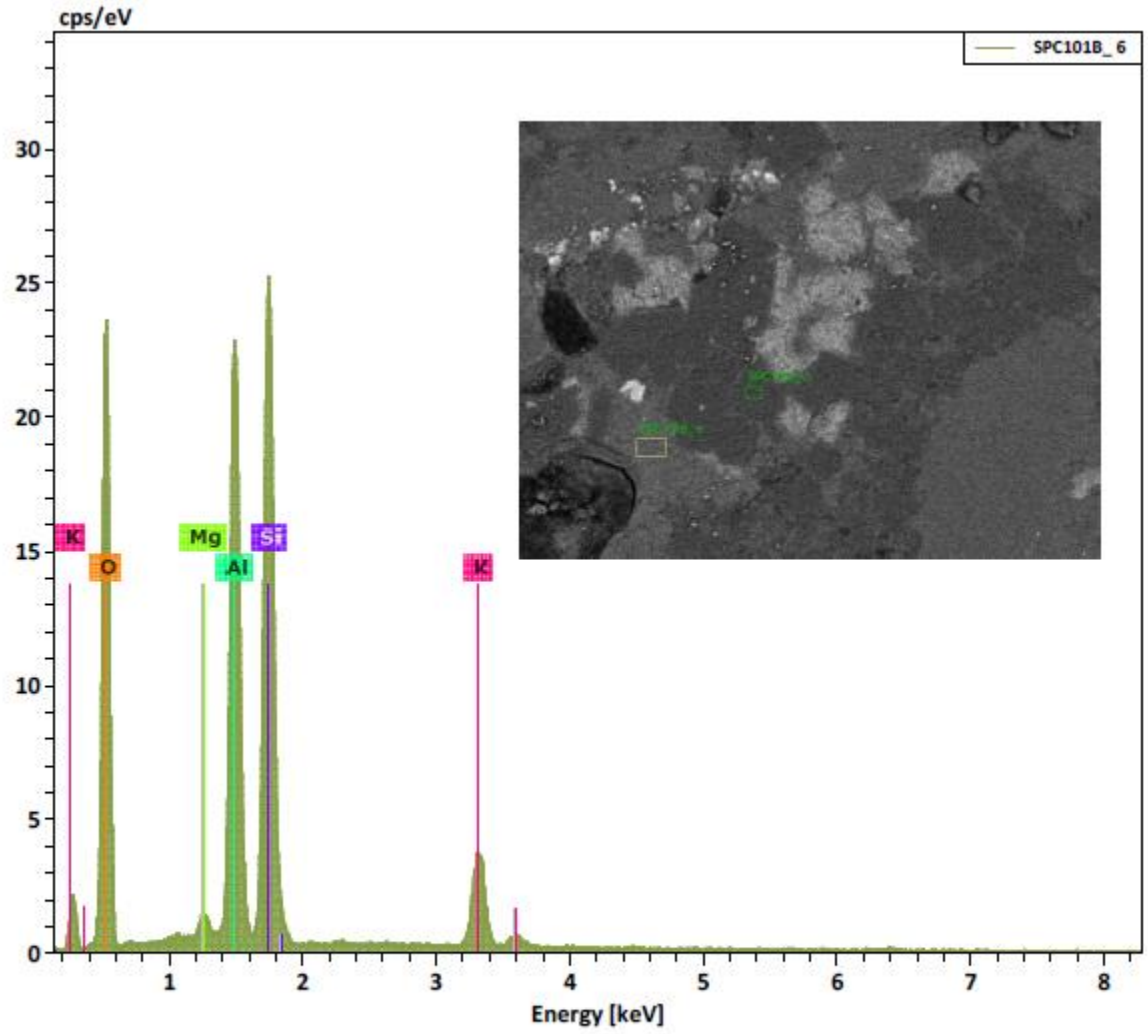

Spectrum	O	Mg	Al	Si	K
SPC101B_6	49.6	0.7	18.7	24.6	6.4

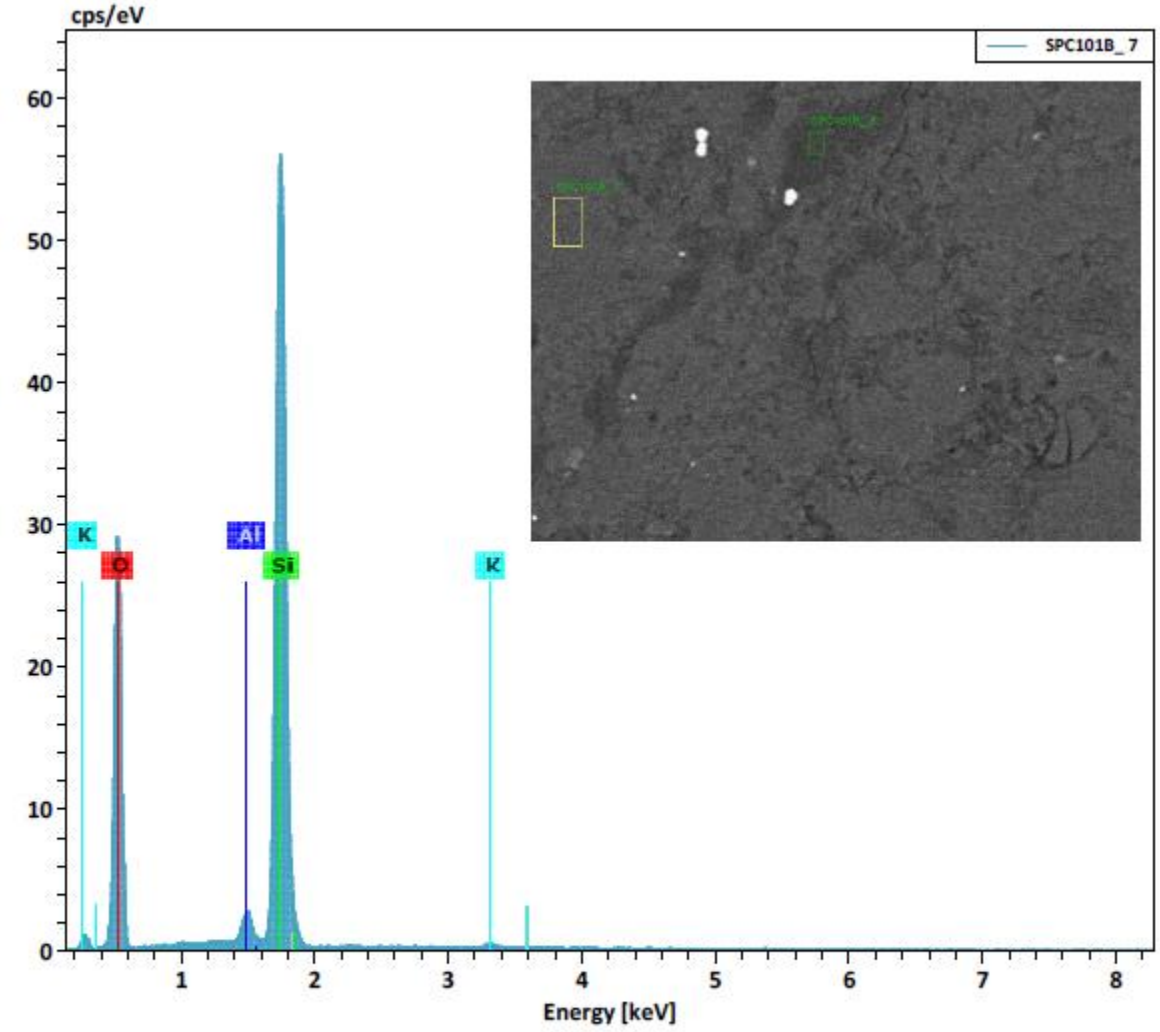

Spectrum	O	Al	Si	K
SPC101B_7	52.4	1.4	45.7	0.4

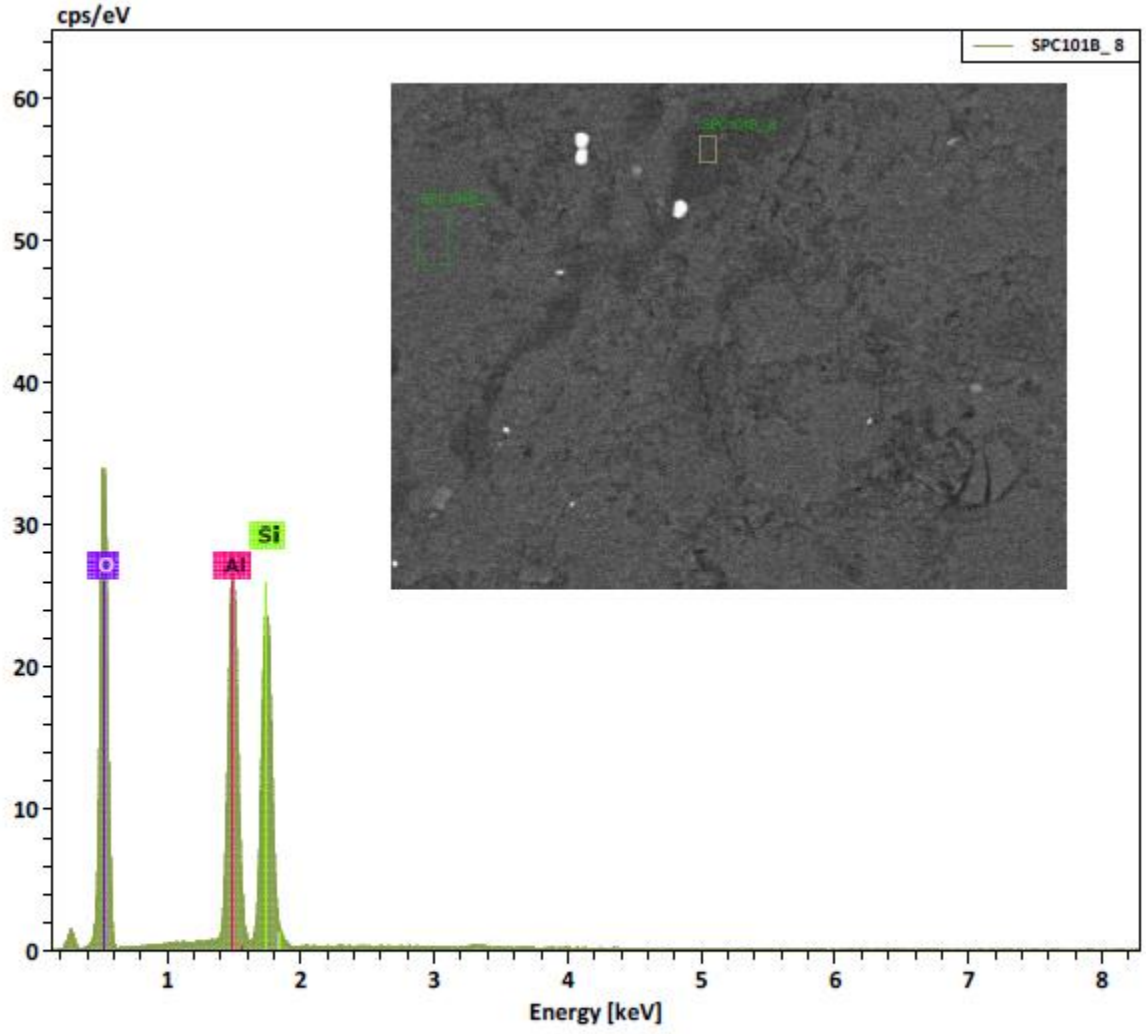

Spectrum	O	Al	Si
SPC101B_ 8	56.1	19.6	24.3

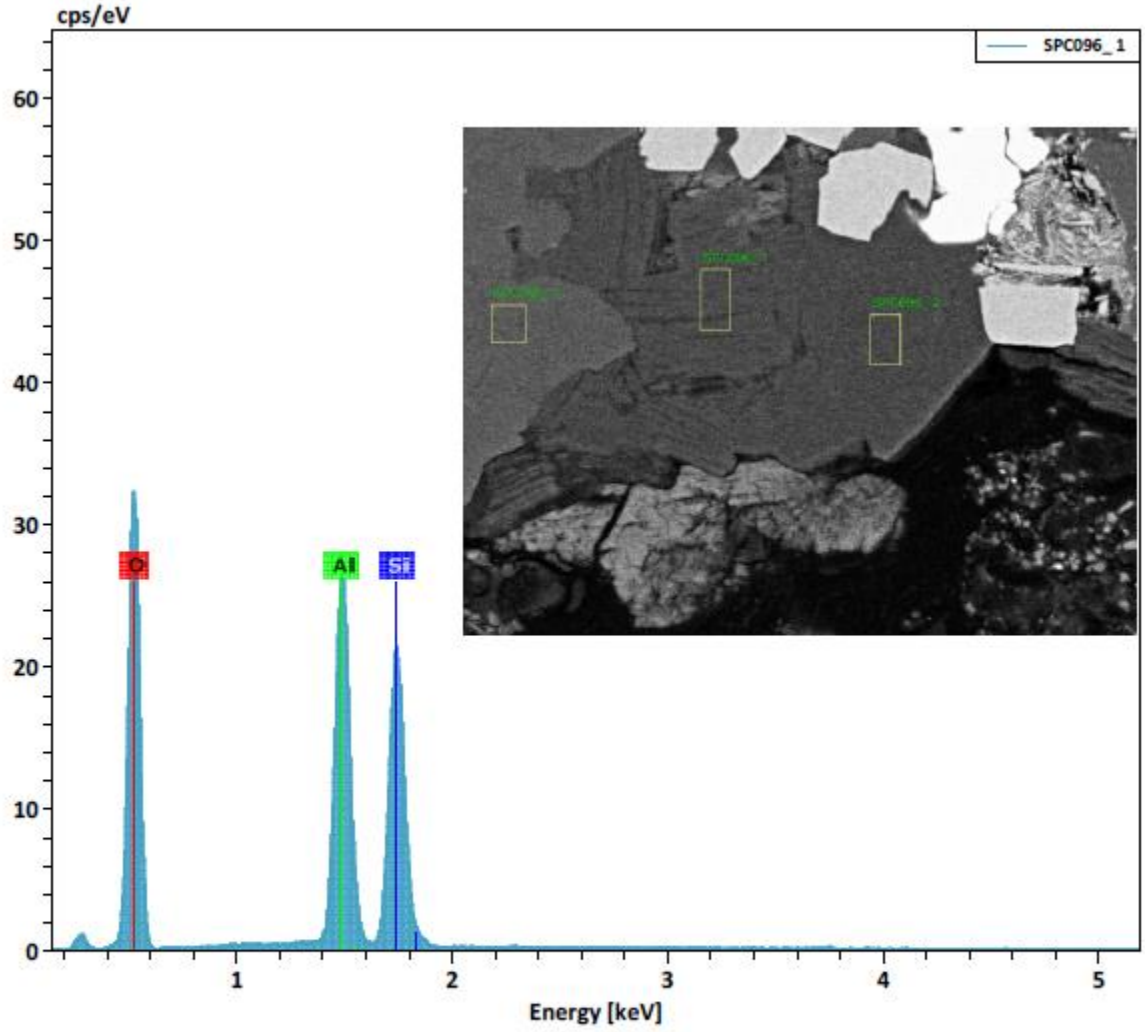

Spectrum	O	Al	Si
SPC096_1	56.4	21.0	22.6

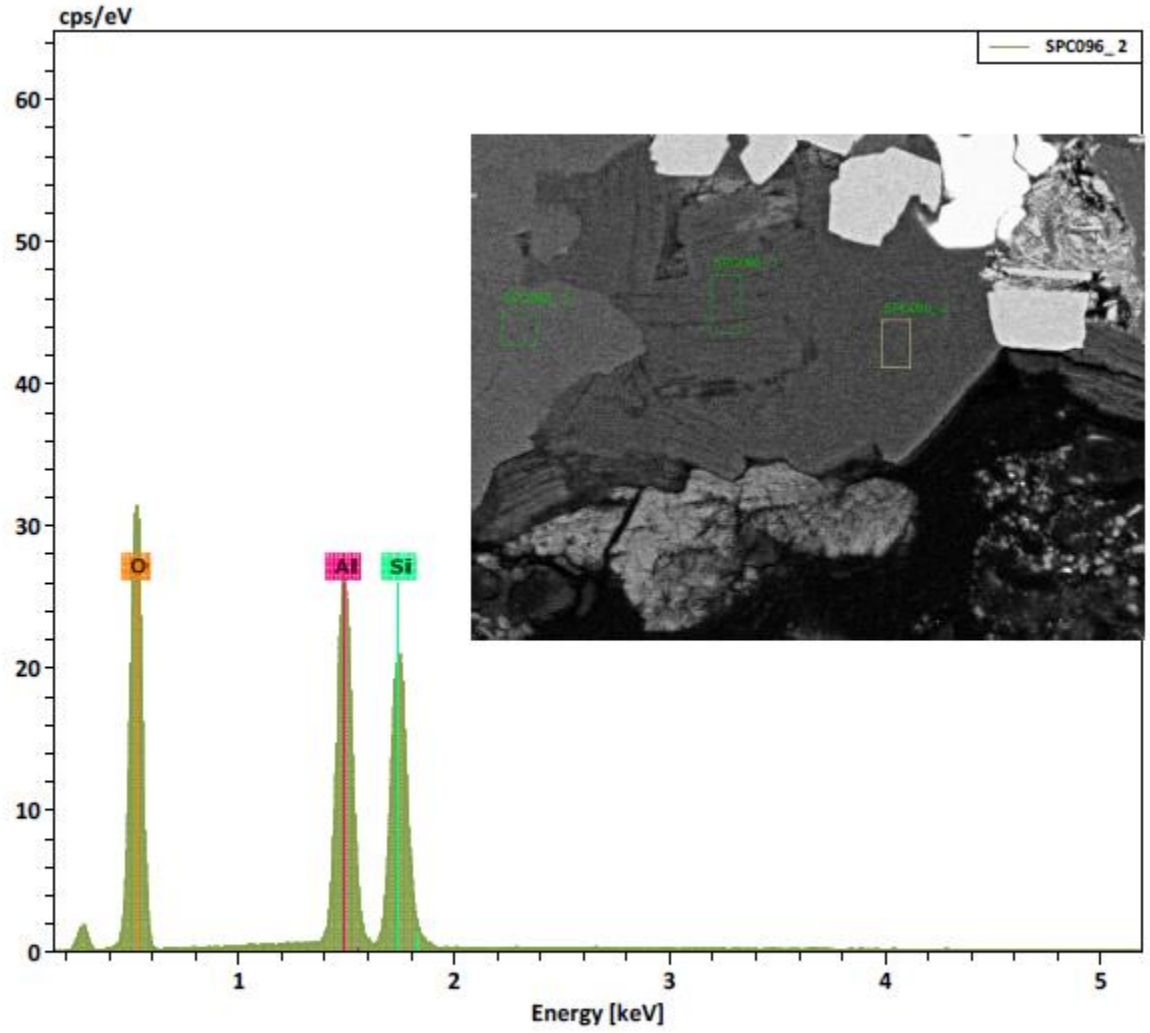

Spectrum	O	Al	Si
SPC096_2	55.8	22.1	22.1

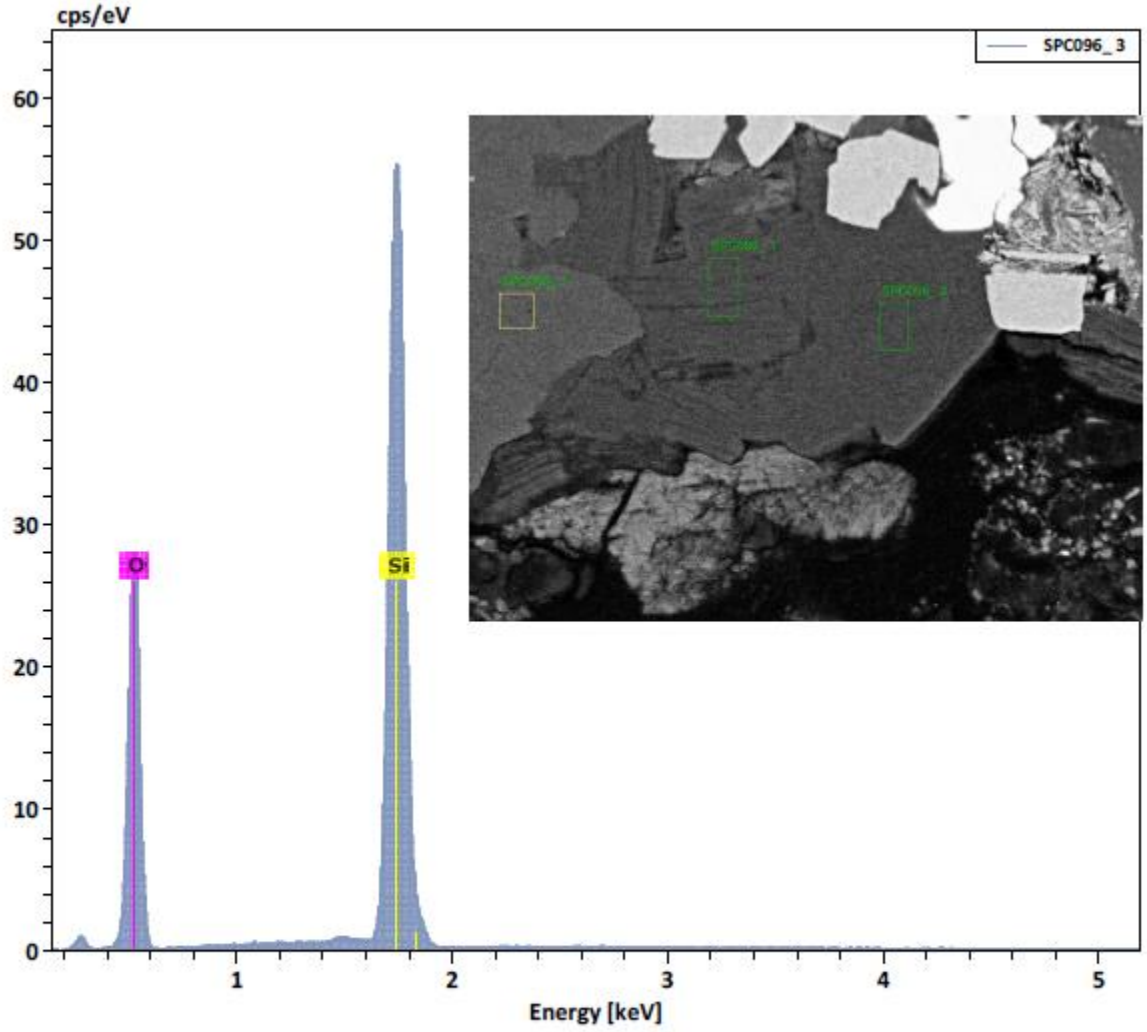

Spectrum	O	Si
SPC096_3	52.6	47.4

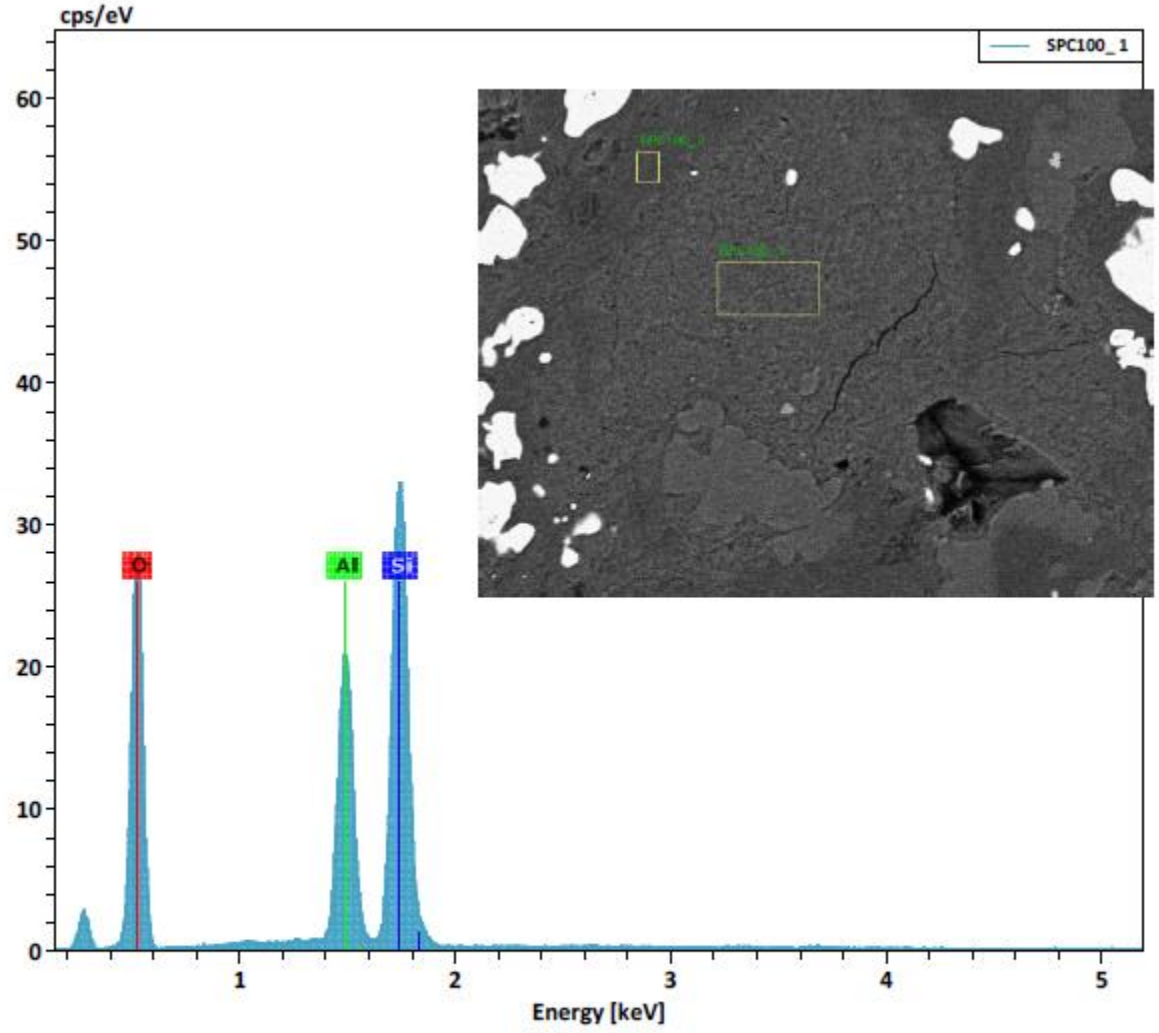

Spectrum	O	Al	Si
SPC100_1	51.4	16.3	32.3

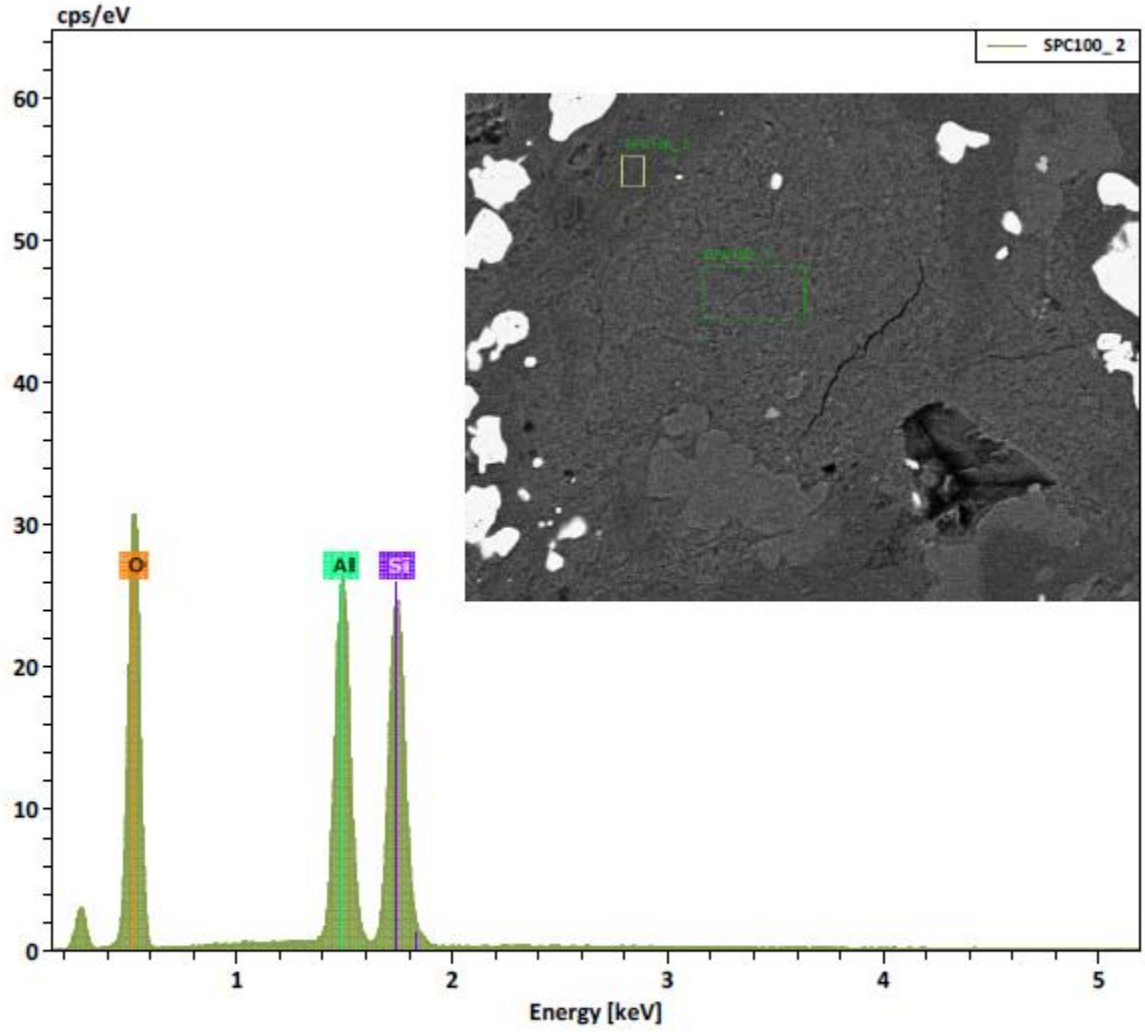

Spectrum	O	Al	Si
SPC100_2	54.3	19.9	25.8

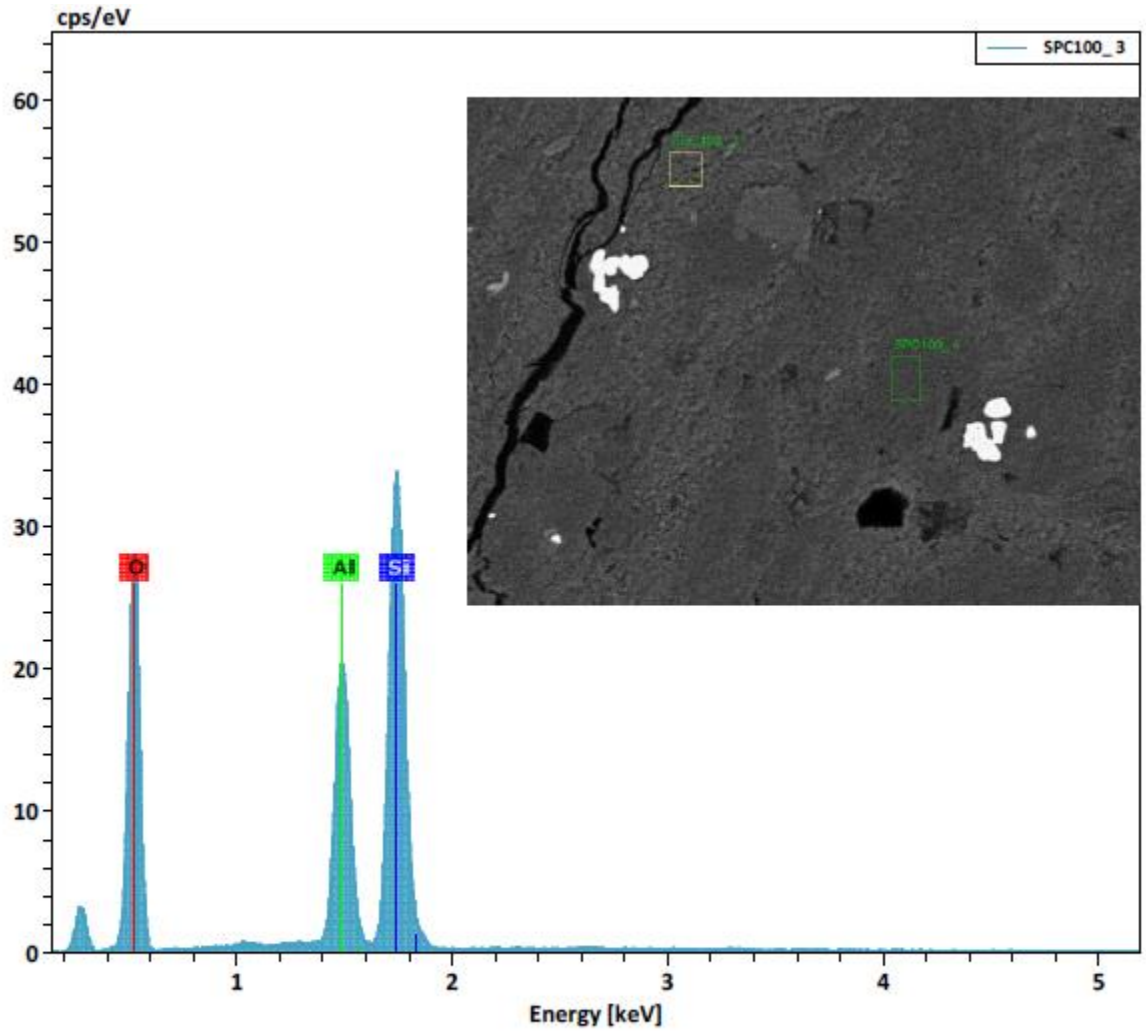

Spectrum	O	Al	Si
SPC100_3	51.3	16.0	32.7

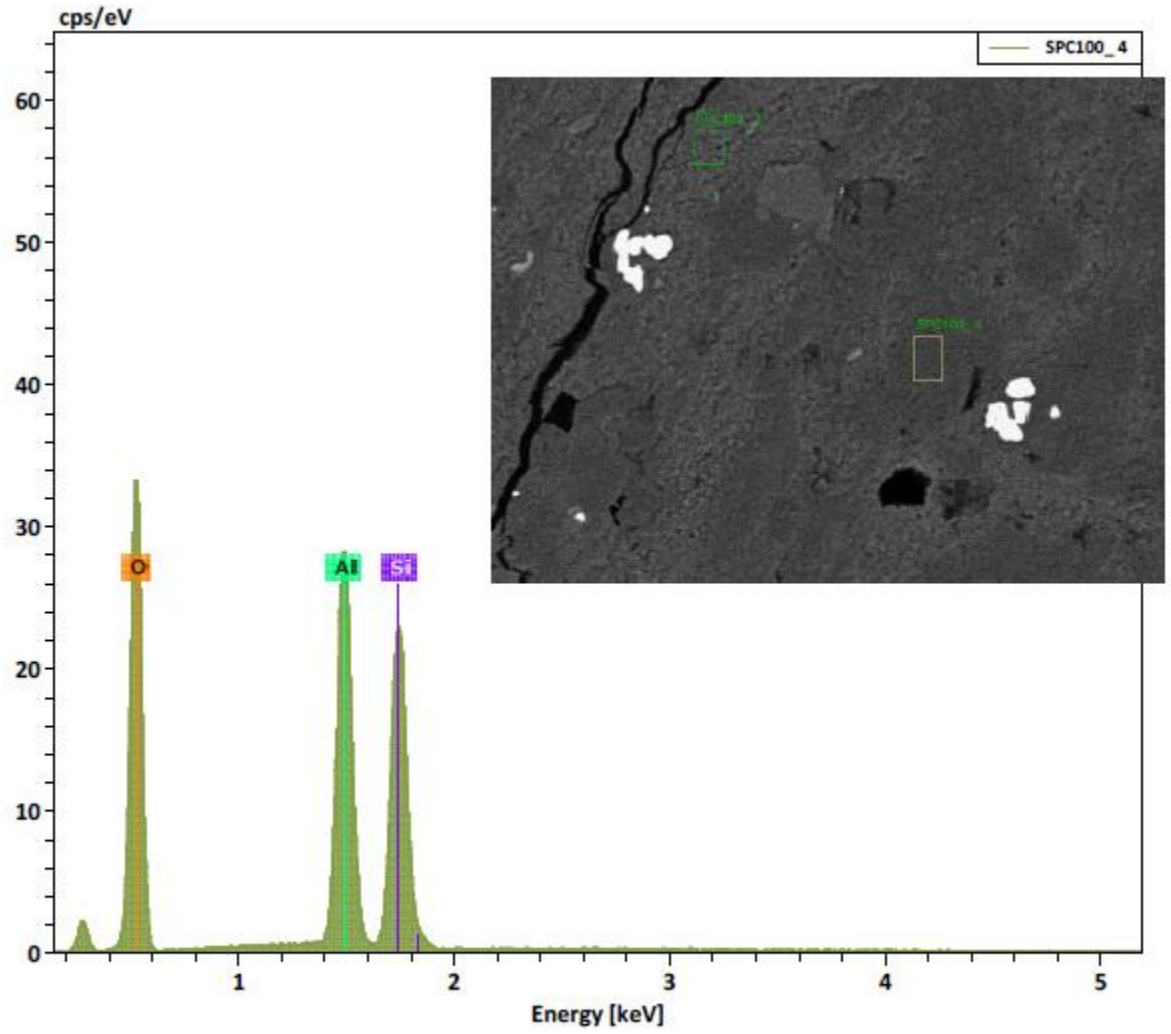

Spectrum	O	Al	Si
SPC100_4	55.4	21.2	23.4

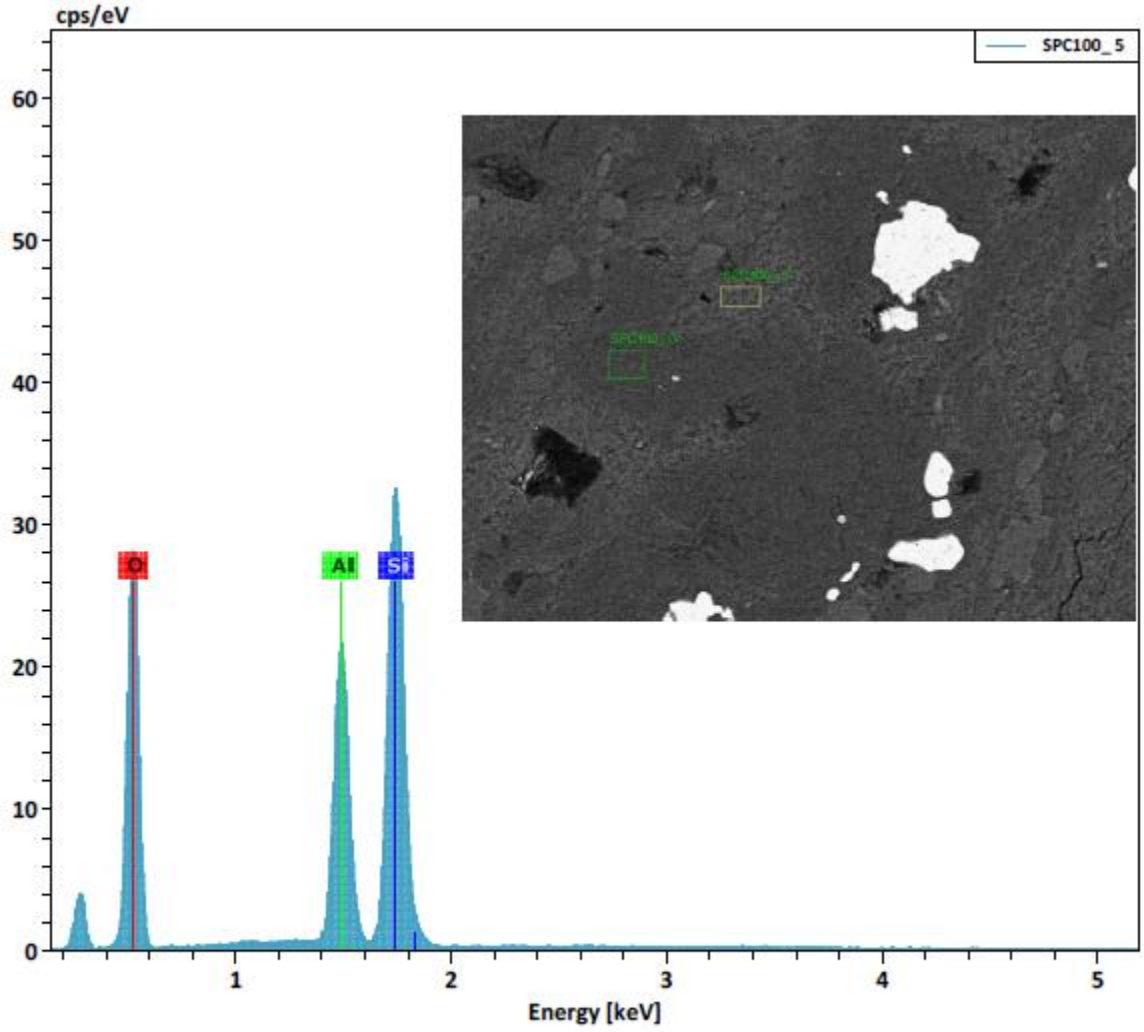

Spectrum	O	Al	Si
SPC100_5	51.6	15.9	32.5

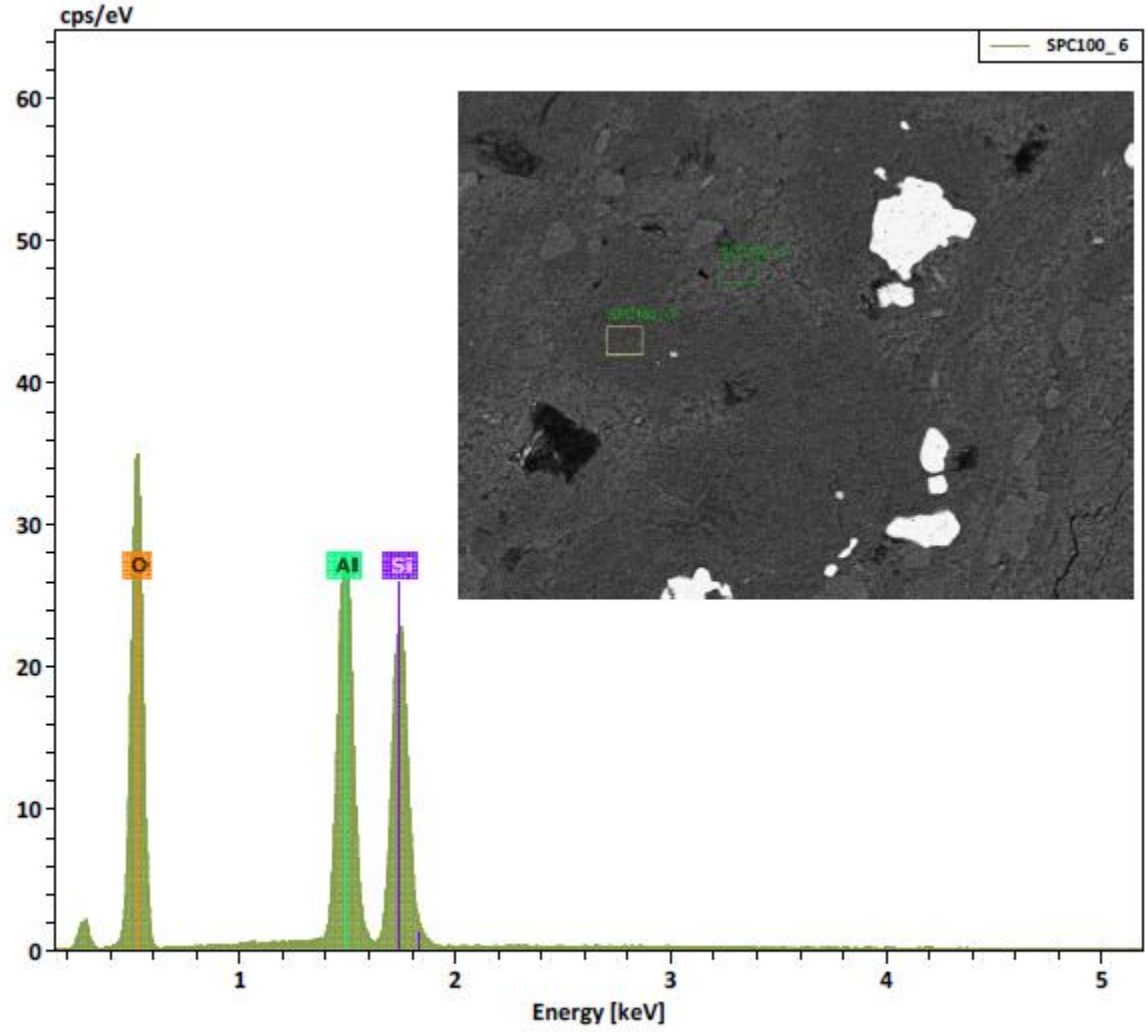

Spectrum	O	Al	Si
SPC100_6	55.9	21.0	23.1

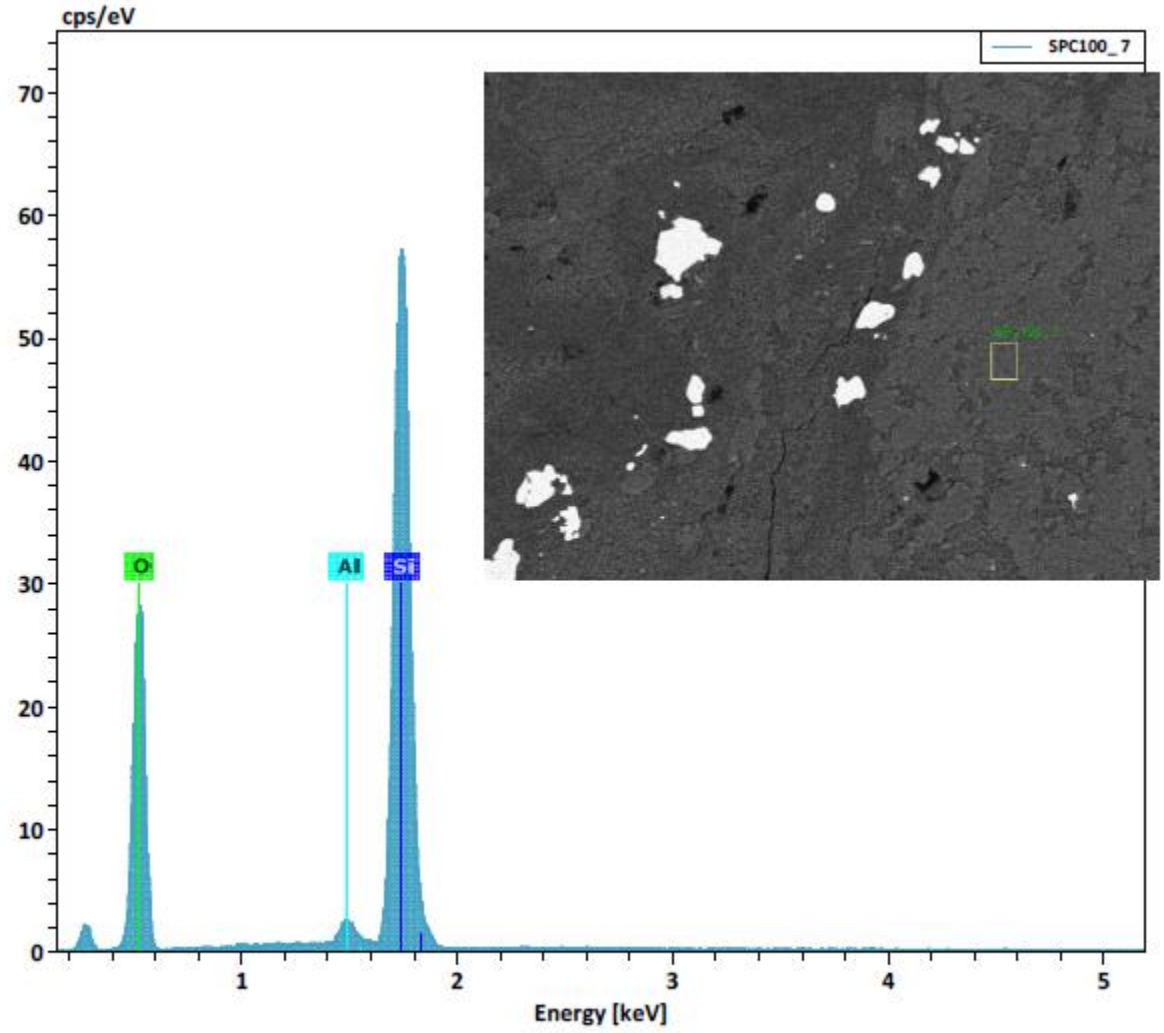

Spectrum	O	Al	Si
SPC100_7	51.6	1.5	47.0

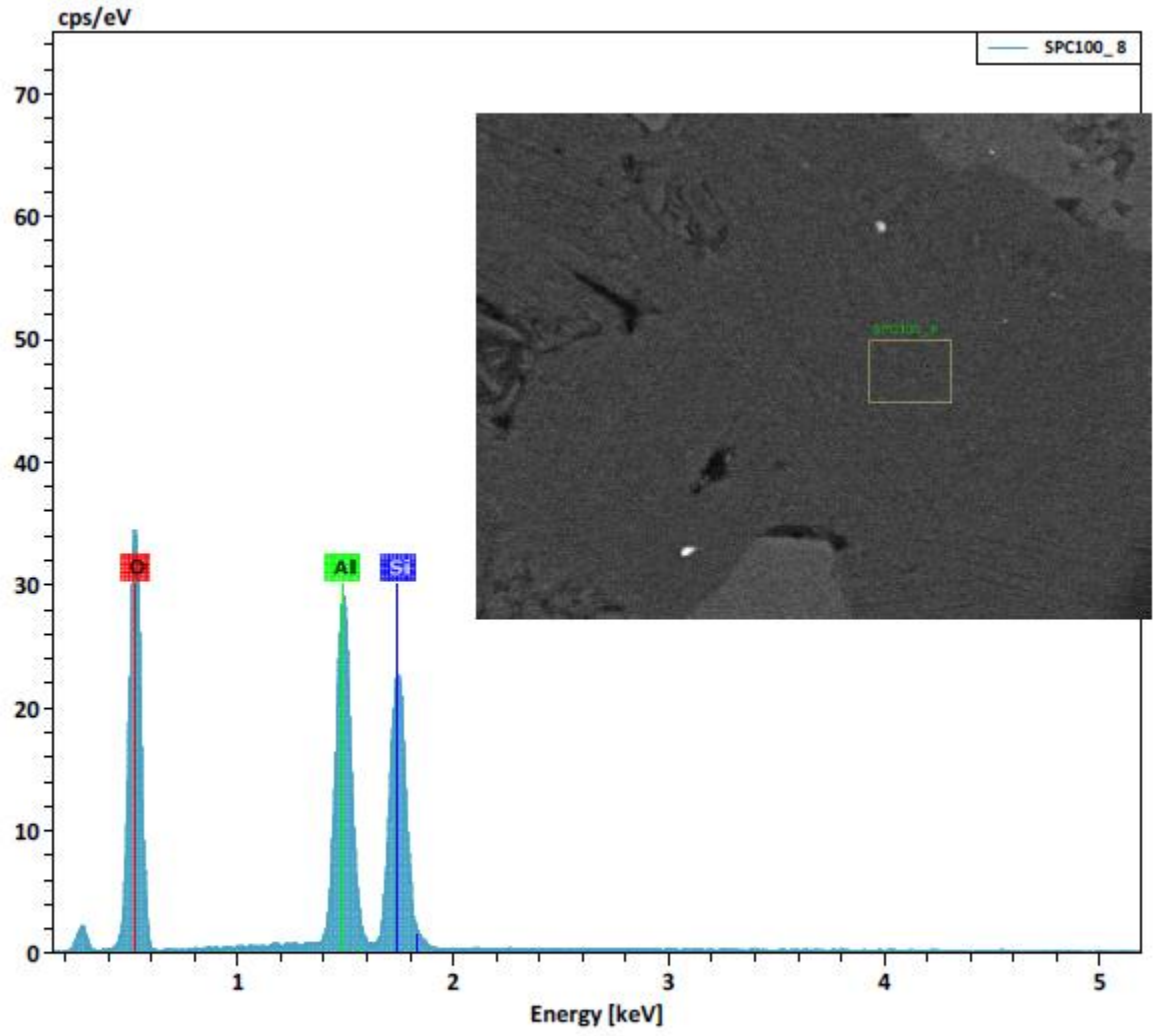

Spectrum	O	Al	Si
SPC100_8	55.8	21.5	22.7

| NodeID | DepthFrom | DepthTo | CollarEast | CollarNorth | SampleType | SWIRMineralsRaw | SWIRMineral_Howat | AlternationAssemblage_mineralsRaw | alMineral1 | alMineral2 | alMineral3 | alMineral4 | alMineral5 | alMineral6 | VNIRMineralsRaw | Reflection | QaQc_Reflect | SWIRMineral | QaQc_Noise | QaQc_Quality | QaQc_Water | WhiteMica_SC | Chlorite_SC | Carbonate_SC | Biotite_SC | Epidote_SC | Kaolinite_SC | Dickite_SC | Halloysite_SC | Amphibole_SC | Montmor_SC | Nontronite_SC | Zeolite_SC | Alunite_SC | CaAlunite_SC | Jarosite_SC | Gypsum_SC | Pyrophyllite_SC | Prehnite_SC | Wotter_ice_SC | Jarosite_mix | FeCarb_xor | Hem_xor | Goeth_xor | Chl_xor | Tourm_xor | Wav_WhMica | KT_WhMica | KT_WHMica | Wav_ChlMin | Type_ChlMin | Wav_Alunite | Int_Alunite | Type_Alunite | Type_Carb | KT_KaolRatio | KT_KaolQ1480 | KT_KaolQ1560 | KaDiWtM | Slope2160 | Wav_Min | D_Main | Wav_AlOH | D_AlOH | Wvl_AlOHM | Wav_AlOHAbs | D_AlOHAbs | Wvl_AlOHAbs | Wav_FeOx | D_FeOx | Wvl_FeOH | Wav_MgOHCb | D_MgOHCb | Wvl_MgOHCb | ReSmectite | Wav_OHAl2200 | D_OHAl2200 | Wvl_OHAl2200 | Wav_Epi1550 | D_Epi1550 | Wav_H2O |
|---|---|---

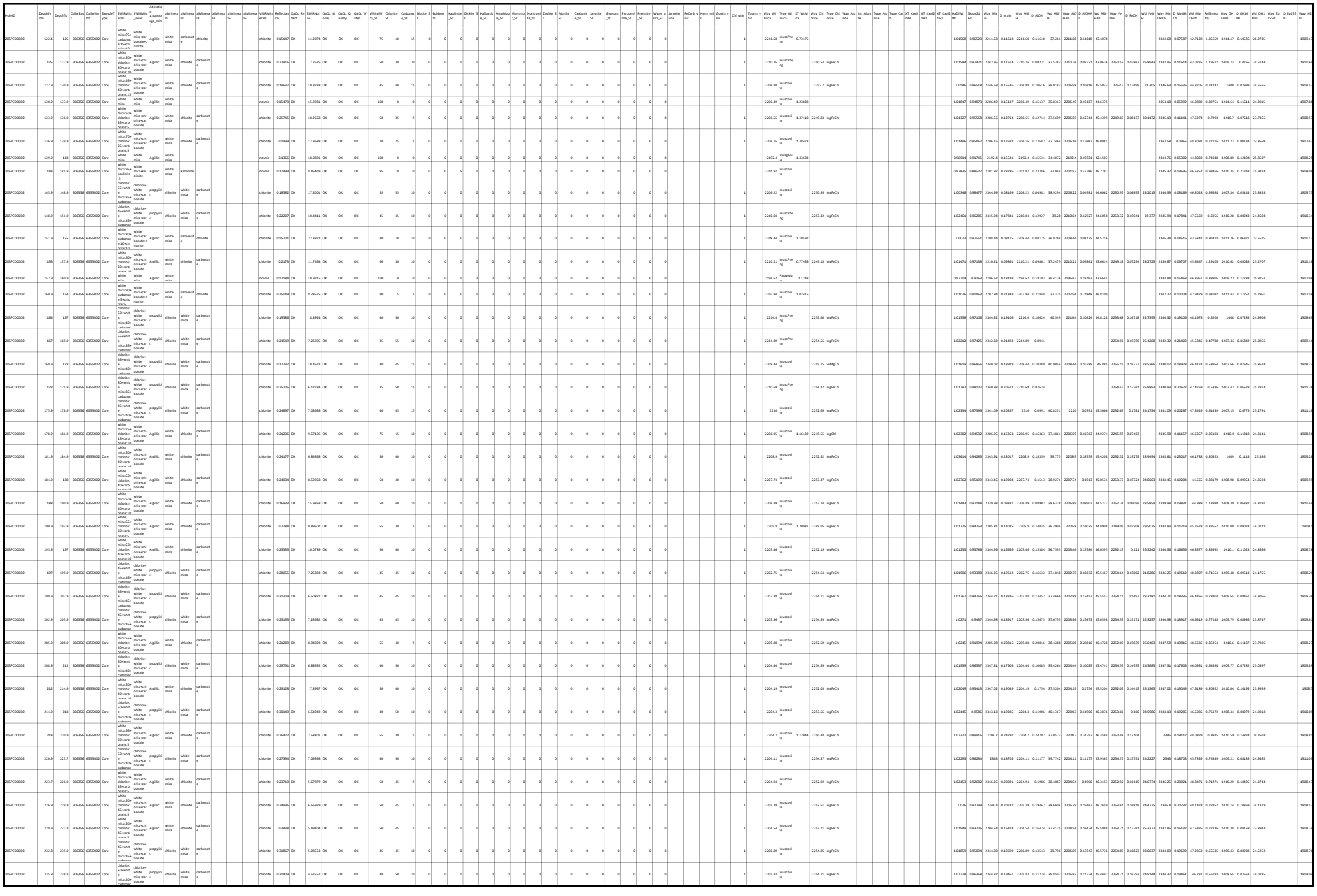

| HoleID | Depth(from) | Depth(to) | CollarEast | CollarNorth | SampleType | SWIRMineralsA | SWIRMineralsB | AlternationAssemblage_mineralsA | aiMineral1 | aiMineral2 | aiMineral3 | aiMineral4 | aiMineral5 | aiMineral6 | VNIRMineralsA | Reflection | QaQc_Reflect | SWIRMineralsC | QaQc_Noise | QaQc_Quality | QaQc_Water | WhiteMica_SC | Chlorite_SC | Carbonate_SC | Biotite_SC | Epidote_SC | Kaolinite_SC | Dickite_SC | Halloysite_SC | Amphibole_SC | Montmor_SC | Nontron_SC | Zeolite_SC | Alunite_SC | CaAlunite_SC | Jarosite_SC | Gypsum_SC | Pyrophyllite_SC | Prehnite_SC | Wollastonite_SC | Jarosite_variation | FeCarb_variation | Hem_vsWr | Goeth_vsWr | Chl_variation | Tourm_vsWr | Wav_WhiteMica | Type_WhiteMica | KT_WMIndex | Wav_ChlIndex | Type_ChlIndex | Wav_AlunIndex | Int_AlunIndex | Type_AlunIndex | Type_CarbIndex | KT_KaoliIndex | KT_KaoQI180 | KT_KaoQI160 | KaDiWtM | Slope2140 | Wav_Min | D_Main | Wav_AlOH | D_AlOH | Wid_AlOH | Wav_AlOH3 | D_AlOH4 | Wid_AlOH4 | Wav_Fe | D_FeOH | Wid_FeOH | Wav_MgOH3b | D_MgOH3b | Wid_MgOH3b | RelSmectite | Wav_OH1600 | D_OH1600 | Wid_OH1600 | Wav_Epi1550 | D_Epi1550 | Wav_H2O |
|---|---|---

| HoleID | DepthFrom | DepthTo | CollarEast | CollarNorth | SampleType | SWIRMineralsNewest | SWIRMineralsNewest | Alteration Assemblage_mins | aiMineral1 | aiMineral2 | aiMineral3 | aiMineral4 | aiMineral5 | aiMineral6 | VNIRMineralsNewest | Reflectance | QaQc_Reflect | SWIRMoose | QaQc_Noise | QaQc_Quality | QaQc_Water | WhiteMica_SC | Chlorite_SC | Carbonate_SC | Biotite_SC | Epidote_SC | Kaolinite_SC | Dickite_SC | Halloysite_SC | Amphibole_SC | Montmor_SC | Nontronite_SC | Zeolite_SC | Alunite_SC | CaAlunite_SC | Jarosite_SC | Gypsum_SC | PyrophyllHine_SC | Prehnite_SC | Wotter_silica_SC | Jarosite_vnir | FeCarb_vnir | Hem_vnir | Goeth_vnir | Chl_vnir | Tourm_vnir | Wav_WhMica | Type_WhMica | KT_WhMica | Wav_ChlorIte | Type_ChlorIte | Wav_Alunite | Int_Alunite | Type_Alunite | Type_Calcite | KT_KaoliniteI | KT_KaoGI160 | KT_KaoGI160 | KaDiWtM | Slope1400 | Wav_Min | D_Main | Wav_AlOHH | D_AlOHi | Wd_AlOHM | Wav_AlOHAll | D_AlOHAll | Wd_AlOHAll | Wav_FeOH | D_FeOxi | Wd_FeOH | Wav_MgOHClb | D_MgOHClb | Wd_MgOHClb | RelSmectite | Wav_OHI1620 | D_OH1480 | Wd_OH1480 | Wav_Epi1550 | D_Epi1550 | Wav_H2O |
|---|---|---

| HoleID | DepthFrom | DepthTo | CollarEast | CollarNorth | SampleType | SWIRMineralS | SWIRMin_newt | Alteration Assemblage_min | alMineral1 | alMineral2 | alMineral3 | alMineral4 | alMineral5 | alMineral6 | VNIRMineralS | Reflectance | QaQc_Reflect | SWIRNoise | QaQc_Noise | QaQc_Quality | QaQc_Water | WhiteMica_SC | Chlorite_SC | Carbonate_SC | Biotite_SC | Epidote_SC | Kaolinite_SC | Dickite_SC | Halloysite_SC | Amphibole_SC | Montmor_SC | Nontronite_SC | Zeolite_SC | Alunite_SC | CaAlunite_SC | Jarosite_SC | Gypsum_SC | PyrophyllineSC | Prehnite_SC | Wotter_silica_SC | Jarosite_vnir | FeCarb_vnir | Hem_vnir | Goeth_vnir | Chl_vnir | Tourm_vnir | Wav_WhMica | Type_WhMica | KT_WMica | Wav_Chlorite | Type_Chlorite | Wav_Alunite | Int_Alunite | Type_Alunite | Type_Carb | KT_KaolGlite | KT_KaolGlite1 | KT_KaolGlite2 | KaDiWtM | Slope2140 | Wav_Min | D_Main | Wav_AlOH | D_AlOH | Wid_AlOH | Wav_AlOHA | D_AlOHA | Wid_AlOHA | Wav_FeOH | D_FeOH | Wid_FeOH | Wav_MgOH | D_MgOHb | Wid_MgOHb | ReSmectite | Wav_OH1600 | D_OH1400 | Wid_OH1400 | Wav_Epi1550 | D_Epi1550 | Wav_H2O |
|---|---|---

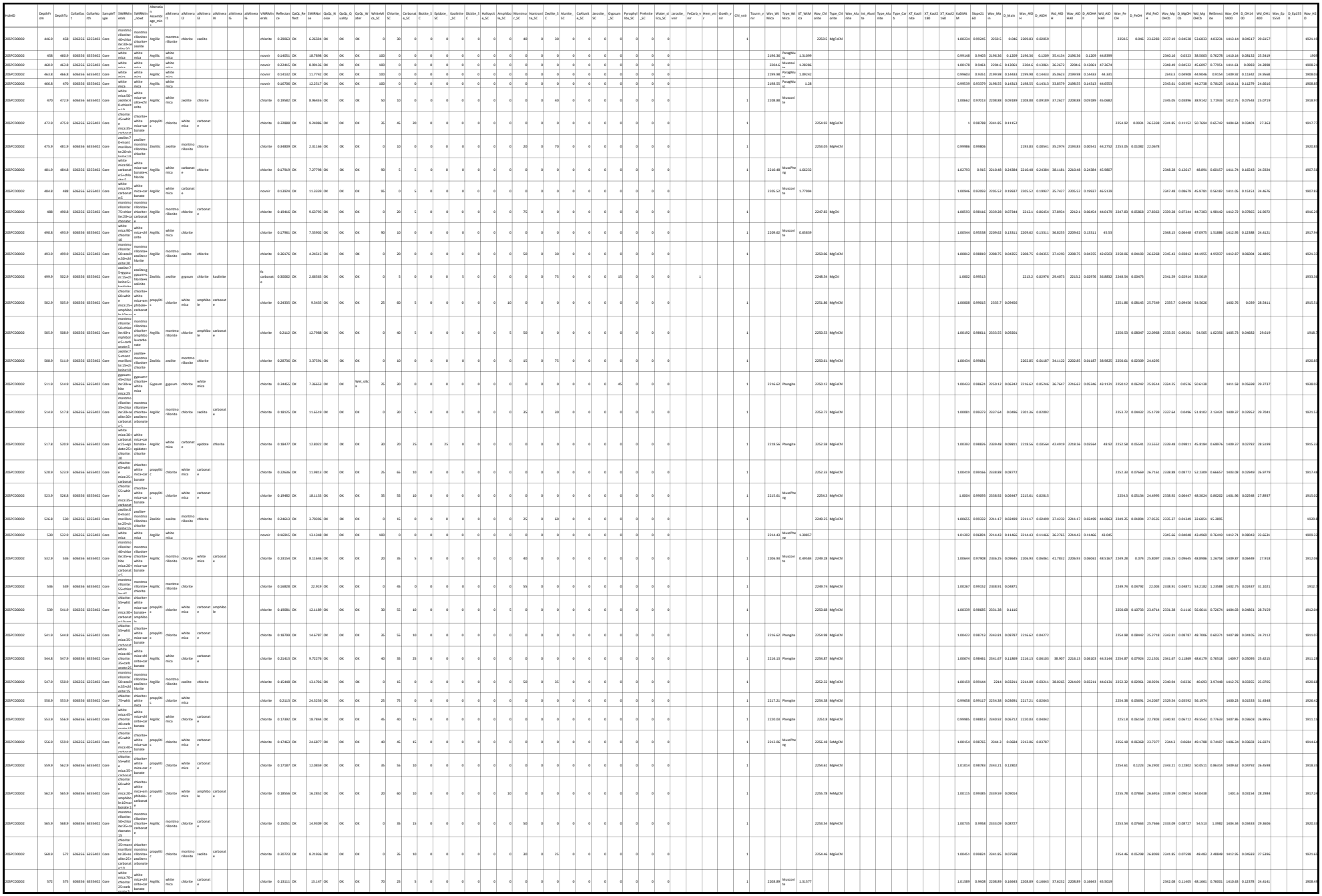

| NodeID | DepthFrom | DepthTo | CollarEast | CollarNorth | SampleType | SWIRMineralsPresent | SWIRMineralsPresent_newest | AlteredAssemblage_mineralsPresent | aiMineralGroup1 | aiMineralGroup2 | aiMineralGroup3 | aiMineralGroup4 | aiMineralGroup5 | aiMineralGroup6 | VNIRMineralsPresent | ReflectanceQuality | QaQc_ReflectanceQuality | QaQc_SWIRNoise | QaQc_NoiseQuality | QaQc_QualityWater | WhiteMicaSC | ChloriteSC | CarbonateSC | BiotiteSC | EpidoteSC | KaoliniteSC | DickiteSC | HalloysiteSC | AmphiboleSC | MontmorilloniteSC | NontroniteSC | ZeoliteSC | AlunitoSC | CaAluniteSC | JarositeSC | GypsumSC | PyrophyllineSC | PrehniteSC | WatteriteSC | JarositeCrystalline | FeClayCrystalline | Hem_veinCrystalline | GoethiteCrystalline | Chl_veinCrystalline | Tourm_veinCrystalline | Wav_WhiteMica | Type_WhiteMica | KT_WIMIca | Wav_Chlorite | Type_Chlorite | Wav_AluminousClay | Type_ClayCrystalline | KT_KaoliniteClay | KT_KaoliniteClay180 | KT_KaoliniteClay360 | KaDiWidth | Slope2160 | Wav_Mgin | D_Main | Wav_AlOH | D_AlOH | Wid_AlOH | Wav_AlOHAll | D_AlOHAll | Wid_AlOHAll | Wav_FeOx | D_FeOx | Wid_FeOx | Wav_MgOHCb | D_MgOHCb | Wid_MgOHCb | RelSmectite | Wav_OHAl2200 | D_OH14800 | Wid_OH1400 | Wav_Epi1550 | D_Epi1550 | Wav_H2O |
|---|---|---

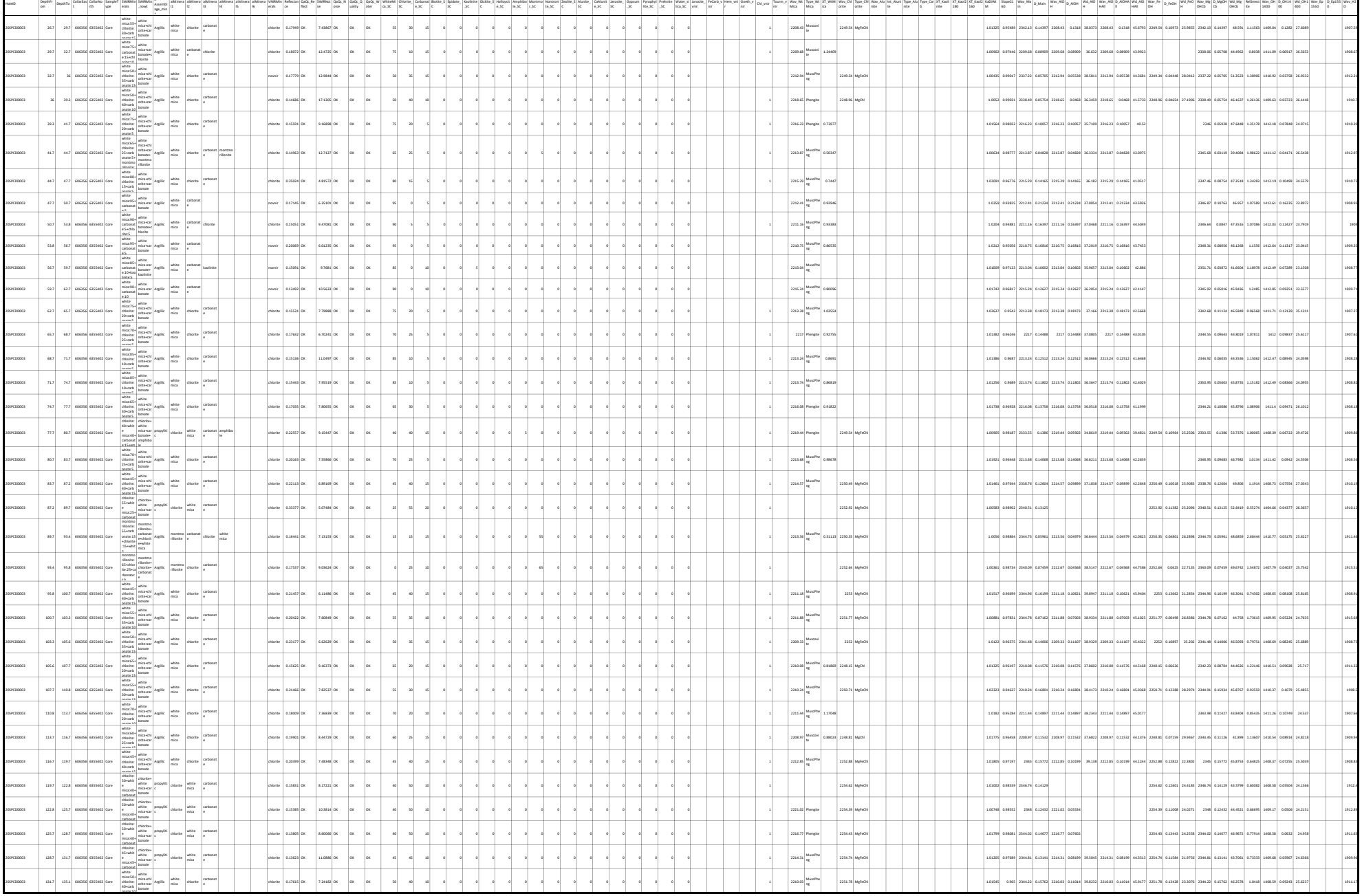

| HoleID | DepthFrom | DepthTo | CollarEast | CollarNorth | SampleType | SWIRMineralsNewE | SWIRMineralsNewE | AlternationAssemblage_mins | aiMineral1 | aiMineral2 | aiMineral3 | aiMineral4 | aiMineral5 | aiMineral6 | VNIRMineralsNewE | ReflectanceQ | QaQc_Reflect | SWIRNoise | QaQc_Noise | QaQc_Quality | QaQc_Water | WhiteMicaSC | Chlorite_SC | Carbonate_SC | Biotite_SC | Epidote_SC | Kaolinite_SC | Dickite_SC | Halloysite_SC | Amphibole_SC | Montmor_SC | Nontronite_SC | Zeolite_SC | Alunite_SC | CaAlunite_SC | Jarosite_SC | Gypsum_SC | PyrophyllineSC | Prehnite_SC | WatericeSC | Jarosite_unsr | FeCarb_unsr | Hem_unsr | Goeth_unsr | Chl_unsr | Tourm_unsr | Wav_WhiMica | Type_WhiMica | KT_WhiMica | Wav_ChlorIntra | Type_ChlorIntra | Wav_Alunite | Int_Alunite | Type_Alunite | Type_Carb | KT_KaoliniteI | KT_KaoliI 180 | KT_KaoliI 160 | KaDiWM | Slope1400 | Wav_Min | D_Main | Wav_AlOHa | D_AlOHa | Wid_AlOHA | Wav_AlOHA43 | D_AlOHA43 | Wid_AlOHA43 | Wav_FeOxide | D_FeOxide | Wid_FeOxide | Wav_MgOHCb | D_MgOHCb | Wid_MgOHCb | ReSmectite | Wav_OHIntra1600 | D_OHIntra1600 | Wid_OHIntra1600 | Wav_Epidote1550 | D_Epidote1550 | Wav_H2O |
|---|---|---

| HoleID | DepthFrom | DepthTo | CollarEast | CollarNorth | SampleType | SWIRMineralsNewE | SWIRMineralsNewE | Alteration Assemblage_mins | aiMineral1 | aiMineral2 | aiMineral3 | aiMineral4 | aiMineral5 | aiMineral6 | VNIRMineralsNewE | Reflectance | QaQc_Reflect | SWIRNoise | QaQc_Noise | QaQc_Quality | QaQc_Water | WhiteMica_SC | Chlorite_SC | Carbonate_SC | Biotite_SC | Epidote_SC | Kaolinite_SC | Dickite_SC | Halloysite_SC | Amphibole_SC | Montmor_SC | Nontronite_SC | Zeolite_SC | Alunite_SC | CaAlunite_SC | Jarosite_SC | Gypsum_SC | PyrophyllineSC | Prehnite_SC | Witter_silica_SC | Jarosite_xnir | FeCarb_xnir | Hem_xnir | Goeth_xnir | Chl_xnir | Tourm_xnir | Wav_WhMica | Type_WhMica | KT_WhMica | Wav_ChlorIte | Type_ChlorIte | Wav_Alunite | Int_Alunite | Type_Alunite | Type_Carb | KT_KaoliniteA | KT_KaoQual180 | KT_KaoQual160 | KaDiWtM | Slope2160 | Wav_Min | D_Main | Wav_AlOH | D_AlOH | Wid_AlOH | Wav_AlOHAll | D_AlOHAll | Wid_AlOHAll | Wav_FeOH | D_FeOH | Wid_FeOH | Wav_MgOHCb | D_MgOHCb | Wid_MgOHCb | RelSmectite | Wav_OHI1620 | D_OHI1630 | Wid_OHI1630 | Wav_Epi1550 | D_Epi1550 | Wav_H2O |
|---|---|---

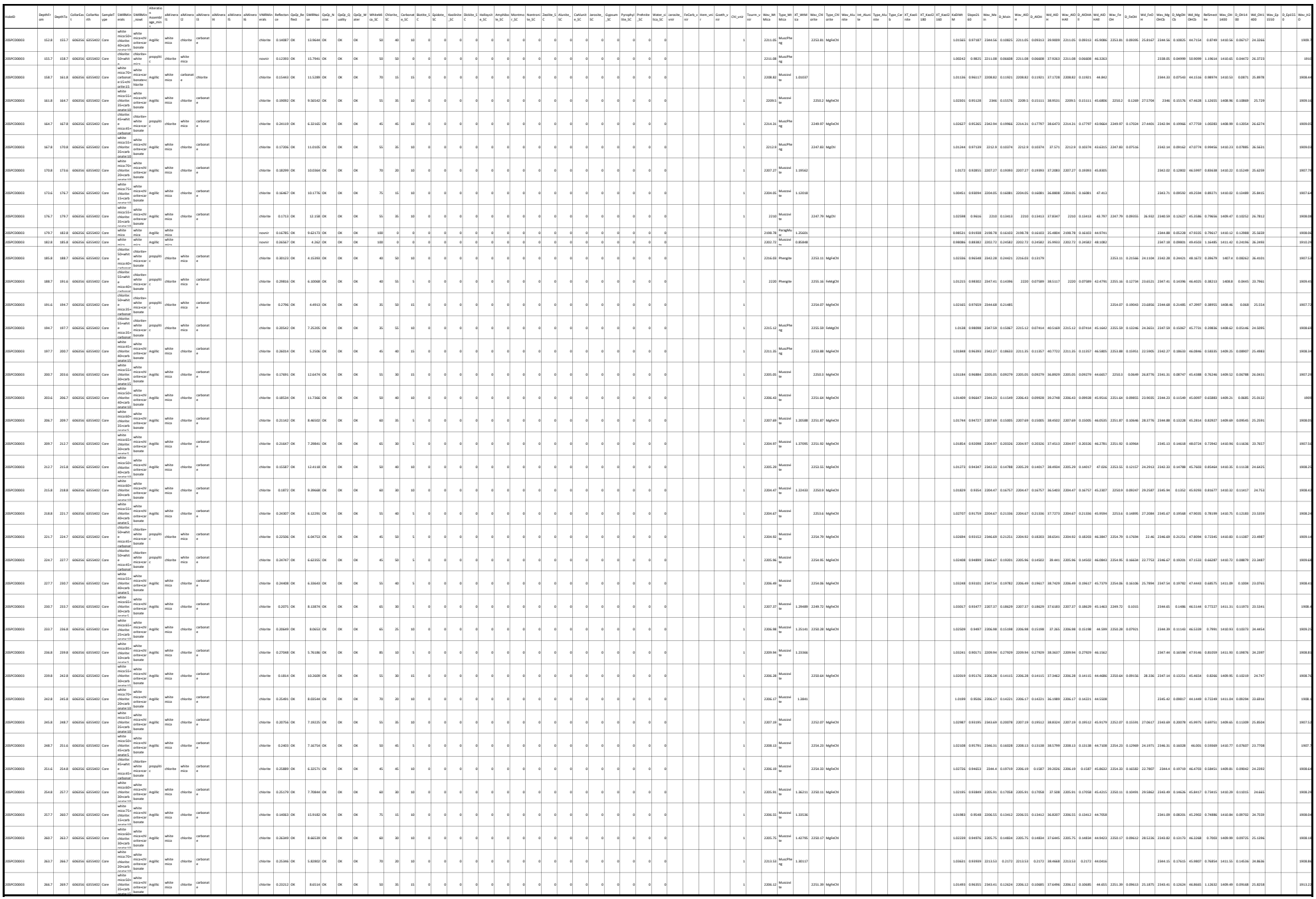

| HoleID | DepthFrom | DepthTo | CollarEast | CollarNorth | SampleType | SWIRMineralsNewE | SWIRMineralsNewE | Alteration Assemblage_mineralsNewE | alMineral1 | alMineral2 | alMineral3 | alMineral4 | alMineral5 | alMineral6 | VNIRMineralsNewE | Reflection | QaQc_Reflect | SWIRNoise | QaQc_Noise | QaQc_Quality | QaQc_Water | WhiteMica_SC | Chlorite_SC | Carbonate_SC | Biotite_SC | Epidote_SC | Kaolinite_SC | Dickite_SC | Halloysite_SC | Amphibole_SC | Montmor_SC | Nontron_SC | Zeolite_SC | Alunite_SC | CaAlunite_SC | Jarosite_SC | Gypsum_SC | Pyrophyl_SC | Prehnite_SC | Wotter_silica_SC | Jarosite_visir | FeCarb_visir | Hem_visir | Goeth_visir | Chl_visir | Tourm_visir | Wav_WhiteMica | Type_WhiteMica | KT_WIMica | Wav_Chlorite | Type_Chlorite | KT_Kaol1 | KT_Kaol2 | KT_Kaol3 | KaDiWall | Slope2to40 | Wav_Min | D_Main | Wav_AlOH | D_AlOH | Wid_AlOH | Wav_AlOHAsd | D_AlOHAsd | Wid_AlOHAsd | Wav_Fe | D_FeOxi | Wid_FeOH | Wav_MgOHCb | D_MgOHCb | Wid_MgOHCb | ReGmed | Wav_OHAl1600 | D_OHAl1600 | Wid_OHAl1600 | Wav_SpAl1550 | D_SpAl1550 | Wav_H2O |
|---|---|---

| NodeID | DepthFrom | DepthTo | CollarEast | CollarNorth | SampleType | SWIRMineralsWet | SWIRMineralsDry | Alteration_Assemblage_mins | aiMineral1 | aiMineral2 | aiMineral3 | aiMineral4 | aiMineral5 | aiMineral6 | VNIRMineralsWet | Reflectance | QaQc_Reflect | SWIRNoise | QaQc_Noise | QaQc_Quality | QaQc_Water | WhiteMica_SC | Chlorite_SC | Carbonate_SC | Biotite_SC | Epidote_SC | Kaolinite_SC | Dickite_SC | Halloysite_SC | Amphibole_SC | Montmor_SC | Nontronite_SC | Zeolite_SC | Alunite_SC | CaAlunite_SC | Jarosite_SC | Gypsum_SC | PyrophyllHite_SC | Prehnite_SC | Wotter_ice_SC | Jarosite_voir | FeCarb_voir | Hem_voir | Goeth_voir | Chl_voir | Tourm_voir | Wav_WhMica | Type_WhMica | KT_WhMica | Wav_ChlorIte | Type_ChlorIte | Wav_Alunite | Int_Alunite | Type_Alunite | Type_Carb | KT_KaoliHite | KT_KaoQI180 | KT_KaoQI160 | KaDiWtM | Slope2140 | Wav_MgOH | D_Main | Wav_AlOH | D_AlOH | Wd_AlOHM | Wav_AlOHAbs | D_AlOHAbs | Wd_AlOHAbs | Wav_FeOxi | D_FeOxi | Wd_FeOH | Wav_MgOHCb | D_MgOHCb | Wd_MgOHCb | ReSmectite | Wav_OH1600 | D_OH1600 | Wd_OH1400 | Wav_Epi1550 | D_Epi1550 | Wav_H2O |
|---|---|---

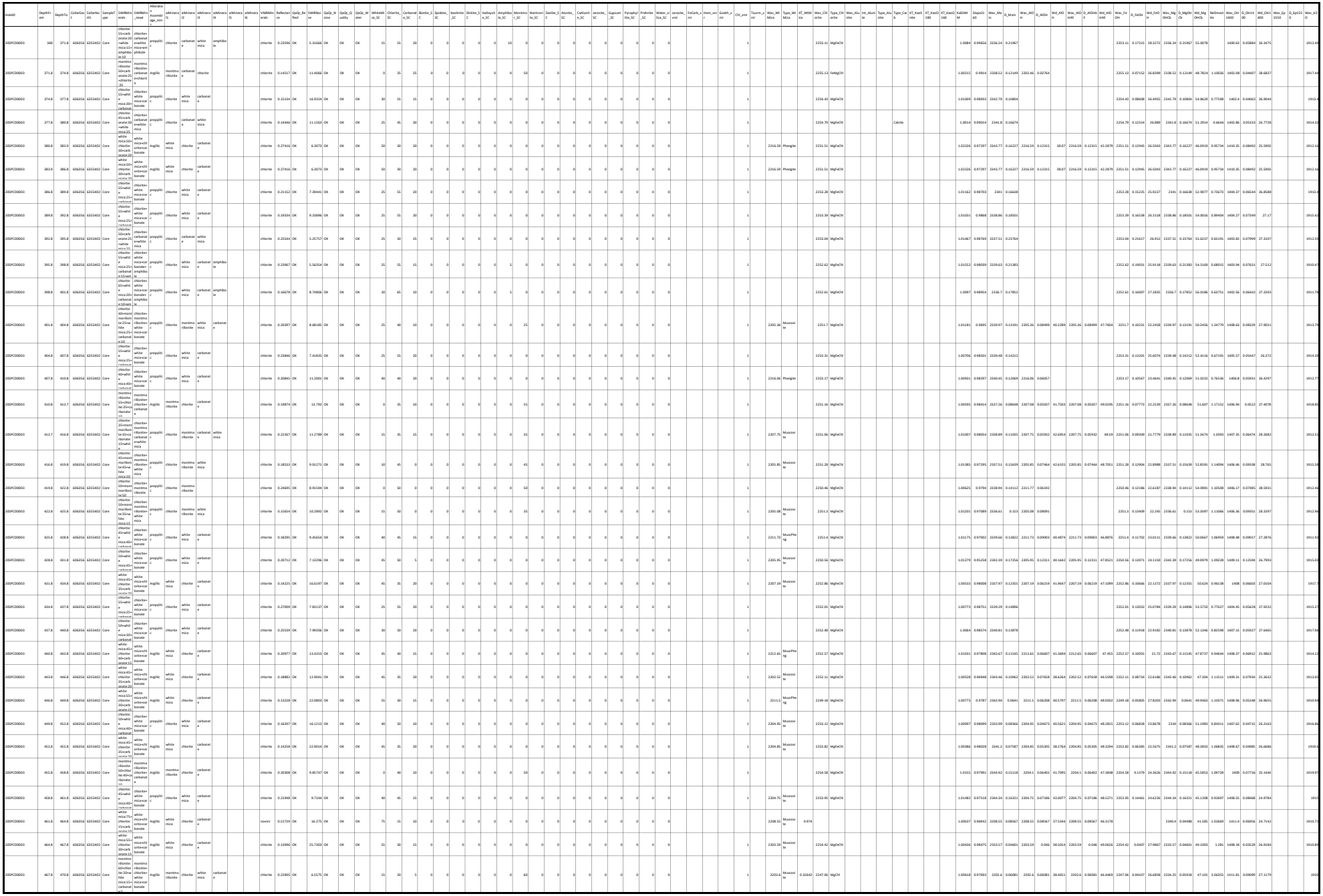

| NodeID | DepthFrom | DepthTo | CollarEast | CollarNorth | SampleType | SWIRMineralsIds | SWIRMineral_Jewel | AlternationAssemblage_mins | aiMineralSI | aiMineralSI2 | aiMineralSI3 | aiMineralSI4 | aiMineralSI5 | aiMineralSI6 | VNIRMineralsIds | Reflectance | QaQc_Reflect | SWIRNoise | QaQc_Noise | QaQc_Quality | QaQc_Water | WhiteMica_SC | Chlorite_SC | Carbonate_SC | Biotite_SC | Epidote_SC | Kaolinite_SC | Dickite_SC | Halloysite_SC | Amphibole_SC | Montmor_SC | Nontronite_SC | Zeolite_SC | Alunite_SC | CaAlunite_SC | Jarosite_SC | Gypsum_SC | PyrophyllHite_SC | Prehnite_SC | Wotter_silica_SC | Jarosite_vnir | FeCarb_vnir | Hem_vnir | Goeth_vnir | Chl_vnir | Tourm_vnir | Wav_WhMica | Type_WhMica | KT_WIMIca | Wav_ChlorIte | Type_ChlorIte | Wav_AluNite | Int_Alunite | Type_AluNite | Type_Calcite | KT_KaoliNite | KT_KaoQI180 | KT_KaoQI360 | KaDiWIM | Slope2160 | Wav_Min | D_Main | Wav_AlOH | D_AlOH | Wid_AlOH | Wav_AlOHAll | D_AlOHAll | Wid_AlOHAll | Wav_FeOH | D_FeOH | Wid_FeOH | Wav_MgOHCb | D_MgOHCb | Wid_MgOHCb | RelSmectite | Wav_OHI1620 | D_OHI1620 | Wid_OHI1400 | Wav_Epi1550 | D_Epi1550 | Wav_H2O | D_H2O |
|---|---|---

| HoleID | DepthFrom | DepthTo | CollarEast | CollarNorth | SampleType | SWIRMineralsNewE | SWIRMineralsNewE | AlternationAssemblage_mins | alMineral1 | alMineral2 | alMineral3 | alMineral4 | alMineral5 | alMineral6 | VNIRMineralsNewE | Reflectance | QaQc_Reflect | SWIRNoise | QaQc_Noise | QaQc_Quality | QaQc_Water | WhiteMica_SC | Chlorite_SC | Carbonate_SC | Biotite_SC | Epidote_SC | Kaolinite_SC | Dickite_SC | Halloysite_SC | Amphibole_SC | Montmor_SC | Nontronite_SC | Zeolite_SC | Alunite_SC | CaAlunite_SC | Jarosite_SC | Gypsum_SC | Pyrophyllite_SC | Prehnite_SC | Wotter_silica_SC | Jarosite_visir | FeCarb_visir | Hem_visir | Goeth_visir | Chl_visir | Tourm_visir | Wav_WhMica | Type_WhMica | KT_WhMica | Wav_Chlorite | Type_Chlorite | Wav_Alunite | Int_Alunite | Type_Alunite | Type_Carb | KT_KaoliniteD1 | KT_KaoD1D2 | KT_KaoD2D3 | KaDiWtM | Slope2to1D | Wav_Min | D_Main | Wav_AlOH | D_AlOH | Wid_AlOH | Wav_AlOHA | D_AlOHA | Wid_AlOHA | Wav_FeOH | D_FeOH | Wid_FeOH | Wav_MgOHCb | D_MgOHCb | Wid_MgOHCb | RelSmectite | Wav_OHD1600 | D_OH1400 | Wid_OH1400 | Wav_Epi1550 | D_Epi1550 | Wav_H2O |
|---|---|---

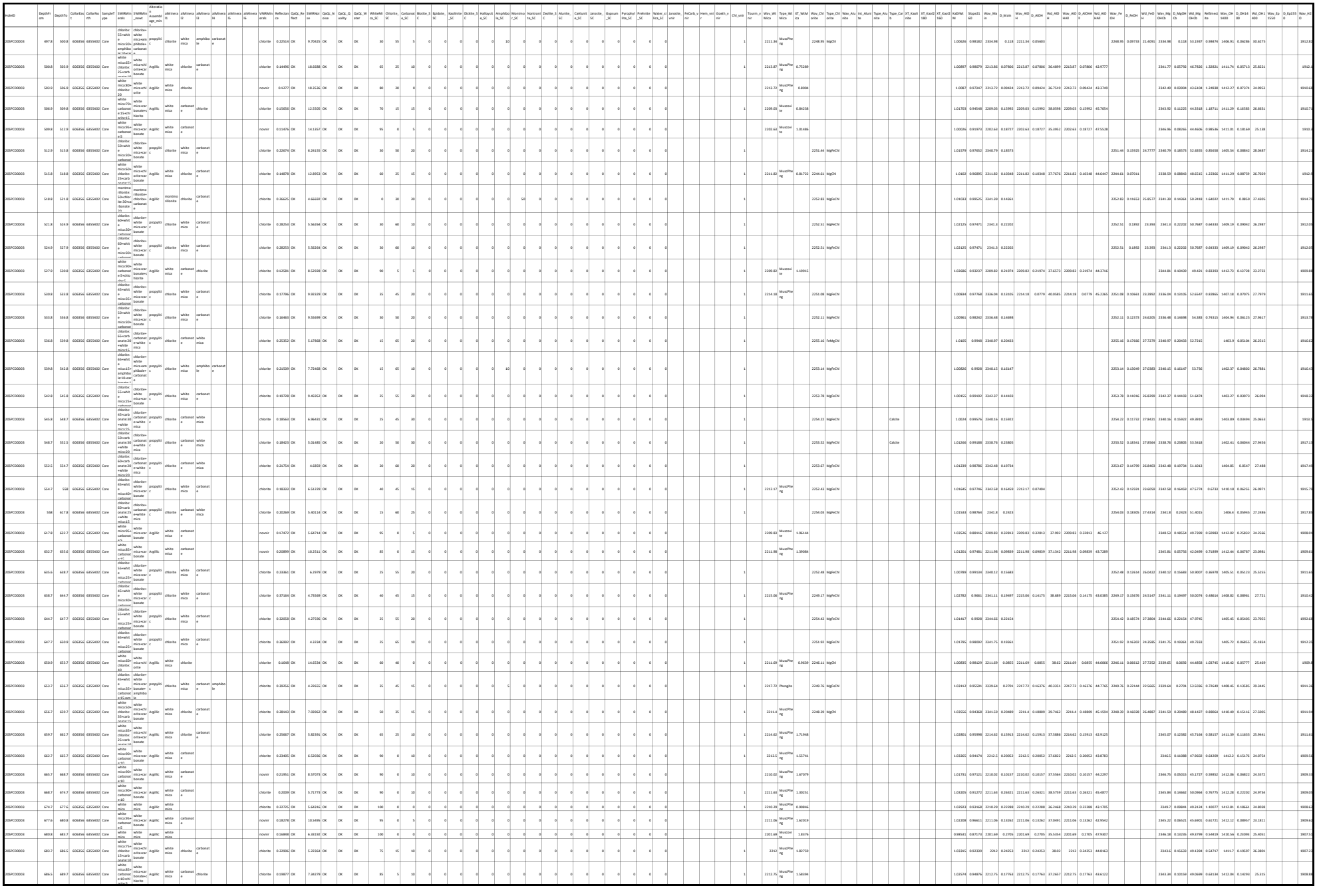

| HoleID | DepthFrom | DepthTo | CollarEast | CollarNorth | SampleType | SWIRMineralsNowell | SWIRMineralsNowell | Alteration Assemblage_mins | aiMineral1 | aiMineral2 | aiMineral3 | aiMineral4 | aiMineral5 | aiMineral6 | VNIRMineralsNowell | ReflectanceQuality | QpQc_ReflectQuality | SWIRMineralsNowell | QpQc_NoiseQuality | QpQc_QualityWater | QpQc_WaterQuality | WhiteMica_SC | Chlorite_SC | Carbonate_SC | Biotite_SC | Epidote_SC | Kaolinite_SC | Dickite_SC | Halloysite_SC | Amphibole_SC | Montmor_SC | Nontronite_SC | Zeolite_SC | Alunite_SC | CaAlunite_SC | Jarosite_SC | Gypsum_SC | PyrophyllHoleSC | Prehnite_SC | Wollastonite_SC | Jarosite_unsure | FeCarb_ox | Hem_unsure | Goeth_xsure | Chl_unsure | Tourm_xsure | Wav_WhMica | Type_WhMica | KT_WIMica | Wav_ChlontIte | Type_ChlontIte | Wav_AlunIte | Int_AlunIte | Type_AlunIte | Type_CarbIb | KT_KaoliIdx | KT_KaoQI180 | KT_KaoQI160 | KaDiWtM | Slope2140 | Wav_MgOH | D_Main | Wav_AlOH | D_AlOHn | Wid_AlOHA | Wav_AlOH2 | D_AlOHw3 | Wid_AlOHA#2 | Wav_FeOH | D_FeOpt | Wid_FeOHW | Wav_MgOHCb | D_MgOHCb | Wid_MgOHCb | ReSmectite | Wav_OH1600 | D_OH1480 | Wid_OH1480 | Wav_Epi1550 | D_Epi1550 | Wav_H2O |
|---|---|---

| NodeID | DepthFrom | DepthTo | CollarCount | CollarNotes | SampleType | SWIRMineralsAssemblage | SWIRMineralsAssemblage_newd | AlternativeAssemblage_mixes | alMineral1 | alMineral2 | alMineral3 | alMineral4 | alMineral5 | alMineral6 | VNIRMineralsAssemblage | Reflectance | QaQc_Reflectance | SWIRNoise | QaQc_Noise | QaQc_Quality | QaQc_Water | WhiteMica_SC | Chlorite_SC | Carbonate_SC | Biotite_SC | Epidote_SC | Kaolinite_SC | Dickite_SC | Halloysite_SC | Amphibole_SC | Montmor_SC | Nontronite_SC | Zeolite_SC | Alunite_SC | CaAlunite_SC | Jarosite_SC | Gypsum_SC | Pyrophyllite_SC | Prehnite_SC | Wotter_silica_SC | Jarosite_visir | FeCarb_visir | Hem_visir | Goeth_visir | Chl_visir | Tourm_visir | Wav_WhiteMica | Type_WhiteMica | KT_WIMIca | Wav_ChlorIntra | Type_ChlorIntra | Wav_AlunIntra | Int_AlunIta | Type_AlunIntra | Type_CarbIta | Type_CarbIta | KT_KaolGlad1 | KT_KaolGlad2 | KaDiWidM | Slope2160 | Wav_MaxIn | D_MaxIn | D_AlOHn | D_AlOHnA | Wvl_AlOHn | Wvl_AlOHnA | D_AlOHnA | Wvl_AlOHnA | Wav_FeOxIn | D_FeOxI | Wvl_FeOxI | Wav_MgOHCb | D_MgOHCb | Wvl_MgOHCb | RelSmectite | Wav_OHIn920 | D_OHIn1400 | Wvl_OHIn1400 | Wav_Epsilon1550 | D_Epsilon1550 | Wav_H2O |
|---|---|---

| HoleID | DepthFrom | DepthTo | CollarEast | CollarNorth | SampleType | SWIRMineralsNewE | SWIRMineralsNewE | Alternation Assemblage_mins | aiMineral1 | aiMineral2 | aiMineral3 | aiMineral4 | aiMineral5 | aiMineral6 | VNIRMineralsNewE | Reflectance | QaQc_Reflect | SWIRNoise | QaQc_Noise | QaQc_Quality | QaQc_Water | WhiteMica_SC | Chlorite_SC | Carbonate_SC | Biotite_SC | Epidote_SC | Kaolinite_SC | Dickite_SC | Halloysite_SC | Amphibole_SC | Montmor_SC | Nontronite_SC | Zeolite_SC | Alunite_SC | CaAlunite_SC | Jarosite_SC | Gypsum_SC | PyrophyllHse_SC | Prehnite_SC | Wotter_silica_SC | Jarosite_visir | FeCarb_visir | Hem_visir | Goeth_visir | Chl_visir | Tourm_visir | Wav_WhMica | Type_WhMica | KT_WIMica | Wav_ChlorIte | Type_ChlorIte | Wav_Alunite | Int_Alunite | Type_Alunite | Type_Carb | KT_KaoliIte | KT_KaoGib | KT_KaoGibM | KaDiWtM | Slope1600 | Wav_Min | D_Main | Wav_AlOH | D_AlOH | Wid_AlOH | Wav_AlOHA | D_AlOHA | Wid_AlOHA | Wav_FeOx | D_FeOx | Wid_FeOH | Wav_MgOHCb | D_MgOHCb | Wid_MgOHCb | ReSmectite | Wav_OHI1600 | D_OHI1600 | Wid_OHI1400 | Wav_Epi2150 | D_Epi2150 | Wav_H2O |
|---|---|---

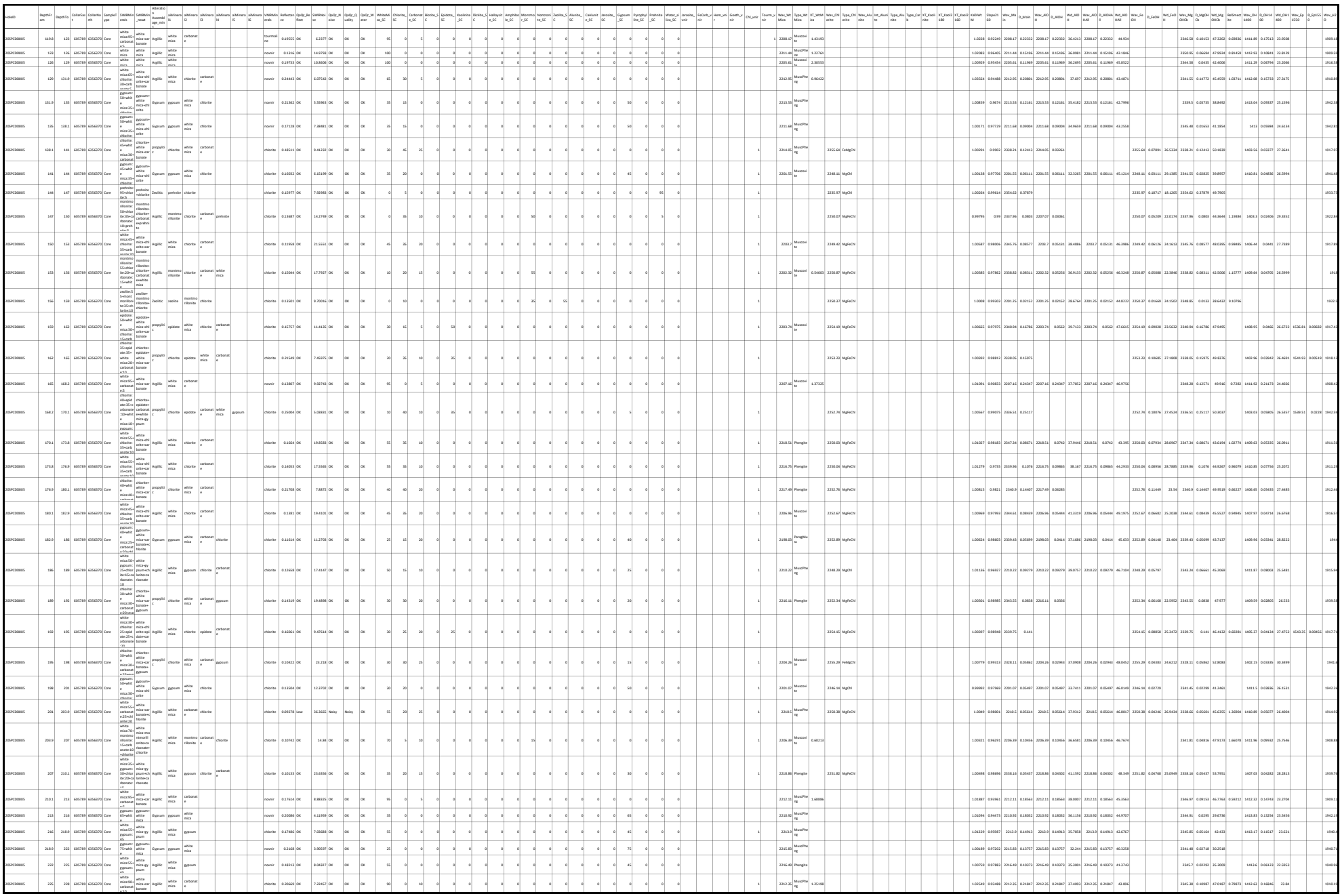

| HoleID | DepthFrom | DepthTo | CollarEast | CollarNorth | SampleType | SWIRMineralogy_newd | SWIRMineralogy_newd | Alteration Assemblage_mins | aiMineral1 | aiMineral2 | aiMineral3 | aiMineral4 | aiMineral5 | aiMineral6 | VNIRMineralogy | Reflection | QaQc_Reflect | SWIRNoise | QaQc_Noise | QaQc_Quality | QaQc_Water | WhiteMica_SC | Chlorite_SC | Carbonate_SC | Biotite_SC | Epidote_SC | Kaolinite_SC | Dickite_SC | Halloysite_SC | Amphibole_SC | Montmor_SC | Nontron_SC | Zeolite_SC | Alunite_SC | CaAlunite_SC | Jarosite_SC | Gypsum_SC | PyrophyllHse_SC | Prehnite_SC | Wotter_silica_SC | Jarosite_var | FeCarb_var | Hem_var | Goeth_var | Chl_var | Tourm_var | Wav_WhMica | Type_WhMica | KT_WhMica | Wav_Chlorite | Type_Chlorite | Wav_Alunite | Int_Alunite | Type_Alunite | Type_Carb | KT_Kaol1 | KT_Kaol2 180 | KT_Kaol3 160 | KaDiWtM | Slope2140 | Wav_Mgin | D_Main | Wav_AlOH | D_AlOH | Wd_AlOHM | Wav_AlOHAll | D_AlOHAll | Wd_AlOHAll | Wav_FeOH | D_FeOH | Wd_FeOH | Wav_MgOHCb | D_MgOHCb | Wd_MgOHCb | RelSmectite | Wav_OHI920 | D_OH1400 | Wd_OH1400 | Wav_Epi1550 | D_Epi1550 | Wav_H2O |
|---|---|---

| HoleID | DepthFrom | DepthTo | CollarEast | CollarNorth | SampleType | SWIRMineralsNewE | SWIRMineralsNewE | Alteration Assemblage_mineralsNewE | aiMineral1 | aiMineral2 | aiMineral3 | aiMineral4 | aiMineral5 | aiMineral6 | VNIRMineralsNewE | Reflectance | QaQc_Reflect | SWIRNoise | QaQc_Noise | QaQc_Quality | QaQc_Water | WhiteMica_SC | Chlorite_SC | Carbonate_SC | Biotite_SC | Epidote_SC | Kaolinite_SC | Dickite_SC | Halloysite_SC | Amphibole_SC | Montmor_SC | Nontronite_SC | Zeolite_SC | Alunite_SC | CaAlunite_SC | Jarosite_SC | Gypsum_SC | Pyrophyllite_SC | Prehnite_SC | Wollastonite_SC | Jarosite_var | FeCarb_var | Hem_var | Goeth_var | Chl_var | Tourm_var | Wav_WhiteMica | KT_WMFit | Type_WhiteMica | Wav_Chlorite | Type_Chlorite | Wav_Alunite | Int_Alunite | Type_Alunite | Type_Carb | KT_KaoliHite | KT_KaoQ180 | KT_KaoQ160 | KaDiWtM | Slope2to60 | Wav_Min | D_Main | Wav_AlOHa | D_AlOHa | Wid_AlOHa | Wav_AlOHMid | D_AlOHMid | Wid_AlOHMid | Wav_FeOH | D_FeOH | Wid_FeOH | Wav_MgOHCb | D_MgOHCb | Wid_MgOHCb | RelSmectite | Wav_OHb1600 | D_OHb1600 | Wid_OHb1600 | Wav_Epi1550 | D_Epi1550 | Wav_H2O |
|---|---|---

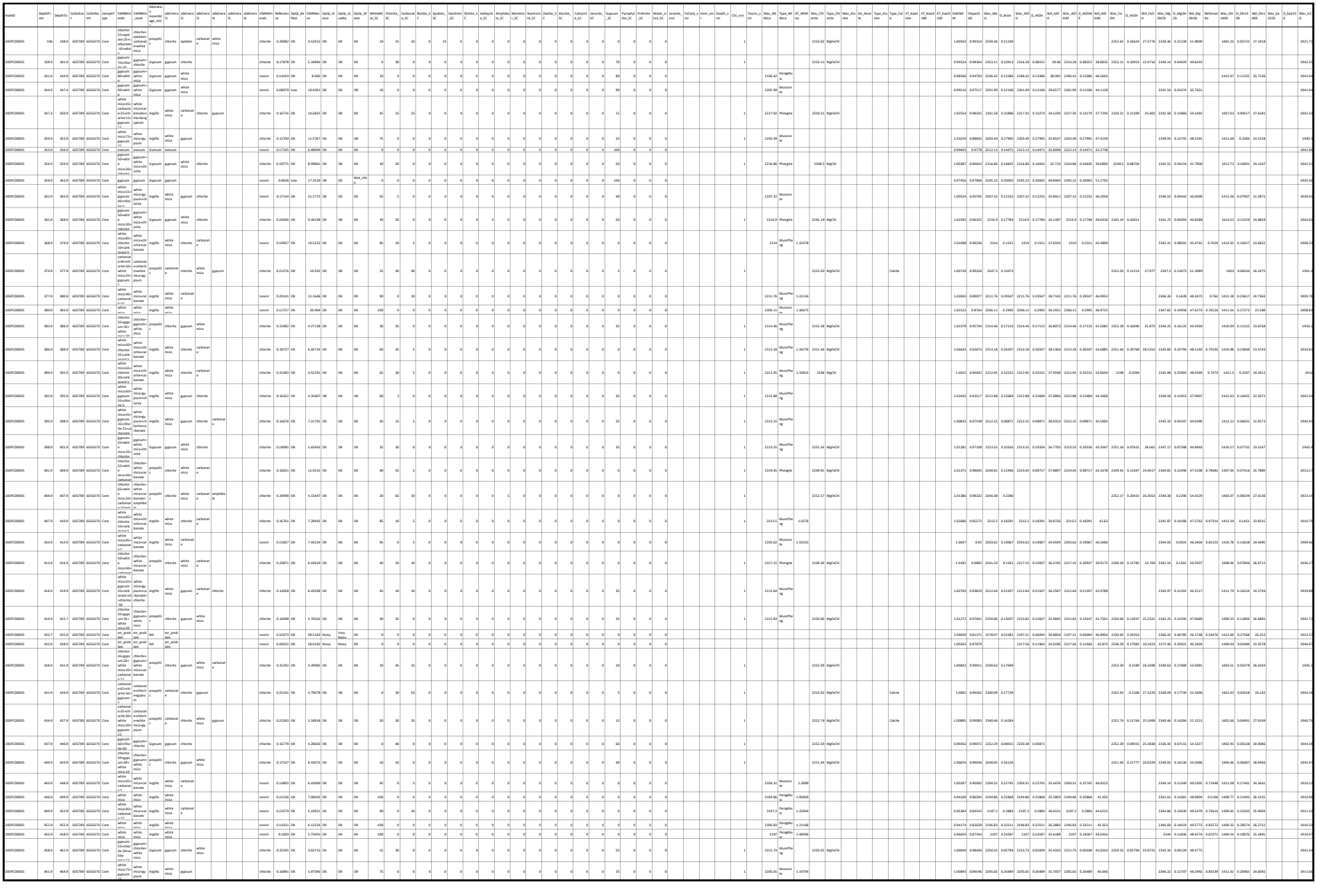

| HoleID | DepthFrom | DepthTo | CollarEast | CollarNorth | SampleType | SWIRMineralsNewE | SWIRMineralsNewE | Alteration Assemblage_mins | idMineral1 | idMineral2 | idMineral3 | idMineral4 | idMineral5 | idMineral6 | VNIRMineralsNewE | Reflectance | QaQc_Reflect | SWIRNoise | QaQc_Noise | QaQc_Quality | QaQc_Water | WhiteMica_SC | Chlorite_SC | Carbonate_SC | Biotite_SC | Epidote_SC | Kaolinite_SC | Dickite_SC | Halloysite_SC | Amphibole_SC | Montmor_SC | Nontronite_SC | Zeolite_SC | Alunite_SC | CaAlunite_SC | Jarosite_SC | Gypsum_SC | PyrophyllHoe_SC | Prehnite_SC | Wotter_silica_SC | Jarosite_unsr | FeCarb_unsr | Hem_unsr | Goeth_unsr | Chl_unsr | Tourm_unsr | Wav_WhMica | Type_WhMica | KT_WhMica | Wav_Chlorite | Type_Chlorite | Wav_Alunite | Int_Alunite | Type_Alunite | Type_Carb | KT_Kaol1 nite | KT_Kaol2 160 | KT_Kaol3 160 | KaDiWtM | Slope2160 | Wav_Mgin | D_Main | Wav_AlOH | D_AlOH | Wid_AlOH | Wav_AlOH4 | D_AlOH4 | Wid_AlOH4 | Wav_Fe Oxi | D_FeOxi | Wid_FeOH | Wav_MgOHCb | D_MgOHCb | Wid_MgOHCb | RelSmectite | Wav_OH 1600 | D_OH14 00 | Wid_OH1 400 | Wav_Epi 1550 | D_Epi155 0 | Wav_H2O |
|---|---|---

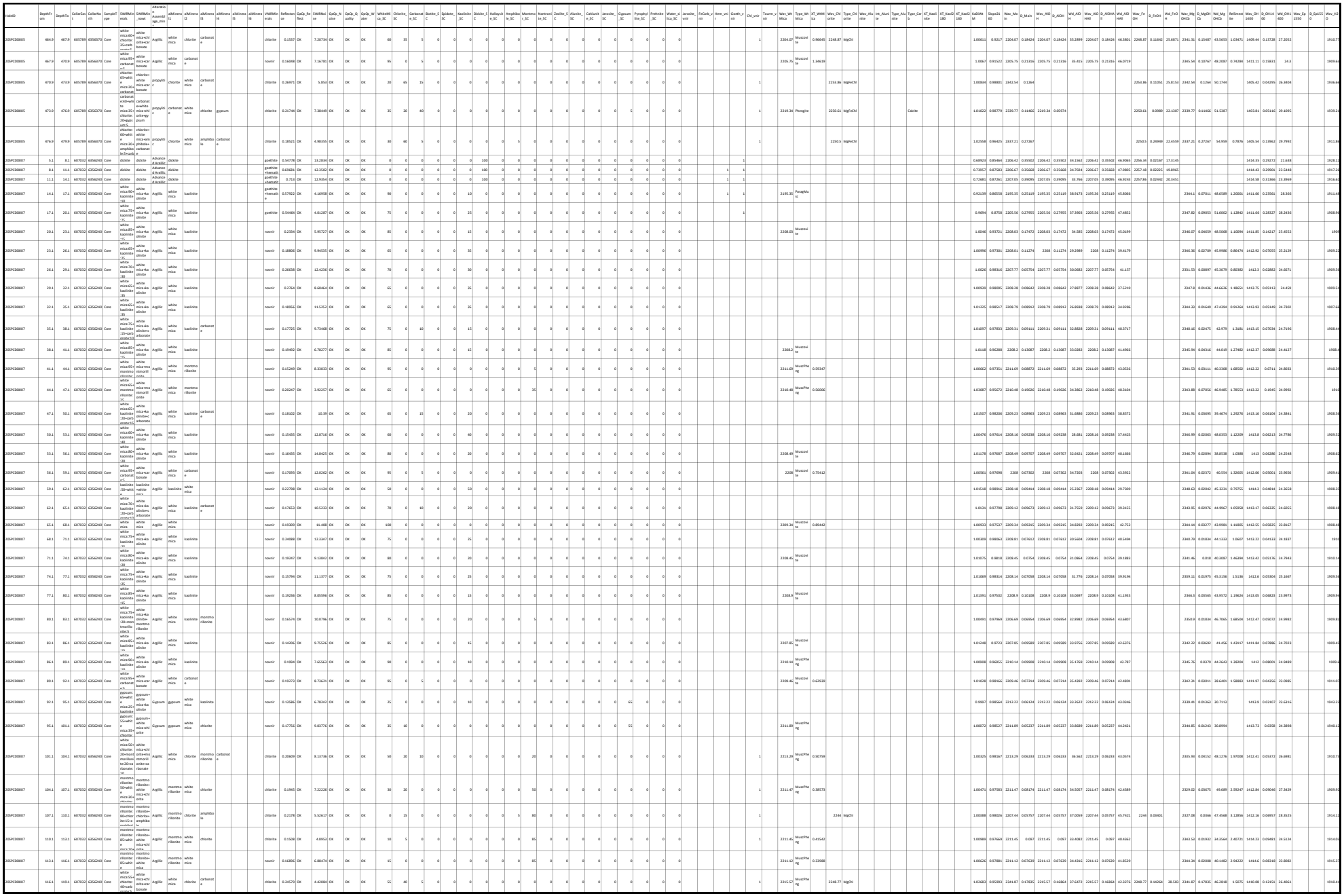

| HoleID | DepthFrom | DepthTo | CollarEast | CollarNorth | SampleType | SWIRMineralS | SWIRMineral_Jewel | AlternationAssemblage_mins | aiMineral1 | aiMineral2 | aiMineral3 | aiMineral4 | aiMineral5 | aiMineral6 | VNIRMineralS | Reflection | QaQc_Reflect | SWIRNoise | QaQc_Noise | QaQc_Quality | QaQc_Water | WhiteMicaSC | Chlorite_SC | Carbonate_SC | Biotite_SC | Epidote_SC | Kaolinite_SC | Dickite_SC | Halloysite_SC | Amphibole_SC | Montmo r_SC | Nontronite_SC | Zeolite_SC | Alunite_SC | CaAlunit e_SC | Jarosite_SC | Gypsum_SC | Pyrophyl lite_SC | Prehnite_SC | Wotter_ol liza_SC | Jarosite_unsr | FeCarb_unsr | Hem_unsr | Goeth_unsr | Chl_unsr | Tourm_unsr | Wav_WhMica | Type_WhMica | KT_WhMica | Wav_Chlorite | Type_Chlorite | Wav_Alunite | Int_Alunite | Type_Alunite | Type_Carb | KT_KaoliniteI | KT_KaoliI 180 | KT_KaoliI 360 | KaDiWtM | Slope1600 | Wav_Min | D_Main | Wav_AlOHmain | D_AlOH | Wd_AlOHmain | Wav_AlOHwid | D_AlOHwid | Wd_AlOHwid | Wav_FeOH | D_FeOH | Wd_FeOHm | Wav_MgOHCb | D_MgOHCb | Wd_MgOHCb | RelSmectite | Wav_OH1600 | D_OH1600 | Wd_OH1400 | Wav_Epi1550 | D_Epi1550 | Wav_H2O |
|---|---|---

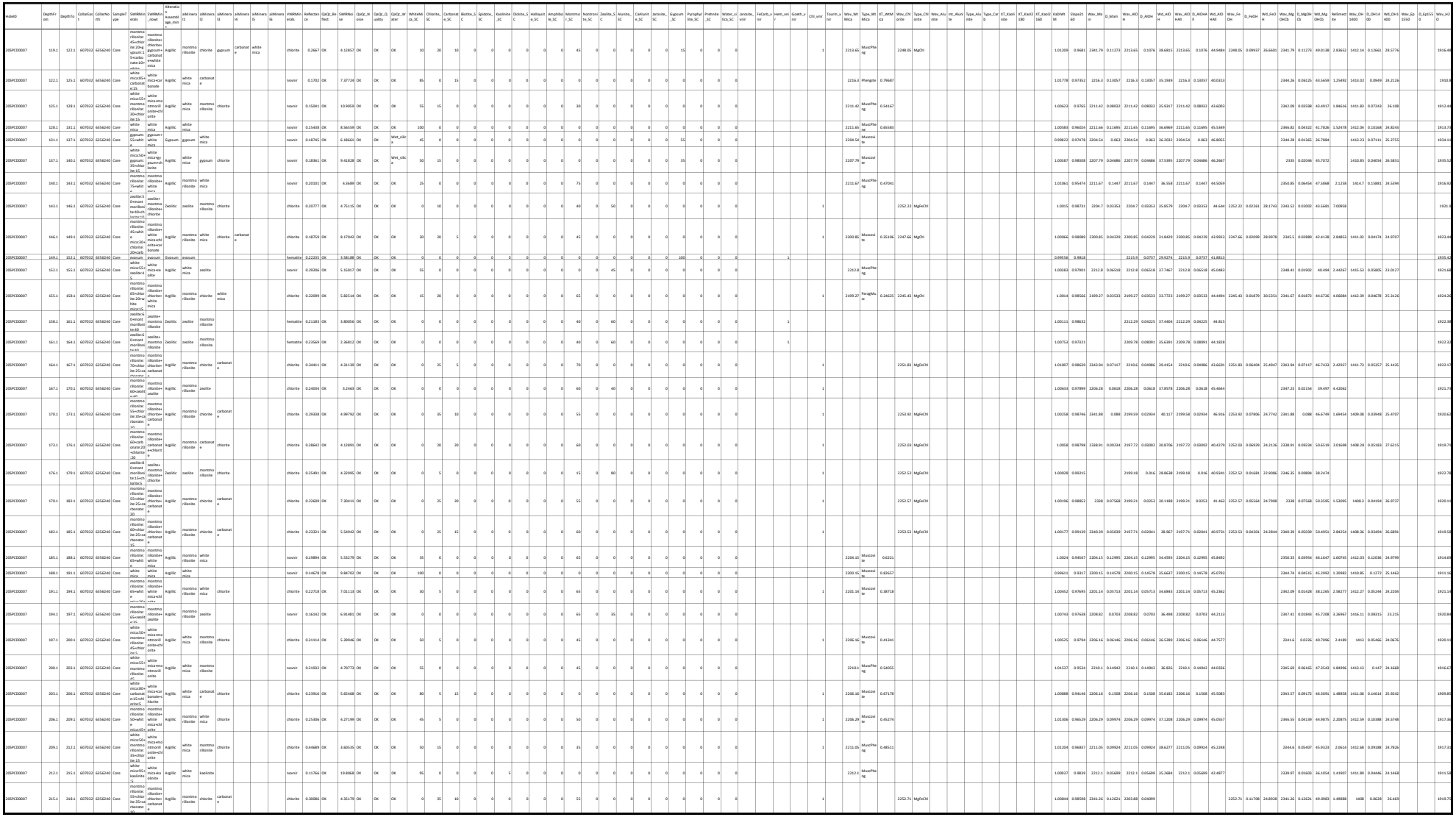

| NodeID | DepthFrom | DepthTo | CollarEast | CollarNorth | SampleType | SWIRMineralsAssemblage | SWIRMineralsAssemblage_newd | AlternationAssemblage_mins | aiMineral1 | aiMineral2 | aiMineral3 | aiMineral4 | aiMineral5 | aiMineral6 | VNIRMineralsAssemblage | Reflectance | QaQc_Reflect | SWIRNoise | QaQc_Noise | QaQc_Quality | QaQc_Water | WhiteMica_SC | Chlorite_SC | Carbonate_SC | Biotite_SC | Epidote_SC | Kaolinite_SC | Dickite_SC | Halloysite_SC | Amphibole_SC | Montmor_SC | Nontronite_SC | Zeolite_SC | Alunite_SC | CaAlunite_SC | Jarosite_SC | Gypsum_SC | PyrophyllHine_SC | Prehnite_SC | WatterIce_SC | Jarosite_var | FeCarb_var | Hem_var | Goeth_var | Chl_var | Tourm_var | Wav_WhiteMica | Type_WhiteMica | KT_WMIca | Wav_Chlorite | Type_Chlorite | Wav_Alunite | Int_Alunite | Type_Alunite | Type_Carb | KT_Kaol1 | KT_Kaol2180 | KT_Kaol3160 | KaDiWtM | Slope1400 | Wav_Mgin | D_Main | Wav_AlOH | D_AlOH | Wvl_AlOHA | Wvl_AlOHA0 | D_AlOHA | Wvl_AlOHA2 | Wav_FeOx | D_FeOx | Wvl_FeOH | Wav_MgOHCb | D_MgOHCb | Wvl_MgOHCb | ReSmectite | Wav_OHIr1600 | D_OHIr1 | Wvl_OHIr1400 | Wav_Epi1550 | D_Epi1550 | Wav_H2O |
|---|---|---

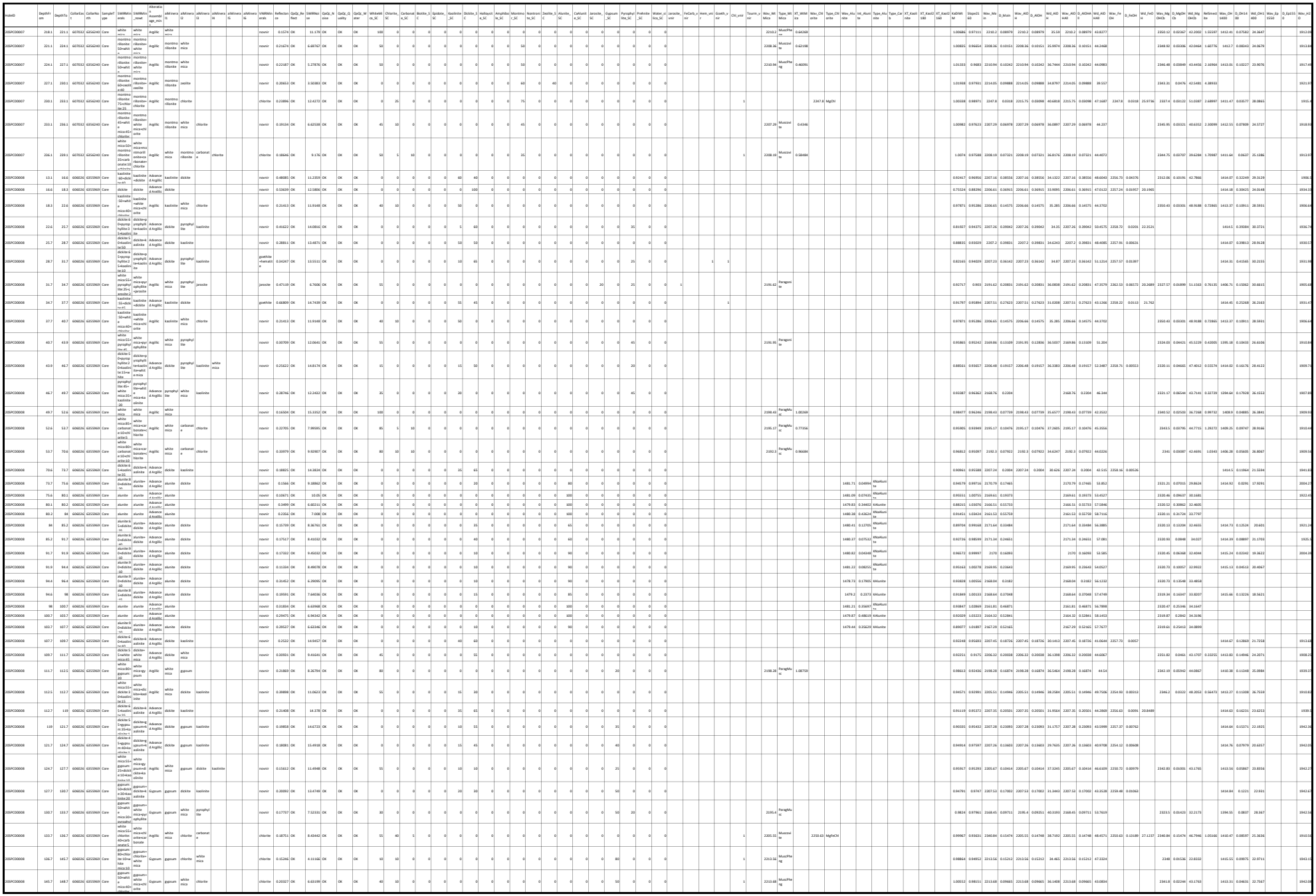

| HoleID | DepthFrom | DepthTo | CollarEast | CollarNorth | SampleType | SWIRMineralsMod | SWIRMineralsNewE | Alteration Assemblage_mins | idMineral1 | idMineral2 | idMineral3 | idMineral4 | idMineral5 | idMineral6 | VNIRMineralsMod | Reflection | QaQc_Reflect | QaQc_Noise | SWIRNoise | QaQc_Noise | QaQc_Quality | QaQc_Water | WhiteMica_SC | Chlorite_SC | Carbonate_SC | Biotite_SC | Epidote_SC | Kaolinite_SC | Dickite_SC | Halloysite_SC | Amphibole_SC | Montmor_SC | Nontronite_SC | Zeolite_SC | Alunite_SC | CaAlunite_SC | Jarosite_SC | Gypsum_SC | Pyrophyllite_SC | Prehnite_SC | Wotter_ice_SC | Jarosite_mix | FeCarb_vor | Hem_vor | Goeth_vor | Chl_vor | Tourm_vor | Wav_WhiteMica | Type_WhiteMica | KT_WMIrca | KT_WMCrystal | Wav_Chlorite | Type_Chlorite | Wav_Alunite | Int_Alunite | Type_Alunite | Type_Carb | KT_KaoliniteP | KT_KaoQual180 | KT_KaoQual360 | KaDiWM | Slope2to60 | Wav_Montm | D_Main | Wav_AlOH | D_AlOHPos | Wid_AlOHM | Wav_AlOHAsd | D_AlOHAsd | Wid_AlOHAsd | Wav_FeOxide | D_FeOxide | Wid_FeOH | Wav_MgOHCb | D_MgOHCb | Wid_MgOHCb | RelSmectite | Wav_OH1600 | D_OH1400 | Wid_OH1400 | Wav_Epi1550 | D_Epi1550 | Wav_H2O |
|---|---|---

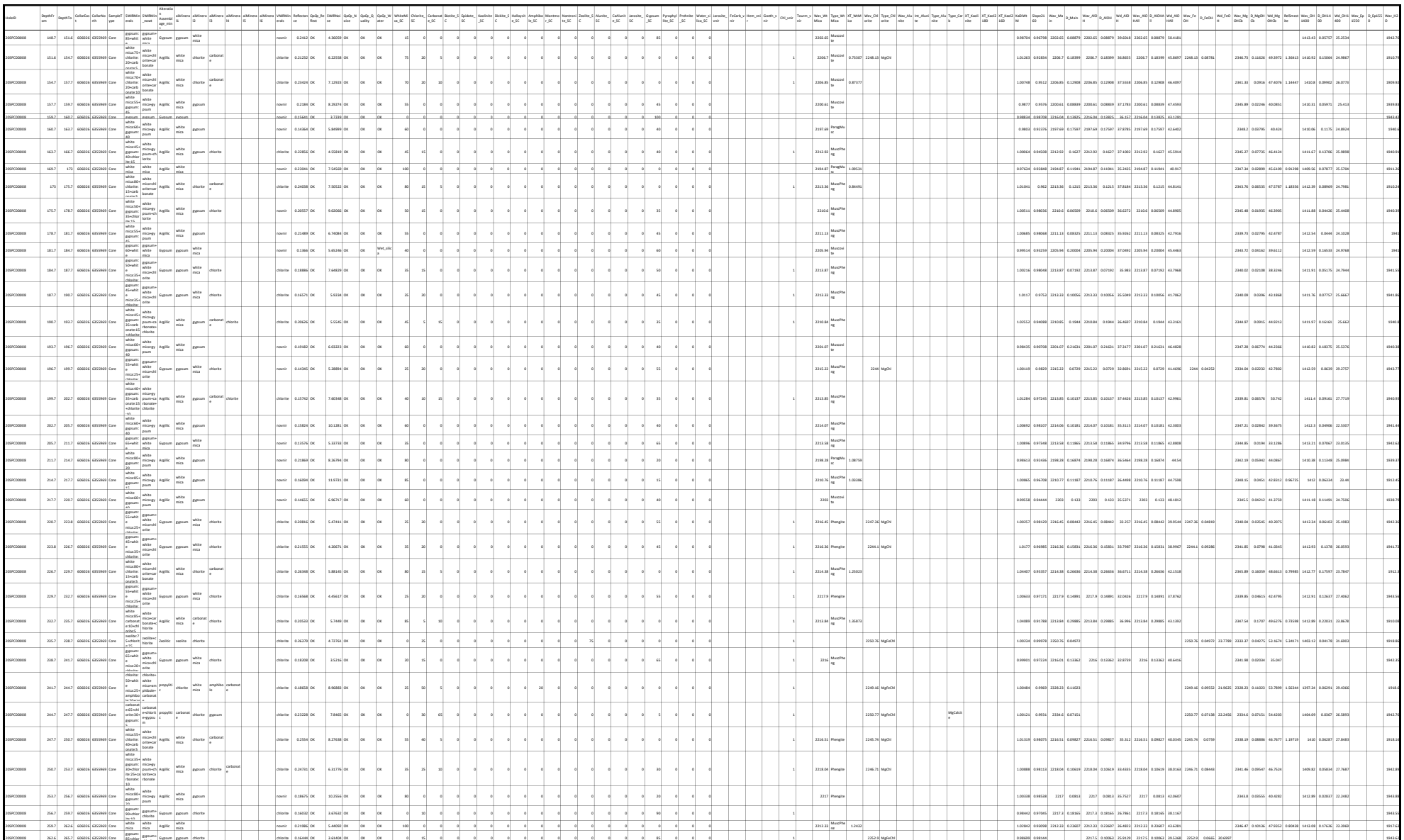

| HoleID | Depth(from) | Depth(to) | CollarEast | CollarNorth | SampleType | SWIRMineralsGroups | SWIRMineralsGroups_newest | AlteredAssemblage_mineralsGroups | alMineralsGroups | alMineralsGroups2 | alMineralsGroups3 | alMineralsGroups4 | alMineralsGroups5 | alMineralsGroups6 | VNIRMineralsGroups | Reflectance | QaQc_Reflectance | QaQc_Noise | QaQc_Quality | QaQc_Water | WhiteMica_SC | Chlorite_SC | Carbonate_SC | Biotite_SC | Epidote_SC | Kaolinite_SC | Dickite_SC | Halloysite_SC | Amphibole_SC | Montmor_SC | Nontronite_SC | Zeolite_SC | Alunite_SC | CaAlunite_SC | Jarosite_SC | Gypsum_SC | PyrophyllHse_SC | Prehnite_SC | Wotter_silica_SC | Jarosite_visir | Type_Carb | FeCarb_visnir | Hem_visnir | Goeth_visnir | Chl_visnir | Tourm_visnir | Wav_WhiMica | Type_WhiMica | KT_WIMica | Wav_Chlorite | Type_Chlorite | Wav_Alunite | Int_Alunite | Type_Alunite | Type_Carb | KT_KaoliHite | KT_KaoGib | KT_KaoGib0 | KaDiWtM | Slope2to0 | Wav_Mgoh | D_Main | Wav_AlOH | D_AlOH | Wid_AlOH | Wav_AlOHA0 | D_AlOHA0 | Wid_AlOHA0 | Wav_FeOx | D_FeOx | Wid_FeOH | Wav_MgOHCb | D_MgOHCb | Wid_MgOHCb | RelSmectite | Wav_OH1600 | D_OH1600 | Wid_OH1600 | Wav_Epi1550 | D_Epi1550 | Wav_H2O |
|---|---|---

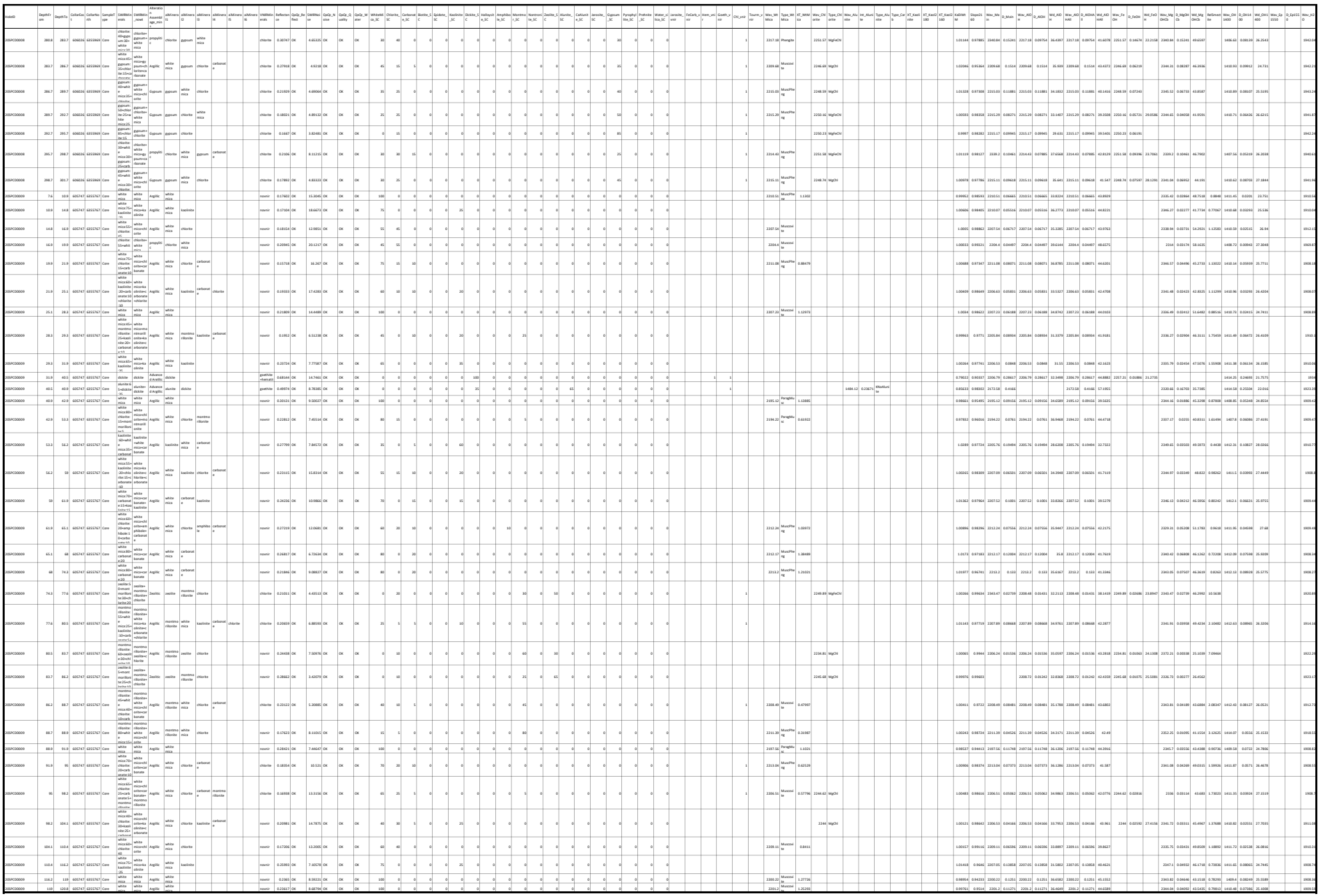

| NodeID | Depth(cm | Depth(cm | CollarDate | CollarNotes | SampleType | SWIRMineralsNotes | SWIRMineral_Need | Alternation Assemblage_mineral | aiMineral1 | aiMineral2 | aiMineral3 | aiMineral4 | aiMineral5 | aiMineral6 | VNIRMineralsNotes | Reflectance | QaQc_Reflect | SWIRNoise | QaQc_Noise | QaQc_Quality | QaQc_Water | WhiteMica_SC | Chlorite_SC | Carbonate_SC | Biotite_SC | Epidote_SC | Kaolinite_SC | Dickite_SC | Halloysite_SC | Amphibole_SC | Montmor_SC | Nontronite_SC | Zeolite_SC | Alunite_SC | CaAlunite_SC | Jarosite_SC | Gypsum_SC | Pyrophyllite_SC | Prehnite_SC | Wotter_silica_SC | Jarosite_visir | FeCarb_visir | Hem_visir | Goeth_visir | Chl_visir | Tourm_visir | Wav_WhiMica | Type_WhiMica | KT_WIMica | Wav_ChlorIntra | Type_ChlorIntra | Wav_Alunite | Int_Alunite | Type_Alunite | Type_Carb | KT_KaoliMet | KT_KaoCl180 | KT_KaoCl160 | KaDiWtM | Slope2160 | Wav_Min | D_Main | Wav_AlOH | D_AlOH | Wd_AlOHM | Wav_AlOHAll | D_AlOHAll | Wd_AlOHAll | Wav_FeOH | D_FeOH | Wd_FeOH | Wav_MgOHCb | D_MgOHCb | Wd_MgOHCb | RelSmectite | Wav_OHH20 | D_OH+H2O | Wd_OH+H2O | Wav_Sp1550 | D_Sp1550 | Wav_H2O |
|---|---|---

| HoleID | Depth(From) | Depth(To) | CollarEast | CollarNorth | SampleType | SWIRMineralsExists | SWIRMineral_Newest | AlteredAssemblage_mins | aiMineral1 | aiMineral2 | aiMineral3 | aiMineral4 | aiMineral5 | aiMineral6 | VNIRMineralsExists | Reflectance | QaQc_Reflect | SWIRNoise | QaQc_Noise | QaQc_Quality | QaQc_Water | WhiteMica_SC | Chlorite_SC | Carbonate_SC | Biotite_SC | Epidote_SC | Kaolinite_SC | Dickite_SC | Halloysite_SC | Amphibole_SC | Montmor_SC | Nontronite_SC | Zeolite_SC | Alunite_SC | CaAlunite_SC | Jarosite_SC | Gypsum_SC | PyrophyllSC | Prehnite_SC | Wotter_silica_SC | Jarosite_mix | FeCarb_mix | Hem_mix | Goeth_mix | Chl_mix | Tourm_mix | Wav_WhiMica | Type_WhiMica | KT_WhiMica | Wav_Chlorite | Type_Chlorite | Wav_Alunite | Int_Alunite | Type_Alunite | Type_Carb | KT_Kaol1nite | KT_Kaol2180 | KT_Kaol3160 | KaDiWtM | Slope1400 | Wav_Min | D_Main | Wav_AlOH | D_AlOH | Wd_AlOH | Wav_AlOHAll | D_AlOHAll | Wd_AlOHAll | Wav_FeOH | D_FeOH | Wd_FeOH | Wav_MgOHCb | D_MgOHCb | Wd_MgOHCb | ReSmectite | Wav_OH1600 | D_OH1400 | Wd_OH1400 | Wav_Epi1550 | D_Epi1550 | Wav_H2O |
|---|---|---

| ModelID | DepthFrom | DepthTo | CollarEast | CollarNorth | SampleType | SWIRMineralsreals | SWIRMineral_newt | AlternationAssemblage_mins | aiMineral1 | aiMineral2 | aiMineral3 | aiMineral4 | aiMineral5 | aiMineral6 | VNIRMineralreals | Reflectance | QaQc_Reflect | SWIRNoise | QaQc_Noise | QaQc_Quality | QaQc_Weather | WhiteMica_SC | Chlorite_SC | Carbonate_SC | Biotite_SC | Epidote_SC | Kaolinite_SC | Dickite_SC | Halloysite_SC | Amphibole_SC | Montmor_SC | Nontron_SC | Zeolite_SC | Alunite_SC | CaAlunite_SC | Jarosite_SC | Gypsum_SC | Pyrophyllite_SC | Prehnite_SC | Wotter_silica_SC | Jarosite_visir | FeCarb_visir | Hem_visir | Goeth_visir | Chl_visir | Tourm_visir | Wav_WhiteMica | Type_WhiteMica | KT_WIMica | Wav_ChlorIntra | Type_ChlorIntra | Wav_AlunIntra | Int_AlunIntra | Type_AlunIntra | Type_CarbIntra | KT_KaoliIntra | KT_KaoG180 | KT_KaoG360 | KaDiWiM | Slope2to60 | Wav_MaxIn | D_MaxIn | Wav_AlOHIn | D_AlOHIn | Wid_AlOHIn | Wav_AlOHAbs | D_AlOHAbs | Wid_AlOHAbs | Wav_FeOxIn | D_FeOxIn | Wid_FeOxIn | Wav_MgOHCls | D_MgOHCls | Wid_MgOHCls | RelSmectite | Wav_OHIn920 | D_OHIn4 | Wid_OHIn500 | Wav_Epi1550 | D_Epi1550 | Wav_H2O |
|---|---|---

| NodeID | DepthFrom | DepthTo | CollarEast | CollarNorth | SampleType | SWIRMineralsGroup | SWIRMineralsSubgroup | SWIRMineralsAssemblage | AlMineral1 | AlMineral2 | AlMineral3 | AlMineral4 | AlMineral5 | AlMineral6 | VNIRMineralsGroup | Reflectance | QaQc_Reflect | SWIRNoise | QaQc_Noise | QaQc_Quality | QaQc_Water | WhiteMica_SC | Chlorite_SC | Carbonate_SC | Biotite_SC | Epidote_SC | Kaolinite_SC | Dickite_SC | Halloysite_SC | Amphibole_SC | Montmor_SC | Nontron_SC | Zeolite_SC | Alunite_SC | CaAlunite_SC | Jarosite_SC | Gypsum_SC | PyrophyHoneSC | Prehnite_SC | Wotter_silica_SC | Jarosite_var | FeCarb_var | Hem_var | Goeth_var | Chl_var | Tourm_var | Wav_WhiteMica | Type_WhiteMica | KT_WMIrca | Wav_Chlorite | Type_Chlorite | Wav_Alunite | Int_Alunite | Type_Alunite | Type_Carb | KT_Kaol1nite | KT_Kaol2180 | KT_Kaol3160 | KaDiWtM | Slope2160 | Wav_Min | D_Main | Wav_AlOH | D_AlOH | Wid_AlOHAll | D_AlOHAll | Wid_AlOHAll | Wav_Fe | D_FeOH | Wid_FeOH | Wav_MgOHCb | D_MgOHCb | Wid_MgOHCb | RelSmectite | Wav_OH1600 | D_OH1600 | Wid_OH1400 | Wav_Epi1550 | D_Epi1550 | Wav_H2O |
|---|---|---

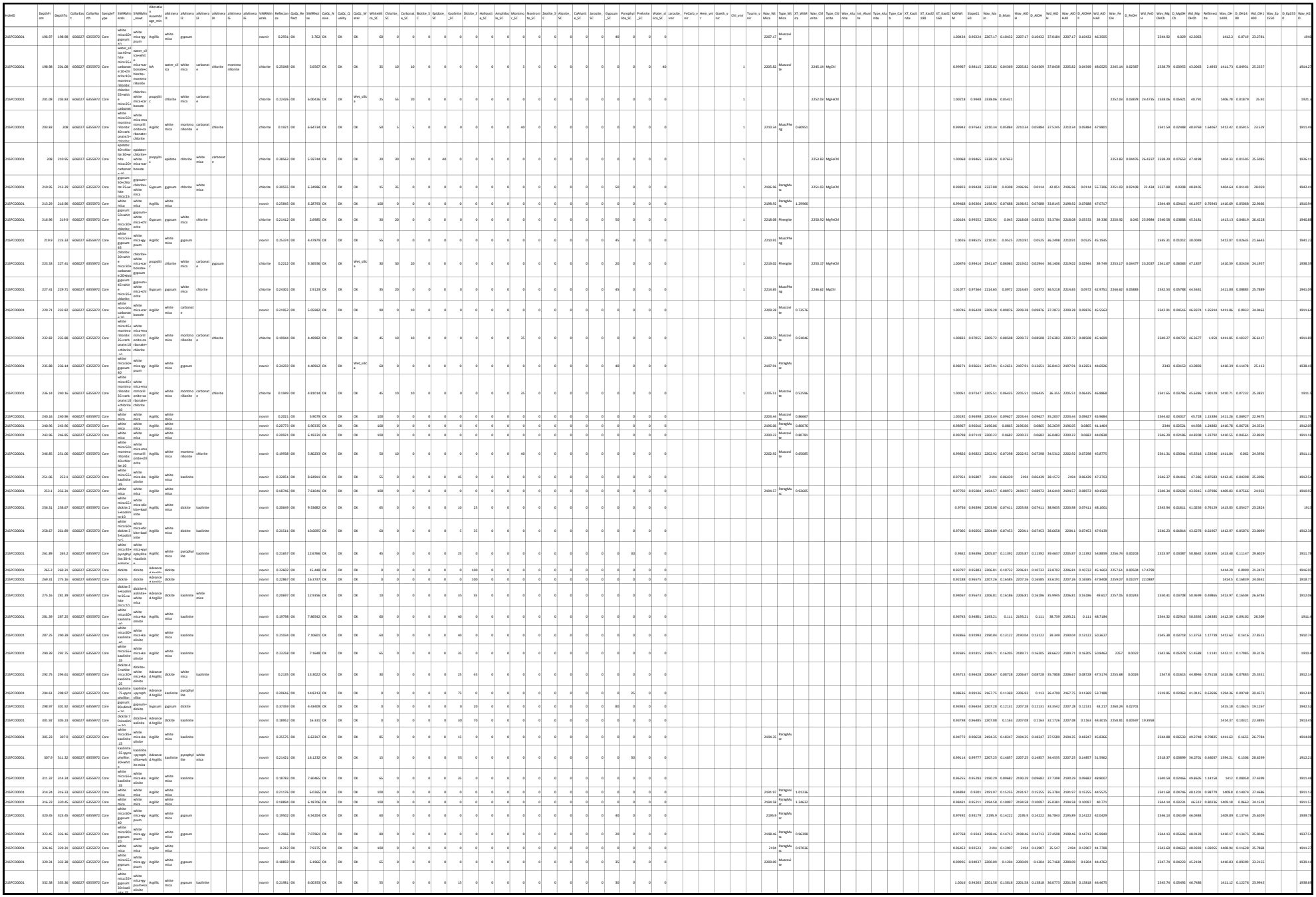

| ModelID | DepthFrom | DepthTo | CollarEast | CollarNorth | SampleType | SWIRMineralsnew | SWIRMineralsnew2 | Alteration Assemblage_mine | aiMineral1 | aiMineral2 | aiMineral3 | aiMineral4 | aiMineral5 | aiMineral6 | VNIRMinerals | Reflection | QaQc_Reflect | SWIRNoise | QaQc_Noise | QaQc_Quality | QaQc_Water | WhiteMica_SC | Chlorite_SC | Carbonate_SC | Biotite_SC | Epidote_SC | Kaolinite_SC | Dickite_SC | Halloysite_SC | Amphibole_SC | Montmor_SC | Nontron_SC | Zeolite_SC | Alunite_SC | CaAlunite_SC | Jarosite_SC | Gypsum_SC | Pyrophyll_SC | Prehnite_SC | Wotter_silica_SC | Jarosite_visir | FeCarb_visir | Hem_visir | Goeth_visir | Chl_visir | Tourm_visir | Wav_WhMica | Type_WhMica | KT_WhMica | Wav_Chlorite | Type_Chlorite | Wav_Alunite | Int_Alunite | Type_Alunite | Type_Carb | KT_Kaolinite | KT_Kaol2180 | KT_Kaol2160 | KaDiWtM | Slope2160 | Wav_Min | D_Main | Wav_AlOH | D_AlOH | Wid_AlOH | Wav_AlOHA | D_AlOHA | Wid_AlOHA | Wav_FeOH | D_FeOH | Wid_FeOH | Wav_MgOH2b | D_MgOH2b | Wid_MgOH2b | RelSmectite | Wav_OH1600 | D_OH1600 | Wid_OH1600 | Wav_Epi1550 | D_Epi1550 | Wav_H2O |
|---|---|---

| NodeID | DepthFrom | DepthTo | CollarCount | CollarNotes | SampleType | SWIRMineralsGroup | SWIRMineral_newest | AlternationAssemblage_mine | aiMineral1 | aiMineral2 | aiMineral3 | aiMineral4 | aiMineral5 | aiMineral6 | VNIRMineralsGroup | Reflectance | QaQc_Reflect | SWIRNoise | QaQc_Noise | QaQc_Quality | QaQc_Water | WhiteMica_SC | Chlorite_SC | Carbonate_SC | Biotite_SC | Epidote_SC | Kaolinite_SC | Dickite_SC | Halloysite_SC | Amphibole_SC | Montmor_SC | Nontronite_SC | Zeolite_SC | Alunite_SC | CaAlunite_SC | Jarosite_SC | Gypsum_SC | Pyrophyllite_SC | Prehnite_SC | Wotter_silica_SC | Jarosite_visir | FeCarb_visir | Hem_visir | Goeth_visir | Chl_visir | Tourm_visir | Wav_WhiMica | Type_WhiMica | KT_WIMica | Wav_Chlorite | Type_Chlorite | Wav_Alunite | Int_Alunite | Type_Alunite | Type_Carb | KT_KaoliniteA | KT_KaoD1180 | KT_KaoD1560 | KaDiWell | Slope2160 | Wav_Min | D_Main | Wav_AlOH | D_AlOH | Wid_AlOH | Wav_AlOHA | D_AlOHA | Wid_AlOHA | Wav_Fe | D_FeOxi | Wid_FeOH | Wav_MgOHCb | D_MgOHCb | Wid_MgOHCb | ReSmectite | Wav_OH1600 | D_OH1600 | Wid_OH1400 | Wav_Epi1550 | D_Epi1550 | Wav_H2O |
|---|---|---

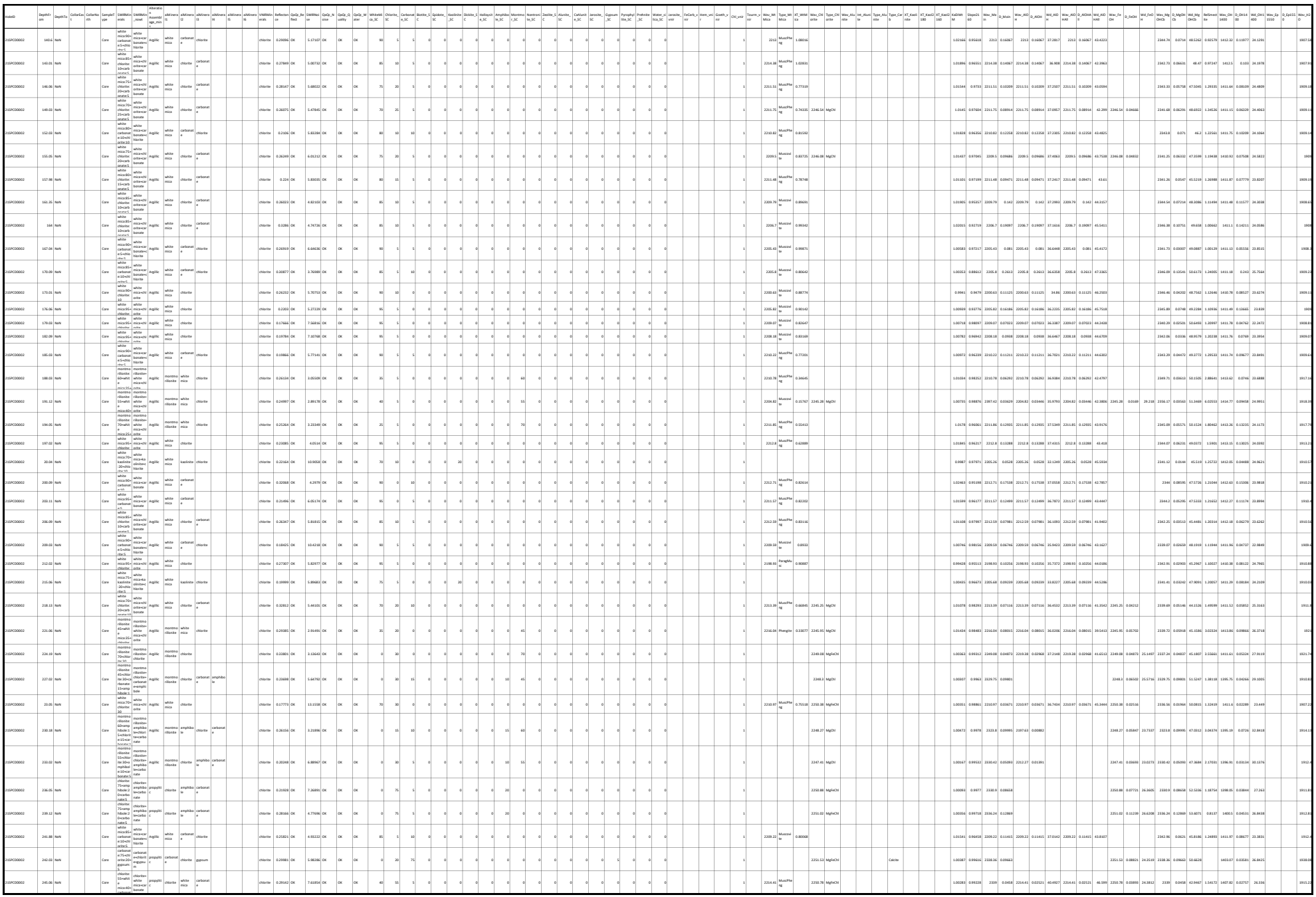

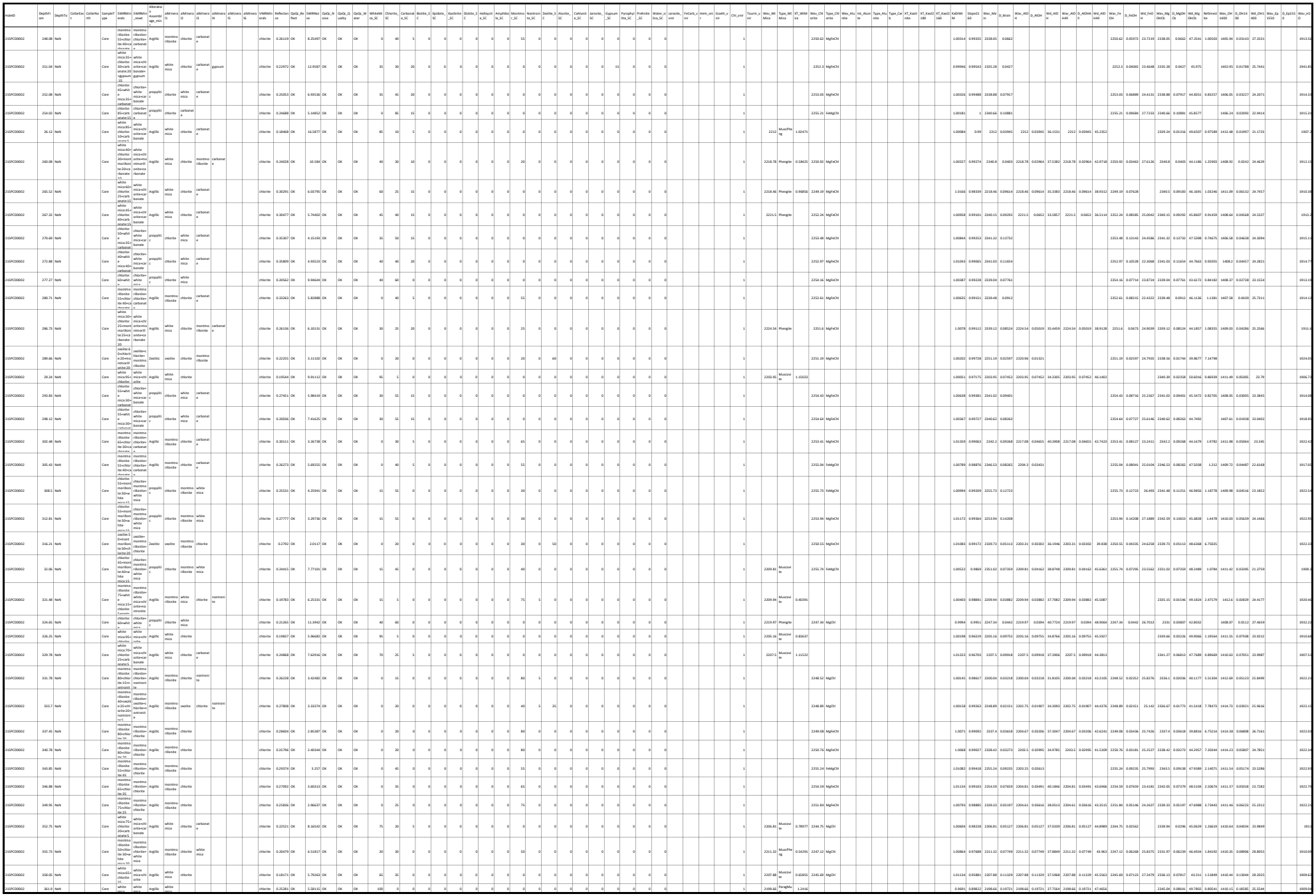

| HoleID | DepthFrom | DepthTo | CollarCount | CollarNotes | SampleType | SWIRMineralsGroups | SWIRMineralsGroups_newest | AlteredAssemblage_mineralogy | aiMineralGroup1 | aiMineralGroup2 | aiMineralGroup3 | aiMineralGroup4 | aiMineralGroup5 | aiMineralGroup6 | VNIRMineralsGroups | Reflectance | QaQc_Reflect | SWIRNoise | QaQc_Noise | QaQc_Quality | QaQc_Water | WhiteMica_SC | Chlorite_SC | Carbonate_SC | Biotite_SC | Epidote_SC | Kaolinite_SC | Dickite_SC | Halloysite_SC | Amphibole_SC | Montmorillonite_SC | Nontronite_SC | Zeolite_SC | Alunite_SC | CaAlunite_SC | Jarosite_SC | Gypsum_SC | Pyrophyllite_SC | Prehnite_SC | Wotter_silica_SC | Jarosite_visir | FeCarb_visir | Hem_visir | Goeth_visir | Chl_visir | Tourm_visir | Wav_WhiteMica | Type_WhiteMica | KT_WMIndex | Wav_Chlorite | Type_Chlorite | Wav_Alunite | Int_Alunite | Type_Alunite | Type_Carb | KT_KaoliIndex | KT_KaoliD1D2 | KT_KaoliD3D2 | KaDiWtM | Slope2140 | Wav_Min | D_Main | Wav_AlOH | D_AlOH | Wid_AlOHM | Wav_AlOHAll | D_AlOHAll | Wid_AlOHAll | Wav_FeOx | D_FeOx | Wid_FeOH | Wav_MgOHCb | D_MgOHCb | Wid_MgOHCb | RelSmectite | Wav_OHH20 | D_OH14H20 | Wid_OH14H20 | Wav_Epi1550 | D_Epi1550 | Wav_H2O |
|---|---|---

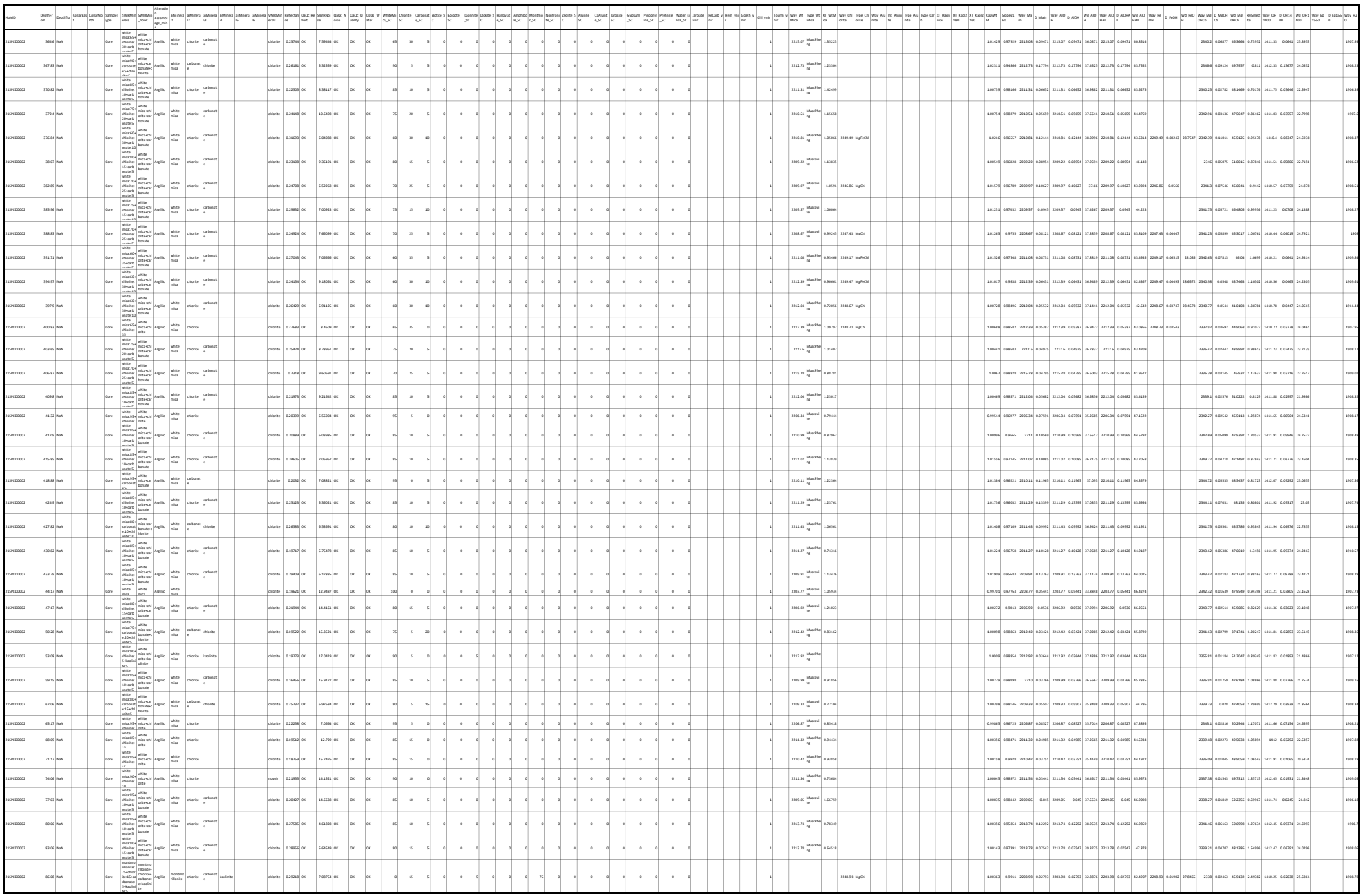

| HoleID | DepthFrom | DepthTo | CollarEast | CollarNorth | SampleType | SWIRMineralsWet | SWIRMineralsDry | Alteration Assemblage_mineral | aiMineral1 | aiMineral2 | aiMineral3 | aiMineral4 | aiMineral5 | aiMineral6 | VNIRMineralsWet | Reflection | QaQc_Reflect | SWIRNose | QaQc_Noise | QaQc_Quality | QaQc_Water | WhiteMica_SC | Chlorite_SC | Carbonate_SC | Biotite_SC | Epidote_SC | Kaolinite_SC | Dickite_SC | Halloysite_SC | Amphibole_SC | Montmor_SC | Nontronite_SC | Zeolite_SC | Alunite_SC | CaAlunite_SC | Jarosite_SC | Gypsum_SC | Pyrophyllite_SC | Prehnite_SC | Wotter_silica_SC | Jarosite_visir | FeCarb_visir | Hem_visir | Goeth_visir | Chl_visir | Tourm_visir | Wav_WhiteMica | Type_WhiteMica | KT_WMIndex | Wav_ChlorIndex | Type_ChlorIndex | Wav_Alunite | Int_Alunite | Type_Alunite | Type_Carb | KT_KaoliIndex | KT_KaoQI380 | KT_KaoQI360 | KaDiWtM | Slope2140 | Wav_Min | D_Main | Wav_AlOH | D_AlOH | Wd_AlOM | Wav_AlOHAbs | D_AlOHAbs | Wd_AlOHAbs | Wav_FeOx | D_FeOx | Wd_FeOH | Wav_MgOHCb | D_MgOHCb | Wd_MgOHCb | RelSmectite | Wav_OHI1600 | D_OHI1400 | Wd_OHI1400 | Wav_Epi1550 | D_Epi1550 | Wav_H2O |
|---|---|---

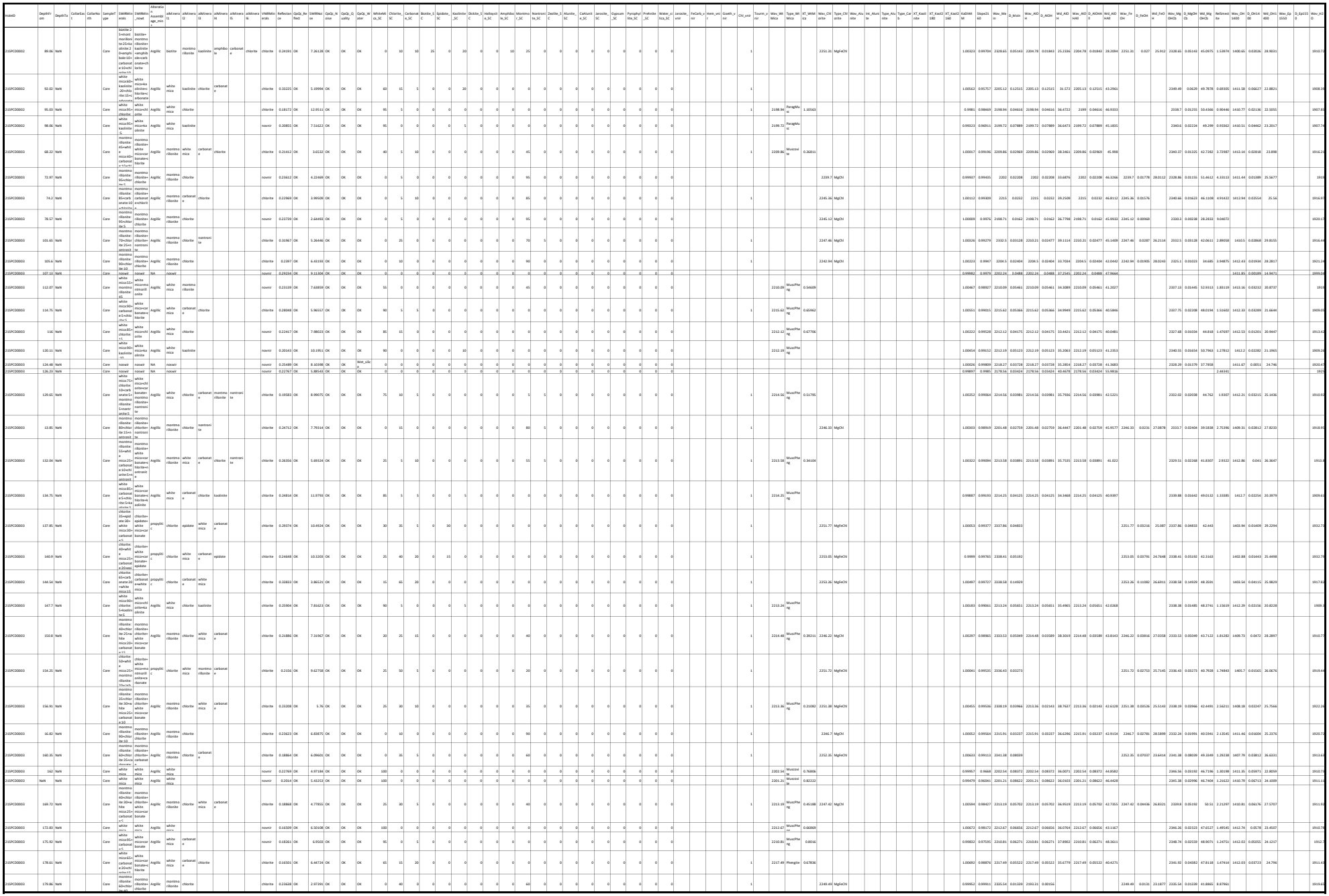

| NodeID | Depth(cm) | Depth(ca | CollarCas | CollarNo | SampleT | SWIRMin | SWIRMin | SWIRMin | Alternati | Assembl | siMineral | siMineral | siMineral | siMineral | siMineral | siMineral | VNIRMin | Reflectan | QaQc_Re | SWIRNoi | QaQc_N | QaQc_Q | QaQc_W | WhiteMi | Chlorite_ | Carbonat | Illonite_S | Epidote_ | Kaolinite | Dickite_S | Halloysit | Amphibo | Montmo | Nontroni | Zeolite_S | Alunite_ | CaAlunit | Jarosite_ | Gypsum | Pyrophyl | Prehnite | Witter_si | Jarosite_ | FeCarb_v | Hem_vni | Goeth_v | Chl_vni | Tourm_v | Wav_Wt | Type_Wt | KT_WtM | Wav_Chl | Type_Chl | Wav_Alu | Int_Alunit | Type_Alu | Type_Car | KT_Kaoli | KT_Kaol | KT_Kaol | KaDiWt | Slope(1 | Wav_Mo | D_Main | Wav_IMO | D_IMOH | Wd_IMO | Wav_IMO | D_IMOHA | Wd_IMO | Wav_Fe | D_FeOxi | Wd_FeO | Wav_Mg | D_MgOH | Wd_Mg | ReSmect | Wav_OH | D_OH14 | Wd_OH1 | Wav_Ep | D_Epi15 | Wav_H2O |
|---|---|---

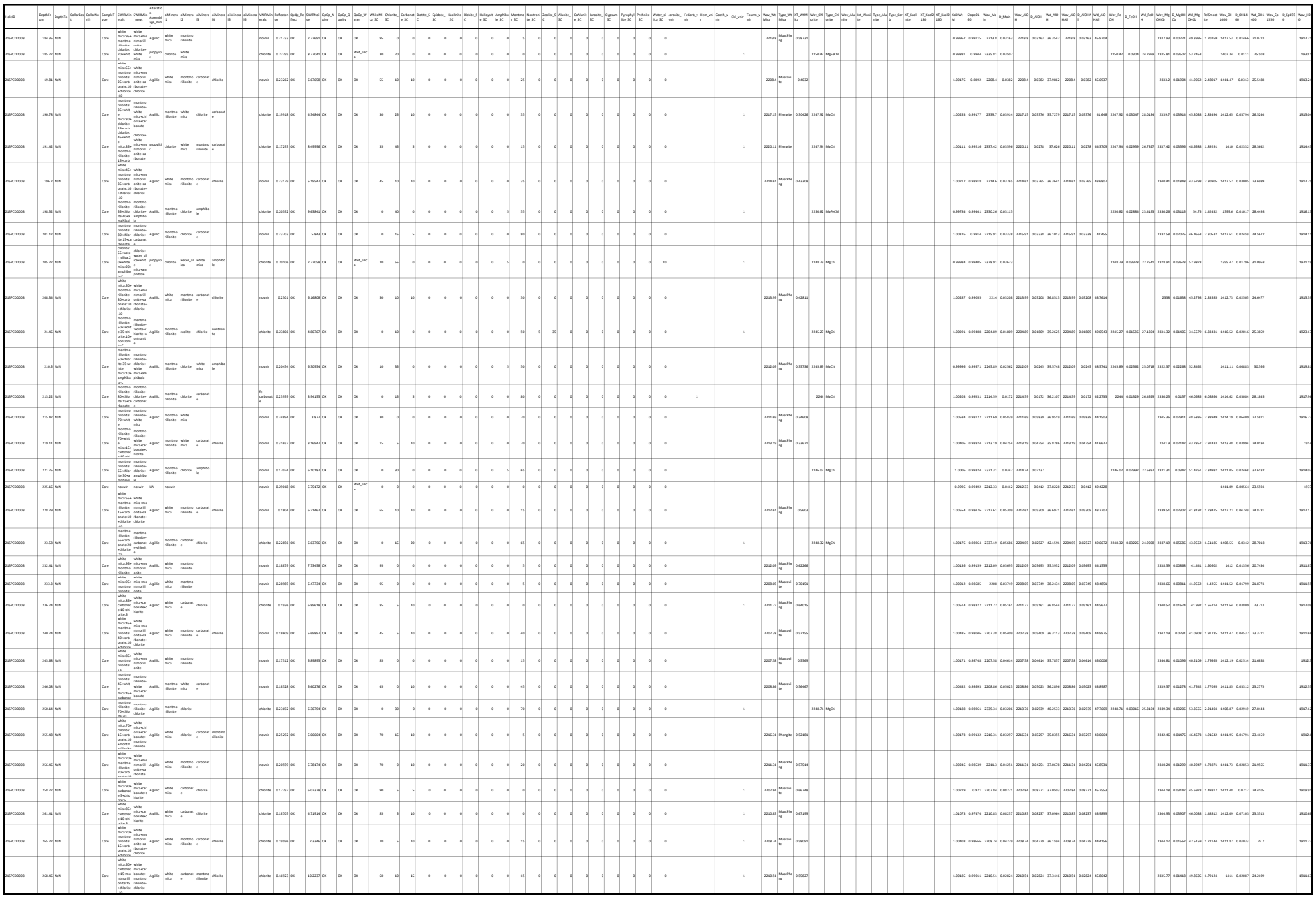

| HoleID | DepthFrom | DepthTo | CollarCarrier | CollarNotes | SampleType | SWIRMineralsDetailed | SWIRMineralsNewest | AlternationAssemblage_mins | aiMineral1 | aiMineral2 | aiMineral3 | aiMineral4 | aiMineral5 | aiMineral6 | VNIRMineralsDetailed | Reflectance | QaQc_Reflect | SWIRNoise | QaQc_Noise | QaQc_Quality | QaQc_Water | WhiteMica_SC | Chlorite_SC | Carbonate_SC | Biotite_SC | Epidote_SC | Kaolinite_SC | Dickite_SC | Halloysite_SC | Amphibole_SC | Montmor_SC | Nontronite_SC | Zeolite_SC | Alunite_SC | CaAlunite_SC | Jarosite_SC | Gypsum_SC | PyrophyllHalite_SC | Prehnite_SC | Wotter_silica_SC | Jarosite_unsr | FeCarb_unsr | Hem_unsr | Goeth_unsr | Chl_unsr | Tourm_unsr | Wav_WhiMica | Type_WhiMica | KT_WhiMica | Wav_Chlorite | Type_Chlorite | Wav_Alunite | Int_Alunite | Type_Alunite | Type_Carb | KT_Kaol1nite | KT_Kaol2180 | KT_Kaol3160 | KaDiWtM | Slope2140 | Wav_Min | D_Main | Wav_AlOH | D_AlOH | Wd_AlOHM | Wav_AlOHAll | D_AlOHAll | Wd_AlOHAll | Wav_FeOH | D_FeOH | Wd_FeOH | Wav_MgOHCb | D_MgOHCb | Wd_MgOHCb | RelSmectite | Wav_OHI1600 | D_OH1600 | Wd_OH1600 | Wav_Epi1550 | D_Epi1550 | Wav_H2O |
|---|---|---

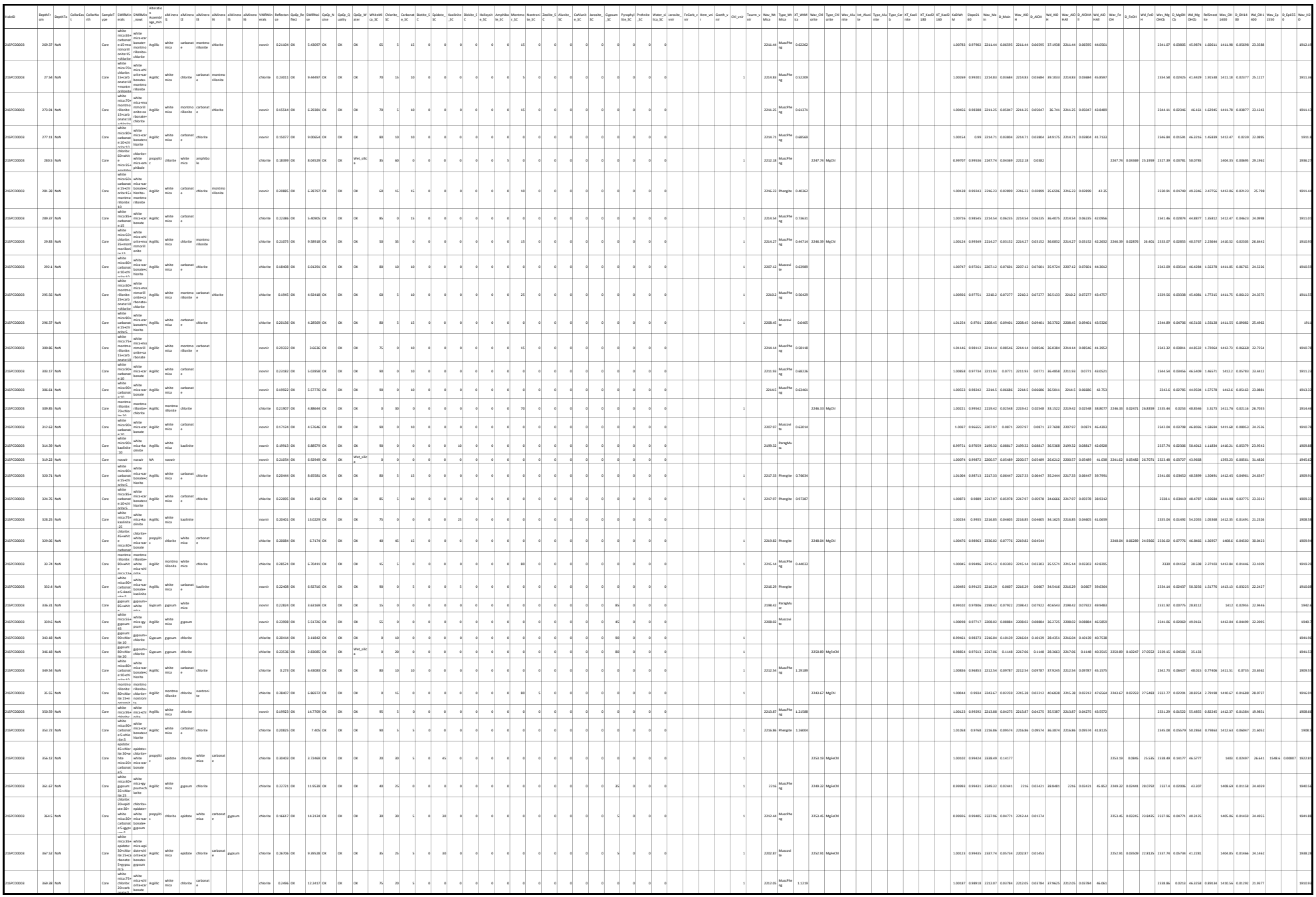

| ModelID | DepthFrom | DepthTo | CollarCount | CollarNotes | SampleType | SWIRMineralsNotes | SWIRMineralsNewest | AlteredAssemblage_mins | aiMineral1 | aiMineral2 | aiMineral3 | aiMineral4 | aiMineral5 | aiMineral6 | VNIRMineralsNotes | ReflectanceQuality | QaQc_ReflectSlope | SWIRNoise | QaQc_NoiseQuality | QaQc_QualityWater | WhiteMica_SC | Chlorite_SC | Carbonate_SC | Biotite_SC | Epidote_SC | Kaolinite_SC | Dickite_SC | Halloysite_SC | Amphibole_SC | Montmor_SC | Nontronite_SC | Zeolite_SC | Alunite_SC | CaAlunite_SC | Jarosite_SC | Gypsum_SC | PyrophyllineSC | Prehnite_SC | Wotter_silica_SC | Jarosite_unsr | FeCarb_unsr | Hem_unsr | Goeth_unsr | Chl_unsr | Tourm_unsr | Wav_WhiteMica | Type_WhiteMica | KT_WMIcka | Wav_ChlorIntra | Type_ChlorIntra | Wav_AluNative | Int_AluniteA | Type_AluniteA | Type_CarbA | KT_KaoliniteA | KT_KaoG1803d0 | KT_KaoG2360 | KaDiWtM | Slope2160 | Wav_MinIn | D_MaIn | Wav_AlOHA | D_AlOHA | Wd_AlOHA | Wav_AlOHA40 | D_AlOHA3 | Wd_AlOHA40 | Wav_FeOxi | D_FeOxi | Wd_FeOxi | Wav_MgOHCb | D_MgOHCb | Wd_MgOHCb | ReiSmectite | Wav_OHI1620 | D_OHI1400 | Wd_OHI1400 | Wav_Epi1550 | D_Epi1550 | Wav_H2O |
|---|---|---

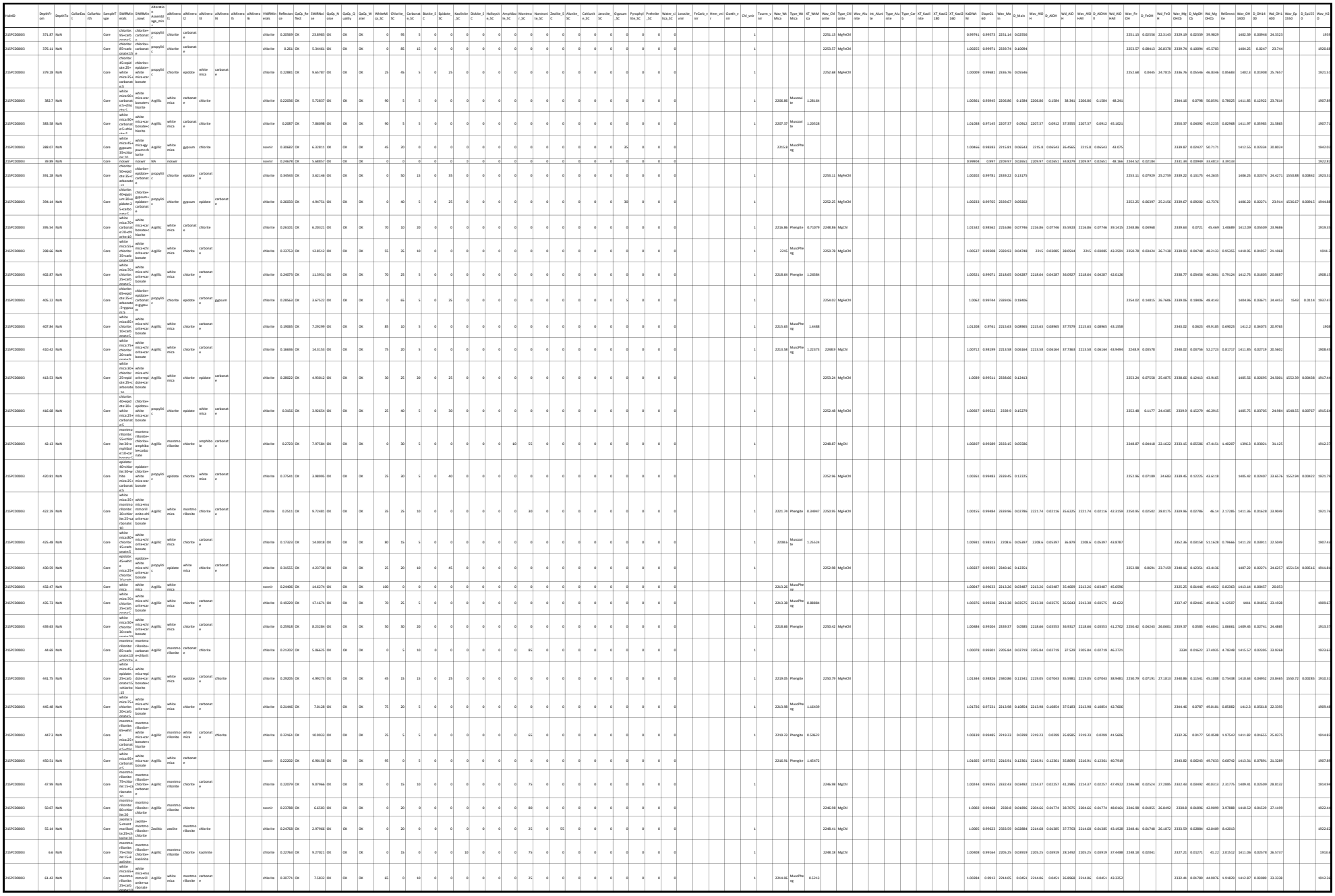

| NodeID | DepthFrom | DepthTo | CollarCount | CollarNotes | SampleType | SWIRMineralsAssemblage | SWIRMineralsAssemblage_newest | AlteredMineralsAssemblage_mixture | aMineral1 | aMineral2 | aMineral3 | aMineral4 | aMineral5 | aMineral6 | VNIRMineralsAssemblage | ReflectanceFeature | QaQc_ReflectanceFeature | SWIRNoise | QaQc_NoiseFeature | QaQc_QualityFeature | QaQc_WaterFeature | WhiteMica_SC | Chlorite_SC | Carbonate_SC | Biotite_SC | Epidote_SC | Kaolinite_SC | Dickite_SC | Halloysite_SC | Amphibole_SC | Montmor_SC | Nontronite_SC | Zeolite_SC | Alunite_SC | CaAlunite_SC | Jarosite_SC | Gypsum_SC | PyrophyllineSC | Prehnite_SC | WatterIce_SC | Jarosite_vnir | FeCarb_vnir | Hem_vnir | Goeth_vnir | Chl_vnir | Tourm_vnir | Wav_WhiteMica | Type_WhiteMica | KT_WMFit | Wav_ChlorFeature | Type_ChlorFeature | Wav_Alunite | Int_Alunite | Type_AluniteFeature | Type_CarbFeature | KT_KaoliniteFeature | KT_KaoGI180 | KT_KaoGI360 | KaDiWtMf | Slope2to60 | Wav_Mgin | D_Main | Wav_AlOH | D_AlOH | Wid_AlOH | Wav_AlOHAnd | D_AlOHAnd | Wid_AlOHAnd | Wav_FeOH | D_FeOH | Wid_FeOH | Wav_MgOHCb | D_MgOHCb | Wid_MgOHCb | RelSmectite | Wav_OHH2O | D_OH14000 | Wid_OH14000 | Wav_Epi1550 | D_Epi1550 | Wav_H2O |
|---|---|---

| NodeID | DepthFrom | DepthTo | CollarCount | CollarNotes | CollarType | SampleType | SWIRMineralsNewE | SWIRMineralsNewE | AlteredAssemblage_mineralsNewE | aiMineralsNewE | aiMineralsNewE | aiMineralsNewE | aiMineralsNewE | aiMineralsNewE | VNIRMineralsNewE | Reflectance | QaQc_Reflect | SWIRNoise | QaQc_Noise | QaQc_Quality | QaQc_Weather | WhiteMica_SC | Chlorite_SC | Carbonate_SC | Biotite_SC | Epidote_SC | Kaolinite_SC | Dickite_SC | Halloysite_SC | Amphibole_SC | Montmor_SC | Nontron_SC | Zeolite_SC | Alunite_SC | CaAlunite_SC | Jarosite_SC | Gypsum_SC | PyrophyllHte_SC | Prehnite_SC | Wotter_ollica_SC | Jarosite_visir | FeCarb_vnir | Hem_visir | Goeth_vnir | Chl_vnir | Tourm_vnir | Wav_WhMica | Type_WhMica | KT_WhMica | KT_KaolGib | KT_KaolGib0 | KaDiWtM | Wav_ChlMin | Type_ChlMin | Wav_AluMin | Type_AluMin | Type_CarbMin | KT_KaolMin | KT_KaolGib0 | KaDiWtM | Slope2140 | Wav_MinMin | D_Main | Wav_AlOHMin | D_AlOHMin | Wav_AlOHMin | Wav_AlOHMin | D_AlOHMin | Wav_AlOHMin | Wav_FeOxMin | D_FeOxMin | Wav_FeOxMin | D_MgOHCrb | Wav_MgOHCrb | D_MgOHCrb | RelSmectite | Wav_OHMin | D_OH1400 | Wav_OH1400 | D_OH1550 | D_Epi1550 | Wav_H2O |
|---|---|---

| NodeID | DepthFrom | DepthTo | CollarCount | CollarNotes | SampleType | SWIRMineralsAssemblage | SWIRMineralsAssemblage_newest | AlteredAssemblage_mins | aiMineral1 | aiMineral2 | aiMineral3 | aiMineral4 | aiMineral5 | aiMineral6 | VNIRMineralsAssemblage | ReflectanceQuality | QaQc_ReflectanceQuality | SWIRNoise | QaQc_NoiseQuality | QaQc_QualityWater | WhiteMica_SC | Chlorite_SC | Carbonate_SC | Biotite_SC | Epidote_SC | Kaolinite_SC | Dickite_SC | Halloysite_SC | Amphibole_SC | Montmor_SC | Nontronite_SC | Zeolite_SC | Alunite_SC | CaAlunite_SC | Jarosite_SC | Gypsum_SC | PyrophyllineSC | Prehnite_SC | WatericeSC | Jarosite_unsorted | FeCarb_vsorted | Hem_vsorted | Goeth_vsorted | Chl_unsorted | Tourm_vsorted | Wav_WhiteMica | Type_WhiteMica | KT_WIMIAcia | Wav_ChlorIntra | Type_ChlorIntra | Wav_AluInte | Int_Alunite | Type_AluInte | Type_Carb | KT_KaoliInte | KT_KaoGI180 | KT_KaoGI360 | KaDiWtM | Slope2160 | Wav_Min | D_Main | Wav_AlOH | D_AlOH | Wid_AlOH | Wav_AlOHA40 | D_AlOHA40 | Wid_AlOHA40 | Wav_FeOx | D_FeOx | Wid_FeOH | Wav_MgChlCb | D_MgChlCb | Wid_MgChlCb | ReSmectite | Wav_OHI400 | D_OHI400 | Wid_OHI400 | Wav_Epi1550 | D_Epi1550 | Wav_H2O |
|---|---|---

| HoleID | DepthFrom | DepthTo | CollarEast | CollarNorth | SampleType | SWIRMineralsNewest | SWIRMineralsNewest | Alteration Assemblage_mins | aiMineral1 | aiMineral2 | aiMineral3 | aiMineral4 | aiMineral5 | aiMineral6 | VNIRMineralsNewest | Reflectance | QaQc_Reflect | SWIRNoise | QaQc_Noise | QaQc_Quality | QaQc_Water | WhiteMica_SC | Chlorite_SC | Carbonate_SC | Biotite_SC | Epidote_SC | Kaolinite_SC | Dickite_SC | Halloysite_SC | Amphibole_SC | Montmor_SC | Nontronite_SC | Zeolite_SC | Alunite_SC | CaAlunite_SC | Jarosite_SC | Gypsum_SC | Pyrophyllite_SC | Prehnite_SC | Witter_silica_SC | Jarosite_vnir | FeCarb_vnir | Hem_vnir | Goeth_vnir | Chl_vnir | Tourm_vnir | Wav_WhiMica | Type_WhiMica | KT_WMica | Wav_Chlorite | Type_Chlorite | Wav_Alunite | Int_Alunite | Type_Alunite | Type_Carb | KT_Kaol1nite | KT_Kaol2180 | KT_Kaol3160 | KaDiWtM | Slope2140 | Wav_Min | D_Main | Wav_AlOH | D_AlOH | Wid_AlOH | Wav_AlOHA0 | D_AlOHA0 | Wid_AlOHA0 | Wav_FeOH | D_FeOH | Wid_FeOH | Wav_MgOH1b | D_MgOH1b | Wid_MgOH1b | RelSmectite | Wav_OH1600 | D_OH1600 | Wid_OH1400 | Wav_Epi1550 | D_Epi1550 | Wav_H2O |
|---|---|---

| NodeID | DepthFrom | DepthTo | CollarCast | CollarNotes | SampleType | SWIRMineralsNotes | SWIRMineralsNewE | AlternationAssemblage_mins | aiMineral1 | aiMineral2 | aiMineral3 | aiMineral4 | aiMineral5 | aiMineral6 | VNIRMineralsNotes | Reflectance | QaQc_Reflect | SWIRNoise | QaQc_Noise | QaQc_Quality | QaQc_Water | WhiteMica_SC | Chlorite_SC | Carbonate_SC | Biotite_SC | Epidote_SC | Kaolinite_SC | Dickite_SC | Halloysite_SC | Amphibole_SC | Montmor_SC | Nontronite_SC | Zeolite_SC | Alunite_SC | CaAlunite_SC | Jarosite_SC | Gypsum_SC | PyrophyllineSC | Prehnite_SC | Wotter_silica_SC | Jarosite_visir | FeCarb_visir | Hem_visir | Goeth_visir | Chl_visir | Tourm_visir | Wav_WhMica | Type_WhMica | KT_WhMica | Wav_ChlorIntre | Type_ChlorIntre | D_Main | Wav_AlOH | D_AlOH | Wid_AlOH | Wav_AlOHAsd | D_AlOHAsd | Wid_AlOHAsd | Wav_FeOH | D_FeOH | Wid_FeOH | Wav_MgOHCb | D_MgOHCb | Wid_MgOHCb | RelSmectite | Wav_OHAl1600 | D_OHAl1600 | Wid_OHAl1600 | Wav_EpIll500 | D_EpIll500 | Wav_H2O |
|---|---|---

| NodeID | DepthFrom | DepthTo | CollarCount | CollarNotes | SampleType | SWIRMineralsRaw | SWIRMineralsCorrected | Alteration Assemblage_mineralsRaw | aiMineralsRaw | aiMineralsQ2 | aiMineralsQ4 | aiMineralsQ6 | aiMineralsQ8 | VNIRMineralsRaw | Reflectance | QaQc_ReflectedRaw | SWIRNoise | QaQc_NoiseRaw | QaQc_Quality | QaQc_Weather | WhiteMica_SC | Chlorite_SC | Carbonate_SC | Biotite_SC | Epidote_SC | Kaolinite_SC | Dickite_SC | Halloysite_SC | Amphibole_SC | Montmor_SC | Nontronite_SC | Zeolite_SC | Alunite_SC | CeMineral_SC | Jarosite_SC | Gypsum_SC | Pyrophyllite_SC | Prehnite_SC | Wotter_silica_SC | Jarosite_visir | FeCarb_visir | Hem_visir | Goeth_visir | Chl_visir | Tourm_visir | Wav_WhiteMica | Type_WhiteMica | KT_WMFlexa | Wav_ChlorinteRaw | Type_ChlorinteRaw | Wav_AluniteRaw | Int_AluniteRaw | Type_AluniteRaw | Type_Carb | KT_KaoliniteRaw | KT_KaoQ1180 | KT_KaoQ1560 | KaDiWtM | Slope2160 | Wav_Min | D_Main | Wav_AlOHRaw | D_AlOH | Wid_AlOHM | Wav_AlOHAbsRaw | D_AlOHAbs | Wid_AlOHAbsM | Wav_FeOxRaw | D_FeOxRaw | Wid_FeOxM | Wav_MgOHRaw | D_MgOHRaw | Wid_MgOHRaw | RelSmectite | Wav_OHRaw1600 | D_OH14001600 | Wid_OH14001600 | Wav_Epi1550 | D_Epi1550 | Wav_H2O |
|---|---|---

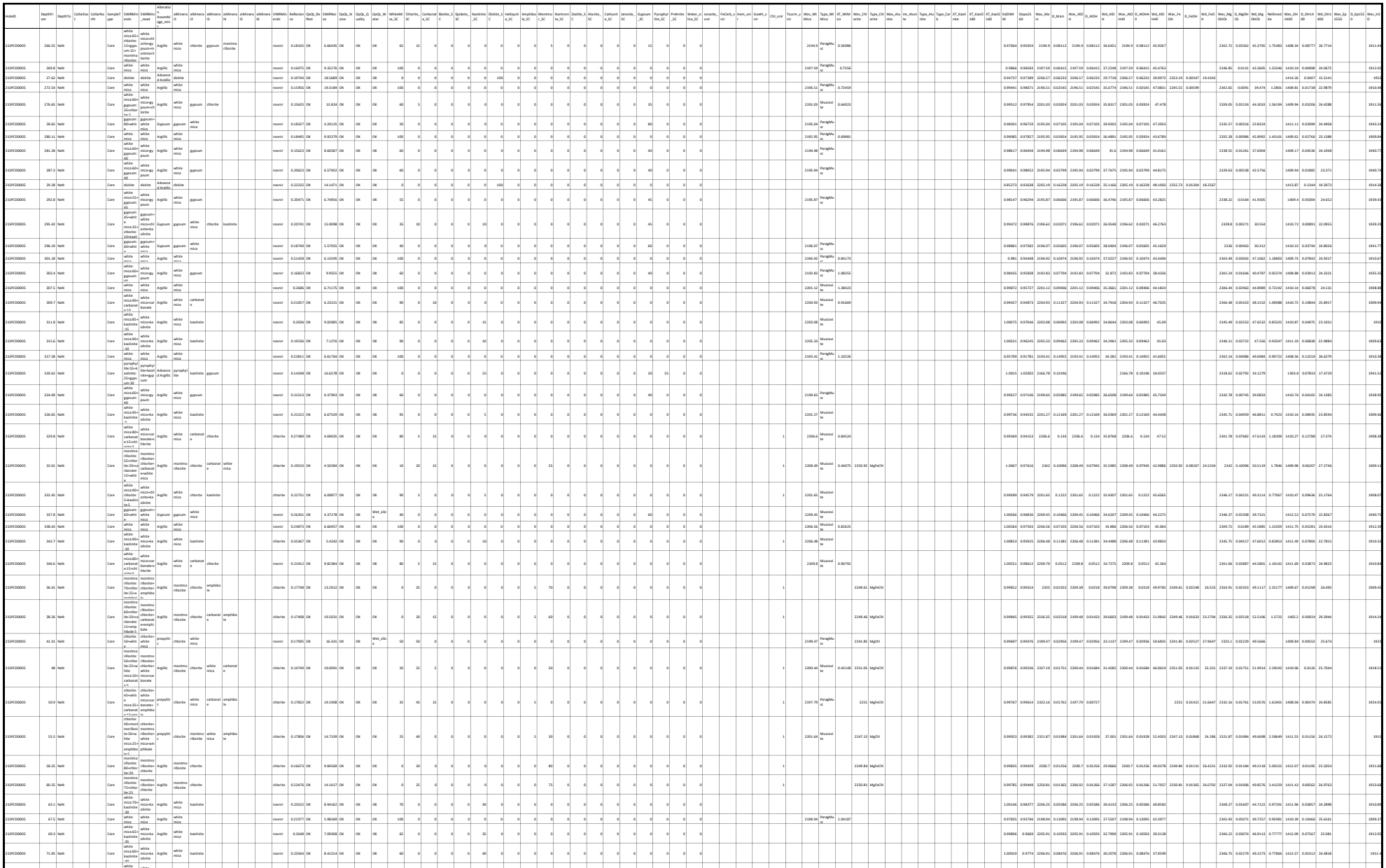

| HoleID | DepthFrom | DepthTo | CollarEast | CollarNorth | SampleType | SWIRMineralsModel | SWIRMineral_newest | AlteredAssemblage_mine | aMineral1 | aMineral2 | aMineral3 | aMineral4 | aMineral5 | aMineral6 | VNIRMineralsModel | Reflectance | QaQc_Reflect | SWIRNoise | QaQc_Noise | QaQc_Quality | QaQc_Water | WhiteMica_SC | Chlorite_SC | Carbonate_SC | Biotite_SC | Epidote_SC | Kaolinite_SC | Dickite_SC | Halloysite_SC | Amphibole_SC | Montmor_SC | Nontronite_SC | Zeolite_SC | Alunite_SC | CaAlunite_SC | Jarosite_SC | Gypsum_SC | PyrophyllineSC | Prehnite_SC | Wotter_silica_SC | Jarosite_mineral | FeCarb_mineral | Hem_mineral | Goeth_mineral | Chl_unmix | Tourm_mineral | Wav_WhiteMica | Type_WhiteMica | KT_WIMIca | Wav_Chlorite | Type_Chlorite | Wav_Alunite | Int_Alunite | Type_Alunite | Type_Carb | KT_KaoliniteA | KT_KaoliniteB | KT_KaoliniteD | KaDiWell | Slope2160 | Wav_Min | D_Main | Wav_AlOH | D_AlOH | Wd_AlOH | Wav_AlOHAll | D_AlOHAll | Wd_AlOHAll | Wav_Fe | D_FeOH | Wd_FeOH | Wav_MgOHCb | D_MgOHCb | Wd_MgOHCb | ReSmectite | Wav_OHStr1600 | D_OH1400 | Wd_OH1400 | Wav_Sp1550 | D_Sp1550 | Wav_H2O |
|---|---|---

| HoleID | Depth(From) | Depth(To) | CollarEast | CollarNorth | SampleType | SWIRMineralsMineral | SWIRMineralsMineral_Caveat | AlteredMineralAssemblage_mineral | alMineral1 | alMineral2 | alMineral3 | alMineral4 | alMineral5 | alMineral6 | VNIRMineralsMineral | Reflection | QaQc_ReflectionFlat | SWIRNoise | QaQc_NoiseSWIR | QaQc_QualityMineral | QaQc_WaterMineral_SC | WhiteMica_SC | Chlorite_SC | Carbonate_SC | Biotite_SC | Epidote_SC | Kaolinite_SC | Dickite_SC | Halloysite_SC | Amphibole_SC | Montmor_SC | Nontronite_SC | Zeolite_SC | Alunite_SC | CaAlunite_SC | Jarosite_SC | Gypsum_SC | PyrophyllHoneyComb_SC | Prehnite_SC | Wotter_silica_SC | Jarosite_mineral | FeCarb_mineral | Hem_mineral | Goeth_mineral | Chl_mineral | Tourm_mineral | Wav_WhiteMica | Type_WhiteMica | KT_WMIndex | Wav_Chlorite | Type_Chlorite | Wav_Alunite | Int_Alunite | Type_Alunite | Type_Carb | KT_KaoliIndex | KT_KaoQI180 | KT_KaoQI160 | KaDiWMM | Slope2160 | Wav_Min | D_Main | Wav_AlOH | D_AlOHn | Wd_AlOHAbs | Wav_AlOHAbs | D_AlOHAbs | Wd_AlOHAbs | Wav_FeOH | D_FeOH | Wd_FeOH | Wav_MgOHCb | D_MgOHCb | Wd_MgOHCb | RelSmectite | Wav_OH1620 | D_OH1460 | Wd_OH1490 | Wav_Epi1550 | D_Epi1550 | Wav_H2O |
|---|---|---

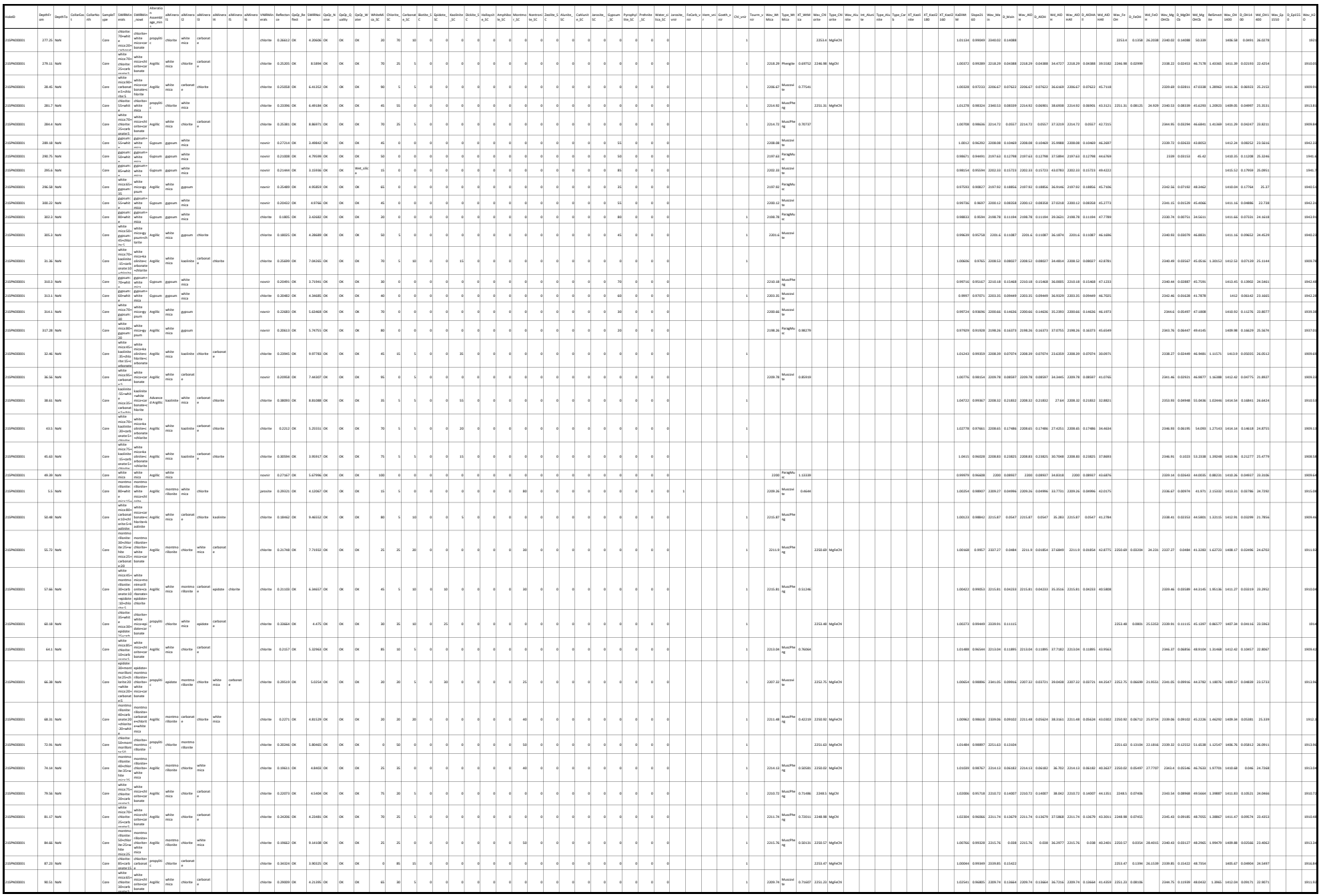

| HoleID | DepthFrom | DepthTo | CollarCount | CollarNotes | SampleType | SWIRMineralsNewest | SWIRMineralsNewest | Alteration Assemblage_mins | aiMineral1 | aiMineral2 | aiMineral3 | aiMineral4 | aiMineral5 | aiMineral6 | VNIRMineralsNewest | Reflection | QaQc_Reflect | SWIRNoise | QaQc_Noise | QaQc_Quality | QaQc_Water | WhiteMica_SC | Chlorite_SC | Carbonate_SC | Biotite_SC | Epidote_SC | Kaolinite_SC | Dickite_SC | Halloysite_SC | Amphibole_SC | Montmor_SC | Nontronite_SC | Zeolite_SC | Alunite_SC | CaAlunite_SC | Jarosite_SC | Gypsum_SC | PyrophyllHoe_SC | Prehnite_SC | Wotter_silica_SC | Jarosite_visir | FeCarb_visir | Hem_visir | Goeth_visir | Chl_visir | Tourm_visir | Wav_WhMica | Type_WhMica | KT_WhMica | Wav_ChlorIntra | Type_ChlorIntra | Wav_AluNote | Int_AluniteNote | Type_AluNote | Type_CarbNote | KT_KaoliNote | KT_KaoQual180 | KT_KaoQual360 | KaDiWtM | Slope2to60 | Wav_MainIn | D_MainIn | Wav_AlOHPeak | D_AlOHPeak | Wd_AlOHAll | Wav_AlOHAll | D_AlOHAll | Wd_AlOHAll | Wav_FeOxide | D_FeOxide | Wd_FeOHPeak | Wav_MgOHCarb | D_MgOHCarb | Wd_MgOHCarb | RelSmectite | Wav_OHIn1600 | D_OHIn1600 | Wd_OHIn1400 | Wav_Epidote1550 | D_Epidote1550 | Wav_H2O |
|---|---|---

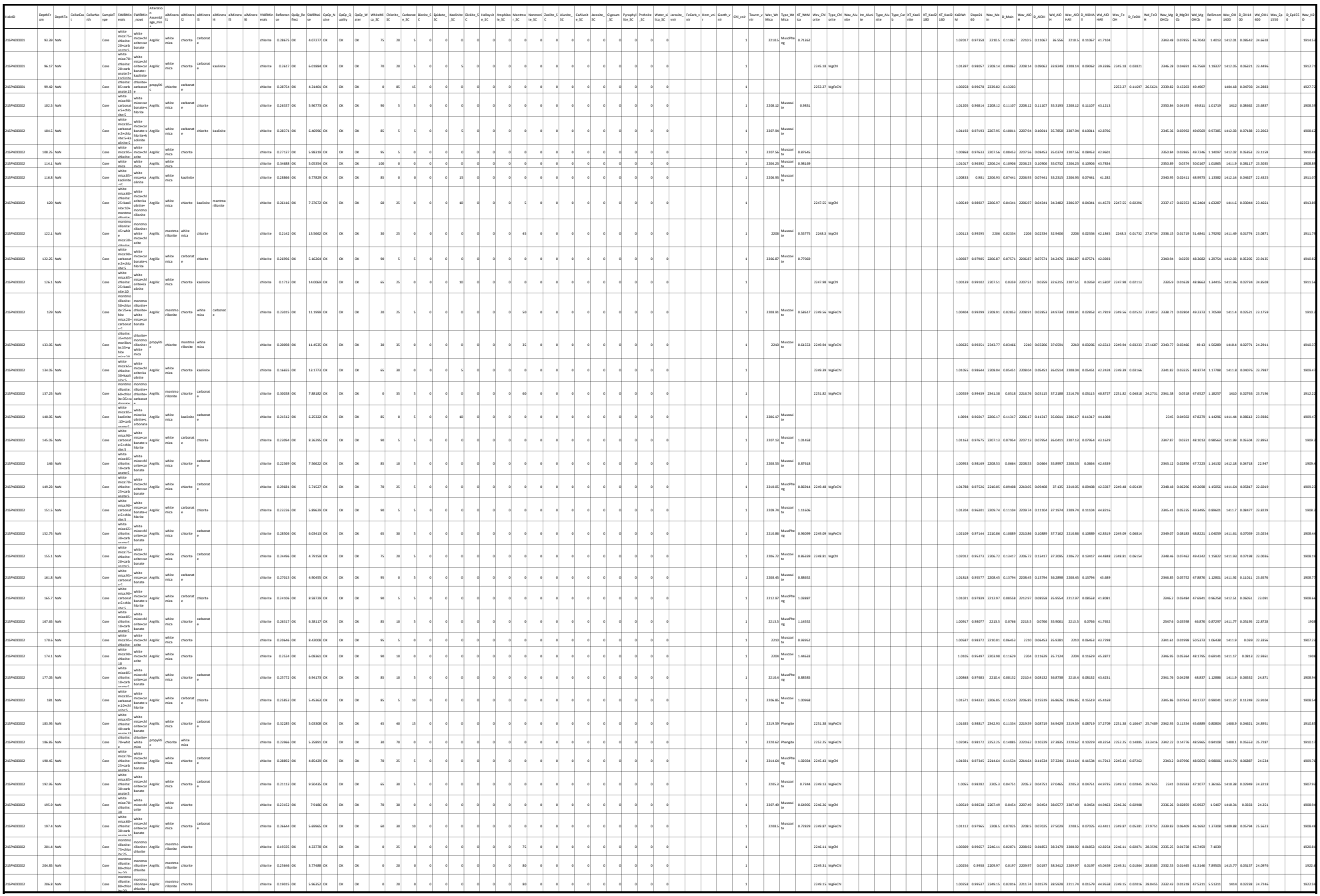

| NodeID | DepthFrom | DepthTo | CollarCount | CollarNotes | SampleType | SWIRMineralsNotes | SWIRMineralsNotes_Newest | AlteredAssemblage_mins | aiMineral1 | aiMineral2 | aiMineral3 | aiMineral4 | aiMineral5 | aiMineral6 | VNIRMineralsNotes | Reflectance | QaQc_Reflect | SWIRNoise | QaQc_Noise | QaQc_Quality | QaQc_Water | WhiteMica_SC | Chlorite_SC | Carbonate_SC | Biotite_SC | Epidote_SC | Kaolinite_SC | Dickite_SC | Halloysite_SC | Amphibole_SC | Montmor_SC | Nontronite_SC | Zeolite_SC | Alunite_SC | CaAlunite_SC | Jarosite_SC | Gypsum_SC | PyrophyllHeight_SC | Prehnite_SC | Wotter_silica_SC | Jarosite_visir | FeCarb_visnir | Hem_visnir | Goeth_visnir | Chl_visnir | Tourm_visnir | Wav_WhiMica | Type_WhiMica | KT_WhiMica | Wav_ChlIntra | Type_ChlIntra | Wav_AluInte | Int_AluInte | Type_AluInte | Type_Carb | KT_KaoliInte | KT_KaoQI180 | KT_KaoQI160 | KaDiWtM | Slope2160 | Wav_MgIn | D_Main | Wav_AlOHInt | D_AlOHInt | Wid_AlOHM | Wav_AlOHAbs | D_AlOHAbs | Wid_AlOHAbs | Wav_FeOxi | D_FeOxi | Wid_FeOxiM | Wav_MgOHCb | D_MgOHCb | Wid_MgOHCb | RelSmectite | Wav_OHI1600 | D_OHI1600 | Wid_OHI1600 | Wav_Epi1550 | D_Epi1550 | Wav_H2O |
|---|---|---

| NodeID | DepthFrom | DepthTo | CollarCoords | CollarNotes | SampleType | SWIRMineralsNewest | SWIRMineral_Newest | AlteredAssemblage_mins | aiMineral1 | aiMineral2 | aiMineral3 | aiMineral4 | aiMineral5 | aiMineral6 | VNIRMineralsNewest | Reflectance | QaQc_Reflect | SWIRNoise | QaQc_Noise | QaQc_Quality | QaQc_Water | WhiteMica_SC | Chlorite_SC | Carbonate_SC | Biotite_SC | Epidote_SC | Kaolinite_SC | Dickite_SC | Halloysite_SC | Amphibole_SC | Montmor_SC | Nontronite_SC | Zeolite_SC | Alunite_SC | CaAlunite_SC | Jarosite_SC | Gypsum_SC | Pyrophyllite_SC | Prehnite_SC | Wotter_silica_SC | Jarosite_visir | FeCarb_visir | Hem_visir | Goeth_visir | Chl_visir | Tourm_visir | Wav_WhMica | Type_WhMica | KT_WhMica | Wav_ChlorIntra | Type_ChlorIntra | Wav_AluInter | Int_AluniIn | Type_AluInter | Type_CarbIn | KT_KaoliInter | KT_KaoQI 180 | KT_KaoQI 160 | KaDiWtM | Slope2160 | Wav_MgIn | D_MgIn | Wav_AlOH | D_AlOHn | Wid_AlOHM | Wav_AlOHAll | D_AlOHAll | Wid_AlOHAll | Wav_FeOxi | D_FeOxi | Wid_FeOH | Wav_MgOHCb | D_MgOHCb | Wid_MgOHCb | RelSmectite | Wav_OHI600 | D_OHI4600 | Wid_OHI4600 | Wav_Epi1550 | D_Epi1550 | Wav_H2O |
|---|---|---

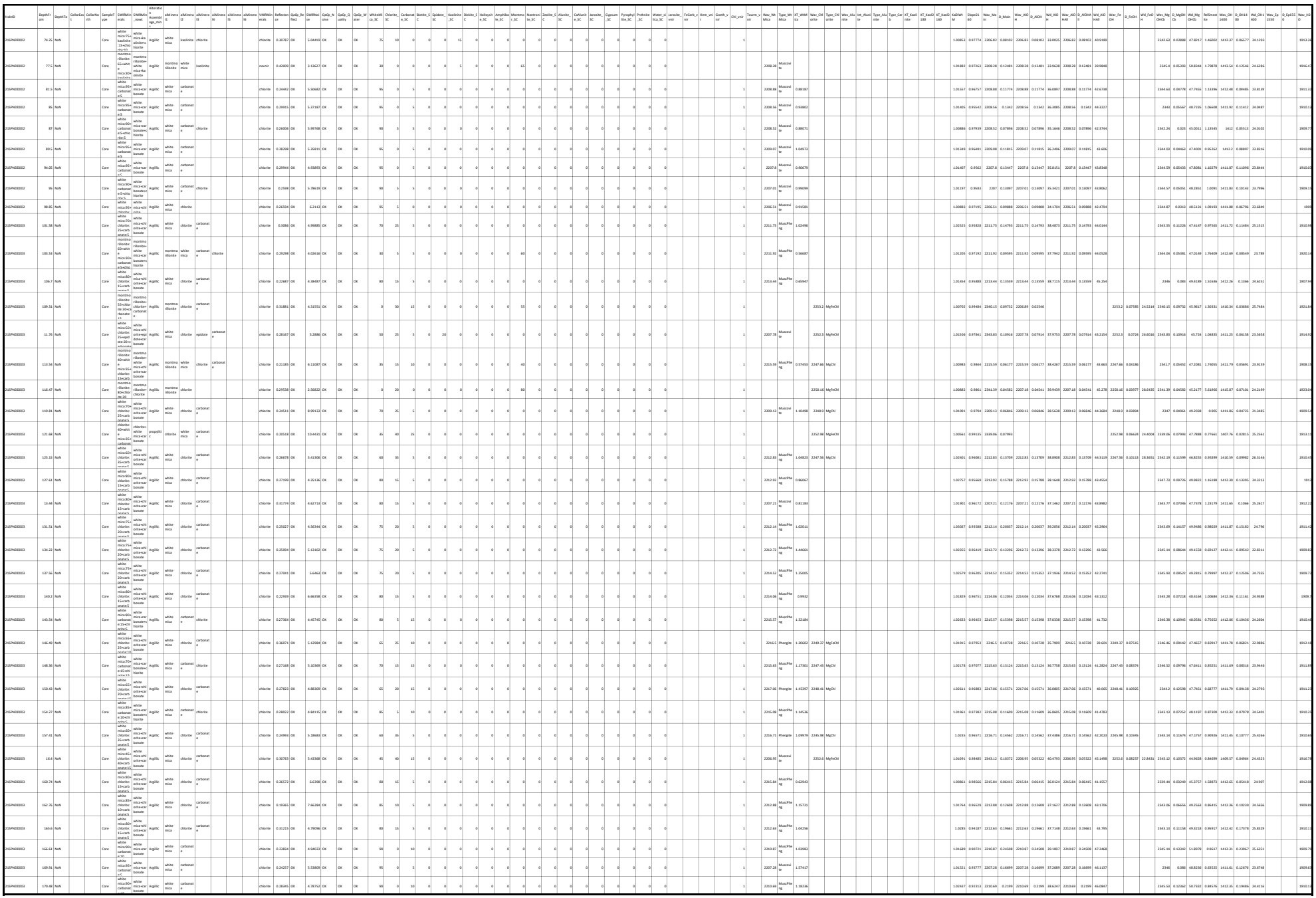

| NodeID | Depth(cm) | Depth.Cm | CollarCast | CollarNotes | SampleType | SWIRMineralsWet | SWIRMineralsDry | SWIRMineral_Dry_Notes | Alternation_Assemblage_minus | aiMineralGroup1 | aiMineralGroup2 | aiMineralGroup3 | aiMineralGroup4 | aiMineralGroup5 | aiMineralGroup6 | VNIRMineralsDry | Reflectance | QaQc_Reflect | SWIRNoise | QaQc_Noise | QaQc_Quality | QaQc_Weather | WhiteMica_SC | Chlorite_SC | Carbonate_SC | Biotite_SC | Epidote_SC | Kaolinite_SC | Dickite_SC | Halloysite_SC | Amphibole_SC | Montmor_SC | Nontronite_SC | Zeolite_SC | Alunite_SC | CaAlunite_SC | Jarosite_SC | Gypsum_SC | Pyrophyllite_SC | Prehnite_SC | Wotter_silica_SC | Jarosite_visir | FeCarb_visir | Hem_visir | Goeth_visir | Chl_visir | Tourm_visir | Wav_WhiteMica | Type_WhiteMica | KT_WMIndex | Wav_ChlorIndex | Type_ChlorIndex | Wav_AluIndex | Int_AluIndex | Type_AluIndex | Type_CarbIndex | KT_KaoIndex | KT_KaoQual180 | KT_KaoQual360 | KaDiWtM | Slope2140 | Wav_MgIn | D_MgIn | Wav_AlOH | D_AlOH | Wd_AlOM | Wav_AlOHAll | D_AlOHAll | Wd_AlOHAll | Wav_FeOx | D_FeOx | Wd_FeOH | Wav_MgOHCb | D_MgOHCb | Wd_MgOHCb | RelSmectite | Wav_OHIndex | D_OH14 00 | Wd_OH1400 | Wav_Epidote | D_Epi550 | D_Epi550 | Wav_H2O |
|---|---|---

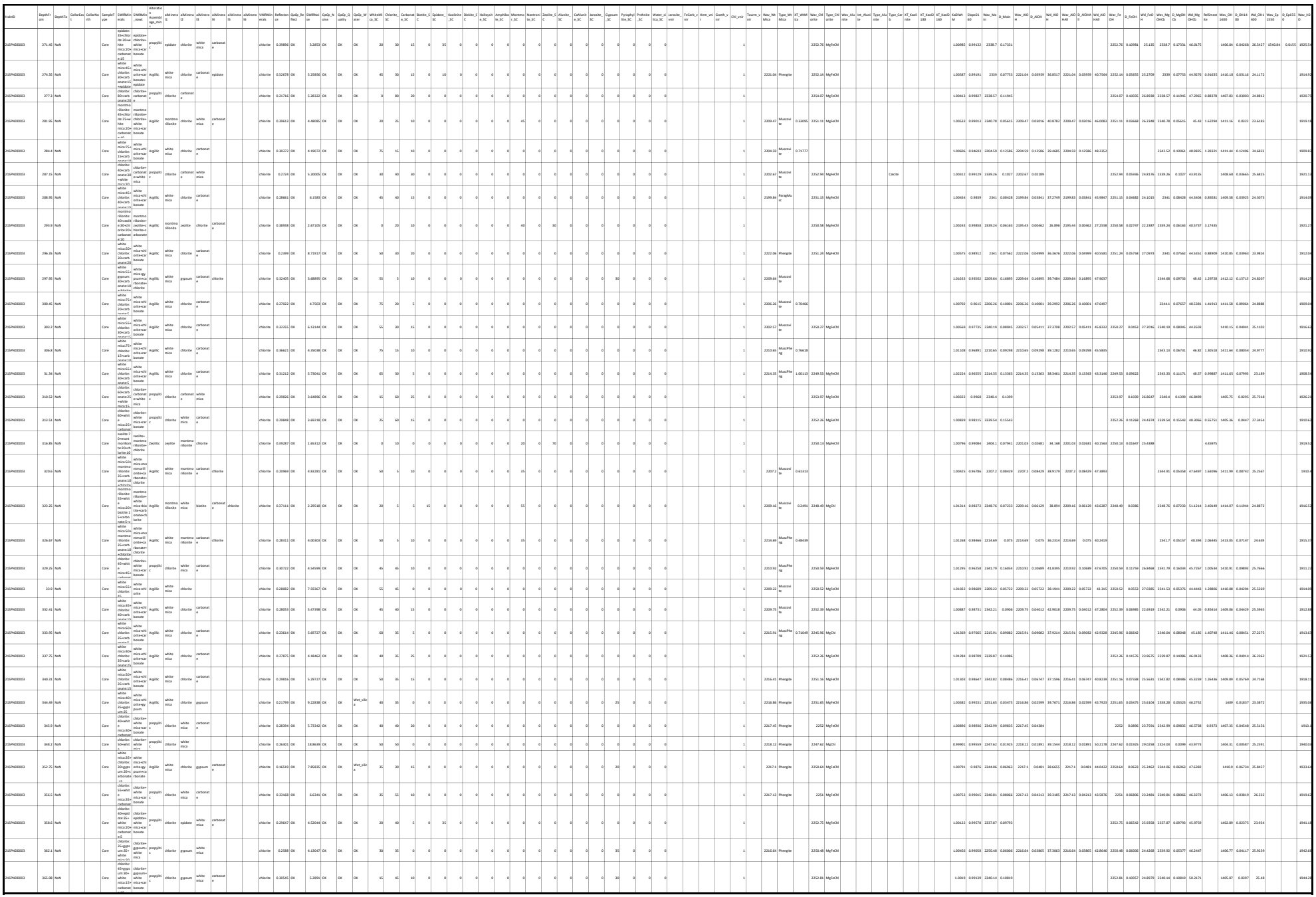

| NodeID | DepthFrom | DepthTo | CollarCast | CollarNotes | SampleType | SWIRMineralsWoodford | SWIRMineralsNewWoodford | AlteredAssemblage_mineralsWoodford | aiMineralsWoodford | aiMineralsWoodford2 | aiMineralsWoodford3 | aiMineralsWoodford4 | aiMineralsWoodford5 | aiMineralsWoodford6 | VNIRMineralsWoodford | ReflectanceWoodford | QaQc_ReflectWoodford | SWIRNoiseWoodford | QaQc_NoiseWoodford | QaQc_QualityWoodford | QaQc_WaterWoodford | WhiteMica_SC | Chlorite_SC | Carbonate_SC | Biotite_SC | Epidote_SC | Kaolinite_SC | Dickite_SC | Halloysite_SC | Amphibole_SC | Montmor_SC | Nontronite_SC | Zeolite_SC | Alunite_SC | CaAlunite_SC | Jarosite_SC | Gypsum_SC | Pyrophyllite_SC | Prehnite_SC | Witherite_SC | Jarosite_variance | FeCarb_vnir | Hem_vnir | Goeth_vnir | Chl_vnir | Tourm_vnir | Wav_WhiteMica | Type_WhiteMica | KT_WIMIca | Wav_Chlorite | Type_Chlorite | Wav_Alunite | Int_Alunite | Type_Alunite | Type_Carb | KT_Kaolinite | KT_Kaol2180 | KT_Kaol3160 | KaDiWtM | Slope2160 | Wav_Min | D_Main | Wav_AlOH | D_AlOH | Wd_AlOHM | Wav_AlOHAki | D_AlOHAki | Wd_AlOHAki | Wav_FeOxi | D_FeOxi | Wd_FeOxi | Wav_MgOHCb | D_MgOHCb | Wd_MgOHCb | RelSmectite | Wav_OHI1670 | D_OHI4 | Wd_OHI1400 | Wav_Epi1550 | D_Epi1550 | Wav_H2O |
|---|---|---

| NodeID | DepthFrom | DepthTo | CollarCount | CollarNotes | SampleType | SWIRMineralsNewest | SWIRMineralsNewest | AlteredAssemblage_mins | aiMineral1 | aiMineral2 | aiMineral3 | aiMineral4 | aiMineral5 | aiMineral6 | VNIRMineralsNewest | Reflection | QaQc_Reflect | SWIRNoise | QaQc_Noise | QaQc_Quality | QaQc_Water | WhiteMica_SC | Chlorite_SC | Carbonate_SC | Biotite_SC | Epidote_SC | Kaolinite_SC | Dickite_SC | Halloysite_SC | Amphibole_SC | Montmor_SC | Nontronite_SC | Zeolite_SC | Alunite_SC | CaAlunite_SC | Jarosite_SC | Gypsum_SC | PyrophyllHine_SC | Prehnite_SC | Wotter_silica_SC | Jarosite_visir | FeCarb_visir | Hem_visir | Goeth_visir | Chl_visir | Tourm_visir | Wav_WhiMica | Type_WhiMica | KT_WIMica | Wav_ChlorIte | Type_ChlorIte | Wav_Alunite | Int_Alunite | Type_Alunite | Type_Carb | KT_KaoliHite | KT_KaoGib | KT_KaoGib0 | KaDiWtM | Slope1400 | Wav_Mgin | D_Main | Wav_AlOH | D_AlOH | Wd_AlOHM | Wav_AlOHAbs | D_AlOHAbs | Wd_AlOHAbs | Wav_FeOH | D_FeOH | Wd_FeOHM | Wav_MgOHCb | D_MgOHCb | Wd_MgOHCb | RelSmectite | Wav_OH1600 | D_OH1400 | Wd_OH1400 | Wav_Epi1550 | D_Epi1550 | Wav_H2O |
|---|---|---

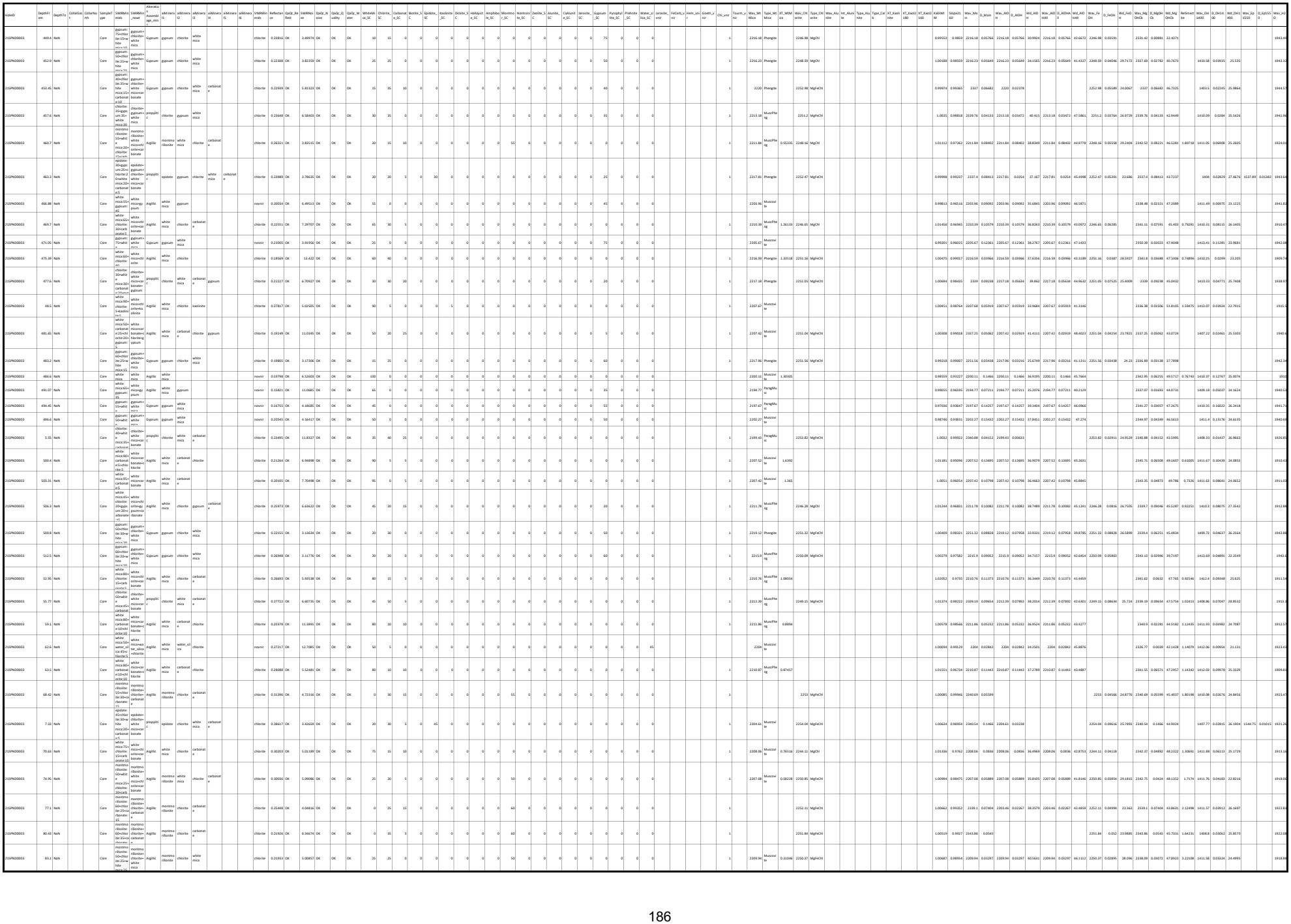

| HoleID | Depth(From) | Depth(To) | CollarCast | CollarNotes | SampleType | SWIRMineralsNewest | SWIRMineralsNewest | Alteration Assemblage_mineralsNewest | idMineral1 | idMineral2 | idMineral3 | idMineral4 | idMineral5 | idMineral6 | VNIRMineralsNewest | Reflectance | QaQc_Reflect | SWIRNoise | QaQc_Noise | QaQc_Quality | QaQc_Water | WhiteMicaSC | Chlorite_SC | Carbonate_SC | Biotite_SC | Epidote_SC | Kaolinite_SC | Dickite_SC | Halloysite_SC | Amphibole_SC | Montmor_SC | Nontronite_SC | Zeolite_SC | Alunite_SC | CaAlunite_SC | Jarosite_SC | Gypsum_SC | PyrophyllHite_SC | Prehnite_SC | Wotter_ice_SC | Jarosite_vnir | FeCarb_vnir | Hem_vnir | Goeth_vnir | Chl_vnir | Tourm_vnir | Wav_WhiMica | Type_WhiMica | KT_WIMica | Wav_ChlorIte | Type_ChlorIte | Wav_Alunite | Int_Alunite | Type_Alunite | Type_Carb | KT_KaoliniteB | KT_KaoG180 | KT_KaoG360 | KaDiWM | Slope2140 | Wav_Min | D_Main | Wav_AlOH | D_AlOH | Wd_AlOM | Wav_AlOH40 | D_AlOH40 | Wd_AlOH40 | Wav_FeOH | D_FeOH | Wd_FeOH | Wav_MgOH2b | D_MgOH2b | Wd_MgOH2b | ReGmectite | Wav_OH1600 | D_OH1600 | Wd_OH1600 | Wav_Epi1550 | D_Epi1550 | Wav_H2O |
|---|---|---

| HoleID | DepthFrom | DepthTo | CollarEast | CollarNorth | SampleType | SWIRMineralsWeak | SWIRMineralsNewest | AlternativeAssemblage_mixes | alMineral1 | alMineral2 | alMineral3 | alMineral4 | alMineral5 | alMineral6 | VNIRMineralsWeak | Reflectance | QaQc_Reflect | SWIRNoise | QaQc_Noise | QaQc_Quality | QaQc_Water | WhiteMica_SC | Chlorite_SC | Carbonate_SC | Biotite_SC | Epidote_SC | Kaolinite_SC | Dickite_SC | Halloysite_SC | Amphibole_SC | Montmor_SC | Nontronite_SC | Zeolite_SC | Alunite_SC | CaAlunite_SC | Jarosite_SC | Gypsum_SC | Pyrophyllite_SC | Prehnite_SC | Wotter_silica_SC | Jarosite_vnir | FeCarb_vnir | Hem_vnir | Goeth_vnir | Chl_vnir | Tourm_vnir | Wav_WhiMica | Type_WhiMica | KT_WMica | Wav_Chlorite | Type_Chlorite | Wav_Alunite | Int_Alunite | Type_Alunite | Type_Carb | KT_KaoliniteA | KT_KaoliniteB | KT_KaoliniteM | KaDiWt | Slope2140 | Wav_Min | D_Main | Wav_AlOH | D_AlOH | Wid_AlOH | Wav_AlOHA | D_AlOHA | Wid_AlOHA | Wav_FeOH | D_FeOH | Wid_FeOH | Wav_MgOHCb | D_MgOHCb | Wid_MgOHCb | ReSmectite | Wav_OH1600 | D_OH1400 | Wid_OH1400 | Wav_Epi1550 | D_Epi1550 | Wav_H2O |
|---|---|---

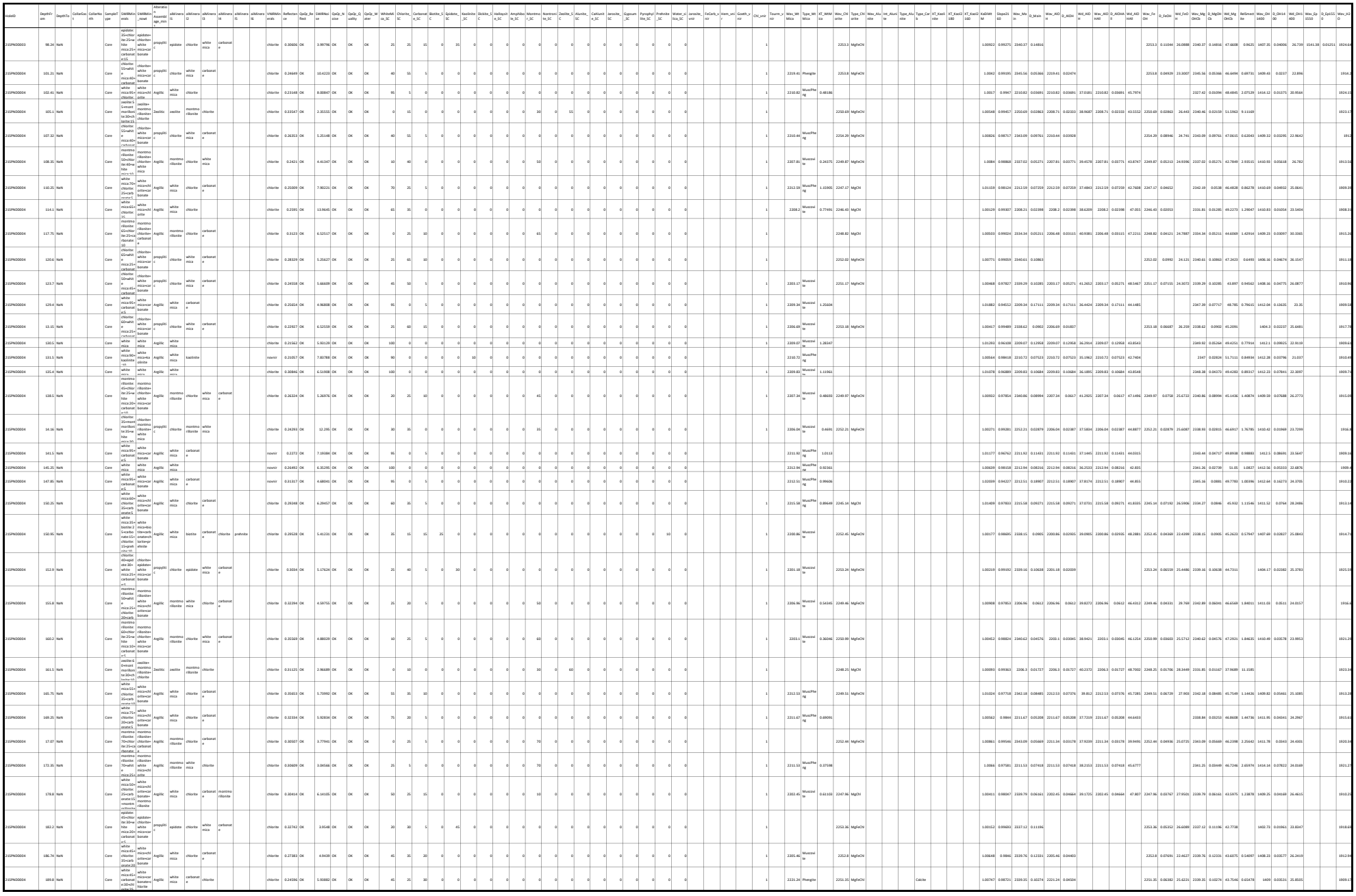

| HoleID | DepthFrom | DepthTo | CollarEast | CollarNorth | SampleType | SWIRMineralsAssemblage_newest | SWIRMineralsAssemblage_newest | AlternationAssemblage_mineralsAssemblage_mineralsAssemblage_minerals

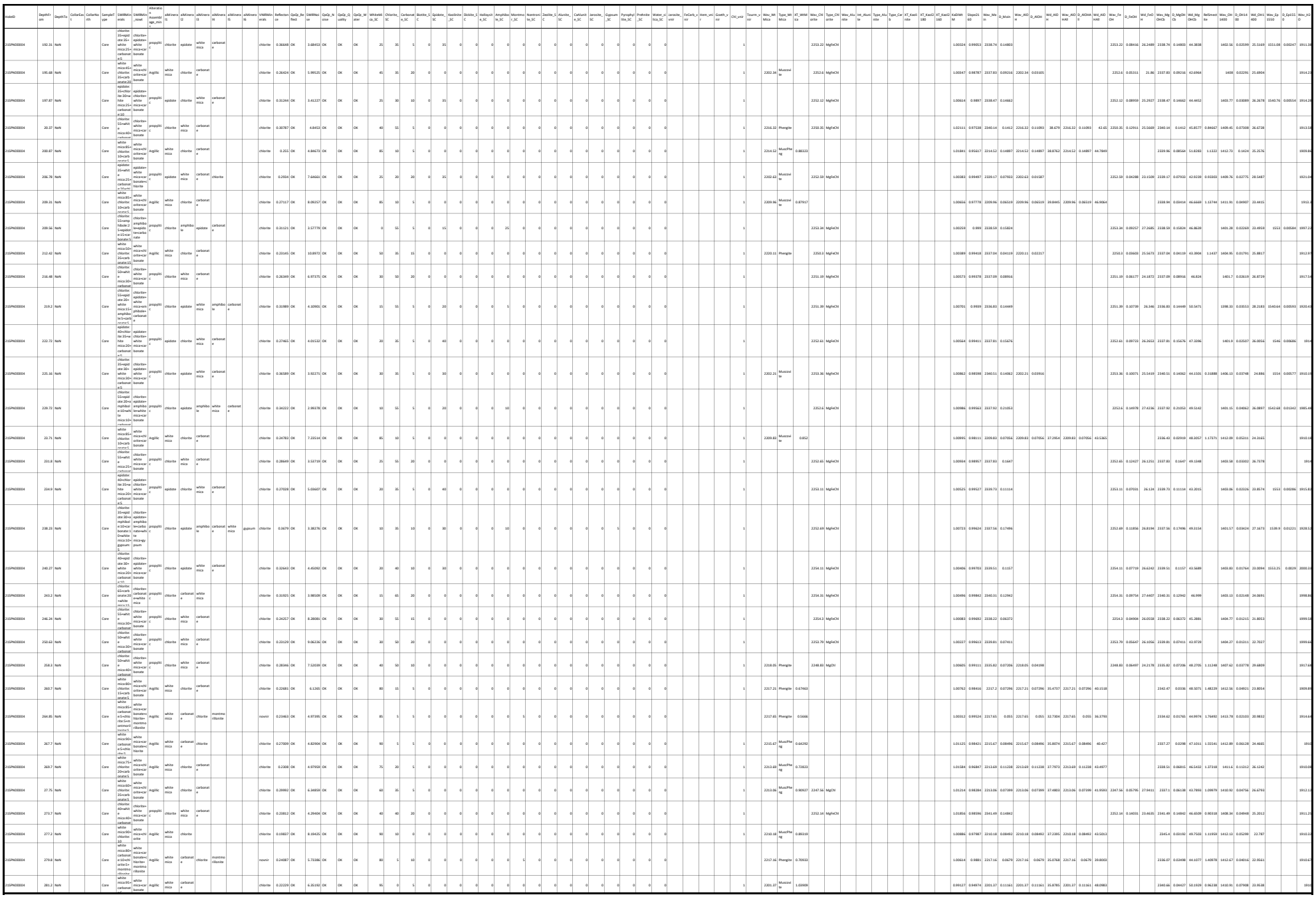

| HoleID | DepthFrom | DepthTo | CollarEast | CollarNorth | SampleType | SWIRMineralsL | SWIRMineral_newL | AlteredAssemblage_mineralsL | aiMineral1 | aiMineral2 | aiMineral3 | aiMineral4 | aiMineral5 | aiMineral6 | VNIRMineralsL | Reflection | OpQc_Reflect | SWIRNoise | OpQc_Noise | OpQc_Quality | OpQc_Water | WhiteMica_SC | Chlorite_SC | Carbonate_SC | Biotite_SC | Epidote_SC | Kaolinite_SC | Dickite_SC | Halloysite_SC | Amphibole_SC | Montmor_SC | Nontronite_SC | Zeolite_SC | Alunite_SC | CaAlunite_SC | Jarosite_SC | Gypsum_SC | PyrophyllHte_SC | Prehnite_SC | Wotter_silica_SC | Jarosite_unsr | FeCarb_unsr | Hem_unsr | Goeth_unsr | Chl_unsr | Tourm_unsr | Wav_WhMica | Type_WhMica | KT_WhMica | Wav_ChlorIte | Type_ChlorIte | Wav_AluNite | Int_AluniteL | Type_AluniteL | Type_CarbL | KT_KaoliniteL | KT_KaoQI180L | KT_KaoQI360L | KaDiWtM | Wav_4100 | Slope2160 | Wav_MgOH | D_MgOH | Wav_MgOHCb | D_MgOHCb | Wd_MgOHCb | RelSmectite | Wav_OH1600 | D_OH1600 | Wd_OH1400 | Wav_Epi1550 | D_Epi1550 | Wav_H2O |
|---|---|---

| HoleID | DepthFrom | DepthTo | CollarEast | CollarNorth | SampleType | SWIRMineralsNowel | SWIRMineralsNowel | Alteration Assemblage_mins | aiMineral1 | aiMineral2 | aiMineral3 | aiMineral4 | aiMineral5 | aiMineral6 | VNIRMineralsNowel | Reflectance | QaQc_Reflect | SWIRNoise | QaQc_Noise | QaQc_Quality | QaQc_Water | WhiteMica_SC | Chlorite_SC | Carbonate_SC | Biotite_SC | Epidote_SC | Kaolinite_SC | Dickite_SC | Halloysite_SC | Amphibole_SC | Montmor_SC | Nontronite_SC | Zeolite_SC | Alunite_SC | CaAlunite_SC | Jarosite_SC | Gypsum_SC | Pyrophyllite_SC | Prehnite_SC | Wotter_silica_SC | Jarosite_visir | FeCarb_visir | Hem_visir | Goeth_visir | Chl_visir | Tourm_visir | Wav_WhiteMica | Type_WhiteMica | KT_WIMica | Wav_Chlorite | Type_Chlorite | Wav_Alunite | Int_Alunite | Type_Alunite | Type_Carb | KT_KaoliniteI | KT_KaoI3180 | KT_KaoI3160 | KaDiWtM | Slope2160 | Wav_Min | D_Main | Wav_AlOH | D_AlOH | Wd_AlOHM | Wav_AlOHAll | D_AlOHAll | Wd_AlOHAll | Wav_Fe | D_FeOxi | Wd_FeOH | Wav_MgChlCb | D_MgOHCb | Wd_MgChlCb | RelSmectite | Wav_OHI600 | D_OHI4 00 | Wd_OHI400 | Wav_Epi1550 | D_Epi1550 | Wav_H2O |
|---|---|---

| Sample | Field ID | Depth_From | Depth_To | Index | Min1 CTAV1 | Mn1 CTAV1 | Mn2 CTAV1 | Mn3 CTAV1 | Mn4 CTAV1 | Mn5 CTAV1 | Mn6 CTAV1 | Mn7 CTAV1 | Mn8 CTAV1 | Mn9 CTAV1 | Mn10 CTAV1 | Mn11 CTAV1 | wn12000 | Sq12000 | wn11000 | wn10000 | Sq11000 | wn9000 | Sq9000 | wn8000 | Sq8000 | wn7000 | Sq7000 | wn6000 | Sq6000 | wn5000 | Sq5000 | wn4000 | Sq4000 | wn3000 | Sq3000 | wn2000 | Sq2000 | wn1000 | Sq1000 | Mn1 Cryst | Mn1 Clays | Mn1 Oxides | Mn1 Carbs | Mn1 Sulfates | Mn1 Phos | Mn1 Halides | Mn1 Sulfides | Mn1 Organics | Mn1 Silicates | Mn1 Zeolites | Mn1 Phyllosilicates | Mn1 Tectosilicates | Mn1 Inosilicates | Mn1 Nesosilicates | Mn1 Sorosilicates | Mn1 Cyclosilicates | Mn1 Unclassified | Mineral 1 | Mineral 2 | Mineral 3 | Alteration Assemblage | *Confidence |
|---|---|---

Sample	Hole ID	Depth_From	Depth_To	Index	Min1 cTotal	Min1 cTotal	Min2 cTotal	Min2 cTotal	Min3 cTotal	Min3 cTotal	Min4 cTotal	Min4 cTotal	Min5 cTotal	Min5 cTotal	Min6 cTotal	Min6 cTotal	Error cTotal	wn1000	hq1000	wn01000	wn2500	hq02500	wn02500	hq02950	wn03500	hq03950	MMCryst	hCl01 mean	hCl01 stanev	Calc Cryst	wn10500	wn10500	wn13000	Depth_From	Min1 cTotal	Min2 cTotal	Min3 cTotal	Mineral 1	Mineral 2	Mineral 3	Alteration Assemblage	*Confidence?
ESSPCD0006_098.00M.asd	20SPCD0006	098.00	099.00	FSPE.20001 ish-102-sm. SAMPLED FROM SIDE OF CORE	Siderite	0.415	Phengite	0.305	Chlorite-FeMg	0.244	300.78	NULL	NULL	NULL	NULL	NULL	2330.16	0.0564	96.197	2251.27	0.0643	2362.42	0.097	97.990	0.39	2.281	0.982	0.999	0.983	2342.42	2251.27	2330.16	098.00	Siderite	Phengite	Chlorite-FeMg	Chlorite			Propylitic	
ESSPCD0006_099.00M.asd	20SPCD0006	099.00	099.00	FSPE.20001 ish-102-sm. SAMPLED FROM SIDE OF CORE	Montmorillonite	0.00	Chlorite-FeMg	0.895	NULL	NULL	NULL	80.996	Aspectral	1	NULL	NULL	500	2251.79	0.0996	96.796	2336.72	0.0516	2360.76	0.0197	99.429	0.082	0.726	0.967	0.99	0.977	2343.76	2336.72	2351.79	099.00	Montmorillonite	Chlorite-FeMg	NULL	Montmorillonite			Argillic	
ESSPCD0006_098.00M.asd	20SPCD0006	098.00	101.40	FSPE.20001 ish-102-sm. SAMPLED FROM SIDE OF CORE	Chlorite-FeMg	0.598	Muscovite	0.402	NULL	NULL	NULL	99.051	Aspectral	1	NULL	NULL	500	2307.48	0.0907	95.006	2316.75	0.0496	2363.08	0.0366	93.288	0.202	0.326	0.962	0.989	0.972	2343.08	2316.75	2307.48	098.00	Chlorite-FeMg	Muscovite	NULL	Muscovite			Argillic	
ESSPCD0006_101.40M.asd	20SPCD0006	101.40	104.00	FSPE.20001 ish-102-sm. SAMPLED FROM SIDE OF CORE	Chlorite-FeMg	0.528	Muscovite	0.477	NULL	NULL	NULL	76.999	Aspectral	1	NULL	NULL	500	2305.58	0.0689	91.239	2338.23	0.0366	2328.12	0.0282	98.608	0.0996	0.491	0.971	0.992	0.979	2338.12	2338.23	2305.58	101.40	Chlorite-FeMg	Muscovite	NULL	Muscovite			Argillic	
ESSPCD0006_104.00M.asd	20SPCD0006	104.00	107.05	FSPE.20001 ish-102-sm. SAMPLED FROM SIDE OF CORE	Siderite	0.405	Muscovite	0.385	NULL	NULL	NULL	86.216	Aspectral	1	NULL	NULL	500	2306.33	0.0918	92.754	2338.09	0.0398	2352.78	0.0358	92.656	0.192	0.284	0.966	0.99	0.977	2332.78	2338.09	2306.33	104.00	Siderite	Muscovite	NULL	Muscovite			Argillic	
ESSPCD0006_107.05M.asd	20SPCD0006	107.05	110.00	FSPE.20001 ish-102-sm. SAMPLED FROM SIDE OF CORE	Aspectral	1	NULL	NULL	NULL	NULL	460.38	NULL	NULL	NULL	NULL	NULL	2306.98	0.0566	25.051	2265.99	0.0198	2326.35	0.00931	26.535	0.257	0.228	0.972	0.987	0.985	2326.35	2265.99	2306.98	107.05	Aspectral	NULL	NULL	Montmorillonite			Argillic	
ESSPCD0006_110.00M.asd	20SPCD0006	110.00	113.05	FSPE.20001 ish-102-sm. SAMPLED FROM SIDE OF CORE	Aspectral	1	NULL	NULL	NULL	NULL	172.55	NULL	NULL	NULL	NULL	NULL	2306.89	0.0383	29.763	NULL	NULL	2325.22	0.00357	28.706	0.207	0.192	0.979	0.992	0.985	2325.22	NULL	2306.89	110.00	Aspectral	NULL	NULL	Montmorillonite			Argillic	
ESSPCD0006_113.05M.asd	20SPCD0006	113.05	116.40	FSPE.20001 ish-102-sm. SAMPLED FROM SIDE OF CORE	Siderite	0.635	Muscovite	0.365	NULL	NULL	NULL	80.096	Aspectral	1	NULL	NULL	500	2305.19	0.0478	27.007	2251.06	0.0376	2309.58	0.0378	96.922	0.111	0.03	0.979	0.992	0.982	2309.58	2251.06	2305.19	113.05	Siderite	Muscovite	NULL	Illite	chlorite		Argillic	
ESSPCD0006_116.40M.asd	20SPCD0006	116.40	119.00	FSPE.20001 ish-102-sm. SAMPLED FROM SIDE OF CORE	Siderite	0.38	Muscovite	0.323	Biotite	0.297	79.92	Aspectral	1	NULL	NULL	NULL	500	2301.86	0.0669	29.821	2250.88	0.0317	2308.11	0.0365	96.494	0.155	0.609	0.966	0.989	0.976	2308.11	2250.88	2301.86	116.40	Siderite	Muscovite	Biotite	Illite	Chlorite		Argillic	
ESSPCD0006_119.00M.asd	20SPCD0006	119.00	122.20	FSPE.20001 ish-102-sm. SAMPLED FROM SIDE OF CORE	Chlorite-FeMg	0.4	Muscovite	0.24	NULL	NULL	NULL	127.58	Aspectral	1	NULL	NULL	500	2301.86	0.0609	32.24	2253.99	0.0508	2302.85	0.0959	99.918	0.133	0.596	0.971	0.992	0.977	2302.85	2253.99	2301.86	119.00	Chlorite-FeMg	Muscovite	NULL	chlorite			Argillic	
ESSPCD0006_122.20M.asd	20SPCD0006	122.20	125.18	FSPE.20001 ish-102-sm. SAMPLED FROM SIDE OF CORE	Muscovite	0.339	Siderite	0.301	NULL	NULL	NULL	190.58	Aspectral	1	NULL	NULL	500	2306.99	0.0975	30.527	NULL	NULL	2302.6	0.0115	32.131	0.236	0.397	0.958	0.986	0.972	2302.6	NULL	2306.99	122.20	Muscovite	Siderite	NULL	Muscovite			Argillic	
ESSPCD0006_125.18M.asd	20SPCD0006	125.18	128.00	FSPE.20001 ish-102-sm. SAMPLED FROM SIDE OF CORE	Muscovite	0.325	Laiviolite	0.175	NULL	NULL	NULL	90.768	Aspectral	1	NULL	NULL	500	2310.6	0.0886	27.081	NULL	NULL	2317.5	0.0142	33.938	0.236	0.42	0.955	0.982	0.97	2317.5	NULL	2310.6	125.18	Muscovite	Laiviolite	NULL	Muscovite			Argillic	
ESSPCD0006_128.00M.asd	20SPCD0006	128.00	131.05	FSPE.20001 ish-102-sm. SAMPLED FROM SIDE OF CORE	Phengilbiotite	0.555	Siderite	0.307	Montmorillonite	0.3	87.092	NULL	NULL	NULL	NULL	NULL	2311.5	0.105	33.893	NULL	NULL	2306.97	0.0362	99.132	0.1	1.016	0.969	0.984	0.963	2306.97	NULL	2311.5	128.00	Phengilbiotite	Siderite	Montmorillonite	Phengilbiotite			Argillic	
ESSPCD0006_131.45M.asd	20SPCD0006	131.45	134.56	FSPE.20001 ish-102-sm. SAMPLED FROM SIDE OF CORE	Phengilbiotite	0.296	Montmorillonite	0.266	Siderite	0.259	119.79	NULL	NULL	NULL	NULL	NULL	2312.56	0.118	33.075	NULL	NULL	2302.65	0.0354	96.462	0.146	0.808	0.956	0.991	0.965	2302.65	NULL	2312.56	131.45	Phengilbiotite	Montmorillonite	Siderite	Phengilbiotite			Argillic	
ESSPCD0006_134.56M.asd	20SPCD0006	134.56	137.00	FSPE.20001 ish-102-sm. SAMPLED FROM SIDE OF CORE	Muscovitebiotite	0.57	Montmorillonite	0.429	NULL	NULL	NULL	89.161	Aspectral	1	NULL	NULL	500	2306.09	0.191	32.287	NULL	NULL	2303.67	0.0797	99.262	0.241	0.793	0.889	0.967	0.92	2303.67	NULL	2306.09	134.56	Muscovitebiotite	Montmorillonite	NULL	Muscovitebiotite			Argillic	
ESSPCD0006_137.00M.asd	20SPCD0006	137.00	140.05	FSPE.20001 ish-102-sm. SAMPLED FROM SIDE OF CORE	Phengilbiotite	0.585	Montmorillonite	0.306	Siderite	0.275	69.48	NULL	NULL	NULL	NULL	NULL	2314.56	0.142	33.49	NULL	NULL	2302.42	0.0562	97.911	0.201	0.707	0.952	0.991	0.961	2302.42	NULL	2314.56	137.00	Phengilbiotite	Montmorillonite	Siderite	Phengilbiotite			Argillic	
ESSPCD0006_140.05M.asd	20SPCD0006	140.05	143.10	FSPE.20001 ish-102-sm. SAMPLED FROM SIDE OF CORE	Aspectral	1	NULL	NULL	NULL	NULL	162.02	NULL	NULL	NULL	NULL	NULL	2306.92	0.0353	30.976	2262.61	0.0233	2319.31	0.00968	26.261	0.266	0.132	0.982	0.997	0.986	2319.31	2262.61	2306.92	140.05	Aspectral	NULL	NULL	muscovite			Argillic	
ESSPCD0006_143.10M.asd	20SPCD0006	143.10	145.98	FSPE.20001 ish-102-sm. SAMPLED FROM SIDE OF CORE	NULL	NULL	NULL	NULL	NULL	NULL	NULL	NULL	NULL	NULL	NULL	NULL	2311.16	0.0687	31.956	2260.98	0.0265	2327.06	0.0151	32.631	0.358	0.192	0.977	0.997	0.99	2327.06	2260.98	2311.16	143.10	NULL	NULL	NULL	muscovite			Argillic	
ESSPCD0006_145.98M.asd	20SPCD0006	145.98	149.00	FSPE.20001 ish-102-sm. SAMPLED FROM SIDE OF CORE	Aspectral	1	NULL	NULL	NULL	NULL	378.36	NULL	NULL	NULL	NULL	NULL	2306.09	0.0351	28.566	2265.62	0.0283	2321.86	0.0132	93.928	0.328	0.102	0.966	0.997	0.987	2321.86	2265.62	2306.09	145.98	Aspectral	NULL	NULL	muscovite			Argillic	
ESSPCD0006_149.00M.asd	20SPCD0006	149.00	152.22	FSPE.20001 ish-102-sm. SAMPLED FROM SIDE OF CORE	NULL	NULL	NULL	NULL	NULL	NULL	NULL	NULL	Aspectral	1	NULL	NULL	500	2306.33	0.0363	25.96	2251.99	0.0205	2302.85	0.0279	97.029	0.245	0.189	0.976	0.991	0.981	2302.85	2251.99	2306.33	149.00	NULL	NULL	NULL	muscovite			Argillic	
ESSPCD0006_152.22M.asd	20SPCD0006	152.22	155.15	FSPE.20001 ish-102-sm. SAMPLED FROM SIDE OF CORE	Siderite	0.362	Biotite	0.284	Muscovite	0.254	139.37	Aspectral	1	NULL	NULL	NULL	500	2302.18	0.0936	25.966	2251.96	0.0165	2302.62	0.0475	99.099	0.245	0.178	0.979	0.996	0.982	2302.62	2251.96	2302.18	152.22	Siderite	Biotite	Muscovite	Muscovitebiotite			Argillic	
ESSPCD0006_155.15M.asd	20SPCD0006	155.15	158.00	FSPE.20001 ish-102-sm. SAMPLED FROM SIDE OF CORE	NULL	NULL	NULL	NULL	NULL	NULL	NULL	NULL	Aspectral	1	NULL	NULL	500	2301.07	0.0176	97.067	2306.79	0.0178	2324.28	0.0166	96.257	0.216	0.0625	0.99	0.998	0.992	2324.28	2306.79	2301.07	155.15	NULL	NULL	NULL	Muscovitebiotite			Argillic	
ESSPCD0006_158.00M.asd	20SPCD0006	158.00	161.98	FSPE.20001 ish-102-sm. SAMPLED FROM SIDE OF CORE	Chlorite-FeMg	0.555	Siderite	0.296	Muscovite	0.255	89.679	NULL	NULL	NULL	NULL	NULL	2305.16	0.067	29.676	2252.32	0.0755	2308.39	0.0977	99.021	0.166	0.411	0.968	0.993	0.975	2308.39	2252.32	2305.16	158.00	Chlorite-FeMg	Siderite	Muscovite	Chlorite-FeMg			Propylitic	
ESSPCD0006_161.98M.asd	20SPCD0006	161.98	164.30	FSPE.20001 ish-102-sm. SAMPLED FROM SIDE OF CORE	Aspectral	1	NULL	NULL	NULL	NULL	410.28	Aspectral	1	NULL	NULL	NULL	500	2306.99	0.0487	26.731	NULL	NULL	2303.06	0.00216	23.727	0.34	0.103	0.979	0.992	0.986	2303.06	NULL	2306.99	161.98	Aspectral	NULL	NULL	Montmorillonite			Argillic	
ESSPCD0006_164.30M.asd	20SPCD0006	164.30	167.00	FSPE.20001 ish-102-sm. SAMPLED FROM SIDE OF CORE	Chlorite-FeMg	0.339	Siderite	0.307	Muscovite	0.215	101.18	NULL	NULL	NULL	NULL	NULL	2305.03	0.056	36.656	2253.76	0.0722	2302.27	0.0975	99.369	0.156	0.269	0.988	0.997	0.986	2302.27	2253.76	2305.03	164.30	Chlorite-FeMg	Siderite	Muscovite	Chlorite-FeMg			Propylitic	
ESSPCD0006_167.00M.asd	20SPCD0006	167.00	170.27	FSPE.20001 ish-102-sm.	Siderite	0.396	Biotite	0.304	Muscovite	0.299	87.661	Aspectral	1	NULL	NULL	NULL	500	2305.89	0.0866	26.053	2253.27	0.0288	2301.08	0.0535	98.296	0.196	0.238	0.979	0.996	0.983	2301.08	2253.27	2305.89	167.00	Siderite	Biotite	Muscovite	Muscovite			Argillic	
ESSPCD0006_170.27M.asd	20SPCD0006	170.27	173.00	FSPE.20001 ish-102-sm.	NULL	NULL	NULL	NULL	NULL	NULL	NULL	NULL	NULL	NULL	NULL	NULL	2306.39	0.0579	31.217	2249.93	0.0366	2307.89	0.0141	32.22	0.132	0.186	0.972	0.989	0.978	2307.89	2249.93	2306.39	170.27	NULL	NULL	NULL	Muscovite			Argillic	
ESSPCD0006_173.00M.asd	20SPCD0006	173.00	176.02	FSPE.20001 ish-102-sm.	Muscovite	0.695	Magnesit	0.305	NULL	NULL	NULL	133.68	Aspectral	1	NULL	NULL	500	2308.3	0.085	33.673	2202.93	0.0357	2307.71	0.0336	91.939	0.155	0.21	0.963	0.995	0.968	2307.71	2202.93	2308.3	173.00	Muscovite	Magnesite	NULL	Muscovite			Argillic	
ESSPCD0006_176.02M.asd	20SPCD0006	176.02	179.00	FSPE.20001 ish-102-sm.	Phengite	0.395	Pyrite	0.305	NULL	NULL	NULL	129.54	NULL	NULL	NULL	NULL	2308.3	0.0927	34.196	2248.58	0.0397	2303.41	0.0726	97.717	0.296	0.313	0.942	0.997	0.968	2303.41	2248.58	2308.3	176.02	Phengite	Pyrite	NULL	Phengite			Argillic	
ESSPCD0006_179.00M.asd	20SPCD0006	179.00	182.00	FSPE.20001 ish-102-sm.	Magnesite	0.305	NULL	NULL	NULL	NULL	172.48	NULL	NULL	NULL	NULL	NULL	2307.32	0.0796	33.529	NULL	NULL	2303.23	0.0235	99.779	0.286	0.28	0.966	0.995	0.97	2303.23	NULL	2307.32	179.00	Magnesite	NULL	NULL	Magnesite			Argillic	
ESSPCD0006_182.00M.asd	20SPCD0006	182.00	185.00	FSPE.20001 ish-102-sm.	Siderite	0.345	Muscovit e-illite	0.292	Montmorillonite	0.292	51.186	NULL	NULL	NULL	NULL	NULL	2308.47	0.129	34.066	NULL	NULL	2303.1	0.098	97.312	0.175	0.716	0.948	0.995	0.956	2303.1	NULL	2308.47	182.00	Siderite	Muscovite-illite	Montmorillonite	Muscovitebiotite			Argillic	
ESSPCD0006_185.00M.asd	20SPCD0006	185.00	188.00	FSPE.20001 ish-102-sm.	Chlorite-FeMg	0.424	Muscovite	0.424	NULL	NULL	NULL	160.14	Aspectral	1	NULL	NULL	500	2308.47	0.0929	36.49	2254.16	0.115	2303.47	0.139	98.936	0.0924	1.002	0.961	0.992	0.967	2303.47	2254.16	2308.47	185.00	Chlorite-FeMg	Muscovite	NULL	Chlorite-FeMg			Propylitic	
ESSPCD0006_188.00M.asd	20SPCD0006	188.00	191.00	FSPE.20001 ish-102-sm.	Chlorite-FeMg	0.356	Muscovit e-illite	0.256	NULL	NULL	NULL	161.09	Aspectral	1	NULL	NULL	500	2315.89	0.0803	99.018	2256.9	0.128	2302.5	0.137	98.087	0.0759	1.066	0.969	0.996	0.972	2302.5	2256.9	2315.89	188.00	Chlorite-FeMg	Muscovite-illite	NULL	Chlorite-FeMg			Propylitic	
ESSPCD0006_191.00M.asd	20SPCD0006	191.00	194.00	FSPE.20001 ish-102-sm.	Muscovite	0.374	Montmorillonite	0.26	Biotite	0.26	126.32	Aspectral	1	NULL	NULL	NULL	500	2311.75	0.123	99.682	2252.87	0.114	2306.08	0.133	99.377	0.0965	1.369	0.959	0.992	0.956	2306.08	2252.87	2311.75	191.00	Muscovite	Montmorillonite	Biotite	Montmorillonite	Muscovite		Propylitic	
ESSPCD0006_194.00M.asd	20SPCD0006	194.00	197.00	FSPE.20001 ish-102-sm.	Chlorite-FeMg	0.444	Montmorillonite	0.324	Muscovite	0.195	116.52	Aspectral	1	NULL	NULL	NULL	500	2311.66	0.111	99.778	2253.17	0.142	2303.05	0.136	97.995	0.135	0.97	0.955	0.99	0.956	2303.05	2253.17	2311.66	194.00	Chlorite-FeMg	Montmorillonite	Muscovite	Chlorite-FeMg			Propylitic	
ESSPCD0006_197.00M.asd	20SPCD0006	197.00	200.00	FSPE.20001 ish-102-sm.	Phengilbiotite	0.444	Siderite	0.256	Montmorillonite	0.256	95.479	NULL	NULL	NULL	NULL	NULL	2310.99	0.187	33.95	NULL	NULL	2303.5	0.091	97.781	0.179	1.004	0.926	0.99	0.953	2303.5	NULL	2310.99	197.00	Phengilbiotite	Siderite	Montmorillonite	Phengilbiotite	Montmorillonite		Argillic	
ESSPCD0006_200.00M.asd	20SPCD0006	200.00	203.00	FSPE.20001 ish-102-sm.	Siderite	0.438	Muscovite	0.295	Phengilbiotite	0.267	103.97	NULL	NULL	NULL	NULL	NULL	2310.89	0.111	34.135	NULL	NULL	2301	0.0757	52.702	0.115	0.922	0.952	0.989	0.963	2301	NULL	2310.89	200.00	Siderite	Muscovite	Phengilbiotite	Phengilbiotite	Montmorillonite		Argillic	
ESSPCD0006_203.00M.asd	20SPCD0006	203.00	206.00	FSPE.20001 ish-102-sm.	Phengilbiotite	0.444	Siderite	0.256	Muscovite	0.256	95.479	NULL	NULL	NULL	NULL	NULL	2310.99	0.187	33.95	NULL	NULL	2303.5	0.091	97.781	0.179	1.004	0.926	0.99	0.953	2303.5	NULL	2310.99	203.00	Phengilbiotite	Siderite	Muscovite	Phengilbiotite	Montmorillonite		Argillic	
ESSPCD0006_206.00M.asd	20SPCD0006	206.00	209.00	FSPE.20001 ish-102-sm.	Montmorillonite	0.395	Muscovit e-illite	0.355	Siderite	0.295	91.298	NULL	NULL	NULL	NULL	NULL	2309.78	0.126	33.84	NULL	NULL	2309.58	0.0377	96.026	0.195	0.768	0.948	0.996	0.964	2309.58	NULL	2309.78	206.00	Montmorillonite	Muscovite-illite	Siderite	Montmorillonite	Muscovite		Argillic	
ESSPCD0006_209.00M.asd	20SPCD0006	209.00	212.00	FSPE.20001 ish-102-sm.	Montmorillonite	0.467	Muscovite	0.224	Chlorite-FeMg	0.224	77.616	NULL	NULL	NULL	NULL	NULL	2310.17	0.183	33.962	NULL	NULL	2305.79	0.0711	97.09	0.235	0.891	0.929	0.986	0.939	2305.79	NULL	2310.17	209.00	Montmorillonite	Muscovite-illite	Chlorite-FeMg	Montmorillonite	Muscovite		Argillic	
ESSPCD0006_212.00M.asd	20SPCD0006	212.00	215.00	FSPE.20001 ish-102-sm.	Montmorillonite	0.407	Muscovite	0.279	Chlorite-FeMg	0.314	102.85	NULL	NULL	NULL	NULL	NULL	2310.56	0.193	33.875	NULL	NULL	2305.23	0.0986	97.715	0.198	1.038	0.92	0.986	0.953	2305.23	NULL	2310.56	212.00	Montmorillonite	Muscovite-illite	Chlorite-FeMg	Montmorillonite	Muscovite		Argillic	
ESSPCD0006_215.00M.asd	20SPCD0006	215.00	218.00	FSPE.20001 ish-102-sm.	Muscovite-illite	0.474	Montmorillonite	0.326	NULL	NULL	NULL	95.457	Aspectral	1	NULL	NULL	500	2306.98	0.273	33.173	NULL	NULL	2306.73	0.133	97.091	0.236	1.265	0.861	0.97	0.888	2306.73	NULL	2306.98	215.00	Muscovite-illite	Montmorillonite	NULL	Muscovite-illite	Montmorillonite		Argillic	
ESSPCD0006_218.00M.asd	20SPCD0006	218.00	221.00	FSPE.20001 ish-102-sm.	Phengilbiotite	0.429	NULL	NULL	NULL	NULL	92.408	Aspectral	1	NULL	NULL	NULL	500	2306.81	0.205	34.215	NULL	NULL	2301.71	0.0625	95.693	0.198	1.136	0.818	0.98	0.927	2301.71	NULL	2306.81	218.00	Phengilbiotite	NULL	NULL	Montmorillonite	Phengilbiotite	Paragonite-illite	Argillic	
ESSPCD0006_221.00M.asd	20SPCD0006	221.00	224.00	FSPE.20001 ish-102-sm.	Dickite	0.737	Chlorite-FeMg	0.263	Kaolinite-WX	0.255	177.42	NULL	NULL	NULL	NULL	NULL	2307.26	0.156	24.983	2258.99	0.0288	2301.77	0.0431	92.525	0.0938	0.476	0.895	0.929	0.964	2301.77	2258.99	2307.26	221.00	Dickite	Kaolinite-WX	Chlorite-Mg	Dickite	Kaolinite-WX		Advanced Argillic	
ESSPCD0006_224.00M.asd	20SPCD0006	224.00	227.00	FSPE.20001 ish-102-sm.	Kaolinite-WX	0.554	Chlorite-FeMg	0.446	NULL	NULL	NULL	164.08	Aspectral	1	NULL	NULL	500	2307.26	0.156	24.983	2258.99	0.0288	2301.77	0.0431	92.525	0.0938	0.476	0.895	0.929	0.964	2301.77	2258.99	2307.26	224.00	Kaolinite-WX	Chlorite-FeMg	NULL	Kaolinite-WX			Advanced Argillic	
ESSPCD0006_227.00M.asd	20SPCD0006	227.00	229.90	FSPE.20001 ish-102-sm.	Paragonite	0.485	NULL	NULL	NULL	NULL	116.68	Aspectral	1	NULL	NULL	NULL	500	2306.77	0.101	32.699	NULL	NULL	2307.86	0.0345	95.703	0.139	1.091	0.899	0.972	0.929	2307.86	NULL	2306.77	227.00	Paragonite	NULL	NULL	Paragonite	Montmorillonite		Argillic	
ESSPCD0006_229.90M.asd	20SPCD0006	229.90	232.00	FSPE.20001 ish-102-sm.	Phengite	0.5	Montmorillonite	0.259	Siderite	0.202	95.712	Aspectral	1	NULL	NULL	NULL	500	2311.35	0.161	33.783	NULL	NULL	2307.6	0.0605	95.968	0.147	1.096	0.903	0.985	0.947	2307.6	NULL	2311.35	229.90	Phengite	Montmorillonite	Siderite	Phengite	Montmorillonite		Argillic	
ESSPCD0006_232.00M.asd	20SPCD0006	232.00	236.00	FSPE.20001 ish-102-sm.	Chlorite-FeMg	0.424	Phengite	0.285	Siderite	0.291	106.98	Aspectral	1	NULL	NULL	NULL	500	2314.82	0.0992	34.705	2251.5	0.131	2309.2	0.168	97.338	0.136	0.801	0.968	0.997	0.973	2309.2	2251.5	2314.82	232.00	Chlorite-FeMg	Phengite	Siderite	Chlorite-FeMg	Phengilbiotite		Propylitic	
ESSPCD0006_236.00M.asd	20SPCD0006	236.00	239.00	FSPE.20001 ish-102-sm.	Chlorite-FeMg	0.444	Muscovite	0.324	Montmorillonite	0.232	116.52	Aspectral	1	NULL	NULL	NULL	500	2311.66	0.111	99.778	2253.17	0.142	2303.05	0.136	97.995	0.135	0.97	0.955	0.99	0.956	2303.05	2253.17	2311.66	236.00	Chlorite-FeMg	Muscovite	Montmorillonite	Chlorite-FeMg			Propylitic	
ESSPCD0006_239.00M.asd	20SPCD0006	239.00	242.00	FSPE.20001 ish-102-sm.	Siderite	0.405	Muscovite	0.385	NULL	NULL	NULL	86.216	Aspectral	1	NULL	NULL	500	2306.33	0.0918	24.754	2338.09	0.0398	2332.78	0.0358	92.656	0.192	0.284	0.966	0.99	0.977	2332.78	2338.09	2306.33	239.00	Siderite	Muscovite	NULL	Muscovite			Argillic	
ESSPCD0006_242.00M.asd	20SPCD0006	242.00	244.80	FSPE.20001 ish-102-sm.	Chlorite-FeMg	0.598	Muscovite	0.402	NULL	NULL	NULL	99.051	Aspectral	1	NULL	NULL	500	2307.48	0.0907	95.006	2316.75	0.0496	2363.08	0.0366	93.288	0.202	0.326	0.962	0.989	0.972	2363.08	2316.75	2307.48	242.00	Chlorite-FeMg	Muscovite	NULL	Muscovite			Argillic	
ESSPCD0006_244.80M.asd	20SPCD0006	244.80	248.00	FSPE.20001 ish-102-sm.	Wood	1	NULL	NULL	NULL	NULL	119.08	Aspectral	1	NULL	NULL	NULL	NULL	NULL	NULL	NULL	NULL	2327.13	0.0116	99.508	0.037	NULL	NULL	0.999	0.989	1.004	2327.13	NULL	NULL	NULL	264.80	Wood	NULL	NULL	NULL			
ESSPCD0006_248.00M.asd	20SPCD0006	248.00	251.00	FSPE.20001 ish-102-sm.	Phengilbiotite	0.345	Montmorillonite	0.325	Ankerite	0.185	109.61	NULL	NULL	NULL	NULL	NULL	2312.1	0.189	33.203	NULL	NULL	2306.99	0.0812	99.996	0.167	1.116	0.903	0.969	0.943	2306.99	NULL	2312.1	248.00	Phengilbiotite	Montmorillonite	Ankerite	Phengilbiotite			Argillic	
ESSPCD0006_251.00M.asd	20SPCD0006	251.00	254.00	FSPE.20001 ish-102-sm.	Siderite	0.374	Muscovite	0.242	Chlorite-FeMg	0.242	70.756	Aspectral	1	NULL	NULL	NULL	500	2314.72	0.143	33.899	NULL	NULL	2307.57	0.0736	99.958	0.185	0.857	0.951	0.992	0.963	2307.57	NULL	2314.72	251.00	Siderite	Muscovite	Chlorite-FeMg	Montmorillonite			Argillic	
ESSPCD0006_254.00M.asd	20SPCD0006	254.00	257.00	FSPE.20001 ish-102-sm.	Siderite	0.291	Chlorite-FeMg	0.291	Muscovite	0.291	108.37	Aspectral	1	NULL	NULL	NULL	500	2314.23	0.0783	96.651	2249.82	0.0825	2309.13	0.0988	95.951	0.107	0.756	0.966	0.992	0.973	2309.13	2249.82	2314.23	254.00	Siderite	Montmorillonite	Chlorite-FeMg	Montmorillonite	Chlorite-FeMg		Argillic	
ESSPCD0006_257.00M.asd	20SPCD0006	257.00	259.00	FSPE.20001 ish-102-sm.	Phengite	0.345	Ankerite	0.275	Chlorite-FeMg	0.275	119.32	Aspectral	1	NULL	NULL	NULL	500	2314.6	0.12	34.426	2249.5	0.105	2302.25	0.117	97.579	0.138	0.902	0.96	0.991	0.969	2302.25	2249.5	2314.6	257.00	Phengite	Ankerite	Chlorite-FeMg	Chlorite-FeMg	Ankerite		Propylitic	
ESSPCD0006_260.00M.asd	20SPCD0006	259.00	260.00	FSPE.20001 ish-102-sm.	Dolomite	1.00	Phengite	0.295	Ankerite	0.188	85.895	Aspectral	1	NULL	NULL	NULL	500	2235.35	0.186	29.632	2242.1	0.0996	2301.42	0.0132	22.186	0.567	0.935	0.907

Sample	Hole ID	Depth_From	Depth_To	Index	Min1 cTotA	Min1 cTotA	Min2 cTotA	Min2 cTotA	Min3 cTotA	Min3 cTotA	Xmin cTotA	Xmin cTotA	Min1 cTotV	Min1 cTotV	Min2 cTotV	Min2 cTotV	Xmin cTotV	wn1000	hq1000	wn1000	wn2350	hq2350	wn2950	hq2950	wn3050	hq3050	Min1 cyc4	Min1 cyc4	Min2 cyc4	Min2 cyc4	Min Cryst	wn2050	wn2250	wn2000	Depth_Fro m	Min1 cTotA	Min1 cTotA1	Min1 cTotA1	Mineral 1	Mineral 2	Mineral 3	Alteration Assemblage	*Confidence?
20PCD0006_410.00M.asd	20PCD0006	410.00	411.00	FSPE.20001 wn.cls2 sec.	Chlorite-Mg	0.241	Montmori llonite	0.241	NULL	NULL	30.532	Aspectral	1	NULL	NULL	500	2253.86	0.09	36.33	2268.66	0.156	2307.76	0.135	39.506	0.14	0.705	0.962	0.971	2307.76	2268.66		2253.86	410.00	Chlorite-Mg	Montmorillonite	NULL	Chlorite-Mg			Propylitic	
20PCD0006_415.00M.asd	20PCD0006	415.00	416.00	FSPE.20001 wn.cls2 sec.	Muscovite050	0.098	Montmori llonite	0.322	Ankerite	0.259	60.600	Aspectral	1	NULL	NULL	500	2213.2	0.181	33.999	NULL	NULL	2306.62	0.138	38.794	0.138	0.98	0.988	0.99	0.969	2306.62	NULL		2213.2	415.00	Muscovite050	Montmorillonite	Ankerite	Muscovite050			Argillic	
20PCD0006_416.00M.asd	20PCD0006	416.00	419.70	FSPE.20001 wn.cls2 sec.	Muscovite050	0.092	Chlorite-Mg	0.242	Montmor illonite	0.292	122.87	Aspectral	1	NULL	NULL	500	2211.35	0.229	34.865	NULL	NULL	2308.52	0.132	40.925	0.268	0.856	0.896	0.979	0.955	2308.52	NULL		2211.35	416.00	Muscovite050	Chlorite-Mg	Montmorillonit e	Muscovite050			Argillic	
20PCD0006_419.70M.asd	20PCD0006	419.70	422.00	FSPE.20001 wn.cls2 sec.	Phengite	0.419	Gypsum	0.387	NULL	NULL	142.81	Aspectral	1	NULL	NULL	500	2217.49	0.105	30.336	NULL	NULL	2305.05	0.0172	31.529	0.236	0.429	0.963	0.986	0.976	2305.05	NULL		2217.49	419.70	Phengite	Gypsum	NULL	Phengite			Argillic	
20PCD0006_422.00M.asd	20PCD0006	422.00	426.45	FSPE.20001 wn.cls2 sec.	Chlorite-FeMg	0.815	Ankerite	0.185	NULL	NULL	254.29	Aspectral	1	NULL	NULL	500	NULL	NULL	NULL	2251.16	0.156	2309.62	0.136	37.022	0.188	NULL		0.979	0.997	0.982	2309.62	2251.16	NULL	422.00	Chlorite-FeMg	Ankerite	NULL	Chlorite-FeMg			Propylitic	
20PCD0006_426.45M.asd	20PCD0006	426.45	428.00	FSPE.20001 wn.cls2 sec.	Chlorite-Mg	0.438	Gypsum	0.4	Montmor illonite	0.261	89.776	NULL	NULL	NULL	NULL	500	2217.84	0.0725	29.663	2265.97	0.0585	2308.35	0.0439	42.35	0.241	0.921	0.97	0.987	0.982	2308.35	2265.97		2217.84	426.45	Chlorite-Mg	Gypsum	Montmorillonit e	Chlorite-Mg			Propylitic	
20PCD0006_428.00M.asd	20PCD0006	428.00	432.30	FSPE.20001 wn.cls2 sec.	Chlorite-FeMg	0.589	Siderite	0.321	Phengite	0.31	133.02	Aspectral	1	NULL	NULL	500	2216.35	0.0727	34.793	2268.99	0.0935	2310.81	0.0806	40.791	0.195	0.98	0.971	0.995	0.976	2310.81	2268.99		2216.35	428.00	Chlorite-FeMg	Siderite	Phengite	Chlorite-FeMg			Propylitic	
20PCD0006_432.30M.asd	20PCD0006	432.30	434.00	FSPE.20001 wn.cls2 sec.	Gypsum	0.418	Chlorite-FeMg	0.275	Montmor illonite	0.275	97.996	Aspectral	1	NULL	NULL	500	2216.16	0.0797	30.865	2262.51	0.015	2308.86	0.0176	30.006	0.252	0.324	0.961	0.985	0.976	2308.86	2262.51		2216.16	432.30	Gypsum	Chlorite-FeMg	Montmorillonit e	Gypsum			Gypsum	
20PCD0006_434.00M.asd	20PCD0006	434.00	437.00	FSPE.20001 wn.cls2 sec.	Phengite	0.398	Siderite	0.2	Chlorite-FeMg	0.272	116.37	Aspectral	1	NULL	NULL	500	2214.79	0.0952	35.921	2268.61	0.0999	2307.43	0.0992	36.05	0.196	0.952	0.965	0.97	2307.43	2268.61		2214.79	434.00	Phengite	Siderite	Chlorite-FeMg	Phengite			Argillic	
20PCD0006_437.00M.asd	20PCD0006	437.00	441.00	FSPE.20001 wn.cls2 sec.	Gypsum	0.602	Chlorite-FeMg	0.179	Phengite	0.169	84.353	Aspectral	1	NULL	NULL	500	2217.1	0.088	29.9	2253.61	0.106	2301.87	0.0836	33.731	0.221	0.97	0.952	0.978	2301.87	2253.61		2217.1	437.00	Gypsum	Phengite	Chlorite-FeMg	Gypsum			Propylitic	
20PCD0006_441.00M.asd	20PCD0006	441.00	443.00	FSPE.20001 wn.cls2 sec.	Phengite	0.736	Siderite	0.256	NULL	NULL	83.256	Aspectral	1	NULL	NULL	500	2212.32	0.127	33.686	NULL	NULL	2308.8	0.0539	36.22	0.136	1.01	0.952	0.99	0.962	2308.8	NULL		2212.32	441.00	Phengite	Siderite	NULL	Phengite			Argillic	
20PCD0006_443.00M.asd	20PCD0006	443.00	446.00	FSPE.20001 wn.cls2 sec.	Gypsum	0.42	Chlorite-FeMg	0.197	Montmor illonite	0.197	111.33	Aspectral	1	NULL	NULL	500	2215.75	0.203	28.871	2252.99	0.127	2305.66	0.0239	29.129	0.423	0.328	0.899	0.952	0.966	2305.66	2252.99		2215.75	443.00	Gypsum	Chlorite-FeMg	Montmorillonit e	Gypsum			Gypsum	
20PCD0006_446.00M.asd	20PCD0006	446.00	448.00	FSPE.20001 wn.cls2 sec.	Gypsum	0.42	Chlorite-FeMg	0.353	NULL	NULL	59.975	Aspectral	1	NULL	NULL	500	2216.39	0.103	25.599	2251.51	0.0962	2308.78	0.0137	18.714	0.636	0.212	0.923	0.955	0.966	2308.78	2251.51		2216.39	446.00	Gypsum	Chlorite-FeMg	NULL	Gypsum			Gypsum	
20PCD0007_239.15M.asd	20PCD0007	239.15	242.18	FSPE.20001 wn.cls2 sec.	Muscovite050	0.092	Montmor illonite	0.265	Ankerite	0.243	109.7	NULL	NULL	NULL	NULL	NULL	2308.76	0.116	34.595	NULL	NULL	2305.91	0.0523	36.958	0.156	0.737	0.95	0.991	0.959	2305.91	NULL		2308.76	239.15	Muscovite050	Montmorillonite	Ankerite	Muscovite050			Argillic	
20PCD0007_242.18M.asd	20PCD0007	242.18	243.18	FSPE.20001 wn.cls2 sec.	Chlorite-FeMg	0.643	Muscovit e	0.189	NULL	NULL	162.96	Aspectral	1	NULL	NULL	500	2210.4	0.0686	36.853	2251.69	0.0895	2309.29	0.0897	35.43	0.107	0.661	0.967	0.995	0.972	2309.29	2251.69		2210.4	242.18	Chlorite-FeMg	Muscovite	NULL	Chlorite-FeMg			Propylitic	
20PCD0007_243.18M.asd	20PCD0007	243.18	250.18	FSPE.20001 wn.cls2 sec.	Chlorite-FeMg	0.653	Phengite	0.347	NULL	NULL	168.75	Aspectral	1	NULL	NULL	500	2212.89	0.123	37.532	2252.54	0.172	2301.38	0.182	39.655	0.166	0.705	0.953	0.996	0.957	2301.38	2252.54		2212.89	243.18	Chlorite-FeMg	Phengite	NULL	Chlorite-FeMg			Propylitic	
20PCD0007_248.18M.asd	20PCD0007	248.18	251.18	FSPE.20001 wn.cls2 sec.	Montmorillon ite	0.598	Muscovit e	0.329	Ankerite	0.073	86.056	Aspectral	1	NULL	NULL	500	2210.12	0.111	34.625	2306.34	0.0686	2309.76	0.0782	35.222	0.179	0.622	0.953	0.993	0.961	2309.76	2306.34		2210.12	248.18	Montmorillonite	Muscovite	Ankerite	Montmorillonite			Argillic	
20PCD0007_251.18M.asd	20PCD0007	251.18	254.18	FSPE.20001 wn.cls2 sec.	Chlorite-FeMg	0.74	Muscovit e	0.26	NULL	NULL	97.456	Aspectral	1	NULL	NULL	500	2209.42	0.168	32.702	2307.31	0.109	2302.71	0.136	37.906	0.216	0.758	0.902	0.985	0.956	2302.71	2307.31		2209.42	251.18	Chlorite-FeMg	Muscovite	NULL	Montmorillonit e			Propylitic	
20PCD0007_254.18M.asd	20PCD0007	254.18	257.18	FSPE.20001 wn.cls2 sec.	Muscovite050	0.092	Chlorite-FeMg	0.287	Montmor illonite	0.287	68.79	NULL	NULL	NULL	NULL	NULL	2307.11	0.193	34.143	NULL	NULL	2310	0.0856	37.577	0.166	0.812	0.96	0.985	0.965	2310	NULL		2307.11	254.18	Muscovite050	Chlorite-FeMg	Montmorillonit e	Muscovite050			Argillic	
20PCD0007_257.18M.asd	20PCD0007	257.18	260.18	FSPE.20001 wn.cls2 sec.	Chlorite-FeMg	0.74	Muscovit e	0.241	NULL	NULL	128.08	Aspectral	1	NULL	NULL	500	2304.39	0.0961	35.115	2252.7	0.114	2301.79	0.118	36.829	0.136	0.697	0.95	0.991	0.959	2301.79	2252.7		2304.39	257.18	Chlorite-FeMg	Muscovite	NULL	Chlorite-FeMg			Propylitic	
20PCD0007_260.18M.asd	20PCD0007	260.18	265.18	FSPE.20001 wn.cls2 sec.	Chlorite-FeMg	0.699	Muscovit e	0.301	NULL	NULL	111.86	Aspectral	1	NULL	NULL	500	2309.59	0.114	36.457	2251.77	0.131	2303.17	0.116	38.191	0.192	0.596	0.951	0.994	0.957	2303.17	2251.77		2309.59	260.18	Chlorite-FeMg	Muscovite	NULL	Chlorite-FeMg			Propylitic	
20PCD0030.asd				FSPE.20001 wn.cls2 sec.	Dickite	0.441	Kaolinite -WX	0.389	NULL	NULL	80.535	Ganthrite	1	NULL	NULL	500	2307.08	0.408	29.795	2257.11	0.0171	2354.62	0.0278	39.598	0.148	2.751	0.678	0.742	0.953	2354.62	2257.11		2307.08		Dickite	Kaolinite-WX	NULL	Dickite			Advanced Argillic	
20PCD0031.asd				FSPE.20001 wn.cls2 sec.	Dickite	1	NULL	NULL	NULL	NULL	82.766	Ganthrite	1	NULL	NULL	597.63	2306.49	0.456	31.081	2257.97	0.0436	2302.58	0.138	30.638	0.13	3.926	0.598	0.737	0.868	2302.58	2257.97		2306.49		Dickite	NULL	NULL	Dickite			Advanced Argillic	
20PCD0032.asd				FSPE.20001 wn.cls2 sec.	Muscovite	1	NULL	NULL	NULL	NULL	20.309	Aspectral	1	NULL	NULL	500	2306.93	0.062	26.695	NULL	NULL	2307.31	0.00758	31.957	0.138	0.266	0.985	0.996	0.987	2307.31	NULL		2306.93		Muscovite	NULL	NULL	Muscovite			Argillic	
20PCD0033.asd				FSPE.20001 wn.cls2 sec.	Muscovite	0.398	Siderite	0.359	Montmor illonite	0.243	20.078	Ganthrite	1	NULL	NULL	165.33	2306.35	0.128	30.579	NULL	NULL	2301.4	0.0376	34.75	0.199	0.321	0.968	0.997	0.973	2301.4	NULL		2306.35		Muscovite	Siderite	Montmorillonit e	Muscovite			Argillic	
20PCD0034.asd				FSPE.20001 wn.cls2 sec.	Muscovite	0.592	Montmor illonite	0.208	Magnesit e	0.201	17.285	Ganthrite	1	NULL	NULL	372.75	2306.47	0.116	31.76	NULL	NULL	2303.51	0.0369	36.66	0.185	0.322	0.999	0.997	0.961	2303.51	NULL		2306.47		Muscovite	Montmorillonite	Magnesite	Muscovite			Argillic	
20PCD0037.asd				FSPE.20001 wn.cls2 sec.	Muscovite	0.308	Magnesit e	0.162	NULL	NULL	30.133	Ganthrite	1	NULL	NULL	85.363	2302.09	0.14	33.157	NULL	NULL	2302.89	0.0356	34.484	0.216	0.511	0.967	0.991	0.956	2302.89	NULL		2302.09		Muscovite	Magnesite	NULL	Muscovite			Argillic	
20PCD0038.asd				FSPE.20001 wn.cls2 sec.	Muscovite	0.441	Montmor illonite	0.325	Dickite	0.177	21.813	Ganthrite	1	NULL	NULL	69.976	2306.57	0.152	35.702	NULL	NULL	2308.29	0.0131	33.975	0.191	0.332	0.996	0.998	0.968	2308.29	NULL		2306.57		Muscovite	Montmorillonite	Dickite	Muscovite			Argillic	
20PCD0039.asd				FSPE.20001 wn.cls2 sec.	Dickite	0.736	Kaolinite -WX	0.264	NULL	NULL	77.437	Ganthrite	1	NULL	NULL	115.61	2306.91	0.186	29.922	2258.86	0.0318	2301.31	0.0735	36.25	0.136	2.636	0.695	0.77	0.899	2301.31	2258.86		2306.91		Dickite	Kaolinite-WX	NULL	Dickite			Advanced Argillic	
20PCD0040.asd				FSPE.20001 wn.cls2 sec.	Alunite-K	0.537	Dickite	0.463	NULL	NULL	62.15	NULL	NULL	NULL	NULL	NULL	NULL	NULL	NULL	2251.16	NULL	2305.22	0.0737	33.213	0.0282	NULL		0.797	0.823	0.959	2305.22	NULL	NULL			Alunite-K	Dickite	NULL	Alunite-K			Advanced Argillic	
20PCD0041.asd				FSPE.20001 wn.cls2 sec.	Dickite	1	NULL	NULL	NULL	NULL	100.87	Ganthrite	1	NULL	NULL	97.488	2306.88	0.359	28.791	2256.83	0.0193	2354.16	0.0677	37.503	0.131	0.111	0.716	0.797	0.899	2354.16	2256.83		2306.88		Dickite	NULL	NULL	Dickite			Advanced Argillic	
20PCD0042.asd				FSPE.20001 wn.cls2 sec.	Chlorite-Fe	0.826	Ankerite	0.174	NULL	NULL	61.389	NULL	NULL	NULL	NULL	NULL	NULL	NULL	NULL	2254.59	0.0928	2302.23	0.0956	36.867	0.198	NULL		0.997	1	0.997	2302.23	2254.59	NULL			Chlorite-Fe	Ankerite	NULL	Chlorite-Fe			Propylitic	
20PCD0043.asd				FSPE.20001 wn.cls2 sec.	Chlorite-FeMg	0.714	Muscovit e	0.286	Magnesit e	0.199	36.982	NULL	NULL	NULL	NULL	NULL	2226.38	0.0276	38.918	2251.18	0.091	2328.67	0.126	49.807	0.377	0.0732	0.996	1	0.956	2328.67	2251.18		2226.38		Chlorite-FeMg	Muscovite	Magnesite	Chlorite-FeMg			Propylitic	
20PCD0044.asd				FSPE.20001 wn.cls2 sec.	Muscovite	0.669	Siderite	0.357	NULL	NULL	22.367	NULL	NULL	NULL	NULL	NULL	2208.5	0.093	31.65	2265	0.0286	2309.65	0.0362	39.718	0.248	0.376	0.965	0.996	0.969	2309.65	2265		2208.5		Muscovite	Siderite	NULL	Muscovite			Argillic	
20PCD0045.asd				FSPE.20001 wn.cls2 sec.	Muscovite	0.429	Siderite	0.332	Montmor illonite	0.239	17.652	Ganthrite	1	NULL	NULL	864.75	2309.48	0.116	32.592	NULL	NULL	2305.3	0.0379	39.719	0.368	0.115	0.965	0.998	0.962	2305.3	NULL		2309.48		Muscovite	Siderite	Montmorillonit e	Muscovite			Argillic	
20PCD0046.asd				FSPE.20001 wn.cls2 sec.	Muscovite050	0.092	Montmor illonite	0.185	Magnesit e	0.185	30.161	Ganthrite	1	NULL	NULL	902.42	2309.58	0.156	32.35	NULL	NULL	2302.66	0.0369	34.502	0.366	0.02	0.999	0.999	0.951	2302.66	NULL		2309.58		Muscovite050	Montmorillonite	Magnesite	Muscovite050			Argillic	
20PCD0047.asd				FSPE.20001 wn.cls2 sec.	Siderite	0.741	Montmor illonite	0.259	NULL	NULL	56.236	NULL	NULL	NULL	NULL	NULL	2206.36	0.0609	29.842	2253.06	0.0535	2303.96	0.0346	43.004	0.101	0.632	0.995	0.957	0.955	2303.96	2253.06		2206.36		Siderite	Montmorillonite	NULL	Siderite			Propylitic	
20PCD0048.asd				FSPE.20001 wn.cls2 sec.	Aspectral	1	NULL	NULL	NULL	NULL	109.09	NULL	NULL	NULL	NULL	NULL	2206.46	0.0259	23.596	2251.26	0.0115	2308.12	0.00586	25.099	0.22	0.118	0.999	0.999	0.956	2308.12	2251.26		2206.46		Aspectral	NULL	NULL	Aspectral			NULL	
20PCD0049.asd				FSPE.20001 wn.cls2 sec.	Aspectral	1	NULL	NULL	NULL	NULL	116.69	NULL	NULL	NULL	NULL	NULL	2200.89	0.0382	30.906	NULL	NULL	2306.55	0.000661	27.129	0.231	0.103	0.979	0.995	0.983	2306.55	NULL		2200.89		Aspectral	NULL	NULL	Aspectral			NULL	
20PCD0050.asd				FSPE.20001 wn.cls2 sec.	NULL	NULL	NULL	NULL	NULL	NULL	NULL	Aspectral	1	NULL	NULL	500	2306.07	0.0853	26.084	NULL	NULL	2300.86	0.00231	37.498	0.138	0.266	0.985	0.995	0.99	2300.86	NULL		2306.07		NULL	NULL	NULL	NULL			NULL	

| Sample_ TSG | Index_TS G | Min1_sTS AS_TSG | Wt1_sTS AS_TSG | Min2_sTS AS_TSG | Wt2_sTS AS_TSG | Error_sTS AS_TSG | kaol_xtal _TSG | k2161_m ean_TSG | k2181_m ean_TSG | w2200_T SG | w2250_T SG | w2350_T SG | width 2200_TS G | width_23 50_TSG | Crystallini ty_Index _2200_TS m | Muscovit e_TSG | Chlorite 2_TSG | Alunite _TSG | White_M ica_NoMi x | Kaolinite _NoMix | Chlorite_ NoMix | Mineral 1_TSG | Mineral 2_TSG | Mineral 3_TSG | Temp C | pH | Mineral Group | Alteration Assemblage | Commen ts | | Sample | SampleID | Date | BestLatit ude | BestLongi tude | BestElevа tion | UTM_Eas t | UTM_No rth | MineralN ame1 | StarRatin g1 | MineralN ame2 | StarRatin g2 | MineralN ame3 | StarRatin g3 | MineralN ame4 | StarRatin g4 | MineralN ame5 | StarRatin g5 | MineralN ame6 | StarRatin g6 | MineralN ame7 | StarRatin g7 | AlFeMg | AlOH | CSM | Fe3i | Fe3t | FeOH | ISM | Kx | MgOH | sampler | type | add_not es |
|---|---|---

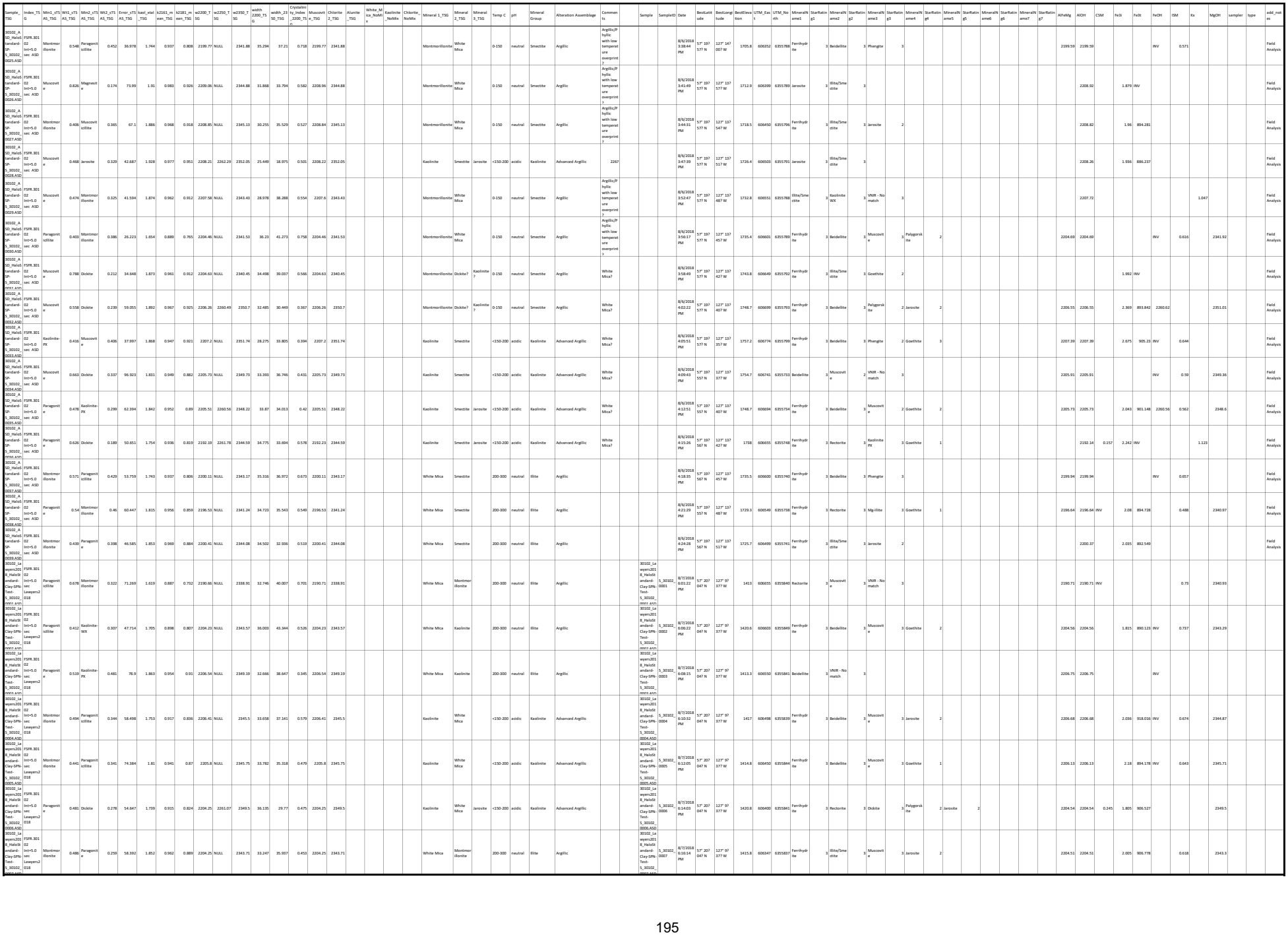

| Sample_TSG | Index_TSG | Min1_sTSA5_TSG | Wt1_sTSA5_TSG | Min2_sTSA5_TSG | Wt2_sTSA5_TSG | Error_sTSA5_TSG | kaol_xtal_TSG | k2161_mean_TSG | k2181_mean_TSG | w2200_TSG | w2250_TSG | w2350_TSG | width_2200_TSG | width_2350_TSG | Crystallinity_Index_2200_TSG | Muscovite_TSG | Chlorite_2_TSG | Alunite_TSG | White_Mica_NoMix | Kaolinite_NoMix | Chlorite_NoMix | Mineral 1_TSG | Mineral 2_TSG | Mineral 3_TSG | Temp C | pH | Mineral Group | Alteration Assemblage | Comments | | Sample | SampleID | Date | BestLatitude | BestLongitude | BestElevation | UTM_East | UTM_North | MineralName1 | StarRating1 | MineralName2 | StarRating2 | MineralName3 | StarRating3 | MineralName4 | StarRating4 | MineralName5 | StarRating5 | MineralName6 | StarRating6 | MineralName7 | StarRating7 | AlFeMg | AlOH | CSM | Fe3i | Fe3t | FeOH | ISM | Kx | MgOH | sampler | type | add_notes |
|---|---|---

| Sample_TSG | Index_TSG | Min1_sTSAS_TSG | Wl1_sTSAS_TSG | Min2_sTSAS_TSG | Wl2_sTSAS_TSG | Error_sTSAS_TSG | kaol_xtal_TSG | k2161_mean_TSG | k2181_mean_TSG | w2200_TSG | w2250_TSG | w2350_TSG | width_2200_TSG | width_2350_TSG | Crystallinity_Index_2200_TSG | Muscovite_TSG | Chlorite_2_TSG | Alunite_TSG | White_Mica_NoMix | Kaolinite_NoMix | Chlorite_NoMix | Mineral 1_TSG | Mineral 2_TSG | Mineral 3_TSG | Temp C | pH | Mineral Group | Alteration Assemblage | Comments | | Sample | SampleID | Date | BestLatitude | BestLongitude | BestElevation | UTM_East | UTM_North | MineralName1 | StarRating1 | MineralName2 | StarRating2 | MineralName3 | StarRating3 | MineralName4 | StarRating4 | MineralName5 | StarRating5 | MineralName6 | StarRating6 | MineralName7 | StarRating7 | AlFeMg | AlOH | CSM | Fe3i | Fe3t | FeOH | ISM | Kx | MgOH | sampler | type | add_notes |
|---|---|---

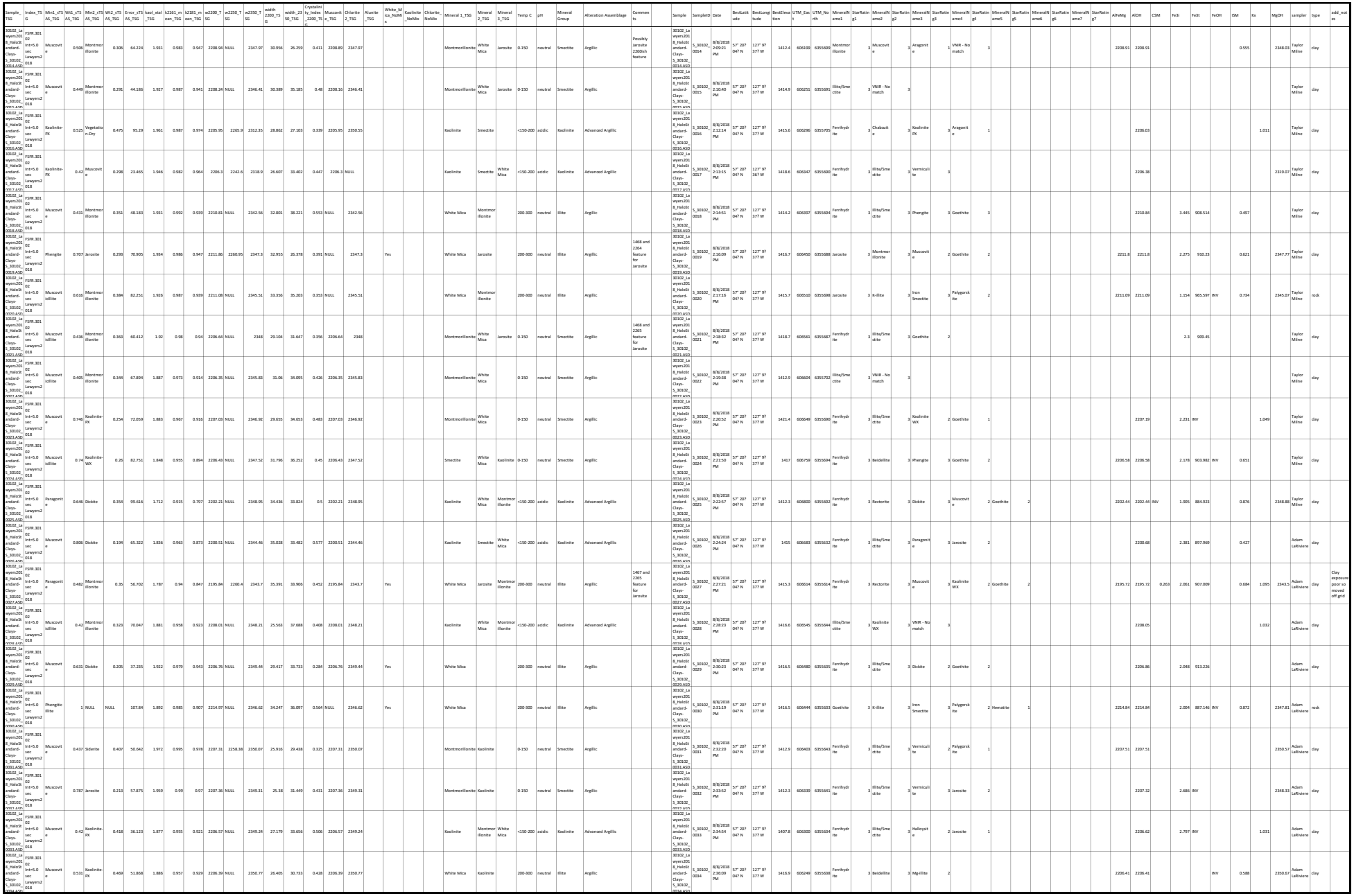

| Sample_TSG | Index_TSG | Min1_sTSAS_TSG | Wt1_sTSAS_TSG | Min2_sTSAS_TSG | Wt2_sTSAS_TSG | Error_sTSAS_TSG | kaol_xtal_TSG | k2161_mean_TSG | k2181_mean_TSG | w2200_TSG | w2250_TSG | w2350_TSG | width_2200_TSG | width_2350_TSG | Crystallinity_Index_2200_TSG | Muscovite_TSG | Chlorite_2_TSG | Alunite_TSG | White_Mica_NoMix | Kaolinite_NoMix | Chlorite_NoMix | Mineral 1_TSG | Mineral 2_TSG | Mineral 3_TSG | Temp C | pH | Mineral Group | Alteration Assemblage | Comments | Sample | SampleID | Date | BestLatitude | BestLongitude | BestElevation | UTM_East | UTM_North | MineralName1 | StarRating1 | MineralName2 | StarRating2 | MineralName3 | StarRating3 | MineralName4 | StarRating4 | MineralName5 | StarRating5 | MineralName6 | StarRating6 | MineralName7 | StarRating7 | AlFeMg | AlOH | CSM | Fe3t | Fe3t | FeOH | ISM | Kx | MgOH | sampler | type | add_notes |
|---|---|---

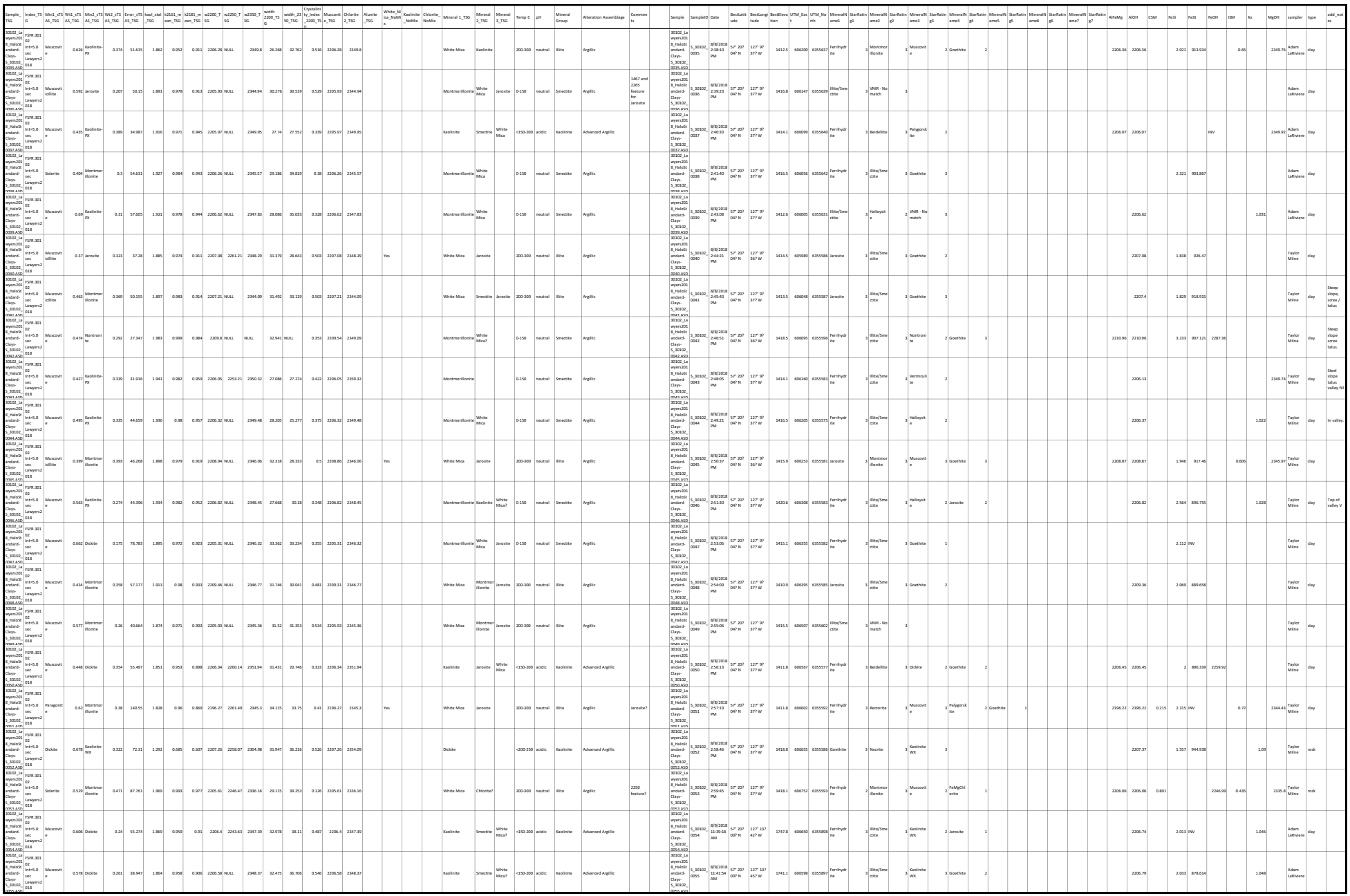

Sample_TSG	Index_TSG	Min1_sTSG	Wt1_sTSG	Min2_sTSG	Wt2_sTSG	Error_sTSG	kaol_xtal_TSG	k2161_mean_TSG	k2181_mean_TSG	w2200_TSG	w2250_TSG	w2350_TSG	width_2200_TSG	width_2350_TSG	Crystallinity_Index_2200_TSG	Muscovite_TSG	Chlorite_2_TSG	Alunite_TSG	White_Mica_NoMix	Kaolinite_NoMix	Chlorite_NoMix	Mineral 1_TSG	Mineral 2_TSG	Mineral 3_TSG	Temp C	pH	Mineral Group	Alteration Assemblage	Comments
30102_Lawyers2018_Halos9andard-Clays-S_30102_0035.ASD	FSFR.30102sct1=5.0 secLawyers2018	Muscovite	0.626	Kaolinite-PX	0.374	51.615	1.862	0.952	0.911	2206.28	NULL	2349.8	26.268	32.762	0.516	2206.28	2349.8					White Mica	Kaolinite		200-300	neutral	Illite	Argillic	
30102_Lawyers2018_Halos9andard-Clays-S_30102_0036.ASD	FSFR.30102sct1=5.0 secLawyers2018	Muscovite	0.592	Jarosite	0.207	50.15	1.891	0.978	0.913	2205.93	NULL	2344.94	30.276	30.519	0.529	2205.93	2344.94					Montmorillonite	White Mica	Jarosite	0-150	neutral	Smectite	Argillic	1467 and 2265 feature for Jarosite
30102_Lawyers2018_Halos9andard-Clays-S_30102_0037.ASD	FSFR.30102sct1=5.0 secLawyers2018	Muscovite	0.435	Kaolinite-PX	0.389	34.987	1.916	0.971	0.945	2205.97	NULL	2349.95	27.74	27.552	0.339	2205.97	2349.95					Kaolinite	Smectite	White Mica	<150-200	acidic	Kaolinite	Advanced Argillic	
30102_Lawyers2018_Halos9andard-Clays-S_30102_0038.ASD	FSFR.30102sct1=5.0 secLawyers2018	Siderite	0.404	Montmorillonite	0.3	54.631	1.927	0.984	0.943	2206.26	NULL	2345.57	29.186	34.819	0.38	2206.26	2345.57					Montmorillonite	White Mica		0-150	neutral	Smectite	Argillic	
30102_Lawyers2018_Halos9andard-Clays-S_30102_0039.ASD	FSFR.30102sct1=5.0 secLawyers2018	Muscovite	0.69	Kaolinite-PX	0.31	57.605	1.921	0.978	0.944	2206.62	NULL	2347.83	28.086	35.033	0.328	2206.62	2347.83					Montmorillonite	White Mica		0-150	neutral	Smectite	Argillic	
30102_Lawyers2018_Halos9andard-Clays-S_30102_0040.ASD	FSFR.30102sct1=5.0 secLawyers2018	Muscovite	0.37	Jarosite	0.323	37.28	1.885	0.974	0.911	2207.08	2261.21	2348.29	31.379	28.643	0.503	2207.08	2348.29		Yes			White Mica	Jarosite		200-300	neutral	Illite	Argillic	
30102_Lawyers2018_Halos9andard-Clays-S_30102_0041.ASD	FSFR.30102sct1=5.0 secLawyers2018	Muscovite	0.463	Montmorillonite	0.369	50.155	1.897	0.983	0.914	2207.21	NULL	2344.09	31.492	33.119	0.503	2207.21	2344.09					White Mica	Smectite	Jarosite	200-300	neutral	Illite	Argillic	
30102_Lawyers2018_Halos9andard-Clays-S_30102_0042.ASD	FSFR.30102sct1=5.0 secLawyers2018	Muscovite	0.474	Nontronite	0.292	27.347	1.983	0.999	0.984	2209.8	NULL	NULL	32.941	NULL	0.353	2209.54	2349.09					Montmorillonite	White Mica?		0-150	neutral	Smectite	Argillic	
30102_Lawyers2018_Halos9andard-Clays-S_30102_0043.ASD	FSFR.30102sct1=5.0 secLawyers2018	Muscovite	0.427	Kaolinite-PX	0.339	31.916	1.941	0.982	0.959	2206.05	2253.21	2350.32	27.086	27.274	0.422	2206.05	2350.32					Montmorillonite			0-150	neutral	Smectite	Argillic	
30102_Lawyers2018_Halos9andard-Clays-S_30102_0044.ASD	FSFR.30102sct1=5.0 secLawyers2018	Muscovite	0.495	Kaolinite-PX	0.335	44.659	1.936	0.98	0.957	2206.32	NULL	2349.48	28.205	25.277	0.375	2206.32	2349.48					Montmorillonite	White Mica		0-150	neutral	Smectite	Argillic	
30102_Lawyers2018_Halos9andard-Clays-S_30102_0045.ASD	FSFR.30102sct1=5.0 secLawyers2018	Muscovite	0.399	Montmorillonite	0.393	46.268	1.898	0.979	0.919	2208.94	NULL	2346.06	32.318	28.333	0.5	2208.86	2346.06		Yes			White Mica	Jarosite		200-300	neutral	Illite	Argillic	
30102_Lawyers2018_Halos9andard-Clays-S_30102_0046.ASD	FSFR.30102sct1=5.0 secLawyers2018	Muscovite	0.563	Kaolinite-PX	0.274	44.396	1.934	0.982	0.952	2206.82	NULL	2348.45	27.668	30.18	0.348	2206.82	2348.45					Montmorillonite	Kaolinite	White Mica?	0-150	neutral	Smectite	Argillic	
30102_Lawyers2018_Halos9andard-Clays-S_30102_0047.ASD	FSFR.30102sct1=5.0 secLawyers2018	Muscovite	0.662	Dickite	0.175	78.783	1.895	0.972	0.923	2205.31	NULL	2346.32	33.362	33.234	0.355	2205.31	2346.32					Montmorillonite	White Mica	Jarosite	0-150	neutral	Smectite	Argillic	
30102_Lawyers2018_Halos9andard-Clays-S_30102_0048.ASD	FSFR.30102sct1=5.0 secLawyers2018	Muscovite	0.434	Montmorillonite	0.358	57.177	1.913	0.98	0.933	2209.46	NULL	2346.77	31.746	30.041	0.481	2209.31	2346.77					White Mica	Montmorillonite	Jarosite	200-300	neutral	Illite	Argillic	
30102_Lawyers2018_Halos9andard-Clays-S_30102_0049.ASD	FSFR.30102sct1=5.0 secLawyers2018	Muscovite	0.577	Montmorillonite	0.26	40.664	1.874	0.971	0.903	2205.93	NULL	2345.36	31.52	31.353	0.534	2205.93	2345.36					White Mica	Montmorillonite	Jarosite	200-300	neutral	Illite	Argillic	
30102_Lawyers2018_Halos9andard-Clays-S_30102_0050.ASD	FSFR.30102sct1=5.0 secLawyers2018	Muscovite	0.448	Dickite	0.354	55.497	1.851	0.953	0.898	2206.34	2260.14	2351.94	31.431	20.746	0.323	2206.34	2351.94					Kaolinite	Jarosite	White Mica	<150-200	acidic	Kaolinite	Advanced Argillic	
30102_Lawyers2018_Halos9andard-Clays-S_30102_0051.ASD	FSFR.30102sct1=5.0 secLawyers2018	Paragonite	0.62	Montmorillonite	0.38	140.55	1.828	0.96	0.869	2196.27	2261.49	2345.3	34.115	33.75	0.41	2196.27	2345.3		Yes			White Mica	Jarosite		200-300	neutral	Illite	Argillic	Jarosite?
30102_Lawyers2018_Halos9andard-Clays-S_30102_0052.ASD	FSFR.30102sct1=5.0 secLawyers2018	Dickite	0.678	Kaolinite-WX	0.322	72.31	1.292	0.685	0.607	2207.26	2258.07	2304.98	31.947	36.216	0.526	2207.26	2354.09					Dickite			<200-250	acidic	Kaolinite	Advanced Argillic	
30102_Lawyers2018_Halos9andard-Clays-S_30102_0053.ASD	FSFR.30102sct1=5.0 secLawyers2018	Siderite	0.529	Montmorillonite	0.471	87.761	1.969	0.993	0.977	2205.61	2246.47	2336.16	29.115	39.253	0.126	2205.61	2336.16					White Mica	Chlorite?		200-300	neutral	Illite	Argillic	2250 feature?
30102_Lawyers2018_Halos9andard-Clays-S_30102_0054.ASD	FSFR.30102sct1=5.0 secLawyers2018	Muscovite	0.606	Dickite	0.24	55.274	1.869	0.959	0.91	2206.4	2243.63	2347.39	32.978	38.11	0.487	2206.4	2347.39					Kaolinite	Smectite	White Mica?	<150-200	acidic	Kaolinite	Advanced Argillic	
30102_Lawyers2018_Halos9andard-Clays-S_30102_0055.ASD	FSFR.30102sct1=5.0 secLawyers2018	Muscovite	0.578	Dickite	0.261	38.947	1.864	0.958	0.906	2206.58	NULL	2348.37	32.475	36.706	0.546	2206.58	2348.37					Kaolinite	Smectite	White Mica?	<150-200	acidic	Kaolinite	Advanced Argillic	

Sample	SampleID	Date	BestLatitude	BestLongitude	BestElevation	UTM_East	UTM_North	MineralName1	StarRating1	MineralName2	StarRating2	MineralName3	StarRating3	MineralName4	StarRating4	MineralName5	StarRating5	MineralName6	StarRating6	MineralName7	StarRating7	AlPerMg	AlOH	CSM	FeSi	FeSt	FeOH	ISM	Kx	MgOH	sampler	type	add_notes
30102_Lawyers2018_Halos9andard-Clays-S_30102_0035.ASD	S_30102_0035	8/8/2018 2:38:10 PM	57° 20' 047 N	127° 97' 377 W	1412.5	606200	6355637	Ferrihydrite	3	Montmorillonite	3	Muscovite	2	Goethite	2							2206.36	2206.36		2.021	913.934			0.65		2349.76	Adam LaFlamme	clay	
30102_Lawyers2018_Halos9andard-Clays-S_30102_0036.ASD	S_30102_0036	8/8/2018 2:39:23 PM	57° 20' 047 N	127° 97' 377 W	1416.8	606147	6355639	Illite/Smectite	3	VNIR - No match	3																					Adam LaFlamme	clay	
30102_Lawyers2018_Halos9andard-Clays-S_30102_0037.ASD	S_30102_0037	8/8/2018 2:40:33 PM	57° 20' 047 N	127° 97' 377 W	1414.1	606099	6355640	Ferrihydrite	3	Beidellite	3	Palygorskite	2									2206.07	2206.07				INV			2349.92	Adam LaFlamme	clay	
30102_Lawyers2018_Halos9andard-Clays-S_30102_0038.ASD	S_30102_0038	8/8/2018 2:41:40 PM	57° 20' 047 N	127° 97' 377 W	1416.5	606056	6355642	Ferrihydrite	3	Illite/Smectite	3	Goethite	3												2.321	903.867						Adam LaFlamme	clay	
30102_Lawyers2018_Halos9andard-Clays-S_30102_0039.ASD	S_30102_0039	8/8/2018 2:43:08 PM	57° 20' 047 N	127° 97' 377 W	1412.6	606005	6355631	Illite/Smectite	3	Halloysite	2	VNIR - No match	3									2206.62							1.031		Adam LaFlamme	clay	
30102_Lawyers2018_Halos9andard-Clays-S_30102_0040.ASD	S_30102_0040	8/8/2018 2:44:21 PM	57° 20' 047 N	127° 97' 367 W	1414.5	605989	6355586	Jarosite	3	Illite/Smectite	3	Goethite	2									2207.08			1.838	926.47						Taylor Milne	clay	
30102_Lawyers2018_Halos9andard-Clays-S_30102_0041.ASD	S_30102_0041	8/8/2018 2:45:43 PM	57° 20' 047 N	127° 97' 377 W	1413.5	606048	6355587	Jarosite	3	Illite/Smectite	3	Goethite	3									2207.4			1.829	918.915						Taylor Milne	clay	Steep slope, scree / talus.
30102_Lawyers2018_Halos9andard-Clays-S_30102_0042.ASD	S_30102_0042	8/8/2018 2:46:51 PM	57° 20' 047 N	127° 97' 367 W	1418.5	606095	6355596	Ferrihydrite	3	Illite/Smectite	3	Nontronite	2	Goethite	3							2210.96	2210.96		3.233	907.121	2287.36					Taylor Milne	clay	Steep slope scree talus.
30102_Lawyers2018_Halos9andard-Clays-S_30102_0043.ASD	S_30102_0043	8/8/2018 2:48:05 PM	57° 20' 047 N	127° 97' 377 W	1414.1	606160	6355583	Ferrihydrite	3	Illite/Smectite	3	Vermiculite	2									2206.13								2349.74	Taylor Milne	clay	Steel slope talus valley fill
30102_Lawyers2018_Halos9andard-Clays-S_30102_0044.ASD	S_30102_0044	8/8/2018 2:49:21 PM	57° 20' 047 N	127° 97' 377 W	1416.5	606205	6355575	Ferrihydrite	3	Illite/Smectite	3	Halloysite	2									2206.37							1.022		Taylor Milne	clay	In valley.
30102_Lawyers2018_Halos9andard-Clays-S_30102_0045.ASD	S_30102_0045	8/8/2018 2:50:37 PM	57° 20' 047 N	127° 97' 367 W	1415.9	606253	6355581	Jarosite	3	Montmorillonite	3	Muscovite	3	Goethite	3							2208.87	2208.87		1.946	917.46		0.606		2345.97	Taylor Milne	clay	
30102_Lawyers2018_Halos9andard-Clays-S_30102_0046.ASD	S_30102_0046	8/8/2018 2:51:10 PM	57° 20' 047 N	127° 97' 377 W	1420.6	606308	6355583	Ferrihydrite	3	Illite/Smectite	3	Halloysite	2	Jarosite	2							2206.82			2.564	896.755			1.028			Taylor Milne	clay	Top of valley V
30102_Lawyers2018_Halos9andard-Clays-S_30102_0047.ASD	S_30102_0047	8/8/2018 2:53:06 PM	57° 20' 047 N	127° 97' 377 W	1415.1	606355	6355582	Ferrihydrite	3	Illite/Smectite	3	Goethite	1												2.112	INV						Taylor Milne	clay	
30102_Lawyers2018_Halos9andard-Clays-S_30102_0048.ASD	S_30102_0048	8/8/2018 2:54:09 PM	57° 20' 047 N	127° 97' 377 W	1410.9	606395	6355585	Jarosite	3	Illite/Smectite	3	Goethite	2									2209.36			2.069	889.658						Taylor Milne	clay	
30102_Lawyers2018_Halos9andard-Clays-S_30102_0049.ASD	S_30102_0049	8/8/2018 2:55:06 PM	57° 20' 047 N	127° 97' 377 W	1415.5	606507	6355602	Illite/Smectite	3	VNIR - No match	3																					Taylor Milne	clay	
30102_Lawyers2018_Halos9andard-Clays-S_30102_0050.ASD	S_30102_0050	8/8/2018 2:56:13 PM	57° 20' 047 N	127° 97' 377 W	1411.8	606567	6355577	Ferrihydrite	3	Beidellite	3	Dickite	2	Goethite	2							2206.45	2206.45		2	896.339	2259.92					Taylor Milne	clay	
30102_Lawyers2018_Halos9andard-Clays-S_30102_0051.ASD	S_30102_0051	8/8/2018 2:57:19 PM	57° 20' 047 N	127° 97' 377 W	1411.8	606602	6355592	Ferrihydrite	3	Rectorite	3	Muscovite	3	Palygorskite	2	Goethite	1					2196.22	2196.22	0.215	2.315	INV		0.72		2344.43	Taylor Milne	clay	
30102_Lawyers2018_Halos9andard-Clays-S_30102_0052.ASD	S_30102_0052	8/8/2018 2:58:46 PM	57° 20' 047 N	127° 97' 377 W	1418.8	606655	6355586	Goethite	3	Nacrite	3	Kaolinite WX	3									2207.37			1.557	944.938			1.09			Taylor Milne	rock	
30102_Lawyers2018_Halos9andard-Clays-S_30102_0053.ASD	S_30102_0053	8/8/2018 2:59:45 PM	57° 20' 047 N	127° 97' 377 W	1418.1	606752	6355593	Ferrihydrite	2	Montmorillonite	3	Muscovite	2	FeMgChlorite	1							2206.06	2206.06	0.801			2246.99	0.435		2335.8	Taylor Milne	rock	
30102_Lawyers2018_Halos9andard-Clays-S_30102_0054.ASD	S_30102_0054	9/8/2018 11:39:18 AM	57° 20' 007 N	127° 13? 427 W	1747.8	606650	6355898	Ferrihydrite	3	Illite/Smectite	3	Kaolinite WX	2	Jarosite	1							2206.74			2.013	INV			1.046			Adam LaFlamme	clay	
30102_Lawyers2018_Halos9andard-Clays-S_30102_0055.ASD	S_30102_0055	9/8/2018 11:41:54 AM	57° 20' 007 N	127° 13? 457 W	1741.1	606598	6355897	Ferrihydrite	3	Illite/Smectite	3	Kaolinite WX	3	Goethite	2							2206.79			2.033	878.614			1.048			Adam LaFlamme	clay	

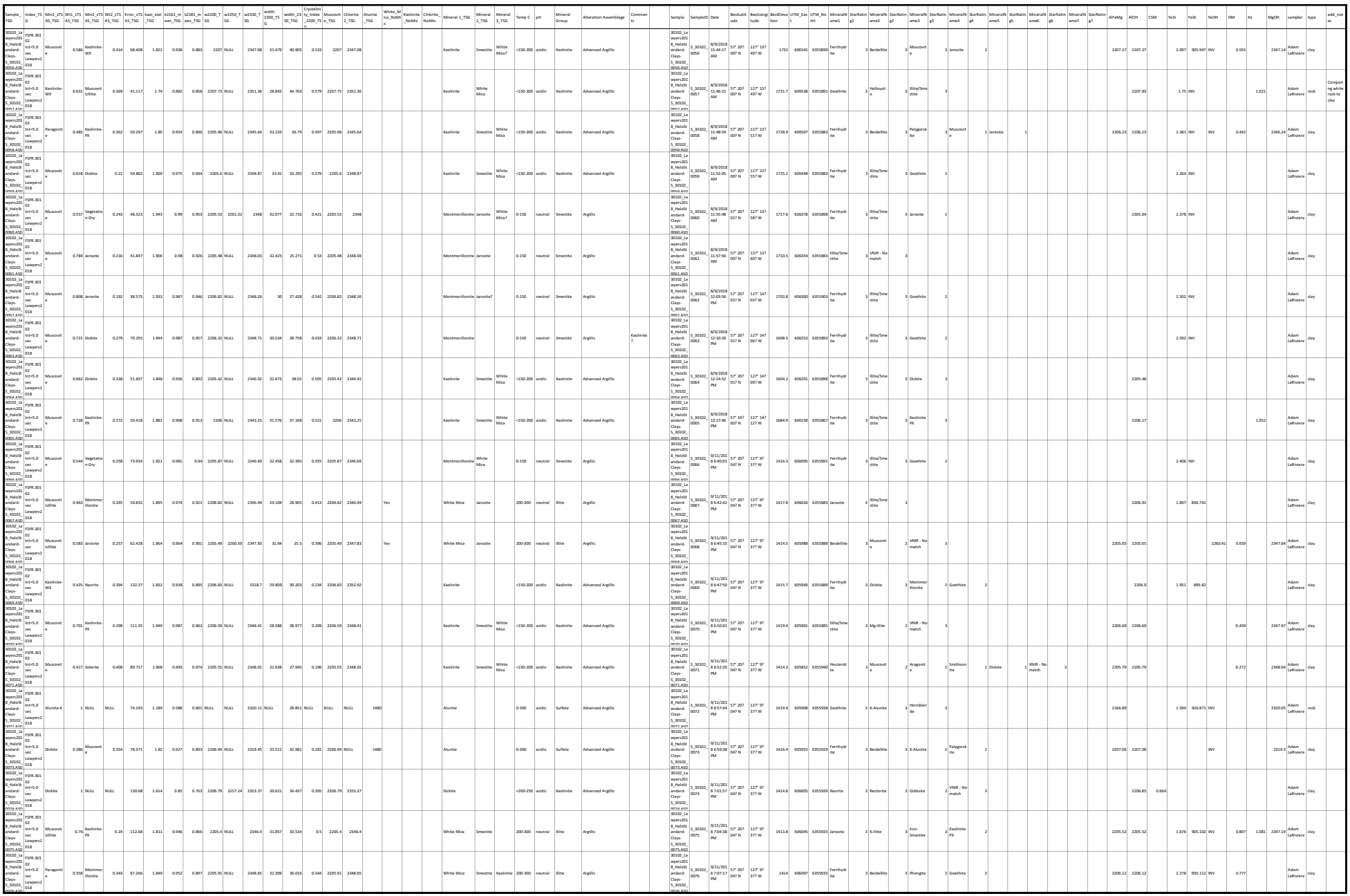

Sample_TSG	Index_TSG	Min1_sTSAS_TSG	Wt1_sTSAS_TSG	Min2_sTSAS_TSG	Wt2_sTSAS_TSG	Error_sTSAS_TSG	kaol_xtal_TSG	k2161_mean_TSG	k2181_mean_TSG	w2200_TSG	w2250_TSG	w2350_TSG	width_2200_TSG	width_2350_TSG	Crystallinity_Index_2200_TSG	Muscovite_TSG	Chlorite_2_TSG	Alunite_TSG	White_Mica_NoMix	Kaolinite_NoMix	Chlorite_NoMix	Mineral 1_TSG	Mineral 2_TSG	Mineral 3_TSG	Temp C	pH	Mineral Group	Alteration Assemblage	Comments
30102_Lawyers2018_Halos9andard-Clays-S_30102_0056.ASD	FSFR.30102 Int=5.0 sec Lawyers2018	Muscovite	0.586	Kaolinite-WX	0.414	68.408	1.822	0.938	0.883	2207	NULL	2347.08	31.479	40.905	0.533	2207	2347.08					Kaolinite	Smectite	White Mica?	<150-200	acidic	Kaolinite	Advanced Argillic	
30102_Lawyers2018_Halos9andard-Clays-S_30102_0057.ASD	FSFR.30102 Int=5.0 sec Lawyers2018	Kaolinite-WX	0.631	Muscovitcillite	0.369	41.117	1.74	0.882	0.858	2207.73	NULL	2351.36	28.842	44.763	0.579	2207.75	2351.36					Kaolinite	White Mica		<150-200	acidic	Kaolinite	Advanced Argillic	
30102_Lawyers2018_Halos9andard-Clays-S_30102_0058.ASD	FSFR.30102 Int=5.0 sec Lawyers2018	Paragonite	0.485	Kaolinite-PX	0.362	50.297	1.85	0.954	0.896	2205.96	NULL	2345.64	33.233	36.79	0.497	2205.96	2345.64					Kaolinite	Smectite	White Mica	<150-200	acidic	Kaolinite	Advanced Argillic	
30102_Lawyers2018_Halos9andard-Clays-S_30102_0059.ASD	FSFR.30102 Int=5.0 sec Lawyers2018	Muscovite	0.618	Dickite	0.21	59.802	1.909	0.975	0.934	2205.6	NULL	2348.87	33.41	33.295	0.379	2205.6	2348.87					Kaolinite	Smectite	White Mica	<150-200	acidic	Kaolinite	Advanced Argillic	
30102_Lawyers2018_Halos9andard-Clays-S_30102_0060.ASD	FSFR.30102 Int=5.0 sec Lawyers2018	Muscovite	0.557	Vegetation-Dry	0.243	48.323	1.943	0.99	0.953	2205.53	2261.32	2348	32.077	22.716	0.421	2205.53	2348					Montmorillonite	Jarosite	White Mica?	0-150	neutral	Smectite	Argillic	
30102_Lawyers2018_Halos9andard-Clays-S_30102_0061.ASD	FSFR.30102 Int=5.0 sec Lawyers2018	Muscovite	0.784	Jarosite	0.216	41.847	1.906	0.98	0.926	2205.48	NULL	2348.03	32.425	25.271	0.53	2205.48	2348.03					Montmorillonite	Jarosite		0-150	neutral	Smectite	Argillic	
30102_Lawyers2018_Halos9andard-Clays-S_30102_0062.ASD	FSFR.30102 Int=5.0 sec Lawyers2018	Muscovite	0.808	Jarosite	0.192	38.575	1.933	0.987	0.946	2206.82	NULL	2348.26	30	27.428	0.542	2206.82	2348.26					Montmorillonite	Jarosite?		0-150	neutral	Smectite	Argillic	
30102_Lawyers2018_Halos9andard-Clays-S_30102_0063.ASD	FSFR.30102 Int=5.0 sec Lawyers2018	Muscovite	0.721	Dickite	0.279	70.255	1.944	0.987	0.957	2206.32	NULL	2348.71	30.534	28.758	0.433	2206.32	2348.71					Montmorillonite			0-150	neutral	Smectite	Argillic	Kaolinite?
30102_Lawyers2018_Halos9andard-Clays-S_30102_0064.ASD	FSFR.30102 Int=5.0 sec Lawyers2018	Muscovite	0.662	Dickite	0.338	51.837	1.848	0.956	0.892	2205.42	NULL	2346.92	32.673	38.01	0.505	2205.42	2346.92					Kaolinite	Smectite	White Mica	<150-200	acidic	Kaolinite	Advanced Argillic	
30102_Lawyers2018_Halos9andard-Clays-S_30102_0065.ASD	FSFR.30102 Int=5.0 sec Lawyers2018	Muscovite	0.728	Kaolinite-PX	0.272	59.418	1.881	0.968	0.913	2206	NULL	2343.25	31.576	37.168	0.521	2206	2343.25					Kaolinite	Smectite	White Mica	<150-200	acidic	Kaolinite	Advanced Argillic	
30102_Lawyers2018_Halos9andard-Clays-S_30102_0066.ASD	FSFR.30102 Int=5.0 sec Lawyers2018	Muscovite	0.544	Vegetation-Dry	0.258	73.934	1.921	0.981	0.94	2205.87	NULL	2346.69	32.458	32.395	0.355	2205.87	2346.69					Montmorillonite		White Mica	0-150	neutral	Smectite	Argillic	
30102_Lawyers2018_Halos9andard-Clays-S_30102_0067.ASD	FSFR.30102 Int=5.0 sec Lawyers2018	Muscovitcillite	0.463	Montmorillonite	0.345	59.832	1.895	0.974	0.921	2206.82	NULL	2346.94	29.109	28.905	0.413	2206.82	2346.94		Yes			White Mica	Jarosite		200-300	neutral	Illite	Argillic	
30102_Lawyers2018_Halos9andard-Clays-S_30102_0068.ASD	FSFR.30102 Int=5.0 sec Lawyers2018	Muscovitcillite	0.583	Jarosite	0.257	62.428	1.864	0.964	0.901	2205.49	2260.39	2347.83	31.94	25.5	0.396	2205.49	2347.83		Yes			White Mica	Jarosite		200-300	neutral	Illite	Argillic	
30102_Lawyers2018_Halos9andard-Clays-S_30102_0069.ASD	FSFR.30102 Int=5.0 sec Lawyers2018	Kaolinite-WX	0.425	Nacrite	0.394	132.37	1.832	0.938	0.895	2206.83	NULL	2318.7	29.809	30.203	0.234	2206.83	2352.62					Kaolinite			<150-200	acidic	Kaolinite	Advanced Argillic	
30102_Lawyers2018_Halos9andard-Clays-S_30102_0070.ASD	FSFR.30102 Int=5.0 sec Lawyers2018	Muscovite	0.701	Kaolinite-PX	0.299	111.35	1.949	0.987	0.962	2206.59	NULL	2348.41	28.588	38.977	0.209	2206.59	2348.41					Kaolinite	Smectite	White Mica	<150-200	acidic	Kaolinite	Advanced Argillic	
30102_Lawyers2018_Halos9andard-Clays-S_30102_0071.ASD	FSFR.30102 Int=5.0 sec Lawyers2018	Muscovite	0.417	Siderite	0.408	89.717	1.968	0.993	0.974	2205.55	NULL	2348.01	31.938	27.945	0.196	2205.55	2348.01					Kaolinite	Smectite	White Mica	<150-200	acidic	Kaolinite	Advanced Argillic	
30102_Lawyers2018_Halos9andard-Clays-S_30102_0072.ASD	FSFR.30102 Int=5.0 sec Lawyers2018	Alunite-K	1	NULL	NULL	74.193	1.189	0.588	0.601	NULL	NULL	2320.11	NULL	28.853	NULL	NULL	NULL	1480				Alunite			0-300	acidic	Sulfate	Advanced Argillic	
30102_Lawyers2018_Halos9andard-Clays-S_30102_0073.ASD	FSFR.30102 Int=5.0 sec Lawyers2018	Dickite	0.386	Muscovite	0.354	78.371	1.82	0.927	0.893	2206.94	NULL	2319.45	35.511	32.981	0.281	2206.94	NULL	1480				Alunite			0-300	acidic	Sulfate	Advanced Argillic	
30102_Lawyers2018_Halos9andard-Clays-S_30102_0074.ASD	FSFR.30102 Int=5.0 sec Lawyers2018	Dickite	1	NULL	NULL	130.68	1.614	0.85	0.763	2206.79	2257.24	2353.37	30.621	34.437	0.395	2206.79	2353.37					Dickite			<200-250	acidic	Kaolinite	Advanced Argillic	
30102_Lawyers2018_Halos9andard-Clays-S_30102_0075.ASD	FSFR.30102 Int=5.0 sec Lawyers2018	Muscovitcillite	0.76	Kaolinite-PX	0.24	112.68	1.811	0.946	0.866	2205.4	NULL	2346.4	31.857	33.534	0.5	2205.4	2346.4					White Mica	Smectite		200-300	neutral	Illite	Argillic	
30102_Lawyers2018_Halos9andard-Clays-S_30102_0076.ASD	FSFR.30102 Int=5.0 sec Lawyers2018	Paragonite	0.358	Montmorillonite	0.343	87.266	1.849	0.952	0.897	2205.91	NULL	2348.65	32.309	36.016	0.344	2205.91	2348.65					White Mica	Smectite	Kaolinite	200-300	neutral	Illite	Argillic	

Sample	SampleID	Date	BestLatitude	BestLongitude	BestElevation	UTM_East	UTM_North	MineralName1	StarRating1	MineralName2	StarRating2	MineralName3	StarRating3	MineralName4	StarRating4	MineralName5	StarRating5	MineralName6	StarRating6	MineralName7	StarRating7	AlFeMg	AlOH	CSM	Fe3i	Fe3t	FeOH	ISM	Kx	MgOH	sampler	type	add_notes
30102_Lawyers2018_Halos9andard-Clays-S_30102_0056.ASD	S_30102_0056	8/9/2018 11:44:17 AM	57° 20' 0.07" N	127° 13' 49.7" W	1732	606541	6355890	Ferrihydrite	3	Beidellite	3	Muscovite	3	Jarosite	2							2207.27	2207.27		2.097	905.947	INV		0.555		2347.14	Adam LaFlamme	clay	
30102_Lawyers2018_Halos9andard-Clays-S_30102_0057.ASD	S_30102_0057	8/9/2018 11:46:15 AM	57° 20' 0.07" N	127° 13' 49.7" W	1731.7	606538	6355891	Goethite	3	Halloysite	3	Illite/Smectite	3									2207.83			1.75	INV			1.021		Adam LaFlamme	rock	Comparing white rock to clay
30102_Lawyers2018_Halos9andard-Clays-S_30102_0058.ASD	S_30102_0058	8/9/2018 11:48:54 AM	57° 20' 0.07" N	127° 13' 51.9" W	1728.9	606507	6355883	Ferrihydrite	3	Beidellite	3	Palygorskite	3	Muscovite	1	Jarosite	1					2206.23	2206.23		2.381	INV	INV		0.442		2346.24	Adam LaFlamme	clay	
30102_Lawyers2018_Halos9andard-Clays-S_30102_0059.ASD	S_30102_0059	8/9/2018 11:52:05 AM	57° 20' 0.07" N	127° 13' 55.7" W	1725.2	606448	6355883	Ferrihydrite	3	Illite/Smectite	3	Goethite	1												2.263	INV						Adam LaFlamme	clay	
30102_Lawyers2018_Halos9andard-Clays-S_30102_0060.ASD	S_30102_0060	8/9/2018 11:55:46 AM	57° 20' 1.7" N	127° 13' 58.9" W	1717.6	606378	6355898	Ferrihydrite	3	Illite/Smectite	3	Jarosite	1									2205.64			2.378	INV						Adam LaFlamme	clay	
30102_Lawyers2018_Halos9andard-Clays-S_30102_0061.ASD	S_30102_0061	8/9/2018 11:57:56 AM	57° 20' 1.7" N	127° 13' 60.7" W	1710.5	606354	6355883	Illite/Smectite	3	VNIR - No match	3																				Adam LaFlamme	clay	
30102_Lawyers2018_Halos9andard-Clays-S_30102_0062.ASD	S_30102_0062	8/9/2018 12:03:56 PM	57° 20' 1.7" N	127° 14' 3.5" W	1703.8	606300	6355903	Ferrihydrite	3	Illite/Smectite	3	Goethite	2												2.502	INV						Adam LaFlamme	clay	
30102_Lawyers2018_Halos9andard-Clays-S_30102_0063.ASD	S_30102_0063	8/9/2018 12:10:26 PM	57° 20' 1.7" N	127° 14' 6.7" W	1698.5	606253	6355893	Ferrihydrite	3	Illite/Smectite	3	Goethite	2												2.592	INV						Adam LaFlamme	clay	
30102_Lawyers2018_Halos9andard-Clays-S_30102_0064.ASD	S_30102_0064	8/9/2018 12:14:52 PM	57° 20' 1.7" N	127° 14' 7.9" W	1694.2	606201	6355898	Illite/Smectite	3	Illite/Smectite	3	Dickite	3									2205.48									Adam LaFlamme	clay	
30102_Lawyers2018_Halos9andard-Clays-S_30102_0065.ASD	S_30102_0065	8/9/2018 12:17:46 PM	57° 19' 7.6" N	127° 14' 7.9" W	1684.9	606158	6355867	Ferrihydrite	3	Illite/Smectite	3	Kaolinite PX	3									2206.17							1.052		Adam LaFlamme	clay	
30102_Lawyers2018_Halos9andard-Clays-S_30102_0066.ASD	S_30102_0066	9/11/2018 6:40:01 PM	57° 20' 0.4" N	127° 9' 37.7" W	1416.3	606095	6355891	Ferrihydrite	3	Illite/Smectite	3	Goethite	2												2.406	INV						Adam LaFlamme	clay	
30102_Lawyers2018_Halos9andard-Clays-S_30102_0067.ASD	S_30102_0067	9/11/2018 6:42:42 PM	57° 20' 0.4" N	127° 9' 37.7" W	1417.8	606026	6355883	Jarosite	3	Illite/Smectite	3											2206.91			1.897	896.741						Adam LaFlamme	clay	
30102_Lawyers2018_Halos9andard-Clays-S_30102_0068.ASD	S_30102_0068	9/11/2018 6:45:11 PM	57° 20' 0.4" N	127° 9' 37.7" W	1414.5	605988	6355888	Beidellite	3	Muscovite	2	VNIR - No match	3									2205.65	2205.65					2260.41	0.659		2347.64	Adam LaFlamme	clay	
30102_Lawyers2018_Halos9andard-Clays-S_30102_0069.ASD	S_30102_0069	9/11/2018 6:47:50 PM	57° 20' 0.4" N	127° 9' 37.7" W	1415.7	605949	6355889	Ferrihydrite	3	Dickite	3	Montmorillonite	2	Goethite	2							2206.9			1.951	885.82						Adam LaFlamme	clay	
30102_Lawyers2018_Halos9andard-Clays-S_30102_0070.ASD	S_30102_0070	9/11/2018 6:50:01 PM	57° 20' 0.4" N	127° 9' 37.7" W	1419.4	605901	6355885	Illite/Smectite	3	Mg-Illite	2	VNIR - No match	3									2206.69	2206.69						0.459		2347.97	Adam LaFlamme	clay	
30102_Lawyers2018_Halos9andard-Clays-S_30102_0071.ASD	S_30102_0071	9/11/2018 6:52:20 PM	57° 20' 0.4" N	127° 9' 37.7" W	1414.3	605852	6355940	Heulandite	3	Muscovite	2	Aragonite	1	Smithsonite	1	Dickite	1	VNIR - No match	3			2205.79	2205.79						0.272		2348.04	Adam LaFlamme	clay	
30102_Lawyers2018_Halos9andard-Clays-S_30102_0072.ASD	S_30102_0072	9/11/2018 6:57:41 PM	57° 20' 0.4" N	127° 9' 37.7" W	1419.4	605908	6355938	Goethite	3	K-Alunite	3	Hornblende	3									2166.89			1.594	926.871	INV				2320.05	Adam LaFlamme	rock	
30102_Lawyers2018_Halos9andard-Clays-S_30102_0073.ASD	S_30102_0073	9/11/2018 6:59:38 PM	57° 20' 0.4" N	127° 9' 37.7" W	1416.4	605955	6355929	Ferrihydrite	3	Beidellite	3	K-Alunite	2	Palygorskite	1							2207.06	2207.06				INV				2319.3	Adam LaFlamme	clay	
30102_Lawyers2018_Halos9andard-Clays-S_30102_0074.ASD	S_30102_0074	9/11/2018 7:01:57 PM	57° 20' 0.4" N	127° 9' 37.7" W	1414.8	606005	6355939	Nacrite	3	Rectorite	3	Gibbsite	2	VNIR - No match	3								2206.85	0.664							Adam LaFlamme	clay	
30102_Lawyers2018_Halos9andard-Clays-S_30102_0075.ASD	S_30102_0075	9/11/2018 7:04:38 PM	57° 20' 0.4" N	127° 9' 37.7" W	1413.8	606045	6355935	Jarosite	3	K-Illite	3	Iron Smectite	3	Kaolinite PX	2							2205.52	2205.52		1.676	905.102	INV		0.807	1.081	2347.19	Adam LaFlamme	clay	
30102_Lawyers2018_Halos9andard-Clays-S_30102_0076.ASD	S_30102_0076	9/11/2018 7:07:17 PM	57° 20' 0.4" N	127° 9' 37.7" W	1414	606097	6355935	Ferrihydrite	3	Beidellite	3	Phengite	2	Goethite	2							2206.12	2206.12		2.278	905.112	INV		0.777			Adam LaFlamme	clay	

| Sample_TSG | Index_TSG | Min1_sTSAS_TSG | Wt1_sTSAS_TSG | Min2_sTSAS_TSG | Wt2_sTSAS_TSG | Error_sTSAS_TSG | kaol_xtal_TSG | kl2161_mean_TSG | kl2181_mean_TSG | w2200_TSG | w2250_TSG | w2350_TSG | width_2200_TSG | width_2350_TSG | Crystallinity_Index_2200_TSG | Muscovite_TSG | Chlorite_2_TSG | Alunite_TSG | White_Mica_NoMix | Kaolinite_NoMix | Chlorite_NoMix | Mineral 1_TSG | Mineral 2_TSG | Mineral 3_TSG | Temp C | pH | Mineral Group | Alteration Assemblage | Comments | Sample | SampleID | Date | BestLatitude | BestLongitude | BestElevation | UTM_East | UTM_North | MineralName1 | StarRating1 | MineralName2 | StarRating2 | MineralName3 | StarRating3 | MineralName4 | StarRating4 | MineralName5 | StarRating5 | MineralName6 | StarRating6 | MineralName7 | StarRating7 | AlFeMg | AlOH | CSM | Fe3i | Fe3t | FeOH | ISM | Kx | MgOH | sampler | type | add_notes |
|---|---|---

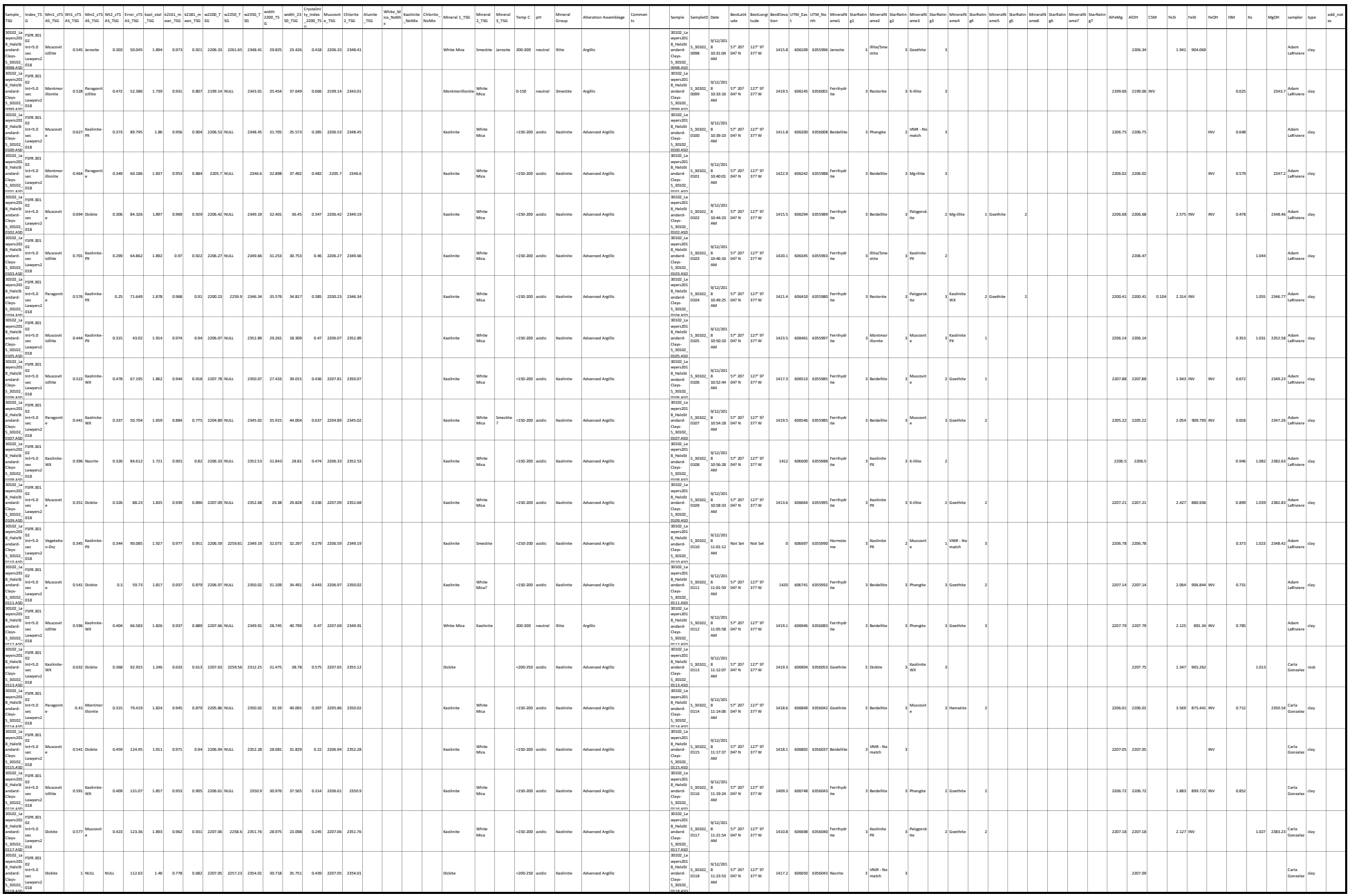

Sample_TSG	Index_TSG	Min1_sTSAS_TSG	Wt1_sTSAS_TSG	Min2_sTSAS_TSG	Wt2_sTSAS_TSG	Error_sTSAS_TSG	kaol_xtal_TSG	k2161_mean_TSG	k2181_mean_TSG	w2200_TSG	w2250_TSG	w2350_TSG	width_2200_TSG	width_2350_TSG	Crystallinity_Index_2200_TSG	Muscovite_TSG	Chlorite_2_TSG	Alunite_TSG	White_Mica_NoMix	Kaolinite_NoMix	Chlorite_NoMix	Mineral 1_TSG	Mineral 2_TSG	Mineral 3_TSG	Temp C	pH	Mineral Group	Alteration Assemblage	Comments
30102_Lawyers2018_HaloSandard-Clays-S_30102_0098.ASD	FSFR.30102.Int>5.0 sec Lawyers2018	Muscovite	0.545	Jarosite	0.303	50.045	1.894	0.973	0.921	2206.33	2261.65	2348.41	29.825	23.426	0.418	2206.33	2348.41					White Mica	Smectite	Jarosite	200-300	neutral	Illite	Argillic	
30102_Lawyers2018_HaloSandard-Clays-S_30102_0099.ASD	FSFR.30102.Int>5.0 sec Lawyers2018	Montmorillonite	0.528	Paragonite	0.472	52.386	1.739	0.931	0.807	2199.14	NULL	2343.01	35.454	37.649	0.666	2199.14	2343.01					Montmorillonite	White Mica		0-150	neutral	Smectite	Argillic	
30102_Lawyers2018_HaloSandard-Clays-S_30102_0100.ASD	FSFR.30102.Int>5.0 sec Lawyers2018	Muscovite	0.627	Kaolinite-PX	0.373	89.795	1.86	0.956	0.904	2206.53	NULL	2348.45	31.705	35.573	0.385	2206.53	2348.45					Kaolinite	White Mica		<150-200	acidic	Kaolinite	Advanced Argillic	
30102_Lawyers2018_HaloSandard-Clays-S_30102_0101.ASD	FSFR.30102.Int>5.0 sec Lawyers2018	Montmorillonite	0.464	Paragonite	0.349	60.186	1.837	0.953	0.884	2205.7	NULL	2346.6	32.898	37.492	0.482	2205.7	2346.6					Kaolinite	White Mica		<150-200	acidic	Kaolinite	Advanced Argillic	
30102_Lawyers2018_HaloSandard-Clays-S_30102_0102.ASD	FSFR.30102.Int>5.0 sec Lawyers2018	Muscovite	0.694	Dickite	0.306	84.326	1.897	0.969	0.929	2206.42	NULL	2349.19	32.401	36.45	0.347	2206.42	2349.19					Kaolinite	White Mica		<150-200	acidic	Kaolinite	Advanced Argillic	
30102_Lawyers2018_HaloSandard-Clays-S_30102_0103.ASD	FSFR.30102.Int>5.0 sec Lawyers2018	Muscovite	0.701	Kaolinite-PX	0.299	64.862	1.892	0.97	0.922	2206.27	NULL	2349.66	31.253	30.753	0.46	2206.27	2349.66					Kaolinite	White Mica		<150-200	acidic	Kaolinite	Advanced Argillic	
30102_Lawyers2018_HaloSandard-Clays-S_30102_0104.ASD	FSFR.30102.Int>5.0 sec Lawyers2018	Paragonite	0.576	Kaolinite-PX	0.25	71.649	1.878	0.968	0.91	2200.23	2259.9	2346.34	35.579	34.817	0.385	2200.23	2346.34					Kaolinite	White Mica		<150-200	acidic	Kaolinite	Advanced Argillic	
30102_Lawyers2018_HaloSandard-Clays-S_30102_0105.ASD	FSFR.30102.Int>5.0 sec Lawyers2018	Muscovite	0.444	Kaolinite-PX	0.315	43.02	1.914	0.974	0.94	2206.07	NULL	2352.89	29.261	18.309	0.47	2206.07	2352.89					Kaolinite	White Mica		<150-200	acidic	Kaolinite	Advanced Argillic	
30102_Lawyers2018_HaloSandard-Clays-S_30102_0106.ASD	FSFR.30102.Int>5.0 sec Lawyers2018	Muscovite	0.522	Kaolinite-WX	0.478	67.195	1.862	0.944	0.918	2207.78	NULL	2350.07	27.433	39.015	0.436	2207.81	2350.07					Kaolinite	White Mica		<150-200	acidic	Kaolinite	Advanced Argillic	
30102_Lawyers2018_HaloSandard-Clays-S_30102_0107.ASD	FSFR.30102.Int>5.0 sec Lawyers2018	Paragonite	0.441	Kaolinite-WX	0.337	50.704	1.659	0.884	0.775	2204.89	NULL	2345.02	35.915	44.004	0.637	2204.89	2345.02					Kaolinite	White Mica	Smectite?	<150-200	acidic	Kaolinite	Advanced Argillic	
30102_Lawyers2018_HaloSandard-Clays-S_30102_0108.ASD	FSFR.30102.Int>5.0 sec Lawyers2018	Kaolinite-WX	0.396	Nacrite	0.326	84.612	1.721	0.901	0.82	2206.33	NULL	2352.53	31.843	28.81	0.474	2206.33	2352.53					Kaolinite	White Mica		<150-200	acidic	Kaolinite	Advanced Argillic	
30102_Lawyers2018_HaloSandard-Clays-S_30102_0109.ASD	FSFR.30102.Int>5.0 sec Lawyers2018	Muscovite	0.351	Dickite	0.326	88.23	1.835	0.939	0.896	2207.09	NULL	2352.68	29.38	29.828	0.336	2207.09	2352.68					Kaolinite	White Mica		<150-200	acidic	Kaolinite	Advanced Argillic	
30102_Lawyers2018_HaloSandard-Clays-S_30102_0110.ASD	FSFR.30102.Int>5.0 sec Lawyers2018	Vegetation-Dry	0.345	Kaolinite-PX	0.344	90.085	1.927	0.977	0.951	2206.59	2259.81	2349.19	32.073	32.297	0.279	2206.59	2349.19					Kaolinite	Smectite		<150-200	acidic	Kaolinite	Advanced Argillic	
30102_Lawyers2018_HaloSandard-Clays-S_30102_0111.ASD	FSFR.30102.Int>5.0 sec Lawyers2018	Muscovite	0.541	Dickite	0.3	59.73	1.817	0.937	0.879	2206.97	NULL	2350.02	31.109	34.491	0.443	2206.97	2350.02					Kaolinite	White Mica?		<150-200	acidic	Kaolinite	Advanced Argillic	
30102_Lawyers2018_HaloSandard-Clays-S_30102_0112.ASD	FSFR.30102.Int>5.0 sec Lawyers2018	Muscovite	0.596	Kaolinite-WX	0.404	66.583	1.826	0.937	0.889	2207.66	NULL	2349.91	28.745	40.799	0.47	2207.69	2349.91					White Mica	Kaolinite		200-300	neutral	Illite	Argillic	
30102_Lawyers2018_HaloSandard-Clays-S_30102_0113.ASD	FSFR.30102.Int>5.0 sec Lawyers2018	Kaolinite-WX	0.632	Dickite	0.368	92.915	1.246	0.633	0.613	2207.63	2259.56	2312.25	31.475	38.78	0.575	2207.65	2355.12					Dickite			<200-250	acidic	Kaolinite	Advanced Argillic	
30102_Lawyers2018_HaloSandard-Clays-S_30102_0114.ASD	FSFR.30102.Int>5.0 sec Lawyers2018	Paragonite	0.41	Montmorillonite	0.315	79.419	1.824	0.945	0.879	2205.86	NULL	2350.02	33.59	40.065	0.397	2205.86	2350.02					Kaolinite	White Mica		<150-200	acidic	Kaolinite	Advanced Argillic	
30102_Lawyers2018_HaloSandard-Clays-S_30102_0115.ASD	FSFR.30102.Int>5.0 sec Lawyers2018	Muscovite	0.541	Dickite	0.459	124.95	1.911	0.971	0.94	2206.94	NULL	2352.28	28.081	31.829	0.22	2206.94	2352.28					Kaolinite	White Mica		<150-200	acidic	Kaolinite	Advanced Argillic	
30102_Lawyers2018_HaloSandard-Clays-S_30102_0116.ASD	FSFR.30102.Int>5.0 sec Lawyers2018	Muscovite	0.591	Kaolinite-WX	0.409	131.07	1.857	0.953	0.905	2206.61	NULL	2350.9	30.976	37.565	0.314	2206.61	2350.9					Kaolinite	White Mica		<150-200	acidic	Kaolinite	Advanced Argillic	
30102_Lawyers2018_HaloSandard-Clays-S_30102_0117.ASD	FSFR.30102.Int>5.0 sec Lawyers2018	Dickite	0.577	Muscovite	0.423	123.36	1.893	0.962	0.931	2207.06	2258.6	2351.76	28.975	23.098	0.245	2207.06	2351.76					Kaolinite	White Mica		<150-200	acidic	Kaolinite	Advanced Argillic	
30102_Lawyers2018_HaloSandard-Clays-S_30102_0118.ASD	FSFR.30102.Int>5.0 sec Lawyers2018	Dickite	1	NULL	NULL	112.63	1.46	0.778	0.682	2207.05	2257.23	2354.01	30.718	35.751	0.439	2207.05	2354.01					Dickite			<200-250	acidic	Kaolinite	Advanced Argillic	

Sample	SampleID	Date	BestLatitude	BestLongitude	BestElevation	UTM_East	UTM_North	MineralName1	StarRating1	MineralName2	StarRating2	MineralName3	StarRating3	MineralName4	StarRating4	MineralName5	StarRating5	MineralName6	StarRating6	MineralName7	StarRating7	AlPerMg	AlOH	CSM	Fe3i	Fe3t	FeOH	ISM	Kx	MgOH	sampler	type	add_notes
30102_Lawyers2018_HaloSandard-Clays-S_30102_0098.ASD	S_30102_0098	9/12/2018 10:31:04 AM	57° 20' 047 N	127° 97' 377 W	1415.8	606109	6355996	Jarosite	3	Illite/Smectite	3	Goethite	3										2206.34		1.941	904.069					Adam LaRiviere	clay	
30102_Lawyers2018_HaloSandard-Clays-S_30102_0099.ASD	S_30102_0099	9/12/2018 10:33:16 AM	57° 20' 047 N	127° 97' 377 W	1419.5	606145	6356001	Fernhydrite	3	Rectorite	3	K-illite	3									2199.06	2199.06	INV				0.625		2343.7	Adam LaRiviere	clay	
30102_Lawyers2018_HaloSandard-Clays-S_30102_0100.ASD	S_30102_0100	9/12/2018 10:39:10 AM	57° 20' 047 N	127° 97' 377 W	1411.8	606200	6356038	Beidellite	3	Phengite	2	VNIR - No match	3									2206.75	2206.75				INV	0.648			Adam LaRiviere	clay	
30102_Lawyers2018_HaloSandard-Clays-S_30102_0101.ASD	S_30102_0101	9/12/2018 10:40:01 AM	57° 20' 047 N	127° 97' 377 W	1422.9	606242	6355988	Fernhydrite	3	Beidellite	3	Mg-illite	3									2206.02	2206.02				INV	0.579		2347.2	Adam LaRiviere	clay	
30102_Lawyers2018_HaloSandard-Clays-S_30102_0102.ASD	S_30102_0102	9/12/2018 10:44:23 AM	57° 20' 047 N	127° 97' 377 W	1415.5	606294	6355989	Fernhydrite	3	Beidellite	3	Palygorskite	2	Mg-illite	1	Goethite	2					2206.68	2206.68		2.575	INV	INV	0.478		2348.46	Adam LaRiviere	clay	
30102_Lawyers2018_HaloSandard-Clays-S_30102_0103.ASD	S_30102_0103	9/12/2018 10:46:16 AM	57° 20' 047 N	127° 97' 377 W	1420.1	606345	6355993	Fernhydrite	3	Illite/Smectite	3	Kaolinite PX	2									2206.47							1.044		Adam LaRiviere	clay	
30102_Lawyers2018_HaloSandard-Clays-S_30102_0104.ASD	S_30102_0104	9/12/2018 10:49:25 AM	57° 20' 047 N	127° 97' 377 W	1421.4	606410	6355980	Fernhydrite	3	Rectorite	3	Palygorskite	3	Kaolinite WX	2	Goethite	2					2200.41	2200.41	0.104	2.314	INV			1.055	2346.77	Adam LaRiviere	clay	
30102_Lawyers2018_HaloSandard-Clays-S_30102_0105.ASD	S_30102_0105	9/12/2018 10:50:10 AM	57° 20' 047 N	127° 97' 377 W	1423.5	606461	6355997	Fernhydrite	3	Montmorillonite	3	Muscovite	3	Kaolinite PX	1							2206.14	2206.14					0.353	1.031	2352.58	Adam LaRiviere	clay	
30102_Lawyers2018_HaloSandard-Clays-S_30102_0106.ASD	S_30102_0106	9/12/2018 10:52:44 AM	57° 20' 047 N	127° 97' 377 W	1417.3	606513	6355985	Fernhydrite	3	Beidellite	3	Muscovite	2	Goethite	1							2207.88	2207.88		1.943	INV	INV	0.672		2349.23	Adam LaRiviere	clay	
30102_Lawyers2018_HaloSandard-Clays-S_30102_0107.ASD	S_30102_0107	9/12/2018 10:54:18 AM	57° 20' 047 N	127° 97' 377 W	1419.5	606546	6355985	Fernhydrite	3	Beidellite	3	Muscovite	3	Goethite	2							2205.22	2205.22		2.054	909.793	INV	0.658		2347.26	Adam LaRiviere	clay	
30102_Lawyers2018_HaloSandard-Clays-S_30102_0108.ASD	S_30102_0108	9/12/2018 10:56:28 AM	57° 20' 047 N	127° 97' 377 W	1412	606600	6355988	Fernhydrite	3	Kaolinite PX	3	K-illite	2									2206.5	2206.5					0.946	1.082	2382.63	Adam LaRiviere	clay	
30102_Lawyers2018_HaloSandard-Clays-S_30102_0109.ASD	S_30102_0109	9/12/2018 10:58:33 AM	57° 20' 047 N	127° 97' 377 W	1413.6	606664	6355995	Fernhydrite	3	Kaolinite PX	3	K-illite	2	Goethite	2							2207.21	2207.21		2.427	880.936		0.899	1.039	2382.83	Adam LaRiviere	clay	
30102_Lawyers2018_HaloSandard-Clays-S_30102_0110.ASD	S_30102_0110	9/12/2018 11:01:12 AM	Not Set	Not Set	0	606697	6355990	Harmotome	3	Kaolinite PX	2	Muscovite	1	VNIR - No match	3							2206.78	2206.78					0.373	1.023	2348.42	Adam LaRiviere	clay	
30102_Lawyers2018_HaloSandard-Clays-S_30102_0111.ASD	S_30102_0111	9/12/2018 11:01:59 AM	57° 20' 047 N	127° 97' 377 W	1420	606741	6355992	Fernhydrite	3	Beidellite	3	Phengite	3	Goethite	2							2207.14	2207.14		2.064	906.844	INV	0.731			Adam LaRiviere	clay	
30102_Lawyers2018_HaloSandard-Clays-S_30102_0112.ASD	S_30102_0112	9/12/2018 11:05:58 AM	57° 20' 047 N	127° 97' 377 W	1419.1	606946	6356083	Fernhydrite	3	Beidellite	3	Phengite	3	Goethite	3							2207.79	2207.79		2.125	891.34	INV	0.785			Adam LaRiviere	clay	
30102_Lawyers2018_HaloSandard-Clays-S_30102_0113.ASD	S_30102_0113	9/12/2018 11:12:07 AM	57° 20' 047 N	127° 97' 377 W	1419.3	606904	6356053	Goethite	3	Dickite	3	Kaolinite WX	3									2207.75			1.347	965.262			1.013		Carla Gonzalez	rock	
30102_Lawyers2018_HaloSandard-Clays-S_30102_0114.ASD	S_30102_0114	9/12/2018 11:14:06 AM	57° 20' 047 N	127° 97' 377 W	1418.6	606849	6356042	Goethite	3	Beidellite	3	Muscovite	3	Hematite	2							2206.01	2206.01		3.569	875.441	INV	0.712		2350.54	Carla Gonzalez	clay	
30102_Lawyers2018_HaloSandard-Clays-S_30102_0115.ASD	S_30102_0115	9/12/2018 11:17:37 AM	57° 20' 047 N	127° 97' 377 W	1418.1	606802	6356037	Beidellite	3	VNIR - No match	3											2207.05	2207.05				INV				Carla Gonzalez	clay	
30102_Lawyers2018_HaloSandard-Clays-S_30102_0116.ASD	S_30102_0116	9/12/2018 11:19:24 AM	57° 20' 047 N	127° 97' 377 W	1409.3	606748	6356043	Fernhydrite	3	Beidellite	3	Phengite	2	Goethite	2							2206.72	2206.72		1.883	899.722	INV	0.852			Carla Gonzalez	clay	
30102_Lawyers2018_HaloSandard-Clays-S_30102_0117.ASD	S_30102_0117	9/12/2018 11:21:54 AM	57° 20' 047 N	127° 97' 377 W	1410.8	606698	6356040	Fernhydrite	3	Kaolinite PX	3	Palygorskite	2	Goethite	2							2207.18	2207.18		2.127	INV			1.027	2383.23	Carla Gonzalez	clay	
30102_Lawyers2018_HaloSandard-Clays-S_30102_0118.ASD	S_30102_0118	9/12/2018 11:23:53 AM	57° 20' 047 N	127° 97' 377 W	1417.2	606650	6356043	Nacrite	3	VNIR - No match	3											2207.09									Carla Gonzalez	clay	

| Sample_TSG | Index_TSG | Min1_sTSAS_TSG | Wt1_sTSAS_TSG | Min2_sTSAS_TSG | Wt2_sTSAS_TSG | Error_sTSAS_TSG | kaol_xtal_TSG | k2161_mean_TSG | k2181_mean_TSG | w2200_TSG | w2250_TSG | w2350_TSG | width_2200_TSG | width_2350_TSG | Crystallinity_Index_2200_TSG | Muscovite_TSG | Chlorite_2_TSG | Alunite_TSG | White_Mica_NoMix | Kaolinite_NoMix | Chlorite_NoMix | Mineral 1_TSG | Mineral 2_TSG | Mineral 3_TSG | Temp C | pH | Mineral Group | Alteration Assemblage | Comments | Sample | SampleID | Date | BestLatitude | BestLongitude | BestElevation | UTM_East | UTM_North | MineralName1 | StarRating1 | MineralName2 | StarRating2 | MineralName3 | StarRating3 | MineralName4 | StarRating4 | MineralName5 | StarRating5 | MineralName6 | StarRating6 | MineralName7 | StarRating7 | AlPerMg | AlOH | CSM | FeSi | FeSt | FeOH | ISM | Kx | MgOH | sampler | type | add_notes |
|---|---|---

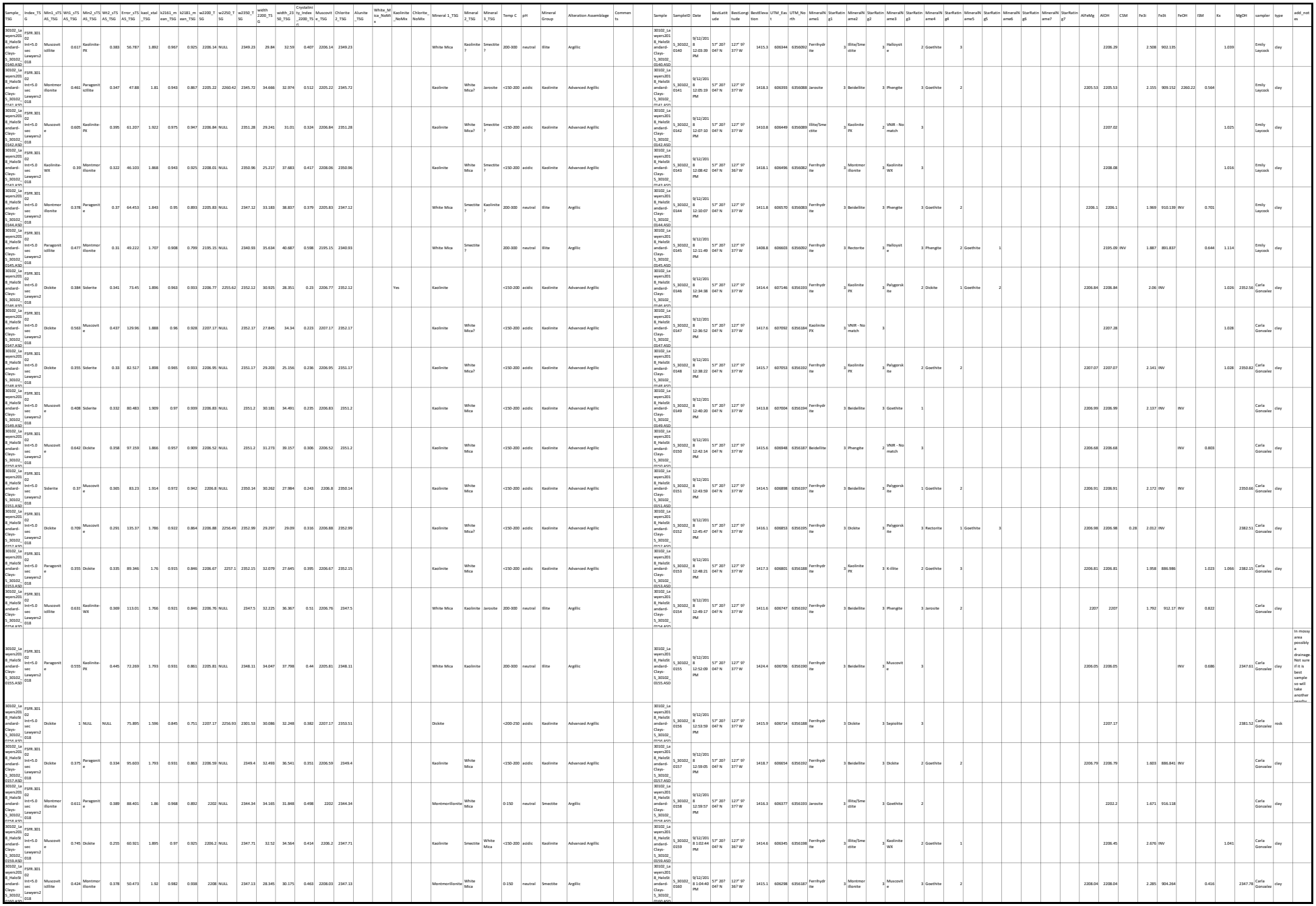

| Sample_TSG | Index_TSG | Min1_sTSAS_TSG | Wt1_sTSAS_TSG | Min2_sTSAS_TSG | Wt2_sTSAS_TSG | Error_sTSAS_TSG | kaol_xtal_TSG | k2161_mean_TSG | k2181_mean_TSG | w2200_TSG | w2250_TSG | w2350_TSG | width_2200_TSG | width_2350_TSG | Crystallinity_Index_2200_TSG | Muscovite_TSG | Chlorite_2_TSG | Alunite_TSG | White_Mica_NoMix | Kaolinite_NoMix | Chlorite_NoMix | Mineral 1_TSG | Mineral 2_TSG | Mineral 3_TSG | Temp C | pH | Mineral Group | Alteration Assemblage | Comments | Sample | SampleID | Date | BestLatitude | BestLongitude | BestElevation | UTM_East | UTM_North | MineralName1 | StarRating1 | MineralName2 | StarRating2 | MineralName3 | StarRating3 | MineralName4 | StarRating4 | MineralName5 | StarRating5 | MineralName6 | StarRating6 | MineralName7 | StarRating7 | AlPeMg | AlOH | CSM | Fe3i | Fe3t | FeOH | ISM | Kx | MgOH | sampler | type | add_notes |
|---|---|---

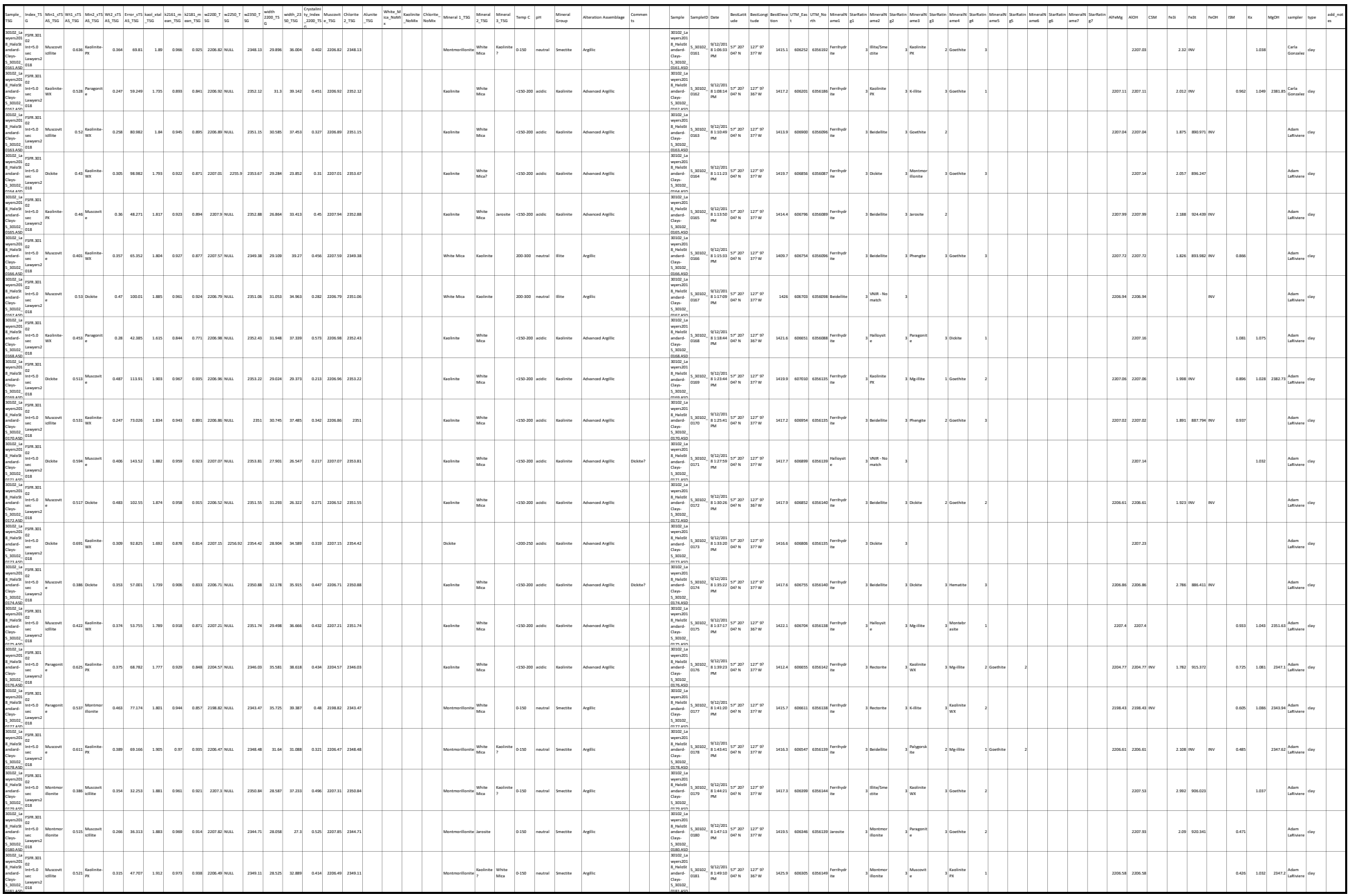

Sample_TSG	Index_TSG	Min1_sTSAS_TSG	Wt1_sTSAS_TSG	Min2_sTSAS_TSG	Wt2_sTSAS_TSG	Error_sTSAS_TSG	kaol_xtal_TSG	k2161_mean_TSG	k2181_mean_TSG	w2200_TSG	w2250_TSG	w2350_TSG	width_2200_TSG	width_2350_TSG	Crystallinity_Index_2200_TSG	Muscovite_TSG	Chlorite_2_TSG	Alunite_TSG	White_Mica_NoMix	Kaolinite_NoMix	Chlorite_NoMix	Mineral 1_TSG	Mineral 2_TSG	Mineral 3_TSG	Temp C	pH	Mineral Group	Alteration Assemblage	Comments
30102_Lawyers2018_Halos9andard-Clays-S_30102_0161.ASD	FSFR.30102.52.Int=5.0 sec Lawyers2018	Muscovite	0.636	Kaolinite-PX	0.364	69.81	1.89	0.966	0.925	2206.82	NULL	2348.13	29.896	36.004	0.402	2206.82	2348.13					Montmorillonite	White Mica	Kaolinite?	0-150	neutral	Smectite	Argillic	
30102_Lawyers2018_Halos9andard-Clays-S_30102_0162.ASD	FSFR.30102.52.Int=5.0 sec Lawyers2018	Kaolinite-WX	0.528	Paragonite	0.247	59.249	1.735	0.893	0.841	2206.92	NULL	2352.12	31.3	39.142	0.451	2206.92	2352.12					Kaolinite	White Mica		<150-200	acidic	Kaolinite	Advanced Argillic	
30102_Lawyers2018_Halos9andard-Clays-S_30102_0163.ASD	FSFR.30102.52.Int=5.0 sec Lawyers2018	Muscovite	0.52	Kaolinite-WX	0.258	80.982	1.84	0.945	0.895	2206.89	NULL	2351.15	30.585	37.453	0.327	2206.89	2351.15					Kaolinite	White Mica		<150-200	acidic	Kaolinite	Advanced Argillic	
30102_Lawyers2018_Halos9andard-Clays-S_30102_0164.ASD	FSFR.30102.52.Int=5.0 sec Lawyers2018	Dickite	0.43	Kaolinite-WX	0.305	98.982	1.793	0.922	0.871	2207.01	2255.9	2353.67	29.284	23.852	0.31	2207.01	2353.67					Kaolinite	White Mica?		<150-200	acidic	Kaolinite	Advanced Argillic	
30102_Lawyers2018_Halos9andard-Clays-S_30102_0165.ASD	FSFR.30102.52.Int=5.0 sec Lawyers2018	Kaolinite-PX	0.46	Muscovite	0.36	48.271	1.817	0.923	0.894	2207.9	NULL	2352.88	26.864	33.413	0.45	2207.94	2352.88					Kaolinite	White Mica	Jarosite	<150-200	acidic	Kaolinite	Advanced Argillic	
30102_Lawyers2018_Halos9andard-Clays-S_30102_0166.ASD	FSFR.30102.52.Int=5.0 sec Lawyers2018	Muscovite	0.401	Kaolinite-WX	0.357	65.352	1.804	0.927	0.877	2207.57	NULL	2349.38	29.109	39.27	0.456	2207.59	2349.38					White Mica	Kaolinite		200-300	neutral	Illite	Argillic	
30102_Lawyers2018_Halos9andard-Clays-S_30102_0167.ASD	FSFR.30102.52.Int=5.0 sec Lawyers2018	Muscovite	0.53	Dickite	0.47	100.01	1.885	0.961	0.924	2206.79	NULL	2351.06	31.053	34.963	0.282	2206.79	2351.06					White Mica	Kaolinite		200-300	neutral	Illite	Argillic	
30102_Lawyers2018_Halos9andard-Clays-S_30102_0168.ASD	FSFR.30102.52.Int=5.0 sec Lawyers2018	Kaolinite-WX	0.453	Paragonite	0.28	42.385	1.615	0.844	0.771	2206.98	NULL	2352.43	31.948	37.339	0.573	2206.98	2352.43					Kaolinite	White Mica		<150-200	acidic	Kaolinite	Advanced Argillic	
30102_Lawyers2018_Halos9andard-Clays-S_30102_0169.ASD	FSFR.30102.52.Int=5.0 sec Lawyers2018	Dickite	0.513	Muscovite	0.487	113.91	1.903	0.967	0.935	2206.96	NULL	2353.22	29.024	29.373	0.213	2206.96	2353.22					Kaolinite	White Mica		<150-200	acidic	Kaolinite	Advanced Argillic	
30102_Lawyers2018_Halos9andard-Clays-S_30102_0170.ASD	FSFR.30102.52.Int=5.0 sec Lawyers2018	Muscovite	0.531	Kaolinite-WX	0.247	73.026	1.834	0.943	0.891	2206.86	NULL	2351	30.745	37.485	0.342	2206.86	2351					Kaolinite	White Mica		<150-200	acidic	Kaolinite	Advanced Argillic	
30102_Lawyers2018_Halos9andard-Clays-S_30102_0171.ASD	FSFR.30102.52.Int=5.0 sec Lawyers2018	Dickite	0.594	Muscovite	0.406	143.52	1.882	0.959	0.923	2207.07	NULL	2353.81	27.901	26.547	0.217	2207.07	2353.81					Kaolinite	White Mica		<150-200	acidic	Kaolinite	Advanced Argillic	Dickite?
30102_Lawyers2018_Halos9andard-Clays-S_30102_0172.ASD	FSFR.30102.52.Int=5.0 sec Lawyers2018	Muscovite	0.517	Dickite	0.483	102.55	1.874	0.958	0.915	2206.52	NULL	2351.55	31.293	26.322	0.271	2206.52	2351.55					Kaolinite	White Mica		<150-200	acidic	Kaolinite	Advanced Argillic	
30102_Lawyers2018_Halos9andard-Clays-S_30102_0173.ASD	FSFR.30102.52.Int=5.0 sec Lawyers2018	Dickite	0.691	Kaolinite-WX	0.309	92.825	1.692	0.878	0.814	2207.15	2256.92	2354.42	28.904	34.589	0.319	2207.15	2354.42					Dickite			<200-250	acidic	Kaolinite	Advanced Argillic	
30102_Lawyers2018_Halos9andard-Clays-S_30102_0174.ASD	FSFR.30102.52.Int=5.0 sec Lawyers2018	Muscovite	0.386	Dickite	0.353	57.001	1.739	0.906	0.833	2206.71	NULL	2350.88	32.178	35.915	0.447	2206.71	2350.88					Kaolinite	White Mica		<150-200	acidic	Kaolinite	Advanced Argillic	Dickite?
30102_Lawyers2018_Halos9andard-Clays-S_30102_0175.ASD	FSFR.30102.52.Int=5.0 sec Lawyers2018	Muscovite	0.422	Kaolinite-WX	0.374	53.755	1.789	0.918	0.871	2207.21	NULL	2351.74	29.498	36.666	0.432	2207.21	2351.74					Kaolinite	White Mica		<150-200	acidic	Kaolinite	Advanced Argillic	
30102_Lawyers2018_Halos9andard-Clays-S_30102_0176.ASD	FSFR.30102.52.Int=5.0 sec Lawyers2018	Paragonite	0.625	Kaolinite-PX	0.375	68.782	1.777	0.929	0.848	2204.57	NULL	2346.03	35.581	38.618	0.434	2204.57	2346.03					Kaolinite	White Mica		<150-200	acidic	Kaolinite	Advanced Argillic	
30102_Lawyers2018_Halos9andard-Clays-S_30102_0177.ASD	FSFR.30102.52.Int=5.0 sec Lawyers2018	Paragonite	0.537	Montmorillonite	0.463	77.174	1.801	0.944	0.857	2198.82	NULL	2343.47	35.725	39.387	0.48	2198.82	2343.47					Montmorillonite	White Mica		0-150	neutral	Smectite	Argillic	
30102_Lawyers2018_Halos9andard-Clays-S_30102_0178.ASD	FSFR.30102.52.Int=5.0 sec Lawyers2018	Muscovite	0.611	Kaolinite-PX	0.389	69.166	1.905	0.97	0.935	2206.47	NULL	2348.48	31.64	31.088	0.321	2206.47	2348.48					Montmorillonite	White Mica	Kaolinite?	0-150	neutral	Smectite	Argillic	
30102_Lawyers2018_Halos9andard-Clays-S_30102_0179.ASD	FSFR.30102.52.Int=5.0 sec Lawyers2018	Montmorillonite	0.386	Muscovite	0.354	32.253	1.881	0.961	0.921	2207.3	NULL	2350.84	28.587	37.233	0.496	2207.31	2350.84					Montmorillonite	White Mica	Kaolinite?	0-150	neutral	Smectite	Argillic	
30102_Lawyers2018_Halos9andard-Clays-S_30102_0180.ASD	FSFR.30102.52.Int=5.0 sec Lawyers2018	Montmorillonite	0.515	Muscovite	0.266	36.313	1.883	0.969	0.914	2207.82	NULL	2344.71	28.058	27.3	0.525	2207.85	2344.71					Montmorillonite	Jarosite		0-150	neutral	Smectite	Argillic	
30102_Lawyers2018_Halos9andard-Clays-S_30102_0181.ASD	FSFR.30102.52.Int=5.0 sec Lawyers2018	Muscovite	0.521	Kaolinite-PX	0.315	47.707	1.912	0.973	0.938	2206.49	NULL	2349.11	28.525	32.889	0.414	2206.49	2349.11					Montmorillonite	Kaolinite?	White Mica	0-150	neutral	Smectite	Argillic	

Sample	SampleID	Date	BestLatitude	BestLongitude	BestElevation	UTM_East	UTM_North	MineralName1	StarRating1	MineralName2	StarRating2	MineralName3	StarRating3	MineralName4	StarRating4	MineralName5	StarRating5	MineralName6	StarRating6	MineralName7	StarRating7	AlOH	CSM	Fe3i	Fe3t	FeOH	ISM	Kx	MgOH	sampler	type	add_notes
30102_Lawyers2018_Halos9andard-Clays-S_30102_0161.ASD	S_30102_0161	9/12/2018 1:06:31 PM	57° 20' 047 N	127° 97' 377 W	1415.1	606252	6356192	Fernihydrite	3	Illite/Smectite	3	Kaolinite PX	2	Goethite	3							2207.03		2.32	INV				1.038		Carla Gonzalez	clay	
30102_Lawyers2018_Halos9andard-Clays-S_30102_0162.ASD	S_30102_0162	9/12/2018 1:08:14 PM	57° 20' 047 N	127° 97' 367 W	1417.2	606201	6356186	Fernihydrite	3	Kaolinite PX	3	K-illite	3	Goethite	1							2207.11	2207.11	2.012	INV			0.962	1.049	2381.85	Carla Gonzalez	clay	
30102_Lawyers2018_Halos9andard-Clays-S_30102_0163.ASD	S_30102_0163	9/12/2018 1:10:40 PM	57° 20' 047 N	127° 97' 377 W	1413.9	606900	6356096	Fernihydrite	3	Beidellite	3	Goethite	2									2207.04	2207.04	1.875	890.971	INV					Adam LaRiviere	clay	
30102_Lawyers2018_Halos9andard-Clays-S_30102_0164.ASD	S_30102_0164	9/12/2018 1:11:23 PM	57° 20' 047 N	127° 97' 377 W	1419.7	606856	6356087	Fernihydrite	3	Dickite	3	Montmorillonite	3	Goethite	3							2207.14		2.057	896.247						Adam LaRiviere	clay	
30102_Lawyers2018_Halos9andard-Clays-S_30102_0165.ASD	S_30102_0165	9/12/2018 1:13:53 PM	57° 20' 047 N	127° 97' 377 W	1414.4	606796	6356089	Fernihydrite	3	Beidellite	3	Jarosite	2									2207.99	2207.99	2.188	924.439	INV					Adam LaRiviere	clay	
30102_Lawyers2018_Halos9andard-Clays-S_30102_0166.ASD	S_30102_0166	9/12/2018 1:15:33 PM	57° 20' 047 N	127° 97' 377 W	1409.7	606754	6356096	Fernihydrite	3	Beidellite	3	Phengite	3	Goethite	3							2207.72	2207.72	1.826	893.982	INV		0.866			Adam LaRiviere	clay	
30102_Lawyers2018_Halos9andard-Clays-S_30102_0167.ASD	S_30102_0167	9/12/2018 1:17:05 PM	57° 20' 047 N	127° 97' 377 W	1426	606703	6356098	Beidellite	3	VNIR - No match	3											2206.94	2206.94				INV				Adam LaRiviere	clay	
30102_Lawyers2018_Halos9andard-Clays-S_30102_0168.ASD	S_30102_0168	9/12/2018 1:18:44 PM	57° 20' 047 N	127° 97' 367 W	1421.6	606651	6356088	Fernihydrite	3	Halloysite	3	Paragonite	3	Dickite	1							2207.16						1.081	1.075		Adam LaRiviere	clay	
30102_Lawyers2018_Halos9andard-Clays-S_30102_0169.ASD	S_30102_0169	9/12/2018 1:23:41 PM	57° 20' 047 N	127° 97' 377 W	1419.9	607010	6356135	Fernihydrite	3	Kaolinite PX	3	Mg-illite	1	Goethite	2							2207.06	2207.06	1.998	INV			0.896	1.028	2382.73	Adam LaRiviere	clay	
30102_Lawyers2018_Halos9andard-Clays-S_30102_0170.ASD	S_30102_0170	9/12/2018 1:25:41 PM	57° 20' 047 N	127° 97' 377 W	1417.2	606954	6356135	Fernihydrite	3	Beidellite	3	Phengite	2	Goethite	3							2207.02	2207.02	1.891	887.794	INV		0.937			Adam LaRiviere	clay	
30102_Lawyers2018_Halos9andard-Clays-S_30102_0171.ASD	S_30102_0171	9/12/2018 1:27:50 PM	57° 20' 047 N	127° 97' 377 W	1417.7	606899	6356139	Halloysite	3	VNIR - No match	3											2207.14							1.032		Adam LaRiviere	clay	
30102_Lawyers2018_Halos9andard-Clays-S_30102_0172.ASD	S_30102_0172	9/12/2018 1:30:26 PM	57° 20' 047 N	127° 97' 367 W	1417.9	606852	6356140	Fernihydrite	3	Beidellite	3	Dickite	2	Goethite	2							2206.61	2206.61	1.923	INV	INV					Adam LaRiviere	clay	
30102_Lawyers2018_Halos9andard-Clays-S_30102_0173.ASD	S_30102_0173	9/12/2018 1:33:20 PM	57° 20' 047 N	127° 97' 377 W	1416.6	606806	6356135	Fernihydrite	3	Dickite	3											2207.23									Adam LaRiviere	clay	
30102_Lawyers2018_Halos9andard-Clays-S_30102_0174.ASD	S_30102_0174	9/12/2018 1:35:22 PM	57° 20' 047 N	127° 97' 377 W	1417.6	606755	6356140	Fernihydrite	3	Beidellite	3	Dickite	3	Hematite	3							2206.86	2206.86	2.786	886.411	INV					Adam LaRiviere	clay	
30102_Lawyers2018_Halos9andard-Clays-S_30102_0175.ASD	S_30102_0175	9/12/2018 1:37:17 PM	57° 20' 047 N	127° 97' 367 W	1422.1	606704	6356138	Fernihydrite	3	Halloysite	3	Mg-illite	3	Montebrasite	1							2207.4	2207.4					0.933	1.043	2351.63	Adam LaRiviere	clay	
30102_Lawyers2018_Halos9andard-Clays-S_30102_0176.ASD	S_30102_0176	9/12/2018 1:39:23 PM	57° 20' 047 N	127° 97' 377 W	1412.4	606655	6356142	Fernihydrite	3	Rectorite	3	Kaolinite WX	3	Mg-illite	2	Goethite	2					2204.77	2204.77	1.782	915.372	INV		0.725	1.081	2347.1	Adam LaRiviere	clay	
30102_Lawyers2018_Halos9andard-Clays-S_30102_0177.ASD	S_30102_0177	9/12/2018 1:41:20 PM	57° 20' 047 N	127° 97' 377 W	1415.7	606611	6356138	Fernihydrite	3	Rectorite	3	K-illite	3	Kaolinite WX	2							2198.43	2198.43	INV				0.605	1.086	2343.94	Adam LaRiviere	clay	
30102_Lawyers2018_Halos9andard-Clays-S_30102_0178.ASD	S_30102_0178	9/12/2018 1:43:41 PM	57° 20' 047 N	127° 97' 377 W	1416.3	606547	6356139	Fernihydrite	3	Beidellite	3	Palygorskite	2	Mg-illite	1	Goethite	2					2206.61	2206.61	2.108	INV	INV		0.485		2347.62	Adam LaRiviere	clay	
30102_Lawyers2018_Halos9andard-Clays-S_30102_0179.ASD	S_30102_0179	9/12/2018 1:44:21 PM	57° 20' 047 N	127° 97' 377 W	1417.3	606399	6356144	Fernihydrite	3	Illite/Smectite	3	Kaolinite WX	3	Goethite	2							2207.53		2.992	906.023				1.037		Adam LaRiviere	clay	
30102_Lawyers2018_Halos9andard-Clays-S_30102_0180.ASD	S_30102_0180	9/12/2018 1:47:13 PM	57° 20' 047 N	127° 97' 377 W	1419.5	606346	6356139	Jarosite	3	Montmorillonite	3	Paragonite	3	Goethite	2							2207.93		2.09	920.341			0.471			Adam LaRiviere	clay	
30102_Lawyers2018_Halos9andard-Clays-S_30102_0181.ASD	S_30102_0181	9/12/2018 1:49:10 PM	57° 20' 047 N	127° 97' 367 W	1425.9	606305	6356149	Fernihydrite	3	Montmorillonite	3	Muscovite	3	Kaolinite PX	1							2206.58	2206.58					0.426	1.032	2347.2	Adam LaRiviere	clay	

| Sample_TSG | Index_TSG | Min1_sTSAS_TSG | Wt1_sTSAS_TSG | Min2_sTSAS_TSG | Wt2_sTSAS_TSG | Error_sTSAS_TSG | kaol_xtal_TSG | kl2161_mean_TSG | kl2181_mean_TSG | w2200_TSG | w2250_TSG | w2350_TSG | width_2200_TSG | width_2350_TSG | Crystallinity_Index_2200_TSG | Muscovite_TSG | Chlorite_2_TSG | Alunite_TSG | White_Mica_NoMix | Kaolinite_NoMix | Chlorite_NoMix | Mineral 1_TSG | Mineral 2_TSG | Mineral 3_TSG | Temp C | pH | Mineral Group | Alteration Assemblage | Commnts | Sample | SampleID | Date | BestLatitude | BestLongitude | BestElevation | UTM_East | UTM_North | MineralName1 | StarRating1 | MineralName2 | StarRating2 | MineralName3 | StarRating3 | MineralName4 | StarRating4 | MineralName5 | StarRating5 | MineralName6 | StarRating6 | MineralName7 | StarRating7 | AlFeMg | AlOH | CSM | Fe3i | Fe3t | FeOH | ISM | Kx | MgOH | sampler | type | add_notes |
|---|---|---

Sample_TSG	Index_TSG	Min1_sTSAS_TSG	Wt1_sTSAS_TSG	Min2_sTSAS_TSG	Wt2_sTSAS_TSG	Error_sTSAS_TSG	kaol_xtal_TSG	kl2161_mean_TSG	kl2181_mean_TSG	w2200_TSG	w2250_TSG	w2350_TSG	width_2200_TSG	width_2350_TSG	Crystallinity_Index_2200_TSG	Muscovite_TSG	Chlorite_2_TSG	Alunite_TSG	White_Mica_NoMix	Kaolinite_NoMix	Chlorite_NoMix	Mineral 1_TSG	Mineral 2_TSG	Mineral 3_TSG	Temp C	pH	Mineral Group	Alteration Assemblage	Comments
30102_Lawyers2018_HaloStandard-Clays-S_30102_0203.ASD	FSFR.30102.Int5.0sec Lawyers2018	0.525	Muscovite	0.475	Dickite	152.81	1.89	0.962	0.928	2207.2	NULL	2352.92	28.235	33.812	0.234	2207.2	2352.92					White Mica	Kaolinite?	Dickite?	200-300	neutral	Illite	Argillic	
30102_Lawyers2018_HaloStandard-Clays-S_30102_0204.ASD	FSFR.30102.Int5.0sec Lawyers2018	0.574	Dickite	0.426	Muscovite	110.01	1.89	0.962	0.928	2206.99	2243.88	2351.38	29.714	29.924	0.257	2206.99	2351.38					White Mica	Kaolinite?	Dickite?	200-300	neutral	Illite	Argillic	
30102_Lawyers2018_HaloStandard-Clays-S_30102_0205.ASD	FSFR.30102.Int5.0sec Lawyers2018	0.509	Dickite	0.491	Muscovite	113.65	1.893	0.964	0.929	2207.15	NULL	2351.41	28.235	34.068	0.24	2207.15	2351.41					White Mica	Kaolinite?	Dickite?	200-300	neutral	Illite	Argillic	
30102_Lawyers2018_HaloStandard-Clays-S_30102_0206.ASD	FSFR.30102.Int5.0sec Lawyers2018	0.533	Dickite	0.467	Muscovite	102.87	1.898	0.966	0.933	2207.04	NULL	2351.61	28.746	32.432	0.256	2207.04	2351.61					White Mica	Kaolinite?	Dickite?	200-300	neutral	Illite	Argillic	
30102_Lawyers2018_HaloStandard-Clays-S_30102_0207.ASD	FSFR.30102.Int5.0sec Lawyers2018	0.548	Dickite	0.452	Muscovite	169.14	1.921	0.973	0.948	2207.24	NULL	2351.94	27.574	35.924	0.194	2207.24	2351.94					White Mica	Kaolinite?	Dickite?	200-300	neutral	Illite	Argillic	
30102_Lawyers2018_HaloStandard-Clays-S_30102_0208.ASD	FSFR.30102.Int5.0sec Lawyers2018	0.372	Kaolinite-WX	0.315	77.697	1.838	0.939	0.899	2207.2	NULL	2352.54	28.954	28.667	0.287	2207.2	2352.54						Kaolinite	White Mica?	Dickite?	<150-200	acidic	Kaolinite	Advanced Argillic	
30102_Lawyers2018_HaloStandard-Clays-S_30102_0209.ASD	FSFR.30102.Int5.0sec Lawyers2018	0.366	Dickite	0.325	73.857	1.877	0.957	0.92	2207	NULL	2350.4	29.472	26.001	0.28	2207	2350.4						Kaolinite	White Mica?	Dickite?	<150-200	acidic	Kaolinite	Advanced Argillic	
30102_Lawyers2018_HaloStandard-Clays-S_30102_0210.ASD	FSFR.30102.Int5.0sec Lawyers2018	0.586	Dickite	0.414	103.4	1.847	0.947	0.9	2206.9	NULL	2351.07	30.216	33.754	0.333	2206.9	2351.07						Kaolinite	White Mica	Dickite?	<150-200	acidic	Kaolinite	Advanced Argillic	
30102_Lawyers2018_HaloStandard-Clays-S_30102_0211.ASD	FSFR.30102.Int5.0sec Lawyers2018	0.545	Dickite	0.455	98.63	1.791	0.927	0.863	2206.62	NULL	2350.36	31.543	37.105	0.394	2206.62	2350.36						Kaolinite	White Mica	Dickite?	<150-200	acidic	Kaolinite	Advanced Argillic	
30102_Lawyers2018_HaloStandard-Clays-S_30102_0212.ASD	FSFR.30102.Int5.0sec Lawyers2018	0.382	Dickite	0.375	76.864	1.756	0.912	0.844	2206.84	NULL	2352.2	30.961	31.852	0.411	2206.84	2352.2						Kaolinite	White Mica	Dickite?	<150-200	acidic	Kaolinite	Advanced Argillic	
30102_Lawyers2018_HaloStandard-Clays-S_30102_0213.ASD	FSFR.30102.Int5.0sec Lawyers2018	0.444	Kaolinite-WX	0.304	Paragonite	56.384	1.593	0.846	0.747	2206.22	NULL	2352.44	33.378	31.34	0.716	2206.22	2352.44					Kaolinite	White Mica	Dickite?	<150-200	acidic	Kaolinite	Advanced Argillic	
30102_Lawyers2018_HaloStandard-Clays-S_30102_0214.ASD	FSFR.30102.Int5.0sec Lawyers2018	0.42	Kaolinite-WX	0.347	Paragonite	83.623	1.787	0.92	0.867	2206.88	NULL	2352.37	31.625	38.9	0.361	2206.88	2352.37					Kaolinite	White Mica	Dickite?	<150-200	acidic	Kaolinite	Advanced Argillic	
30102_Lawyers2018_HaloStandard-Clays-S_30102_0215.ASD	FSFR.30102.Int5.0sec Lawyers2018	0.7	Montmorillonite	0.3	151.06	1.664	0.907	0.757	2195.91	NULL	2343.02	33.353	38.646	0.491	2195.91	2343.02			Yes				White Mica			200-300	neutral	Illite	Argillic	
30102_Lawyers2018_HaloStandard-Clays-S_30102_0216.ASD	FSFR.30102.Int5.0sec Lawyers2018	0.473	Kaolinite-WX	0.323	Paragonite	87.848	1.691	0.879	0.812	2207.01	2261.43	2351.8	32.342	28.152	0.501	2207.01	2351.8					Kaolinite	White Mica	Jarosite	<150-200	acidic	Kaolinite	Advanced Argillic	
30102_Lawyers2018_HaloStandard-Clays-S_30102_0217.ASD	FSFR.30102.Int5.0sec Lawyers2018	0.727	Dickite	0.273	84.656	1.867	0.961	0.906	2205.93	NULL	2346.84	32.271	35.741	0.406	2205.93	2346.84						Montmorillonite	White Mica	Kaolinite?	0-150	neutral	Smectite	Argillic	
30102_Lawyers2018_HaloStandard-Clays-S_30102_0218.ASD	FSFR.30102.Int5.0sec Lawyers2018	0.62	Kaolinite-PX	0.38	63.588	1.908	0.971	0.937	2206.2	NULL	2349.02	29.614	38.362	0.293	2206.2	2349.02						Montmorillonite	White Mica	Kaolinite?	0-150	neutral	Smectite	Argillic	
30102_Lawyers2018_HaloStandard-Clays-S_30102_0219.ASD	FSFR.30102.Int5.0sec Lawyers2018	0.597	Dickite	0.403	90.751	1.922	0.976	0.946	2206.77	NULL	2350.82	29.328	33.996	0.25	2206.77	2350.82						Montmorillonite	White Mica	Kaolinite	0-150	neutral	Smectite	Argillic	
30102_Lawyers2018_HaloStandard-Clays-S_30102_0220.ASD	FSFR.30102.Int5.0sec Lawyers2018	0.515	Chlorite-FeMg	0.265	Muscovite	70.691	1.943	0.983	0.96	2205.32	2250.22	2340.74	26.492	38.222	0.381	2205.32	2340.74			Yes		Chlorite	Montmorillonite	White Mica	0-300	neutral	Mica	Propylitic	
30102_Lawyers2018_HaloStandard-Clays-S_30102_0221.ASD	FSFR.30102.Int5.0sec Lawyers2018	0.687	Dickite	0.313	72.959	1.886	0.967	0.918	2206.37	NULL	2348.44	32.24	34.646	0.359	2206.37	2348.44						Montmorillonite	Kaolinite	White Mica	0-150	neutral	Smectite	Argillic	
30102_Lawyers2018_HaloStandard-Clays-S_30102_0222.ASD	FSFR.30102.Int5.0sec Lawyers2018	0.585	Muscovite	0.415	Kaolinite-PX	78.174	1.91	0.973	0.937	2206.85	NULL	2350.05	28.353	35.278	0.315	2206.85	2350.05					Montmorillonite	Kaolinite	White Mica	0-150	neutral	Smectite	Argillic	
30102_Lawyers2018_HaloStandard-Clays-S_30102_0223.ASD	FSFR.30102.Int5.0sec Lawyers2018	0.527	Montmorillonite	0.29	64.524	1.689	0.908	0.781	2192.41	NULL	2341.1	35.674	38.876	0.611	2192.43	2341.1							White Mica	Smectite	200-300	neutral	Illite	Argillic	

Sample	SampleID	Date	BestLatitude	BestLongitude	BestElevation	UTM_East	UTM_North	MineralName1	StarRating1	MineralName2	StarRating2	MineralName3	StarRating3	MineralName4	StarRating4	MineralName5	StarRating5	MineralName6	StarRating6	MineralName7	StarRating7	AlPerMg	AlOH	CSM	Fe3i	Fe3t	FeOH	ISM	Kx	MgOH	sampler	type	add_notes
30102_Lawyers2018_HaloStandard-Clays-S_30102_0203.ASD	S_30102_0203	9/12/2018 4:49:31 PM	57° 20' 04" N	127° 9' 37" W	1419.7	607054	6356236	Kaolinite PX	3	K-illite	2	VNIR - No match	3									2207.27	2207.27								Adam LaRiviere	clay	
30102_Lawyers2018_HaloStandard-Clays-S_30102_0204.ASD	S_30102_0204	9/12/2018 4:51:09 PM	57° 20' 04" N	127° 9' 37" W	1421.2	607096	6356240	Kaolinite PX	3	Palygorskite	2	VNIR - No match	3									2207.09	2207.09						1.03	2382.96	Adam LaRiviere	clay	
30102_Lawyers2018_HaloStandard-Clays-S_30102_0205.ASD	S_30102_0205	9/12/2018 4:52:38 PM	57° 20' 04" N	127° 9' 37" W	1415	607146	6356239	Kaolinite PX	3	Mg-illite	2	VNIR - No match	3									2207.24	2207.24						0.891	1.032	2352.34	Adam LaRiviere	clay	
30102_Lawyers2018_HaloStandard-Clays-S_30102_0206.ASD	S_30102_0206	9/12/2018 5:00:54 PM	57° 20' 04" N	127° 9' 37" W	1417	607154	6356350	Beidellite	3	VNIR - No match	3											2207.14	2207.14				INV				Adam LaRiviere	clay	
30102_Lawyers2018_HaloStandard-Clays-S_30102_0207.ASD	S_30102_0207	9/12/2018 5:02:33 PM	57° 20' 04" N	127° 9' 37" W	1418.6	607104	6356340	Beidellite	3	VNIR - No match	3											2207.33	2207.33				INV				Adam LaRiviere	clay	
30102_Lawyers2018_HaloStandard-Clays-S_30102_0208.ASD	S_30102_0208	9/12/2018 5:07:45 PM	57° 20' 04" N	127° 9' 37" W	1417	607054	6356332	Ferrihydrite	3	Kaolinite PX	3	Goethite	2									2207.26			2.073	INV			1.036		Adam LaRiviere	clay	
30102_Lawyers2018_HaloStandard-Clays-S_30102_0209.ASD	S_30102_0209	9/12/2018 5:08:20 PM	57° 20' 04" N	127° 9' 37" W	1419.8	607008	6356347	Ferrihydrite	3	Kaolinite PX	3	Mg-illite	2	Goethite	2							2207.13	2207.13		2.156	INV			0.805	1.034	2350.39	Adam LaRiviere	clay	
30102_Lawyers2018_HaloStandard-Clays-S_30102_0210.ASD	S_30102_0210	9/12/2018 5:10:10 PM	57° 20' 04" N	127° 9' 37" W	1414.8	606959	6356337	Beidellite	3	Phengite	2	VNIR - No match	3									2207.03	2207.03				INV		0.872		Adam LaRiviere	clay	
30102_Lawyers2018_HaloStandard-Clays-S_30102_0211.ASD	S_30102_0211	9/12/2018 5:11:45 PM	57° 20' 04" N	127° 9' 37" W	1420.4	606902	6356337	Ferrihydrite	3	Beidellite	3	Dickite	2	Goethite	3							2206.75	2206.75		2.127	894.003	INV					Adam LaRiviere	clay	
30102_Lawyers2018_HaloStandard-Clays-S_30102_0212.ASD	S_30102_0212	9/12/2018 5:13:05 PM	57° 20' 04" N	127° 9' 37" W	1421.2	606849	6356343	Ferrihydrite	3	Kaolinite PX	3	K-illite	2	Goethite	3							2206.97	2206.97		2.162	885.156			1.07	1.066	2352.67	Adam LaRiviere	clay	
30102_Lawyers2018_HaloStandard-Clays-S_30102_0213.ASD	S_30102_0213	9/12/2018 5:14:46 PM	57° 20' 04" N	127° 9' 37" W	1412.1	606159	6356192	Hematite	3	Beidellite	3	Goethite	2									2206.44	2206.44		4.191	893.72	INV					Carla Gonzalez	clay	
30102_Lawyers2018_HaloStandard-Clays-S_30102_0214.ASD	S_30102_0214	9/12/2018 5:17:33 PM	57° 20' 04" N	127° 9' 37" W	1416.1	606103	6356188	Kaolinite PX	3	K-illite	3	VNIR - No match	3									2207.1	2207.1						0.983	1.049	2381.37	Carla Gonzalez	clay	
30102_Lawyers2018_HaloStandard-Clays-S_30102_0215.ASD	S_30102_0215	9/12/2018 5:18:41 PM	57° 20' 04" N	127° 9' 37" W	1415.8	606047	6356190	Ferrihydrite	3	Goethite	2											2195.88	2195.88		1.848	INV			1.634		2343.56	Carla Gonzalez	clay	
30102_Lawyers2018_HaloStandard-Clays-S_30102_0216.ASD	S_30102_0216	9/12/2018 5:20:38 PM	57° 20' 04" N	127° 9' 37" W	1417.7	606002	6356184	Ferrihydrite	3	K-illite	3	Jarosite	2									2207.24	2207.24		2.078	908.224			1.006	1.066	2382.57	Carla Gonzalez	clay	
30102_Lawyers2018_HaloStandard-Clays-S_30102_0217.ASD	S_30102_0217	9/12/2018 5:22:16 PM	57° 20' 04" N	127° 9' 37" W	1417.5	605960	6356191	Ferrihydrite	3	Beidellite	3	Mg-illite	2	Goethite	2							2206.09	2206.09		2.227	INV	INV		0.574		2346.49	Carla Gonzalez	clay	
30102_Lawyers2018_HaloStandard-Clays-S_30102_0218.ASD	S_30102_0218	9/12/2018 5:24:17 PM	57° 20' 04" N	127° 9' 37" W	1421.2	605897	6356178	Ferrihydrite	3	Beidellite	3	Mg-illite	2									2206.31	2206.31				INV		0.601		2349.05	Carla Gonzalez	clay	
30102_Lawyers2018_HaloStandard-Clays-S_30102_0219.ASD	S_30102_0219	9/12/2018 5:26:44 PM	57° 20' 04" N	127° 9' 37" W	1417.9	605848	6356180	Ferrihydrite	3	Beidellite	3	Palygorskite	2	Goethite	1							2206.86	2206.86		2.11	INV	INV				2351.03	Carla Gonzalez	clay	
30102_Lawyers2018_HaloStandard-Clays-S_30102_0220.ASD	S_30102_0220	9/12/2018 5:28:54 PM	57° 20' 04" N	127° 9' 37" W	1415.4	605759	6356181	Heulandite	3	Muscovite	2	FeMgChlorite	1	Kaolinite PX	1	VNIR - No match	3					2205.53	2205.53	0.426			2249.45	0.387	1.021	2340.83	Carla Gonzalez	rock	
30102_Lawyers2018_HaloStandard-Clays-S_30102_0221.ASD	S_30102_0221	9/12/2018 5:30:17 PM	57° 20' 04" N	127° 9' 37" W	1418.4	605705	6356182	Ferrihydrite	3	Illite/Smectite	3	Dickite	2	Goethite	2							2206.56			2.479	INV						Carla Gonzalez	clay	
30102_Lawyers2018_HaloStandard-Clays-S_30102_0222.ASD	S_30102_0222	9/12/2018 5:31:58 PM	57° 20' 04" N	127° 9' 37" W	1408	605652	6356186	Illite/Smectite	3	Dickite	2	VNIR - No match	3									2206.95									Carla Gonzalez	clay	
30102_Lawyers2018_HaloStandard-Clays-S_30102_0223.ASD	S_30102_0223	9/12/2018 5:33:44 PM	57° 20' 04" N	127° 9' 37" W	1416.1	607145	6356287	Ferrihydrite	3	Rectorite	3	Muscovite	3	Jarosite	1							2192.4	2192.4	INV	1.913	902.112			0.659		2342.75	Carla Gonzalez	clay	

| Sample_TSG | Index_TSG | Min1_sTSAS_TSG | Wt1_sTSAS_TSG | Min2_sTSAS_TSG | Wt2_sTSAS_TSG | Error_sTSAS_TSG | kaol_xtal_TSG | k2161_mean_TSG | k2181_mean_TSG | w2200_TSG | w2250_TSG | w2350_TSG | width_2200_TSG | width_2350_TSG | Crystallinity_Index_2200_TSG | Muscovite_TSG | Chlorite_2_TSG | Alunite_TSG | White_Mica_NoMix | Kaolinite_NoMix | Chlorite_NoMix | Mineral 1_TSG | Mineral 2_TSG | Mineral 3_TSG | Temp C | pH | Mineral Group | Alteration Assemblage | Comments | Sample | SampleID | Date | BestLatitude | BestLongitude | BestElevation | UTM_East | UTM_North | MineralName1 | StarRating1 | MineralName2 | StarRating2 | MineralName3 | StarRating3 | MineralName4 | StarRating4 | MineralName5 | StarRating5 | MineralName6 | StarRating6 | MineralName7 | StarRating7 | AlFeMg | AlOH | CSM | Fe3i | Fe3t | FeOH | ISM | Kx | MgOH | sampler | type | add_notes |
|---|---|---

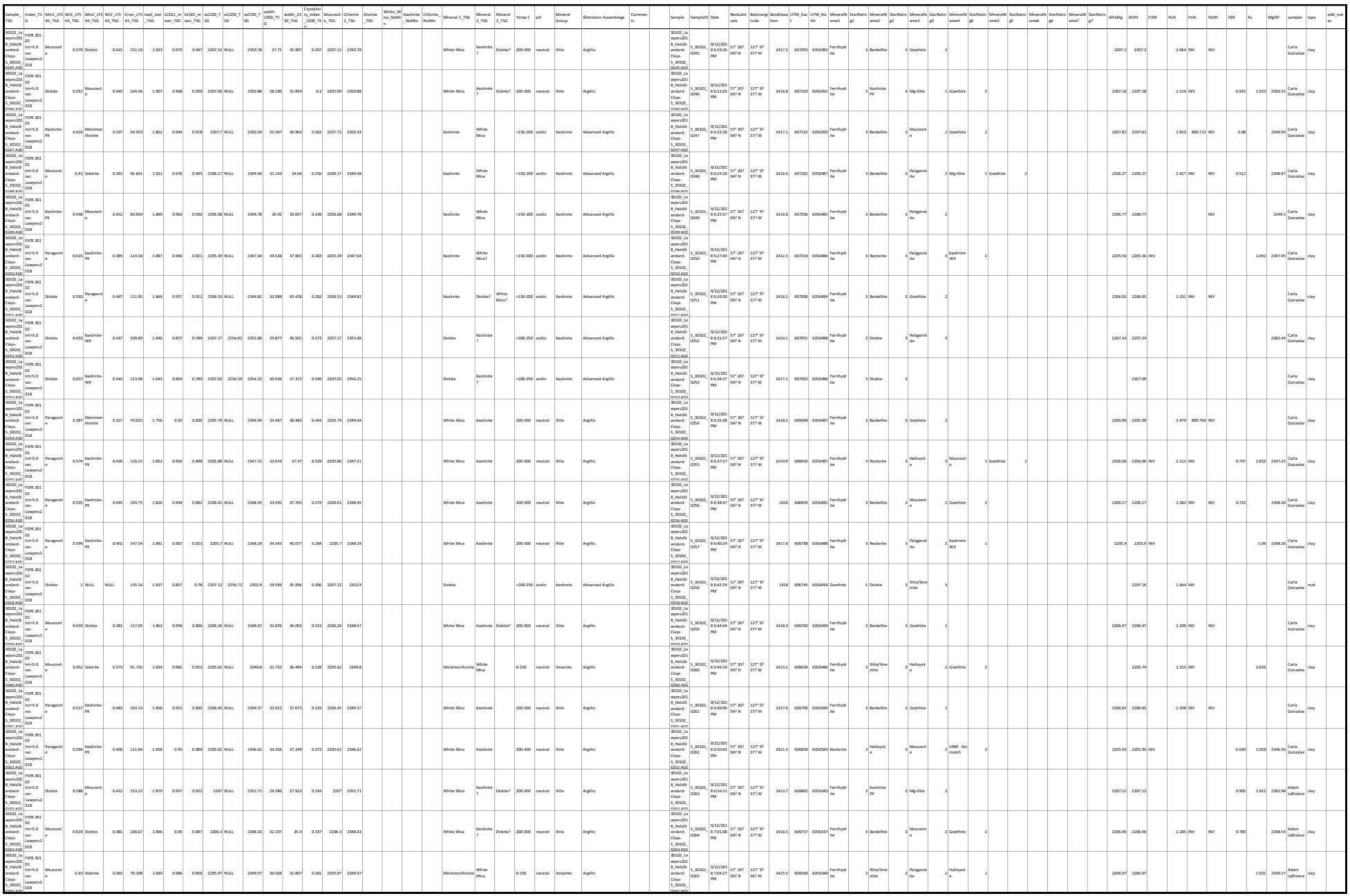

Sample_TSG	Index_TSG	Min1_sTSAS_TSG	Wt1_sTSAS_TSG	Min2_sTSAS_TSG	Wt2_sTSAS_TSG	Error_sTSAS_TSG	kaol_xtal_TSG	k2161_mean_TSG	k2181_mean_TSG	w2200_TSG	w2250_TSG	w2350_TSG	width_2200_TSG	width_2350_TSG	Crystallinity_Index_2200_TSG	Muscovite_TSG	Chlorite_2_TSG	Alunite_TSG	White_Mica_NoMix	Kaolinite_NoMix	Chlorite_NoMix	Mineral 1_TSG	Mineral 2_TSG	Mineral 3_TSG	Temp C	pH	Mineral Group	Alteration Assemblage	Comments
30102_Lawyers2018_Halos9andard-Clays-S_30102_0245.ASD	FSFR.30102 Int=5.0 sec Lawyers2018	Muscovite	0.579	Dickite	0.421	151.19	1.923	0.975	0.947	2207.12	NULL	2350.78	27.71	35.997	0.207	2207.12	2350.78					White Mica	Kaolinite?	Dickite?	200-300	neutral	Illite	Argillic	
30102_Lawyers2018_Halos9andard-Clays-S_30102_0246.ASD	FSFR.30102 Int=5.0 sec Lawyers2018	Dickite	0.557	Muscovite	0.443	164.46	1.907	0.968	0.939	2207.09	NULL	2350.88	28.196	31.894	0.2	2207.09	2350.88					White Mica	Kaolinite?	Dickite?	200-300	neutral	Illite	Argillic	
30102_Lawyers2018_Halos9andard-Clays-S_30102_0247.ASD	FSFR.30102 Int=5.0 sec Lawyers2018	Kaolinite-PX	0.419	Montmorillonite	0.297	59.353	1.862	0.944	0.918	2207.7	NULL	2350.34	25.567	39.964	0.362	2207.72	2350.34					Kaolinite	White Mica		<150-200	acidic	Kaolinite	Advanced Argillic	
30102_Lawyers2018_Halos9andard-Clays-S_30102_0248.ASD	FSFR.30102 Int=5.0 sec Lawyers2018	Muscovite	0.41	Siderite	0.363	92.641	1.921	0.976	0.945	2206.17	NULL	2349.44	31.143	34.04	0.256	2206.17	2349.44					Kaolinite	White Mica		<150-200	acidic	Kaolinite	Advanced Argillic	
30102_Lawyers2018_Halos9andard-Clays-S_30102_0249.ASD	FSFR.30102 Int=5.0 sec Lawyers2018	Kaolinite-PX	0.548	Muscovite	0.452	60.904	1.899	0.963	0.936	2206.68	NULL	2349.78	26.92	33.057	0.339	2206.68	2349.78					Kaolinite	White Mica		<150-200	acidic	Kaolinite	Advanced Argillic	
30102_Lawyers2018_Halos9andard-Clays-S_30102_0250.ASD	FSFR.30102 Int=5.0 sec Lawyers2018	Paragonite	0.615	Kaolinite-PX	0.385	114.58	1.887	0.966	0.921	2205.39	NULL	2347.64	34.528	37.993	0.303	2205.39	2347.64					Kaolinite	White Mica?		<150-200	acidic	Kaolinite	Advanced Argillic	
30102_Lawyers2018_Halos9andard-Clays-S_30102_0251.ASD	FSFR.30102 Int=5.0 sec Lawyers2018	Dickite	0.533	Paragonite	0.467	111.95	1.869	0.957	0.912	2206.53	NULL	2349.82	32.089	43.428	0.282	2206.53	2349.82					Kaolinite	Dickite?	White Mica?	<150-200	acidic	Kaolinite	Advanced Argillic	
30102_Lawyers2018_Halos9andard-Clays-S_30102_0252.ASD	FSFR.30102 Int=5.0 sec Lawyers2018	Dickite	0.653	Kaolinite-WX	0.347	109.89	1.646	0.857	0.789	2207.17	2256.81	2353.86	29.877	40.501	0.373	2207.17	2353.86					Dickite	Kaolinite?		<200-250	acidic	Kaolinite	Advanced Argillic	
30102_Lawyers2018_Halos9andard-Clays-S_30102_0253.ASD	FSFR.30102 Int=5.0 sec Lawyers2018	Dickite	0.657	Kaolinite-WX	0.343	113.98	1.643	0.854	0.789	2207.02	2256.59	2354.25	30.026	37.372	0.349	2207.02	2354.25					Dickite	Kaolinite?		<200-250	acidic	Kaolinite	Advanced Argillic	
30102_Lawyers2018_Halos9andard-Clays-S_30102_0254.ASD	FSFR.30102 Int=5.0 sec Lawyers2018	Paragonite	0.387	Montmorillonite	0.327	74.025	1.756	0.92	0.836	2205.79	NULL	2349.04	33.467	38.483	0.464	2205.79	2349.04					White Mica	Kaolinite		200-300	neutral	Illite	Argillic	
30102_Lawyers2018_Halos9andard-Clays-S_30102_0255.ASD	FSFR.30102 Int=5.0 sec Lawyers2018	Paragonite	0.574	Kaolinite-PX	0.426	116.21	1.852	0.954	0.898	2205.86	NULL	2347.21	33.674	37.37	0.329	2205.86	2347.21					White Mica	Kaolinite		200-300	neutral	Illite	Argillic	
30102_Lawyers2018_Halos9andard-Clays-S_30102_0256.ASD	FSFR.30102 Int=5.0 sec Lawyers2018	Paragonite	0.555	Kaolinite-PX	0.445	104.75	1.826	0.944	0.882	2206.01	NULL	2348.45	33.545	37.703	0.374	2206.01	2348.45					White Mica	Kaolinite		200-300	neutral	Illite	Argillic	
30102_Lawyers2018_Halos9andard-Clays-S_30102_0257.ASD	FSFR.30102 Int=5.0 sec Lawyers2018	Paragonite	0.599	Kaolinite-PX	0.401	147.54	1.891	0.967	0.923	2205.7	NULL	2348.29	34.343	40.077	0.284	2205.7	2348.29					White Mica	Kaolinite		200-300	neutral	Illite	Argillic	
30102_Lawyers2018_Halos9andard-Clays-S_30102_0258.ASD	FSFR.30102 Int=5.0 sec Lawyers2018	Dickite	1	NULL	NULL	135.34	1.637	0.857	0.78	2207.12	2256.72	2302.9	29.599	35.936	0.396	2207.12	2353.9					Dickite			<200-250	acidic	Kaolinite	Advanced Argillic	
30102_Lawyers2018_Halos9andard-Clays-S_30102_0259.ASD	FSFR.30102 Int=5.0 sec Lawyers2018	Muscovite	0.619	Dickite	0.381	117.05	1.862	0.956	0.906	2206.26	NULL	2348.67	32.876	36.003	0.323	2206.26	2348.67					White Mica	Kaolinite	Dickite?	200-300	neutral	Illite	Argillic	
30102_Lawyers2018_Halos9andard-Clays-S_30102_0260.ASD	FSFR.30102 Int=5.0 sec Lawyers2018	Muscovite	0.452	Siderite	0.373	91.716	1.934	0.981	0.953	2205.62	NULL	2349.8	31.732	36.494	0.228	2205.62	2349.8					Montmorillonite	White Mica		0-150	neutral	Smectite	Argillic	
30102_Lawyers2018_Halos9andard-Clays-S_30102_0261.ASD	FSFR.30102 Int=5.0 sec Lawyers2018	Paragonite	0.517	Kaolinite-PX	0.483	103.14	1.856	0.951	0.905	2206.45	NULL	2349.37	32.912	37.673	0.329	2206.45	2349.37					White Mica	Kaolinite		200-300	neutral	Illite	Argillic	
30102_Lawyers2018_Halos9andard-Clays-S_30102_0262.ASD	FSFR.30102 Int=5.0 sec Lawyers2018	Paragonite	0.594	Kaolinite-PX	0.406	111.84	1.838	0.95	0.889	2205.62	NULL	2346.62	34.256	37.249	0.373	2205.62	2346.62					White Mica	Kaolinite		200-300	neutral	Illite	Argillic	
30102_Lawyers2018_Halos9andard-Clays-S_30102_0263.ASD	FSFR.30102 Int=5.0 sec Lawyers2018	Dickite	0.588	Muscovite	0.412	153.22	1.879	0.957	0.922	2207	NULL	2351.71	29.396	27.923	0.243	2207	2351.71					White Mica	Kaolinite?	Dickite?	200-300	neutral	Illite	Argillic	
30102_Lawyers2018_Halos9andard-Clays-S_30102_0264.ASD	FSFR.30102 Int=5.0 sec Lawyers2018	Muscovite	0.619	Dickite	0.381	106.67	1.846	0.95	0.897	2206.3	NULL	2348.33	32.197	35.9	0.337	2206.3	2348.33					White Mica	Kaolinite?	Dickite?	200-300	neutral	Illite	Argillic	
30102_Lawyers2018_Halos9andard-Clays-S_30102_0265.ASD	FSFR.30102 Int=5.0 sec Lawyers2018	Muscovite	0.43	Siderite	0.383	70.198	1.939	0.984	0.956	2205.97	NULL	2349.57	30.504	32.007	0.281	2205.97	2349.57					Montmorillonite	White Mica		0-150	neutral	Smectite	Argillic	

Sample	SampleID	Date	BestLatitude	BestLongitude	BestElevation	UTM_East	UTM_North	MineralName1	StarRating1	MineralName2	StarRating2	MineralName3	StarRating3	MineralName4	StarRating4	MineralName5	StarRating5	MineralName6	StarRating6	MineralName7	StarRating7	AlFeMg	AlOH	CSM	Fe3i	Fe3t	FeOH	ISM	Kx	MgOH	sampler	type	add_notes
30102_Lawyers2018_Halos9andard-Clays-S_30102_0245.ASD	S_30102_0245	9/12/2018 6:19:26 PM	57° 20' 04? N	127° 9' 37? W	1417.2	607055	6356383	Fernhydrite	3	Beidellite	3	Goethite	2									2207.2	2207.2		2.064	INV	INV				Carla Gonzalez	clay	
30102_Lawyers2018_Halos9andard-Clays-S_30102_0246.ASD	S_30102_0246	9/12/2018 6:21:02 PM	57° 20' 04? N	127° 9' 37? W	1416.8	607103	6356391	Fernhydrite	3	Kaolinite PX	3	Mg-illite	1	Goethite	2							2207.18	2207.18		2.114	INV			0.932	1.025	2350.53	Carla Gonzalez	clay	
30102_Lawyers2018_Halos9andard-Clays-S_30102_0247.ASD	S_30102_0247	9/12/2018 6:22:28 PM	57° 20' 04? N	127° 9' 37? W	1417.1	607132	6356393	Fernhydrite	3	Beidellite	3	Muscovite	2	Goethite	2							2207.81	2207.81		1.953	890.712	INV		0.88		2349.93	Carla Gonzalez	clay	
30102_Lawyers2018_Halos9andard-Clays-S_30102_0248.ASD	S_30102_0248	9/12/2018 6:24:20 PM	57° 20' 04? N	127° 9' 37? W	1416.6	607201	6356487	Fernhydrite	3	Beidellite	3	Palygorskite	2	Mg-illite	1	Goethite	2					2206.27	2206.27		2.427	INV	INV		0.512		2348.87	Carla Gonzalez	clay	
30102_Lawyers2018_Halos9andard-Clays-S_30102_0249.ASD	S_30102_0249	9/12/2018 6:25:57 PM	57° 20' 04? N	127° 9' 37? W	1416.8	607256	6356485	Fernhydrite	3	Beidellite	3	Palygorskite	2									2206.77	2206.77				INV				2349.5	Carla Gonzalez	clay	
30102_Lawyers2018_Halos9andard-Clays-S_30102_0250.ASD	S_30102_0250	9/12/2018 6:27:44 PM	57° 20' 04? N	127° 9' 37? W	1412.5	607154	6356486	Fernhydrite	3	Rectorite	3	Palygorskite	3	Kaolinite WX	2							2205.56	2205.56	INV					1.042	2347.95	Carla Gonzalez	clay	
30102_Lawyers2018_Halos9andard-Clays-S_30102_0251.ASD	S_30102_0251	9/12/2018 6:29:30 PM	57° 20' 04? N	127° 9' 37? W	1418.1	607090	6356484	Fernhydrite	3	Beidellite	3	Goethite	2									2206.65	2206.65		2.231	INV	INV				Carla Gonzalez	clay	
30102_Lawyers2018_Halos9andard-Clays-S_30102_0252.ASD	S_30102_0252	9/12/2018 6:31:57 PM	57° 20' 04? N	127° 9' 37? W	1410.1	607051	6356488	Fernhydrite	3	Dickite	3	Palygorskite	3									2207.24	2207.24							2382.44	Carla Gonzalez	clay	
30102_Lawyers2018_Halos9andard-Clays-S_30102_0253.ASD	S_30102_0253	9/12/2018 6:34:27 PM	57° 20' 04? N	127° 9' 37? W	1417.1	607002	6356488	Fernhydrite	3	Dickite	3												2207.09								Carla Gonzalez	clay	
30102_Lawyers2018_Halos9andard-Clays-S_30102_0254.ASD	S_30102_0254	9/12/2018 6:35:38 PM	57° 20' 04? N	127° 9' 37? W	1418.1	606949	6356487	Fernhydrite	3	Beidellite	3	Goethite	2									2205.99	2205.99		2.479	890.764	INV					Carla Gonzalez	clay	
30102_Lawyers2018_Halos9andard-Clays-S_30102_0255.ASD	S_30102_0255	9/12/2018 6:37:17 PM	57° 20' 04? N	127° 9' 37? W	1419.9	606910	6356487	Fernhydrite	3	Rectorite	3	Halloysite	3	Muscovite	1	Goethite	1					2206.06	2206.06	INV	2.112	INV			0.707	1.053	2347.25	Carla Gonzalez	clay	
30102_Lawyers2018_Halos9andard-Clays-S_30102_0256.ASD	S_30102_0256	9/12/2018 6:38:47 PM	57° 20' 04? N	127° 9' 37? W	1418	606854	6356481	Fernhydrite	3	Beidellite	3	Muscovite	2	Goethite	2							2206.17	2206.17		2.282	INV	INV		0.732		2348.26	Carla Gonzalez	clay	
30102_Lawyers2018_Halos9andard-Clays-S_30102_0257.ASD	S_30102_0257	9/12/2018 6:40:24 PM	57° 20' 04? N	127° 9' 37? W	1417.8	606798	6356488	Fernhydrite	3	Rectorite	3	Palygorskite	2	Kaolinite WX	1							2205.9	2205.9	INV					1.04	2348.26	Carla Gonzalez	clay	
30102_Lawyers2018_Halos9andard-Clays-S_30102_0258.ASD	S_30102_0258	9/12/2018 6:42:19 PM	57° 20' 04? N	127° 9' 37? W	1418	606745	6356494	Goethite	3	Dickite	3	Illite/Smectite	3										2207.16		1.664	INV						Carla Gonzalez	rock	
30102_Lawyers2018_Halos9andard-Clays-S_30102_0259.ASD	S_30102_0259	9/12/2018 6:44:44 PM	57° 20' 04? N	127° 9' 37? W	1418.3	606700	6356490	Fernhydrite	3	Beidellite	3	Goethite	1									2206.47	2206.47		2.299	INV	INV				Carla Gonzalez	clay	
30102_Lawyers2018_Halos9andard-Clays-S_30102_0260.ASD	S_30102_0260	9/12/2018 6:46:19 PM	57° 20' 04? N	127° 9' 37? W	1413.1	606639	6356486	Fernhydrite	3	Illite/Smectite	3	Halloysite	2	Goethite	2							2205.74			2.153	INV				1.026		Carla Gonzalez	clay	
30102_Lawyers2018_Halos9andard-Clays-S_30102_0261.ASD	S_30102_0261	9/12/2018 6:49:08 PM	57° 20' 04? N	127° 9' 37? W	1417.6	606796	6356584	Fernhydrite	3	Beidellite	3	Goethite	1									2206.65	2206.65		2.208	INV	INV					Carla Gonzalez	clay	
30102_Lawyers2018_Halos9andard-Clays-S_30102_0262.ASD	S_30102_0262	9/12/2018 6:50:42 PM	57° 20' 04? N	127° 9' 37? W	1421.3	606839	6356583	Rectorite	3	Halloysite	3	Muscovite	2	VNIR - No match	3							2205.93	2205.93	INV				0.693	1.058	2346.56	Carla Gonzalez	clay	
30102_Lawyers2018_Halos9andard-Clays-S_30102_0263.ASD	S_30102_0263	9/12/2018 6:54:31 PM	57° 20' 04? N	127° 9' 37? W	1413.7	606805	6356343	Fernhydrite	3	Kaolinite PX	3	Mg-illite	2									2207.12	2207.12						0.905	1.031	2382.98	Adam LaRiviere	clay	
30102_Lawyers2018_Halos9andard-Clays-S_30102_0264.ASD	S_30102_0264	9/12/2018 7:01:08 PM	57° 20' 04? N	127° 9' 37? W	1416.5	606757	6356337	Fernhydrite	3	Beidellite	3	Muscovite	2	Goethite	2							2206.46	2206.46		2.185	INV	INV		0.789		2348.54	Adam LaRiviere	clay	
30102_Lawyers2018_Halos9andard-Clays-S_30102_0265.ASD	S_30102_0265	9/12/2018 7:04:27 PM	57° 20' 04? N	127° 9' 36? W	1415.5	606500	6356340	Fernhydrite	3	Illite/Smectite	3	Palygorskite	2	Halloysite	1							2206.07	2206.07							1.025	2349.17	Adam LaRiviere	clay	

Sample_TSG	Index_TSG	Min1_sTSAS_TSG	Wt1_sTSAS_TSG	Min2_sTSAS_TSG	Wt2_sTSAS_TSG	Error_sTSAS_TSG	kaol_xtal_TSG	k2161_mean_TSG	k2181_mean_TSG	w2200_TSG	w2250_TSG	w2350_TSG	width_2200_TSG	width_2350_TSG	Crystallinity_Index_2200_TSG	Muscovite_TSG	Chlorite_2_TSG	Alunite_TSG	White_Mica_NoMix	Kaolinite_NoMix	Chlorite_NoMix	Mineral 1_TSG	Mineral 2_TSG	Mineral 3_TSG	Temp C	pH	Mineral Group	Alteration Assemblage	Comments
30102_Lawyers2018_Halos9andard-Clays-S_30102_0266.ASD	FSFR.30102.Int=5.0 sec Lawyers2018	Montmorillonite	0.529	Paragonite	0.248	90.53	1.927	0.983	0.944	2204.65	2257.99	2350.1	31.65	30.327	0.262	2204.65	2350.1					Montmorillonite	Jarosite		0-150	neutral	Smectite	Argillic	
30102_Lawyers2018_Halos9andard-Clays-S_30102_0267.ASD	FSFR.30102.Int=5.0 sec Lawyers2018	Montmorillonite	0.393	Muscovite	0.167	46.54	1.861	0.966	0.895	2206.11	NULL	2347.14	30.405	33.262	0.547	2206.11	2347.14					Montmorillonite	White Mica		0-150	neutral	Smectite	Argillic	
30102_Lawyers2018_Halos9andard-Clays-S_30102_0268.ASD	FSFR.30102.Int=5.0 sec Lawyers2018	Montmorillonite	0.423	Muscovite	0.324	58.454	1.874	0.969	0.905	2206.07	NULL	2345.85	30.358	31.141	0.528	2206.07	2345.85					Montmorillonite	White Mica		0-150	neutral	Smectite	Argillic	
30102_Lawyers2018_Halos9andard-Clays-S_30102_0269.ASD	FSFR.30102.Int=5.0 sec Lawyers2018	Muscovite	0.623	Kaolinite-PX	0.377	78.06	1.906	0.971	0.934	2206.7	NULL	2348.49	29.728	29.541	0.428	2206.7	2348.49					Montmorillonite	White Mica	Kaolinite?	0-150	neutral	Smectite	Argillic	
30102_Lawyers2018_Halos9andard-Clays-S_30102_0270.ASD	FSFR.30102.Int=5.0 sec Lawyers2018	Muscovite	0.53	Kaolinite-PX	0.314	52.44	1.853	0.954	0.9	2207.16	NULL	2346.56	30.322	31.699	0.489	2207.16	2346.56					Montmorillonite	White Mica	Kaolinite?	0-150	neutral	Smectite	Argillic	
30102_Lawyers2018_Halos9andard-Clays-S_30102_0271.ASD	FSFR.30102.Int=5.0 sec Lawyers2018	Muscovite	0.582	Dickite	0.418	99.485	1.912	0.972	0.94	2206.64	NULL	2350.33	29.889	33.923	0.227	2206.64	2350.33					Kaolinite	White Mica		<150-200	acidic	Kaolinite	Advanced Argillic	
30102_Lawyers2018_Halos9andard-Clays-S_30102_0272.ASD	FSFR.30102.Int=5.0 sec Lawyers2018	Muscovite	1	NULL	NULL	108.19	1.868	0.973	0.894	2203.83	NULL	2345.83	32.594	36.801	0.377	2203.83	2345.83		Yes			White Mica			200-300	neutral	Illite	Argillic	
30102_Lawyers2018_Halos9andard-Clays-S_30102_0273.ASD	FSFR.30102.Int=5.0 sec Lawyers2018	Muscovite	0.761	Kaolinite-PX	0.239	68.109	1.897	0.973	0.924	2202.18	NULL	2345.9	32.872	37.171	0.287	2202.18	2345.9					White Mica	Kaolinite		200-300	neutral	Illite	Argillic	
30102_Lawyers2018_Halos9andard-Clays-S_30102_0274.ASD	FSFR.30102.Int=5.0 sec Lawyers2018	Muscovite	0.642	Kaolinite-PX	0.358	59.646	1.888	0.966	0.922	2206.25	NULL	2349.14	31.389	35.454	0.376	2206.25	2349.14					White Mica	Kaolinite		200-300	neutral	Illite	Argillic	
30102_Lawyers2018_Halos9andard-Clays-S_30102_0275.ASD	FSFR.30102.Int=5.0 sec Lawyers2018	Montmorillonite	0.378	Kaolinite-WX	0.36	41.511	1.715	0.891	0.823	2207.15	NULL	2347.24	31.097	42.623	0.662	2207.15	2347.24					White Mica	Kaolinite		200-300	neutral	Illite	Argillic	
30102_Lawyers2018_Halos9andard-Clays-S_30102_0276.ASD	FSFR.30102.Int=5.0 sec Lawyers2018	Dickite	0.659	Muscovite	0.341	87.862	1.758	0.914	0.844	2206.78	NULL	2352.19	30.829	24.529	0.371	2206.78	2352.19					Dickite			<200-250	acidic	Kaolinite	Advanced Argillic	
30102_Lawyers2018_Halos9andard-Clays-S_30102_0277.ASD	FSFR.30102.Int=5.0 sec Lawyers2018	Muscovite	0.728	Dickite	0.272	97.751	1.891	0.968	0.922	2206.02	NULL	2348.22	31.563	31.424	0.316	2206.02	2348.22					White Mica	Dickite?	Kaolinite?	200-300	neutral	Illite	Argillic	
30102_Lawyers2018_Halos9andard-Clays-S_30102_0278.ASD	FSFR.30102.Int=5.0 sec Lawyers2018	Paragonite	0.442	Montmorillonite	0.364	69.468	1.762	0.927	0.835	2204.37	NULL	2344.52	35.213	38.27	0.506	2204.37	2344.52					White Mica	Kaolinite		200-300	neutral	Illite	Argillic	
30102_Lawyers2018_Halos9andard-Clays-S_30102_0279.ASD	FSFR.30102.Int=5.0 sec Lawyers2018	Dickite	0.435	Paragonite	0.327	78.086	1.836	0.944	0.892	2206.71	2256.46	2310.06	31.451	32.671	0.365	2206.71	2349.99					White Mica	Dickite?	Kaolinite?	200-300	neutral	Illite	Argillic	
30102_Lawyers2018_Halos9andard-Clays-S_30102_0280.ASD	FSFR.30102.Int=5.0 sec Lawyers2018	Paragonite	0.417	Dickite	0.296	91.6	1.816	0.942	0.874	2205.82	NULL	2348.55	33.688	36.18	0.363	2205.82	2348.55					White Mica	Dickite?	Kaolinite?	200-300	neutral	Illite	Argillic	
30102_Lawyers2018_Halos9andard-Clays-S_30102_0281.ASD	FSFR.30102.Int=5.0 sec Lawyers2018	Muscovite	0.545	Dickite	0.455	112.26	1.872	0.959	0.912	2206.49	NULL	2349.21	31.906	30.049	0.293	2206.49	2349.21					White Mica	Dickite?	Kaolinite?	200-300	neutral	Illite	Argillic	
30102_Lawyers2018_Halos9andard-Clays-S_30102_0282.ASD	FSFR.30102.Int=5.0 sec Lawyers2018	Muscovite	0.341	Kaolinite-WX	0.335	83.579	1.822	0.933	0.888	2207	NULL	2352.46	30.176	33.876	0.301	2207	2352.46					White Mica	Kaolinite		200-300	neutral	Illite	Argillic	
30102_Lawyers2018_Halos9andard-Clays-S_30102_0283.ASD	FSFR.30102.Int=5.0 sec Lawyers2018	Nacrite	0.597	Kaolinite-WX	0.403	189.76	1.736	0.902	0.834	2206.65	2256.22	2353.05	29.602	35.822	0.285	2206.65	2353.05					Dickite	Kaolinite?		<200-250	acidic	Kaolinite	Advanced Argillic	
30102_Lawyers2018_Halos9andard-Clays-S_30102_0284.ASD	FSFR.30102.Int=5.0 sec Lawyers2018	Dickite	0.384	Muscovite	0.349	66.854	1.78	0.919	0.861	2206.9	NULL	2321.18	31.037	40.325	0.355	2206.9	2351.59					White Mica	Dickite?	Kaolinite?	200-300	neutral	Illite	Argillic	
30102_Lawyers2018_Halos9andard-Clays-S_30102_0285.ASD	FSFR.30102.Int=5.0 sec Lawyers2018	Dickite	0.828	Alunite-Na	0.172	106.38	1.699	0.878	0.821	2207.05	2256.46	2314.5	30.583	34.859	0.344	2207.05	2352.43	1483				Dickite	Alunite?		<200-250	acidic	Kaolinite	Advanced Argillic	
30102_Lawyers2018_Halos9andard-Clays-S_30102_0286.ASD	FSFR.30102.Int=5.0 sec Lawyers2018	Kaolinite-PX	0.458	Paragonite	0.307	67.367	1.864	0.952	0.913	2206.73	NULL	2348.94	31.114	43.704	0.336	2206.73	2348.94					White Mica	Kaolinite		200-300	neutral	Illite	Argillic	

Sample	SampleID	Date	BestLatitude	BestLongitude	BestElevation	UTM_East	UTM_North	MineralName1	StarRating1	MineralName2	StarRating2	MineralName3	StarRating3	MineralName4	StarRating4	MineralName5	StarRating5	MineralName6	StarRating6	MineralName7	StarRating7	AlFeMg	AlOH	CSM	Fe3i	Fe3t	FeOH	ISM	Kx	MgOH	sampler	type	add_notes
30102_Lawyers2018_Halos9andard-Clays-S_30102_0266.ASD	S_30102_0266	9/12/2018 7:06:04 PM	57° 20' 047 N	127° 97' 377 W	1412.9	606686	6356338	Jarosite	3	Montmorillonite	3	Goethite	3										2204.72		1.664	907.956					Adam LaRiviere	clay	
30102_Lawyers2018_Halos9andard-Clays-S_30102_0267.ASD	S_30102_0267	9/12/2018 7:08:41 PM	57° 20' 047 N	127° 97' 377 W	1419.2	606448	6356336	Fernhydrite	3	Montmorillonite	3	Muscovite	3	Goethite	2								2206.08	2206.08	2.24	891.83		0.538		2347.35	Adam LaRiviere	clay	
30102_Lawyers2018_Halos9andard-Clays-S_30102_0268.ASD	S_30102_0268	9/12/2018 7:10:03 PM	57° 20' 047 N	127° 97' 377 W	1413.7	606403	6356332	Fernhydrite	3	Montmorillonite	3	Muscovite	3	Goethite	2								2206.12	2206.12	2.125	894.172		0.489		2345.38	Adam LaRiviere	clay	
30102_Lawyers2018_Halos9andard-Clays-S_30102_0269.ASD	S_30102_0269	9/12/2018 7:12:14 PM	57° 20' 047 N	127° 97' 377 W	1418.9	606208	6356348	Fernhydrite	3	Montmorillonite	3	Kaolinite PX	3	Muscovite	1	Goethite	2						2206.79	2206.79	2.349	INV		0.391	1.033	2347.46	Adam LaRiviere	clay	
30102_Lawyers2018_Halos9andard-Clays-S_30102_0270.ASD	S_30102_0270	9/12/2018 7:13:41 PM	57° 20' 047 N	127° 97' 377 W	1417.5	606034	6356341	Beidellite	3	Mg-illite	3	VNIR - No match	3										2207.28	2207.28			INV	0.55		2346.78	Adam LaRiviere	clay	
30102_Lawyers2018_Halos9andard-Clays-S_30102_0271.ASD	S_30102_0271	9/12/2018 7:15:48 PM	57° 20' 047 N	127° 97' 377 W	1421.5	605946	6356353	Beidellite	3	VNIR - No match	3												2206.77	2206.77			INV				Adam LaRiviere	clay	
30102_Lawyers2018_Halos9andard-Clays-S_30102_0272.ASD	S_30102_0272	9/12/2018 7:17:45 PM	57° 20' 047 N	127° 97' 377 W	1416.4	605849	6356334	Fernhydrite	3	Palygorskite	3												2203.77	2203.77				0.942		2345.46	Adam LaRiviere	clay	
30102_Lawyers2018_Halos9andard-Clays-S_30102_0273.ASD	S_30102_0273	9/12/2018 7:22:26 PM	57° 20' 047 N	127° 97' 377 W	1417.7	605957	6356426	Fernhydrite	3	Rectorite	3	Mg-illite	2	Halloysite	1	Goethite	3						2202.11	2202.11	2.115	INV		0.644	1.046	2347.64	Adam LaRiviere	clay	
30102_Lawyers2018_Halos9andard-Clays-S_30102_0274.ASD	S_30102_0274	9/12/2018 7:24:01 PM	57° 20' 047 N	127° 97' 377 W	1417.9	605997	6356428	Fernhydrite	3	Beidellite	3	Palygorskite	2	Goethite	2								2206.39	2206.39	2.438	902.968	INV			2350.06	Adam LaRiviere	clay	
30102_Lawyers2018_Halos9andard-Clays-S_30102_0275.ASD	S_30102_0275	9/12/2018 7:26:05 PM	57° 20' 047 N	127° 97' 377 W	1416.6	606058	6356428	Fernhydrite	3	Beidellite	3												2207.4	2207.4			INV				Adam LaRiviere	clay	
30102_Lawyers2018_Halos9andard-Clays-S_30102_0276.ASD	S_30102_0276	9/12/2018 7:27:31 PM	57° 20' 047 N	127° 97' 377 W	1419	606249	6356437	Fernhydrite	3	Halloysite	3	Goethite	2										2206.86		1.979	INV			1.066		Adam LaRiviere	clay	
30102_Lawyers2018_Halos9andard-Clays-S_30102_0277.ASD	S_30102_0277	9/12/2018 7:29:11 PM	57° 20' 047 N	127° 97' 377 W	1418.5	606360	6356447	Fernhydrite	3	Beidellite	3	Mg-illite	2	Goethite	2								2206.13	2206.13	2.192	INV	INV	0.658		2348.13	Adam LaRiviere	clay	
30102_Lawyers2018_Halos9andard-Clays-S_30102_0278.ASD	S_30102_0278	9/12/2018 7:30:41 PM	57° 20' 047 N	127° 97' 377 W	1416.9	606749	6356438	Fernhydrite	3	Rectorite	3	Phengite	3	Kaolinite WX	2	Goethite	1						2204.59	INV	1.986	892.714		0.757	1.094		Adam LaRiviere	clay	
30102_Lawyers2018_Halos9andard-Clays-S_30102_0279.ASD	S_30102_0279	9/13/2018 10:09:43 AM	57° 20' 047 N	127° 97' 377 W	1418.1	606804	6356442	Beidellite	3	VNIR - No match	3												2206.86	2206.86			INV				Adam LaRiviere	clay	
30102_Lawyers2018_Halos9andard-Clays-S_30102_0280.ASD	S_30102_0280	9/13/2018 10:21:59 AM	57° 20' 047 N	127° 97' 377 W	1423.1	606848	6356443	Fernhydrite	3	Beidellite	3	Muscovite	2	Goethite	2								2206.01	2206.01	2.126	884.866	INV	0.794		2348.72	Adam LaRiviere	clay	
30102_Lawyers2018_Halos9andard-Clays-S_30102_0281.ASD	S_30102_0281	9/13/2018 10:24:38 AM	57° 20' 047 N	127° 97' 377 W	1413.3	606897	6356444	Fernhydrite	3	Beidellite	3	Goethite	2										2206.65	2206.65	2.055	INV	INV				Adam LaRiviere	clay	
30102_Lawyers2018_Halos9andard-Clays-S_30102_0282.ASD	S_30102_0282	9/13/2018 10:26:22 AM	57° 20' 047 N	127° 97' 377 W	1422.7	606953	6356438	Fernhydrite	3	Kaolinite PX	3	Goethite	3										2207.13		2.018	883.879			1.041		Adam LaRiviere	clay	
30102_Lawyers2018_Halos9andard-Clays-S_30102_0283.ASD	S_30102_0283	9/13/2018 10:28:31 AM	57° 20' 047 N	127° 97' 377 W	1418.9	606997	6356438	Nacrite	3	Rectorite	3	VNIR - No match	3										2206.69	0.597							Adam LaRiviere	clay	
30102_Lawyers2018_Halos9andard-Clays-S_30102_0284.ASD	S_30102_0284	9/13/2018 10:31:12 AM	57° 20' 047 N	127° 97' 377 W	1418.1	607046	6356445	Fernhydrite	3	Halloysite	3	Nacrite	2	Palygorskite	1								2207.01	2207.01					1.055	2382.22	Adam LaRiviere	clay	
30102_Lawyers2018_Halos9andard-Clays-S_30102_0285.ASD	S_30102_0285	9/13/2018 10:33:42 AM	57° 20' 047 N	127° 97' 377 W	1417.4	607094	6356442	Fernhydrite	3	Dickite	3	Palygorskite	3										2207.14	2207.14						2383.04	Adam LaRiviere	clay	
30102_Lawyers2018_Halos9andard-Clays-S_30102_0286.ASD	S_30102_0286	9/13/2018 10:35:45 AM	57° 20' 047 N	127° 97' 377 W	1418.7	607151	6356442	Fernhydrite	3	Beidellite	3												2206.84	2206.84			INV				Adam LaRiviere	clay	

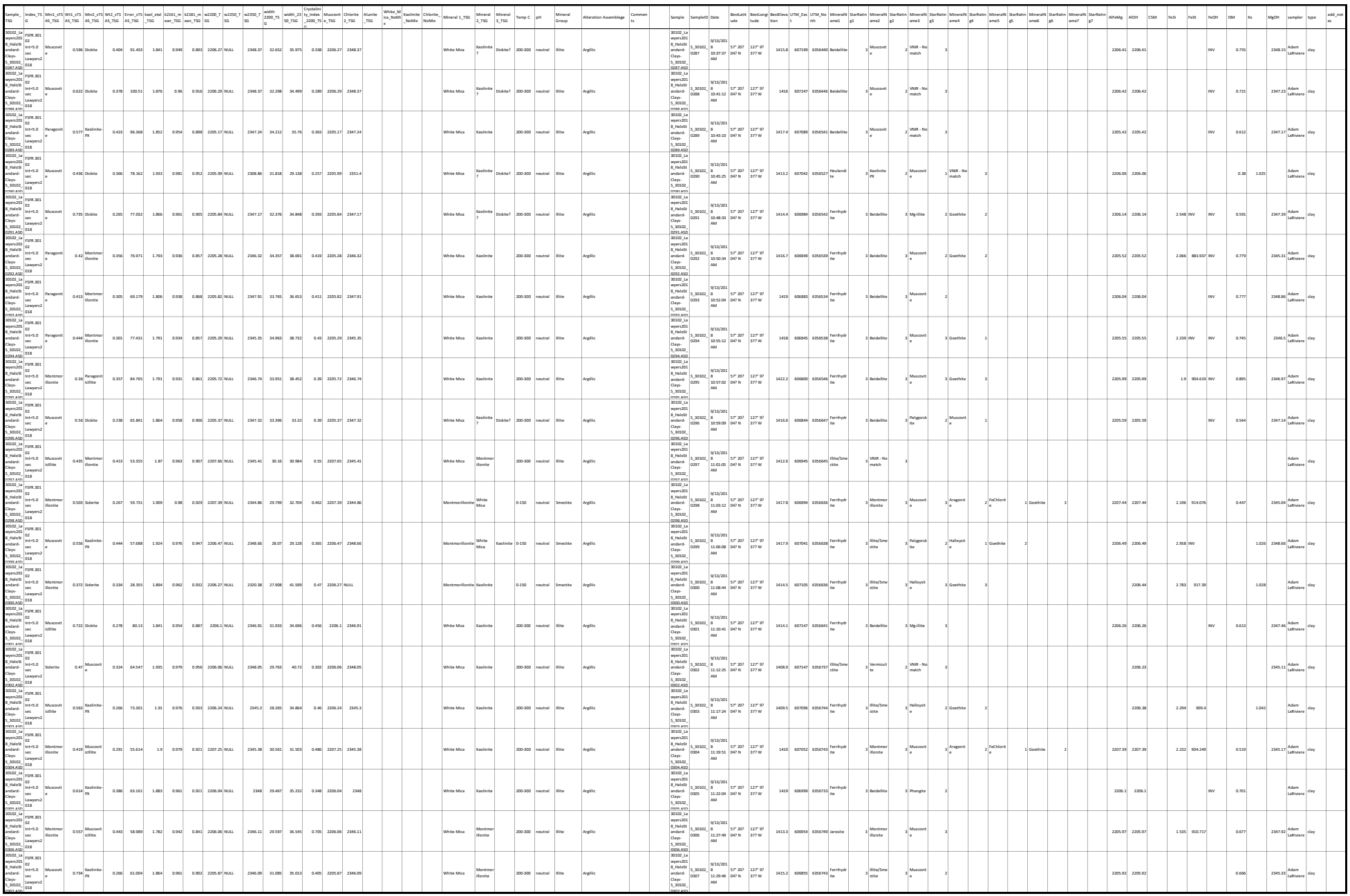

Sample_TSG	Index_TSG	Min1_sTSG	Wt1_sTSG	Min2_sTSG	Wt2_sTSG	Error_sTSG	kaol_xtal_TSG	k2161_mean_TSG	k2181_mean_TSG	w2200_TSG	w2250_TSG	w2350_TSG	width_2200_TSG	width_2350_TSG	Crystallinity_Index_2200_TSG	Muscovite_TSG	Chlorite_2_TSG	Alunite_TSG	White_Mica_NoMix	Kaolinite_NoMix	Chlorite_NoMix	Mineral 1_TSG	Mineral 2_TSG	Mineral 3_TSG	Temp C	pH	Mineral Group	Alteration Assemblage	Comments
30102_Lawyers2018_HaloSmectite-Clays-S_30102_0287.ASD	ESPIR.30102int+5.0 sec Lawyers2018	Muscovite	0.596	Dickite	0.404	91.433	1.841	0.949	0.893	2206.27	NULL	2348.37	32.652	35.975	0.338	2206.27	2348.37					White Mica	Kaolinite?	Dickite?	200-300	neutral	Illite	Argillic	
30102_Lawyers2018_HaloSmectite-Clays-S_30102_0288.ASD	ESPIR.30102int+5.0 sec Lawyers2018	Muscovite	0.622	Dickite	0.378	100.51	1.876	0.96	0.916	2206.29	NULL	2348.37	32.298	34.499	0.289	2206.29	2348.37					White Mica	Kaolinite?	Dickite?	200-300	neutral	Illite	Argillic	
30102_Lawyers2018_HaloSmectite-Clays-S_30102_0289.ASD	ESPIR.30102int+5.0 sec Lawyers2018	Paragonite	0.577	Kaolinite-PX	0.423	96.368	1.852	0.954	0.898	2205.17	NULL	2347.24	34.212	35.76	0.363	2205.17	2347.24					White Mica	Kaolinite		200-300	neutral	Illite	Argillic	
30102_Lawyers2018_HaloSmectite-Clays-S_30102_0290.ASD	ESPIR.30102int+5.0 sec Lawyers2018	Muscovite	0.436	Dickite	0.366	78.162	1.933	0.981	0.952	2205.99	NULL	2308.86	31.818	29.138	0.257	2205.99	2351.4					White Mica	Kaolinite?	Dickite?	200-300	neutral	Illite	Argillic	
30102_Lawyers2018_HaloSmectite-Clays-S_30102_0291.ASD	ESPIR.30102int+5.0 sec Lawyers2018	Muscovite	0.735	Dickite	0.265	77.032	1.866	0.961	0.905	2205.84	NULL	2347.17	32.376	34.848	0.393	2205.84	2347.17					White Mica	Kaolinite?	Dickite?	200-300	neutral	Illite	Argillic	
30102_Lawyers2018_HaloSmectite-Clays-S_30102_0292.ASD	ESPIR.30102int+5.0 sec Lawyers2018	Paragonite	0.42	Montmorillonite	0.356	76.971	1.793	0.936	0.857	2205.28	NULL	2346.32	34.357	38.691	0.419	2205.28	2346.32					White Mica	Kaolinite		200-300	neutral	Illite	Argillic	
30102_Lawyers2018_HaloSmectite-Clays-S_30102_0293.ASD	ESPIR.30102int+5.0 sec Lawyers2018	Paragonite	0.413	Montmorillonite	0.305	69.179	1.806	0.938	0.868	2205.82	NULL	2347.91	33.765	36.653	0.411	2205.82	2347.91					White Mica	Kaolinite		200-300	neutral	Illite	Argillic	
30102_Lawyers2018_HaloSmectite-Clays-S_30102_0294.ASD	ESPIR.30102int+5.0 sec Lawyers2018	Paragonite	0.444	Montmorillonite	0.301	77.431	1.791	0.934	0.857	2205.29	NULL	2345.35	34.963	38.732	0.43	2205.29	2345.35					White Mica	Kaolinite		200-300	neutral	Illite	Argillic	
30102_Lawyers2018_HaloSmectite-Clays-S_30102_0295.ASD	ESPIR.30102int+5.0 sec Lawyers2018	Montmorillonite	0.36	Paragonite\tIllite	0.357	84.765	1.791	0.931	0.861	2205.72	NULL	2346.74	33.951	38.452	0.39	2205.72	2346.74					White Mica	Kaolinite		200-300	neutral	Illite	Argillic	
30102_Lawyers2018_HaloSmectite-Clays-S_30102_0296.ASD	ESPIR.30102int+5.0 sec Lawyers2018	Muscovite	0.56	Dickite	0.238	65.841	1.864	0.958	0.906	2205.37	NULL	2347.32	33.396	33.32	0.39	2205.37	2347.32					White Mica	Kaolinite?	Dickite?	200-300	neutral	Illite	Argillic	
30102_Lawyers2018_HaloSmectite-Clays-S_30102_0297.ASD	ESPIR.30102int+5.0 sec Lawyers2018	Muscovite\tIllite	0.435	Montmorillonite	0.413	53.355	1.87	0.963	0.907	2207.66	NULL	2345.41	30.16	30.984	0.55	2207.65	2345.41					White Mica	Montmorillonite		200-300	neutral	Illite	Argillic	
30102_Lawyers2018_HaloSmectite-Clays-S_30102_0298.ASD	ESPIR.30102int+5.0 sec Lawyers2018	Montmorillonite	0.503	Siderite	0.267	59.731	1.909	0.98	0.929	2207.39	NULL	2344.86	29.799	32.704	0.462	2207.39	2344.86					Montmorillonite	White Mica		0-150	neutral	Smectite	Argillic	
30102_Lawyers2018_HaloSmectite-Clays-S_30102_0299.ASD	ESPIR.30102int+5.0 sec Lawyers2018	Muscovite	0.556	Kaolinite-PX	0.444	57.688	1.924	0.976	0.947	2206.47	NULL	2348.66	28.07	29.128	0.365	2206.47	2348.66					Montmorillonite	White Mica	Kaolinite	0-150	neutral	Smectite	Argillic	
30102_Lawyers2018_HaloSmectite-Clays-S_30102_0300.ASD	ESPIR.30102int+5.0 sec Lawyers2018	Montmorillonite	0.372	Siderite	0.334	28.355	1.894	0.962	0.932	2206.27	NULL	2320.38	27.908	41.599	0.47	2206.27	NULL					Montmorillonite	Kaolinite		0-150	neutral	Smectite	Argillic	
30102_Lawyers2018_HaloSmectite-Clays-S_30102_0301.ASD	ESPIR.30102int+5.0 sec Lawyers2018	Muscovite\tIllite	0.722	Dickite	0.278	80.13	1.841	0.954	0.887	2206.1	NULL	2346.91	31.933	34.696	0.456	2206.1	2346.91					White Mica	Kaolinite		200-300	neutral	Illite	Argillic	
30102_Lawyers2018_HaloSmectite-Clays-S_30102_0302.ASD	ESPIR.30102int+5.0 sec Lawyers2018	Siderite	0.47	Muscovite	0.324	64.547	1.935	0.979	0.956	2206.06	NULL	2348.05	29.763	40.72	0.302	2206.06	2348.05					White Mica	Kaolinite		200-300	neutral	Illite	Argillic	
30102_Lawyers2018_HaloSmectite-Clays-S_30102_0303.ASD	ESPIR.30102int+5.0 sec Lawyers2018	Muscovite\tIllite	0.563	Kaolinite-PX	0.266	73.301	1.91	0.976	0.933	2206.24	NULL	2345.3	28.265	34.864	0.46	2206.24	2345.3					White Mica	Kaolinite		200-300	neutral	Illite	Argillic	
30102_Lawyers2018_HaloSmectite-Clays-S_30102_0304.ASD	ESPIR.30102int+5.0 sec Lawyers2018	Montmorillonite	0.419	Muscovite\tIllite	0.291	55.614	1.9	0.979	0.921	2207.25	NULL	2345.38	30.561	31.503	0.486	2207.25	2345.38					White Mica	Kaolinite		200-300	neutral	Illite	Argillic	
30102_Lawyers2018_HaloSmectite-Clays-S_30102_0305.ASD	ESPIR.30102int+5.0 sec Lawyers2018	Muscovite	0.614	Kaolinite-PX	0.386	63.161	1.883	0.961	0.921	2206.04	NULL	2348	29.467	35.232	0.348	2206.04	2348					White Mica	Kaolinite		200-300	neutral	Illite	Argillic	
30102_Lawyers2018_HaloSmectite-Clays-S_30102_0306.ASD	ESPIR.30102int+5.0 sec Lawyers2018	Montmorillonite	0.557	Muscovite\tIllite	0.443	58.989	1.782	0.942	0.841	2206.06	NULL	2346.11	29.597	36.545	0.705	2206.06	2346.11					White Mica	Montmorillonite		200-300	neutral	Illite	Argillic	
30102_Lawyers2018_HaloSmectite-Clays-S_30102_0307.ASD	ESPIR.30102int+5.0 sec Lawyers2018	Muscovite	0.734	Kaolinite-PX	0.266	61.004	1.864	0.961	0.902	2205.87	NULL	2346.09	31.085	35.013	0.405	2205.87	2346.09					White Mica	Montmorillonite		200-300	neutral	Illite	Argillic	

Sample	SampleID	Date	BestLatitude	BestLongitude	BestElevation	UTM_East	UTM_North	MineralName1	StarRating1	MineralName2	StarRating2	MineralName3	StarRating3	MineralName4	StarRating4	MineralName5	StarRating5	MineralName6	StarRating6	MineralName7	StarRating7	AlPerMg	AlOH	CSM	FeSi	FeSt	FeOH	ISM	Kx	MgOH	sampler	type	add_notes
30102_Lawyers2018_HaloSmectite-Clays-S_30102_0287.ASD	S_30102_0287	9/13/2018 10:37:37 AM	57° 20' 047 N	127° 97' 377 W	1415.8	607199	6356440	Beidellite	3	Muscovite	2	VNIR - No match	3									2206.41	2206.41							2348.15	Adam LaRiviere	clay	
30102_Lawyers2018_HaloSmectite-Clays-S_30102_0288.ASD	S_30102_0288	9/13/2018 10:41:12 AM	57° 20' 047 N	127° 97' 377 W	1416	607247	6356446	Beidellite	3	Muscovite	2	VNIR - No match	3									2206.42	2206.42				INV		0.721	2347.23	Adam LaRiviere	clay	
30102_Lawyers2018_HaloSmectite-Clays-S_30102_0289.ASD	S_30102_0289	9/13/2018 10:43:10 AM	57° 20' 047 N	127° 97' 377 W	1417.4	607089	6356541	Beidellite	3	Muscovite	2	VNIR - No match	3									2205.42	2205.42				INV		0.612	2347.17	Adam LaRiviere	clay	
30102_Lawyers2018_HaloSmectite-Clays-S_30102_0290.ASD	S_30102_0290	9/13/2018 10:45:25 AM	57° 20' 047 N	127° 97' 377 W	1413.2	607042	6356527	Heulandite	3	Kaolinite PX	2	Muscovite	1	VNIR - No match	3							2206.06	2206.06						0.38	1.025		Adam LaRiviere	clay	
30102_Lawyers2018_HaloSmectite-Clays-S_30102_0291.ASD	S_30102_0291	9/13/2018 10:48:33 AM	57° 20' 047 N	127° 97' 377 W	1414.4	606984	6356542	Ferrihydrite	3	Beidellite	3	Mg-illite	2	Goethite	2							2206.14	2206.14		2.548	INV	INV		0.591	2347.39	Adam LaRiviere	clay	
30102_Lawyers2018_HaloSmectite-Clays-S_30102_0292.ASD	S_30102_0292	9/13/2018 10:50:34 AM	57° 20' 047 N	127° 97' 377 W	1416.7	606949	6356539	Ferrihydrite	3	Beidellite	3	Muscovite	2	Goethite	2							2205.52	2205.52		2.066	883.937	INV		0.779	2345.31	Adam LaRiviere	clay	
30102_Lawyers2018_HaloSmectite-Clays-S_30102_0293.ASD	S_30102_0293	9/13/2018 10:52:04 AM	57° 20' 047 N	127° 97' 377 W	1419	606883	6356534	Ferrihydrite	3	Beidellite	3	Muscovite	2									2206.04	2206.04				INV		0.777	2348.86	Adam LaRiviere	clay	
30102_Lawyers2018_HaloSmectite-Clays-S_30102_0294.ASD	S_30102_0294	9/13/2018 10:55:12 AM	57° 20' 047 N	127° 97' 377 W	1418	606845	6356538	Ferrihydrite	3	Beidellite	3	Muscovite	3	Goethite	1							2205.55	2205.55		2.239	INV	INV		0.745	2346.5	Adam LaRiviere	clay	
30102_Lawyers2018_HaloSmectite-Clays-S_30102_0295.ASD	S_30102_0295	9/13/2018 10:57:02 AM	57° 20' 047 N	127° 97' 377 W	1422.2	606800	6356546	Ferrihydrite	3	Beidellite	3	Muscovite	3	Goethite	3							2205.99	2205.99		1.9	904.619	INV		0.895	2346.97	Adam LaRiviere	clay	
30102_Lawyers2018_HaloSmectite-Clays-S_30102_0296.ASD	S_30102_0296	9/13/2018 10:59:09 AM	57° 20' 047 N	127° 97' 377 W	1416.6	606844	6356647	Ferrihydrite	3	Beidellite	3	Palygorskite	2	Muscovite	1							2205.59	2205.59				INV		0.544	2347.14	Adam LaRiviere	clay	
30102_Lawyers2018_HaloSmectite-Clays-S_30102_0297.ASD	S_30102_0297	9/13/2018 11:01:05 AM	57° 20' 047 N	127° 97' 377 W	1412.6	606945	6356645	Illite/Smectite	3	VNIR - No match	3																				Adam LaRiviere	clay	
30102_Lawyers2018_HaloSmectite-Clays-S_30102_0298.ASD	S_30102_0298	9/13/2018 11:03:12 AM	57° 20' 047 N	127° 97' 377 W	1417.8	606994	6356636	Ferrihydrite	3	Montmorillonite	3	Muscovite	3	Aragonite	2	FeChlorite	1	Goethite	3			2207.44	2207.44		2.196	914.076			0.447	2345.04	Adam LaRiviere	clay	
30102_Lawyers2018_HaloSmectite-Clays-S_30102_0299.ASD	S_30102_0299	9/13/2018 11:06:08 AM	57° 20' 047 N	127° 97' 377 W	1417.9	607041	6356638	Ferrihydrite	3	Illite/Smectite	3	Palygorskite	2	Halloysite	1	Goethite	2					2206.49	2206.49		2.958	INV				2348.86	Adam LaRiviere	clay	
30102_Lawyers2018_HaloSmectite-Clays-S_30102_0300.ASD	S_30102_0300	9/13/2018 11:08:44 AM	57° 20' 047 N	127° 97' 377 W	1414.5	607105	6356636	Ferrihydrite	3	Illite/Smectite	3	Halloysite	3	Goethite	3							2206.44			2.783	917.39			1.028		Adam LaRiviere	clay	
30102_Lawyers2018_HaloSmectite-Clays-S_30102_0301.ASD	S_30102_0301	9/13/2018 11:10:41 AM	57° 20' 047 N	127° 97' 377 W	1414.1	607147	6356641	Ferrihydrite	3	Beidellite	3	Mg-illite	3									2206.26	2206.26				INV		0.613	2347.46	Adam LaRiviere	clay	
30102_Lawyers2018_HaloSmectite-Clays-S_30102_0302.ASD	S_30102_0302	9/13/2018 11:12:25 AM	57° 20' 047 N	127° 97' 377 W	1408.9	607147	6356737	Illite/Smectite	3	Vermiculite	2	VNIR - No match	3										2206.23							2345.11	Adam LaRiviere	clay	
30102_Lawyers2018_HaloSmectite-Clays-S_30102_0303.ASD	S_30102_0303	9/13/2018 11:17:24 AM	57° 20' 047 N	127° 97' 377 W	1409.5	607096	6356744	Ferrihydrite	3	Illite/Smectite	3	Halloysite	2	Goethite	2								2206.38		2.294	909.4			1.042		Adam LaRiviere	clay	
30102_Lawyers2018_HaloSmectite-Clays-S_30102_0304.ASD	S_30102_0304	9/13/2018 11:19:51 AM	57° 20' 047 N	127° 97' 377 W	1410	607052	6356743	Ferrihydrite	3	Montmorillonite	3	Muscovite	3	Aragonite	2	FeChlorite	1	Goethite	2			2207.39	2207.39		2.232	904.249			0.519	2345.17	Adam LaRiviere	clay	
30102_Lawyers2018_HaloSmectite-Clays-S_30102_0305.ASD	S_30102_0305	9/13/2018 11:22:04 AM	57° 20' 047 N	127° 97' 377 W	1419	606999	6356733	Ferrihydrite	3	Beidellite	3	Phengite	2									2206.1	2206.1				INV		0.701		Adam LaRiviere	clay	
30102_Lawyers2018_HaloSmectite-Clays-S_30102_0306.ASD	S_30102_0306	9/13/2018 11:27:49 AM	57° 20' 047 N	127° 97' 377 W	1413.3	606954	6356749	Jarosite	3	Montmorillonite	3	Muscovite	3									2205.97	2205.97		1.535	910.717			0.677	2347.92	Adam LaRiviere	clay	
30102_Lawyers2018_HaloSmectite-Clays-S_30102_0307.ASD	S_30102_0307	9/13/2018 11:29:46 AM	57° 20' 047 N	127° 97' 377 W	1415.2	606855	6356743	Ferrihydrite	3	Illite/Smectite	3	Muscovite	2									2205.92	2205.92						0.666	2345.33	Adam LaRiviere	clay	

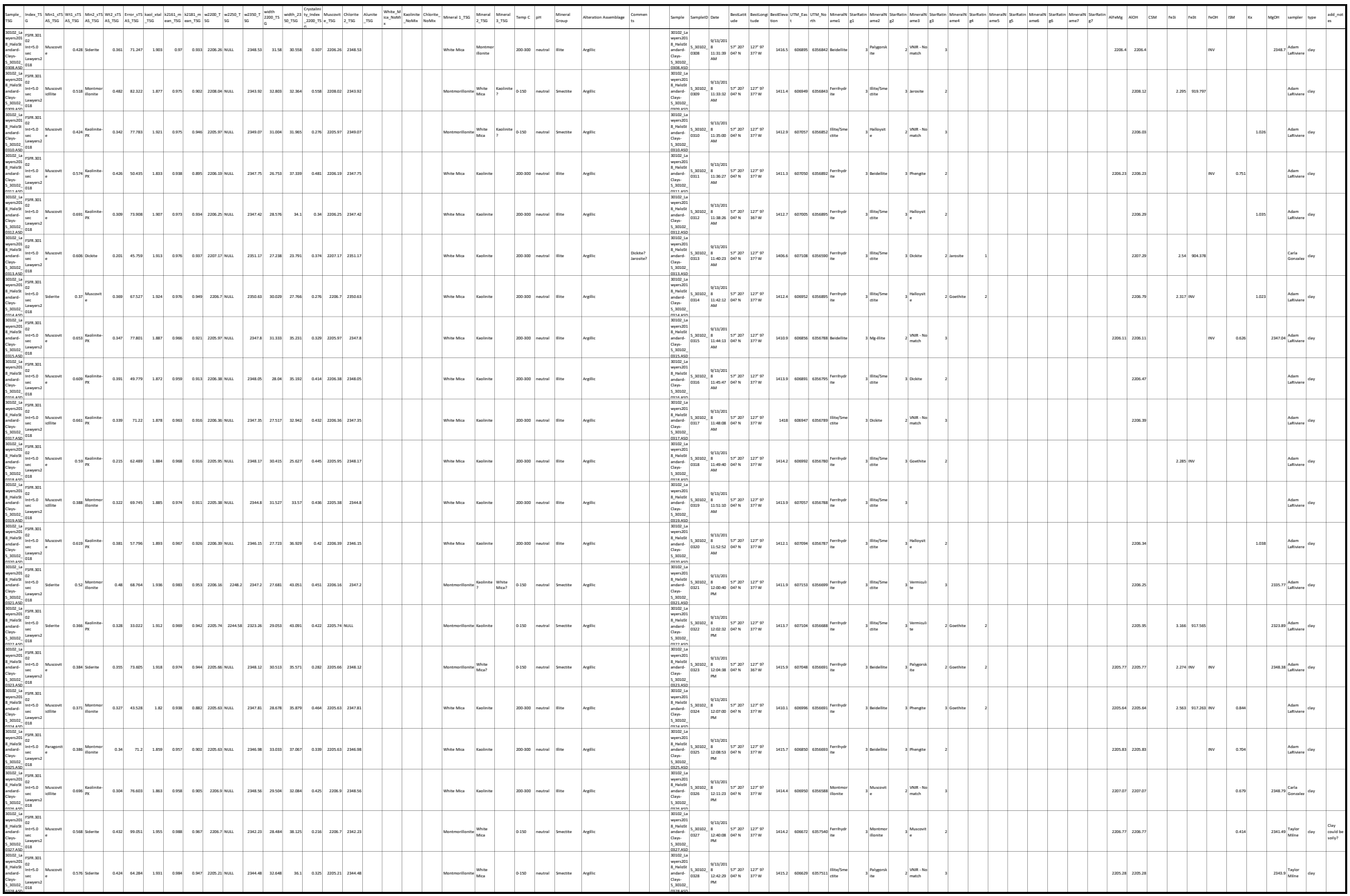

| Sample_TSG | Index_TSG | Min1_sTSAS_TSG | Wt1_sTSAS_TSG | Min2_sTSAS_TSG | Wt2_sTSAS_TSG | Error_sTSAS_TSG | kaol_xtal_TSG | kl2161_mean_TSG | kl2181_mean_TSG | w2200_TSG | w2250_TSG | w2350_TSG | width_2200_TSG | width_2350_TSG | Crystallinity_Index_2200_TSG | Muscovite_TSG | Chlorite_2_TSG | Alunite_TSG | White_Mica_NoMix | Kaolinite_NoMix | Chlorite_NoMix | Mineral 1_TSG | Mineral 2_TSG | Mineral 3_TSG | Temp C | pH | Mineral Group | Alteration Assemblage | Comments | Sample | SampleID | Date | BestLatitude | BestLongitude | BestElevation | UTM_East | UTM_North | MineralName1 | StarRating1 | MineralName2 | StarRating2 | MineralName3 | StarRating3 | MineralName4 | StarRating4 | MineralName5 | StarRating5 | MineralName6 | StarRating6 | MineralName7 | StarRating7 | AlFeMg | AlOH | CSM | Fe3t | Fe3t | FeOH | ISM | Kx | MgOH | sampler | type | add_notes |
|---|---|---

Sample_TSG	Index_TSG	Min1_sTSAS_TSG	Wt1_sTSAS_TSG	Min2_sTSAS_TSG	Wt2_sTSAS_TSG	Error_sTSAS_TSG	kaol_xtal_TSG	k2161_mean_TSG	k2181_mean_TSG	w2200_TSG	w2250_TSG	w2350_TSG	width_2200_TSG	width_2350_TSG	Crystallinity_Index_2200_TSG	Muscovite_TSG	Chlorite_2_TSG	Alunite_TSG	White_Mica_NoMix	Kaolinite_NoMix	Chlorite_NoMix	Mineral 1_TSG	Mineral 2_TSG	Mineral 3_TSG	Temp C	pH	Mineral Group	Alteration Assemblage	Comments
30102_Lawyers2018_HaloSandard-Clays-S_30102_0329.ASD	FSFR.30102.52.Int=5.0 sec Lawyers2018	Muscovite	0.652	Dickite	0.348	72.411	1.898	0.97	0.928	2206.2	NULL	2346.37	31.624	38.105	0.316	2206.2	2346.37					Montmorillonite	White Mica	Kaolinite	0-150	neutral	Smectite	Argillic	
30102_Lawyers2018_HaloSandard-Clays-S_30102_0330.ASD	FSFR.30102.52.Int=5.0 sec Lawyers2018	Muscovite	0.531	Siderite	0.469	73.632	1.96	0.992	0.968	2206.37	NULL	2347.37	30.201	34.66	0.242	2206.37	2347.37					Montmorillonite	White Mica	Kaolinite	0-150	neutral	Smectite	Argillic	
30102_Lawyers2018_HaloSandard-Clays-S_30102_0331.ASD	FSFR.30102.52.Int=5.0 sec Lawyers2018	Muscovite	0.519	Illite	0.481	53.546	1.89	0.973	0.917	2207.59	NULL	2347.1	30.297	36.931	0.453	2207.58	2347.1					Montmorillonite	White Mica		200-300	neutral	Illite	Argillic	
30102_Lawyers2018_HaloSandard-Clays-S_30102_0332.ASD	FSFR.30102.52.Int=5.0 sec Lawyers2018	Muscovite	0.574	Siderite	0.426	77.697	1.946	0.987	0.959	2206.43	NULL	2347.51	28.783	36.174	0.248	2206.43	2347.51					Montmorillonite	White Mica		200-300	neutral	Illite	Argillic	
30102_Lawyers2018_HaloSandard-Clays-S_30102_0333.ASD	FSFR.30102.52.Int=5.0 sec Lawyers2018	Muscovite	0.772	Kaolinite-PX	0.228	76.005	1.91	0.977	0.933	2205.59	NULL	2345.98	31.618	34.873	0.32	2205.59	2345.98					Montmorillonite	White Mica		200-300	neutral	Illite	Argillic	
30102_Lawyers2018_HaloSandard-Clays-S_30102_0334.ASD	FSFR.30102.52.Int=5.0 sec Lawyers2018	Muscovite	0.647	Kaolinite-PX	0.353	108.66	1.945	0.985	0.96	2206.37	NULL	2352.18	29.453	32.861	0.236	2206.37	2352.18					Kaolinite	White Mica		200-300	neutral	Illite	Argillic	
30102_Lawyers2018_HaloSandard-Clays-S_30102_0335.ASD	FSFR.30102.52.Int=5.0 sec Lawyers2018	Muscovite	0.786	Dickite	0.214	69.286	1.902	0.974	0.928	2205.14	NULL	2345.18	32.904	36.773	0.304	2205.14	2345.18					Kaolinite?	White Mica		200-300	neutral	Illite	Argillic	
30102_Lawyers2018_HaloSandard-Clays-S_30102_0336.ASD	FSFR.30102.52.Int=5.0 sec Lawyers2018	Muscovite	0.775	Kaolinite-PX	0.225	95.687	1.908	0.977	0.931	2205.75	NULL	2344.15	31.007	35.52	0.312	2205.75	2344.15					Kaolinite	White Mica		200-300	neutral	Illite	Argillic	
30102_Lawyers2018_HaloSandard-Clays-S_30102_0337.ASD	FSFR.30102.52.Int=5.0 sec Lawyers2018	Muscovite	0.66	Siderite	0.34	53.829	1.916	0.98	0.937	2205.29	NULL	2344.26	31.563	35.511	0.273	2205.29	2344.26		Yes				White Mica		200-300	neutral	Illite	Argillic	
30102_Lawyers2018_HaloSandard-Clays-S_30102_0338.ASD	FSFR.30102.52.Int=5.0 sec Lawyers2018	Muscovite	0.635	Kaolinite-PX	0.365	49.288	1.877	0.965	0.912	2205.88	NULL	2347.95	31.405	35.934	0.343	2205.88	2347.95					Kaolinite?	White Mica		200-300	neutral	Illite	Argillic	
30102_Lawyers2018_HaloSandard-Clays-S_30102_0339.ASD	FSFR.30102.52.Int=5.0 sec Lawyers2018	Muscovite	0.526	Wood	0.474	17.678	1.987	0.999	0.988	2204.69	2266.47	2312.07	29.883	23.755	0.26	2204.69	2351.9						White Mica		200-300	neutral	Illite	Argillic	
30102_Lawyers2018_HaloSandard-Clays-S_30102_0340.ASD	FSFR.30102.52.Int=5.0 sec Lawyers2018	Muscovite	0.564	Vegetation-Dry	0.247	50.278	1.926	0.982	0.944	2205.36	NULL	2346.71	33.457	34.447	0.316	2205.36	2346.71		Yes				White Mica		200-300	neutral	Illite	Argillic	
30102_Lawyers2018_HaloSandard-Clays-S_30102_0341.ASD	FSFR.30102.52.Int=5.0 sec Lawyers2018	Muscovite	0.74	Dickite	0.26	39.069	1.922	0.979	0.943	2205.2	NULL	2342.26	33.875	39.222	0.281	2205.2	2342.26					Kaolinite	White Mica		200-300	neutral	Illite	Argillic	
30102_Lawyers2018_HaloSandard-Clays-S_30102_0342.ASD	FSFR.30102.52.Int=5.0 sec Lawyers2018	Muscovite	0.76	Dickite	0.24	63.183	1.928	0.982	0.946	2205.22	NULL	2345.28	33.266	35.958	0.262	2205.22	2345.28					Kaolinite	White Mica		200-300	neutral	Illite	Argillic	
30102_Lawyers2018_HaloSandard-Clays-S_30102_0343.ASD	FSFR.30102.52.Int=5.0 sec Lawyers2018	Muscovite	0.744	Dickite	0.256	52.365	1.896	0.972	0.925	2205.15	NULL	2347.34	33.528	33.918	0.335	2205.15	2347.34					Kaolinite	White Mica		200-300	neutral	Illite	Argillic	
30102_Lawyers2018_HaloSandard-Clays-S_30102_0344.ASD	FSFR.30102.52.Int=5.0 sec Lawyers2018	Muscovite	0.775	Dickite	0.225	70.08	1.881	0.969	0.911	2203.67	NULL	2345.55	34.631	35.72	0.338	2203.67	2345.55					Kaolinite	White Mica		200-300	neutral	Illite	Argillic	
30102_Lawyers2018_HaloSandard-Clays-S_30102_0345.ASD	FSFR.30102.52.Int=5.0 sec Lawyers2018	Muscovite	0.768	Dickite	0.232	32.759	1.899	0.974	0.925	2205.13	NULL	2344.64	32.722	36.189	0.413	2205.13	2344.64					Kaolinite	White Mica		200-300	neutral	Illite	Argillic	
30102_Lawyers2018_HaloSandard-Clays-S_30102_0346.ASD	FSFR.30102.52.Int=5.0 sec Lawyers2018	Muscovite	0.7	Dickite	0.3	61.99	1.881	0.964	0.917	2206.05	NULL	2342.86	32.314	42.03	0.321	2206.05	2342.86					Kaolinite	White Mica		200-300	neutral	Illite	Argillic	
30102_Lawyers2018_HaloSandard-Clays-S_30102_0347.ASD	FSFR.30102.52.Int=5.0 sec Lawyers2018	Jarosite	0.447	Muscovite	0.35	48.626	1.909	0.977	0.933	2207.84	2262.99	NULL	32.223	NULL	0.268	2207.84	2350.58		Yes			Jarosite	White Mica			acidic	Sulfate	Argillic	
30102_Lawyers2018_HaloSandard-Clays-S_30102_0348.ASD	FSFR.30102.52.Int=5.0 sec Lawyers2018	Montmorillonite	0.411	Muscovite	0.404	51.406	1.907	0.975	0.932	2206.54	NULL	2348.17	27.866	28.894	0.443	2206.54	2348.17					Montmorillonite	White Mica		0-150	neutral	Smectite	Argillic	
30102_Lawyers2018_HaloSandard-Clays-S_30102_0349.ASD	FSFR.30102.52.Int=5.0 sec Lawyers2018	Muscovite	0.392	Montmorillonite	0.358	54.851	1.925	0.983	0.943	2207.77	NULL	2347.8	30.052	26.687	0.381	2207.75	2347.8					Montmorillonite	White Mica	Jarosite	0-150	neutral	Smectite	Argillic	

Sample	SampleID	Date	BestLatitude	BestLongitude	BestElevation	UTM_East	UTM_North	MineralName1	StarRating1	MineralName2	StarRating2	MineralName3	StarRating3	MineralName4	StarRating4	MineralName5	StarRating5	MineralName6	StarRating6	MineralName7	StarRating7	AlFeMg	AlOH	CSM	Fe3i	Fe3t	FeOH	ISM	Kx	MgOH	sampler	type	add_notes
30102_Lawyers2018_HaloSandard-Clays-S_30102_0329.ASD	S_30102_0329	9/13/2018 12:45:08 PM	57° 20' 047 N	127° 97' 377 W	1419.6	606578	6357473	Beidellite	3	Palygorskite	2	Muscovite	1	VNIR - No match	3							2206.28	2206.28							2346.72	Taylor Mine	clay	
30102_Lawyers2018_HaloSandard-Clays-S_30102_0330.ASD	S_30102_0331	9/13/2018 12:49:16 PM	57° 20' 047 N	127° 97' 377 W	1417.5	606488	6357414	Fernhydrite	3	Illite/Smectite	3																				Taylor Mine	clay	
30102_Lawyers2018_HaloSandard-Clays-S_30102_0332.ASD	S_30102_0332	9/13/2018 12:51:42 PM	57° 20' 047 N	127° 97' 377 W	1413.5	606429	6357380	Fernhydrite	3	Montmorillonite	3	Muscovite	2	Goethite	2							2206.51	2206.51		2.257	INV			0.454		2347.04	Taylor Mine	clay	
30102_Lawyers2018_HaloSandard-Clays-S_30102_0333.ASD	S_30102_0333	9/13/2018 12:53:43 PM	57° 20' 047 N	127° 97' 377 W	1415.6	606364	6357341	Fernhydrite	3	Illite/Smectite	3	Muscovite	2	Goethite	2							2205.49	2205.49		2.113	INV			0.523		2347.01	Taylor Mine	clay	
30102_Lawyers2018_HaloSandard-Clays-S_30102_0334.ASD	S_30102_0334	9/13/2018 12:56:00 PM	57° 20' 047 N	127° 97' 377 W	1417.5	606296	6357302	Montmorillonite	3	Muscovite	2	VNIR - No match	3									2206.4	2206.4						0.418		2352.14	Taylor Mine	clay	
30102_Lawyers2018_HaloSandard-Clays-S_30102_0335.ASD	S_30102_0335	9/13/2018 12:58:23 PM	57° 20' 047 N	127° 97' 377 W	1415.4	606247	6357255	Fernhydrite	3	Rectorite	3	Mg-illite	3	Kaolinite WX	1	Goethite	2					2205.19	2205.19	INV	2.226	INV			0.586	1.043	2346.14	Taylor Mine	clay	
30102_Lawyers2018_HaloSandard-Clays-S_30102_0336.ASD	S_30102_0336	9/13/2018 1:01:48 PM	57° 20' 047 N	127° 97' 377 W	1417.8	606178	6357209	Montmorillonite	3	Muscovite	2	VNIR - No match	3									2205.94	2205.94						0.602		2343.31	Taylor Mine	clay	Wet and sandy
30102_Lawyers2018_HaloSandard-Clays-S_30102_0337.ASD	S_30102_0337	9/13/2018 1:04:05 PM	57° 20' 047 N	127° 97' 377 W	1418	606117	6357204	Fernhydrite	3	Rectorite	3	Mg-illite	2	Muscovite	1	Goethite	3					2205.64	2205.64	INV	2.373	927.997			0.643		2344.27	Taylor Mine	clay	Sandy
30102_Lawyers2018_HaloSandard-Clays-S_30102_0338.ASD	S_30102_0338	9/13/2018 1:06:41 PM	57° 20' 047 N	127° 97' 377 W	1422.9	605944	6357236	Beidellite	3	Phengite	2	Goethite	2									2206.09	2206.09		2.395	908.845	INV		0.687			Taylor Mine	clay	
30102_Lawyers2018_HaloSandard-Clays-S_30102_0339.ASD	S_30102_0339	9/13/2018 1:09:21 PM	57° 20' 047 N	127° 97' 377 W	1420.4	606016	6357216	Fernhydrite	3	Chabazite	3	Illite/Smectite	2	Goethite	2										3.424	911.08						Taylor Mine	clay	
30102_Lawyers2018_HaloSandard-Clays-S_30102_0340.ASD	S_30102_0340	9/13/2018 1:11:56 PM	57° 20' 047 N	127° 97' 377 W	1410.4	605913	6357190	Fernhydrite	3	Illite/Smectite	3	Goethite	3												2.914	INV						Taylor Mine	clay	
30102_Lawyers2018_HaloSandard-Clays-S_30102_0341.ASD	S_30102_0341	9/13/2018 1:13:40 PM	57° 20' 047 N	127° 97' 367 W	1421.6	605895	6357123	Fernhydrite	3	Illite/Smectite	3																				Taylor Mine	clay	
30102_Lawyers2018_HaloSandard-Clays-S_30102_0342.ASD	S_30102_0342	9/13/2018 1:16:07 PM	57° 20' 047 N	127° 97' 367 W	1425	605896	6357030	Fernhydrite	3	Rectorite	3	Palygorskite	2	Mg-illite	1							2205.57	2205.57	INV					0.464		2343.99	Taylor Mine	clay	
30102_Lawyers2018_HaloSandard-Clays-S_30102_0343.ASD	S_30102_0343	9/13/2018 1:19:50 PM	57° 20' 047 N	127° 97' 377 W	1414.4	605940	6356984	Fernhydrite	3	Rectorite	3	Palygorskite	2	Muscovite	1							2205.24	2205.24	INV					0.506		2347.8	Taylor Mine	clay	
30102_Lawyers2018_HaloSandard-Clays-S_30102_0344.ASD	S_30102_0344	9/13/2018 1:21:35 PM	57° 20' 047 N	127° 97' 377 W	1413.6	605958	6356941	Fernhydrite	3	Rectorite	3	Mg-illite	3	Halloysite	1							2204.13	2204.13	INV					0.592	1.055	2346.04	Taylor Mine	clay	
30102_Lawyers2018_HaloSandard-Clays-S_30102_0345.ASD	S_30102_0345	9/13/2018 1:23:49 PM	57° 20' 047 N	127° 97' 377 W	1414.1	605949	6356886	Fernhydrite	3	Illite/Smectite	3																				Taylor Mine	clay	
30102_Lawyers2018_HaloSandard-Clays-S_30102_0346.ASD	S_30102_0346	9/13/2018 1:26:30 PM	57° 20' 047 N	127° 97' 377 W	1415.1	605893	6356789	Fernhydrite	3	Beidellite	3	Mg-illite	2	Goethite	2							2206.13	2206.13		2.348	886.404	INV		0.65		2342.56	Taylor Mine	clay	
30102_Lawyers2018_HaloSandard-Clays-S_30102_0347.ASD	S_30102_0347	9/13/2018 1:29:09 PM	57° 20' 047 N	127° 97' 367 W	1426.9	605445	6356706	Jarosite	3	K-illite	3	Goethite	3									2262.9	2207.91		2.465	919.742			0.882			Taylor Mine	clay	
30102_Lawyers2018_HaloSandard-Clays-S_30102_0348.ASD	S_30102_0348	9/13/2018 1:34:49 PM	57° 20' 047 N	127° 97' 377 W	1418.5	606906	6354522	Fernhydrite	3	Illite/Smectite	3																				Taylor Mine	clay	
30102_Lawyers2018_HaloSandard-Clays-S_30102_0349.ASD	S_30102_0349	9/13/2018 1:37:03 PM	57° 20' 047 N	127° 97' 367 W	1418.5	606861	6354550	Montmorillonite	3	Muscovite	3	Gibbsite	1	VNIR - No match	3							2207.7	2207.7						0.534		2347.06	Taylor Mine	clay	
30102_Lawyers2018_HaloSandard-Clays-S_30102_0350.ASD	S_30102_0350	9/13/2018 1:39:03 PM	57° 20' 047 N	127° 97' 377 W	1416.4	606799	6354557	Fernhydrite	3	Illite/Smectite	3	Jarosite	2										2206.7		1.923	908.881						Taylor Mine	clay	

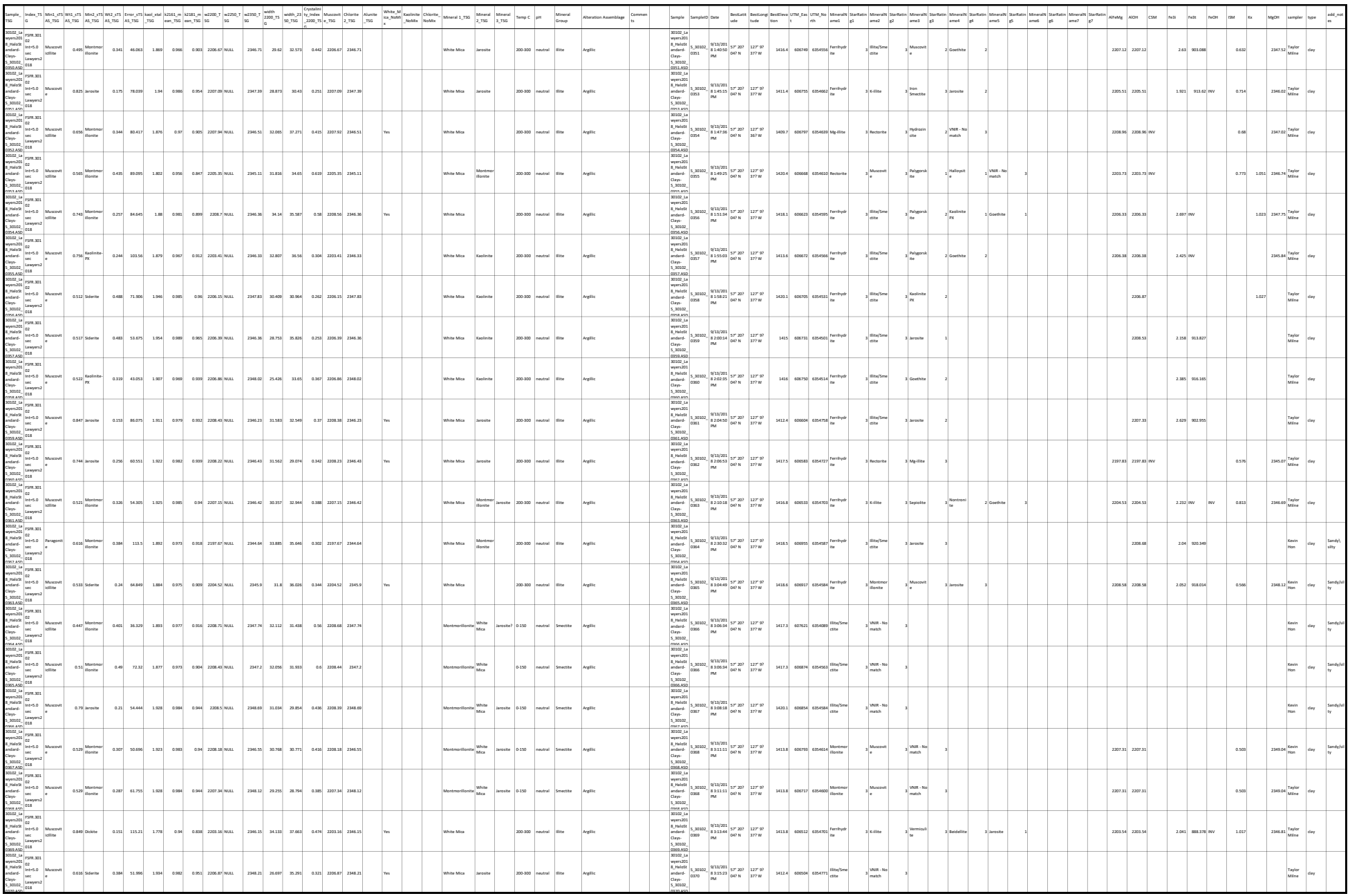

Sample_TSG	Index_TSG	Min1_sTSG	Wt1_sTSG	Min2_sTSG	Wt2_sTSG	Error_sTSG	kaol_xtal_TSG	k2161_mean_TSG	k2181_mean_TSG	w2200_TSG	w2250_TSG	w2350_TSG	width_2200_TSG	width_2350_TSG	Crystallinity_Index_2200_TSG	Muscovite_TSG	Chlorite_2_TSG	Alunite_TSG	White_kaolinite_NoMix	Kaolinite_NoMix	Chlorite_NoMix	Mineral 1_TSG	Mineral 2_TSG	Mineral 3_TSG	Temp C	pH	Mineral Group	Alteration Assemblage	Comments
30102_Lawyers2018_HaloSandard-Clays-S_30102_0350.ASD	ESPR.30102 Int=5.0 sec Lawyers2018	Muscovite	0.495	Montmorillonite	0.341	46.063	1.869	0.966	0.903	2206.67	NULL	2346.71	29.62	32.573	0.442	2206.67	2346.71					White Mica	Jarosite		200-300	neutral	Illite	Argillic	
30102_Lawyers2018_HaloSandard-Clays-S_30102_0351.ASD	ESPR.30102 Int=5.0 sec Lawyers2018	Muscovite	0.825	Jarosite	0.175	78.039	1.94	0.986	0.954	2207.09	NULL	2347.39	28.873	30.43	0.251	2207.09	2347.39					White Mica	Jarosite		200-300	neutral	Illite	Argillic	
30102_Lawyers2018_HaloSandard-Clays-S_30102_0352.ASD	ESPR.30102 Int=5.0 sec Lawyers2018	Muscovite	0.656	Montmorillonite	0.344	80.417	1.876	0.97	0.905	2207.94	NULL	2346.51	32.085	37.271	0.415	2207.92	2346.51		Yes			White Mica			200-300	neutral	Illite	Argillic	
30102_Lawyers2018_HaloSandard-Clays-S_30102_0353.ASD	ESPR.30102 Int=5.0 sec Lawyers2018	Muscovite	0.565	Montmorillonite	0.435	89.095	1.802	0.956	0.847	2205.35	NULL	2345.11	31.816	34.65	0.619	2205.35	2345.11					White Mica	Montmorillonite		200-300	neutral	Illite	Argillic	
30102_Lawyers2018_HaloSandard-Clays-S_30102_0354.ASD	ESPR.30102 Int=5.0 sec Lawyers2018	Muscovite	0.743	Montmorillonite	0.257	84.645	1.88	0.981	0.899	2208.7	NULL	2346.36	34.14	35.587	0.58	2208.56	2346.36		Yes			White Mica			200-300	neutral	Illite	Argillic	
30102_Lawyers2018_HaloSandard-Clays-S_30102_0355.ASD	ESPR.30102 Int=5.0 sec Lawyers2018	Muscovite	0.756	Kaolinite-PX	0.244	103.56	1.879	0.967	0.912	2203.41	NULL	2346.33	32.807	36.56	0.304	2203.41	2346.33					White Mica	Kaolinite		200-300	neutral	Illite	Argillic	
30102_Lawyers2018_HaloSandard-Clays-S_30102_0356.ASD	ESPR.30102 Int=5.0 sec Lawyers2018	Muscovite	0.512	Siderite	0.488	71.906	1.946	0.985	0.96	2206.15	NULL	2347.83	30.409	30.964	0.262	2206.15	2347.83					White Mica	Kaolinite		200-300	neutral	Illite	Argillic	
30102_Lawyers2018_HaloSandard-Clays-S_30102_0357.ASD	ESPR.30102 Int=5.0 sec Lawyers2018	Muscovite	0.517	Siderite	0.483	53.675	1.954	0.989	0.965	2206.39	NULL	2346.36	28.753	35.826	0.253	2206.39	2346.36					White Mica	Kaolinite		200-300	neutral	Illite	Argillic	
30102_Lawyers2018_HaloSandard-Clays-S_30102_0358.ASD	ESPR.30102 Int=5.0 sec Lawyers2018	Muscovite	0.522	Kaolinite-PX	0.319	43.053	1.907	0.969	0.939	2206.86	NULL	2348.02	25.426	33.65	0.367	2206.86	2348.02					White Mica	Kaolinite		200-300	neutral	Illite	Argillic	
30102_Lawyers2018_HaloSandard-Clays-S_30102_0359.ASD	ESPR.30102 Int=5.0 sec Lawyers2018	Muscovite	0.847	Jarosite	0.153	86.075	1.911	0.979	0.932	2208.43	NULL	2346.23	31.583	32.549	0.37	2208.38	2346.23		Yes			White Mica	Jarosite		200-300	neutral	Illite	Argillic	
30102_Lawyers2018_HaloSandard-Clays-S_30102_0360.ASD	ESPR.30102 Int=5.0 sec Lawyers2018	Muscovite	0.744	Jarosite	0.256	60.551	1.922	0.982	0.939	2208.22	NULL	2346.43	31.562	29.074	0.342	2208.23	2346.43		Yes			White Mica	Jarosite		200-300	neutral	Illite	Argillic	
30102_Lawyers2018_HaloSandard-Clays-S_30102_0361.ASD	ESPR.30102 Int=5.0 sec Lawyers2018	Muscovite	0.521	Montmorillonite	0.326	54.305	1.925	0.985	0.94	2207.15	NULL	2346.42	30.357	32.944	0.388	2207.15	2346.42					White Mica	Montmorillonite	Jarosite	200-300	neutral	Illite	Argillic	
30102_Lawyers2018_HaloSandard-Clays-S_30102_0362.ASD	ESPR.30102 Int=5.0 sec Lawyers2018	Paragonite	0.616	Montmorillonite	0.384	113.5	1.892	0.973	0.918	2197.67	NULL	2344.64	33.885	35.646	0.302	2197.67	2344.64					White Mica	Montmorillonite		200-300	neutral	Illite	Argillic	
30102_Lawyers2018_HaloSandard-Clays-S_30102_0363.ASD	ESPR.30102 Int=5.0 sec Lawyers2018	Muscovite	0.533	Siderite	0.24	64.849	1.884	0.975	0.909	2204.52	NULL	2345.9	31.8	36.026	0.344	2204.52	2345.9		Yes			White Mica			200-300	neutral	Illite	Argillic	
30102_Lawyers2018_HaloSandard-Clays-S_30102_0364.ASD	ESPR.30102 Int=5.0 sec Lawyers2018	Muscovite	0.447	Montmorillonite	0.401	36.329	1.893	0.977	0.916	2208.71	NULL	2347.74	32.112	31.438	0.56	2208.68	2347.74					White Mica	Montmorillonite	Jarosite?	0-150	neutral	Smectite	Argillic	
30102_Lawyers2018_HaloSandard-Clays-S_30102_0365.ASD	ESPR.30102 Int=5.0 sec Lawyers2018	Muscovite	0.53	Montmorillonite	0.49	72.32	1.877	0.973	0.904	2208.43	NULL	2347.2	32.056	31.933	0.6	2208.44	2347.2					White Mica	Montmorillonite		0-150	neutral	Smectite	Argillic	
30102_Lawyers2018_HaloSandard-Clays-S_30102_0366.ASD	ESPR.30102 Int=5.0 sec Lawyers2018	Muscovite	0.79	Jarosite	0.21	54.444	1.928	0.984	0.944	2208.5	NULL	2348.69	31.034	29.854	0.436	2208.39	2348.69					White Mica	Montmorillonite	Jarosite	0-150	neutral	Smectite	Argillic	
30102_Lawyers2018_HaloSandard-Clays-S_30102_0367.ASD	ESPR.30102 Int=5.0 sec Lawyers2018	Muscovite	0.529	Montmorillonite	0.307	50.696	1.923	0.983	0.94	2208.18	NULL	2346.55	30.768	30.771	0.416	2208.18	2346.55					White Mica	Montmorillonite	Jarosite	0-150	neutral	Smectite	Argillic	
30102_Lawyers2018_HaloSandard-Clays-S_30102_0368.ASD	ESPR.30102 Int=5.0 sec Lawyers2018	Muscovite	0.529	Montmorillonite	0.287	61.755	1.928	0.984	0.944	2207.34	NULL	2348.12	29.255	28.794	0.385	2207.34	2348.12					White Mica	Montmorillonite	Jarosite	0-150	neutral	Smectite	Argillic	
30102_Lawyers2018_HaloSandard-Clays-S_30102_0369.ASD	ESPR.30102 Int=5.0 sec Lawyers2018	Muscovite	0.849	Dickite	0.151	115.21	1.778	0.94	0.838	2203.16	NULL	2346.15	34.133	37.663	0.474	2203.16	2346.15		Yes			White Mica			200-300	neutral	Illite	Argillic	
30102_Lawyers2018_HaloSandard-Clays-S_30102_0370.ASD	ESPR.30102 Int=5.0 sec Lawyers2018	Muscovite	0.616	Siderite	0.384	51.996	1.934	0.982	0.951	2206.87	NULL	2348.21	26.697	35.291	0.321	2206.87	2348.21		Yes			White Mica	Jarosite		200-300	neutral	Illite	Argillic	

Sample	SampleID	Date	BestLatitude	BestLongitude	BestElevation	UTM_East	UTM_North	MineralName1	StarRating1	MineralName2	StarRating2	MineralName3	StarRating3	MineralName4	StarRating4	MineralName5	StarRating5	MineralName6	StarRating6	MineralName7	StarRating7	AlPerMg	AlOH	CSM	Fe3i	Fe3t	FeOH	ISM	Kx	MgOH	sampler	type	add_notes
30102_Lawyers2018_HaloSandard-Clays-S_30102_0351.ASD	S_30102_0351	9/13/2018 1:40:50 PM	57° 20' 047 N	127° 9' 377 W	1416.4	606749	6354556	Ferrihydrite	3	Illite/Smectite	3	Muscovite	2	Goethite	2							2207.12	2207.12		2.63	903.088		0.632		2347.52	Taylor Milne	clay	
30102_Lawyers2018_HaloSandard-Clays-S_30102_0352.ASD	S_30102_0352	9/13/2018 1:45:15 PM	57° 20' 047 N	127° 9' 377 W	1411.4	606755	6354662	Ferrihydrite	3	K-illite	3	Iron Smectite	3	Jarosite	2							2205.51	2205.51		1.921	911.62	INV	0.714		2346.02	Taylor Milne	clay	
30102_Lawyers2018_HaloSandard-Clays-S_30102_0353.ASD	S_30102_0353	9/13/2018 1:47:35 PM	57° 20' 047 N	127° 9' 367 W	1409.7	606797	6354639	Mg-illite	3	Rectorite	3	Hydrozincite	2	VNIR - No match	3							2208.96	2208.96	INV				0.68		2347.02	Taylor Milne	clay	
30102_Lawyers2018_HaloSandard-Clays-S_30102_0354.ASD	S_30102_0354	9/13/2018 1:49:25 PM	57° 20' 047 N	127° 9' 377 W	1420.4	606668	6354610	Rectorite	3	Muscovite	3	Palygorskite	1	Halloysite	1	VNIR - No match	3					2203.73	2203.73	INV					0.773	1.051	2346.74	Taylor Milne	clay	
30102_Lawyers2018_HaloSandard-Clays-S_30102_0355.ASD	S_30102_0355	9/13/2018 1:51:34 PM	57° 20' 047 N	127° 9' 377 W	1418.1	606623	6354595	Ferrihydrite	3	Illite/Smectite	3	Palygorskite	2	Kaolinite PX	1	Goethite	1					2206.33	2206.33		2.697	INV			1.023	2347.75	Taylor Milne	clay	
30102_Lawyers2018_HaloSandard-Clays-S_30102_0356.ASD	S_30102_0356	9/13/2018 1:55:03 PM	57° 20' 047 N	127° 9' 377 W	1413.6	606672	6354566	Ferrihydrite	3	Illite/Smectite	3	Palygorskite	2	Goethite	2							2206.38	2206.38		2.425	INV				2345.84	Taylor Milne	clay	
30102_Lawyers2018_HaloSandard-Clays-S_30102_0357.ASD	S_30102_0357	9/13/2018 1:58:21 PM	57° 20' 047 N	127° 9' 377 W	1420.1	606705	6354531	Ferrihydrite	3	Illite/Smectite	3	Kaolinite PX	2									2206.87							1.027		Taylor Milne	clay	
30102_Lawyers2018_HaloSandard-Clays-S_30102_0358.ASD	S_30102_0358	9/13/2018 2:00:14 PM	57° 20' 047 N	127° 9' 377 W	1415	606731	6354501	Ferrihydrite	3	Illite/Smectite	3	Jarosite	1									2208.53			2.358	913.827					Taylor Milne	clay	
30102_Lawyers2018_HaloSandard-Clays-S_30102_0359.ASD	S_30102_0359	9/13/2018 2:02:31 PM	57° 20' 047 N	127° 9' 377 W	1416	606750	6354514	Ferrihydrite	3	Illite/Smectite	3	Goethite	2												2.385	916.165					Taylor Milne	clay	
30102_Lawyers2018_HaloSandard-Clays-S_30102_0360.ASD	S_30102_0360	9/13/2018 2:04:50 PM	57° 20' 047 N	127° 9' 377 W	1412.4	606604	6354758	Ferrihydrite	3	Illite/Smectite	3	Jarosite	2									2207.33			2.629	902.955					Taylor Milne	clay	
30102_Lawyers2018_HaloSandard-Clays-S_30102_0361.ASD	S_30102_0361	9/13/2018 2:06:53 PM	57° 20' 047 N	127° 9' 377 W	1417.5	606583	6354727	Ferrihydrite	3	Rectorite	3	Mg-illite	3									2197.83	2197.83	INV				0.576		2345.07	Taylor Milne	clay	
30102_Lawyers2018_HaloSandard-Clays-S_30102_0362.ASD	S_30102_0362	9/13/2018 2:10:18 PM	57° 20' 047 N	127° 9' 377 W	1416.8	606533	6354703	Ferrihydrite	3	K-illite	3	Sepiolite	3	Nontronite	2	Goethite	3					2204.53	2204.53		2.232	INV	INV	0.813		2346.69	Taylor Milne	clay	
30102_Lawyers2018_HaloSandard-Clays-S_30102_0363.ASD	S_30102_0363	9/13/2018 2:30:31 PM	57° 20' 047 N	127° 9' 377 W	1418.5	606955	6354587	Ferrihydrite	3	Illite/Smectite	3	Jarosite	3									2208.68			2.04	920.349					Kevin Hon	clay	Sandy\, silty
30102_Lawyers2018_HaloSandard-Clays-S_30102_0364.ASD	S_30102_0364	9/13/2018 3:04:49 PM	57° 20' 047 N	127° 9' 377 W	1418.6	606917	6354584	Ferrihydrite	3	Montmorillonite	3	Muscovite	3	Jarosite	3							2208.58	2208.58		2.052	918.014		0.566		2348.12	Kevin Hon	clay	Sandy\silty
30102_Lawyers2018_HaloSandard-Clays-S_30102_0365.ASD	S_30102_0365	9/13/2018 3:06:34 PM	57° 20' 047 N	127° 9' 377 W	1417.3	607621	6354089	Illite/Smectite	3	VNIR - No match	3																				Kevin Hon	clay	Sandy\silty
30102_Lawyers2018_HaloSandard-Clays-S_30102_0366.ASD	S_30102_0366	9/13/2018 3:06:34 PM	57° 20' 047 N	127° 9' 377 W	1417.3	606874	6354563	Illite/Smectite	3	VNIR - No match	3																				Kevin Hon	clay	Sandy\silty
30102_Lawyers2018_HaloSandard-Clays-S_30102_0367.ASD	S_30102_0367	9/13/2018 3:08:14 PM	57° 20' 047 N	127° 9' 377 W	1420.1	606854	6354584	Illite/Smectite	3	VNIR - No match	3																				Kevin Hon	clay	Sandy\silty
30102_Lawyers2018_HaloSandard-Clays-S_30102_0368.ASD	S_30102_0368	9/13/2018 3:11:11 PM	57° 20' 047 N	127° 9' 377 W	1413.8	606793	6354614	Montmorillonite	3	Muscovite	3	VNIR - No match	3									2207.31	2207.31					0.503		2349.04	Kevin Hon	clay	Sandy\silty
30102_Lawyers2018_HaloSandard-Clays-S_30102_0369.ASD	S_30102_0369	9/13/2018 3:11:11 PM	57° 20' 047 N	127° 9' 377 W	1413.8	606717	6354600	Montmorillonite	3	Muscovite	3	VNIR - No match	3									2207.31	2207.31					0.503		2349.04	Taylor Milne	clay	
30102_Lawyers2018_HaloSandard-Clays-S_30102_0370.ASD	S_30102_0369	9/13/2018 3:13:44 PM	57° 20' 047 N	127° 9' 377 W	1413.8	606512	6354701	Ferrihydrite	3	K-illite	3	Vermiculite	3	Beidellite	3	Jarosite	1					2203.54	2203.54		2.041	888.378	INV	1.017		2346.81	Taylor Milne	clay	
30102_Lawyers2018_HaloSandard-Clays-S_30102_0371.ASD	S_30102_0370	9/13/2018 3:15:23 PM	57° 20' 047 N	127° 9' 377 W	1412.4	606504	6354771	Illite/Smectite	3	VNIR - No match	3																				Taylor Milne	clay	

| Sample_TSG | Index_TSG | Min1_sTSAS_TSG | Wt1_sTSAS_TSG | Min2_sTSAS_TSG | Wt2_sTSAS_TSG | Error_sTSAS_TSG | kaol_xtal_TSG | k2161_mean_TSG | k2181_mean_TSG | w2200_TSG | w2250_TSG | w2350_TSG | width_2200_TSG | width_2350_TSG | Crystallinity_Index_2200_TSG | Muscovite_TSG | Chlorite_2_TSG | Alunite_TSG | White_Mica_NoMix | Kaolinite_NoMix | Chlorite_NoMix | Mineral 1_TSG | Mineral 2_TSG | Mineral 3_TSG | Temp C | pH | Mineral Group | Alteration Assemblage | Commnts | | Sample | SampleID | Date | BestLatitude | BestLongitude | BestElevation | UTM_East | UTM_North | MineralName1 | StarRating1 | MineralName2 | StarRating2 | MineralName3 | StarRating3 | MineralName4 | StarRating4 | MineralName5 | StarRating5 | MineralName6 | StarRating6 | MineralName7 | StarRating7 | AlFeMg | AlOH | CSM | Fe3t | Fe3t | FeOH | ISM | Kx | MgOH | sampler | type | add_notes |
|---|---|---

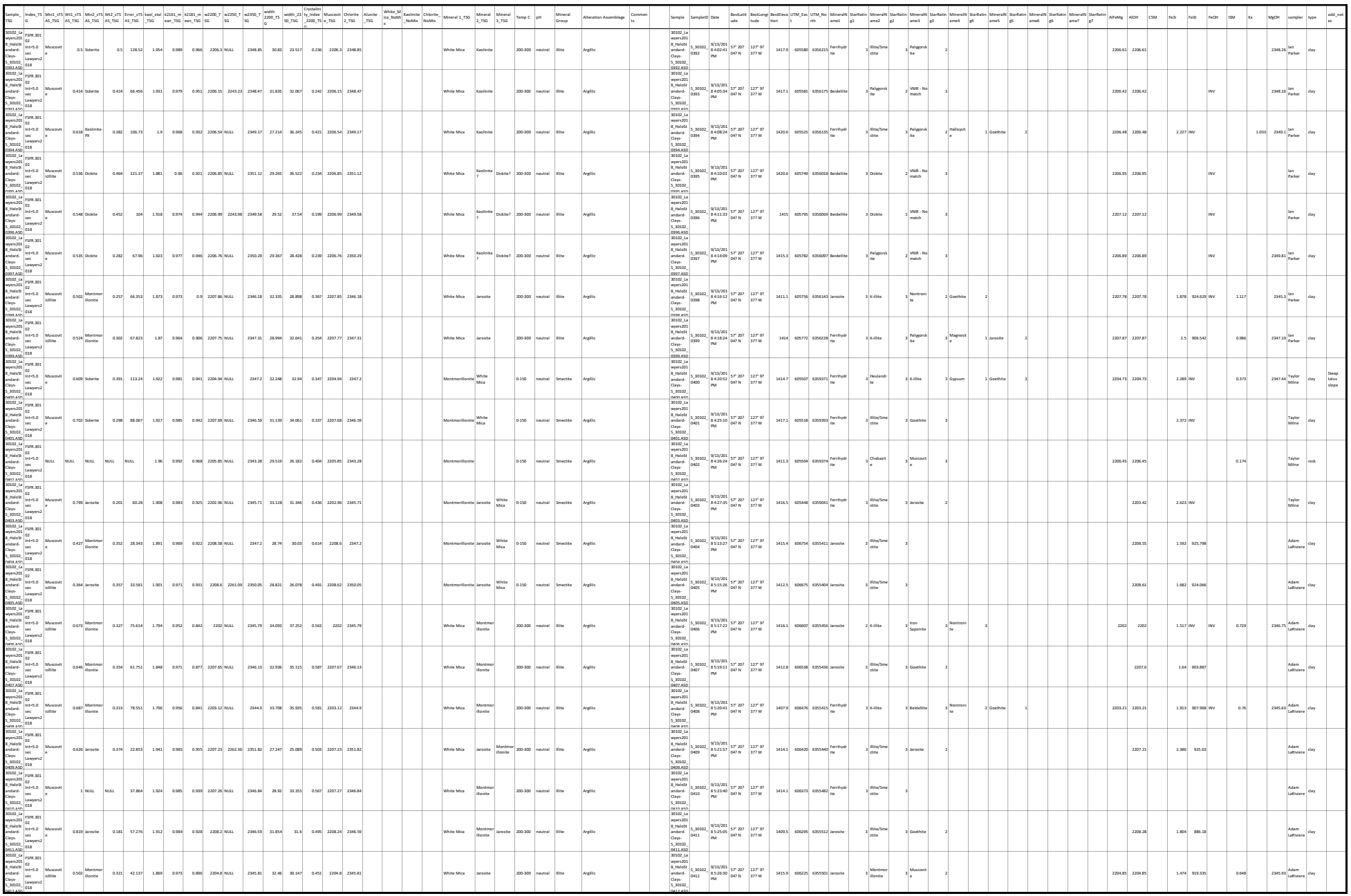

Sample_TSG	Index_TSG	Min1_sTSG	Wt1_sTSG	Min2_sTSG	Wt2_sTSG	Error_sTSG	kaol_xtal_TSG	k2161_mean_TSG	k2181_mean_TSG	w2200_TSG	w2250_TSG	w2350_TSG	width_2200_TSG	width_2350_TSG	Crystallinity_Index_2200_TSG	Muscovite_TSG	Chlorite_2_TSG	Alunite_TSG	White_kaolinite_NoMix	Kaolinite_NoMix	Chlorite_NoMix	Mineral 1_TSG	Mineral 2_TSG	Mineral 3_TSG	Temp C	pH	Mineral Group	Alteration Assemblage	Comments
30102_Lawyers2018_Halos9andard-Clays-S_30102_0392.ASD	FSFR.30102.52.Int=5.0 sec Lawyers2018	Muscovite	0.5	Siderite	0.5	128.52	1.954	0.989	0.966	2206.3	NULL	2348.85	30.83	23.517	0.236	2206.3	2348.85					White Mica	Kaolinite		200-300	neutral	Illite	Argillic	
30102_Lawyers2018_Halos9andard-Clays-S_30102_0393.ASD	FSFR.30102.52.Int=5.0 sec Lawyers2018	Muscovite	0.414	Siderite	0.414	66.456	1.931	0.979	0.951	2206.15	2243.23	2348.47	31.835	32.067	0.242	2206.15	2348.47					White Mica	Kaolinite		200-300	neutral	Illite	Argillic	
30102_Lawyers2018_Halos9andard-Clays-S_30102_0394.ASD	FSFR.30102.52.Int=5.0 sec Lawyers2018	Muscovite	0.618	Kaolinite-PX	0.382	106.73	1.9	0.968	0.932	2206.54	NULL	2349.17	27.214	36.245	0.421	2206.54	2349.17					White Mica	Kaolinite		200-300	neutral	Illite	Argillic	
30102_Lawyers2018_Halos9andard-Clays-S_30102_0395.ASD	FSFR.30102.52.Int=5.0 sec Lawyers2018	Muscovite	0.536	Dickite	0.464	121.37	1.881	0.96	0.921	2206.85	NULL	2351.12	29.265	36.522	0.234	2206.85	2351.12					White Mica	Kaolinite?	Dickite?	200-300	neutral	Illite	Argillic	
30102_Lawyers2018_Halos9andard-Clays-S_30102_0396.ASD	FSFR.30102.52.Int=5.0 sec Lawyers2018	Muscovite	0.548	Dickite	0.452	104	1.918	0.974	0.944	2206.99	2243.98	2349.58	29.52	37.54	0.199	2206.99	2349.58					White Mica	Kaolinite?	Dickite?	200-300	neutral	Illite	Argillic	
30102_Lawyers2018_Halos9andard-Clays-S_30102_0397.ASD	FSFR.30102.52.Int=5.0 sec Lawyers2018	Muscovite	0.535	Dickite	0.282	67.96	1.923	0.977	0.946	2206.76	NULL	2350.29	29.367	28.428	0.239	2206.76	2350.29					White Mica	Kaolinite?	Dickite?	200-300	neutral	Illite	Argillic	
30102_Lawyers2018_Halos9andard-Clays-S_30102_0398.ASD	FSFR.30102.52.Int=5.0 sec Lawyers2018	Muscovite	0.502	Montmorillonite	0.257	66.353	1.873	0.973	0.9	2207.86	NULL	2346.18	32.335	28.898	0.367	2207.85	2346.18					White Mica	Jarosite		200-300	neutral	Illite	Argillic	
30102_Lawyers2018_Halos9andard-Clays-S_30102_0399.ASD	FSFR.30102.52.Int=5.0 sec Lawyers2018	Muscovite	0.524	Montmorillonite	0.302	67.823	1.87	0.964	0.906	2207.75	NULL	2347.31	28.994	32.641	0.354	2207.77	2347.31					White Mica	Jarosite		200-300	neutral	Illite	Argillic	
30102_Lawyers2018_Halos9andard-Clays-S_30102_0400.ASD	FSFR.30102.52.Int=5.0 sec Lawyers2018	Muscovite	0.609	Siderite	0.391	113.24	1.922	0.981	0.941	2204.94	NULL	2347.2	32.248	32.94	0.347	2204.94	2347.2					Montmorillonite	White Mica		0-150	neutral	Smectite	Argillic	
30102_Lawyers2018_Halos9andard-Clays-S_30102_0401.ASD	FSFR.30102.52.Int=5.0 sec Lawyers2018	Muscovite	0.702	Siderite	0.298	88.067	1.927	0.985	0.942	2207.69	NULL	2346.59	31.139	34.061	0.337	2207.68	2346.59					Montmorillonite	White Mica		0-150	neutral	Smectite	Argillic	
30102_Lawyers2018_Halos9andard-Clays-S_30102_0402.ASD	FSFR.30102.52.Int=5.0 sec Lawyers2018	NULL	NULL	NULL	NULL	NULL	1.96	0.992	0.968	2205.85	NULL	2343.28	29.519	26.182	0.404	2205.85	2343.28					Montmorillonite			0-150	neutral	Smectite	Argillic	
30102_Lawyers2018_Halos9andard-Clays-S_30102_0403.ASD	FSFR.30102.52.Int=5.0 sec Lawyers2018	Muscovite	0.799	Jarosite	0.201	60.28	1.908	0.983	0.925	2202.96	NULL	2345.71	33.128	31.346	0.436	2202.96	2345.71					Montmorillonite	Jarosite	White Mica	0-150	neutral	Smectite	Argillic	
30102_Lawyers2018_Halos9andard-Clays-S_30102_0404.ASD	FSFR.30102.52.Int=5.0 sec Lawyers2018	Muscovite	0.427	Montmorillonite	0.352	28.343	1.891	0.969	0.922	2208.58	NULL	2347.2	28.74	30.03	0.614	2208.6	2347.2					Montmorillonite	Jarosite	White Mica	0-150	neutral	Smectite	Argillic	
30102_Lawyers2018_Halos9andard-Clays-S_30102_0405.ASD	FSFR.30102.52.Int=5.0 sec Lawyers2018	Muscovite	0.364	Jarosite	0.357	33.581	1.901	0.971	0.931	2208.6	2261.09	2350.05	28.821	26.078	0.491	2208.62	2350.05					Montmorillonite	Jarosite	White Mica	0-150	neutral	Smectite	Argillic	
30102_Lawyers2018_Halos9andard-Clays-S_30102_0406.ASD	FSFR.30102.52.Int=5.0 sec Lawyers2018	Muscovite	0.673	Montmorillonite	0.327	75.614	1.794	0.952	0.842	2202	NULL	2345.79	34.093	37.252	0.563	2202	2345.79					White Mica	Montmorillonite		200-300	neutral	Illite	Argillic	
30102_Lawyers2018_Halos9andard-Clays-S_30102_0407.ASD	FSFR.30102.52.Int=5.0 sec Lawyers2018	Muscovite	0.646	Montmorillonite	0.354	61.751	1.848	0.971	0.877	2207.65	NULL	2346.13	32.936	35.115	0.587	2207.67	2346.13					White Mica	Montmorillonite		200-300	neutral	Illite	Argillic	
30102_Lawyers2018_Halos9andard-Clays-S_30102_0408.ASD	FSFR.30102.52.Int=5.0 sec Lawyers2018	Muscovite	0.687	Montmorillonite	0.313	78.551	1.796	0.956	0.841	2203.12	NULL	2344.9	33.708	35.935	0.581	2203.12	2344.9					White Mica	Montmorillonite		200-300	neutral	Illite	Argillic	
30102_Lawyers2018_Halos9andard-Clays-S_30102_0409.ASD	FSFR.30102.52.Int=5.0 sec Lawyers2018	Muscovite	0.626	Jarosite	0.374	22.853	1.941	0.985	0.955	2207.23	2262.36	2351.82	27.247	25.089	0.503	2207.23	2351.82					White Mica	Jarosite	Montmorillonite	200-300	neutral	Illite	Argillic	
30102_Lawyers2018_Halos9andard-Clays-S_30102_0410.ASD	FSFR.30102.52.Int=5.0 sec Lawyers2018	Muscovite	1	NULL	NULL	37.864	1.924	0.985	0.939	2207.26	NULL	2346.84	28.92	33.355	0.567	2207.27	2346.84					White Mica	Montmorillonite		200-300	neutral	Illite	Argillic	
30102_Lawyers2018_Halos9andard-Clays-S_30102_0411.ASD	FSFR.30102.52.Int=5.0 sec Lawyers2018	Muscovite	0.819	Jarosite	0.181	57.276	1.912	0.984	0.928	2208.2	NULL	2346.59	31.854	31.6	0.495	2208.24	2346.59					White Mica	Montmorillonite	Jarosite	200-300	neutral	Illite	Argillic	
30102_Lawyers2018_Halos9andard-Clays-S_30102_0412.ASD	FSFR.30102.52.Int=5.0 sec Lawyers2018	Muscovite	0.502	Montmorillonite	0.321	42.137	1.869	0.973	0.896	2204.8	NULL	2345.81	32.46	30.147	0.451	2204.8	2345.81					White Mica	Jarosite		200-300	neutral	Illite	Argillic	

Sample	SampleID	Date	BestLatitude	BestLongitude	BestElevation	UTM_East	UTM_North	MineralName1	StarRating1	MineralName2	StarRating2	MineralName3	StarRating3	MineralName4	StarRating4	MineralName5	StarRating5	MineralName6	StarRating6	MineralName7	StarRating7	AlFeMg	AlOH	CSM	Fe3i	Fe3t	FeOH	ISM	Kx	MgOH	sampler	type	add_notes
30102_Lawyers2018_Halos9andard-Clays-S_30102_0392.ASD	S_30102_0392	9/13/2018 4:02:41 PM	57° 20' 047 N	127° 97' 377 W	1417.9	605580	6356215	Ferrihydrite	3	Illite/Smectite	3	Palygorskite	2									2206.61	2206.61							2348.26	Ian Parker	clay	
30102_Lawyers2018_Halos9andard-Clays-S_30102_0393.ASD	S_30102_0393	9/13/2018 4:05:34 PM	57° 20' 047 N	127° 97' 377 W	1417.1	605581	6356175	Beidellite	3	Palygorskite	2	VNIR - No match	3									2206.42	2206.42				INV			2348.16	Ian Parker	clay	
30102_Lawyers2018_Halos9andard-Clays-S_30102_0394.ASD	S_30102_0394	9/13/2018 4:08:26 PM	57° 20' 047 N	127° 97' 377 W	1420.6	605525	6356135	Ferrihydrite	3	Palygorskite	2	Halloysite	1	Goethite	2							2206.48	2206.48		2.227	INV			1.033	2349.1	Ian Parker	clay	
30102_Lawyers2018_Halos9andard-Clays-S_30102_0395.ASD	S_30102_0395	9/13/2018 4:10:01 PM	57° 20' 047 N	127° 97' 377 W	1420.6	605749	6356018	Beidellite	3	Dickite	2	VNIR - No match	3									2206.95	2206.95				INV				Ian Parker	clay	
30102_Lawyers2018_Halos9andard-Clays-S_30102_0396.ASD	S_30102_0396	9/13/2018 4:11:31 PM	57° 20' 047 N	127° 97' 377 W	1415	605795	6356069	Beidellite	3	Dickite	1	VNIR - No match	3									2207.12	2207.12				INV				Ian Parker	clay	
30102_Lawyers2018_Halos9andard-Clays-S_30102_0397.ASD	S_30102_0397	9/13/2018 4:14:09 PM	57° 20' 047 N	127° 97' 377 W	1415.3	605782	6356097	Beidellite	3	Palygorskite	2	VNIR - No match	3									2206.89	2206.89				INV			2349.81	Ian Parker	clay	
30102_Lawyers2018_Halos9andard-Clays-S_30102_0398.ASD	S_30102_0398	9/13/2018 4:16:12 PM	57° 20' 047 N	127° 97' 377 W	1411.1	605756	6356143	Jarosite	3	K-illite	3	Nontronite	2	Goethite	2							2207.78	2207.78		1.878	924.629	INV	1.117		2345.3	Ian Parker	clay	
30102_Lawyers2018_Halos9andard-Clays-S_30102_0399.ASD	S_30102_0399	9/13/2018 4:18:24 PM	57° 20' 047 N	127° 97' 377 W	1414	605772	6356228	Ferrihydrite	3	K-illite	3	Palygorskite	3	Magnesite	1	Jarosite	2					2207.87	2207.87		2.5	906.542		0.986		2347.19	Ian Parker	clay	
30102_Lawyers2018_Halos9andard-Clays-S_30102_0400.ASD	S_30102_0400	9/13/2018 4:20:52 PM	57° 20' 047 N	127° 97' 377 W	1414.7	605507	6359371	Ferrihydrite	3	Heulandite	3	K-illite	3	Gypsum	1	Goethite	3					2204.73	2204.73		2.289	INV		0.373		2347.44	Taylor Milne	clay	Steep talus slope
30102_Lawyers2018_Halos9andard-Clays-S_30102_0401.ASD	S_30102_0401	9/13/2018 4:25:10 PM	57° 20' 047 N	127° 97' 377 W	1417.1	605518	6359393	Ferrihydrite	3	Illite/Smectite	3	Goethite	3									2207.87	2207.87		2.372	INV					Taylor Milne	clay	
30102_Lawyers2018_Halos9andard-Clays-S_30102_0402.ASD	S_30102_0402	9/13/2018 4:26:26 PM	57° 20' 047 N	127° 97' 377 W	1411.3	605504	6359374	Ferrihydrite	3	Chabazite	3	Muscovite	3									2206.45	2206.45					0.174			Taylor Milne	rock	
30102_Lawyers2018_Halos9andard-Clays-S_30102_0403.ASD	S_30102_0403	9/13/2018 4:27:35 PM	57° 20' 047 N	127° 97' 377 W	1416.5	605448	6359041	Ferrihydrite	3	Illite/Smectite	3	Jarosite	2									2203.42			2.623	INV					Taylor Milne	clay	
30102_Lawyers2018_Halos9andard-Clays-S_30102_0404.ASD	S_30102_0404	9/13/2018 5:13:27 PM	57° 20' 047 N	127° 97' 377 W	1415.4	606754	6355411	Jarosite	3	Illite/Smectite	3											2208.55			1.592	925.798					Adam LaRiviere	clay	
30102_Lawyers2018_Halos9andard-Clays-S_30102_0405.ASD	S_30102_0405	9/13/2018 5:15:26 PM	57° 20' 047 N	127° 97' 377 W	1412.5	606675	6355404	Jarosite	3	Illite/Smectite	3											2208.61			1.682	924.066					Adam LaRiviere	clay	
30102_Lawyers2018_Halos9andard-Clays-S_30102_0406.ASD	S_30102_0406	9/13/2018 5:17:22 PM	57° 20' 047 N	127° 97' 377 W	1416.1	606607	6355456	Jarosite	2	K-illite	3	Iron Saponite	3	Nontronite	3							2202	2202		1.517	INV	INV	0.729		2346.75	Adam LaRiviere	clay	
30102_Lawyers2018_Halos9andard-Clays-S_30102_0407.ASD	S_30102_0407	9/13/2018 5:19:11 PM	57° 20' 047 N	127° 97' 377 W	1412.8	606538	6355436	Jarosite	3	Illite/Smectite	3	Goethite	2									2207.6			1.64	903.887					Adam LaRiviere	clay	
30102_Lawyers2018_Halos9andard-Clays-S_30102_0408.ASD	S_30102_0408	9/13/2018 5:20:41 PM	57° 20' 047 N	127° 97' 377 W	1407.9	606476	6355415	Ferrihydrite	3	K-illite	3	Beidellite	3	Nontronite	2	Goethite	1					2203.21	2203.21		1.913	907.968	INV	0.76		2345.63	Adam LaRiviere	clay	
30102_Lawyers2018_Halos9andard-Clays-S_30102_0409.ASD	S_30102_0409	9/13/2018 5:21:57 PM	57° 20' 047 N	127° 97' 377 W	1414.1	606420	6355440	Ferrihydrite	3	Illite/Smectite	3	Jarosite	2									2207.21			2.386	925.63					Adam LaRiviere	clay	
30102_Lawyers2018_Halos9andard-Clays-S_30102_0410.ASD	S_30102_0410	9/13/2018 5:23:45 PM	57° 20' 047 N	127° 97' 377 W	1414.1	606373	6355482	Ferrihydrite	3	Illite/Smectite	3																				Adam LaRiviere	clay	
30102_Lawyers2018_Halos9andard-Clays-S_30102_0411.ASD	S_30102_0411	9/13/2018 5:25:05 PM	57° 20' 047 N	127° 97' 377 W	1409.5	606295	6355512	Jarosite	3	Illite/Smectite	3	Goethite	2									2208.28			1.804	886.18					Adam LaRiviere	clay	
30102_Lawyers2018_Halos9andard-Clays-S_30102_0412.ASD	S_30102_0412	9/13/2018 5:26:30 PM	57° 20' 047 N	127° 97' 377 W	1415.9	606225	6355501	Jarosite	3	Montmorillonite	3	Muscovite	2									2204.85	2204.85		1.474	919.335		0.648		2345.93	Adam LaRiviere	clay	

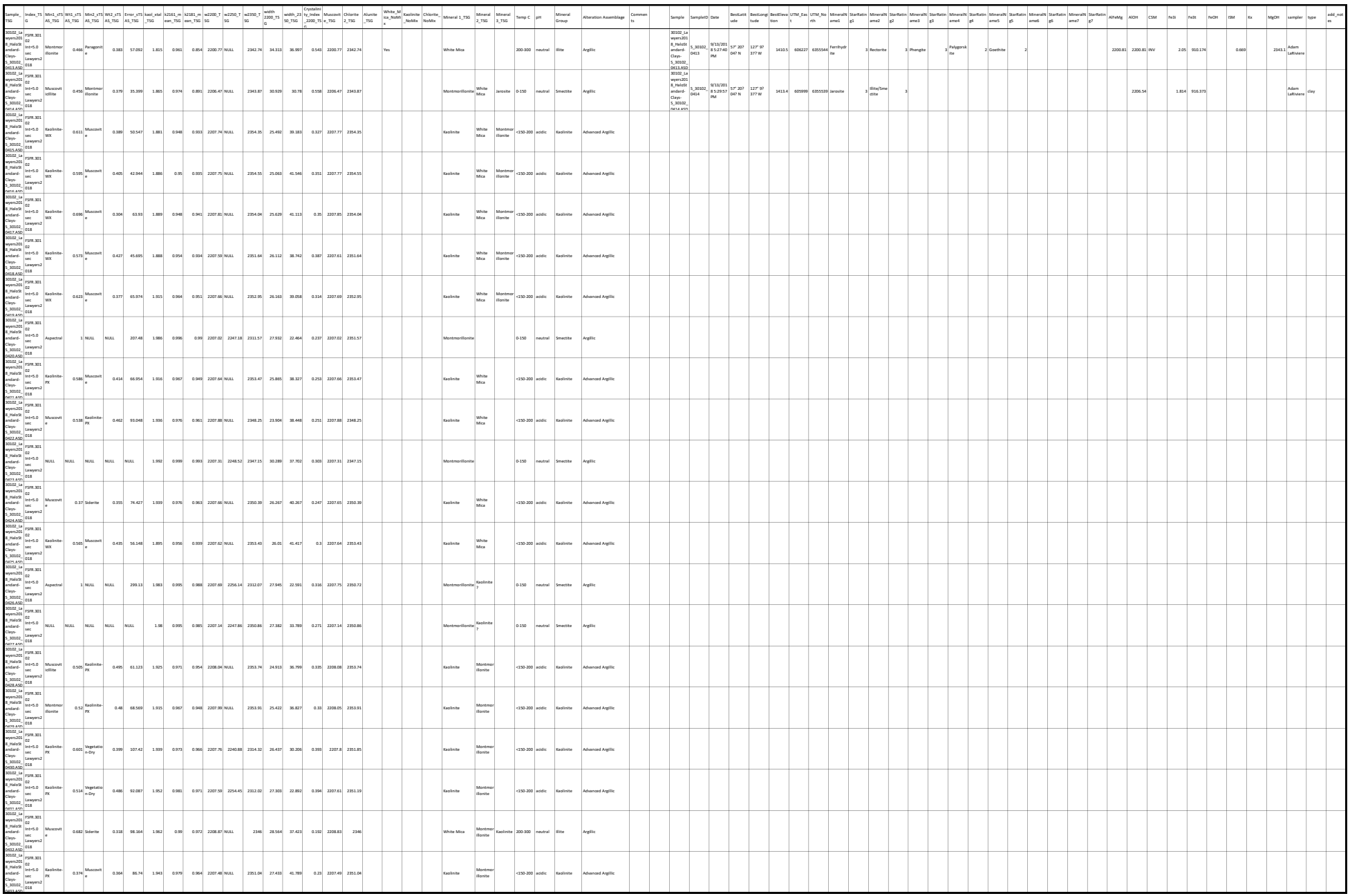

| Sample_TSG | Index_TSG | Min1_sTSAS_TSG | Wt1_sTSAS_TSG | Min2_sTSAS_TSG | Wt2_sTSAS_TSG | Error_sTSAS_TSG | kaol_xtal_TSG | k2161_mean_TSG | k2181_mean_TSG | w2200_TSG | w2250_TSG | w2350_TSG | width_2200_TSG | width_2350_TSG | Crystallinity_Index_2200_TSG | Muscovite_TSG | Chlorite_2_TSG | Alunite_TSG | White_Mica_NoMix | Kaolinite_NoMix | Chlorite_NoMix | Mineral 1_TSG | Mineral 2_TSG | Mineral 3_TSG | Temp C | pH | Mineral Group | Alteration Assemblage | Comments | | Sample | SampleID | Date | BestLatitude | BestLongitude | BestElevation | UTM_East | UTM_North | MineralName1 | StarRating1 | MineralName2 | StarRating2 | MineralName3 | StarRating3 | MineralName4 | StarRating4 | MineralName5 | StarRating5 | MineralName6 | StarRating6 | MineralName7 | StarRating7 | AlFeMg | AlOH | CSM | Fe3i | Fe3t | FeOH | ISM | Kx | MgOH | sampler | type | add_notes |
|---|---|---

| Sample_TSG | Index_TSG | Min1_sTSAS_TSG | Wl1_sTSAS_TSG | Min2_sTSAS_TSG | Wl2_sTSAS_TSG | Error_sTSAS_TSG | kaol_xtal_TSG | k2161_mean_TSG | k2181_mean_TSG | w2200_TSG | w2250_TSG | w2350_TSG | width_2200_TSG | width_2350_TSG | Crystallinity_Index_2200_TSG | Muscovite_TSG | Chlorite2_TSG | Alunite_TSG | White_Mica_NoMix | Kaolinite_NoMix | Chlorite_NoMix | Mineral 1_TSG | Mineral 2_TSG | Mineral 3_TSG | Temp C | pH | Mineral Group | Alteration Assemblage | Comments | | Sample | SampleID | Date | BestLatitude | BestLongitude | BestElevation | UTM_East | UTM_North | MineralName1 | StarRating1 | MineralName2 | StarRating2 | MineralName3 | StarRating3 | MineralName4 | StarRating4 | MineralName5 | StarRating5 | MineralName6 | StarRating6 | MineralName7 | StarRating7 | AlFeMg | AlOH | CSM | FeSi | FeSt | FeOH | ISM | Kx | MgOH | sampler | type | add_notes |
|---|---|---